IJAO The International Journal of Artificial Organs

Abstract

ESAO-IFAO Congress

The International Journal of Artificial Organs
2024, Vol. 47(7) 421–565

DOI: 10.1177/03913988241279540
journals.sagepub.com/home/jao
Sage

INFLUENCE OF LENGTH OF SIDE HOLE PORTION AND INTERVAL OF SIDE HOLES IN DRAINAGE CANNULAE FOR V-V ECMO: EFFECT ON RECIRCULATION RATE AND BLOOD OXYGENATION

Konomi Togo (1)

1. Teikyo Heisei University, Japan

Introduction: We employ veno-venous extracorporeal membrane oxygenation (V-V ECMO) to address severe respiratory failure. In V-V ECMO, a variable proportion of oxygenated blood from the return cannula enters the drainage cannula. This condition is known as recirculation. Increased recirculation rates may result in insufficient blood oxygenation. Cannula design may influence recirculation rates. Therefore, in this study, I investigated the effects of the length of the side hole portion and the intervals of the side holes in drainage cannulae on the recirculation rate and blood oxygenation.

Methods: As shown in Figure 1, I manufactured drainage cannulae with side holes, respectively.

I inserted drainage and return cannulae into the simulated circuit, positioning the tip of the drainage cannula in the atrium and the return cannula in the superior vena cava. I filled the simulated circuit, including the venous reservoir, with 5 L of porcine blood. Prior to initiating ECMO, I adjusted the blood oxygen saturation to 60 ± 5% and the partial pressure of carbon dioxide to 70 ± 10 mmHg.

After initiating ECMO, I measured the recirculation rate and the arterial oxygen pressure (PaO2).

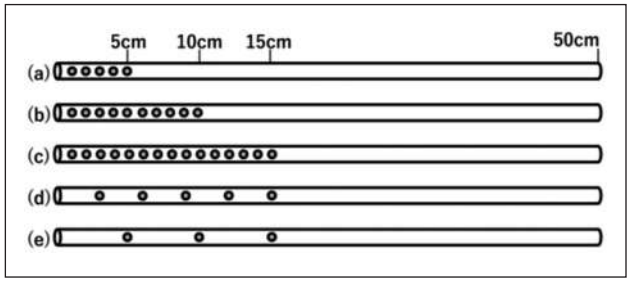

Figure 1. Cannulae.
I designed side holes as depicted in (a) through (e), respectively: (a) at 1 cm intervals from the tip to 5 cm [5cm], (b) at 1 cm intervals from the tip to 10 cm [10cm], (c) at 1 cm intervals from the tip to 15 cm [15cm], (d) at 3 cm intervals from the tip to 15 cm [3cm intervals], (e) at 5 cm intervals from the tip to 15 cm [5cm intervals]. All side holes were 2 mm in diameter.

Results: The recirculation rate and PaO2 were as follows: (a) 5 cm: 54 ± 5 % and 95 ± 7 mmHg; (b) 10 cm: 38 ± 1 % and 139 ± 8 mmHg; (c) 15 cm: 31 ± 1 % and 166 ± 6 mmHg; (d) 3 cm intervals: 34 ± 1 % and 154 ± 7 mmHg; (e) 5 cm intervals: 39 ± 1 % and 134 ± 7 mmHg, respectively (n = 6).

Discussion: Among the cannulae evaluated, (c) 15 cm demonstrated the lowest recirculation rate and best blood oxygenation, followed by cannula with (d) 3 cm intervals. Despite having a greater number of side holes, the (b) 10 cm cannula resulted in lower blood oxygenation compared to the (d) 3 cm intervals cannula. In V-V ECMO, it has been reported that blood is predominantly drained from the bottom portion of the drainage cannula rather than the tip [1]. Based on this, I inferred that a cannula with a longer side hole portion drained more unoxygenated blood, resulting in more efficient blood oxygenation.

Conclusion: In V-V ECMO, we should use cannulae with long side hole portions.

Reference

1. JA Lindholm, J Thorac Dis, 10:S606-S612, 2018.

Acknowledgements

I am grateful to Professor Akihiro C. Yamashita for his advice.

CHANGES IN THE GLOMERULAR MACROPHAGE INDEX (GMI) BETWEEN TWO CONSECUTIVE BIOPSIES AND THE ASSOCIATION TO RENAL TRANSPLANT GRAFT SURVIVAL

Salmir Nasic[1,2], Johan Mölne[3,4], Marie Eriksson[5], Bernd Stegmayr[6], Henri Afghahi[2,7], Björn Peters[2,7]

[1]Region Västra Götaland, Skaraborg Hospital, Research, Education, Development and Innovation Department, Skövde; [2]Department of Molecular and Clinical Medicine, Institute of Medicine, the Sahlgrenska Academy at University of Gothenburg, Gothenburg; [3]Institute of Biomedicine, Department of Laboratory Medicine, University of Gothenburg, Gothenburg; [4]Region Västra Götaland, Sahlgrenska University Hospital, Clinical Pathology, Gothenburg; [5]Department of Statistics, Umeå School of Business, Economics and Statistics, Umeå University, Umeå;[6]Public Health and Clinical Medicine Umeå University, Umeå; [7]Region Västra Götaland, Skaraborg Hospital, Department of Nephrology, Skövde; all in Sweden

Introduction: Macrophages in kidney transplants were shown to be involved in inflammatory processes in transplants, and higher numbers are associated with worsened graft survival [1].

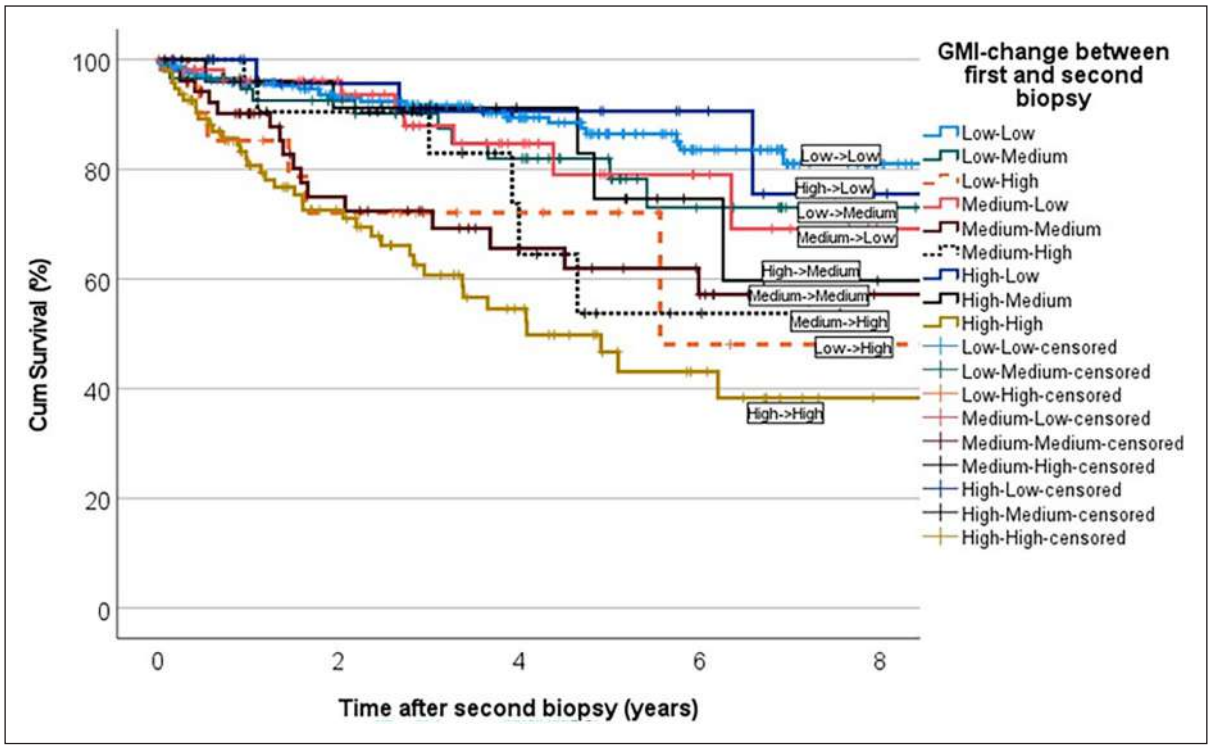

Figure 1. Graft survival (Kaplan-Meier curve) according to GMI-change between the first and second biopsy.

The aim of the study was to investigate if changes exist in the levels of glomerular macrophage index (GMI) between two consecutive kidney transplant biopsies, and if so to determine their potential impact on graft survival.

Methods: The study included 623 patients with two consecutive biopsies performed on the same renal graft. The median time between the first and second biopsies was 86 days. GMI was defined as the average number of macrophages in ten glomeruli and was categorized into three GMI classes: ≤1.8 Low, 1.9-4.5 Medium, and ≥4.6 High. This division yielded nine possible switches between the first and second biopsies (Low-Low, Low-Medium, etc.). Death censored graft survival was analyzed by a Cox-regressions adjusted for age and sex. Hazard ratios (HR) with 95% confidence interval (CI) are presented.

Results: The worst graft survival was observed in the High-High group, and the best graft survival was observed in the Low-Low and High-Low groups (Figure 1). Compared to the High-High group, a reduction of risk was observed in nearly all other decreasing groups (reductions between 65% and 80% of graft loss). The risk for graft-loss was lower in the Low-Low (HR=0.24, CI 0.13-0.46), Low-Medium (HR=0.25, CI 0.11-0.55), Medium-Low (HR=0.29, CI 0.11-0.77) and the High-Low GMI (HR=0.31, CI 0.10-0.98) groups compared to the High-High group as the reference adjusted for covariates.

Discussion: Our findings suggest that high or increasing GMI levels are associated with shorter graft survival, whereas low or decreasing GMI levels are associated with longer graft survival. The present study indicates that the extent of macrophage involvement may change in some grafts and if reduced from High to Low levels could be associated with less graft loss. This indicates that clinicians should aim to lower the extent of macrophage involvement.

Reference

1. Mölne J et al, Clin Transplant, 36(12):e14816, 2022.

Acknowledgements

The authors are grateful to the patients and staff who performed the data collection for enabling this study. Further, the authors are grateful to the Research Fund (FoUUI) at Skaraborg Hospital, Skövde, Sweden, and the Healthcare Board, Region Västra Götaland, Sweden and Njurföreningen Norrland, Sweden.

A BIOREACTOR TO INVESTIGATE THE MECHANICAL INFLUENCE ON CELL MINERALIZATION IN LATTICE BONE IMPLANTS

Erik Kornfellner (1), Matthias Vostatek (1), Elettra Verin (1), Martin Stoiber (1,2), Francesco Moscato (1,2,3)

1. Medical University of Vienna, Austria; 2. Ludwig Boltzmann Institute for Cardiovascular Research, Austria; 3. Austrian Cluster for Tissue Regeneration, Austria

Introduction: Bone implants require a considerable period of time until they become integrated within the native bone [1]. In this context, implants with lattice structures are becoming increasingly interesting because of their macroporosity and thus potentially improved osteoconductive properties [2, 3]. However, understanding the implant's healing dynamics and its dependency on mechanical loads necessitates knowledge of how cells behave within the lattice geometries. Therefore, a bioreactor reproducing mechanical loads on cell-seeded lattice structures, concurrently allowing mechanical properties measurement over time as results extracellular bone matrix calcification would be valuable. This work presents such a bioreactor design and its working principles.

Methods: A reservoir for a human mesenchymal stem cell culture was manufactured using 3D printing with biocompatible resins. The rod-shaped material samples were also 3D printed, including lattice

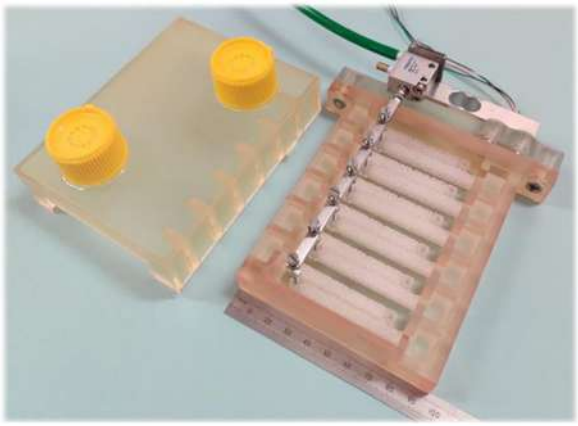

Figure 1. Photo of the bioreactor. Placed on the left side is the lid with ventilated caps. The bioreactor on the right side of the image contains 12 specimens with lattices, of which 6 will be mechanically stimulated. Attached to this is the pneumatic actuator and the load cell to measure the force applied to the specimen.

structures, that can be inserted into this reservoir. A pneumatic cylinder was installed to induce controlled deformation at one end of the samples, which were thus subjected to bending. A load cell and temperature-compensated bridge circuit were incorporated to measure the force exerted by the pneumatic cylinder on the lattice samples. A microcontroller was employed to dictate the stimulation patterns and store the measurement results.

Results: The bioreactor can accommodate a total of twelve rod-shaped samples with a size of 50×8×5 mm³. Among these, six samples can be bent with a stroke of up to 5 mm. The remaining six samples are not stimulated and serve as a control. All stimulated samples are attached to a single axis, and the force on all six samples is measured collectively. The load cell can handle a force of up to 50 N, which can be measured with a resolution of 24 bits. The entire bioreactor can be housed in a static incubator. The bioreactor features a lid with air filters to prevent contamination while allowing air circulation. Only thin cables for measurement and a hose for compressed air need to be led into the incubator, while all other components remain outside. There is no exchange of air between the incubator and the compressed air for the pneumatic cylinder.

Discussion: The bioreactor has successfully undergone and passed a 72-hour durability tests and the first cell experiments with this bioreactor will begin shortly. This bioreactor enables both static and dynamic mechanical testing. Moreover, the samples can be easily extracted, enabling further examination, such as microscopical analysis and staining to detect calcium deposits. This also includes the possibility to evaluate cell responses to mechanical stimuli in both static and dynamic conditions. We anticipate obtaining insightful findings about the alterations in lattice structures induced by bone cells. Insights that would have been unattainable without the aid of such a specialized bioreactor.

References

1. T. Albrektsson et al, JSM Dent. Surg. Vol. 2, No. 3, 2017
2. C. Ghayor et al, Front. Physiol., Vol. 9, 2018
3. F. E. Weber, Tissue Eng. Part B Rev., Vol. 25, No. 5, 2019

Acknowledgements

The authors thankfully acknowledge the support from Stefan Tögel, who provided us access to the cell laboratory for preliminary testing. The construction of the bioreactor was partially funded by the ZMPBME-MedUni Wien Φocus Grant and the INKplant project (FFG grant number: 877452).

A SYSTEMATIC REVIEW OF KNOWN INHIBITORS OF VASCULAR CALCIFICATION IN CHRONIC KIDNEY DISEASE

Jana Holmar (1), Annika Adoberg (1,2), Liisi Leis (1,2), Merike Luman (1,2), Fredrik Uhlin (1,3), Ivo Fridolin (1)

1. Tallinn University of Technology, Department of Health Technologies, Tallinn, Estonia; 2. Centre of Nephrology, North Estonia Medical Centre, Tallinn, Estonia; 3. Linköping University, Department of Health, Medicine and Caring Sciences, Linköping, Sweden

Introduction: Approximately 13% of the population suffers from chronic kidney disease (CKD) globally. Furthermore, about half of the patients with CKD stages 4-5 encounter and eventually die from cardiovascular disease (CVD) [1]. The overwhelming part of the treatment for CKD stage 5 (end-stage renal disease -ESRD) patients for replacing kidney function is hemodialysis. The global number of individuals receiving dialysis treatment reached 2.7 million in 2016 and is estimated to reach 5.4 million by the year 2030 [2]. The occurrence of vascular calcification (VC), deposition of calcium salts in the form of hydroxyapatite in the vascular wall, increases with age in the general population, but is highly frequent and markedly accelerated in patients with CKD [3]. KDIGO (Kidney Disease: Improving Global Outcomes) CKD guidelines suggest considering the patients with advanced CKD (stages 3–5) and VC at the highest CVD risk [4]. More prevalent VC in CKD is believed to result from a disturbed balance between inhibitors and inducers of calcification. During dialysis therapy, uremic toxins are filtered out from the blood regularly. However, during the procedure, all the substances fitting the cut-off size of the dialysis membranes are transported to spent dialysate, among them many beneficial substances (including the inhibitors of vascular calcification). Washout of proteins e.g. albumin (MW 66 kDa) is considered to be a disadvantage of the more effective dialysis [5]. The cut-off value for the older type of membranes is about 3 000 Da, in the case of newer membranes it is around 15 000 Da and in super high-flux dialysis, it can reach 65 000 Da [6]. It is likely that many of VC inhibitors are removed during dialysis therapy, however it is not monitored. We performed a systematic review of literature to collect information about the substances with proved inhibitory effect on VC as a first step towards monitoring the inhibitors removal to make modifications or interventions to improve the inducers-inhibitors balance and thereby help improve these patients' quality of life.

Methods: An advanced search in PubMed and Web of Science was performed to identify existing research in August, 2023, and March, 2024. The systematic review was registered in the PROSPERO database. The search strategy is given in figure 1. Altogether, 177 papers were added to the extensive analysis. Vascular calcification inhibitors were divided in different categories and tables.

Results: Endogenous inhibitors in patients with CKD are fetuin-A, matrix Gla protein, osteoprotegerin, osteopontin, vitamin D, sclerostin, FGF23, magnesium and klotho. Additionally, substances that have shown potential in further research, growth factors, medications, and plant-origin inhibitors were systematized.

Discussion: Measuring the levels of inhibitors that are most probably dialyzed or estimating how serum levels of VC inhibitors during hemodialysis are in relationship with removed uremic toxins would expand further knowledge towards patient-tailored treatment.

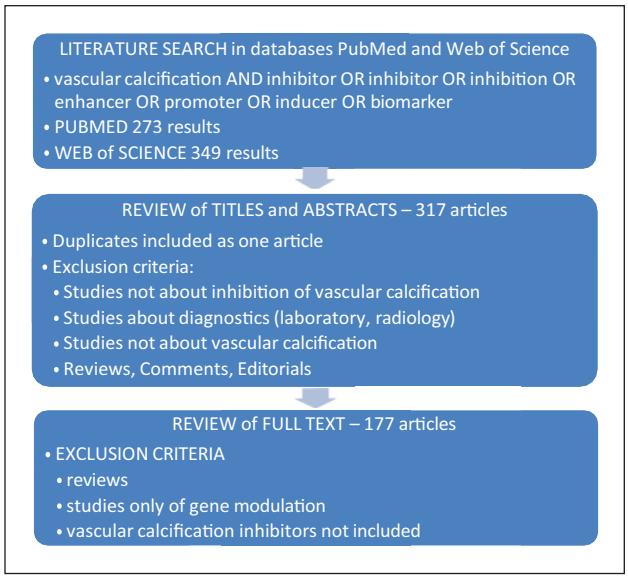

Figure 1. The search strategy.

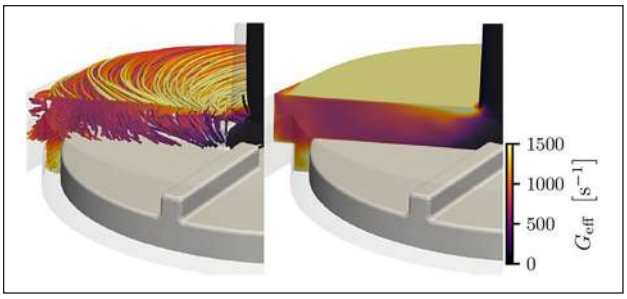

Figure 1. Effective shear rate as predicted by the Lagrangian (left) and Eulerian (right) formulation in a simple blood pump.

Table 1. Execution times of simulations on 192 cores.

Simulation	Time
CFD	20 h
Full-order Eulerian morphology	4000 h
Tank-treading Eulerian morphology	8 min

References

1. Hill, N.R. et al, PLOS ONE, 11, e0158765, 2016.
2. Himmelfarb, J. et al, Nat Rev Nephrol 16, 573–585, 2020.
3. Ruderman, I. et al, Semin Dial, 31, 487-499,2018.
4. Drüeke, T.B., Nephrol Ther, 6, 149-150, 2010.
5. Gayrard, N. et al, PLOS ONE, 12, e0171179, 2017.
6. Olczyk, P. et al, Polim Med, 48, 57-63, 2018.

Acknowledgements

The research was funded by the Estonian Research Council grant PSG819.

AN EFFICIENT COMPUTATIONAL MODEL FOR STRAIN-BASED HEMOLYSIS PREDICTION IN EULERIAN FRAME

Nico Dirkes, Marek Behr

Chair for Computational Analysis for Technical Systems, RWTH Aachen University, Schinkelstr. 2, 52062 Aachen, Germany

Introduction: Flow-induced red blood cell damage (hemolysis) is a key factor in the design process of blood-handling medical devices, such as ventricular assist devices. The numerical prediction of this phenomenon is based on computational fluid dynamics (CFD) simulations. The most basic hemolysis models post-process the CFD results by directly applying empirical correlations to fluid stress (stress-based models). More recent models use the CFD results to explicitly resolve cell deformation (strain-based models). A disadvantage is that these models are typically written in a Lagrangian formulation, i.e., they require particle tracing. This can lead to gaps in coverage and a selection bias. In addition, they are generally expensive to evaluate if they explicitly resolve membrane structure and deformation. They are thus not well-suited for the design of real-world mechanical circulatory support systems.

Methods: We present the new tank-treading morphology model (TTM), a more practical strain-based hemolysis model. It takes into account the characteristic membrane deformation time of red blood cells and allows for an Eulerian formulation. The equations are derived in detail in [1]. As a result, we obtain a field for the effective shear rate Geff(x,t). This effective shear rate is a measure for the instantaneous membrane strain of red blood cells. It can be evaluated at every point x inside the domain and for every time t. This enables designers of medical devices to evaluate precisely where the most hemolysis occurs.

The Eulerian formulation is implemented as part of our in-house multi-physics finite element code [1]. We additionally provide an open-source Python code HemTracer [2] to apply our model in Lagrangian frame and compare it to other common hemolysis models.

Results: We apply our model to a selection of test cases, among them a simple three-dimensional blood pump. We compare the Eulerian formulation to the Lagrangian formulation in Figure 1. The Lagrangian solution exhibits gaps in coverage. In particular, the region around the inner tips of the impeller blades is not penetrated by any of the selected red blood cells.

As Table 1 shows, our new model, the TTM, is two orders of magnitude faster than the CFD simulation and four orders of magnitude faster than a comparable Eulerian strain-based hemolysis model.

Discussion: In contrast to Eulerian stress-based models, the TTM is able to capture the viscoelastic behavior of the cell membrane by resolving cell deformation time. Compared to Lagrangian strain-based models, the TTM is computationally more efficient and does not require tracking individual cells, enabling a more effective analysis of localized hemolysis. These qualities will make it a valuable tool for the design process of future generations of medical devices.

References

1. Dirkes et al., Comput. Methods Appl. Mech. Engrg. 426:116979, 2024
2. https://github.com/nicodirkes/HemTracer

Acknowledgements

This work was funded by the Deutsche Forschungsgemeinschaft (DFG, German Research Foundation) through grant 333849990/GRK2379 (IRTG Modern Inverse Problems).

MORPHOLOGICAL CHARACTERIZATION OF HEALTHY AND PATHOLOGICAL MUSCLES BY OPTICAL COHERENCE TOMOGRAPHY AND IMAGE ANALYSIS

J.F. Escobar-Huertas (1,2), J.J. Vaca-González (3), D.A. Garzón-Alvarado (2), Olfa Trabelsi (1)

1. Université de technologie de Compiègne, CNRS, Biomechanics and Bioengineering, Centre de Recherche Royallieu, CS 60319 -60203 Compiègne Cedex, France. 2. Numerical Methods and Modeling Research Group (GNUM), Universidad Nacional de Colombia, Bogotá, Colombia. 3. Escuela de pregrado, Dirección Académica, Vicerrectoría de Sede, Universidad Nacional de Colombia, Sede la Paz, Cesar, Colombia.

Introduction: Skeletal muscle comprises 40% of total body mass of mammals containing 50 to 75% of the body's protein [1], [2]. The most prevalent genetic muscle disease affecting children is Duchene muscular dystrophy (DMD) [1]. A new nondestructive technique called Optical Coherence Tomography (OCT) for morphological and mechanical characterization of tissues was used. OCT is a non-invasive optical method founded on the interferometry principle. In biological tissues, high scattering results in a loss of contrast, particularly for OCT images. Accordingly, several studies have used clearing agents (CA) to replace interstitial fluids [3],[4]. Accordingly, a morphological characterization of healthy and DMD rat muscles by OCT technique with Iodixanol (IOD) as CA was developed. By employing this 3D imaging method, we conducted a detailed description of structural differences of muscles. Additionally, as the tissue is preserved it could be used for upcoming mechanical tests.

Methods: Optical Coherence Tomography (OCT) imaging: An OCT system (Thorlabs OCT-TEL220C1) with a wavelength of 1.300nm, was used to assess the three-dimensional microstructure architecture of the sample. Muscles were thawed at room temperature in PBS. Then, muscles were fixed in a biaxial test machine by jaws and a preconditioning process was carried out. Thereafter, muscles were immersed in IOD for the clearing process and image acquisition was performed. The Weka tool in ImageJ was used to segmentate muscle fibers. **Muscle isolation:** Wistar rats, were used in this study. The protocol used in the present study complies with the principles of animal care and the French ethical rules of veterinary authorities (Council of Europe No. 123, Strasbourg 1985). Extensor digitorum longus (EDL) and soleus muscles were isolated from healthy and pathological rats for the analysis. **Statistical analysis:** The statistical analysis was performed using R software. A Mann-Whitney U test for a non-parametric population was performed to determine differences between control and DMD muscles fibers.

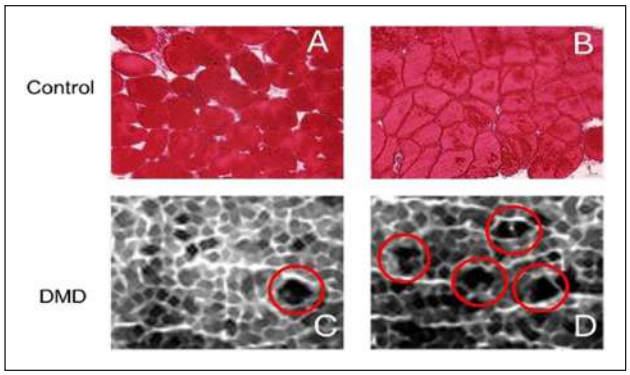

Figure 1. A,B) Histologies of soleus healthy muscles. C,D) OCT images of pathological EDL muscles (red circles).

Results: Increase of homogeneous refractive index across the muscle and reduction of the scattering coefficient were induced by IOD. OCT images obtained after the filtering and the machine learning (Weka) are shown in Figure 1. Muscle fibers, in EDL control muscles, have a homogeneous shape and geometry. However, it can be observed that there are more round-shaped muscle fibers (red circles) in DMD muscles due to the symptoms and evolution of the pathology (Figure 1). Statistical differences of muscle fibers diameter and ECM area were analyzed. Results evidenced an increase in the number of fibers greater than 45 µm (Figure 2).

Discussion: The application of new techniques like OCT enables to visualize and quantify the microscopic architecture of the healthy and pathological muscles without affecting the tissue, which gives the possibility to preserve the sample for further uses such as mechanical testing or molecular characterization. IOD as clearing agent enables us to develop a statistical analysis of muscle fibers morphology and extracellular matrix quantity for healthy or pathological muscles. The OCT, the image segmentation, and statistical analysis applied allowed us to characterize accurately pathological tissues like DMD muscles.

References

1. J. F. Escobar-Huertas et al, Cytoskeleton, 1–18, 2024.
2. K. Grzelkowska-Kowalczyk, InTech, 2016, pp. 1–22.
3. M. Maillet et al, Ann Biomed Eng, 1–14, Jun. 2023.
4. V. A. Acosta Santamaría et al, Front Mech Eng, 1– 14, 2018.

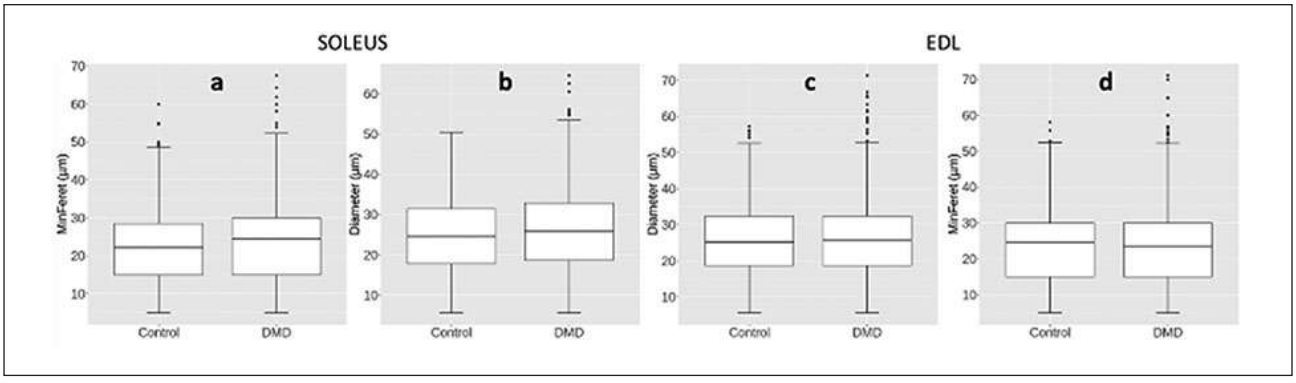

Figure 2. Minferet and diameter boxplots of healthy and pathological fiber for the soleus and EDL muscle.

FABRICATING HUMANS: ETHICAL AND REGULATORY ISSUES

Elena Salvaterra

[1]*ISOPROG Somatolink EPFP research network, Italy*

Introduction: 3D bioprinting of tissues and organs is considered the 4th industrial revolution in the field of medicine and biotechnology. The successful transplantation of an ear printed via 3D, performed in 2022 in the USA, confirmed the potential of this technology to transform regenerative medicine and surgery. However, bioprinting raises important ethical and legal issues that deserve a special attention. Considering that 3D bioprinting makes possible to fabricate body parts on demand, it is necessary to analyze at least the following issues: first, the ethical legitimacy of the human fabrication. What are the ethical conditions legitimizing the printing of vital tissues and organs for transplantation or regeneration? Then, to what extent is ethical using this technology for medical purposes? Biofabrication has the capacity to generate new human species as well as to overcome the natural boundaries of the human life. Where should it be drawn a threshold, if any? Further issues relate to the legal aspects of bioprinting and raises specific questions about a) the ownership of 3D bio-constructs, b) the consent to the medical uses of 3d bioprinting, c) the privacy protection, d) the intellectual property rights. This presentation aims to analyze these issues looking at the potentiality of 3D bioprinting to develop commercial profitable fabrics of vital human body parts.

Materials and methods: An analysis of articles discussing the ethical and legal issues related to 3D bioprinting was performed. This analysis was conducted by searching pertaining articles via google scholars and selecting them trough specific keywords as biofabrication, 3d bioprinting, immortal life, digital twins, ethichal issues, regulations. It was a typical desk analysis including papers published both in indexed and non indexed journals.

Results: The number of articles considering the ethical and legal issues related to 3D bioprinting is still limited. 3D bioprinting is mostly anlaysed in engineering, biomedical, technical perspectives. Though these aspects are analysed deeply both in ethical and legal issues. There is not a consensus on the classification of the orgnaism deriving from bioprinting (is it a new species or not?), however there is a main position on the refusal of the immortal life as “product” of bioprinting for ethical reasons. Other aspects ethically and legally considered are a) informed consent, b) privacy protection, c) IPRs. Lack of specific regulations on 3D organ bioprinting is a shared point on international level.

Conclusions: Considering the rapid advances of human bioprinting, as witnessed in the international literature, ther is a pressing demand to ethically classify and regulate the “products” of this technology per sé and as parts of the human body. There is also the need to identify procedures governing informed consent, the privacy protection, the IPRs.

From the IPR perspective, there is a pressing request to identify regulations clarifying how bioprinting and its products should be considered both in medical practice and market.

References

1. Wallace G.G., R. Cornok, C. O’ Connell, et al. (2014). 3D bioprinting. Printing parts for bodies. Australia: ARC Centre of Excellence for Electromaterials Science.
2. Kirillova A., S. Bushev, A. Abubakirov, et al. (2020). Bioethical and legal issues in 3D Bioprinting. *Int J Bioprint* 6(3):272.
3. Atala A. (2011). Tissue engineering of human bladder. *Br Med Bull* 97: 81-104.
4. Ricci G., F. Gibelli, A. Sirignano. (2023). Three-dimensional bioprinting of human organs and tissues: bioethical and medico-legal implications examined through a Scoping Review. *Bioengineering* 10 (9): 1052.

RESVERALOGUES PROTECT HEPG2 CELLS AGAINST CELLULAR SENESCENCE INDUCED BY HEPATOTOXIC METABOLITES

Neda Heidari, Richard Faragher, Susan Sandeman

School of Applied Sciences, University of Brighton, England

Introduction: Progressive liver disease and dysfunction cause toxic metabolites including ammonia and unconjugated bilirubin to accumulate in plasma. As the population ages alternatives to liver transplantation become increasingly important. One approach for use as a bridge to transplant or recovery is the use of bioartificial liver systems (BALS) containing primary or immortalised hepatocytes as ex-vivo replacements or supports for endogenous liver function. However, exposure to the hepatotoxic metabolites present in plasma causes the rapid failure of these cells to carry out their primary metabolic functions despite remaining viable [1,2]. Hypothesing that components of the hepatotoxic mixture of metabolites and cytokines that accumulate in plasma during liver failure induce cellular senescence and that this altered phenotype drives the failure to detoxify patient plasma in BALS leading to device and clinical endpoint failure.

Methods: HepG2 cell populations, grown in both standard two-dimensional tissue culture systems(2-D) and three-dimensional cultures (3-D) on novel alginate-modified HEMA-MBA cryogels, were exposed to physiologically reflective concentrations of hepatotoxic metabolites and cytokines for six hours. Following treatment, cultures were profiled for growth fraction (by EdU and Ki67 labelling), and senescent fraction (QPCR for p53,p16 and p21 as well as senescence-associated-β galactosidase). Albumin and urea synthesis was measured at 2-D and 3-D surfaces after exposure to hepatotoxins. Simultaneously the potential for SIRT1 activating and non-activating resveralogues to protect HepG2 populations from hepatotoxic metabolites were evaluated.

Results: HepG2 cells were forced into senescence by the toxic metabolites in under six hours (as measured by loss of thymidine analogue incorporation EdU or detectable Ki67 staining) which is associated with a ten to twenty-fold reduction in the capacity of the cultures to synthesise albumin or urea (figure1). This state of senescence induced by liver toxins (SILT) can be prevented by preincubation with either 2-5μM resveratrol, or a series of novel resveralogues with differential capacities to scavenge radicals and activate SIRT1.

Discussion: Senescence Induced by Liver Toxins appears to be a previously unrecognised but critical barrier to the deployment of BALS and to the development of artificial organs more generally which can now be overcome using small molecules that are safe for human use at concentrations readily achievable *in vivo*.

References

1. Abrahamse et al, International journal of artificial organs, 25(10) (2002), pp. 966-974.
2. Struecker et al, Nature Reviews Gastroenterology and Hepatology. 11(3) (2014) pp166-176.

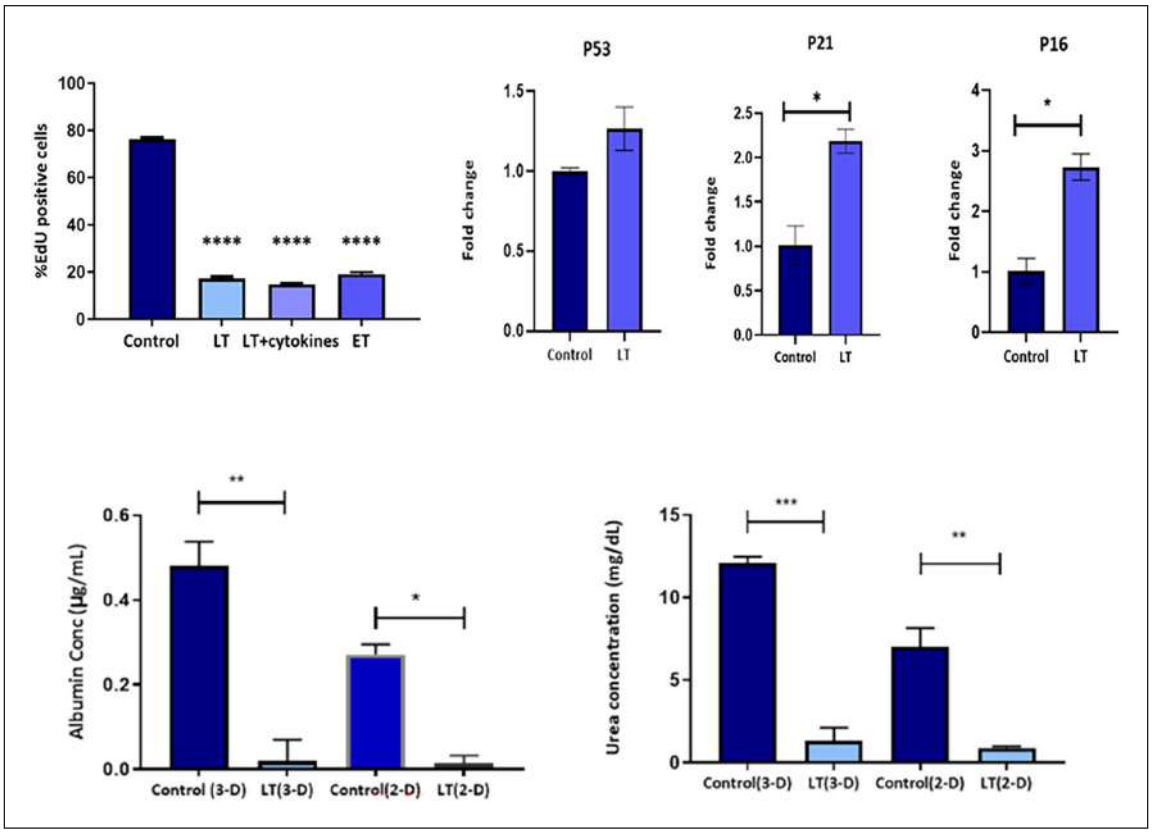

Figure 1. Six-hour treatment with liver toxins cocktail (LT) induces senescence in HepG2 cells as efficiently as etoposide treatment (ET) as measured by loss of labelling index (top left) and induction of the classical senescence markers p21 and p16 (top right). Senescence triggers loss of urea and albumin synthesis in HepG2 (bottom left & right) in both 2-(2-D) or 3-dimensional cultures (3-D). All data ±SD, *p<0.05,**p<0.01, ****p<0.001,****p < 0.0001.*

CONSTRUCTION AND MANUFACTURING OF AN MRI-READY EXPERIMENTAL SETUP WITH A PHANTOM HEART MODEL

Moritz Wiegand (1,2), Tim Bierewirtz (1,2), Lukas Obermeier (1,2), Leonid Goubergrits (1,2,3) and Katharina Vellguth (1,2)

1. Institute of Computerassisted Cardiovascular Medicine, Deutsches Herzzentrum der Charité, Germany; 2. Charité, Germany; 3. Einstein Center Digital Future, Germany

Introduction: CFD simulations using patient-specific geometries are a promising tool for diagnostics and treatment planning of heart diseases. To validate these simulations, 3D flow field measurement is necessary. This data can be obtained with a time-resolved phase contrast MRI using 3D velocity encoding. A verification study of the in silico computed intracardiac blood flow with a 4D-flow MRI was lately performed by Obermeier et al. [1]. However, the image quality of a human subject may be impaired by movements, irregular heart frequency and low dwell times in the MRI. To obtain data without these disturbances, we developed an MRI-ready experimental beating left heart phantom.

Methods: The phantom model is fabricated metal free to exclude interference with its magnetic field. A backup tank around the phantom model ensures leakage free operating.

The phantom model is made in the end-systolic shape and planted into a fluid filled, 3D-printed geometry of the LV in end-diastolic shape, which is connected to an MRI-compatible pump Shelly Medical Imaging Technologies, London, Canada). Therewith, the pressure around the flexible phantom can be changed to achieve physiological movement and thus recreating realistic hemodynamics in the ventricle.

The heart geometry of the phantom model was taken from the MRI-data of subject 3 from Obermeier et al. [1] and adapted, using the CAD software SOLIDWORKS® 2023 (Dassault Systemes Deutschland GmbH, Stuttgart, Germany).

The LV phantom is made from polyvinyl alcohol (PVA) based hydrogel (10% PVA, 10% glycerol, 80% water), cast into 3D-printed molds and hardened through three freezing-thawing cycles lasting 24 hours each. The PVA based hydrogel was chosen due to its elastic and robust behavior ensuring a changeable ventricular volume during the heart cycle. As it is made of similar substances as the blood mimicking fluid (60% water and 40% glycerol), the frequency shift between the materials inside the MRI can be kept to a minimum.

Both aortic and mitral valve were thermoformed from a 1 mm thick polyurethane film. They were manufactured in an almost closed state to ensure a correct shape and proper closing. Threads, acting as chordae tendineae were added and anchored in the ventricular tissue to avoid severe regurgitation.

Figure 1. Cross-sectional view of the phantom model. 2D cine MRI image.

Results: First measurements were performed in a MAGNETOM Cima.X 3T MRI (Siemans Healthineers AG, Germany). The first acquired images show a high image quality, that is often not achievable in human subjects.

Discussion: The phantom model fulfils the requirements of MRI-compatibility, cyclic movement of the ventricle and to a broad extend the functionality of the aortic and mitral valve. However, there is room for improvement, to create a more realistic setup and thus including the influence of the complexity of the LV and valves geometry and motion. For example, the mitral valve has a stenosis, and the movement of the flexible ventricle is currently mostly in longitudinal direction. Improvements on the mentioned functionalities and other minor fixes will be addressed prior to further measurements, which are planned to be performed in future.

Reference

1. Obermeier et al., Verification Study of in Silico Computed Intracardiac Blood Flow With 4D Flow MRI, IEEE Transactions on Biomedical Engineering, 10.1109/TBME.2024.3381212 , 2024

Acknowledgements

We thank Dr. rer. nat. S. Schmitter and D. H. Dillinger for active support and expertise during the measurements at the Physikalisch Technische Bundesanstalt This work was supported by the German Research Foundation (DFG) as part of the SPP2311 under Grant No. 465178743.

INCLUDING THE SECRETOME OF MESENCHYMAL STEM CELLS IN MULTIPLE MYELOMA *IN VITRO* MODELS.

Nadia García-Parra (1), Lora Mincheva Topalova (2), Lourdes Cordón (3,4), Amparo Sempere Talens (3,5), José Luis Gómez Ribelles (1,6)

1. Centre for Biomaterials and Tissue Engineering, Universitat Politècnica de València, Valencia, Spain; 2. Institute of Biophysics and Biomedical Engineering, Bulgarian Academy of Sciences, Sofia, Bulgaria; 3. Biomedical Research Center Networking in Cancer (CIBERONC), Carlos III Institute, Spain; 4. Hematology Research Group, Instituto de Investigación Sanitaria La Fe, Valencia, Spain; 5. Hematology Department, Hospital Universitario y Politécnico La Fe, Valencia, Spain; 6. Biomedical Research Center Networking in Bioengineering, Biomaterials and Nanomedicine (CIBER-BBN), Spain

Introduction: Multiple myeloma (MM) is a hematologic malignancy characterized by the accumulation of neoplastic plasma cells (NPCs) in the bone marrow (BM). Despite advances in treatment, most patients develop drug resistance (DR) and become refractory to therapies. In the BM microenviroenment, bone marrow mesenchymal stem cells (MSC) play a key role in NPCs proliferation and DR. A large part of the effect exerted by MSC is due to the secretion of soluble factors, collectively known as the secretome. In the field of MM, replacing MSC for their secretome would eliminate some of the problems associated with MSC and NPCs in co-culture. However, numerous studies indicate that there are differences between the secretome of MSC from healthy individuals and from patients with MM, due to the transformation of the MSC by the NPCs. For these reasons, our objective is to isolate the secretome of MSC, previously transformed or not with RPMI8226 cells (a MM cell line) and to study the effect of the secretome in RPMI8226 cells.

Methods: Human bone marrow MSC were purchased from Promocell and RPMI8226 cells from the American Type Culture Collection (ATCC). MSC at passage 2 were co-cultured with RPMI8226 cells in a 1:3 proportion for 72h in RPMI 1640 media (Sigma), after which the RPMI8226 were washed out with DPBS. MSC were kept in culture for another 72h in DMEM High Glucose media (Biowest). We obtained the secretome of the transformed and non-transformed MSC (MT and MNT, in advance) and performed ELISA assays to quantify the levels of Interleukin 6 (IL-6) and Interleukin 10 (IL-10), often increased in MSC from MM patients. We also obtained the secretome of RPMI8226 (RNT) and the RPMI8226 washed from the MSC co-culure (RT).The secretome was concentrated 10-15X with centrifuge columns with a 300kDa threshold (AMICON®). To study the effect of the secretome on the RPMI8226 cell line, cells were cultured for 7 days with two different secretome concentrations. Viability and proliferation on days 3 and 6 were studied by trypan counting and MTS assays, respectively. Cell supernatants were collected on day 7 its cytokines were quantified by a Human Inflammatory Cytokine Bead Array (BD Biosciences) Assay in a flow cytometer (BD FACSCanto™ II).

Results: We observed an increase in IL-10 concentration in the secretome of transformed MSCs, MT, compared to the rest of the conditions. On the other hand, concentration of IL-10 in the MM cells that have been in co-culture with MSCs, what we call RT, was higher than in non-transformed, RNT, and both were higher than MNT. We observed no differences in terms of viability nor proliferation among the RPMI8226 supplemented with the different secretomes. However, an increase in the IL-8 production of RPMI8226 was observed when treated with secretome isolated from MT and MNT, regardless the concentration.

Discussion: The increased IL-10 concentrarion in MT compared to MNT could indicate the induction of a phenotype transformed by the RPMI8226. However, when the secretome of MT or MNT cells is added to RPMI8226 culture both trigger IL-8 production but with no significant difference between them. On the other hand, the addition of MSC secretome to mesenchymal cell culture does not seem to have an influence on the proliferation of myeloma cells in culture. Additional experiments are required to study if there is a differential effect between MT and MNT secretomes.

Acknowledgements

We thank Inmaculada García-Briega for her help in the cell culture and flow cytometry experiments. This work has been supported by PID2022-138572OB-C41 project funded by MCIN/AEI/10.13039/501100011033/ FEDER, UE. The research was also supported by CIBER – Consorcio Centro de Investigación Biomédica en Red -CB06/01/1026, Instituto de Salud Carlos III, Ministerio de Ciencia e Innovación. In addition, this research was supported by a grant from the Scientific Foundation of the Spanish Association Against Cancer and its headquarters in Valencia.

IN-VITRO THROMBOGENICITY TESTING FOR ECLS OXYGENATORS – FEASIBILITY, RELIABILITY AND REPRODUCIBILITY

Lasse J. Strudthoff, Pia Hefer, Michael Neidlin, Marlene Schadow, Thomas Schmitz-Rode, Ulrich Steinseifer, Felix Hesselmann*, Johanna C. Clauser

All Institute of Applied Medical Engineering, Helmholtz Institute, University Hospital RWTH Aachen, Germany

Introduction: Hemostatic complications limit the maximum duration of the clinical application of ECLS, normally days or weeks. Decreasing the circuit thrombogenicity remains the Gordian Knot of the therapy and the oxygenator is a major contributor [1]. However, in-vivo-experiments are the only near-to-conclusive testing modality to evaluate the thrombogenicity of oxygenator designs, but they are expensive, slow, and ethically problematic [2]. Our group is currently developing an in-vitro-setup for referential testing of oxygenator variants.

Materials and Methods: We performed in vitro experiments with recirculating porcine whole blood. Two identical circuits were run for 5 hours using blood from the same donor animal. Each circuit comprised the oxygenator with integrated heat exchanger and centrifugal blood pump, a miniaturized blood reservoir, ports for blood sampling and pressure measurements, as well as flow meters. The oxygenators were specifically manufactured HLS 7.0 that have passed the identical production line as commercial devices but omitting the coating step. Throughout the experiment, the flow in each circuit was kept constant. We continuously measured temperature, pump rotations as well as pressures pre-pump, between pump and oxygenator, and post-oxygenator. The setup is depicted on Figure 1.

Further, we took ten blood samples from each circuit distributed over each experiment day. The samples were analyzed using ROTEM (INTEM, HepNATEM), aggregometer, hemogram, BGA, coagulometer (Fibrinogen, FXII), photometer (hemolysis). So far, in 22 experiments, we tested 44 uncoated Maquet HLS 7.0. To prove the validity of our experiment design, the last 8 experiment days were conducted entirely identical, with one exception: For 4/8 of the experiments, we deliberately omitted the usage of an advanced blood selection protocol with the intention to create negative controls, i.e. experiment runs without hemostatic events.

Results: It is feasible to create spontaneous hemostatic events in vitro and in only 5 hours experiment run time, with all logistical and resource-related benefits. Comparing parameters such as blood gases, temperature or hematocrit proves identical circuit conditions. It is also possible, to achieve these spontaneous events reliably. In the final series, we reliably achieved hemostatic events presenting on form of rising pressure differentials and validated by characteristic parameters like platelets, fibrinogen, leukocytes, etc.

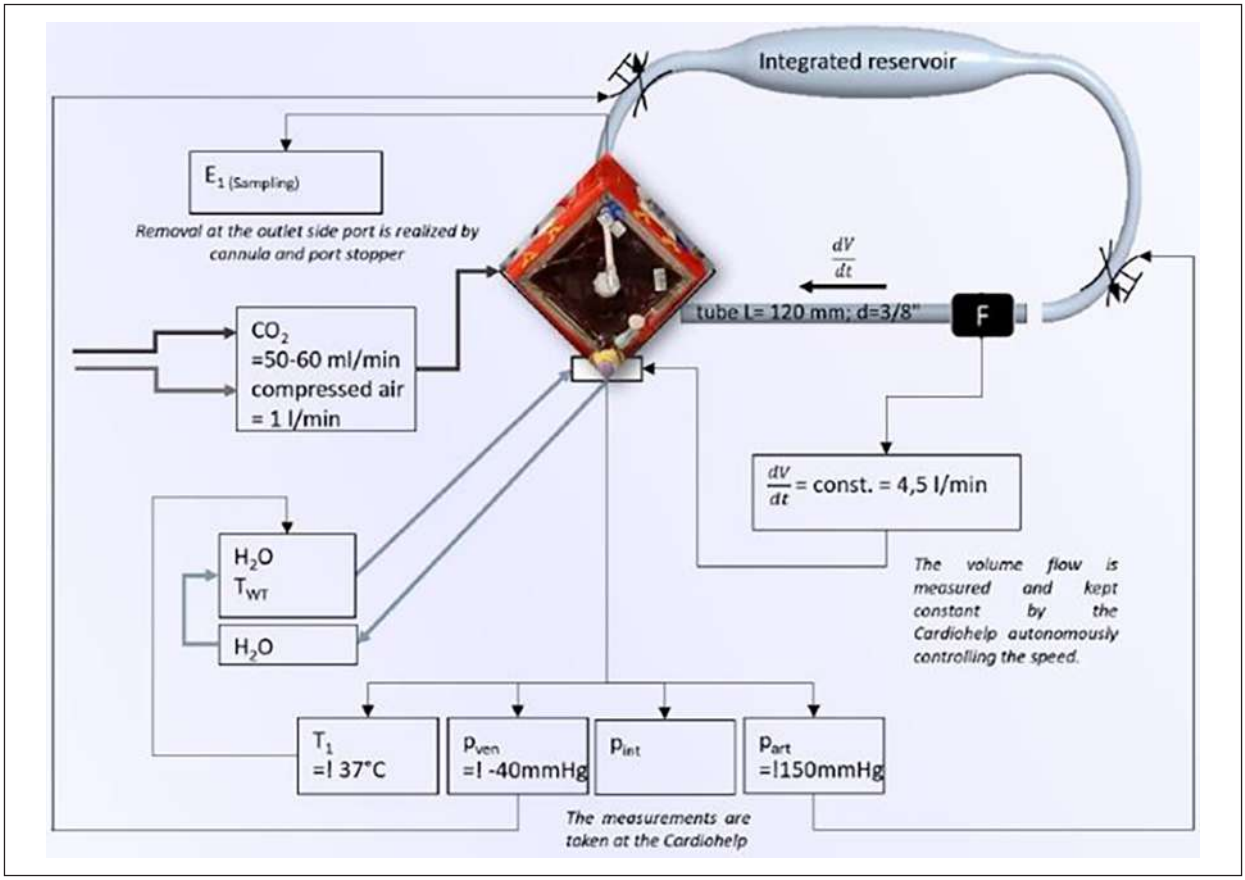

Figure 1. Schematic of experiment setup.

4/4 experiment days with the advanced blood selection protocol yielded positive experiment course, 3/4 experiment days without the advanced blood selection protocol yielded negative controls, as intended. All paired test circuits behaved highly similar in both positive and negative experiment runs for continuous and discrete parameters, showing reproducibility.

Discussion: Our data shows that it is *feasible* to *reliably* and *reproducibly* create hemostatic events using porcine whole blood from the slaughterhouse in two identical circuits in a short time frame of only 5 hours. All measured parameters show high conformity. Thrombogenicity is difficult to quantify in form of an isolated value. As also known from similar test setups (e.g. hemolysis in heart assist systems), referential tests can, nonetheless, offer important insight.

Due to the negative controls, we can qualitatively compare readings during hemostatic events against inherent or autologous processes.

Our results are highly promising that, for the first time, such a test setup can be standardized for the thrombogenicity evaluation of ECLS oxygenators.

References

1. Murphy DA et al. ECMO-hemostatic complications. *Transfus Med Rev* 2015;29(2):90–101
2. Sarode DN, Roy S. In Vitro models for thrombogenicity testing of blood-recirculating medical devices. *Expert Rev Med Devices* 2019;16(7):603–16

Acknowledgements

We thank Dr. Felix Wald, Mr. Thorsten Zipser and Dr. Michaela Obst, all Getinge SE, for their collaboration in this project. This work was financially supported by Getinge SE. We specifically thank Getinge for producing laboratory-grade devices without hemocompatible coating.

NEW STRATEGIES OF HEPARIN IMMOBILIZATION TO IMPROVE BLOOD COMPATIBILITY OF TITANIUM

Janna Kuchinka (1), Thomas Groth (1, 2)

1. Department Biomedical Materials, Martin Luther University Halle-Wittenberg, Germany, 2. Interdisciplinary Center of Material Science Halle, Germany

Introduction: Acute and chronic heart failure are major challenges in modern medicine. Ventricular assist devices (VAD) made of titanium (Ti) alloys as implantable axial pumps have provided solutions to keep patients alive. Long-term application of VAD requires systemic anticoagulation, which decreases the risk of thrombosis but increases that of bleeding. Particularly, the cannula inserted in the ventricular region is prone to thrombotic complications. Therefore, we studied here strategies to improve the blood compatibility of Ti by durable covalent or adsorptive binding of heparin.

Methods: Glass slides were coated with Ti by metal vapor deposition used as model substrata. Subsequently, Ti was oxidized using UV light. Modification of Ti-coated slides was done with organosilanes (OS) providing amino groups for side-on of non-fractionated (HepA) or end-on of degraded (HepB) immobilization of heparin (Hep) [1]. An additional sacrificial coating of Hep was achieved by adsorption of multilayers (PEM) combining polycations with anti-bacterial properties and non-fractionated heparin (pA/Hep; CHI/Hep) [2]. Blood compatibility studies of these coatings was performed with a Factor Xa assay (FXa), [3] a commercial aPTT assay, and by platelet (PLT) adhesion studies [4].

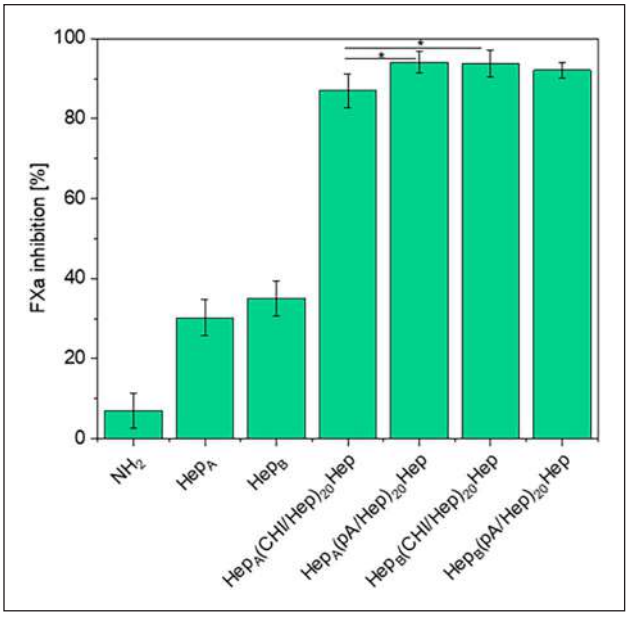

Figure 1. Inhibition of factor Xa by heparinization.

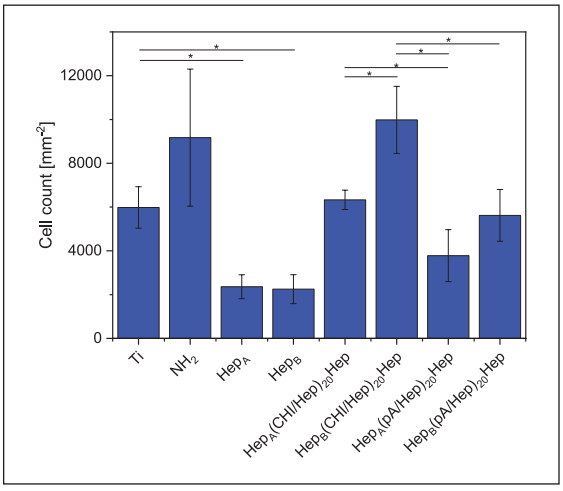

Figure 2. Reduction of platelet adhesion on coatings.

Results: Fig. 1 shows the results of FXa assay with an inhibition of its activity already achieved by covalent binding. Indeed, the inhibition was almost complete when a sacrificial layer of heparin was bound as multilayer in combination with polycations like chitosan (CHI). Studies with whole blood clotting assay aPTT yielded comparable results showing that covalently attached heparin, both side-on and end-on bound, prolong clotting times significantly in comparison to oxidized Ti while addition of a sacrificial Hep as PEM inhibited coagulation of human plasma completely.

PLT adhesion studies were conducted showing that Ti and the OS layer (NH_2) were thrombogenic while platelet number was low on surfaces with covalently bound Hep. PEM with Hep as polyanion increased PLT adhesion, particularly with CHI as polycation which indicated that the

flow conditions might be an important further parameter since PLT assay was done under static conditions.

Discussion: The covalent immobilization of OS enabled the durable covalent binding of Hep either in side-on or end-on fashion. The negative charge of the bound Hep also permitted the adsorption of PEM with Hep as polyanion providing a release system with additional anticoagulant activity. Interaction of covalently bound Hep with anti-thrombin III enabled not only direct inactivation of FXa but also increased blood clotting times, particularly when with PEM releasing Hep. The negative charge of covalently bound Hep also decreased PLT adhesion significantly compared to plain Ti.

References

1. Köwitsch et al. Biotech. Appl. Biochem. 58:376-389, 2011.
2. Aggarwal & Groth, JBMR 102: 4224-4233, 2014.
3. Groth & Wagenknecht, Biomaterials 22: 1227-1234, 2001.
4. Huang et al, Marcomol. Biosci. 11:131-140, 2011.

Acknowledgements

This work was supported by grant Gr1290/13-1 to T.G. from Deutsche Forschungsgemeinschaft. We are grateful to Prof. Dmitry Telyshev from MIET Moscow for co-initiating this project.

GHOST CELLS AS A TWO-PHASE BLOOD ANALOG FLUID — VISUALIZATION OF MECHANICAL HEMOLYSIS

Benjamin J. Schürmann (1), Pia Creutz (1), Sebastian V. Jansen (1), Thomas Schmitz-Rode (1), Ulrich Steinseifer (1), Johanna C. Clauser (1)

[1]Department of Cardiovascular Engineering, Institute of Applied Medical Engineering, Medical Faculty, RWTH Aachen University, Forckenbeckstr. 55, Aachen, 52074, Germany

Background: In designing mechanical circulatory support systems, minimizing hemolysis and thrombosis is crucial. Traditional methods for assessing hemolysis in in-vitro blood experiments are time-consuming and provide only quantitative data. Therefore, we are working on the Fluorescent Hemolysis Detection to locally resolve hemolysis within a mechanical circulatory support system.

Methods: Fluorescent Hemolysis Detection involves a two-phase blood analog fluid made from ghost cells, erythrocytes devoid of hemoglobin and loaded with calcium ions targeted by an extracellular calcium-indicator (Cal590 potassium salt, AAT Bioquest). Upon hemolysis, calcium and indicator bind to each other and thereby exhibit an increased fluorescence signal under laser excitement.

Mechanical hemolysis is induced with high shear stresses in the FDA pump, running at an operational point of 3500 RPM and a volume flow of 2.5 L min^{-1}, inducing a pressure difference of 350 mmHg. A laser sheet at 532 nm excites the fluorescent indicator in the pump, and the fluorescent signal is captured optically using a high-speed camera (Flowsense EO, Dantec Dynamics). Additionally, samples undergo analysis for blood count, free plasma hemoglobin, and fluorescent signal. The pump is also operated with blood to compare the hemolysis with ghost cells.

Results: The free plasma hemoglobin exhibits an increase over time for both ghost cells and blood. The normalized hemolysis index for ghost cells surpassed that of blood. Moreover, the fluorescent signal of the ghost cells fluid obtained by the camera (Figure 1) increased by 21 % in mean brightness over the pump's operational duration.

Conclusion: Our study highlights the hemolysis differences between ghost cells and blood, demonstrating the visibility of increased hemolysis in the FDA pump, which is made visible with the Fluorescent Hemolysis Detection.

Further data analysis will determine if locally resolved hemolysis detection is possible.

Acknowledgements:

Funded by the German Research Foundation DFG (STE 1680/12-2)

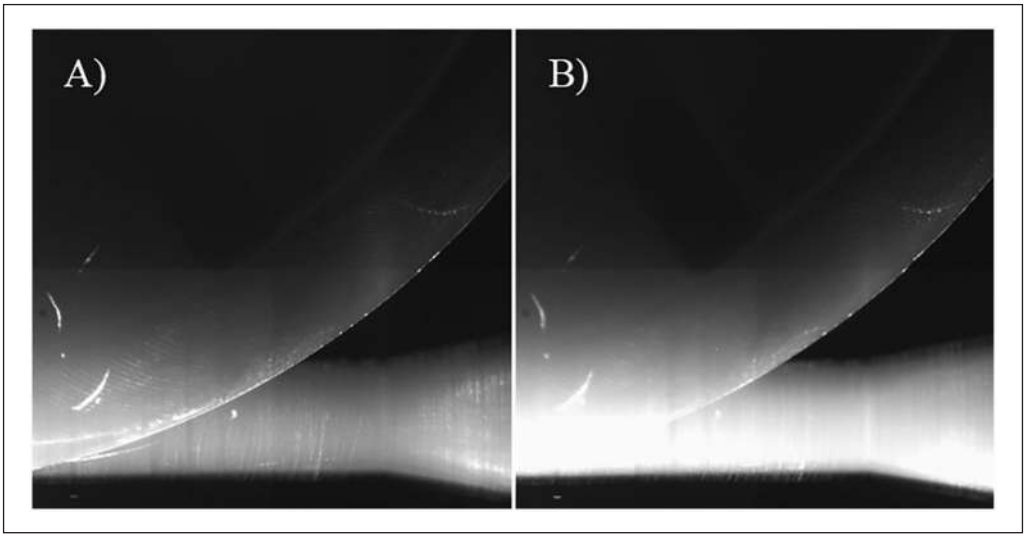

Figure 1. Fluorescent Hemolysis Detection shown in the outlet area of the FDA Pump: A) start of runtime, B) after 13 minutes at 3500 RPM, 2.5 L min^{-1} and 350 mmHg pressure drop.

UNDERSTANDING THE ROLE OF HIGH-FREQUENCY VASCULAR VIBRATIONS IN ARTERIOVENOUS FISTULA FAILURE

Luca Soliveri (1,2), Sofia Poloni (3), Michela Bozzetto (1), Giulia Cabrini (3), Andrea Remuzzi (3), Kristian Valen-Sendstad (4)

1. Istituto di Ricerche Farmacologiche Mario Negri IRCCS, Italy; 2. Politecnico di Milano, Italy; 3. University of Bergamo, Italy; 4. Simula Research Laboratory, Norway

Introduction: Native arteriovenous fistula (AVF) is the preferred vascular access for hemodialysis, yet 40% of them fail within 1 year after surgery [1] mainly due to stenosis. We have recently shown that transitional flow induces vibrations in the AVF vein wall at frequencies exceeding hundreds of Hz, and suggested that the associated mechanical stresses may directly impact the mechanobiology of smooth muscles cells [2]. The aim of this fluid-structure interaction (FSI) longitudinal study is to explore the relation between high-frequency vascular vibrations and adverse AVF wall remodeling.

Methods: Contrast-free magnetic resonance imaging and Doppler Ultrasounds measurements were performed at multiple timepoints (up to 1 year) in six patients with a native radio-cephalic AVF. Two patients underwent successful maturation and long-term patency, whereas the others experienced complications, characterized by either stenosis or excessive dilatation. AVF geometries were reconstructed from medical images and meshes of about 200,000 tetrahedral elements were generated.

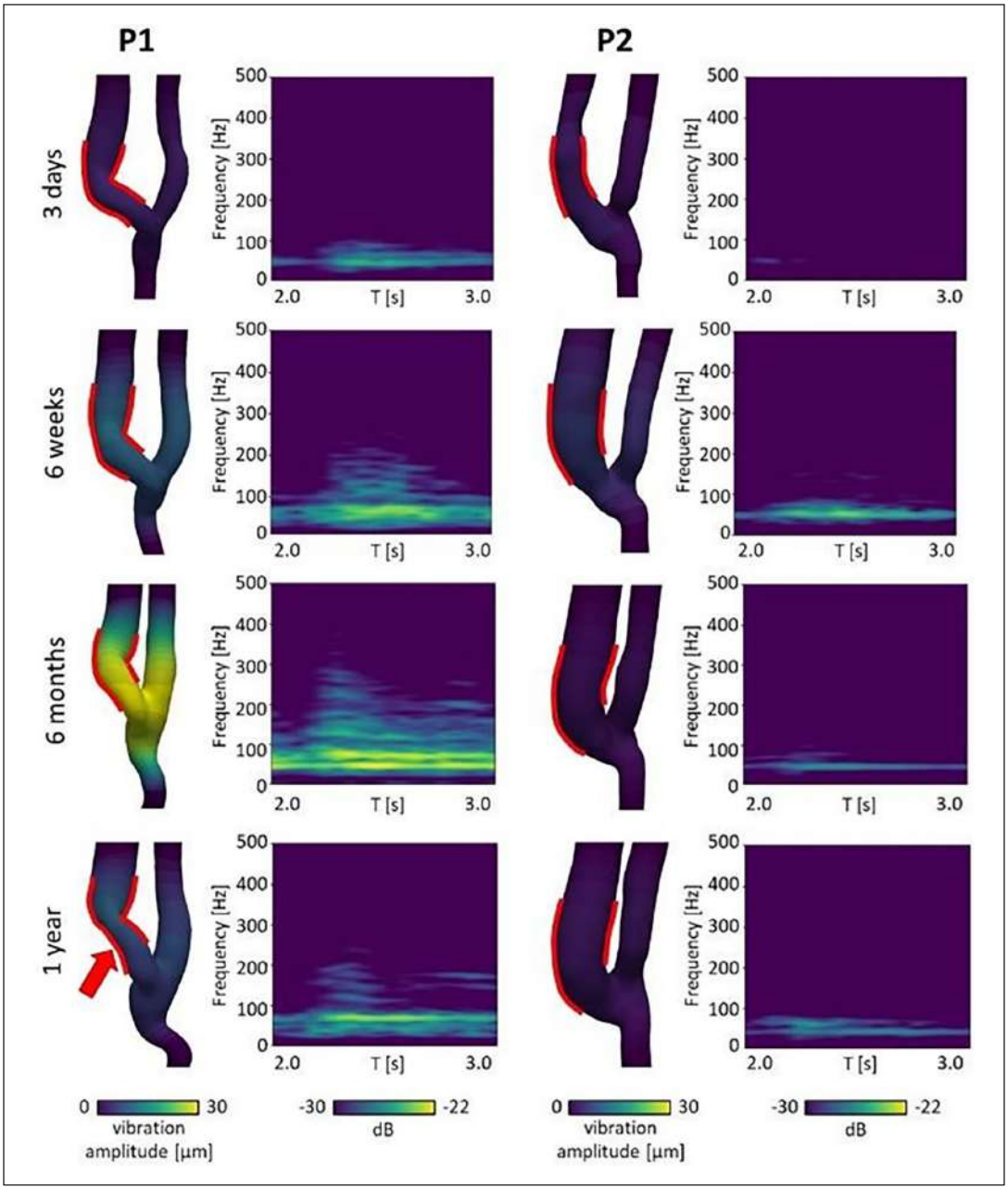

Figure 1. Time-averaged vibration amplitude maps and wall displacement spectrograms extracted in the juxta-anastomotic vein (region between the red lines) for two representative patients at four timepoints.

Fully coupled 2nd order accurate space/time centred high-fidelity FSI simulations were conducted using turtleFSI [3] with a time discretization of 0.1 ms. Patient-specific inflow and pressure were incorporated, and the distinct properties of artery and vein were modeled with a 3-term Mooney-Rivlin model. The simulations also accounted for the stiffening and thickening of the vein during maturation. The perivascular tissue was modeled with Robin boundary conditions. The computed vascular displacement was high-pass filtered using a frequency threshold of 25 Hz to isolate the vibrations from the inflation due to pressure pulsation. Wall displacement spectrograms were generated to illustrate the evolution of high-frequency content over the cardiac cycle [4].

Results: Patients with AVF complications exhibit significantly higher vibration amplitudes with respect to those experiencing good patency (median [IQR] = 11.5 μm [5.8−23.7 μm] vs. 2.7 μm [1.8−6.9 μm], $p < 0.05$), along with a visibly enhanced spectral content up to 500 Hz. *Figure 1* represents the outcomes for two representative patients, P1 exhibiting vein stenosis at 1 year, and P2 with successful long-term patency.

Discussion: Results indicate the presence of significantly higher vibration amplitudes in patients who experienced AVF complications compared to those with successful maturation and long-term patency. Our findings indicate distinct vibration responses associated to different clinical outcomes, suggesting a potential association between high-frequency vascular vibrations and adverse AVF remodeling. If validated in a larger cohort, this finding could hold significant implications for clinical management. The possibility of identifying AVFs at risk of failure through vibration monitoring could enable surgeons to timely intervene, thereby enhancing AVF clinical outcomes.

References

1. Bozzetto M et al, JVA, 24.5: 1061-1068, 2023.
2. Bozzetto M et al, Phys Eng Sci Med, 1-11, 2023.
3. Bergersen A W et al, JOSS, 5.50: 2089, 2020.
4. Bruneau D et al, Nat Commun Med, 3.1:163, 2023.

TOWARDS THE PERSONALIZATION OF THE DIALYTIC THERAPY: AN EXPLAINABLE APPROACH TO PREVENT INTRADIALYTIC HYPOTENSION

Giustina Casagrande (1) Cristiana Larizza (2), Antonino Nocera (2), Silvana Quaglini (2), Riccardo Bellazzi (2), Andrea Ambrosini (3), Pietro Cippà (4), Carla Colturi (5), Gianvincenzo Melfa (6), Reto Venzin (7), Maria Laura Costantino (1)

1. Dpt. of Chemistry, Materials and Chemical Engineering, Politecnico di Milano, Milano, Italy; 2. Dpt.of Electrical, Computer, and Biomedical Engineering, University of Pavia, Italy; 3. Renal Transplant Unit, Azienda Ospedaliera Ospedale di Circolo e Fondazione Macchi, ASST Sette Laghi, Varese, Italy; 4. Unit of Nephrology, Ente Ospedaliero Cantonale, Lugano, Switzerland; 5. Division of Nephrology, ASST Valtellina e Alto Lario, Sondrio, Italy; 6. Division of Nephrology, Ospedale Sant'Anna, ASST Lariana, Como, Italy; 7. Division of Nephrology, Dpt.of Internal Medicine, Cantonal Hospital Graubünden, Chur, Switzerland.

Introduction: Intradialytic hypotension (IDH) is one of the most common complications occurring in haemodialysis (HD) patients. Several works have analysed its epidemiological impact, trying to identify predictors of IDH onset with risk calculators. Deriving suitable risk models is a complex task, further emphasized by the absence of a consensus definition of IDH as mentioned by several authors [1], [2], [3].

A pre-dialysis robust evaluation of the risk of IDH onset may suggest proper session settings, avoiding later emergency interventions. This work aims to analyse the IDH definitions associated with increased mortality in the medium-long-term horizon and assess their predictability with data already available at the start of the haemodialysis treatment.

Methods: A multi-centric database, made available by Interreg DialysIS and InterACTIVE-HD 2.0 projects was used. Among the definitions of IDH in the most recent literature, we have considered the ones associated with an increase in mortality in the medium to long term: ΔSBP40 by Shoji et al. [4]; Nadir90 and Nadir100-90 by Flythe et al. [5], ΔSBP30-Nadir90 by Sands et al. [6]. The overlap between them was initially investigated. We first developed linear, explainable, machine learning models by using the entire dataset. Further, we move to a neural network, applied to subsets of data, gradually including groups of features, to maintain explanability. Subsets were characterized by semantically related sets of predictors. SHapley Additive exPlanation (SHAP) analysis was used to evaluate the significance of the variables and their influence on IDH.

Results: Nadir90 and Nadir100-90 IDH definitions have the highest incidence (27.78% and 28.81% respectively).

ΔSBP40 has an incidence of 22.55%, while ΔSBP30-Nadir 90 of 12.49%.

The results of the preliminary analyses with linear models did not bring statistically significant results (Accuracy, Precision, Recall, and F1<0.8), justifying the choice of non-linear, more complex models. The most informative features by SHAP differ for each definition, with some commonality. Among the patient-related variables, the presence of cardiopathy, together with low pre-dialytic pressure and advanced age are all risk factors for IDH, as well as a low Sodium plasmatic concentration at the dialysis start.

Looking at the dialysate composition, low Chloride concentration is related to hypotension all over the definitions. A low calcium concentration seems associated with Nadir 100-90 episodes; in contrast, a high Calcium concentration correlates with ΔSBP40 and ΔSBP30-Nadir90 definitions.

Discussion: The results confirm the importance of some predictors already reported in the literature but also highlight the importance of the treatment settings (electrolyte concentrations and other dialyzer parameters), thus demonstrating that the in-depth analysis of pre-dialysis data is promising for the prediction of intradialytic hypotension. The limitations that have emerged from the use of linear machine-learning models suggest the need for more complex machine-learning models, which, unfortunately, are black boxes. The proposed approach, of gradual inclusion of features, could be used in order not to lose explainability while using complex models. Creating the conditions to be able to move from a predictive to a preventive approach is a great challenge.

References

1. L.S.Q.N. Ngankem et al., Int J Med Inform, 2023, doi: 10.1016/j.ijmedinf.2022.104975.
2. J.C. Huang et al., Comput Methods Programs Biomed, 2020, doi: 10.1016/j.cmpb.2020.105536.
3. H. Lee et al., NDT 2023, doi: 10.1093/ndt/gfad064.
4. Shoji et al., Kidney Int, 2004, doi: 10.1111/J.1523-1755.2004.00812.X.
5. J.E. Flythe, et al., J Am Soc Nephrol, 2015, doi: 10.1681/ASN.2014020222.
6. J.J. Sands et al., Hemodial Int, 2014, doi: 10.1111/HDI.12138.

Acknowledgements

The work was funded in the framework of the INTERACTIVE-HD2.0 project, cross-border cooperation program INTERREG IT/CH 2014-2020, Grant ID 1441882.

PROTEOMIC PROFILING AND IDENTIFICATION OF PATHOPHYSIOLOGICAL MEDIATORS OF FRIEDREICH'S ATAXIA (FRDA)

J. Rafeya[1], K. Reetz[2], K. Schütt[3], J. Jankowski[1,4], V. Jankowski[1]

[1]Institute for Molecular Cardiovascular Research, University Hospital Aachen, RWTH, Germany, [2]Clinic for Neurology, University Hospital Aachen, RWTH, Germany, [3]Department of Internal Medicine I – Cardiology, University Hospital Aachen, RWTH Germany, [4]School for Cardiovascular Diseases, Maastricht University, Maastricht, The Netherlands

Introduction: Friedreich ataxia is a neuro-degenerative, autosomal recessive disease, which is clinically characterized by loss of coordination, ataxia, along with cardiomyopathy, scoliosis, and an increased risk of diabetes [1]. The disease is manifested due to a GAA expansion mutation on the intron of *FXN* gene, resulting in a reduction of functional frataxin in cells [2]. The project aims to identify the unknown pathophysiological mediators involved in the genesis and progression of Friedreich ataxia along with generating a proteomic profile of the patients.

Method: The samples were split into four major cohorts of healthy, patient, fibrotic patient, and non-fibrotic patients.

Proteins from the plasma and urine samples were separated with gel-electrophoresis. Mass spectrometry (MS1 & MS2) analyses were performed to determine the proteomic profile of the samples with the Mascot Search Engine. A targeted MS analysis focused was conducted by focusing on frataxin and Neurofilament light chain (NFL) in sample cohorts.

Result: Frataxin level had been reduced in the patient cohort compared to healthy cohort (Figure 2, A). However, there was no significant change in frataxin level between the fibrotic and non-fibrotic patients (Figure 2, B). Finally, frataxin was detected in urine (Figure 2, C) in a reduced level compared to plasma.

NFL level had been increased in almost all FRDA patients, except for five patients (Figure 3, C). There was also no significant change in the NFL level between the fibrotic and non-fibrotic patients (Figure 3, B). NFL was also detected in urine (Figure 3, C) and the protein level was lower compared to the plasma NFL level.

Discussion: Frataxin reduction in patient cohort correlates with the notion that FRDA is a frataxin deficiency disease [3]. Increase of NFL in most of the patients indicated increased axonal damage associated with the disease. The relatively lower NFL in five samples can be because NFL level stabilizes toward the later stage of a neurodegenerative disease even though it increases during the early phase of the disease [4].

None of the frataxin and NFL had a significant difference between the fibrotic and non-fibrotic cohorts indicating irrelevance of these proteins to fibrosis progression.

The detection of frataxin and NFL in the urine, albeit at a reduced level was one of the most interesting findings as there is no prior literature article describing this phenomenon. Focusing on this might lead to a new revelation associated with the pathophysiology of the FRDA disease.

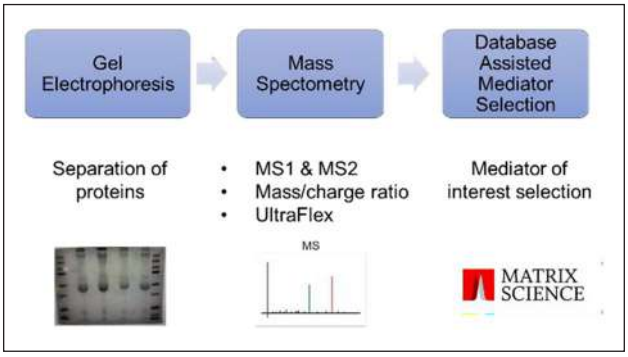

Figure 1. The workflow utilized to obtain the data for the project.

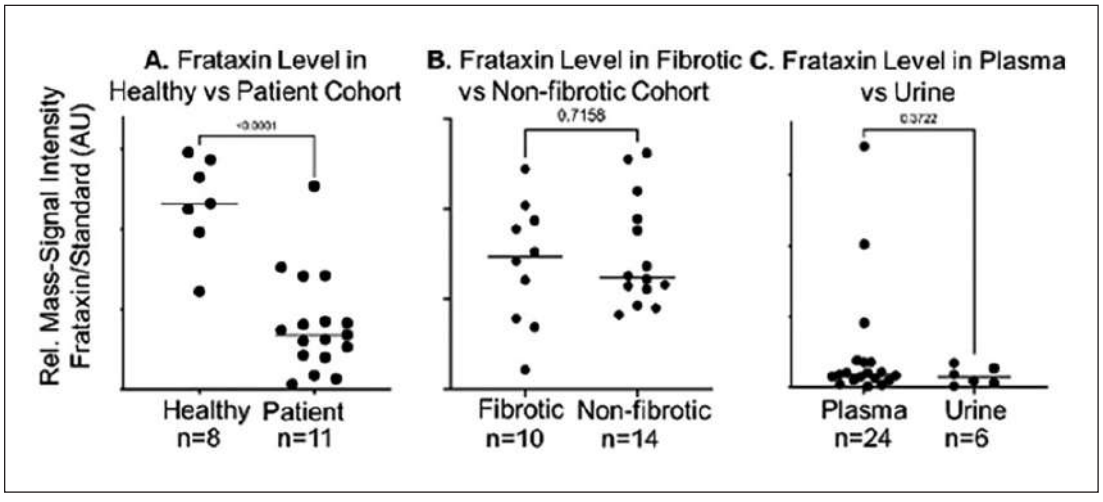

Figure 2. Frataxin level in different sample cohorts demonstrating A). Decrease of frataxin in patient, B). No significant change of frataxin between fibrotic and non-fibrotic patients, C). Detection of frataxin in urine.

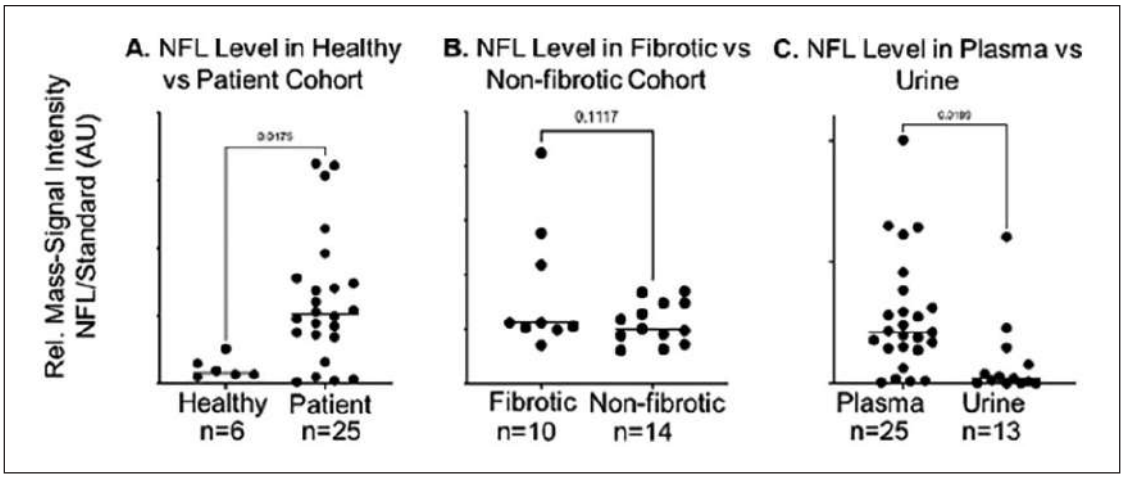

Figure 3. NFL level in different sample cohort indicating A. Increase of NFL in most of the patients, B. No significant change of NFL between fibrotic and non-fibrotic patients, C. Detection of NFL in urine.

References

1. Lynch et al, J. Multidiscip. Healthc., pp.1645-1658, 2021.
2. Gavriilaki et al, The Cerebellum, 1-20, 2023
3. Doni et al, Cell Death Dis, 14(12), p.805, 2023.
4. Zhang et al, Front Neurol., 13, p.833507, 2022.

COMPLIANCE-BASED LUMPED PARAMETER MODEL FOR OPTIMIZING EXTERNAL VENTRICULAR ASSIST DEVICES

Kristóf Sárosi, Thomas Kummer, Patrick Jenny

Institute of Fluid Dynamics, Department of Mechanical and Process Engineering, ETH Zürich, Switzerland

Introduction: Optimizing external ventricular assist devices (VADs) poses challenges due to their complex interaction with heart tissue. As these devices drive the flow in the circulation with compressing the heart, their optimization requires information on the mechanical properties and behavior of the tissue. Currently, computationally expensive finite element models (FEM) or experiments provide the only framework for device optimization.

Methods: Building upon the work of Kummer et al. [1], we propose a more efficient framework based on a lumped parameter model that characterizes the heart through compliances. Unlike existing 0D models, ours employs a general compliance model, eliminating the need for predefined time-varying pressure [2], compliance [3] parameters, or coupling with higher-dimensional models [4]. We introduce a predefined actuation displacement boundary condition, which our compliance model translates into a source term to generate pressure and flow in the circulation.

Considering a simple relation between the volume change in the ventricles and the pressure inside them (p) and displacement of the patches (L), we define the following model:

$$\Delta V = f\left(p_l, p_r, L\right)$$

Applying the chain rule to obtain the rate of change of the volume, we are left with three unknown parameters per ventricle.

$$\frac{dV_l}{dt} = c_{ll}\frac{dp_l}{dt} + c_{lr}\frac{dp_r}{dt} + e_l\frac{dL}{dt}$$

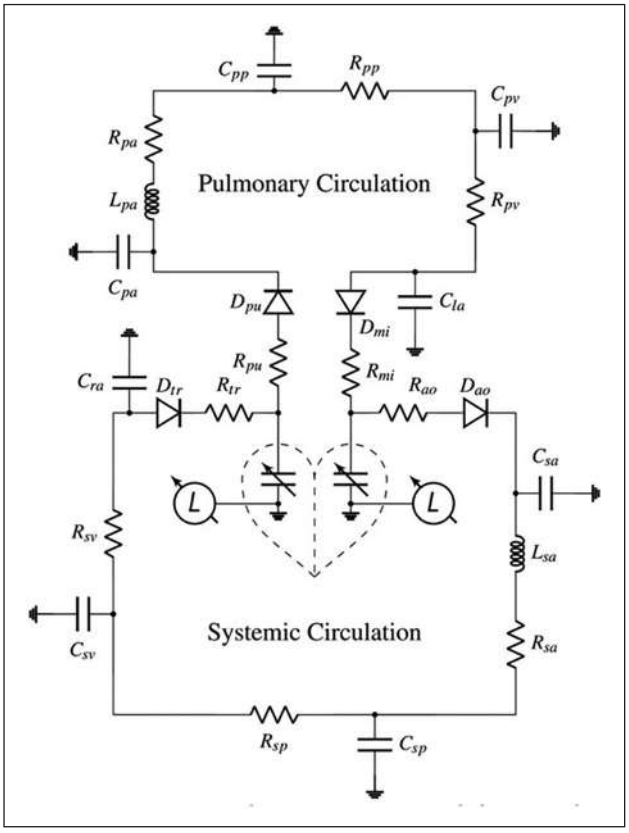

Figure 1. Lumped parameter model extending the work of Kummer et al. [1] A compliance-based approach replaces the FEM-lumped parameter coupling. A displacement boundary condition drives circulatory flow via left and right ventricular compliance models.

However, obtaining a robust ventricular compliance model is challenging due to limited heart compliance data and the influence of interactions with the VAD. We address this by combining results from Kummer's FEM model [1] with experimental data.

Results: Our model can produce results similarly to already existing 0D models without coupling with higher dimensional models or predefined model parameters. This approach also highlights the sensitivity of models that rely on predefined parameters. Our framework offers detailed insights into pressure, flow rate, volume, and valve states throughout the circulatory system. Solutions are stable, and the compliance model can be fine-tuned for accurate physiological flow properties.

Discussion: This compliance-based lumped parameter approach provides a powerful tool for optimizing external VADs such as Corinnova. Characterizing the heart through compliance provides a novel approach for 0D models and understanding the macro-mechanical properties of the heart alike. By incorporating data-driven ventricular compliance models, we aim to obtain the physiological pressure and volume information critical for device optimization and ultimately, improved patient outcomes.

References

1. Kummer et al, Cardiovasc Eng Tech, **13**: 764–782, 2022.
2. Milišić V, Quarteroni A. ESAIM: Mathematical Modelling and Numerical Analysis. **38(4)**:613-632, 2004.
3. Ursino M., Am J Physiol., **275(5)**: 1733-44, 1998.
4. Cicci et al, Int J Numer Meth Biomed Engng, **40(1)**: e3783, 2024.

COLD ATMOSPHERIC PLASMA THERAPY: A NOVEL TREATMENT FOR BERLIN HEART EXCOR CANNULA INFECTIONS

Johanna Schachl (1), Markus Königshofer (2), Martin Stoiber (2,4), Martina Socha (1), Christian Grasl (2,4), Theodor Abart (1), Ina Michel-Behnke (3), Dominik Wiedemann (1), Julia Riebandt (1), Daniel Zimpfer (1), Thomas Schlöglhofer (1,2,4)

1. Department of Cardiac Surgery, Medical University of Vienna, Vienna, Austria; 2. Center for Medical Physics and Biomedical Engineering, Medical University of Vienna, Vienna, Austria; 3. Department of Pediatric Cardiology, Medical University of Vienna, Vienna, Austria; 4. Ludwig Boltzmann Institute for Cardiovascular Research, Vienna, Austria

Introduction: Cold atmospheric plasma (CAP) therapy has been recognized as an effective treatment option for reducing bacterial load in chronic wounds, such as ventricular assist device (VAD) driveline exit-site infections [1]. Currently, there have been no reports on the safety and efficacy of CAP therapy for cannula infections and inflammations in paracorporeal pulsatile VADs.

Methods: The mechanical properties of Berlin Heart EXCOR cannulas were tested in-vitro both before and after Cold Atmospheric Plasma (CAP) treatment (SteriPlas, Adtec Healthcare Limited, UK) to investigate possible material alterations (Figure 1A).

A ring tensile test (Figure 2) was conducted on 20 untreated and 20 CAP-treated (5 min) EXCOR cannulas (Ø12mm) to assess the force at the breaking point of the cannulas (Fmax), at 25% (F25%), and 50% (F50%) of the maximum displacement.

Additionally, scanning electron microscope (SEM) micrographs were taken for both groups to examine any surface changes. Finally, the case of a 13-year-old male EXCOR patient with cannula infections, treated with CAP over 100 days, is presented (Figure 1B).

Results: The in-vitro measurements revealed no statistically significant differences in mechanical strength between the control and CAP groups for F25% (8.18±0.36 N vs. 8.02±0.43 N, p=0.21), F50% (16.87±1.07 N vs. 16.38±1.32 N, p=0.21), and FMAX (44.55±3.24 N vs. 42.83±4.32 N, p=0.16). Additionally, no surface structure alterations were identified in the SEM micrographs. The patient's cannula exit sites showed visible improvement in DESTINE wound staging (Figure 3), along with a reduction in bacterial load and inflammatory parameters after CAP treatment, all achieved without any observed side effects.

Figure 1. CAP treatment of (A) EXCOR cannula samples in-vitro and (B) in-vivo of a pediatric EXCOR patient.

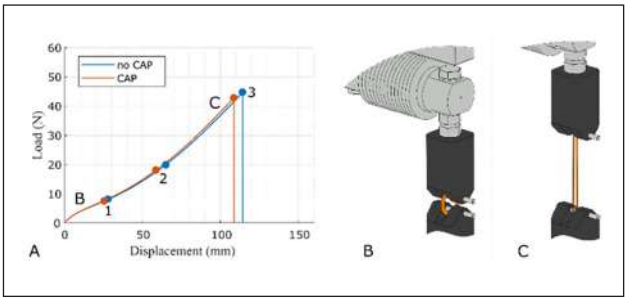

Figure 2. (A) Example tensile test curve, (B) Setup with ring sample at start of measurement and (C) stretched ring during measurement. (1) Force at 25% and (2) 50% of maximum displacement, and (3) maximum force at specimen breaking point. CAP: Cold Atmospheric Plasma.

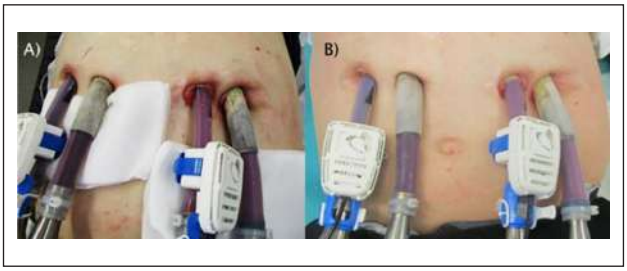

Figure 3. In-vivo situation (DESTINE 2) at the beginning (A) and end of CAP treatment (B).

Discussion: The in-vitro assessments indicated that there were no notable alterations in the mechanical strength or surface structure of the EXCOR cannulas after CAP treatment. The clinical utilization of CAP therapy proved to be safe and effective as an adjuvant treatment for EXCOR cannula exit-site infections.

Reference

1. Hilker L, von Woedtke T, Weltmann KD, Wollert HG. Cold atmospheric plasma: a new tool for the treatment of superficial driveline infections. Eur J Cardiothorac Surg. 2017;51:186–7.

DEEP LEARNING-BASED KOOPMAN ANALYSIS FOR THE PREDICTION OF MULTI-BEAT CARDIOVASCULAR DYNAMICS

Lars Berend Brandt (1,2), Francesco Moscato (1,3,4), Arjan Kuijper (2,5), Max Haberbusch (1,3)

1. Center for Medical Physics and Biomedical Engineering, Medical University of Vienna, Austria; 2. Department of Computer Science, Technical University Darmstadt, Germany; 3. Ludwig Boltzmann Institute for Cardiovascular Research, Austria; 4. Austrian Institute for Tissue Regeneration, Austria; 5. Fraunhofer Institute for Computer Graphics Research IGD, Germany

Introduction: The use of mathematical models in the cardiovascular domain is increasingly recognized for their potential in predicting diseases, planning therapies, and controlling medical devices. These models are usually composed of nonlinear ordinary differential equations (ODEs) that necessitate numerical solutions. However, this requirement often makes the solving process time-intensive, constraining their practical applications. For instance, employing these models within a model-predictive control algorithm for cardiac assistive devices demands predictions of multiple heartbeats within a second, a task challenging when using complex ODEs. Previously, we showed the potential of simplifying a lumped-parameter cardiovascular model using deep learning-based Koopman analysis for single heartbeats [1]. Here we present our preliminary findings on expanding the methodology to multiple heartbeats.

Methods: The dataset was generated using a previously established lumped-parameter cardiovascular system model [2]. In total, 100 simulations of 10 s were performed for varying initial conditions, extracting 18 different hemodynamic signals of interest, including flows, pressures, and volumes in the heart and the circulatory system. All signals were sampled at 50 Hz and stored for further use. The data was z-normalized and split in ratio 8:1:1 into training, validation, and test sets, respectively. Each time series in the training set was split into sequences of 1 s with an overlap of 20 ms using a sliding window approach.

Following the work of Lusch et al. [3], a deep auto-encoder (4 layers, 30 hidden units) was used to transform the data into an intermediate space to linearize the system's dynamics. The transformed states were then fed into a second neural network (3 fully connected dense layers with 10 hidden units each). This network was employed to identify a finite set of Eigenvalues estimating the Koopman operator K. The obtained matrix K is applied to predict future time steps of the hemodynamic states in the intermediate space. Finally, the results are transformed back into the original space using the decoder network.

To evaluate the network's prediction accuracy, the root mean squared error (RMSE) between prediction and ground truth was calculated for all normalized sequences in the test dataset. To assess the computational performance of the reduced model, the time required to predict 10 heartbeats was calculated.

Results: Predicting 10 heartbeats (500 time steps) given only the initial condition resulted in an average z-normalized RMSE of 0.13 over the whole test set (Figure 1). For the predictions on an AMD Ryzen 7 PRO 4750U, the reduced model takes on average 0.78 s compared to 12.5 s using the full model. The variance of all obtained eigenvalues was below 1×10^{-6}, indicating the linearity of the reduced system.

Discussion: The approach previously employed for a single heartbeat [1] was effectively applied for 10 heartbeats, highlighted by low RMSE and variance in Eigenvalues. The computational time of 0.78 s required for the prediction of 10 heartbeats represents a speed-up of factor 16 compared to the lumped-parameter model. Furthermore, it lies within a range suitable for use in model-predictive assays to control medical devices like neuroprostheses or circulatory assist devices.

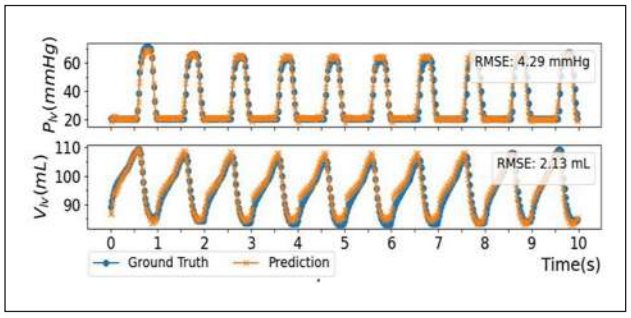

Figure 1. Reduced model prediction versus ground truth of left ventricular pressure (Plv) and volume (Vlv) for 10 s.

Current work is directed towards the prediction of longer sequences with a particular emphasis on robustness against parameter changes, and optimization of network architecture to further enhance accuracy and computational performance.

References

1. Haberbusch et al, ASAIO Journal, 69.2:113, 2023.
2. Haberbusch et al, Front Physiol, 11:579449, 2020.
3. Lusch et al, Nature Communications, 9:4950, 2018.

Acknowledgements

This work was supported by the project PREVENT (H-463816/2023) funded by the City of Vienna.

REMOVAL EFFICIENCY COMPARISSON BETWEEN ACETATE AND CITRATE BASED DIALYZATE IN ONLINE HEMODIAFILTRATION AND EXPANDED HEMODIALYSIS.

Miquel Gomez (1), Diana Rodriguez (2), Marta Arias-Guillén (1,2), Jose-Jesús Broseta (1), Lida Rodas (2), Francisco Maduell (1,2).

1. Laboratori Experimental de Nefrologia i Trasplantament Renal (LENIT), Fundació Clínic per la Recerca Biomédica-Institut d'Investigacions Biomèdiques August Pi I Sunyer (IDIBAPS), Barcelona, Spain. 2. Nephrology Department, Hospital Clinic de Barcelona, Spain.

Introduction: Hemodialysis treatment with bicarbonate dialyzate requires an acidic solution to prevent salt precipitation. Acetic (AC) or citric acid (CT) based dialyzate is preferred according to the treatment modality. The former is implemented in intermittent hemodialysis whereas the latter is relegated to continuous treatments for its calcium chelating properties, enhancing anticoagulation. In addition, CT dialyzate is related to clinical benefits [1] by reducing hyperacetatemia and also showed reduced membrane adsorption of proteins [2], allowing improved removal efficiency. The effect of dialyzate composition together with the enlarged pore size of medium cut-off membranes used in expanded hemodialysis (HDx) on the removal properties have been scarcely explored [3]. Here we compare the removal outcomes between AC and CT dialysate in online hemodiafiltration (HDF) and HDx treatments.

Methods: 12 clinically stable chronic patients in hemodialysis underwent their mid-three-weekly-scheduled treatment using Fx-80 Cordiax, Solacea-19 and Theranova-400 dialyzers combined with Fresenius smartbag 211,50 AC or CT-based dialyzate (6 treatments per patient)

Table 1. Mean± SD values of RR(%) for the different performed treatments. * p<0,05 vs. Fx-80 CT.

Filter	Dzte.	BUN	β -micro	Alb	TP
Fx-80	AC	81±5	80±6	7±7	9±8
	CT	80±5	82±5	9±6	9±6
Sol-19	AC	82±9	79±8	9±7	9±7
	CT	82±5	80±5	9±6	9±6
Ther.	AC	80±7	76±6*	9±6	9±6
	CT	81±3	77±5*	11±10	10±8

in a FMC 5008 device. Session parameters such as blood, dialyzate and substitution flow, as well as ultrafiltration rate, total ultrafiltration, transmembrane pressure (TMP), convective volume (CV), blood processed, treatment duration, initial and final hematocrit and hemoglobin, urea dialysance (K), Kt and Kt/V were recorded. Additionally, treatment pre (C_{pre}) and post (C_{post}) blood samples were taken to calculate the reduction ratio, RR(%), of BUN, β_2-microglobulin, albumin and total proteins (TP) by Equation (1), being C_{post} corrected for all molecules except BUN by Bergström&Wehle [4]. Data was compared by ANOVA for repetitive data and Bonferroni posthoc test.

$$RR(\%) = \frac{C_{pre} - C_{post}}{C_{pre}}.100 \quad (1)$$

Results: Statistical differences were found for TMP, CV and substitution flow when comparing HDF to HDx treatments (p<0,01) but were not translated into significant outcomes for K (p=0,370), Kt (p=0,457) and Kt/V (p=0,504). Regarding removal efficiency, no significance was found in the RR for BUN (p=0,542), albumin (p=0,717) and total proteins (p=0,932) between hemodialyzers and dialyzates (Table 1). In the case of β_2-microglobulin, differences were found between Fx-80 CT and both Theranova-400 AC and CT treatments (p<0,05), but not between AC and CT for the same hemodialyzer.

Discussion: HDF and HDx treatments with CT dialyzate proved well tolerated and have similar removal outcomes as compared to AC. Our results support the implementation of CT in stable patients undergoing intermittent hemodialysis. However, further studies are needed to analyze the adsorption properties of hemodialyzers under CT dialyzate.

References

1. Gabutti, L. et al. BMC Nephrol. 10, 7, 2009.
2. Mares, J. et al. Artif. Organs 43, 1092–1103, 2019.
3. Vrečko, M. M. et al. BMC Nephrol. 23, 1–5, 2022.
4. Bergström, J. & Wehle, B. Lancet 329, 628–629, 1987.

Acknowledgements

This work was funded by Instituto de Salud Carlos III, grant nº exp PI22/00243, Fondos Feder, "una manera de hacer Europa".

A BIOMIMETIC APPROACH FOR VASCULAR PROSTHESES FOR UNIVENTRICULAR HEARTS

Marc Mueller (1), Jan Drexler, (1), Bente Thamsen (2), Marcus Granegger (2) Birgit Glasmacher (1)

1. Institute for Multiphase Processes, Leibniz University Hannover, Germany; 2. Christian Doppler Lab for Mechanical Circulatory Support, Medical University Vienna, Austria

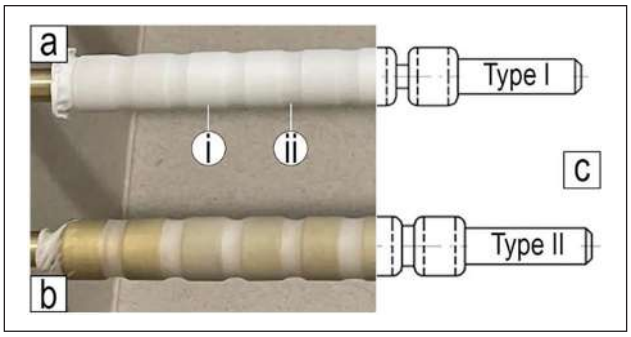

Figure 1. Custom made electrospinning collector for the fabrication of anti-kinking vascular scaffolds. Evaporation of the solvent was completed after 48 h of drying (a) and was previously evident in transparent fibers (b). Scaffolds show a combination of randomly deposited (i) and orientated fibers (ii, gap-spinning).

Introduction: Avoiding kinking of vascular prostheses poses a particular challenge for complex surgical procedures such as in Fontan patients[1]. In this study a biomimetic approach is pursued and combines it with electrospinning to produce a novel vascular scaffold with anti-kinking properties (Fig. 1a).

Methods: Two different electrospinning collectors (Fig. 1c, d=10 mm; l=150 mm) inspired by the caterpillar structure were used, combining the deposition of unaligned fiber segments (stability) with gap-spinning segments (flexibility). The groove depth to ensure the gap spinning effect was varied (Fig. 1c, 1.5 mm vs. 3 mm).

Electrospinning was performed with a 6 w/w% polyure-thane-polycaprolcatone copolymer (MDI-Polyes-ter/Polyether Polyurethane, Sigma Aldrich) in a 1:1 v/v mixture of dimethylformamide and tetrahydrofuran (Carl Roth). The flow rate was kept at 1.5 ml/h, voltage at 18 kV, distance at 170 mm and the spinning duration was 120 min. In a subsequent process, the unaligned fiber segments were additionally coated with silicone. Fiber diameter and morphology were examined via scanning electron microscopy (SEM, S3400-N, Hitachi), wall thickness, delamination and quality of the silicone reinforcement via light microscopy (Axio Discovery V12, Carl Zeiss). To determine the flow properties under bending, a test setup (double distilled water, 37 °C, p=50 mmHg) was used to measure the change in flow rate as a function of the bending angle. The flow rate was measured for 30s for bending angles from 0° to 120° in 15° steps.

Results: The use of different collector types resulted in mean fiber diameters of 1.8 µm and 2.3 µm respectively. Clear morphological differences between the segments could be detected, with the gap spinning areas showing an expected alignment of the fibers. No delamination was detected between the fiber layer and the silicone reinforcement. The mean wall thicknesses for the electrospun layer were 80 µm and 85 µm respectively and was increased to 200 mm for both types by the silicone rein-forcement. Both types showed a linear decrease in flow rate (R^2=0.95 and 0.99) as a function of the bending angle (Fig. 2). The decrease in flow rate was at its maximum for both prostheses at a bending angle of 120°. The decrease was only 95.5 % and 94.5 % of the initial value at 0° bending.

Discussion: The collector design used has been successful both in the modification of the fiber microstructure and in the optimization of the bending properties. No influence of the groove depth on the bending properties was observed. The additional reinforcement structure using silicone showed high integrity and no signs of delamination. It further

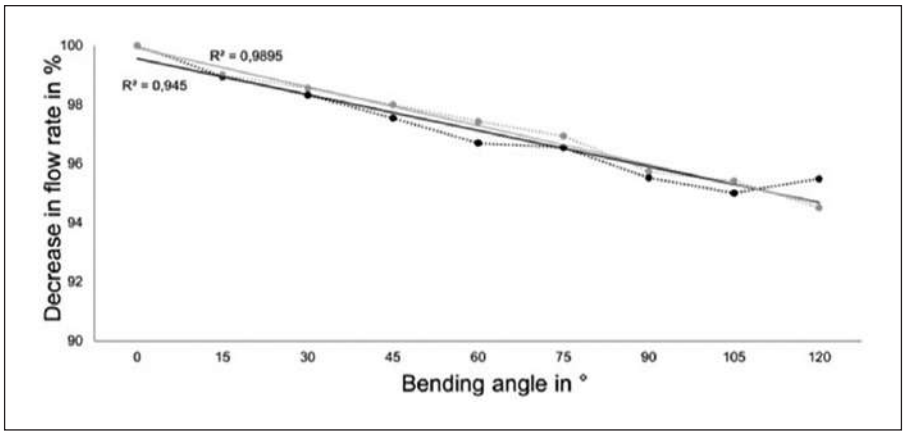

Figure 2. Bending properties of both collector types showed a linear relationship between bending angle and decrease in flow rate (n=3).

improved the bending properties as well as the resistance to compression. At the same time, it is potentially a suitable reinforcement for suturing to the vascular system.

Further investigations are focusing on the transfer of the process to the medical grade polyurethane Carbothane 3585A (Lubrizol) and further performance testing.

Reference

1. Escher A. et al. Semin Thorac Cardiovasc Surg. 2022 Spring;34(1): 238-248.

Acknowledgements

The authors thank our students Michael Guenther and Julia Panitz for their support in this study. This work was funded by the Leibniz Young Investigator Grants.

IN SITU TISSUE ENGINEERED HEART VALVE BASED ON WOVEN TEXTILE SCAFFOLD

Thomas Schmitz-Rode[1], Sebastian Jansen[1], Jan Niklas Thiel[1], Michael Neidlin[1], Torsten Hüner[2], Stefan Jockenhövel[1], Ulrich Steinseifer[1]

1. Institute of Applied Medical Engineering – AME, Helmholtz Institute for Biomedical Engineering, RWTH Aachen University, Aachen, Germany, 2. ac.biomed GmbH, Aachen, Germany

Figure 1. Textile heart valve scaffold tested with 200 million load cycles.

Introduction: Bioprostheses with leaflets made from decellularized animal tissue represent the current state of the art in heart valve replacement. These valves are prone to calcification and structural degeneration, which limits their lifespan and requires repeated surgical interventions. The goal of this project is to investigate a leaflet scaffold based on a load-oriented woven textile. It is designed to provide structural integrity and can be further processed with a hemocompatible and bioactive coating for in situ tissue engineering.

Methods: Mechanical testing was used to preselect the fabric configuration, followed by porosity testing. The woven scaffolds were coated with TPU chloroform (Carbothane PC-3585A, Lubrizol) and mounted in a balloon expandable TAVI stent. Accelerated wear tests were performed under simulated physiological load in a LinA testing device (AME-HIA and ac.biomed GmbH). The function of the leaflets and signs of wear were assessed by high-speed camera recordings, photography and microscopic examination. Favorable textile scaffoldstent designs were tested with a higher number of load cycles. In addition, finite element analysis (FEA) was performed to investigate the stresses in the leaflet material and individual warp threads at the leaflet-stent interface during valve closure.

Results: After design optimization, current lab samples withstand more than 200 million load cycles. Critical failure zones, especially near the commissures, have been mitigated by adapting the weave pattern and the way the weave is attached to the stent. The FEA revealed areas of high stresses in the woven textile and quantified the influence of stent flexibility on the load dynamics. The latest R&D results on these aspects will be presented.

Conclusions: Current results promise to achieve reasonable durability of a valve composed of woven leaflet scaffolds. Further hemocompatibility, cell colonization, and calcification testing are required to confirm suitability as an in situ heart valve replacement.

TRANSLATION OF IN-SILICO ANIMAL TRIAL TO HUMAN CONDITIONS: PULMONARY ARTERY PRESSURE SENSOR HEMODYNAMICS

Leonid Goubergrits (1), Pavlo Yevtushenko (1), Adriano Schlief (1), Jan Romberg (2), Titus Kuehne (1), Andreas Arndt (2), and Jan Bruening (1)

1. Institute of Computer-assisted Cardiovascular Medicine, Deutsches Herzzentrum der Charité, Germany; 2. Biotronik, Germany

Introduction: Heart failure (HF) is a leading cause of death and hospitalization with high prevalence of 1-2% [1]. Recently pulmonary artery pressure sensors (PAPS) were proposed to detect earlier acute decompensation that can ideally be mitigated by pharmaceutical treatment. A novel PAPS designed to be implanted in the left or right PA is currently under development. Preclinical evaluation of safety and efficacy in frames of bench tests and animal trials is necessary for any novel medical device. However, animal trials are still limited with respect to the information that can be assessed and their translation towards use in humans is challenging. The aim of the study presented here was to investigate a translation of in silico animal trial [2] towards humans. This is required since conditions differs among different species [3]. Respective, intra-arterial hemodynamics before and after virtual device implantation in human PAs was simulated using CFD and hemodynamic parameters in animal and human PA were compared.

Materials and Methods: The study based initially on the chronic animal trial: 20 PAPS (one in the left and one in the right PA) were implanted in 10 pigs (app. weight of 60 kg). CT acquisition, which was done before and after implantation was used for in silico image-based CFD analysis of the porcine PA hemodynamics with and without PAPS [2]. To compare hemodynamics in porcine and human PA, human PA geometries were selected from a retrospective cohort using similarity of geometric parameters (lengths and diameters of all three major PA segments, LPA-RPA bifurcation angle, and number of side branches) as measured by L1 norm. Finally, 20 PAPS were virtually implanted into the human PA aiming to mimic pairwise implantation sites in porcine PA of the animal trial (see figure 1).

PA hemodynamics with and without PAPS was analyzed based on transient blood flow simulations performed using STAR-CCM+ flow solver (15.04, Siemens PLM, USA). Blood was modelled as an incompressible fluid with a shear-rate dependent viscosity following a Carreau-Yasuda model. A k-omega SST turbulence model is used to account for turbulent effects. Flow rate curves at the main PA of pigs and humans were generated synthetically using a hybrid approach considering weights for definition of heart rates (HR) and cardiac outputs (CO), whereas patient-specific HR and CO were used in humans. Three parameters were evaluated: time-averaged wall shear stress (TAWSS) and oscillating shear index (OSI), which are parameters associated with a risk of thrombus formation as well as pressure drop caused by the PAPS.

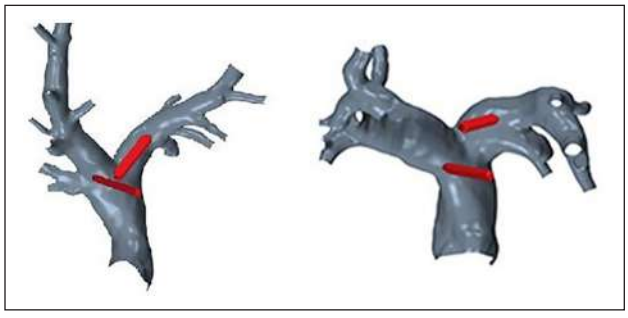

Figure 1. Left: porcine PA with two implanted PAPS. Right: human PA with similar implanted sensors.

Results: We found significantly larger diameters (left Pa: 18±1.3 mm vs. 14±1.7 mm; right PA: 20±1.2 mm vs. 15±2.0 mm) and larger bifurcation angle (89±8° vs. 80±7°) in humans. Comparing boundary conditions, we found significantly lower HR in humans with 65±6.0 bpm vs. 100±2.9 bpm, whereas no significant differences in CO (4.3±1.2 L/min vs. 4.7±0.2 L/min).

We found significantly higher TAWSS in human PA after implantation (pre: 1.38[1.11] Pa; post: 1.44[1.15] Pa), which is clinically neglectable. No significant difference was found for the OSI (pre: 0.16[0.07]; post: 0.15[0.07]). In the human PA TAWSS was significantly lower as in the porcine, whereas OSI significantly higher. PAPS implanted in the human PA causes relatively low averaged pressure drop of 0.8±0.8 mmHg, which non-significantly differs from the pressure drop calculated in porcine PA with 0.7±1.1 mmHg.

Summarizing, we found significant difference in hemodynamics between porcine and human PA that is probably associated with lower protection against thrombosis risk under human conditions. Despite these differences both in silico studies (porcine and human) found no higher thrombosis risk due to PAPS.

References

1. Retrum JH et al. Circ Cardiovasc Qual Outcomes. 6:171– 7, 2013.
2. Bruening J et al. Front. Cardiovasc. Med., 10:1193209, 2023.
3. Goubergrits L et al. Scientific Reports, 13:20211, 2023.

Acknowledgements

This work has been funded under the European Union's Horizon 2020 programme under Grant No. 101017578

ACCURACY OF THE HEARTMATE 3 FLOW ESTIMATION

Theodor Abart (1), Marko Grujic (1), Michael Röhrich (2), Philipp Aigner (1), Stefan Jakubek(3), Daniel Zimpfer (1), Marcus Granegger (1)

1. Christian Doppler Laboratory for Mechanical Circuit Support, Department of Cardiac Surgery, Medical University of Vienna, Austria; 2. Department of Anesthesia, Intensive Care Medicine and Pain Medicine, Medical University of Vienna, Austria, 3. Division of Control and Process Automation, Institute of Mechanics and Mechatronics, Vienna University of Technology, Vienna, Austria

Introduction: Despite advances in fully magnetically levitated left ventricular assist devices (LVADs) [1], the lack of hemodynamic sensors limits the understanding of the patient's cardiovascular condition. However, for advanced diagnostics (e.g. cardiac function, aortic valve opening) and automated speed adaptations, assessment of hemodynamic parameters is crucial. The aim of this study was to evaluate the accuracy of the flow estimator of the clinically available LVAD, the HeartMate 3 (HM3), and evaluate its performance across static and dynamic conditions.

Methods: Experiments were performed at five speeds (3-7 krpm) and three fluid viscosities (2.5, 3.5 and 4.5 mPa*s) using a previously described hybrid mock circulatory loop (HMCL).[2] For static measurements, pump flow was increased stepwise from -1 L/min until no head pressure was generated. Realistic partial and full support scenarios were investigated by coupling virtual patients with the HMCL. Pressures, flows and pump parameters were recorded. Relationships between these parameters and specifically the estimated and measured flow were derived to understand

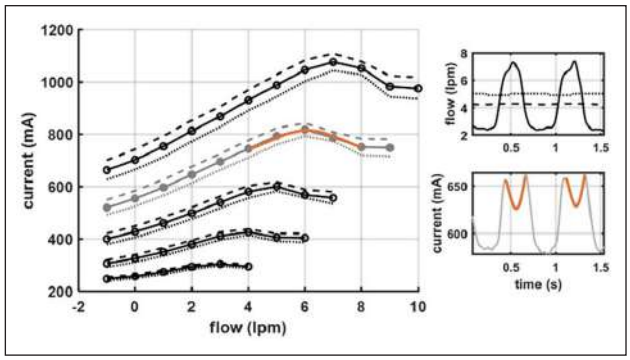

Figure 1. left: Static relationship between measured pump flow and current (bottom to top: 3k, 4k, 5k, 6k, 7 krpm; dotted: 2.5; solid: 3.5; dashed 4.5 mPa*s. Right: Measured (solid black), mean (dashed) and estimated (dotted) flow and current (grey) at 80 bpm, 5.4 krpm and a viscosity of 3.5 mPa*s during partial support. Non-monotonic behavior of current marked in orange.

the underlying working principle of the flow estimator and its accuracy. The Pulsatility Index (PI) as an indicator for flow waveform amplitude was investigated.

Results: Static measurements showed that at each speed (for each viscosity within this speed) the correlation between estimated pump flow and motor current was high ($r^2 > 0.99$, $p<0.001$), indicating that estimated flow is based on speed, current and viscosity. The current exhibits a non-monotonic behavior at higher flows (Figure 1), which is reflected in the estimated pump flow signal, leading to large deviations between estimated and measured pump flow in this region (e.g. -3.5 L/min at 6 krpm and 2.5 mPa*s). Accuracy of the flow estimator in terms of the root-mean-square-error (RMSE) was 1.63 L/min. In typical full support scenarios, the virtual patient's mean flow was overestimated by 1.41±0.44 L/min (41%), in partial support conditions by 0.65±0.41 L/min (18%) on average. During partial support, PI values are up to 48% smaller than they would be with a monotonic current that does not decrease at higher flow values.

Discussion: The HM3 flow estimator calculates flow based on current, speed, and viscosity. The flow signal is overestimated at low flows and underestimated at high flows by up to +2.3 L/min and -3.5 L/min, respectively. These discrepancies can be explained by a non-monotonic relationship between current and pump flow, which renders flow estimation challenging. This non-monotonic behavior also affects PI calculation as an indicator for the amplitude of pump flow: whereas the PI may indicate trends in pulsatility in the linear portion of the relationship (i.e. in full support conditions), it does not adequately represent pulsatility in partial support conditions. The clinically used HM3 parameters should be interpreted with caution and have limitations regarding the assessment of parameters related to cardiac function.

References

1. Mehra *et al.*, *JAMA*, 328, no. 12, 1233–1242. 2022.
2. Bender *et al.*, *IEEE Trans. Biomed. Eng.*, pp. 1–12, 2023,

Acknowledgements

The financial support by the Austrian Federal Ministry of Labour and Economy, the National Foundation for Research, Technology and Development and the Christian Doppler Research Association is gratefully acknowledged.

THE HEART HACKATHON: NURTURING THE NEXT GENERATION IN CARDIOVASCULAR INNOVATION.

Nina Langer (1,2), Thi K. Dao (2,3), Dinasha Wimalasiri (2,4), Ethan Grooby (2,5), Sarah N. Trembley (2), Taylah Banham (1,2), Shaun D. Gregory (1,2,6)

1. Cardio-Respiratory Engineering and Technology Laboratory (CREATElab), Department of Mechanical and Aerospace Engineering, Monash University, Melbourne, VIC, Australia; 2. The Heart Hackathon, International Society of Mechanical Circulatory Support, Houston, Texas, United States of America, 3. Vascular Pathophysiology and Therapeutics Group, Victorian Heart Hospital, Victorian Heart Institute, Monash University, Melbourne, VIC, Australia, 4. Women's Health Group, The Ritchie Centre, Hudson Institute of Medical Research, Department of Obstetrics and Gynaecology, Monash University, Melbourne, VIC, Australia, 5. Biomedical Signal Processing Research Lab, Department of Electrical and Computer Systems Engineering, Monash University, Melbourne, VIC, Australia, 6. The Centre for Biomedical Technologies and School of Mechanical, Medical and Process Engineering, Queensland University of Technology, Brisbane, QLD, Australia

Introduction: Heart Failure (HF) is a leading cause of death globally [1]. With its increasing prevalence and a lack of donor hearts [2], device-based alternatives are required. Total artificial hearts (TAH) can bridge a HF patient until a donor's heart is available. The only commercially available TAH to date was FDA-approved 10 years ago [3], which emphasises a lack of innovation for device-based solutions. To promote new ideas in the field of mechanical circulatory support for HF patients, a student competition, the Heart Hackathon, was developed. This global biomedical engineering design competition aimed to generate a platform for novel ideas and contribute to the development of novel approaches to train the next generation of cardiovascular engineers.

Methods: The ideation process was shaped by interviews with university team leads for established engineering student competitions e.g. Formula Student (motorsport) and University Rover Challenge (Mars rover), focusing on determining an appropriate competition structure, timeline and requirements for competing teams as well as submissions. Based on these discussions, the competition development was broken into four core steps: an online event where teams pitch their concepts, two report submissions, and the grand final. The organising committee was built from the existing structure of the Monash Young Medtech Innovators (MYMI) to lay the groundwork, while the final organising committee is an independent group divided into the lead, engagement, marketing, operations and partnerships divisions. The implementation of the competition included the definition of rules and regulations, IP and NDA arrangements, marketing (HeartHackathon.com), a press release, and global outreach to academic institutions as well as online webinars and workshops. The Heart Hackathon was then merged with the International Society for Mechanical Circulatory Support (ISMCS).

Results: The Heart Hackathon has grown to 9 teams across five continents, constituting over 300 students. Through memberships of the competing teams, ISMCS membership was increased by 22% in 2023, and 50 competing students attended the annual meeting of ISMCS 2023 (Dallas) in person, representing 20% of the conference attendees. Competing teams have received substantial recognition via channels including the Duke of Edinburgh (UK), the Excellence Prize for Scientific Research and the Romanian Healthcare Awards -Medical Innovation of the Year (Romania), and the 2023 UNSW Engineering Education Festival -Winner of the VIP impact competition (Australia). The Heart Hackathon was subsequently integrated into the curriculum of five Universities and directly led to five job interviews for student members to date.

Discussion: Currently, the Heart Hackathon is at a pivotal point of retaining current teams and sponsors while growing and adapting to accommodate teams with varying levels of experience and resources. This competition has created greater public and university awareness of the need for TAH innovation and provided a framework for biomedical engineering students to develop novel approaches for mechanical HF support. The implementation of this competition in university curricula solidifies the longevity and engagement to this need, and enhances biomedical engineering degree courses by providing hands-on experience to students and connecting them to international experts in the field.

References

1. G. Savarese et al, Cardiovascular Research, vol. 119, no. 6, pp. 1453–1453, 2023.
2. M. Cameli, E. et al, Front. Cardiovasc. Med., vol. 10, p. 1290011, 2023.
3. T. Lee and G. Torregrossa, Elsevier, pp. 545–557, 2018.

EXPERIMENTAL AND NUMERICAL ANALYSIS OF THE PARTICLE-AND CELL MIGRATION IN GAP-LIKE FLOWS OF VENTRICULAR ASSIST DEVICES

Finn Knüppel (1), Sasha Malchow (1), Ang Sun (3), Jeanette Hussong (3), Alexander Hartmann (2), Frank-Hendrik Wurm (1), Benjamin Torner (1)

1. Institute of Turbomachinery, University of Rostock, Rostock, Germany, 2. Institute of Clinical Chemistry and Laboratory Medicine, Rostock University Medical Center, Rostock, Germany, 3. Institute for Fluid Mechanics and Aerodynamics, Technical University of Darmstadt, Darmstadt, Germany

Introduction: Patients with advanced terminal heart failure require a donor heart or a technical solution of a ventricular assist device (VAD). A VAD pumps blood from the left ventricle into the artery. To generate the required pressure, the impeller rotates at several thousand revolutions per minute. These high rotational speeds and speed gradients affect the blood. Blood consists of a low-viscosity plasma and high-viscosity cellular components. To minimise damage or activation of the blood components, it is important to numerically identify areas of high stress in a VAD (e.g. bearing regions or side chamber of radial impellers). In these simulations, a single-phase blood analog fluid is used, which has a similar density and viscosity as blood. Nevertheless, this assumption can lead to a deviation, especially in narrow gaps. In gaps between 7-300 µm, the particles migrate to the center of the vessel, and a low-density layer of plasma forms between the wall and the cells. It is known in medicine as the cell-free layer (CFL). After the successful optical analysis of the particle migration, the influence of particle migration in a stationary channel under the flow conditions of a VAD gap (Re ~ 100; 150µm) was investigated both experimentally and numerically

Methods: To better understand the flow in narrow gaps, these flow conditions were adapted to a stationary narrow gap-like flow of ventricular assist devices. Optical analysis, wall shear stress, and pressure measurements were used to study particle migration and flow behavior in these confined spaces. Various Reynolds numbers were tested (50-150), which represent typical flow conditions that prevail in VAD gaps. Various blood with different hematocrits and blood analog fluids were used. In addition, a numerical model was developed based on the optical measurement and particle distribution over the channel height. This takes into account the effect of cell migration based on the change in viscosity over the height of the channel.

Results: A cell-free layer was found in all tested particulate fluids, leading to a reduction in stress and pressure loss compared to single-phase fluid without a cell-free layer. The numerical results were compared with the previously measured experimental results with particle-laden blood analog fluids and with newly recorded blood measurements with particle volume fractions up to 5% (Re = 50 to 150). A good agreement was found between the numerical simulations and the experiments on wall shear stress and pressure losses. Furthermore, it can be seen that the shear stress in the fluid decreases as well.

Discussion: The results in our experimental setup led to the hypothesis that the CFL-formation and stress reduction are also present in the narrow gaps of VADs. A satisfactory agreement was attained between the experimental observations and the numerical results. Now it is possible to predict numerically the impact of particle migration on the flow.

FIRST CO-CULTURE OF HUMAN DURAL FIBROBLASTS AND ADIPOSE STEM CELLS FOR DURA MATER TISSUE-ENGINEERING

Jean-Philippe Tosiani (1), Nathalia Oderich Muniz (1), Timothée Baudequin (1)

1. Université de technologie de Compiègne, CNRS, BMBI (Biomechanics and Bioengineering), Centre de recherche Royallieu -CS 60 319 -60 203 Compiègne Cedex, France

Introduction: The dura mater, the meninges' outermost layer, acts as a semi-rigid barrier between the central nervous system and bone tissues [1]. Its limited healing ability and tendency to form scar tissue can lead to complications after neurosurgery and dural resection. Advancements in dural tissue engineering could enhance our understanding of this interface and help create in vitro models and implantable scaffolds for dura mater repair. One challenge is to develop a co-culture model using human dural fibroblasts (HDufs) and adipose-derived stem cells (ASC52telo) differentiated into osteoblasts, aiming to mimic natural tissue environments and study cell interactions. Here, we present the phenotype analysis results for HDufs and ASC52telo after up to one month of co-culture.

Methods: Two co-culture methods, indirect (separate compartments) and direct (mixed), were conducted using HDufs and ASC52telo. Initially, cells were cultured in an optimized proliferation medium for one week. Then, a three-week period followed with or without osteogenic factors (dexamethasone, ascorbic acid, and beta-glycerophosphate). To assess the effects of co-culture methods and osteogenic stimulation on the behavior of HDufs and ASC52telo, qPCR, immuno-fluorescence, ALP staining, and alizarin red staining were performed at 14 and 28 days. Monoculture controls were conducted to validate the study.

Results and Discussion: The results revealed increased expression of osteogenic genes and bone biomarkers during co-culture, indicating stem cell maturation into osteoblasts even without differentiation factors (Figure 1A), suggesting a beneficial impact of HDufs interaction on this process. Regarding HDufs' functionality in long-term co-culture, they exhibited a notable phenotype change: increased expression of dura mater periosteal layer-related markers and Crapb2 decrease, specific of the dural border cell layer [2] (native dura deepest layer). The dural fibroblast marker FxyD5 was expressed all along till the co-culture end (Figure 1B and C).

Conclusion: Long-term co-culture of HDufs and ASC52telo proved stable, ensuring survival and functionality of both cell types. The synergy between them facilitated stem cell differentiation into mature osteoblasts while inducing phenotypic changes in HDufs resembling native tissue. These findings support the potential of this co-culture model for in vitro dura mater studies and as a substitute testing model for in vivo purposes. Next, we plan to validate these results with 3D scaffold co-culture.

References

1. Vandenabeele et al, J Anat, 189:417–30, 1996.
2. Farmer and al.,Nat Commun, 12:4797, 2021

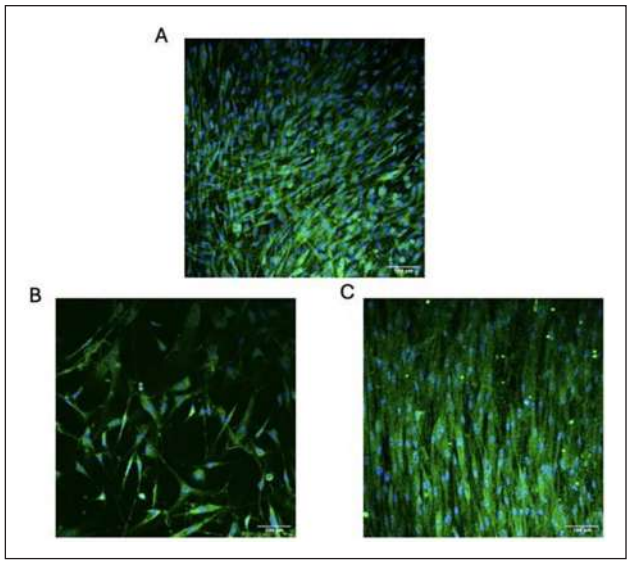

Figure 1. Representative immunostaining of (A) osteocalcin (green) in ASC52telo at day 28, (B) FXYD5 (green) in HDufs at day 14, and (C) day 28 in monoculture exposed to co-culture medium without factors. Blue: cell nuclei (DAPI).

Acknowledgements

The authors acknowledge financial support from ANR (ANR JCJC DuraLayer), MESR, and UTC Direction à la Recherche (Appel Jeunes Chercheurs). Special thanks to Léa Tonini and Chloé Pelletier for their contributions to preliminary studies.

PEPTIDES MEDIATED ORGAN-CROSSTALK: ROLE OF ADRENAL GLANDS IN VASCULAR CALCIFICATION AND BONE METABOLISM.

Shruti Bhargava (1), Erik Merckelbach (1), Vera Jankowski (1), Àngel Argilés (2), Joachim Jankowski (1, 2)

[1]Institute of Molecular Cardiovascular Research, Medical Faculty, RWTH Aachen University, Germany, [2]Experimental Vascular Pathology, Cardiovascular Research Institute Maastricht (CARIM), University of Maastricht, The Netherlands. [3]RD-Néphrologie and EA7288 University of Montpellier, France

Introduction: Adrenal glands are a source of numerous bioactive peptides/mediators which have varied functions in the body like mediation and progression of diseases (1).

Patients receiving dialysis for chronic kidney disease frequently experience osteoporosis along with cardiovascular issues like vascular calcification. Identification of adrenal glands released mediators, which impact disease progression will lead to the establishment of novel therapeutic targets.

Methods: To identify potential mediators originating from adrenal glands, mass spectrometric analysis was conducted, and the results were compared with relevant databases. Chromatographic fractions derived from bovine adrenal glands were tested for their effect on vascular calcification processes using *in vitro, ex vivo,* and *in vivo* rat model of elastocalcinosis (VDN). Further, the bones from the rats were analyzed for structural changes resulting from the administration of CBF.

Results: This research identified an endogenous peptide, Calcification blocking factor (CBF), released from the adrenal gland, which was investigated with regard to it's role in vascular calcification and bone mineralization. Treatment with CBF effectively reduced the calcium content in cells, thoracic aortic rings cultured under calcifying conditions, and aortas from elastocalcinosis animal models. CBF exerts its protective effects by inhibiting the transdifferentiation of aortic smooth muscle cells into osteoblast-like cells, which are responsible for driving the progression of vascular calcification. CBF interacts with the sodium-dependent phosphate transporter PIT-1 and hinders NF-κB activation and the BMP2/p-SMAD pathway, all implicated in vascular calcification. CBF treatment reduced arterial stiffness in elastocalcinosis animals. CKD patients, susceptible to vascular calcification, showed decreased CBF concentration in serum.The 19-amino acid peptide is derived from the enzymatic cleavage of the adrenal protein chromograninA by calpain1 and kallikrein. Further analysis revealed that a specific 6-8 amino acid sequence within the 19-amino acid peptide serves as the active site responsible for the calcification-blocking properties of CBF (2).

Discussion: Our findings suggest that CBF, a novel inhibitor of vascular calcification derived from the adrenal glands inhibits vascular calcification by inhibiting smooth muscle cells transdifferentiation. However, the mechanism by which it improves bone mineralization needs to be further investigated.

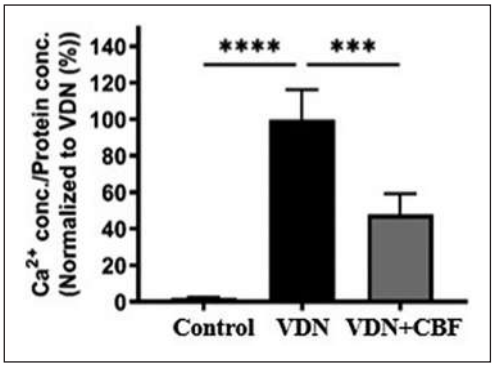

Figure 1. Calcium content was quantified in aorta isolated from control, VDN and VDN rats treated with CBF. VDN rats have a higher calcium content in aortas as compared to control rats. VDN rats treated with CBF show a lower calcium content as compared to untreated VDN rats.

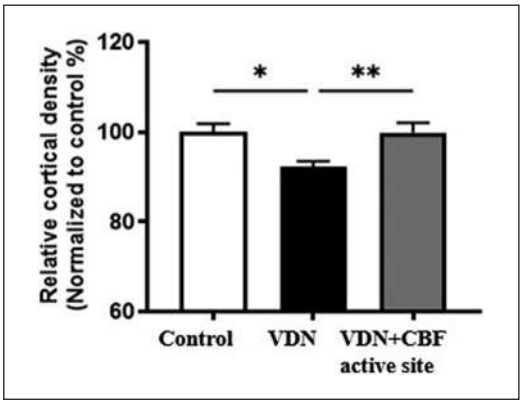

Figure 2. The tibia from controls, VDN and VDN rats treated with CBF active site were scanned using a microCT and bone mineral density was quantified. VDN rats showed a marked reduction in bone mineral density. Treatment of VDN rats with CBF active site led to an increase in bone density as compared to VDN rats.

References

1. Wang H, Dass C. Characterization of bioactive peptides in bovine adrenal medulla by a combination of fast HPLC and ESI-MS. Peptides. 2002 Dec;23(12):2143-50. doi: 10.1016/s0196-9781(02)00257-7. PMID: 12535692.
2. Orth-Alampour S, Gayrard N, Salem S, Bhargava S, Jankowski V, Jover B, Notarnicola C, Noels H, van der Vorst EPC, Kuppe C, Wolf M, Goettsch C, Theelen W, Bruck H, Fliser D, Loscalzo J, Wu Z, Marx N, Zidek W, Argilés À, Jankowski J. Prevention of vascular calcification by the endogenous chromogranin A-derived mediator that inhibits osteogenic transdifferentiation. Basic Res Cardiol. 2021 Oct 13;116(1):57. doi: 10.1007/s00395-021-00899-z. PMID: 34647168; PMCID: PMC8514386.

Acknowledgements

The authors were supported by grants from Deutsche Forschungsgemeinschaft (DFG) (SFB TRR 219; C-04, S-03, M-05; Project-ID: 322900939), the Federal Ministry of Education and Research (MIVAKA) (LS-2-1-001), and the European Union EU-ITN-H2020 to "INTRICARE" (722609) and "CaReSyAn" (764474).

PYRIDOXAL-5'-PHOSPHATE: A NEW THERAPEUTIC DRUG FOR THE TREATMENT OF HYPERTENSION

Michaela Lellig (1), Juan Muñoz-Castañeda (2), Juliane Hermann (1), Heidi Noels (1), Mariano Rodriguez (2), Martin Tepel (3), Joachim Jankowski (1), Vera Jankowski (1)

1. Institute for Molecular Cardiovascular Research (IMCAR), Department of University Hospital Aachen, Aachen, Germany. 2. Maimonides Institute for Biomedical Research (IMIBIC), Cordoba, Spain. 3. Department of Nephrology, Odense University Hospital, Odense, Denmark

Introduction: Although hypertension is a worldwide health problem, treatment options in low-income countries are still limited, resulting in high mortality. Therefore, the development of new therapeutic drugs that are affordable and accessible to everyone is still an urgent need. Since angiotensin II is one of the essential vasoconstrictive peptides in the human organism, we analyzed the impact of its posttranslational modification to pyruvamide-angiotensin II by pyridoxal-5'-phosphate on blood pressure. Pyridoxal-5'-phosphate is a less expensive vitamin B6 derivative and therefore could be a novel, cost-effective drug for the treatment of hypertension.

Methods: The post-translational modification of angiotensin II to pyruvamide-angiotensin II by pyridoxal-5'-phosphate was investigated *in vitro* by mass spectrometry. The calcium ion influx into vascular smooth muscle cells, which were treated with angiotensin II or pyruvamide-angiotensin II, respectively, was also investigated *in vitro*. In *ex vivo* experiments, the vasoconstrictive effect of angiotensin II and pyruvamide-angiotensin II was analyzed by using the bioassay of the isolated perfused rat kidneys. To validate the effect of pyridoxal-5'-phosphate *in vivo*, spontaneously hypertensive rats (SHR) were administered pyridoxal-5'-phosphate by using mini-osmotic pumps. Additionally, Wistar Kyoto rats (WKY) were divided into two groups: one receiving pyridoxal-5'-phosphate alone and the other receiving pyridoxal-5'-phosphate along with angiotensin II administration. Blood pressure was measured time-dependently.

Results: Angiotensin II, incubated with pyridoxal-5'-phosphate, was post-translationally modified to pyruvamide-angiotensin II. In vascular smooth muscle cells, the calcium ion influx after stimulation with pyruvamide-angiotensin II was significantly decreased compared to angiotensin II. The perfusion pressure of isolated perfused rat kidney increased less by pyruvamide-angiotensin II than by unmodified angiotensin II. The systolic and diastolic blood pressure of spontaneously hypertensive rats treated with pyridoxal-5'-phosphate decreased after three days of treatment significantly. The blood pressure of Wistar Kyoto rats treated with angiotensin II increased to hypertensive values, while the blood pressure of Wistar Kyoto rats co-treated with angiotensin II and pyridoxal-5'-phosphate was not increased.

Discussion: Pyridoxal-5'-phosphate significantly decreased blood pressure and might be a cost-effective drug for hypertension treatment. Respectively, an increased pyridoxal-5'-phosphate intake recommendation in the form of vitamin B6 intake might have a decreasing effect on blood pressure in the hypertensive population.

USING AI AND MULTIPHYSICS-SIMULATIONS TO PERFORM VIRTUAL (PRE)CLINICAL TESTING IN THE WEB-BROWSER

Simon J Sonntag (1), Gloria Zörnack (1), Diogo F. Almeida (1), Kristian Debus (1) Wen-Yang Chu (1)

1. Virtonomy GmbH, Germany

Introduction: The demand for innovative and effective medical devices continues to grow, accompanied by increasing development costs in terms of time and profitability. Addressing these challenges, the introduction of technology-enabled device testing alternatives offers a solution by refining and potentially eliminating the need for animal and human testing, while simultaneously making the process cost-effective, efficient, and safe. This transition is strongly supported by regulatory agencies such as the FDA.

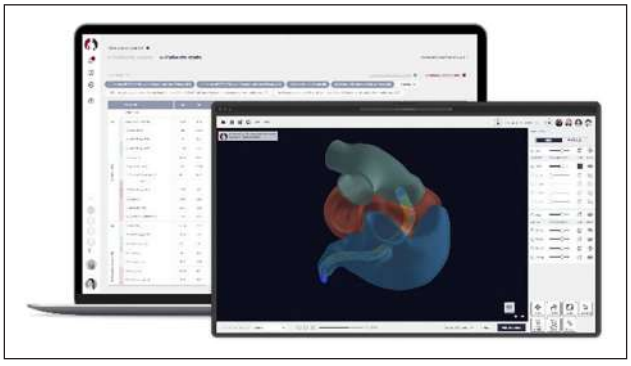

Figure 1. User interface of the web-based software v-Patients.

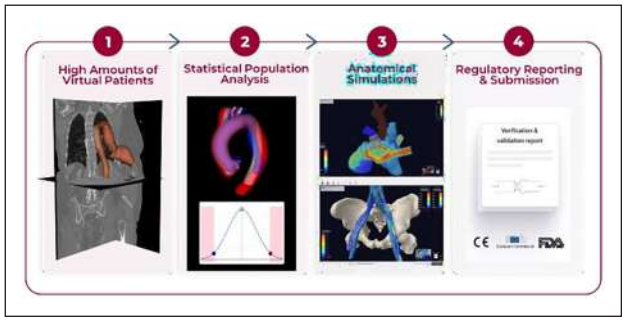

Figure 2. Methodology of v-Patients - from clinical data to digital evidence.

Methods: Virtonomy has developed v-Patients, a pioneering cloud-based technology that leverages digital twin capabilities. This platform empowers developers of cardiovascular medical devices to conduct virtual testing, simulating device performance in their target population using real-world evidence data from humans and animals. By integrating deep learning, statistical analytics, high-performance computing, and simulation, this approach progressively replaces traditional pre-clinical and clinical evidence with digital evidence throughout the entire device development lifecycle, resulting in reduced costs and enhanced resource efficiency.

v-Patients has already demonstrated successful application in the design and approval processes of novel mitral and tricuspid heart valve repair and replacement devices, percutaneous atrial shunt systems, and delivery catheters, as well as Ventricular Assist Devices and Total Artificial Hearts. Virtual studies conducted with v-Patients enable verification of design decisions, estimation of worst-case scenarios for sizes and variants, identification of suitable animal models, virtual testing on a large number of patients, determination and justification of anatomical and morphological eligibility criteria for sub-population selection, and completion of virtual clinical trials incorporating extensive patient data and simulations. These virtual studies pave the way for planning first-in-human studies and significantly reducing the number of actual patients involved.

Results: In successful submissions to regulatory bodies such as the FDA, European Notified Bodies, and other associations, virtual studies have demonstrated the ability to achieve results that may have been unattainable with conventional approaches. They reduce the risk and expense associated with the trial-and-error process, while enhancing evaluation confidence to ensure product safety prior to first-in-human studies and clinical trials.

IN-SILICO REPLACEMENT OF SINGLE-LUMEN CANNULA BENCH TESTING ACCORDING TO ISO 18193:2021

Simon J Sonntag (1), Weiyi Kong (1), John W. Benjamin (1), Fabien Péan (1), Yu-Chung Liao (1), Bence Z. Rochlitz (1)

1. Virtonomy GmbH, Germany

Introduction: Cannula systems are essential for extracorporeal membrane oxygenation (ECMO) allowing adequate blood flow. To replace the costly bench testing for single-lumen cannulas (SLCs), we develop a validated in-silico replacement.

Materials and Methods: The ISO 18193:2021 standard describes three main bench tests for SLCs: pressure drop (PD), blood cell damage, and collapse resistance. We present a computational fluid dynamics (CFD) model of the PD test based on our novel Smoothed Particle Hydrodynamics (SPH) framework able to capture turbulent characteristics like Large Eddy Simulations.

The PD test is conducted according to [1] complying with the ISO 18193:2021 standard (Fig. 1). PD simulations of a selected commercial 19Fr/23cm SLC are performed for multiple operating flow rate range data points.

Results: The PD-flow rate simulation data shows close agreement with the literature reference. The relative error of the pressure drop results is in the range of 3%, indicating the accuracy and regulatory utility of the SPH computations.

Discussion and Conclusions: We showed that the in-silico model (Fig. 3) provides accurate results to replace the physical bench test, significantly

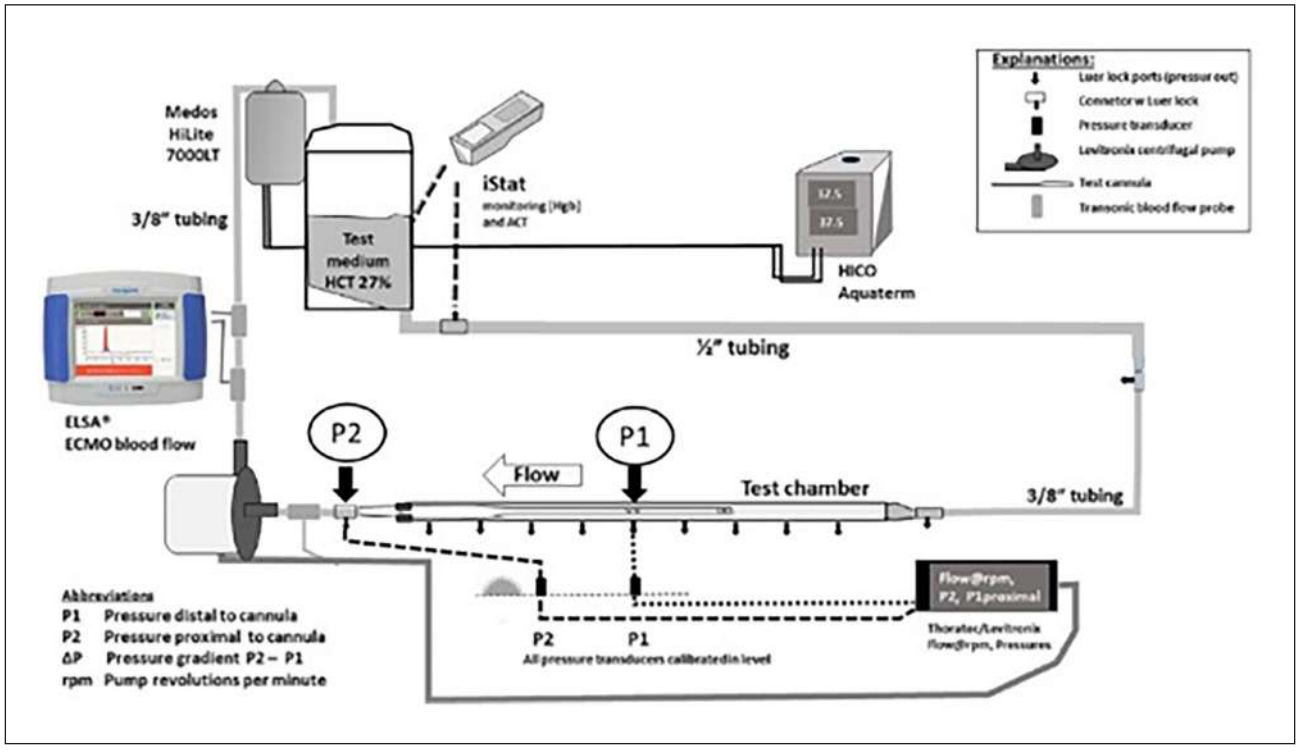

Figure 1. PD test setup [1].

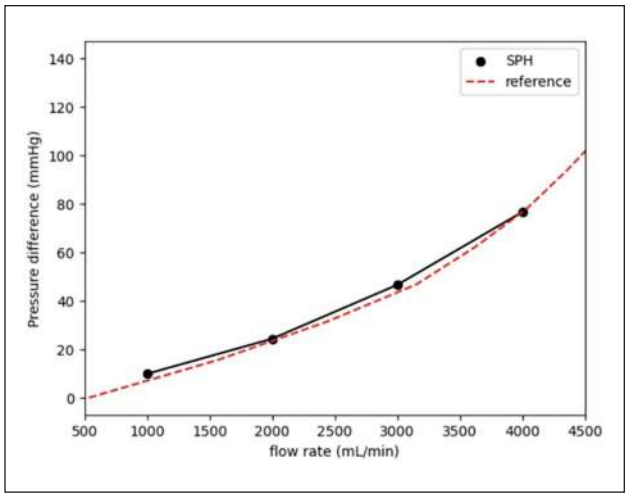

Figure 2. PD under different flow rates for the selected commercial SLC (19Fr/23cm). Red: bench test data from [1] and black: SPH simulation results.

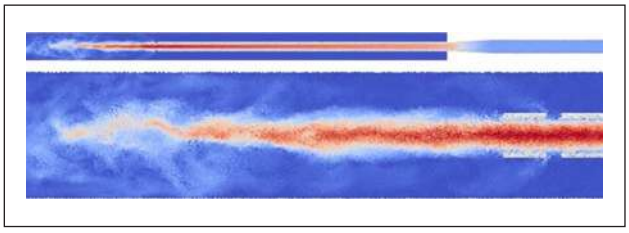

Figure 3. Velocity distribution in the developed arterial SLC flow field (flow rate: 1 L/min). Scale: 0-1.2 m/s from blue to red.

reducing time and cost. Therefore, it allows cannula manufacturers to replace in-vitro tests streamlining development and optimization times. Thanks to thorough validation, the model presents benefits for the regulatory approval process like indicating substantial equivalency to predicate devices.

Reference

1. Broman, L. M., et al. "Pressure and flow properties of cannulae for extracorporeal membrane oxygenation I: return (arterial) cannulae". Perfusion, 2019, Vol. 34(1S) 58–64. DOI: 10.1177/0267659119830521.

ANTICOAGULATION REGIMEN IN PATIENTS WITH IMPELLA SUPPORTED CARDIOGENIC SHOCK

Hiroaki Yamamoto(1), Hiroki Kono(1), Kaoru Matsuura(1), Michiko Watanabe(1), Tomohiko Inui(1), Hiroki Ikeuchi(1), Tomoyoshi Kanda(1), Togo Iwahana(2), Yoshio Kobayashi(2), Goro Matsumiya(1),

1. The department of cardiovascular surgery, Chiba university hospital, Chiba, Japan. 2. The department of cardiology, Chiba university hospital, Chiba, Japan

Background: Impella (Abiomed, USA) is a useful mechanical circulatory support system for the management of cardiogenic shock with a wide range of etiologies. On the other hand, anticoagulation management is often difficult, and fatal complications including thromboembolic and bleeding events are the major limitation of this therapy.

Objective: In this study, we aimed to explore the optimal anticoagulation regimen to prevent thromboembolic and bleeding complications during the Impella support.

Methods: A total of 71 patients, who received Impella 2.5 (n=9), CP (n=56), 5.0 (n=3), and 5.5 (n=3) between July 2018 and April 2024 were retrospectively analyzed. Patient group was divided into 2 groups depending on the time of device use and anticoagulation regimen; the early period (before August 2022, group E, n=47) and the late period (after September 2022, group L, n=24). Patients in group E were managed with unfractionated heparin aiming at higher therapeutic range (aPTT ratio 2.0-2.5) and those in group L were managed aiming at lower therapeutic level (an APTT ratio of 1.5-2.0 during Impella support. Results: Mean age (60.1 vs 57.7 years; p=0.5254), acute myocardial infarction (53.19%, 54.17%; p=0.9379), ECPELLA (78.72%, 79.19%; p=0.9654), and duration of Impella use (10.29, 17.33 days; p=0. 1191) did not differ significantly between the groups. There was no significant difference in bleeding requiring transfusion (51.06%, 45.83%; p=0.6765) or cerebral hemorrhage (17.02%, 12.50%; p=0.7390), but there was a trend toward fewer cases in the group L. Thromboembolic events occurred in 3 (group E) and 0 (group L) patients. No significant difference was found in in-hospital mortality (48.94%, 54.55%; p=0.6639). After matching, group E and group L have each 22 patients, and there are no statistically significant difference in bleeding(50%, 40.91%; p=0.7626), cerebral hemorrhage(22.73%, 13.64%; p=0.6981) and thromboembolic events(4.55%, 0%; p=1.000). These events tend to be lower in group L.

Conclusion: Lowering heparin dose aiming at the target APTT ratio to 1.5-2.0x tended to decrease bleeding complications without increasing thromboembolic events in Impella supported patients.

Table 1. Patients characteristics and events. No statiscally significant difference.

	Group E (n=47)	Group L (n=24)
Age(years)	60.19±2.22	57.75±3.11
Bleeding	24(51.06%)	11(45.83%)
Cerebral hemorrhage	8(17.02%)	3(12.50%)
Thromboem -bolic event	3(6.38%)	0(0%)

Table 2. After Propensity score matching, patients characteristics and events. No statiscally significant difference.

	Group E (n=22)	Group L (n=22)
Age(years)	58.59±3.12	58.81±3.12
Bleeding	11(50%)	9(40.91%)
Cerebral hemorrhage	5(22.73%)	3(13.64%)
Thromboem -bolic event	1(4.55%)	0(0%)

Acknowledgements

No Acknowlegments

DIGITAL LIGHT PROCESSING OF PHOTO-CROSSLINKABLE HYDROGELS TOWARDS AN EQUINE VASCULAR WALL MODEL

Ianina Pokholenko[1,2,3], Marguerite Meeremans[1,2], Nele Pien [1,2], Catharina De Schauwer[2], Sandra Van Vlierberghe[1]

[1] Polymer Chemistry & Biomaterials Group, Centre of Macromolecular Chemistry (CMaC), Department of Organic and Macromolecular Chemistry, Ghent University, Belgium, [2] Faculty of Veterinary Medicine, Department of Translational Physiology, Infectiology and Public Health, Ghent University, Belgium, [3] Institute of Molecular Biology and Genetics of NAS of Ukraine, Ukraine

Introduction: Type 2 diabetes, a metabolic disorder characterized by impaired insulin secretion and action, has currently reached the scale of a global pandemic. It remains one of the leading causes of blindness, end-stage renal disease, lower limb amputation, and cardiovascular disease [1]. Similar to diabetes in humans, horses can suffer from equine metabolic syndrome (EMS) [2], which is also associated with obesity, insulin dysregulation, and vascular wall changes. A suitable *in vitro* vascular wall model for drug screening is needed to improve the treatment of both equine and human patients. The ideal vascular tissue engineering structure must generally resemble all mechanical and biological properties similar to native vessels while being non-thrombogenic and non-immunogenic, making the choice of material crucial. Polymers made from acrylate-endcapped urethane-based polymer precursor (AUP) with a polyethylene glycol (PEG) backbone, called AUPPEGs, combine the characteristics of polyurethanes and PEG, and the polymer properties can be relatively easily tuned [3]. Therefore, the present study aimed to evaluate the effects of coating AUPPEG scaffolds manufactured via digital light processing (DLP) with collagen or gelatine derivatives on their cell-interactive properties towards equine adipose-derived mesenchymal stem cells (eqAT-MSCs) and endothelial cells (eqECs).

Methods: Diacrylate end-capped urethane-based PEG (AUP2PEG) was synthesized via a 2-step modification of PEG (2000 g mol^{-1}) as reported previously [3]. The 3D scaffolds were fabricated using DLP printing (resin solution: 30 wt% AUP2PEG, 10 mol% LiTPO-L, 1 mol% tartrazine, solvent: ultra-pure water; printing parameters: irradiation time 4 s; 23.72 mW/cm^2 light intensity). The surface of the scaffolds was coated with gelatin methacryloyl (GelMA) or bovine atelocollagen. The GelMA coating was applied exploiting a protocol described earlier [4]. The atelocollagen coating was applied by immersion of Argon plasma-activated scaffolds (0.5 min at pressure 0.8 mbar, and a power 100 W, after the plasma treatment, the scaffolds were exposed to the ambient atmosphere for 20 min) in a bovine atelocollagen type I solution (1 mg/mL in 0.01 M acetic acid, without subsequent chemical crosslinking). The eqAT-MSC and eqEC, isolated using enzymatic digestion techniques, were seeded onto the scaffolds at a density of 20,000 cells/ cm^2 or 10,000 cells/cm^2, respectively. A calcein-AM/PI staining was performed to evaluate the viability of the cells. The ability of the eqAD-MSC to differentiate adipogenically and osteogenically on the scaffolds was assessed as described earlier [5].

Results: Both GelMA and atelocollagen coatings improved the short-term (up to 7 days post-seeding) cytocompatibility of DLP-printed AUP2PEG-based scaffolds for eqECs and eqAD-MSCs compared to the uncoated scaffolds. However, during further cultivation (up to 21 days post-seeding), partially adherent spheroid-like aggregates of the eqECs and eqAD-MSCs were detected on the atelocollagen-coated scaffolds. Considering that the cells remained viable, the observed phenomena could be due to the detachment of the coating from the surface. Both GelMA and atelocollagen coating supported adipogenic and osteogenic differentiation of eqAD-MSCs. To mimic diabetic/EMS conditions, the GelMA-coated AUP2PEG scaffolds were incubated in a high glucose medium (35 mM glucose). Short-term cultivation (72 hours) of eqECs in a high glucose medium significantly reduced the number of viable cells attached to the surface compared to cultivation in a low glucose medium (5 mM glucose). In conclusion, our results indicate that GelMA-coated DLP-printed AUP2PEG scaffolds support eqEC and eqAD-MSC cultures.

References

1. Reed J, et al. Diabetes Metab Syndr Obes, 14: 3567–3602, 2021.
2. Morgan RA, et al. Veterinary Record, 177: 173-179, 2015.
3. Arslan A. et al. I WO2020094621A1, 2019.
4. De Jaerghere E., et al. Biomaterials, 158:95-105, 2018.
5. Heyman E, et al. Front. Vet. Sci. 9:98704, 2022

Acknowledgments

The authors would like to acknowledge the financial support from the Special Research Fund (BOF, Ghent University) and FEBS in the framework of Ukrainian Short-Term Fellowships.

VERIFICATION OF THE EFFECT OF PULSATILE FLOW FROM A BLOOD PUMP ON THROMBUS FORMATION IN A MEMBRANE OXYGENATOR

Tatsuki Fujiwara (1), Hironobu Sakurai (1), Wataru Hijikata (2), Daiki Toda (2), Hiro Kato (2), Katsuhiro Ohuchi (3), Orolzod Bumerdene (1), Tomoyuki Fujita (1)

1. Department of Cardiovascular Surgery, Tokyo Medical and Dental University (TMDU), Japan; 2. Department of Mechanical Engineering, Tokyo Institute of Technology, Japan; 3. Department of Clinical Engineering, Faculty of Medical Science, Juntendo University, Japan

Introduction: Thrombus formation in the ECMO circuit can cause embolism and impaired gas exchange in the oxygenator. Anticoagulant for the prevention of thrombus formation in the circuits carry the risk of bleeding complications. We have studied the effect of controlling the driving conditions of centrifugal blood pumps to inhibit thrombus formation in the circuit. In this study, we modified a commercially available centrifugal pump control device and verified the effect of the generated pulsatile flow on thrombus formation in the oxygenator in acute animal experiments.

Methods: Eight pigs were used in this study. One pig was fitted with two venous–arterial ECMO circuits (one by jugular vein and carotid artery, one by femoral vein and artery) under general anesthesia, and the thrombi formed in each oxygenator were compared [1]. The MERA HCF-MP23H was used as the centrifugal pump and the MERA NHP Excelung NSH-R as the oxygenator (SENKO Medical Instrument Mfg. Co., Ltd., Tokyo, Japan). To create a pulsatile flow, a motor speed control system was installed in the driver of the centrifugal pump. The driving conditions for each circuit were set to steady and pulsatile flow, and the average flow rate was matched at 2 L / min. Under the pulsating flow conditions, the pump speed was controlled so that the pattern was a steady flow plus a half-wave rectified waveform (sinusoidal waveform with the negative portion set to zero). Heparin was administered only during cannulation, and protamine was administered when the circulation stabilized, and no anticoagulants were used during extracorporeal circulation. Thrombus formation in the oxygenator was assessed using indocyanine green (ICG) fluorescence imaging every hour, with constant observation by the naked eye during circulation [2]. After the

circulation was stopped, the blood was replaced with saline solution for observation, and the oxygenator was cut to observe internal thrombus formation.

Results: Intraoperative sacking occurred in two of the eight cases, so the final evaluation could not be performed in these cases. In 6 cases, pulsatile flow could be created by controlling the centrifugal pump speed in a stable manner. In the thrombus evaluation after cessation of circulation, there was a tendency for less thrombus formation in the pulsatile flow circuit than in the steady flow circuit in all six pigs.

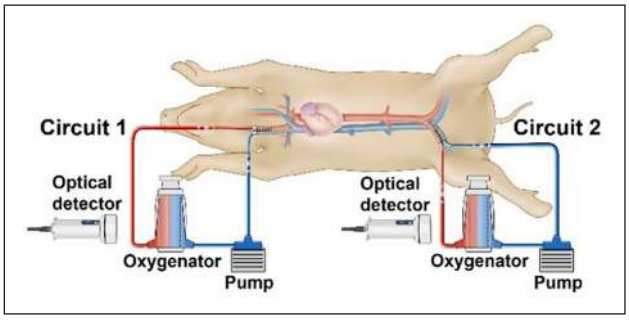

Figure 1. Two venous–arterial ECMO circuits were installed in the cervical and femoral regions of the same animal. The oxygenators are observed with both the naked eye and Indocyanine green (ICG) fluorescence imaging during circulation.

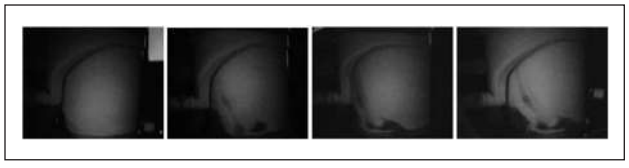

Figure 2. ICG fluorescence imaging shows changes in thrombi formation within the oxygenators

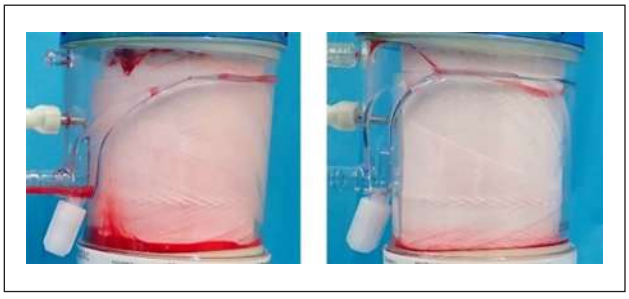

Figure 3. Left photo is the oxygenator used in the steady flow conditions. Right photo is the oxygenator used in the pulsatile flow conditions.

Discussion: This technology improves the anti-thrombogenicity of ECMO circuits by controlling pump speed and creating pulsatile flow. We believe that the originality of this technology is that it can be introduced into existing commercially available ECMO devices without new product development.

References

1. Sakurai H et al, Artif Organs, 47:77-87, 2023
2. Sakurai H et al, Artif Organs, 45:1173-1182, 2021

AN EYE ON USABILITY: SIMULATION BASED HUMAN FACTORS EVALUATION OF LEFT VENTRICULAR ASSIST DEVICE PERIPHERALS

Gregor Widhalm (1), Theodor Abart (1), Katharina Ebenberger (1), Angelika Berger (2), Julia Riebandt (1), Dominik Wiedemann (1), Daniel Zimpfer (1), Michael Wagner (2), Thomas Schlöglhofer (1,3,4)

1. Department of Cardiac Surgery, Medical University of Vienna, Vienna, Austria; 2. Division of Neonatology, Pediatric Intensive Care and Neuropediatrics, Department of Pediatrics, Comprehensive Center for Pediatrics, Medical University of Vienna, Vienna, Austria; 3. Center for Medical Physics and Biomedical Engineering, Medical University of Vienna, Vienna, Austria; 4. Ludwig Boltzmann Institute for Cardiovascular Research, Vienna, Austria

Introduction: Thanks to advancements in left ventricular assist device (LVAD) technology and management over the last decades, the currently available HeartMate 3 LVAD (HM3) shows excellent clinical outcomes with a 1-year survival of 85.9% [1]. However, constrained usability of wearables remains as a challenge in LVAD therapy [2, 3]. The aim of this study was to comparatively assess the usability of CorWave (CW) peripheral prototypes and HM3 wearables in simulated scenarios.

Methods: This cross-sectional single center cohort simulation study involved former LVAD patients post heart transplantation (HTX) and laypeople without LVAD handling experience. Subjects were provided with either HM3 or CW peripherals and instructed to complete six predefined scenarios. The simulation setting included a 4-perspective room video and first-person eye tracking recordings (see Figure 1). Outcome measures were defined as initial success rates, time to success during two attempts, pump-off duration and an 18-item post scenario survey.

Results: Forty-six untrained subjects (30 HM3 vs. 16 CW, median age 63.5 (IQR = 10.0) vs. 60.0 (16.0) years, $p = 0.41$; 53% former LVAD patients, $p = 0.76$) were enrolled and completed 276 scenarios, revealing higher initial success rates for the CW group (92.7% vs. HM3 80.6%, $p = 0.008$).

The change of power supply revealed highest complexity for the HM3 cohort, resulting in ten unintended driveline disconnections, five times higher time to success ($p < 0.001$) and three times lower initial success rates when compared to the CW cohort. Controller exchange success rates were comparable, however both time to success and pump-off durations were twice as long for the HM3 ($p \leq 0.005$, see Table 1). While more CW subjects perceived the cable lengths as appropriate (81% vs. HM3 67%, $p = 0.001$), 41% of the participants agreed on too heavy peripherals ($p = 0.85$).

Discussion: This study emphasizes the user centered design benefits of the novel CW concept compared to HM3 peripherals, promising to enhance both quality of life and safety of future LVAD patients.

Figure 1. Exemplary four-perspective room recording combined with eye tracking perspective.

Table 1. Initial success rates and time to success within two attempts per simulated scenario, stratified by cohorts. HM3: HeartMate 3; CW: CorWave.

Simulated scenario	Initial success rate n (%)			Time to success (two attempts) Median (IQR), seconds		
	CW	HM3	p-value	CW	HM3	p-value
Battery exchange in normal light	16 (100%)	27 (90.0%)	0.54	16.5 (8.5)	32.5 (18.8)	**<0.001**
Power supply change to AC power	15 (93.8%)	8 (26.7%)	**<0.001**	48.0 (30.3)	260.0 (158.0)	**<0.001**
Driveline dis-and reconnection	11 (68.8%)	23 (76.7%)	0.73	41.5 (49.3)	41.5 (44.0)	0.29
Controller exchange	15 (93.8%)	27 (90.0%)	0.79	31.0 (32.0)	83.0 (63.5)	**<0.001**
Battery exchange in dim light	16 (100%)	30 (100%)	-	12.0 (7.3)	21.0 (19.0)	**0.001**
Battery exchange within carry bag	15 (93.8%)	30 (100%)	0.35	40.5 (24.8)	75.0 (45.0)	**<0.001**

References

1. Jorde et al., Ann Thorac Surg, 117(1):33-44, 2024.
2. Schlöglhofer et al., J Heart Lung Transplant, 42(4):466-477, 2023.
3. Dunn et al., Ann Biomed Eng, 47(12):2431-2488, 2019

CORRELATION ANALYSIS OF GLOMERULAR FILTRATION RATE VALUES OBTAINED BY NUCLEAR MEDICINE METHOD VERSUS ESTIMATED MATHEMATICAL EQUATIONS IN KIDNEY RECIPIENTS FROM LIVING AND DECEASED DONORS

Zhaklina Sterjova-Markovska[1], Irena Rambabova Bushljetikj[1], Lada Trajceska[1], Galina Severova[1], Julijana Usprcov[1], Aleksandra Canevska[1], Tanja Makazlieva[2], Aleksandra Peshevska[2], Emilija Rambabova[3], Goce Spasovski[1]

[1]University clinic for nephrology, Faculty of Medicine, University Ss. Cyril and Methodius, Skopje, R.of North Macedonia, [2]Institute of Pathophysiology and Nuclear Medicine, Faculty of Medicine, University Ss. Cyril and Methodius, Skopje, R. of North Macedonia, [3]University Goce Delcev, Shtip, R.of N. Macedonia

Introduction: Glomerular filtration rate (GFR) is a crucial indicator of kidney function and is essential for the diagnosis, monitoring, and management of various renal conditions. Nuclear medicine methods play an important role in accurate assessment of GFR. [1,2] The aim of this study was to make a correlation analysis of measured (mGFR) in kidney recipients from living and deceased donors obtained by three plasma sample method (TPSM) after i.v. application of [99mTc]Tc-DTPA.as a reference method vs. estimated (eGFR) by using the mathematical equations: Chronic Kidney Disease Epidemiology Collaboration (CKD EPI) 2021 and Modification of Diet in Renal Disease (MDRD).

Material and methods: 49 kidney recipients from living and deceased donors, from the first to the third year after kidney transplantation, 35 (71.43%) men and 14 (28.57%) women, participated in the study. A correlation analysis were made between the values of mGFR obtained by using the nuclear medicine method with TPSM [3] and eGFR obtained by mathematical equations: CKD epi 2021 and MDRD.

Results: Patients age ranged from 18 to 66 years, their mean age was 42.6±10.6 years. The highest values for GFR were obtained with the GFR method according to CKDepi 2021 (54.57±17.2 ml/min/1.73m2), followed by the GFR method according to MDRD (47.17±16.7 ml/min/1,73m2), and TPSM (46.8±23.0 ml/min/1.73m2), respectivly. (Table 1) The results of the Repeated Measures ANOVA analysis showed that the mean value of GFR was statistically significantly different between at least two of the analyzed methods [(F(dftime 2, dfError (time)96)=27.81 p<0.0001). Post-hoc analysis with Bonferoni correction showed significantly higher GFR values obtained by CKD epi 2021 method in corelation to the TPSM values and values obtained by MDRD method (p<0.0001), while the difference between the GFR values obtained by TPSM and

MDRD was statistically insignificant (p=1.0). (table 2) Overall between the reference method according to TPSM and GFR according to CKDepi 2021 and MDRD, a statistically significant positive linear correlation and connection was noticed,(r=0.84854 and r=0.85613, p<0.0001, respectively).(Fig.1, 2)

Conclusion: GFR determined by slope-intercept method according to TPSM correlates strongly with

GFR values obtained by mathematical equations (CKD epi 2021 and MDRD) and can be routinely used to for precise GFR values in clinical practice. In the absence of a larger series of subjects, the challenge to accurately calculate GFR without a gold standard remains and no single method can be taken as a valid one to assess GFR.

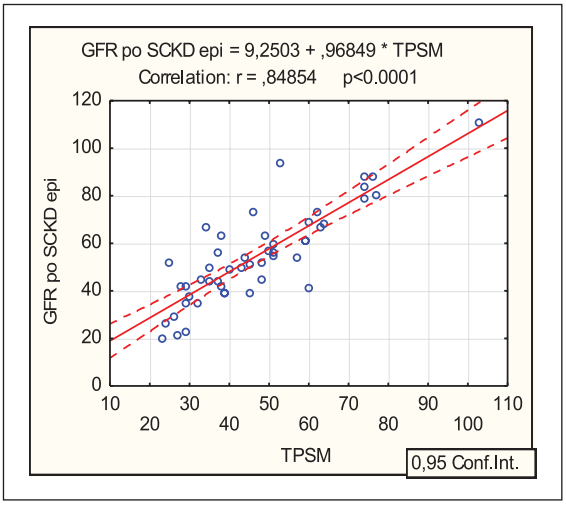

Figure 1. Correlation between GFR values obtained by TPSM and CKD epi 2021

TPSM-Triple plasma sample nuclear method for obtaining mGFR; CKD epi 2021-Chronic kidney disease epidemiology collaboration equation for obtaining eGFR

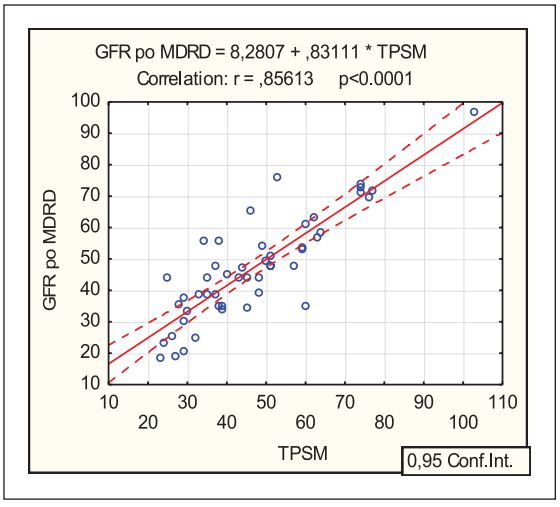

Figure 2. Correlation between GFR values obtained by TPSM and MDRD

TPSM-Triple plasma sample nuclear method for obtaining mGFR; MDRD-Modification of Diet in Renal Disease for obtaining eGFR.

Table 1. Statistical parametars for GFR.

Statistical parametars for GFR					
	mean ± SD	min- max	Std. Error	95% Confidence Interval	
				Lower Bound	Upper Bound
TPSM	46,79 ± 17,2	23 – 103	2,454	41,863	51,729
CKDepi 2021	54,57 ± 19,6	20 – 111	2,800	48,941	60,202
MDRD	47,17 ± 16,7	18,3 – 96,6	2,382	42,384	51,963

TPSM-Triple plasma sample nuclear method for obtaining mGFR; CKD epi 2021-Chronic kidney disease epidemiology collaboration equation for obtaining eGFR; ; MDRD-Modification of Diet in Renal Disease for obtaining eGFR.

Table 2. Repeated Measures ANOVA, Adjustment for multiple comparisons: Bonferroni.

Pairwise Comparisons						
method		Mean Difference	Standard Error	Sig.[b]	95% Confidence Interval for Difference	
					Lower Bound	Upper Bound
TPSM	CKD epi 2021	-7,776	1,484	0,000	-11,457)	-4,094
	MDRD	-0,378	1,299	1,000	-3,600)	2,844
CKDepi 2021	MDRD	7,398	,508	0,000	6,137	8,659

TPSM-Triple plasma sample nuclear method for obtaining mGFR; CKD epi 2021-Chronic kidney disease epidemiology collaboration equation for obtaining eGFR; ; MDRD-Modification of Diet in Renal Disease for obtaining eGFR.

References

1. Summary of Recommendation Statements. Kidney Int Suppl (2011). 2013 Jan;3(1):5-14. doi: 10.1038/kisup.2012.77. PMID: 25598998; PMCID: PMC4284512.
2. Vidal-Petiot E et al, Comparison of 51Cr-EDTA and 99mTc-DTPA for glomerular filtration rate measurement. J Nephrol. 2021 Jun;34(3): 729-737. doi: 10.1007/s40620-020-00932-9. Epub 2021 Mar 4. PMID: 33661505.
3. Fleming JS et al, British Nuclear Medicine Society. Guidelines for the measurement of glomerular filtration rate using plasma sampling. Nucl Med Commun. 2004 Aug;25(8):759-69. doi: 10.1097/01.mnm.0000136715.71820.4a. PMID: 15266169.

ECMO PAL V-V: DEEP NEURAL NETWORK FOR VENOVENOUS ECMO PROGNOSTICATION

Andrew Stephens (1,2), Michael Šeman (1), Arne Diehl (3), David Pilcher (3), Vincent Pellegrino (3), Ryan Barbaro (4), Daniel Brodie (5), Shaun Gregory (1,2), Carol Hodgson (3,6)

1. Advanced Cardiorespiratory Engineering Laboratory, Australia; 2. Queensland University of Technology, Australia; 3. Alfred Hospital, Australia; 4. University of Michigan, USA; 5. Johns Hopkins University, USA; 6. Monash University, Australia

Background: Venovenous extracorporeal membrane oxygenation (V-V ECMO) is a lifesaving therapy for critical lung failure. ECMO is a highly complex and expensive procedure and is fraught with complications and potential adverse events. Patient selection and prognostication is essential to ensure good treatment outcomes and effective allocation of hospital resources. Previously, V-V ECMO prognostication scores have been developed, including RESP, PRESERVE, and PREDICT-VV [1]–[3].

Previously published scores have been based on traditional statistical methods, which may not accurately model the complex variable interactions present during ECMO therapy [4]. Artificial intelligence (AI) can model complex non-linear interactions between multiple patient variables and has been used successfully over a range of

Table 1. Top predictive variables for V-V ECMO survival outcome. The influence on survival to hospital discharge with variable increases is either positive (improves survival) or negative (reduces survival).

Variable Name	Predictive Power	Survival Influence
Age	0.05	Negative
COVID	0.04	Negative
Lactate	0.02	Negative
Time Intubate	0.02	Negative
pH	0.02	Positive

medical prognostication applications. The aim of this research was to investigate an AI model for V-V ECMO outcomes prediction based on a large international dataset.

Methods: The Extracorporeal Life Support Organization (ELSO) registry was used for training and initial validation of the model. 15,602 adult V-V ECMO patients from 590 ECMO centres were used for model training and testing. Initially, 116 pre-ECMO variables were analyzed. *Random Forest permutation importance* was used to identify variables with modest prognostic power (> 0.001). Deep neural networks were explored using hyperparameter optimization via *Tree-Structured Parzen estimation*. Initial internal validation was performed using five-fold cross-validation. Metrics of interest were sensitivity, positive predictive power (precision), and area under the receiver operating characteristic (AUC). The variable of interest was survival to hospital discharge.

Results: A deep neural network (ECMO Predictive Algorithm -ECMO PAL V-V) was developed. Five-fold validation demonstrated a sensitivity and precision to hospital survival of 80 ± 1 % and 70 ± 1%, respectively. AUC was found to be 0.73 ± 0.01. The five most predictive variables were age, COVID status, lactate, how long the patient was intubated prior to ECMO, and pH (Table 1).

Conclusion: This research aimed to investigate an AI tool for VV-ECMO outcomes prediction. Our tool (ECMO PAL) demonstrated good sensitivity and precision in predicting hospital survival over internal five-fold validation. Interestingly, the model reliably predicted ECMO survival but had more difficulty predicting mortality. This finding contrasts our previously developed AI venoarterial ECMO prediction model [4]. ECMO PAL development is ongoing, with further optimizations and external validation underway. ECMO PAL V-V will eventually be incorporated into our existing ECMO PAL framework and hosted as a free online web app (ecmo-pal.icu).

References

[1] M. Schmidt *et al.*, "Predicting survival after extracorporeal membrane oxygenation for severe acute respiratory failure: The Respiratory Extracorporeal Membrane Oxygenation Survival Prediction (RESP) score," *Am. J. Respir. Crit. Care Med.*, vol. 189, no. 11, pp. 1374–1382, 2014, doi: 10.1164/rccm.201311-2023OC.

[2] M. Schmidt *et al.*, "The PRESERVE mortality risk score and analysis of long-term outcomes after extracorporeal membrane oxygenation for severe acute respiratory distress syndrome," *Intensive Care Med.*, vol. 39, no. 10, pp. 1704–1713, 2013, doi: 10.1007/s00134-013-3037-2.

[3] J. Rilinger *et al.*, "A Mortality Prediction Score for Patients With Veno-Venous Extracorporeal Membrane Oxygenation (VV-ECMO): The PREDICT VV-ECMO Score," *ASAIO J.*, pp. 293– 298, 2023, doi: 10.1097/mat.0000000000002088.

[4] A. F. Stephens *et al.*, "ECMO PAL: using deep neural networks for survival prediction in venoarterial extracorporeal membrane oxygenation," *Intensive Care Med.*, vol. 49, no. 9, pp. 1090–1099, Sep. 2023, doi: 10.1007/s00134-023-07157-x.

HEMODYNAMIC PERFORMANCE OF VENO-PULMONARY ECMO IN A MOCK CIRCULATORY LOOP.

Prashant Chand (1), Avishka Wickramarachchi (1) Andrew Stephens (1), Hakeem Yusuff (2,3), Vasileios Zochios (4,5), Chris Joyce (6), Kiran Shekar (7), Shaun Gregory (1,8)

1. Cardio-Respiratory Engineering and Technology Laboratory, Department of Mechanical and Aerospace Engineering, Monash University, Australia; 2. Department of Respiratory Sciences, University of Leicester, UK; 3. NIHR Leicester Biomedical Research Centre, Glenfield Hospital, Leicester, UK; 4. Department of Cardiovascular Sciences, University of Leicester, Leicester, UK; 5. University hospitals of Leicester NHS Trust, Glenfield Hospital ECMO Unit, Leicester, UK; 6. Princess Alexandra Hospital, Australia; 7. Prince Charles Hospital, Australia; 8. Centre for Biomedical Technologies and School of Mechanical, Medical, and Process Engineering, Queensland University of Technology, Australia

Introduction: Veno-Pulmonary extracorporeal membrane oxygenation (VP ECMO) is a treatment strategy that provides right ventricular (RV) and respiratory support to patients. VP ECMO provides pulmonary circulation support by directing flow into the pulmonary artery (PA) with negligible recirculation [1]. The hemodynamic impact of direct non-pulsatile flow in the pulmonary vasculature of an acute respiratory distress syndrome patient with RV failure is not well represented in the current literature. The aim of this in-vitro study is to explore the hemodynamic effects of different flow rates in a mock circulatory loop (MCL). This MCL simulates patients with varying levels of abnormal RV function at different pulmonary hypertension (PH) states.

Methods: A VP ECMO circuit was connected to a MCL via the right atrial (RA) and pulmonary artery (PA) chambers using a 23 Fr drainage and 17 Fr pulmonary arterial cannula, respectively. The MCL was used to simulate patients with various levels of RV function (normal to severe dysfunction) and pulmonary hypertension by adjusting the pulmonary vascular resistance (PVR) from 100-600 dynes/sec/cm^{-5}. The hemodynamic response in each of these clinical scenarios at different levels of ECMO flow rates was recorded (1-5 L/min).

Results: VP ECMO was able to successfully perfuse the pulmonary circulation and maintain adequate cardiac output. Mean pulmonary artery pressures (mPAP) were observed to increase -with a steeper gradient in patients with higher PVR. At flow rates of 3-4 L/min, mPAP values increased beyond 35 mmHg in the simulated patient with mild RV injury and high PVR (> 300).

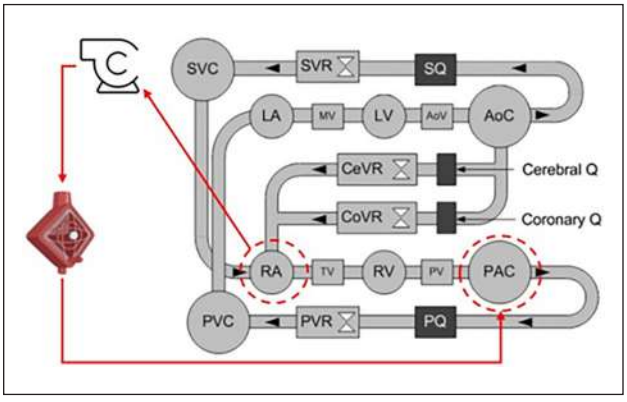

Figure 1. VP ECMO and the MCL experimental setup.

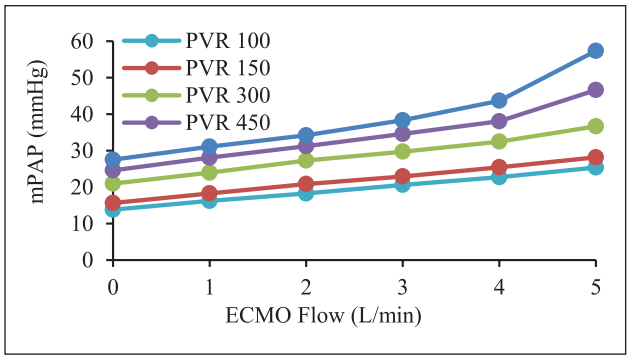

Figure 2. Graph of mean pulmonary artery pressures against ECMO flow rate for a patient with abnormal RV function and various degree of pulmonary hypertension.

Left atrial pressures also increased with increasing ECMO flowrates. However, the RA pressures decreased. Additionally, the pulmonary arterial pulsatility index (PAPi) decreased with increasing ECMO flow rates. There was complete loss of pulsatility at lower flow rates for patients with high PVR, suggesting a correlation with PH. The prolonged loss of PAPi in certain groups of patients has been shown to have a negative impact on ECMO weaning outcomes [2].

Discussion: Although VP ECMO potentially offers significant cardiac and respiratory support to patients without recirculation challenges, careful consideration is required when selecting patients for this treatment modality. At high ECMO flows, mPAP values increase significantly, and this could potentially result in irreversible damage to the pulmonary vasculature, causing pulmonary hemorrhage. Unlike veno-venous ECMO, VP support cannot be run at very high flows (> 4 L/min), and this may affect its ability to maintain blood gas exchange. Therefore, this study shows that PVR as well as RV function, in addition to respiratory support, need to be considered when selecting VP flow rates to prevent damage to the pulmonary vascular bed and ensure successful liberation from ECMO.

References

1. Zochios. V et al, Asaio, 69:511-518, 2023.
2. Martin-Suarez. S et al, J Clinical Medicine, 11:4353, 2022.

DEVELOPMENT OF NON-INVASIVE CIRCUIT PRESSURE ESTIMATION METHOD FOR EXTRACORPOREAL CIRCULATION CIRCUIT

Hirohito Sumikura (1), Yuto Tamura (1), Kei Ota (2), (3), Akihiko Homma (1)

1. Graduate school of Science and Engineering, Graduate School of Tokyo Denki University, Japan; 2. School of Medicine, St. Marianna University, Japan; 3. Tokyo D Tower Hospital, Japan

Introduction: In the extracorporeal circulation circuit, measurement of circuit pressure is important to detect abnormalities in the circuit such as a venous drainage failure or thrombus formation in an oxygenator. Generally, the circuit pressure is measured using a branch such as a connector. However, there is a risk of thrombus formation at the tubing-connector junctions [1]. The polyvinyl chloride (PVC) tubing which is used in the circuit is slightly deformed by the circuit pressure. Therefore, we are developing the circuit pressure estimation method from the tubing displacement. The PVC tubing is viscoelastic body and tubing displacement was gradually changed over time due to creep. The purpose of this study is to estimate the circuit pressure from the tubing displacement by considering the creep.

Methods: A measurement equipment consisted of a displacement sensor (Z4D-F04A, Omron) and a fixing jig (Fig. 1). The experimental circuit composed of the measurement equipment, two kinds of 3/8 inch PVC tubing (Tube A: Mera Exceline S, Senko Medical Instrument Mfg. Co./ Tube B: LH tube, JMS Co.), a centrifugal pump, a pressure sensor, a pinch cock, and a thermostatic bath. The working fluid is tap water. The tubing displacement was measured for 4 hours with the circuit pressure kept constant at -100 mmHg. The same experiment was conducted by changing the tube. A viscoelastic body can be modeled using a spring as an elastic element and a dashpot as a viscous element. Therefore, a three-element model which consists of a single spring and a Voigt element was created and derived following formula.

$$P = \frac{D}{\frac{1}{E_0} + \frac{1}{E_1}\left(1 - e^{-\frac{E_1}{\eta}t}\right)} \quad (1)$$

where P is the Estimated circuit pressure, D is the Tube displacement, E_0 and E_1 are the Viscosity coefficient, η is the Elastic coefficient. The above parameters were calculated from each experimental data.

Results: Figure 2 shows the results of tubing displacement for 4 hours experiments. Each tubing displacement was gradually increased over time due to creep. The amount of displacement at Tube A was large compared to that at Tube B. Figure 3 shows the estimated circuit

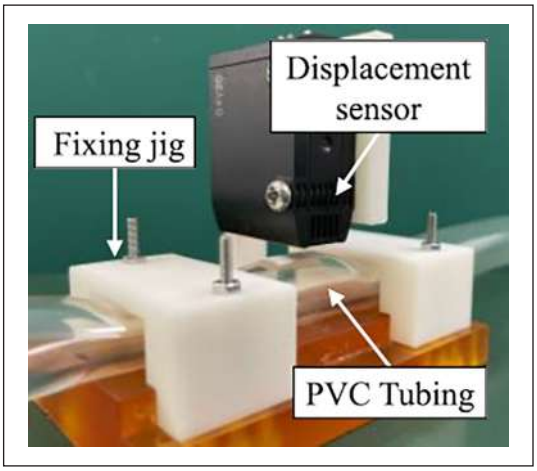

Figure 1. Photograph of measurement equipment.

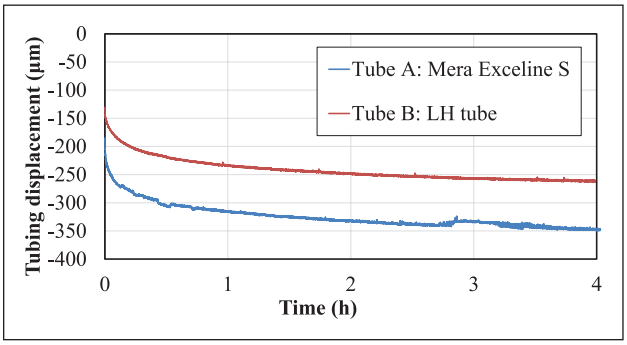

Figure 2. Results of each tubing displacement.

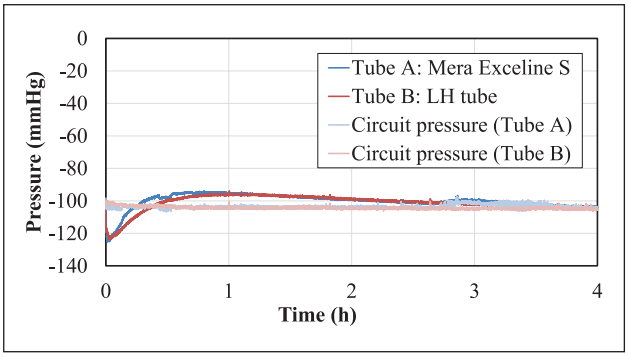

Figure 3. Results of each estimated circuit pressure.

pressure using estimated formula (1). The maximum error rates for Tube A and B were 20.98 and 22.05 %, and the error rates at 4 hours were 0.47 and 0.67 %, respectively.

Discussion and Conclusion: Although the amount of tubing displacement in Tube A and B was different, the estimated circuit pressures showed similar trends. The error rates were large immediately after the start of the measurement and gradually decreased over time. It was suggested that it is possible to non-invasively estimate circuit pressure from the tubing displacement. We consider that this method is useful for improving safety of the extracorporeal circulation circuit.

Reference

1. Susan M Hastings et al, ASAIO J, 63:86-92, 2017

Acknowledgements

This work was supported by MEXT KAKENHI Grant Number JP21K08873.

FUNCTIONAL EVALUATION OF STRUCTURAL CHARACTERISTICS OF A PEDIATRIC PULMONARY VALVED CONDUIT

Kenji Suzuki (1), Hirohito Sumikura (2), Yuki Oikawa (2), Shun-ichiro Sakamoto (1)

1. Department of Cardiovascular Surgery, Nippon Medical School Musashikosugi Hospital, Japan; 2. Graduate school of Science and Engineering, Graduate School of Tokyo Denki University, Japan

Background: Pulmonary valved conduits are used for reconstructing the right ventricular outflow tract in infancy. However, valve dysfunction often arises from stenosis and regurgitation caused by thrombus formation around the valve and decreased mobility of the valve leaflet. To address this, we developed a valved conduit based on the ePTFE bicuspid valve [1], which has a hinge in the center of the posterior wall of the right ventricular outflow tract and opens when the valve leaflet folds into the center and closes when the valve leaflet widens and adheres to the conduit wall; the following two structures were added: 1) A bulging sinus was formed in the anterior portion of the conduit to capture diastolic blood flow and promote adequate closure of the valve leaflet.

2) A fenestration at the right ventricular end of the valve leaflet was added to relieve blood stasis and prevent thrombus formation.

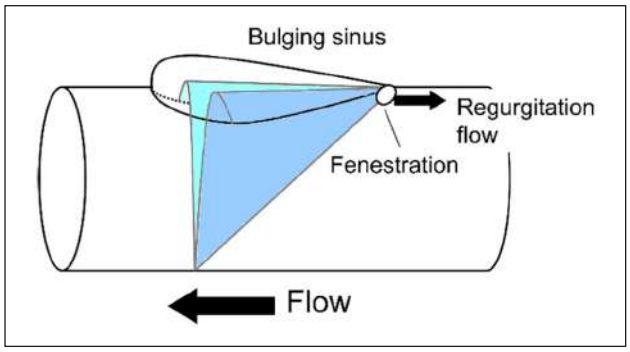

Figure 1. Schema of the proposed conduit.

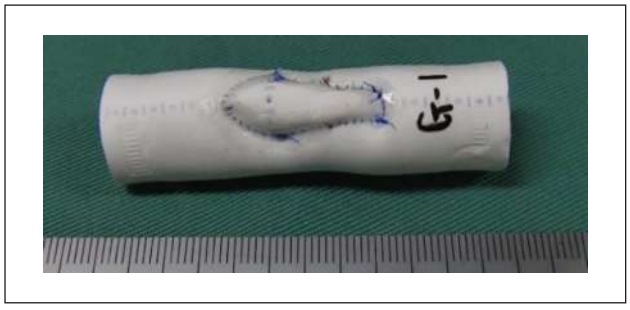

Figure 2. Appearance of the proposed conduit.

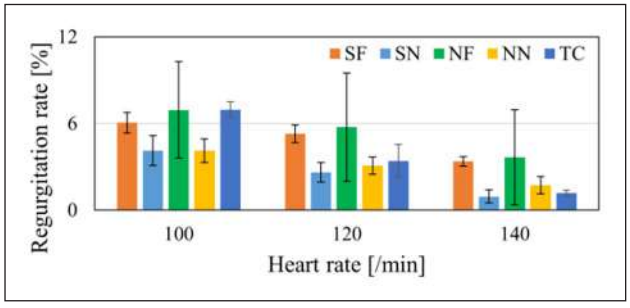

Figure 3. Regurgitation rate.

Objective: To evaluate the function of the bulging sinus and fenestration in the conduit using the developed pulmonary valve.

Methods: The developed conduits (14-mm-diameter ePTFE conduit with a 0.1-mm ePTFE seat valve leaflet sewn on; with bulging sinus and fenestration: SF valve, with bulging sinus and without fenestration; SN valve, without bulging sinus and with fenestration; NF valve, without bulging sinus and fenestration; NN valve, all n = 3) and the ePTFE tricuspid-valved conduit used at our institute (TC valve, n=3) were observed. Each conduit was incorporated into a right heart simulated mock circulation (flow rate, 700 mL/min; pulmonary artery pressure, 20–30/7–8 mmHg) to simulate hemodynamics in infancy, and the regurgitation rate (leakage volume/progressive flow) and pressure gradients before and after the valve were evaluated.

Results: At heart rates of 100/min, 120/min, and 140/min, the regurgitation rates (%) were 6.1, 5.3, and 3.4 for SF valve; 4.1, 2.6, and 0.9 for SN valve; 6.9, 5.7, and 3.7

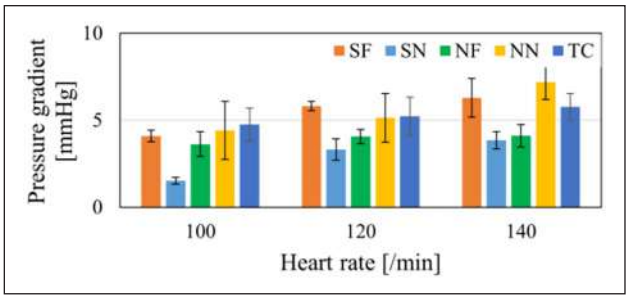

Figure 4. Pressure gradient.

for NF valve; 4.1, 3.1, and 1.7 for NN valve; and 7.0, 3.4, and 1.2 for TC valve, respectively.

Pressure gradients (mmHg) were 4.1, 5.8, and 6.3 for SF valve; 1.5, 3.3, and 3.9 for SN valve; 3.6, 4.1, and 4.1 for NF valve; 4.4, 5.1, and 7.2 for NN valve; and 4.7, 5.2, and 5.8 for TC valve, respectively.

Conclusion: The presence of fenestration was correlated with a relatively high regurgitation rate, while a bulging sinus tended to lower the regurgitation rate. Pressure ranges remained low and acceptable for clinical use, although the trend was not constant. The valve leaflets and conduit geometry can improve valve function.

Reference

1. Nunn GR et al, J Thorac Cardiovasc Surg, 136:290-296, 2008.

IN VIVO TISSUE-ENGINEERED ALLOGENEIC CONNECTIVE TISSUE MEMBRANES AS VASCULAR GRAFTS: OPTIMIZATION OF DECELLULARIZATION AND ANIMAL TRANSPLANTATION EXPERIMENTS.

Tasturo Gondai (1), Masashi Yamanami (1), Hidetake Kawajiri (1), Tomoya Inoue (1), Keiichi Kanda (1), Satoshi Gojo (2), Shinichiro Oda (1).

1. Department of Cardiovascular Surgery, Kyoto Prefectural University of Medicine, Japan; 2. Department of Regenerative Medicine, Kyoto Prefectural University of Medicine, Japan

Introduction: Aiming for ideal vascular grafts, we have developed the autologous connective tissue grafts constructed in subcutaneous spaces of patients. In 2014, we clinically applied this technology in pediatric pulmonary artery patch augmentation, reporting favorable outcomes. [1] However, the formation of reliable connective tissue membranes may be challenging in high-risk pediatric patients due to limited subcutaneous areas and insufficient regeneration activities. Therefore, we began exploring the option of graft creation in healthy parents for allogeneic transplantation to their children. Furthermore, simplification and shortening of the decellularization process are indispensable to achieve same-day transplantation in the operating room. This study focuses on optimizing decellularization process and conducting preliminary animal transplantation experiments.

Methods: Silicone rod molds were implanted subcutaneously in beagle dogs for four weeks, after which the formed connective tissue tubes were excised. These tissue tubes were decellularized using a 1% sodium lauryl ether sulfate (SLES) solution with horizontal shaking (2h/1h/30min). Following decellularization, DNA quantification and tensile strength measurements in the short-axis direction were performed. The tissues were then trimmed into sheets and transplanted as allogeneic patches into another beagle dog's carotid artery. Post-transplantation assessments were conducted using ultrasound, and the grafts were excised after three months.

Results: Decellularization for more than one hour was required to ensure the complete removal of cellular components from the connective tissue membranes. Tensile strength measurements indicated no significant differences before and after decellularization. During three month-implantation, the grafts did not develop aneurysmal dilation. After extraction, Morphological examination exhibited no thrombus formation of the luminal surface, which was covered with smooth neointima.

Discussion: We successfully simplified and shortened the decellularization process using shaking methods compared to previous perfusion methods.[2] The decellularized connective tissue membranes maintained mechanical properties and excellent regenerative performance comparable to previous autografts, which suggests their potential as substitutes for allogeneic vascular grafts.

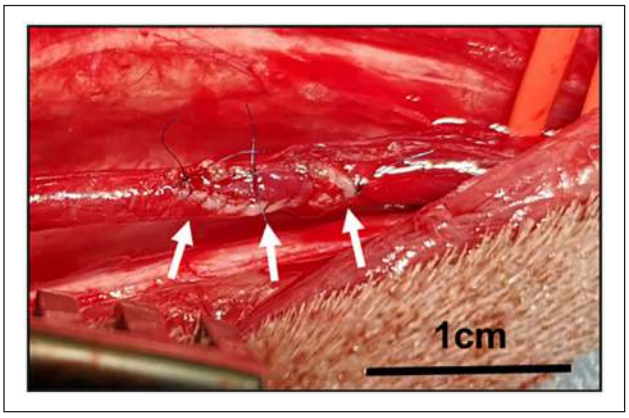

Figure 1. Implantation of patch grafts. Decellularized connective tissues were trimmed to an elliptical sheets of 10 × 8 mm. The resulting sheets were allo-transplanted as vascular patches.

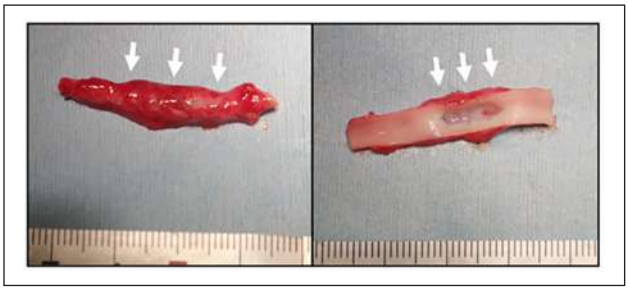

Figure 2. Macroscopic observation of harvested grafts at 3 months after implantation. The inner surfaces of the grafts were almost completely covered with neointima (right).

References

1. Kato N et al, Ann Thorac Surg, 102(4):1387-1390, 2016.
2. Yamanami M et al, Artif Organs, 46(4):633-642, 2022.

Acknowledgements

This study was supported by the Japan Society for the Promotion of Science (JSPS) KAKENHI grants JP19H03742, JP20H03767, and 20K09151 from the Ministry of Education, Culture, Sports, Science and Technology (MEXT) of Japan.

DEVELOPMENT OF EXTRALUMINAL FLOW OXYGENATOR FOR A RAT CPB MODEL

Shunsuke Uchiyama (1) , Hirohito Sumikura (1) , Yutaka Fuji (2) , Akihiko Homma (1)

1. Graduate school of Science and Engineering, Graduate School of Tokyo Denki University, Japan; 2. Department of Clinical Engineering and Medical Technology, Niigata University of Health and Welfare, Japan.

Introduction: Currently, a rat cardiopulmonary bypass (CPB) model is used to study the mechanism of biological reaction during CPB [1]. This study was used the intraluminal flow oxygenator in view of the blood volume of the rats. However, the extraluminal flow oxygenator are used in actual clinical practice. Therefore, the application of the extraluminal flow oxygenator to the rat CPB model would be possible to simulate the CPB close to the clinical conditions.

The purpose of this study is to develop the extraluminal flow oxygenator applicable to rat CPB model. In this study, the extraluminal flow oxygenator was prototyped, and biochemical and inflammatory markers were evaluated using the rat CPB model.

Methods: The extraluminal flow oxygenator was consisted of an acrylic housing, gas caps, a polyurethane polymer, and a polypropylene hollow fibre membrane (HFM) bundle. The HFM bundle porosity, effective membrane surface area, and priming volume were 30 %, 0.023 m^2, 2.7 mL, respectively. The rat CPB model consisted of the extraluminal flow oxygenator, a polyvinyl chloride tubing line, and a roller pump. The priming volume of this system was 8 mL.

The experiments were divided into 3 groups: SHAM group (n=5), a CPB with intraluminal flow oxygenator (n=7), and a CPB with extraluminal flow oxygenator (n=7). The SHAM group only underwent the surgery. After the start of the experiment, pump flow was maintained 60 mL/kg/min, and blood samples were collected three time points: before the start of circulation, 60 minutes and 120 minutes after the start of circulation (end of experiment). Biochemical markers, cytokines (TNF-α, IL-6, IL-10), PLT count were measured for evaluation. This study was conducted with the approval of the Niigata University of Health and Welfare Animal Care and Use Committee.

Table 1. Hemodynamics, blood gases partial pressures before and during CPB with extraluminal flow oxygenator.

	Pre	60min	120min
MAP (mmHg)	104±13	82±12	75±14
HR (beat/min)	384±34	361±20	358±30
PaO_2 (mmHg)	101±11	273±56	268±55
$PaCO_2$ (mmHg)	39±4	35±4	35±4
Hb (g/dL)	15.4±1.1	9.6±1.6	9.5±1.4

In the CPB with extraluminal flow oxygenator group at 60 and 120 minutes after the start of circulation, the PLT count was significantly preserved compared to the CPB with intraluminal flow oxygenator group. However, TNF-α, IL-10, and IL-6 were not significantly different in each CPB groups (Fig. 1(a)-(d)).

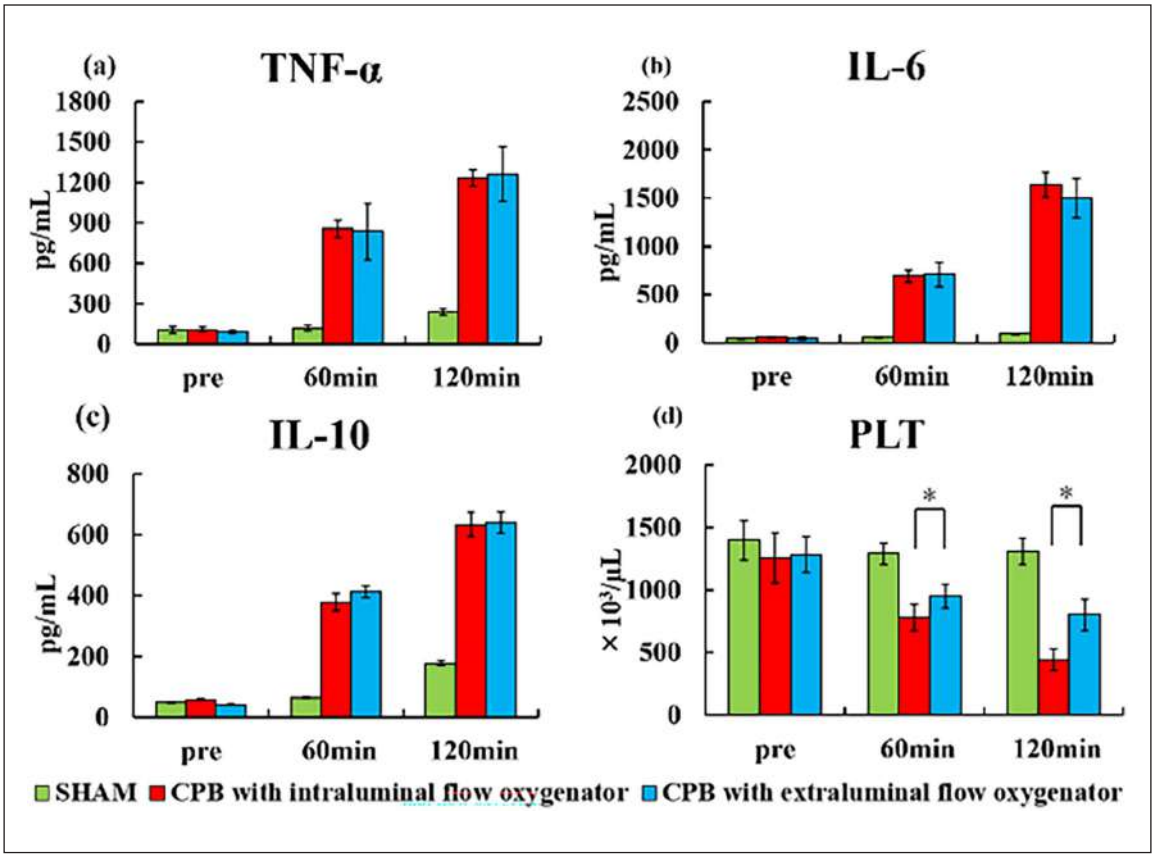

Figure 1. Inflammatory markers: TNF-α, IL-6, IL-10, and PLT in all of groups during the experiments. *P < 0.05 versus CPB with intraluminal flow oxygenator at the same periods. (mean ± SD).

Results: Table 1 presents the changes in hemodynamics, PaO2 and PaCO2, in CPB with extraluminal flow oxygenator during the experiments (mean ± standard deviation (SD)). The blood pressure and the Hb were maintained around 75 mmHg and 9.5 %, respectively, and the CPB was maintained without blood transfusion. It was possible to confirm oxygenation and carbon dioxide removal from the blood.

Discussion: The extraluminal flow oxygenator has lower pressure drop than the intraluminal flow oxygenator, it is possible that PLT was preserved in the extraluminal flow oxygenator. Hemodynamics were maintained in the CPB with extraluminal flow oxygenator group, and there was no significant difference in the inflammatory markers in each CPB group. Therefore, it is suggested that the developed extraluminal flow oxygenator is applicable to rat CPB model.

Reference

1. Yutaka Fujii et al, Artificial Organs, 37:1034-1040, 2013.

ABOUT THE EFFICIENCY OF THE INTRACARDIAC FLOWS: A COMPUTATIONAL STUDY OF THE MITRAL VALVE EFFECT

Franck Nicoud (1,2), Salomé Bru (1), Simon Mendez (1)

1. IMAG, Univ. Montpellier, CNRS, Montpellier, France; 2. Institut Universitaire de France, Paris, France

Introduction: During each cardiac cycle, the left heart receives around 60 ml of fresh blood from the lungs and expels the same amount into the systemic circulation via the aorta. It is expected that the efficiency of this process is somehow linked to the normal/pathological evolution of the heart. Disturbances in the electrophysiological processes leading to muscle contraction can very likely induce energy loss, as can the way in which blood flows through the heart. For example, the well-organized vortex that develops in the left ventricle at end-diastole is believed to ease energy conservation and blood ejection during systole [1], whereas turbulence is a source of extra dissipation. The aim of this work is to quantify the extent to which the structure of the intraventricular flow impacts the amount of energy dissipated during each cardiac cycle.

Methods: The study relies heavily on the numerical strategy developed by Chnafa et al. [2], where a time-evolving 3D mesh consistent with the actual motion of the left heart is generated from medical images (CT Scan or MRI) using segmentation and registration algorithms. The mitral valve is modeled as proposed in [3] and its effect on flow is reproduced using an Immersed Boundary Method (IBM) [4]; a similar IBM is used to model the aortic valve as a simple planar object introduced during the diastolic phase to prevent blood backflow from the aorta. The resulting computational domain includes the four pulmonary veins, the left atrium and ventricle, the ascending aorta, in addition to the two valves mentioned above. The Navier-Stokes equations are then solved using an arbitrary Lagrangian-Eulerian framework as implemented in the widely validated YALES2BIO in-house solver [5], with an appropriate description of turbulence by Large Eddy Simulation [6].

For the patient-specific geometry of [2], four mitral valve (MV) geometries were considered to produce different types of intraventricular flow - see Table 1.

Table 1. Characteristics of the 4 MV considered.

REF	Case A	Case B	Case C
Normal MV	Anterior jet deflection	Wider opening	Smaller opening

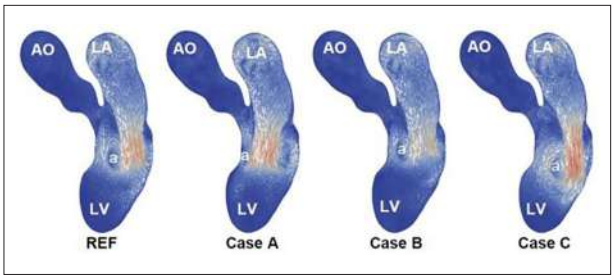

Figure 1. Phase-averaged velocity at mid-diastole. Long-axis cut. LV: left ventricle; AO: Aorta; LA: Left atrium.

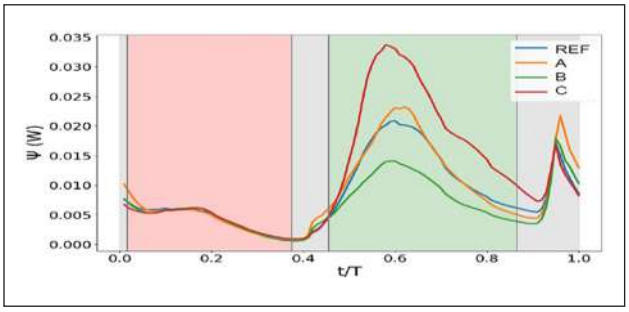

Figure 2. Ventricle integrated viscous dissipation.

Results: Phase-averaged velocity fields for the four cases considered are shown in Figure 1 to illustrate that flow structure is indeed strongly affected by mitral valve geometry. Compared with REF, Cases A to C clearly show the deflection, widening and restriction of the E-wave jet that fills the ventricle in mid-diastole.

The phased-averaged viscous dissipation integrated over the ventricle is displayed in Figure 2; Case C is the least energy-efficient geometry, while jet deflection (case A) has virtually no effect, and jet widening (case B) significantly reduces energy losses.

Discussion: According to the above results, intra-ventricular turbulent activity (closely related to viscous dissipation -not shown -and measurable by MRI [7]), is a good biomarker of mitral valve function. Still, integrating the curves in Fig. 2 over the cardiac cycle shows that the amount of energy dissipated (6.5 mJ for Case B; 11.5 mJ for Case C) is always a small fraction (< 2%) of the total energy expended by the ventricle. These results suggest that, in absence of regurgitation, cardiac efficiency is unaffected by mitral valve function.

References

1. Cimino et al., Eur. J. Fluid Mech. B/fluids, 35:40-46, 2012
2. Chnafa et al., Comp. and Fluids, 94:173–187, 2014.
3. Domenichini & Pedrizzetti, CVET, 6:95-104, 2015
4. Sigüenza et al., J. Comp. Phys., 322: 723-746, 2016
5. https://imag.umontpellier.fr/~yales2bio/
6. Nicoud et al., Phys. Fluids, 23(8): 085106, 2011
7. Dyverfeldt et al., J. Mag. Res. Imag., 56(4) : 850-858, 2006

Acknowledgements

This work was supported by grant ANR-21-CE19-0034-02 from the French research agency ANR.

BLOOD-DERIVED ANTIMICROBIAL PEPTIDES FOR MANUFACTURING ANTISEPTIC MEDICAL SURFACES

Stephan Harm (1), Jennifer Zottl (1), Denisa Cont (1,2), Claudia Schildböck (1), Viktoria Weber (1)

1. Department for Biomedical Research, University for Continuing Education Krems, Austria; 2. Department Physiology, Pharmacology and Microbiology, Karl Landsteiner University, Austria

Introduction: The aim of this study was to functionalize surfaces with endpoint attached (EPA) heparin to incorporate blood-derived cationic antimicrobial peptides and proteins (AMPs) to form an antiseptic surface.

Methods: A adsorbent consisting of carboxylated polyacrylamide (PA) was functionalized with EPA-heparin using the method described by Larm et al [1]. Heparin functionalization was performed using unfractionated heparin (PA-UFH) and low molecular weight heparin (PA-LMWH). The functionalized adsorbents were incubated with human blood for 4 hours, during which neutrophil-derived cationic AMPs bound to the surface, which resembles the glycocalyx lining the human endothelium. The functionalized adsorber was packed into a 1 ml column to measure the clearance of *Staphylococcus aureus*. An aliquot of 6 ml human serum albumin solution (HSA 4%) spiked with 50,000 colony forming units (CFU)/ml of *S. aureus* was pumped through the column, and CFUs were determined pre and post column (Figure 1). A non-functionalized PA adsorbent and a commercial available heparin functionalized adsorbent (Seraph100, ExThera Medical, Martinez, US) were included in this study. An empty column served as control.

Results: Both, the non-modified and the heparin-functionalized adsorbent, pre-incubated in human whole blood, showed a significant reduction in *S. aureus* CFUs, while the same adsorbents pre-incubated in physiological saline showed no significant pathogen clearance (Figure 2).

Discussion: These findings highlight the vital role of the endothelial glycocalyx and its interaction with AMPs in infection, leading to the formation of a protective shield around the site of infection. Potential applications include pre-impregnating medical implants with human blood-derived antimicrobial substances to enhance blood compatibility and reduce the risk of infection. Additionally, EPA-heparin functionalized adsorbents could be integrated into extracorporeal blood purification systems, mimicking the endothelial glycocalyx, to deplete heparin-binding cytotoxic compounds, such as histones, platelet factor 4 or platelet-derived extracellular vesicles in sepsis patients.

Reference

[1] *Biomater Med Devices Artif Organs* 1983, 11, (2-3), 161-73.

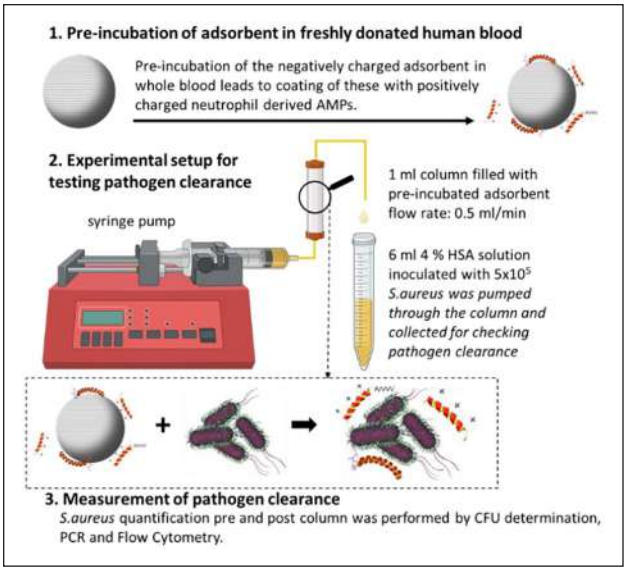

Figure 1. Setup of the dynamic model for pathogen clearance of heparin functionalized adsorbents.

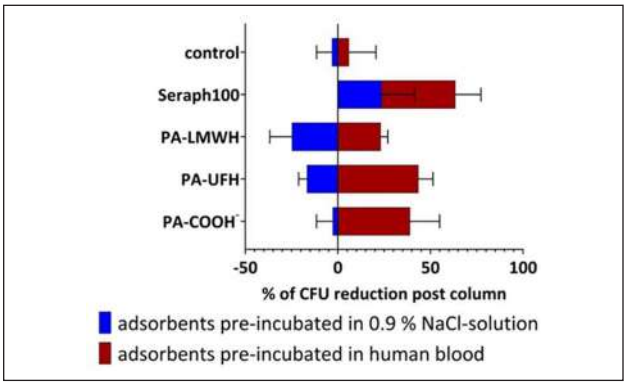

Figure 2. The graph illustrates the percentage decrease in colony forming units per milliliter (CFUs/ml) of the S. aureus suspension after the single pass through the column. An empty column without adsorbents served as control.

NUMERICAL SIMULATION OF PLATELETS ADHESION ON STRUCTURED ARTIFICIAL SURFACES

Corentin Raveleau (1), Marlene Schadow (2), Michael Neidlin (2), Johanna C. Clauser (2), Simon Mendez (1), Franck Nicoud (1,3)

1. IMAG, University of Montpellier, CNRS, France; 2. Department of Cardiovascular Engineering, Institute of Applied Medical Engineering, University Hospital RWTH Aachen University, Aachen; 3. Institut Universitaire de France, IUF, France

Context: As cardiovascular diseases are the first cause of death worldwide, providing efficient medical devices to treat these diseases is a main concern in the biomedical engineering field. However, because these devices are directly interacting with the blood, their hemocompatibility must be ensured. This is one of the most important challenges to their development and side treatment with anti-coagulant is currently needed to prevent thrombus formation at the surface of the blood contacting devices. In an effort towards increased hemocompatibility of such devices, artificial surface structures in the micrometer range have been shown to influence the thrombogenicity of the surface although this effect is not well characterized and understood [1]. This abstract presents the preliminary outcomes of an on-going computational study aiming at better understanding how the platelets adhesion, the key mechanism in thrombus initiation, can be affected by the presence of micro-structurations over the material surface. This is a joint effort including an experimental component addressed in the companion paper by Schadow et al. 2024 [2].

Methods: The numerical model is implemented in the YALES2BIO solver developed at IMAG (https://imag.umontpellier.fr/~yales2bio/) and dedicated to the simulation of blood flows [3].

The fluid movement is described by the incompressible Navier-Stokes continuity and momentum equations:

$$\nabla \cdot \mathbf{u} = 0 \tag{1}$$

$$\rho \frac{D\mathbf{u}}{Dt} = -\nabla p + \mu \nabla^2 \mathbf{u} + \mathbf{f}(\mathbf{x},t) \tag{2}$$

$$f_i(\mathbf{x},t) = F_i \Delta(\mathbf{x} - \mathbf{Y}(t)) + G_{ij} \frac{\partial}{\partial x_j} \Delta_d(\mathbf{x} - \mathbf{Y}(t)) \tag{3}$$

The force $\mathbf{f}(\mathbf{x},t)$ present in the momentum equation (2) and detailed in equation (3) accounts for the presence of a particle in the flow as prescribed by the Force Coupling Method [4]. The external forces and torque as well as the incompressibility constraint are transmitted from the particle to the fluid via two ellipsoidal Gaussian envelopes Δ and Δ_d, centered at the particle center of mass **Y,** whose width are related to the particle dimensions to match chosen physical properties of the particle.

The linear velocity of each particle is measured as the average velocity under the Gaussian envelope (4) and is used to update the position of the particle at each numerical time step by integration of equation (5):

$$\mathbf{u}_p = \int_\Omega \mathbf{u}(\mathbf{x},t)\Delta(\mathbf{x}-\mathbf{Y}(t))dv \tag{4}$$

$$\frac{d\mathbf{Y}}{dt} = \mathbf{u}_p \tag{5}$$

A similar work is done to update the particle orientation by measuring the angular velocity of the particle from the fluid vorticity.

Results: The numerical model has been validated against results from the literature regarding the dynamics of ellipsoidal particles in shear flows. In absence of solid boundary wall, the model reproduces the rotation of the particle in a way fully consistent with the theoretical Jeffery's orbit [4]. Close to a planar wall, results obtained for an aspect ratio equal to 0.5 are in good agreement with the computational results from Hsu & Ganatos [5]. The methodology is now applied to cases where the wall is micro-structured (see Figure 1) and short-range adhesion forces are present. Our results show differences in flow characteristics depending on surface structures that might be responsible for positive and negative effects on the hemocompatibility of structured surfaces. The corresponding results will be presented at the conference, should the paper be accepted.

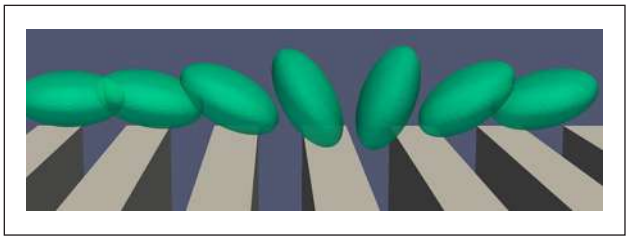

Figure 1. Numerical model of platelet transport over grooves implemented in YALESBIO. A surface of the particle dimensions is used for visualization.

References

1. Kuchinka et al., Bioengineering, 8:215, 2021.
2. Schadow et al., ESAO Submission abstract, 2024.
3. Mendez et al., Bio Flow in Large Vessel, 183-206, 2022.
4. Liu et al., J Computational Physics, 228:3559-3581, 2009.
5. Jeffery, Proc. R. Soc. Lond. A 102:161–179, 1922.
6. Hsu & Ganatos, J Fluid Mec, 268:267-292, 1997.

Acknowledgements

This work has been initiated during the Extreme CFD Workshop & Hackathon (https://ecfd.coria-cfd.fr). It is part of the THROMBOSURF project co-funded by Agence Nationale de la Recherche (ANR-21-CE45-0035-02) and DFG.

PERSONALIZED 3D ANATOMICAL MODEL FOR PULMONARY SURGERY

Giulia Gamberini[1,2], Selene Tognarelli[2], Arianna Menciassi[1,2]

1. Health Science Interdisciplinary Centre, Scuola Superiore Sant'Anna, Italy; 2. The BioRobotics Institute, Scuola Superiore Sant'Anna, Italy;

Introduction: Lung cancer is the most common type of tumour and the leading cause of cancer death worldwide [1]. Patients with early-stage non-small cell lung cancer should be treated with minimally invasive techniques, whenever possible [2]. The most used technics are segmentectomy (excision of a section of a lung lobe) and lobectomy (removal of an entire lobe). Both techniques require isolation and resection of hilar structures including pulmonary arteries, pulmonary veins and bronchi [3]. Vascular and bronchial anatomical variations are common, thus knowledge of them could aid in planning and performing interventional procedures [4]. 3D printing and cast moulding technologies are rapidly growing and transforming the medical industry and they could be useful in developing models for surgical planning and training in lung procedures [5].

This work introduces a personalized 3D anatomical model for planning lung lobectomy surgical interventions. The objective is to provide surgeons with a 3D representation of the lung anatomy and pulmonary vascular structures involved in lung lobectomy. This model could be used by surgeons to understand and study the patient anatomy and the possible anatomical variations prior to the surgical operation. In addition, the model could be used for educational purposes, and for training and retraining on specific surgical skills, such as pulmonary vessel isolation and resection, which are commonly done during pulmonary surgery procedures.

Methods: Figure 1 summarises the steps to create the patient's personalized 3D model. Starting from the segmentation of the anatomical structures by using a high-resolution CT scan, the 3D Slicer software, along with the available *CTACardio* CT scan, was utilized for obtaining the patient's anatomical model. The images were segmented using the *Paint* and *Grow from seed* functions. The first one allowed to select the anatomical regions of interest, the second one to reconstruct the 3D anatomical model. The obtained meshes were imported in Fusion 360 (Autodesk, USA) for 3D design. The meshes were refined to obtain *high* resolution to identify the smallest structures (diameter of 2 mm) and assure printability. Being vascular structures prone to anatomical variations, we focused on those structures. The model can be made both of rigid and soft materials. The rigid version accurately replicates the patient's anatomy, while the soft one allows to create high-fidelity replicas in terms of biomechanical properties. The rigid model is 3D printed without any additional step, obtaining a complete model of the anatomy (blue part of Figure 1). For the soft replica, a mould of the model must be first fabricated for silicone injection. To choose the right silicone, biomechanical data from porcine samples were used as reference [6]. The soft replica, alone or combined with anatomical

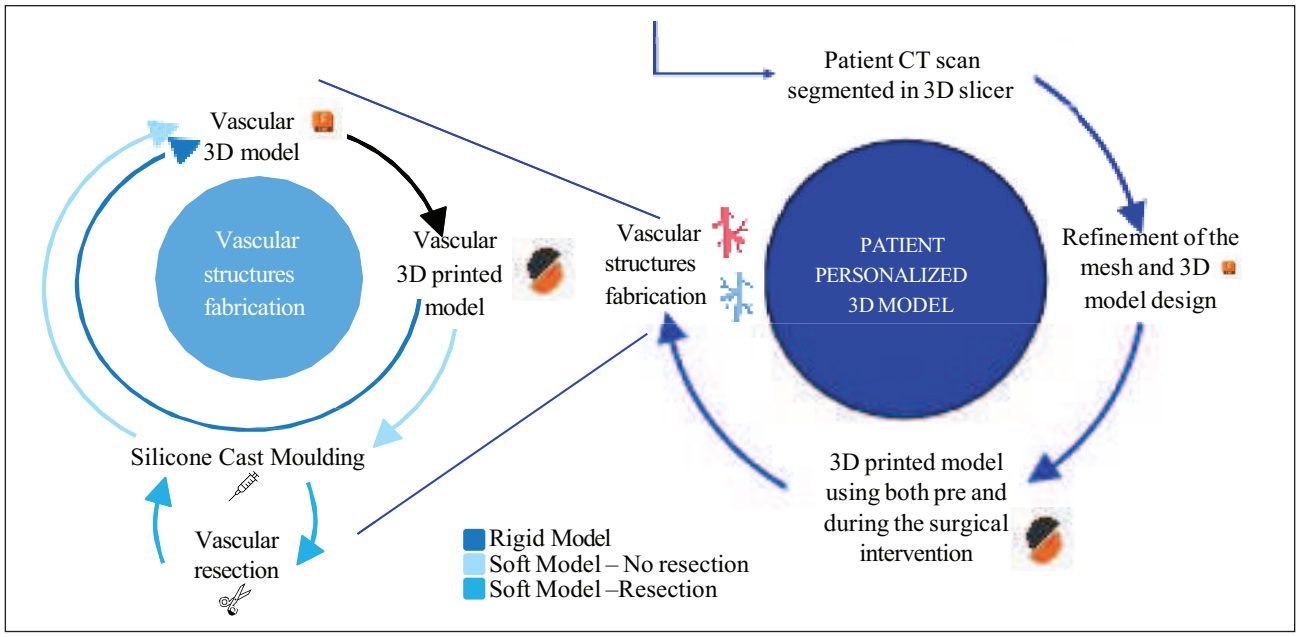

Figure 1. Schematic representation of the procedure to realize the patient personalized 3D model.

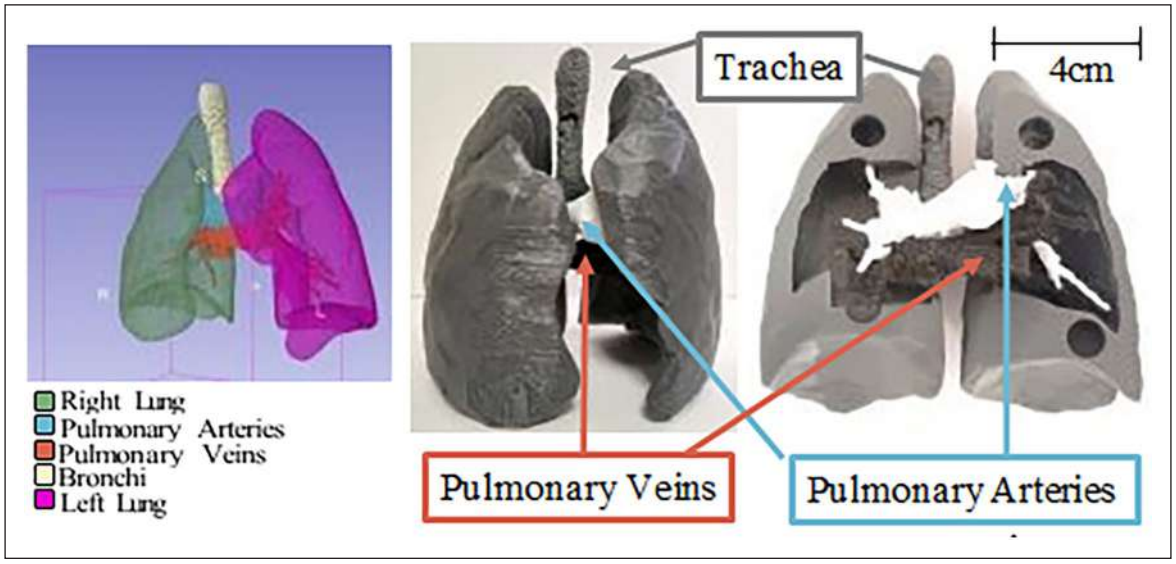

Figure 2. Segmentation of the lungs and vascular structures in 3D Slicer and 3D printed representation.

rigid components, could be also used as a smart training platform for residents and young surgeons. However, once the isolation and resection tasks are performed on the model, it becomes single-used. This is explained in the light blue part of Figure 1.

Results: In Figure 2, the printed patient-specific model -in scale 1:2 -is depicted along with the 3D representation of the rigid components. The mould for the soft replica was also realized and 3D printed using Polylactic acid for further silicone injection. Considering the mechanical properties of porcine vein and artery, Smooth On Silicones, e.g. Ecoflex 00-30, were chosen providing a good compromise in terms of flexibility and biomechanical properties.

Discussion: The presented work introduces a patient-specific 3D model of lungs and hilar structures. The model can be proposed both for surgical intervention planning and surgical training.

References

1. https://gco.iarc.who.int (visited on the 15th of April 2024).
2. Chiappetta, M. et al, Curr Oncology, 30:7773–7776, 2023.
3. Batıhan G., IntechOpen, 2023.
4. Kandathil, A. et al, Cardiov Diagn Ther 8:201-207, 2018.
5. Mamo B. H. et al, J Mech Beh of Biom Mat 143, 2023.
6. Gamberini G. et al, Sci Rep 14, 4779, 2024.

AUTOMATED INSULIN DETECTION BY A MIP SENSOR INTEGRATED IN A MICROFLUIDIC FLOW CELL

Tanja Zidarič (1), Boštjan Vihar (1), Tina Maver (1), Steffen Winkler (2), Natalie Plewka (2), Janina Bahnemann (2), Uroš Maver (1)

1. University of Maribor, Faculty of Medicine, Institute of Biomedical Sciences, Slovenia; 2. University of Augsburg, Chair of Technical Biology, Institute of Physics, Germany

Introduction: Accurate monitoring and quantitative evaluation of biophysical and biochemical parameters within the micro-environment remain critical for validating a microphysiological system's (MPS's) ability to faithfully emulate human tissue or organ function [1-3]. Biosensor integration presents an interesting option for achieving such monitoring An alternative to conventional biosensors based on natural receptors are molecularly imprinted polymers (MIPs) that are more stable in changing environments (e.g. pH, temperature). MIPs involve the formation of specific cavities in a 3D polymer network, which mimic the shape and chemical features of the target molecules [4, 5]. Their compatibility with inline readouts makes MIPs an excellent candidate for integration into microfluidic systems and MPS platforms. With this work, we aimed to integrate a MIP biosensor into a 3D-printed microfluidic flow cell for fully automated and inline detection of insulin.

Methods: The surface of a screen-printed electrode (SPCE) was modified *in situ* with an insulin-imprinted polymer (Figure 1) [6], which was coupled with an automated chip system. Cyclic voltammetry (CV) was used to characterize the electroanalytical response of the assembled in-sulin-imprinted SPCE automated chip. The measurements were performed in the presence of a $[Fe(CN)6]^{3-/4-}$ redox probe. Several parameters were optimized to obtain the linear relationship between signal and insulin concentration in the physiological range. The performance of the automated MIP-SPCE chip was evaluated by quantification of insulin using the multiple standard addition method.

The microfluidic chips were fabricated using high-resolution MultiJet 3D printing and post-processed according to Enders *et al*. [9].

Results: The microfluidic system used for automated calibration and sampling of the MIP-insulin sensor is presented in Figure 2. The chip includes a MIP sensor flow cell, an HC micromixer, a bubble trap, a magnetic valve for sampling and several connection ports.

All calibration experiments (n = 5) showed a linear response in the range of 20.0–70.0 pM insulin (mean R^2 = 0.99). In addition, the automatization of sampling (using a multiple standard addition method) (n = 5) also proved to be successful, as the recovery of calculated insulin values were 87.4 to 90.6 %.

Conclusion: These positive results motivate further validations of the proposed automated MIP-insulin chip for online detection of insulin in *in vitro* pancreatic models. Moreover, the 3D-printed microfluidic system can easily be customized to apply MIP-based monitoring to other MPSs.

References

[1] Fuchs et al, ACS Biomater. Sci. Eng. 7(7)2923-2948, 2021.
[2] Aziz et al, Bioengineering 4(2) 39, 2017.
[3] M.M. Modena et al, ACS chem. biol. 13(7) 1767-1784, 2018.
[4] H. Kavand et al, Advanced Materials 34(17) 2107876, 2022.
[5] L. Mou et al, Lab on a Chip 22(20) 3801-3816, 2022.
[6] Y. Saylan et al, Sensors 19(6) 1279, 2019.
[7] M. Cieplak et al, Trends in biotechnology 34(11) 922-941, 2016.
[8] T. Zidarič et al, Analyst 148(5) 1102-1115, 2023.
[9] Enders et al, Small 15(2) (2019) 1804326.

Acknowledgements

The authors acknowledge the financial support from the Slovenian Research Agency for Research (grant numbers: P3-0036, J1-2470, and Z2-8168),

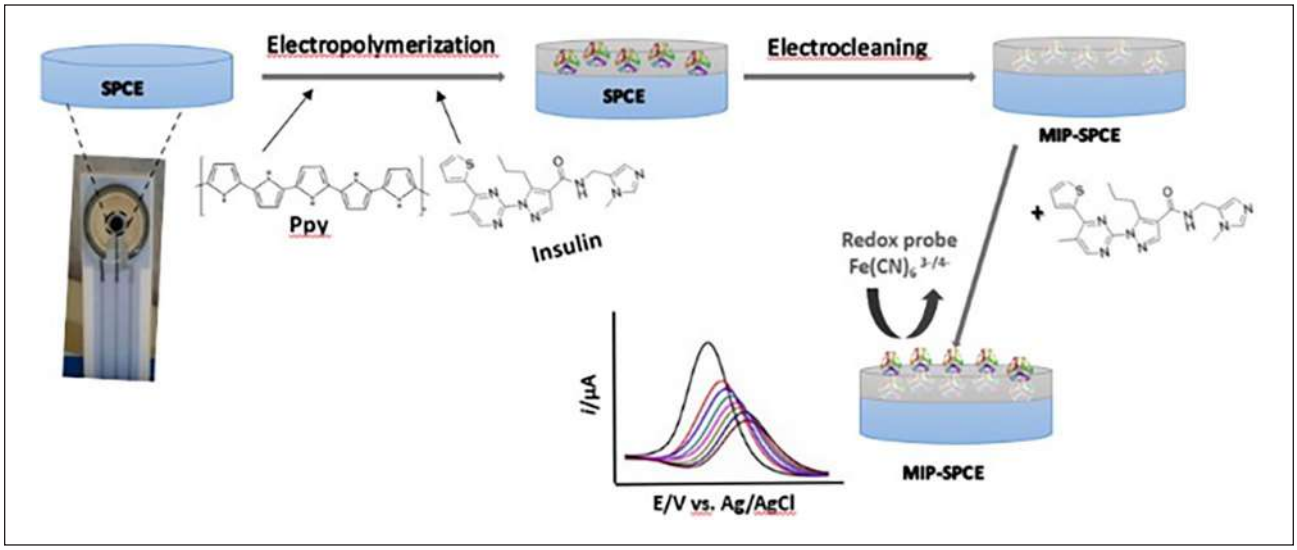

Figure 1. The concept of electrosynthesized MIP prep-aration for insulin detection.

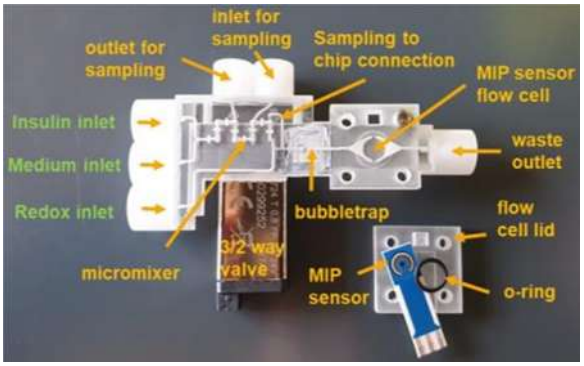

Figure 2. Setup of the microfluidic flow cell for MIP in-tegration, sensor calibration and sampling.

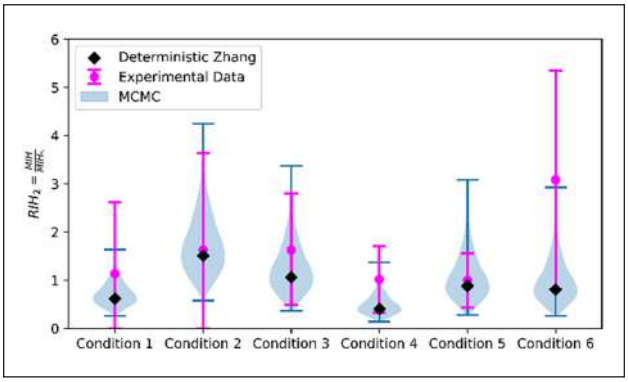

Figure 1. Experimental hemolysis results of [4] in magenta, with numerical prediction of original, deterministic Zhang et al. [2] model (black) and probabilistic MCMC predictions in form of a violine plot (blue).

IMPLEMENTATION OF EXPERIMENTAL UNCERTAINTY TO IMPROVE HEMOLYSIS MODELING IN CARDIOVASCULAR DEVICES

Christopher Blum (1), Ulrich Steinseifer (1), Michael Neidlin (1)

1. Department of Cardiovascular Engineering, Institute of Applied Medical Engineering, RWTH Aachen University, Aachen

Introduction: Despite the widespread use of numerical hemolysis models in biomedical engineering, these models fail to account for the inherent uncertainty in their underlying experimental data. However, uncertainty quantification is of paramount importance in computational modeling of medical devices as emphasized by recent guidance document of the US Food & Drug Administration [1]. The current gold standard for hemolysis modeling is to conduct an experiment of controlled exposure time and shear stress at different operating points and to record the resultant hemolysis index (HI). To build a numerical model, a power law(equation 1) is fitted through all data points.

$$HI = C * ShearStress^{\beta} * Time^{\alpha} \quad (1)$$

In this process all information of the underlying experimental variability gets lost and the resulting hemolysis model only represents a mean state of hemolysis. This study proposes a universally applicable method to implement variation of experimental data into numerical models of hemolysis through the Markov Chain Monte Carlo (MCMC) method.

Methods: We applied the MCMC method to an experimental hemolysis data set [2], conducting 50,000 samples across four chains to derive stochastical distributions for the fitting parameters C, α, and β. These distributions were then utilized in a non-intrusive polynomial chaos expansion to create a reduced order model for hemolysis calculation in the FDA pump benchmark simulation [3]. This approach allowed for fast sampling from MCMC posterior distributions to estimate hemolysis variability across different operating points of the FDA blood pump. We then compared model predictions to published multi-laboratory data of hemolysis in the FDA pump [4].

Results: The analysis exposed the non-uniqueness of traditional model fitting, identifying multiple local minima in the sum of squared errors from least squares fitting. MCMC results yielded a constant, optimal C=3.515e-5 and approximately normally distributed α and β with means of approximately 0.49 and 1.55, respectively. With this, the MCMC model closely matched mean and variance of experimental data [4] in most of the conditions, particularly when comparing relative performance across different operating conditions of the pump (Figure 1). In contrast to this, the conventional approach (deterministic Zhang in Figure 1) does not allow to compute the variation of hemolysis in the FDA pump.

Discussion: This study successfully demonstrates how the inherent uncertainty in hemolysis experiments can be captured and implemented into numerical blood damage models. It further shows that incorporating fitting parameter variability through MCMC substantially enhance the robustness of hemolysis model prediction. The current gold standard of relative comparisons is strengthened by incorporating the variance of the underlying experiments, providing a stronger foundation for comparing simulated hemolysis outcomes with in-vivo experiments. The developed method can easily incorporate further experimental datasets encompassing various stress types, donor species, and a higher number of repetitions. Such an approach has the potential to set a new standard of predictive accuracy in hemolysis modeling.

References

1. FDA,Assessing the Credibility of Computational Modeling and Simulation in Medical Device Submissions, 2023
2. Zhang et al, Artif Organs., 35(12):1180-6,2014.
3. Malinauskas et al, ASAIO J., 63(2):150-160, 2017.
4. Ponnaluri et al, Ann Biomed Eng.,51(1):253-269,2023

Acknowledgements

Funded by the Deutsche Forschungsgemeinschaft (DFG, German Research Foundation) – project number 467133626

ISOLATION AND IDENTIFICATION OF UNKNOWN MEDIATORS AFFECTING CARDIOVASCULAR FUNCTION

James Lohman, Joachim Jankowski, Vera Jankowski

Institute for Molecular Cardiovascular Research, University Hospital RWTH Aachen

Introduction: Cardiovascular Disease (CVD) covers a wide range of disorders and dysfunctions, and a growing global issue as the leading cause of death worldwide. Heart Failure (HF) is recognized as the most

serious CVD complication, carrying a high rate of mortality. Risk of CVD and HF are correlated to several factors, but the rate of incidence is not fully explained by those risks. The underlying biochemical mechanism responsible for HF and it is probable that HF in relation to CVD may be the result of one or more unidentified proteins in the blood.

In previous work from this lab, key peptides were identified in the plasma of pigs which proved to have a strong bradycardiac effect which could lead to HF, primarily those from the protein Peptide YY (PYY). The frequency in hearts of rats were severely reduced in each case when exposed to key peptides from PYY, indicating that they have a negative inotropic effect.

Methods: Samples of blood plasma from patients were split into 3 cohorts: patients with CVD experiencing cardiac episodes (decompensated), patients with CVD after those episodes, in absence of symptoms (compensated), and healthy patients with no history of CVD. Proteins in the blood plasma from each patient were first deprotonated, then separated and isolated using a series of chromatographic techniques including size exclusion, ion exchange, and reverse-phase separation. Mass spectrometry analyses (MS and MS/MS) were then performed to screen the samples for the targeted peptides. Upon detecting the presence of the targeted peptides with MS, the identities were confirmed via MS/MS fragmentation techniques and correlated to the contributing parent proteins.

Results: Fragments of PYY2 have been observed in decompensated samples. One fragment of interest can be observed in **Figure 1A**, corresponding to m/z peak at 687 Da. In **Figure 2** the MS/MS confirmation for the fragment is displayed, identifying it as a peptide with the sequence **PEAPGEDA** unique within the neuropeptide-Y family of proteins to PYY2.

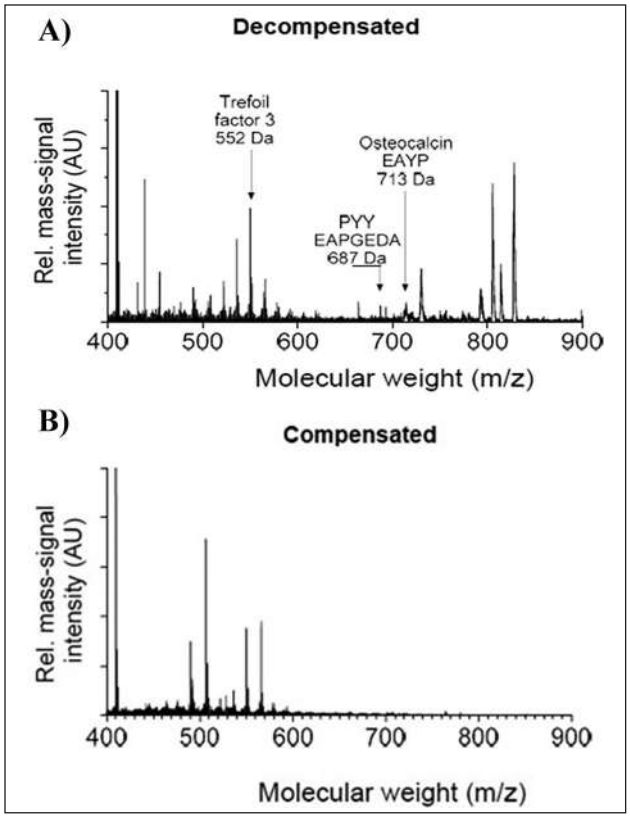

Figure 1 Characteristic MS mass spectrogram of isolated proteins from a A) decompensated and B) compensated CVD patient.

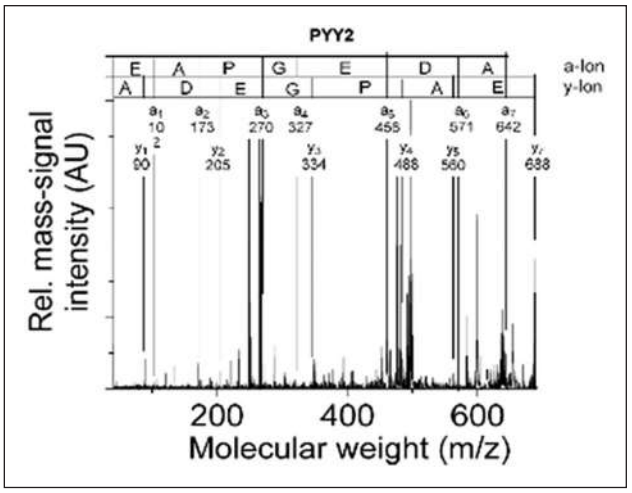

Figure 2. MS/MS of 687 Da mass peak found in decompensated patient.

The presence of sub-fragments of the parent peak indicates that the peptide sequenc is present and among other sequences identified with the same technique, providing strong evidence for the presence of PYY2, within the decompensated patient sample. It is notable that peaks at 687 Da are absent in compensated samples (**Figure 1B**).

Discussion: The hormone PYY2 was observed to be prevalent within decompensated patients. The PYY2 sequence is largely concurrent with the peptide observed to affect heart frequency in pigs. Determining the concentration of PYY2 is an on-going task and investigation of the cardiovascular effects of the protein will be elucidated using physiological assays.

DEVELOPMENT OF AGGRESSIVE TREATMENT TO ADMINISTER DRUGS DIRECTLY INTO THE TRACHEA OF PATIENTS ON ECMO

Yusuke Inoue, Yasushi Sato, Takeshi Terazawa, Tomoki Nagayoshi, Yoshiaki Takewa

Advanced Medical Engineering Research Center, Asahikawa Medical University, Japan

Background: Severe cases of novel coronavirus infection (COVID-19) cause acute respiratory distress syndrome (ARDS); there is no treatment for ARDS and patients are fitted with extracorporeal membrane artificial lungs (ECMO). The increase in the number of patients on ECMO during a pandemic will result in medical collapse due to a shortage of medical staff, hospital beds, and medical equipment. In addition, ECMO is not a device to treat the lungs, but rather a medical device that rests the patient's own lungs and promotes recovery. Therefore, patients with ECMO need a long hospital stay before they can recover. Early weaning from ECMO and improving the life-saving rate is an urgent issue. We have drafted a new treatment modality that promotes early pulmonary recovery by administering drugs directly into the lungs through the trachea. To evaluate the efficacy and safety of this new treatment using ECMO, an experimental animal model of the same size as humans is needed, but there are no experimental animal models available to evaluate the proposed new treatment. In addition, large animal experiments using viruses such as COVID-19 are extremely difficult. Therefore, the purpose of this study is to establish a large animal model that can evaluate aggressive pulmonary therapies that administer drugs transbronchially on ECMO support and to evaluate their efficacy.

Methods: Twelve adult Saanen goats were used. Anesthesia was induced with ketaral and maintained via mechanical ventilation with isoflurane in oxygen gas. After heparin was injected via vein as anticoagulation, the right carotid artery and right jugular vein were exposed, a de-bleeding cannula was inserted from the vein into the right atrium area, and a sending cannula was inserted into the carotid artery. Next, a centrifugal pump and a membrane artificial lung primed by saline were connected to the cannula. Lipopolysaccharide (LPS) as an endotoxin was then injected intravenously (70-100ug/kg) to induce sepsis and create a model of acute lung disease[1-4]. Pressure sensors and catheters were used to continuously measure pressure in the pulmonary artery, left ventricle, and aorta in an observational manner. Oxygen saturation before and after lung and in the artificial lung was measured intermittently. X-ray angiography was performed to observe pulmonary blood flow. Hourly lung tissue sampling was performed to histologically evaluate alveolar, bronchiolar and vascular morphology. In order to minimize the influence of individual animal differences in evaluating the effects of the drug, different conditions were set up and compared in the left and right lungs. Using a two-way intubation tube, only the left lung was administered the therapeutic drug through the trachea, while the right lung was not administered the drug as a control. 2 hours after administration of LPS, the drug (nafamostat mesylate 150 mg) was administered into the lung through the trachea.

Results: Immediately after LPS was administered intravenously, there was a rapid increase in pulmonary arterial pressure. Pulmonary arterial pressure required 30 -60 minutes to return to normal values. A few minutes after the pulmonary artery pressure increased, aortic pressure decreased gradually. Angiography at that time showed markedly reduced pulmonary artery blood flow. Blood gas studies also showed a marked decrease in the partial pressure of oxygen in the blood immediately after the introduction of LPS. When blood flow could no longer be maintained due to the decrease in aortic pressure, ECMO was driven to maintain blood flow, and peripheral blood oxygen saturation recovered to the normal range after ECMO was driven. Histological evaluation showed blood and plasma leakage around blood vessels and inflammation in the lungs treated with LPS compared to normal lungs. The degree of inflammation was lower in the left lung treated with the therapeutic agent than in the right lung that was not treated.

Conclusions: Results of 12 animal studies showed that after endotoxin (LPS) administration, pulmonary hypertension due to vasoconstriction and a marked decrease in pulmonary blood flow and blood oxygen saturation were induced. Histological evaluation showed plasma leakage from peribronchial vessels after LPS administration. Comparison of the left and right lungs showed a difference in the degree of inflammation, allowing evaluation of the efficacy of this treatment method. We succeeded in establishing a model of acute severe lung disease caused by endotoxin and in creating an animal model in which the new treatment method could be evaluated.

References

1. M. Engel, et al. Respir Res, 21: 209, 2020
2. Matute-Bello G, et al. Am J Physiol Cell Mol Physiol, 295: L379-99, 2008
3. Rosenthal CDO, et al. Crit Care Med. 26(5):912-6, 1998
4. Lindenkov PHH, et al. Ped Res, 57(3):371-7, 2005

THE BONE-KIDNEY-AXIS: INVESTIGATING A NEW MEDIATOR OF CKD-INDUCED BONE DYSTROPHIE

Erik Merckelbach[1], Joachim Jankowski[1], Nathalie Gayrard[2], Ángel Argilés[2], Shruti Bhargava[1]

[1]Institute for Molecular Cardiovascular Research (IMCAR), University Hospital RWTH Aachen, Germany; [2]RD-Néphrologie and EA7288, University of Montpellier, France

Introduction: Mineral bone disease (MBD) and cardiovascular disease in patients suffering from chronic kidney disease (CKD) are a prime example of organ cross-talk [1]. Kidney impairments lead to hyperphosphatemia and uremia, promoting vascular calcification as well as bone disorders like osteoporosis [2]. The complex interplay between CKD, MBD, and the vascular system is thus labeled CKD-MBD. The chromogranin A derived calcification blocking factor (CBF) has already been established as an inhibitor of vascular calcification, but nothing is known of its effect on bone health [3].

In this project MBD was investigated in animal models of vascular calcification and atherosclerosis as well as the mediating effect of CBF on the bone.

Methods: To investigate the effect of CKD on bone quality, vascular calcification was induced in rats via vitamin D3 and nicotine treatment (VDN). The structure and bone mineral density of tibia from VDN rats with and without CBF treatment were analyzed via micro-computed tomography (micro-CT) scans. In detail, the bone mineral density of the trabecular and cortical bone, as well as the trabecular thickness, number, porosity, cortical thickness and medullary volume were analyzed.

Results: VDN animals without additional treatment showed significant changes in bone structure and bone mineral density of the tibia. The mineral density of the trabecular bone was increased by 86 % in VDN rats compared to control animals (p=0.01). The trabecular number of VDN rats increased by 128 % (p=0.0009), while the trabecular porosity decreased by 15 % (p=0.0055). The mineral density of the cortical bone decreased by 8 % (p=0.005), while the cortical porosity was increased by 10 % (p=0.0068) and cortical thickness decreased by 22 % (p=0.0048). Conversely, the medullary volume increased by 47 % (p≤0.0001). These changes were in all cases negated to non-significance compared to the control, when the rats were additionally treated with CBF.

Discussion: In our study, we were able to comprehensively show the changes in bone mineral density and bone structure in the tibia of rats suffering from vascular calcification. In addition, preventive treatment with CBF proved to inhibit any changes in bone structure and mineral # density, effectively preserving the healthy state of the bone. Based on these results, CBF presents a novel mediator of not only vascular calcification but also MBD, highlighting it as a possible treatment target in CKD-MBD.

References

1. Hu, Lilio et al, Int J Mol Sci, vol. 23, 20 12223, 2022.
2. Hou, Yi-Chou et al, Clin Chim Acta, vol. 23, 2018.
3. Orth-Alampour, Setareh et al, Basic Res Cardiol, 116(1): 57, 2021.

CRYOPRESERVATION OF IN VITRO LIVER MODEL USING HEPARG CELLS FOR TOXICOLOGICAL STUDIES.

Meschini (1), Leclerc (2), Sakai (2), Legallais (1), Pereira (1)

1. Université de technologie de Compiègne, CNRS, BMBI (Biomechanics and Bioengineering), Centre de recherche Royallieu -CS 60 319 -60 203 Compiègne Cedex, France; 2. University of Tokyo, Graduate school of Engineering, Sakai-Nishikawa Laboratory, 7-3-1 Hongo, City of Bunkyo, Tokyo

Introduction: Animal experimentation raises ethical and scientific concerns, with in vitro models offering an alternative. However, constructing these models faces challenges such as limited biomass availability and delayed establishment. Among the different biological

sources available, immortalized human cell lines are commonly used. Regarding liver engineering, HepaRG cells are valuable for studying drug metabolism, toxicity, and liver diseases due to their physiological relevance. Relatively expensive, this cell type requires prolonged differentiation, and exhibit batch variability.

Cryopreservation of living systems aims to maintain the viability and functionality of these systems while storing them over long periods [1]. Controlled-rate cryopreservation allows the sample to cool at a cell-specific controlled rate to minimize cellular damage caused by the formation of intracellular ice formation [2], and excessive dehydration. This method depends on several parameters, such as the utilization of a specific cryopreservation agent (permeating or non-permeating cryoprotective agents (CPAs) as well as single or combined CPA solutions), CPA loading duration, temperature ramp, addition of chemical factors [3], or the use of protective biomaterials [4]. The optimization of each of these parameters depends on the cell type as well as the organization of the cells.

The aim of this project was to use controlled rate freezing technologies in order to overcome technical obstacles related to inter-batch viability and create a ready to use *in vitro* liver model for toxicological studies.

Methods: HepaRG cell line was encapsulated with alginate serving as a cryoprotectant at a concentration of 1.E6 cells/mL of alginate. The samples were divided into two groups : one group undergoing conventional cryopreservation consisting of addition of CPA agent, 15 minutes of equilibration time at 4°C prior to 24H at -80°C into cell freezing container and transfer into nitrogen tank for long storage. The second group underwent controlled-rate freezing, following the same protocol as the first group, except using CryoMed™, allowing the sample to cool at a rate of -0.3°C/min until reaching -80°C. Five different CPA agents were used in order to compare the effects of CPA on cell activity. Metabolic assays were conducted on the samples prior to cryopreservation and after thawing.

Results and Discussion: Results of cell activity on encapsulated HepaRG reported comparing global cell activity (Figure 1) as well as CYP activity depending on the cryopreservation technique and the CPA used.

Conclusion: Samples undergoing controlled rate freezing presents better cell metabolism compared to conventional cryopreservation regardless of the choice of CPA used. The choice of CPA used thus has an impact on different metabolism (data not shown). Depending on the metabolism of interest, the choice of CPA used is also a parameter to optimize.

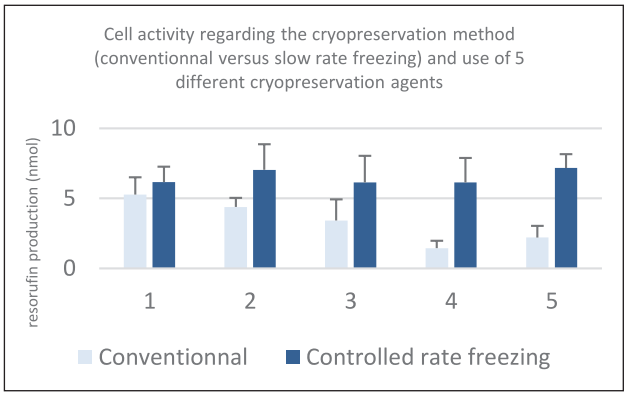

Figure 2. Mesured resorufin production witnessing cell activity by PrestoBlue™ Assay. Two conditions were tested, conventional cryopreservation (light blue), and controlled rate freezing (dark blue).

This study will be extended to other cell line (IPSC-derived liver cells) and cell types (stellate cells, LSECs) as well as several cooling rates will be tested in order to optimize the best cryopreservation program for each cell type.

References

1. Peter Mazur, Cryobiology, 1970
2. Ware, *et al*, Biotechniques 879-80, 882-3, 2005
3. Inui *et al*, PloS One, *18*(5), e0285783, 2023
4. Kilbride *et al.,* Tissue Engineering Part C Methods, 23(8), 455–464, 2017

Acknowledgements

We thank the Pr.Sakai and the Pr.Nishikawa for their welcome in the Sakai-Nishikawa laboratory and their collaboration. This work was supported half by DOT Chair and Université de Technologie de Compiègne (1/2) and Région des Hauts-de-France (1/2).

DEVELOPMENT OF MINIMALLY INVASIVE IMPLANTABLE AUTOLOGOUS TISSUE-ENGINEERED HERAT VALVE FOR CONGENITAL HEART DISEASE

Yasushi Sato (1), Yusuke Inoue (1), Takeshi Terazawa (1), Tomoki Nagayoshi (1), Kazuto Fujimoto (2), Isao Shiraishi (2), Ken Takamatsu (3), Kunio Ohta (3), Yoshiaki Takewa (1)

1. Advanced Medical Engineering Research Center, Asahikawa Medical University, Japan; 2. Department of Pediatric Cardiology, National Cerebral and Cardiovascular Center, Japan; 3. Tamachi Industries Co. Ltd., Japan

Objective: In congenital heart disease (CHD), such as tetralogy of Fallot, artificial materials are commonly used to reconstruct blood vessels and heart valves. However, these materials deteriorate over time and often fail to function within a few years after surgery. As a result, patients who undergo heart valve surgery in childhood for CHD often require multiple reoperations, highlighting the need for alternative approaches to reduce the risks associated with open heart surgery. In this situation, transcatheter valve implantation has emerged as the preferred option. Our study focuses on the development of an autologous tissue-engineered prosthetic heart valve, named Biovalve, utilizing an “in body tissue architecture” approach [1, 2]. In this approach, a tissue-forming mold is implanted subcutaneously, and the connective tissue that forms around the mold serves as the implantation material. Biovalve is an autologous collagen tissue with high biocompatibility and tissue regeneration potential [3]. It is promising for CHD patients due to its potential for tissue regeneration and long-term valve function, offering a viable alternative to multiple surgical procedures. This study aims to develop Biovalves equipped with self-expandable stents, implant them in large animals using a transcatheter technique, and evaluate both their valve function and tissue structure.

Methods: We utilized 3D printed plastic molds in conjunction with shape memory alloy stents, embedding them subcutaneously in goats. Following a period of 2-3 months, the molds were extracted along with the surrounding tissue. By removing the plastic components, we isolated heart valve-like tissues composed of autologous connective tissue (Biovalves) with integrated stents. Subsequently, the stent Biovalve was inserted into a delivery catheter and implanted into a goat pulmonary valve through the right ventricular apex.

Results: Using a mold encapsulating the stent, we obtained a stent-integrated Biovalve in which the stent was covered with autologous

tissue. Both the stents and Biovalve tissues exhibited strong adherence and remained securely in place even under crimping conditions. The Biovalves were successfully implanted with minimal complications, showing no significant stenosis or regurgitation. Despite the absence of anticoagulation therapy post-implantation, there were no findings of thrombosis. After 6 months of implantation, the Biovalve was harvested, and the valve leaflets had retained their morphology, with no thrombi observed on their surfaces. Furthermore, the Biovalves were integrated with the surrounding tissue. Histological examination revealed a gradual migration of host cells into the Biovalve tissue, indicating ongoing tissue remodeling.

Conclusions: The Biovalve with a stent can be implanted with minimal invasiveness, offering the potential for long-term functionality due to tissue regeneration post-implantation. This innovation holds promise for the treatment of CHD and presents an attractive alternative to traditional surgical interventions.

References

1. Hayashida et al, J Thorac Cardiovasc Surg, 134:152–9, 2007.
2. Nakayama et al, J Biomed Mater Res B, 103:1–11, 2015.
3. Takewa et al, ASAIO Journal, 64:395-405, 2018.

Acknowledgments

This research was supported by AMED under Grant Number JP23he0422026.

UNRAVEL NOVEL MECHANISMS RESPONSIBLE FOR CKD INDUCED ENDOTHELIAL CELL DYSFUNCTION

Sonja Vondenhoff[1,2], Tobias Henning[1], Sarah Knapp[1], Constance Baaten[1,2], Heidi Noels[1,2]

1. Institute for Molecular Cardiovascular Research (IMCAR), University Hospital RWTH Aachen, Germany; 2. Department of Biochemistry, Cardiovascular Research Institute Maastricht (CARIM), Maastricht University, the Netherlands

Introduction: The endothelial layer plays an important role in vascular integrity and cardiovascular health. Chronic kidney disease (CKD) disturbs endothelial hemostasis due to the present low-grade inflammation and uremic environment. The endothelium of CKD patients therefore reflects a vasoconstrictive, pro-inflammatory, pro-atherosclerotic as well as a prothrombotic endothelial phenotype [1-2]. To which extent CKD affects the crosstalk between endothelium and immune cells is not fully understood and requires further investigation in order to ultimately reduce the thrombotic and hemorrhagic risk of CKD patients. Therefore, we aim to reveal molecular mechanisms responsible for the increased thrombotic risk in CKD patients by elucidating the disturbed crosstalk between endothelium, platelets, and neutrophils.

Methods: For the experiments three different endothelial cell types were used: human aortic endothelial cells (HAoECs), human dermal microvascular endothelial cells (HDMECs) and human coronary artery endothelial cells (HCAECs). Cells were cultured under static conditions or under flow with a mixture of seven out of twenty uremic toxins with the highest fold increase in CKD 5 patients on dialysis (data is based on the EUTOX data base). The mixture contained Phenylacetic acid, Hippuric acid, Indoxylsulfate, Kynurenic acid, Para-cresyl-sulfate, Methylguanidine and Guanidinosuccinic acid. In the first step essential intracellular processes were analyzed to determine the extent of induced endothelial cell dysfunction. With a special regard on the metabolic activity and processes linked to the cellular metabolism like autophagy, endoplasmic reticulum stress and ROS production, as readouts qPCR and Western Blot were performed.

In the second step, the cultivation of endothelial cells under flow was established, and the confluency of the endothelial cell layer was analyzed using VE-Cadherin immunofluorescent staining.

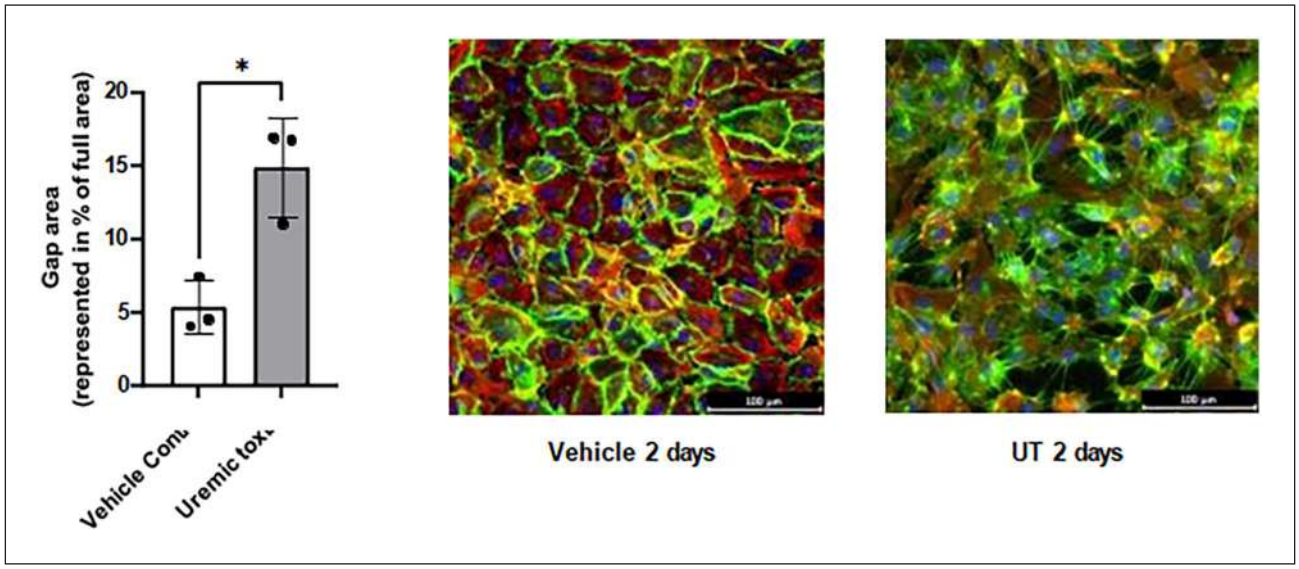

Figure 1. Uremic toxins induce endothelial cell dysfunction by influencing the endothelial cell-cell contact. Data shown as mean ± SD, n=3, using unpaired t-test with Welch's correction (* $p<0.05$).

Results: A decreased metabolic activity in HAoECs and HDMECs was observed after 5 days of treatment which was not due to increased cell death.

The analysis of cellular processes linked to decreased metabolic activity revealed an impaired autophagic flux upon uremic toxins treatment. Furthermore, the combination of uremic toxins and TNFα lead to increased protein levels of NOX-2 being an important protein contributing to the cellular ROS production.

Moreover, we observed that the treatment of uremic toxins leads to morphological changes. Endothelial cells treated with uremic toxins under static conditions displayed dense cell clusters as well as enlarged and flattened cells. The treatment under flow with uremic toxins influenced the cell-cell contact leading to a significantly increased gap area between uremic endothelial compared to untreated cells.

Discussion: Our data showed that the usage of seven relevant uremic toxins leads to endothelial cell dysfunction characterized by a reduced metabolic activity, which is partly due to impaired autophagic flux, increased ROS production as well as decreased cell-cell communication. Currently RNAseq is ongoing to reveal new molecular targets that explain the disturbed interaction between neutrophils, platelets, and endothelial cells.

References

1. Constance C F M J Baaten et al, Circ Res., 14;132(8):970-992, 2023.
2. Sonja Vondenhoff et al, Herz., 49(2):95-104, 2024.

CONDITIONING OF LUNGS FROM GGTA1-KO PIGS APPLYING EX VIVO MACHINE PERFUSION

Robert Ramm (1,2); Klaus Hoeffler (1,2); Nathalie Roters (1,2); Philipp Felgendreff (3); Joerg Mengwasser (3); Saleh Tavil (1); Akylbek Saipbaev (1); Wilfried Kues (4); Patrick Zardo (1,2); Arjang Ruhparwar (1,2); Tobias Goecke (1,2)

1. Hannover Medical School, Department for Cardiac, Thoracic, Transplantation and Vascular Surgery, Hannover, Germany; 2. Lower Saxony Centre for Biomedical Engineering, Implant Research and Development, Hannover, Germany; 3. Hannover Medical School, Department for General, Visceral and Transplant Surgery, Hannover, Germany; 4. Federal Research Institute for Animal Health, Neustadt, Germany

Introduction: Despite considerable progress, artificial devices like ECMO can keep patients alive, but are not suited as destination therapy for patients suffering from end stage lung disease. Allogeneic lung transplantation is still the best therapeutic option, but due to shortage of human donor lungs, not all patients in need can be treated.

Therefore, novel destination therapies for lung failure are needed such as the use of pig lungs for xenotransplantation purposes.

In this study, lungs from genetically modified pigs were used in order to establish an *ex vivo* lung perfusion (EVLP) protocol that will allow the conditioning of lungs in future xenotransplantation experiments.

Methods: Four GGTA1-KO pigs were used for lung retrieval after euthanasia (DCD) and flushed with ice cold Perfadex Plus solution according to standard procedure. After cold storage of 2 hours lungs were hooked to a clinically approved EVLP system primed with Steen solution. After establishing the perfusion, lungs were warmed and ventilated. After 2 hours of perfusion human erythrocytes were added to the system for further 15 minutes of perfusion.

Results: We found that lung retrieval without anticoagulation treatment of the donor is feasible and all four GGTA1-KO pig lungs exhibited very good performance during 2 hours of perfusion with Steen solution. However, the addition of human erythrocytes caused a stark increase in pulmonary resistance, which normalized after further 15 to 20 minutes of perfusion. After perfusion with human erythrocytes the lungs became edematous.

Conclusion: *Ex vivo* perfusion of genetically pig lungs using a clinically approved system and solutions is feasible, ever after DCD, and can be used as model to study and improve the interaction with human blood components.

Acknowledgements

This work was supported by grant CORE 100 from the Ministry for Science and Culture of Lower Saxony, coordinated from the Hannover Medical School Transplant Center.

PREVENTION OF PUMP THROMBUS USING CIRCULAR VIBRATION OF MAGLEV IMPELLER —OPTIMIZATION OF VIBRATION CONDITION—

Wataru Hijikata (1), Kohei Hatakenaka (1), Tatsuki Fujiwara (2), Hironobu Sakurai (2), Tomoyuki Fujita (2), Katsuhiro Ohuchi (3), Yusuke Inoue (4)

1. Department of Mechanical Engineering, Tokyo Institute of Technology, Japan; 2. Department of Cardiovascular Surgery, Tokyo Medical and Dental University, Japan; 3. Department of Clinical Engineering, Juntendo University, Japan; 4. Advanced Medical Engineering Research Center, Asahikawa Medical University, Japan

Introduction: Centrifugal blood pumps used in extracorporeal membrane oxygenation (ECMO) as well as ventricular assist devices (VADs) are composed of engineering materials and have a risk of thrombus when blood has contact with their material surface. Although pump geometries based on fluid dynamics, biocompatible materials, and anti-thrombogenic coatings have been developed, complete anticoagulation-free prevention of thrombosis has not yet been achieved. To solve this issue, we have developed an anti-thrombogenic technology in which a magnetically levitated (maglev) impeller is vibrated in orbital motion to inhibit adhesion of blood components to the impeller surface [1]-[3]. This technology can be used in combination with above-mentioned conventional anti-thrombogenic technologies and is expected to reduce the use of anticoagulants. In this study, we conducted in vitro experiments to determine the optimum vibration conditions for preventing pump thrombus.

Methods: Two maglev centrifugal blood pumps [4] are connected in parallel to a mock circulatory loop consisting of a reservoir and a flow resistance, and filled with porcine blood anticoagulated with heparin. One pump was operated without circular vibration, and the other was operated with vibration of an amplitude A of 5 μm to 30 μm and a frequency f of 70 Hz to 280 Hz. The experiments were conducted twice under all vibration conditions. The 10 points marked on the impeller surface were photographed using a microscope before and after the experiment, and the brightness was set to a threshold value so that the areas of adhesion of blood components were black and the areas exposed on the impeller surface were white. The blood adhesion prevention rate (*BAPR*) was calculated using *Sw/o* (areas of blood components adhered without vibration) and *Sw/* (areas of blood components adhered with vibration) by the following equation.

$$BAPR = (Sw/o - Sw/) / Sw/o \quad (1)$$

Results: The experimental results showed that either the larger amplitude A or the higher frequency f of the vibration increased *BAPR*. Physically, the inhibition of blood adhesion is thought to be due to a change in the shear

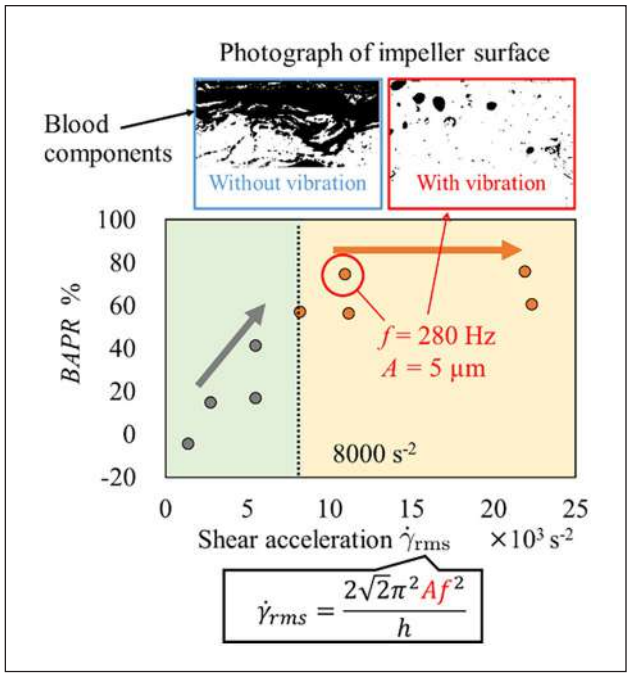

Figure 1. BAPR against shear acceleration generated by maglev impeller vibration. High BAPR was achieved when the shear acceleration was higher than 8000 s^{-2}.

rate acting between the material surface and the blood. As shown in Figure 1, the relationship between the "shear acceleration" (the rate of change of shear rate), which can be expressed as a function of *A* and *f*, and *BAPR* was investigated. The results show that regardless of the values of *A* and *f* separately, a high *BAPR* was obtained when the shear acceleration exceeds 8000 s^{-2}.

Discussion: Shear acceleration of 8000 s^{-2} or higher was identified as a vibration parameter that can achieve a high *BAPR*. This result suggests that not only blood pumps but also any material in contact with blood can be subjected to a certain level of microvibration from the viewpoint of "shear acceleration" to prevent blood adhesion. The outcome is also considered to be a highly versatile result.

References

1. K. Hatakenaka et al, Artif Organs, 47:425-431, 2023.
2. W. Hijikata et al, Artif Organs, 44:596-603, 2020.
3. T. Murashige et al, Artif Organs, 43:849-859, 2019.
4. W. Hijikata et al, Artif Organs, 32:351-540, 2008.

Acknowledgements

This work was supported by JSPE KAKENHI JP 23H00157.

THE EFFECT OF SELECTED ANTIOXIDANTS ON PRODUCTION OF REACTIVE OXYGEN SPECIES BY HUVECS CULTURED *IN VITRO*.

Piotr Ladyzynski (1), Anna Ciechnowska (1), Stanislawa Sabalinska (1)

Nalecz Institute of Biocybernetics and Biomedical Engineering, Poland

Introduction: High concentrations of glucose can lead to endothelial dysfunction, partly due to increased production of reactive oxygen species (ROS) by endothelial cells [1]. This dysfunction may potentially be counteracted by administering antioxidant therapy [2]. Understanding this mechanism underscores the importance of managing glucose levels effectively to maintain endothelial health. In studying endothelial cell behavior *in vivo*, a common approach involves using *in vitro* cultures of the human umbilical vein endothelial cells (HUVECs) as a model system [3].

The aim of this work was to assess the impact of selected antioxidants on ROS production by HUVECs culture *in vitro* under static conditions.

Methods: HUVECs were isolated from umbilical veins obtained by Caesarean section. Cells after the second passage were cultured in the modified M199 medium with normal (5 mM) or high (30 mM) glucose levels, along with three antioxidants: Rutin (100 mM), Coenzyme Q10 (10 mM) or Vitamin C (100 mM). Cultures in 6 replicates have been conducted in an incubator under standard conditions (temp. 37°C, humidified atmosphere with 5% CO2). ROS levels were measured after 7 and 14 days using flow cytometry and the DCFH-DA assay. ROS production is expressed with respect to ROS levels in reference cultures without the addition of any antioxidant.

Results: Figure 1 shows the relative ROS production by HUVECs cultured for 7 and 14 days in the medium with selected antioxidants and normal glucose concentration.

In cultures with normal glucose level, none of the antioxidants reduced ROS production after 7 days, but after 14 days, Rutin significantly decreased ROS levels (1.4-fold).

Figure 2 shows the relative ROS production by HUVECs cultured for 7 and 14 days in the medium with selected antioxidants and high glucose concentration.

In cultures with high glucose level, Coenzyme Q10 and Vitamin C were the most effective antioxidants in reducing ROS levels after 7 and 14 days, respectively. The most significant decrease of ROS levels was observed in cultures with Vitamin C after 14 days (2.5-fold).

Discussion: Our findings demonstrate that the effectiveness of antioxidants in modulating ROS production by HUVECs varies depending on the antioxidant, glucose concentration, and culture duration.

These results underscore the complexity of antioxidant-ROS interactions and emphasize the importance of considering multiple factors during *in vitro* studies.

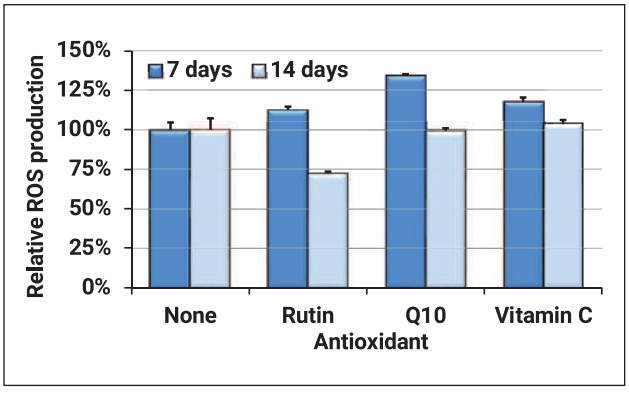

Figure 1. Relative ROS production (Mean ± SD) by HUVECs cultured for 7 and 14 days in the medium with normal glucose level and selected antioxidants.

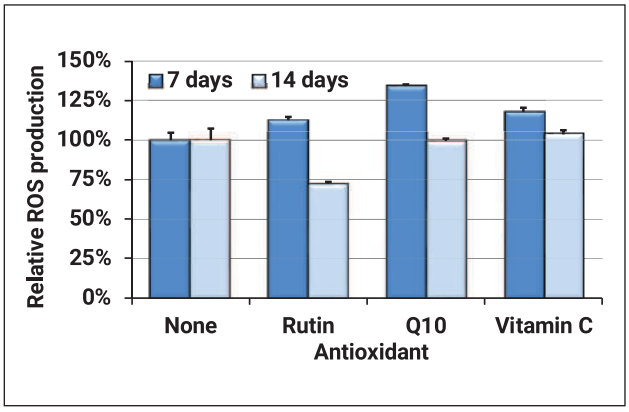

Figure 2. Relative ROS production (Mean ± SD) by HUVECs cultured for 7 and 14 days in the medium with high glucose level and selected antioxidants.

References

1. An Y et al, Cardiovasc Diabetol, 22:237, 2023.
2. González P et al, Int J Mol Sci, 24:9352, 2023.
3. Ciechanowska A et al, Biocybern Biomed Eng, 41:1390-1405, 2021.

Acknowledgements

This work was supported by grant no. 2017/27/B/ST7/00269 from the National Science Centre, Poland.

INDOXYL SULFATE CLEARANCE RISES WITH TEMPERATURE: BUT IS THERE A HYSTERESIS EFFECT?

João Brás (1), Fokko Wieringa (1,2), Emma Sünnen (1), Jeroen Vollenbroek (1,2,3), Karin Gerritsen (1)

1. Department of Nephrology and Hypertension, University Medical Centre Utrecht, Utrecht, The Netherlands; 2. IMEC, Holst Centre, 5656 AE Eindhoven, The Netherlands; 3. BIOS Lab on a Chip Group, MESA + Institute, University of Twente, Hallenweg 15, 7522 NH Enschede, The Netherlands

Introduction: Current hemodialysis methods inefficiently remove protein-bound uremic toxins (PBUTs, which are strongly bound to plasma proteins like albumin) leading to complications such as cardiovascular disease and uremic syndrome. Several PBUT removal strategies are currently explored, such as the use of chemical displacers, adsorbents, increased ionic strength or pH variations [1], but still require more research before reaching clinical use. In this work, we investigated whether increased albumin temperature (up to 42°C) may improve Indoxyl Sulfate (IS) removal, as albumin-IS binding is known to be temperature dependent (higher temperatures lead to lower bound fractions) [2].

Methods: Fig. 1 shows the used setup, where caprylate-stabilized, isotonic infusible albumin solution (40g/L) was spiked with IS (60µM) and dialyzed (Polyflux 2H) against fresh bicarbonate dialysate (Dirinco BV). Both dialysate and albumin solutions were recirculated throughout the test. Real-time dialysate IS concentration was measured with an in-line fluorescence sensor (OptoFluid Tech., Estonia). After 30 mins stabilization, dialysate IS levels reached equilibrium, after which temperature was stepwise increased and then decreased (Fig. 2).

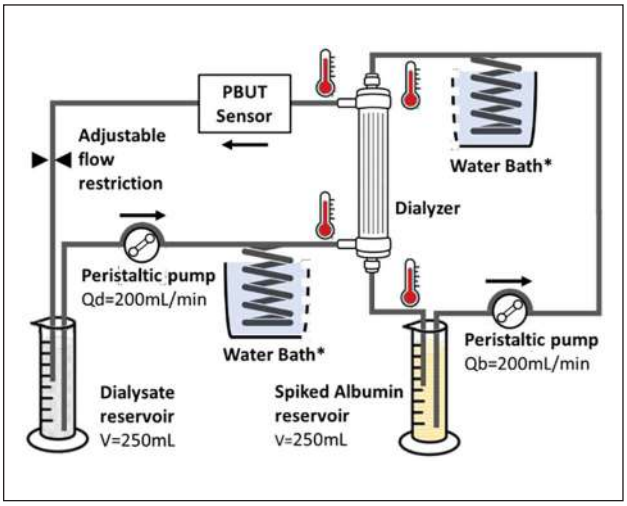

Figure 1. Experimental setup. Qd = dialysate flow; Qb = albumin flow. *One water bath held both coils. We drew both coils separately for circuit clarity.

Both solutions were heated by coiled tubing sections in the *same* water bath. Thermocouples monitored all 4 dialyzer connectors. Free IS fractions were derived from the PBUT sensor readings using Eq. 1:

$$\text{Free Fraction}_{IS} = \frac{C_{IS,free}}{C_{IS,total}} \quad (1)$$

Where: CIS,free is 2x the sensor reading with the system in equilibrium, and CIS,total was determined with HPLC.

Results:

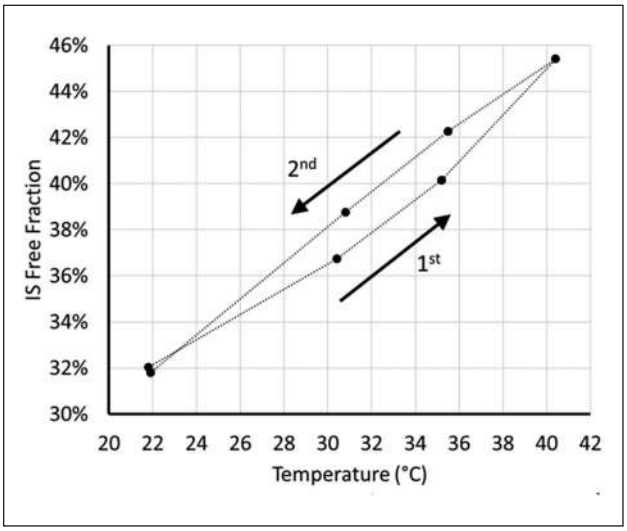

Figure 2. Effect of increasing (1st) and decreasing (2nd) temperature on Indoxyl Sulfate free fraction.

Discussion: Temperature-enhanced PBUT removal works and might be desirable because it doesn't break circuit sterility, is reversible and looks technically combinable with current HD machines. However, our results reveal a peculiar hysteresis-like behavior with a convex/concave shape

which we'd like to discuss during the ESAO ALBUNET session. Existing literature is scarce and suggests a linear behavior (but based at just 3 temperatures) [2]. We present work-in-progress. More research, with repetitive temperature cycles, seems needed regarding the -here observed -"hysteresis-like" effect, as well as regarding long-term blood integrity, maximum safe blood temperature and other possible side effects.

References

1. Sánchez-Ospina D. et al, J. Clin. Med, 13:1428, 2024.
2. Deltombe O. et al, Anal. Methods, 9:1935-1940, 2017.

Acknowledgements

We thank the ALBUNET group for their advice regarding the use of albumin in this work.
This project was funded by a KidneyX Artificial Kidney Prize (project name: MI-TRAM).

VASOCONSTRICTION INHIBITING FACTOR: AN ENDOGENOUS NEW CALCIMIMETIC OF THE CALCIUM-SENSING RECEPTOR THAT INHIBITS VASCULAR CALCIFICATION

Sofia de la Puente Secades (1,2), Dustin Mikolajetz (1), Nathalie Gayrard (3), Juliane Hermann (1), Vera Jankowski (1), Khaleda Alghamdi (4), Àngel Argilés Ciscart (3), Turgay Saritas (5), Leon Schurgers (2), Donald Ward (4), Joachim Jankowski (1,2), Setareh Orth-Alampour (1)

1. Institute for Molecular Cardiovascular Research (IMCAR), University Hospital RWTH Aachen, Germany; 2. Cardiovascular Research Institute (CARIM), Maastricht, the Netherlands; 3. INSERM, Montpellier, France; 4. Institute for Collaborative Research on Ageing, Manchester, United Kingdom; 5. Division of Nephrology and Clinical Immunology, University Hospital RWTH Aachen, Germany

Introduction: Patients with chronic kidney disease (CKD), have an increased risk of cardiovascular disease due to the massively accelerated calcification they develop [1]. Vascular calcification is a highly regulated process mediated by different inducers and inhibitors [2]. The peptide 'vasoconstriction inhibiting factor' (VIF) was recently discovered and described as an inhibitor of the angiotensin II-induced vasoconstriction [3]. Angiotensin II inhibits calcium deposition [4], but VIF effect on vascular calcification is still unknown.

Methods: The effect of VIF was analysed *in vitro* in human aortic smooth muscle cells (hAoSMCs) and *ex vivo* in rat aortic rings, both cultivated under high phosphate concentrations. VIF was also studied *in vivo* in rats treated with vitamin D and nicotine (VDN) as calcification model. HEK-293 cells overexpressing calcium-sensing receptor were used for the study of VIF receptor.

Results: VIF inhibits calcium deposition in all the models studied. Furthermore, in hAoSMC VIF reduces the production of ROS and the initiation of diverse cascades in the cells, like activation of inflammatory cytokines and MAPK kinases, which in turn trigger the expression of various genes involved in the development of vascular calcification. Furthermore, in presence of VIF the population of apoptotic cells, directly linked to vascular calcification, is decreased. Calcium-sensing receptor (CaSR) has been found as VIF binding partner. The production of the calcification inhibitor, carboxy-Matrix Gla Proteins (cMGP) is increased when VIF is given to hAoSMCs and VDN rats. Moreover, CKD patients with extensive calcification show negative correlation between calcification score and VIF concentration

Discussion: VIF is a new potent endogenous inhibitor of vascular calcification that acts as a calcimimetic of the CaSR, leading to an increase production of cMGP. This finding represents a basis for a new target for the prevention and therapy of patients with increased vascular calcification and shows an encouraging perspective for the future.

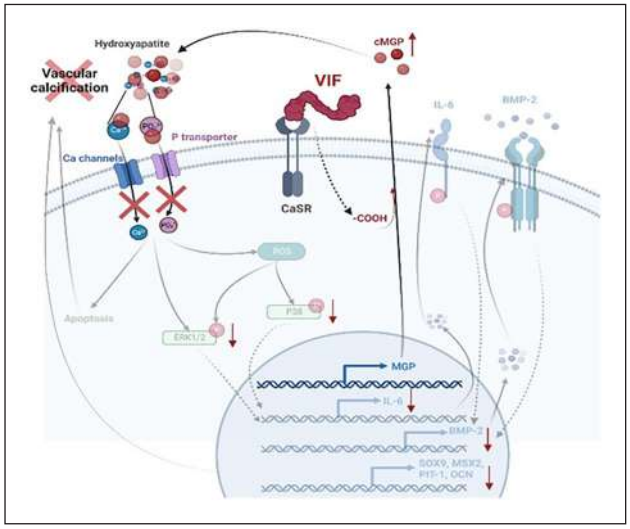

Figure 1. The VIF peptide mechanism to inhibit vascular calcification: When the VIF peptide is added to calcified environment, it acts as a calcimimetic of CaSR and increases cMGP production, which after binding to the hydroxyapatite crystal, reduce calcium influx andt inhibits the activation of calcification pathways (ROS production, kinase activation secretion of inflammatory cytokines, activation of calcification-related genes and apoptosis).

References

1. Chen J et al, JAMA Cardiol 2:635-643, 2017.
2. Lee SJ et al, Int J Mol Sci 21, 2020.
3. Salem S et al, Circulation 131:1426-1434, 2015.
4. Herencia et al, Eur J Clin Invest 45:1129-1144, 2015

Acknowledgements

This work was supported by a grant from the German Research Foundation (DFG, SFB/TRR219 project C-04, the European Union's Horizon 2020 research and innovation program EU-ITN CaReSyAn (764474).

MINIPUMP – INVESTIGATING THE BOUNDARIES OF CONVENTIONAL ROTARY PUMP DESIGN

Lars Fischer (1), Florian Huber (1), Ulrich Steinseifer(1), Lasse Strudthoff (1), Michael Neidlin (1)

1. Department of Cardiovascular Engineering, Institute of Applied Medical Engineering, Medical Faculty, RWTH Aachen University

Introduction: Blood pumps are designed and optimized for a static target operation condition; in that an optimum in efficiency and hemocompatibility is achieved [1,2]. Off-design operation is associated with decreased performance and elevated risk of adverse events [3-4].

Depending on application, low flow rates combined with high pressure heads are required— as present in rodent sized or neonatal extracorporeal life support circuits [5,6]. According to literature, such operation conditions necessitate non-rotary pump designs that are not appropriate for blood pumps [1,2]. Therefore, this study investigates the applicability and boundaries of conventional rotary pump design methodologies for a target operation condition of Q = 70 mL/min and Δp = 115 mmHg, for flow rate and pressure difference, respectively.

Methods: A conventional design approach based on a combination of analytical turbomachinery equations and empirical correlations as described by [1,2] was used for calculation of initial pump dimensions. Additional design requirements encompass in-house manufacturability, low priming volume, bearing's long-term stability, magnetic propulsion, connectivity to 3/16" tubing, and the presence of washout holes to mitigate blood stagnation. Computational fluid dynamics was utilized for design optimization. An in-house manufactured pump head was analyzed for its hydraulic performance and compared to a commercial blood pump. The testing circuit is displayed in Figure 1.

Results: The MiniPump's priming volume is 5.4 mL, 56.1% smaller than the Deltastream DP3 rotary blood pump. Figure 2 shows the HQ-curves of the initial, and optimized MiniPump design, compared to a DP3 as reference. Conventionally calculated initial dimensions failed to meet the performance requirements.

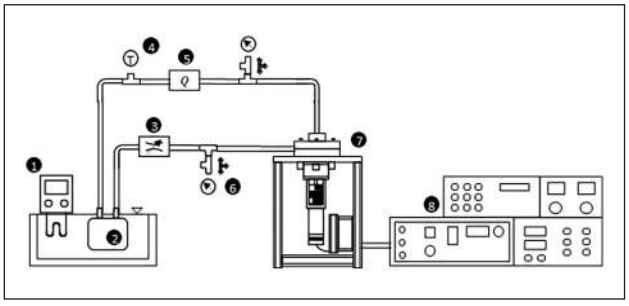

Figure 1. 1) tempered water bath, 2) flexible reservoir, clamp, 4) temperature sensor, 5) flow sensor, 6) pressure sensor, 7) pump head, and 8) data acquisition.

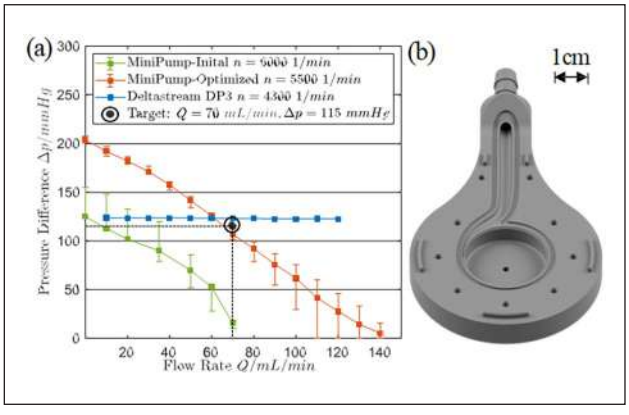

Figure 2. NHQ-curves (a), MiniPump lower housing (b). Computational optimization and adjustment lead to a suitable design, satisfying targeted requirements. The key design parameters are presented in Table 1.

Table 1. MiniPump's key design parameters.

Parameter	Unit	Initial	Optimized
Blade number	N/A	10	6
Inner diameter	mm	2	2.4
Outer diameter	mm	17,5	25
Blade inlet angle	deg	40	36
Blade outlet angle	deg	21,3	24.5
Blade width	mm	0,45	0.6

Discussion: Conventional rotary pump design methodologies fail to provide appropriate design parameters for the targeted operation range. The presented results show that the optimized MiniPump achieves the desired hydraulic performance. In comparison, the throttled Deltastream DP3 shows lower sensitivity to flow rate variations. Future work will assess and evaluate the MiniPump's hemolysis potential in comparison to a DP3 pump.

References

1. Guelich et al., Springer, ISBN: 3642128238, 2010.
2. Stepanoff et al., Krieger Publishing, ISBN: 0894647237, 1992.
3. Hahne et al., ASAIO Journal, DOI: 10.1097/MAT.0000000000002181, 2024
4. Schöps et al., Journal of Translational Medicine, DOI: 10.1186/s12967-020-02599-z, 2021
5. Studthoff et al., Micromachines, DOI: 10.3390/mi14040800, 2023
6. Kiserud et al., Elsevier, DOI: 10.1016/B978-0-323-35214-7.00058-5, 2017

Acknowledgements

This work was supported by the German Research Foundation (DFG) SPP 2014 program. Computations were performed with computing resources granted by RWTH Aachen University under project rwth1611.

LAGRANGIAN HEMOLYSIS MODELING IN PATIENT-SPECIFIC AORTIC BLOOD FLOW ALTERED BY AORTIC VALVE STENOSIS

Tianai Wang[1], Christian Berwanger[1], Christine Quast[2], Florian Bönner[2], Malte Kelm[2,3], Teresa Lemainque[4], Ulrich Steinseifer[1], Michael Neidlin[1]

(1) Department of Cardiovascular Engineering, Institute of Applied Medical Engineering, Medical Faculty, RWTH Aachen University, Aachen, Germany, (2) Department of Cardiology, Pulmonary Diseases and Vascular Medicine, Heinrich-Heine University, Düsseldorf, Germany, (3) CARID, Cardiovascular Research Institute Düsseldorf, Heinrich-Heine University, Düsseldorf, Germany, (4) Department of Diagnostic and Interventional Radiology, University Hospital RWTH Aachen, Germany

Introduction: The presence of aortic valve stenosis (AS) leads to an alteration of supravalvular flow patterns. These pathological hemodynamics are hypothesized to induce elevated membrane stresses on red blood cells (RBCs). In order to elucidate the time and location of highest damage induced by AS, a Lagrangian-based blood damage analysis, commonly carried out for blood-contacting medical devices, was implemented in patient-specific 4D Flow MRI-based CFD models for a group (n = 3) of healthy subjects and a group (n = 3) of patients suffering from severe AS.

Methods: Computational models of subject-specific aortic geometries were created using in-vivo medical imaging data. Temporally and spatially resolved boundary conditions taken from 4D Flow MRI measurements were implemented and particles seeded at the aortic orifice inlet throughout the cardiac cycle. After validating the in-silico results with the in-vivo measurements, the occurring RBC damage was quantified for both the pathological and physiological flows using established Lagrangian power-law formulations. Here, the acting shear stresses on individual particle tracks representing the movement of RBCs through the aortic arch were integrated over time. These insights were used to determine the extent and hemodynamic cause of flow-induced cell damage in AS.

Results: The overall feasibility of the 4D Flow MRI-based CFD simulation was proven with excellent agreement between the in-vivo and in-silico velocity fields on cross-sectional planes throughout the aortic arch and an overall correlation coefficient R^2 of 0.9 (Figure 1).

The subsequent hemolysis analysis showed elevated exposure times and shear stress values on RBCs in the AS cohort, compared to the healthy group. This also resulted in higher hemolysis values, as shown in Figure 2.

Further, the mean exposure time of erythrocytes in physiological aortic flow is marked in red, as reference. This underlines the longer exposure times of RBCs during AS caused by highly disturbed blood flow.

Finally, the time and location of highest damage were identified to occur during late systole/deceleration, in the pathological turbulent flow regions within the bulk flow of the ascending aorta.

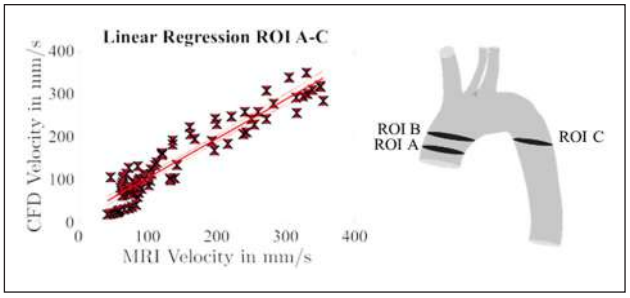

Figure 1. Linear correlation between MRI and CFD velocities on ROI A-C for an AS case.

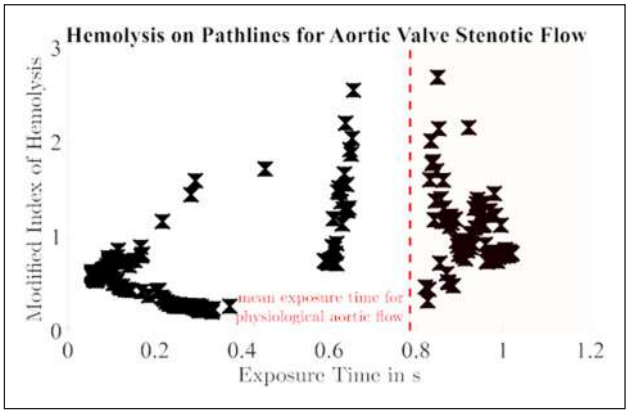

Figure 2. Hemolysis values for a selection of aortic stenotic pathlines and their corresponding exposure duration. The index of hemolysis is multiplied by 10e7 to aid the visualization (MIH).

Discussion: In summary, a methodology to generate a 4D Flow MRI-based numerical fluid simulation model of AS flow within the aortic arch was developed and validated. Turbulent flow features within the free stream of the decelerating ascending aortic jet have been identified as the most prominent contributors towards RBC damage. Future work will validate the results in a larger cohort size and investigate the potential restoration of physiological flow structures through clinical interventions.

Acknowledgements

This study was funded by Studienstiftung des Deutschen Volkes (PhD Fellowship, German Academic Scholarship Foundation).

AUTOMATIC HEART DISEASE PREDICTION USING MODAL DECOMPOSITION AND MASKED AUTOENCODERS FOR LIMITED ECHOCARDIOGRAPHY DATABASES

Andrés Bell-Navas (1), Nourelhouda Groun (1, 2), María Villalba-Orero (3, 4), Enrique Lara-Pezzi (3), Jesús Garicano-Mena (1, 5), Soledad Le Clainche (1, 5)

1. ETSI Aeronáutica y del Espacio, Universidad Politécnica de Madrid, 28040, Madrid, Spain; 2. ETSI Telecomunicación, Universidad Politécnica de Madrid, 28040, Madrid, Spain; 3. Centro Nacional de Investigaciones Cardiovasculares (CNIC), 28029, Madrid, Spain; 4. Facultad de Veterinaria – Universidad Complutense de Madrid, 28040, Madrid, Spain; 5. Center for Computational Simulation (CCS), 28660, Boadilla del Monte, Spain

Introduction: Heart diseases constitute the main cause of international human defunction (around 18 million deaths per year [1]). Also considering the increase of available medical data, much pressure is therefore put on the health industry to develop systems for early and accurate heart disease recognition. This has motivated the development of several deep learning frameworks, mainly employing echocardiography data. However, the majority of approaches are based on Convolutional Neural Networks (CNNs). In addition, these systems typically handle a single disease, or a closely related family of them [2].

Methods: In this contribution, an automatic system based on a novel deep learning framework which analyzes echocardiography videos in real time is proposed. This system addresses two related tasks. The first one is the prediction of the time in which a heart failure happens. The second task involves the heart disease recognition. The system is composed of two stages. The first one is aimed to create a large database from different sources of echocardiography videos. This allows the training of machine learning-based frameworks, including deep learning algorithms. This stage also includes the use of the Higher Order Dynamic Mode Decomposition (HODMD) algorithm [3], for the first time to the authors' knowledge in the medical field [4] for both data augmentation and feature extraction. The second stage builds and trains a Masked Autoencoder (MAE), adapted for an effective training from scratch, even with limited databases. This designed MAE analyzes the images from an echocardiography video to automatically estimate the heart state. In addition, it also estimates the time in which a heart failure will happen.

Results: Table 1 shows the estimation time performance using Vision Transformers (ViTs), the proposed MAE, and the impact of the HODMD algorithm. The proposed MAE achieves the best results, with a lower estimation error. In addition, the HODMD algorithm further improves performance, demonstrating its potential for data augmentation and feature extraction.

Table 1. Comparison of the estimation time performance.

Algorithm	HODMD included	Estimation error (months)	# Training images
ViT		5.44	31211
MAE		5.15	31211
MAE	×	4.65	74974

Discussion: The results demonstrate that the proposed system is superior and the HODMD algorithm effective for the prediction of the time of heart failures.

References

1. World Health Organization, Cardiovascular Diseases (CVDs), https://www.who.int/news-room/fact-sheets/detail/cardiovascular-diseases-(cvds), 1999.
2. Vafaeezadeh et al, CarpNet: Transformer for mitral valve disease classification in echocardiographic videos, Int. J. Imaging Syst. Technol., 33(5):1505-1514, 2023.
3. Le Clainche, S., & Vega, J. M., Higher order dynamic mode decomposition, SIADS, 16(2):882-925, 2017.
4. Groun et al, Higher Order Dynamic Mode decomposition: From fluid dynamics to heart disease analysis, Comput. Biol. Med., 144:105384, 2022.

Acknowledgements

This work was supported by Grant TED2021-129774B-C21 and by Grant PLEC2022-009235, funded by MCIN/AEI/10.13039/501100011033 and by the European Union "NextGenerationEU"/PRTR.

THE EMBOLESS® VENOUS CHAMBER EFFICIENTLY REDUCES AIR BUBBLES. A RANDOMIZED STUDY OF CHRONIC HEMODIALYSIS (HD) PATIENTS.

Ulf Forsberg (1), Per Jonsson (1), Bernd Stegmayr (1)

1. Umea University, Dept. Public Health and Clinical Medicine, Umea, Sweden

Introduction: When blood passes the extracorporeal circuit, air microbubbles (MBs) enter the patient and end up as microemboli in lung, heart, and brain [1]. The MB exposure has no medical purpose and is considered as bio-incompatibility. Selection of venous chambers with higher removal rate of MBs are warranted to reduce the risks with air bio-incompatibility. A previous in vitro comparison of four frequently used venous chambers in clinical practice showed the Fresenius 5008 (F5008) to best reduce contamination of MB [2].

The primary aim of this clinical study was to compare (F5008) and the Emboless® venous chambers (Fig 1) regarding the elimination of MBs in the return bloodline of chronic dialysis patients during hemodialysis (HD).

Methods: Twenty patients performed 80 sessions as cross-over hemodialysis randomized to half of each (40 pairs) using the F5008 versus the Emboless venous chamber bloodline. Eight of the patients also performed 32 study hemodiafiltrations (HDF). MBs were measured with an ultrasound device (within the size range 20-500µm) at the 'Inlet' and 'Outlet' bloodline of the venous chamber. The non-parametric Wilcoxon test pairwise compared percentage elimination of MBs between the two venous chambers. ClinicalTrials.gov (NCT06168539)

Results: Numerous MBs enter the Inlet line during 30 minutes of HD (Table 1). During HD, the median reduction of numbers of MBs between all size ranges in the Outlet versus the Inlet was 39% with the F5008 and 76% with the Emboless venous chambers (p<0.001). During HDF, the reduction was 28% with the F5008 and 70% with the Emboless (p<0.001).

Discussion and Conclusion: Fewer MBs and subsequently fewer microemboli entered the bloodline of the patients using the Emboless® compared to the Fresenius 5008 venous chamber during hemodialysis and during HDF. Venous chambers with higher removal rate of MBs will reduce the extent of air bio-incompatibility.

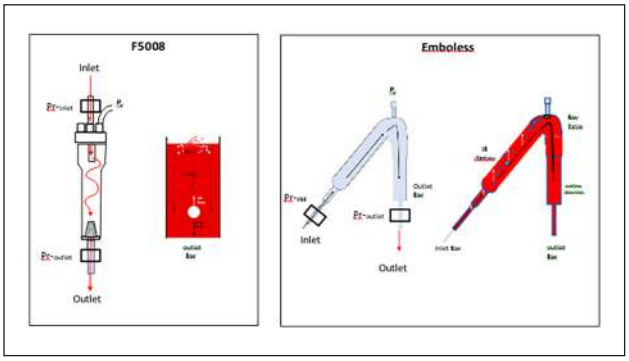

Figure 1. modified after Jonsson et al. [2]: Displayed to the left the blood flow through the F5008 and MB visualized in white with lift force versus drag force. To the right Emboless® with the blood flow from below the left side to the top, then turning downwards at the right side. The upward flow helps white MBs to rise to the top.

Table 1. Median (range) numbers of MBs/30 minutes of dialysis. MBs measured at the Inlet line of F5008 versus Emboless in 40 paired dialyses.

	HD-F5008	HD-Emboless	p-value
MBs Inlet/30min Each 40 pairs	2318 (250-18619)	2151 (362-39903)	0.657

Equations

$$\text{Change in MBs (\%)} = 100*(MB_{Outlet}-MB_{Inlet})/MB_{Inlet} \quad (1)$$

References

1. Forsberg U, Jonsson P, Stegmayr B (2023) Microemboli induced by air bubbles may be deposited in organs as a consequence of contamination during medical care. Clin Kidney J 16: 159-166. doi:10.1093/ckj/sfac217.
2. Jonsson P, Stegmayr C, Stegmayr B, Forsberg U (2023) Venous chambers in clinical use for hemodialysis have limited capacity to eliminate microbubbles from entering the return bloodline: An in vitro study. Artif Organs 47: 961-970. doi:10.1111/aor.14495.

Acknowledgements

We thank staff from the Clinical Trial Center at the University Hospital Umea for monitoring the study. This work was supported by grant from Vinnova and MedTech4Health Funding Agency.
Forsberg U, Jonsson P, Stegmayr B (2023) Microemboli induced by air bubbles may be deposited in organs as a consequence of contamination during medical care. Clin Kidney J 16: 159-166. doi:10.1093/ckj/sfac217.

Jonsson P, Stegmayr C, Stegmayr B, Forsberg U (2023) Venous chambers in clinical use for hemodialysis have limited capacity to eliminate microbubbles from entering the return bloodline: An in vitro study. Artif Organs 47: 961-970. doi:10.1111/aor.14495.

HEMOCOMPATIBILITY OF ROTODYNAMIC BLOOD PUMPS UNDER REALISTIC OPERATION CONDITIONS

Xiangyu He (1); Krishnaraj Narayanaswamy (1); Michael B. Fischer (2); Leonie Schmitt (1); Barbara Messner (1); Stefan Jakubek (3); Daniel Zimpfer (1); Marcus Granegger (1)

1. Christian Doppler Laboratory for Mechanical Circulatory Support, Department of Cardiac Surgery, Medical University of Vienna, Austria; 2. Department of Blood Group Serology and Transfusion Medicine, Medical University of Vienna, Vienna, Austria; 3. Division of Control and Process Automation, Institute of Mechanics and Mechatronics, TU Wien, Vienna, Austria.

Introduction: The operating conditions of rotodynamic blood pumps significantly influence in-vitro hemocompatibility of blood pumps in terms of the normalized index of hemolysis (NIH). Elevated NIH was observed at lower pump flow rates and higher pump speeds [1]. However, these in-vitro investigations were restricted to static pump flow conditions. Realistic pulsatile conditions in patients which may lead to periodic low flows or even flow reversal during the diastolic phase and high flows during the systolic phase of the cardiac cycle were not reflected in these in vitro setups [2]. The aim of this study was to determine hemolytic effects of realistic pulsatile operating conditions within the HeartMate 3 (HM3, Abbott Inc, Chicago, USA).

Methods: Pulsatile blood experiments were performed in a hybrid mock circulatory loop (HMCL) with citrated human blood from hemochromatosis patients. Briefly, the HMCL applies realistic simulated pressure waveforms to a running pump via a pneumatic-hydraulic interface [3]. For two pump speed settings (typical: 5600rpm and off-design: 4800rpm) with targeted mean flow rates of 4.3L/min and 2.5L/min, respectively, three different conditions were investigated: high pulsatile, low pulsatile and constant flow. Experiments were conducted for 12 hours with a change in operating condition every 4 hours. Delta free hemoglobin ($dfHb_{30min}$) and NIH were assessed every 30 minutes. In addition, blood cell counts were evaluated every hour.

Results: Six experiments were performed for each pump speed setting. The mean flow rate and pulsatile flow ranges are presented in Table 1. There was no significant difference of $dfHb_{30min}$ and NIH for the three conditions in both typical as well as off-design pump speed setting (Table 1). However, between the two pump speed settings, the differences in $dfHb_{30min}$ reached statistical significance (0.49±0.20 vs 0.69±0.24 mg/dL, p=0.01), with a trend towards higher NIH for the off-design pump setting (2.81±1.08 vs 2.19±0.72). Blood cell count remained stable over the course of the experiments.

Discussion: This study investigated the effects of pulsatile operating conditions on hemolysis at different pump speeds. The results demonstrated that at the same speed and same mean flow rate, the amplitude of flow pulsatility did not affect $dfHb_{30min}$ and NIH. Even periodic occurrences of low flow rates/flow reversals during diastole (with high statically determined NIH values) in the off-design condition did not significantly impact hemolysis. This finding can be explained by the fact that $dfHb_{30min}$ at each speed setting does not considerably change with flow rate, and NIH is calculated as the ratio between $dfHb_{30min}$ and mean flow rate, leading to similar results, almost independently from flow pulsatility.

A comparison of $dfHb_{30min}$ and NIH values for the two different pump speed settings revealed a significant difference in $dfHb_{30min}$ (higher in the typical speed setting) and NIH (higher in the off-design speed setting, which can be explained by the effect of different pump speeds ($dfHb_{30min}$) and residence times at lower flows (NIH). Further assessment for microparticles, vWf cleavage, and platelet activation is required to elucidate the impact of periodic pulsatile flow conditions on blood trauma and thrombogenicity.

Table 1. Mean flow rate and pulsatile flow range for three conditions of each pump setting together with the calculated NIH value (expressed as mean ± SD).

		Constant flow	Low pulsatile flow	High pulsatile flow
Typical pump setting 5600rpm	Mean flow (L/min)	4.27 ± 0.03	4.27 ± 0.03	4.29 ± 0.04
	Pulsatility range (L/min)	-	-5.03±0.03 - 3.75±0.03	2.68±0.15 - 6.57±0.31
	NIH (mg/100L)	2.35 ± 0.89	1.81 ± 0.51	2.40 ± 0.67
Off-designed pump setting 4800rpm	Mean flow (L/min)	2.38 ± 0.07	2.38 ± 0.02	2.51 ± 0.13
	Pulsatility range (L/min)	-	0.96±0.04 - 4.37±0.07	-0.38±0.17 -6.61±0.17
	NIH (mg/100L)	2.65 ± 2.03	2.55 ± 0.34	2.74 ± 1.61

References

1. Escher et al, IEEE Trans Biomed Eng, 69(8): 2423-2432, 2022.
2. Belkin et al, J Card Fail, 28(5): 845-862, 2022.
3. Bender et al, IEEE Trans Biomed Eng, Dec 22;PP, 2023.

Acknowledgement

The financial support by the Austrian Federal Ministry of Labour and Economy, the National Foundation for Research, Technology and Development and the Christian Doppler Research Association is gratefully acknowledged.

MIMICKING LIVER MICROENVIRONMENT IN A 3D IN VITRO MODEL: COLLAGEN HYDROGELS FUNCTIONALIZED WITH FIBRONECTIN

Estela Sanchez-Gonzalez (1,2), Manuel Salmeron-Sanchez (1,2,3), Gloria Gallego-Ferrer (1,2), Laia Tolosa (2,4)

1. Centre for Biomaterials and Tissue Engineering (CBIT), Universitat Politècnica de València, Valencia, Spain; 2. Biomedical Research Networking Center on Bioengineering, Biomaterials and Nanomedicine (CIBER-BBN), Valencia, Spain; 3. Centre for the Cellular Microenvironment, University of Glasgow, Glasgow, United Kingdom; 4. Experimental Hepatology Unit, Health Research Institute La Fe (IIS La Fe), Valencia, Spain.

Introduction: Current liver *in vitro* models exhibit numerous limitations and low similarity with the native organ, as they fail in the replication of the 3D microstructure and composition found *in vivo.* Therefore, the

design of three-dimensional (3D) models that mimic the liver matrix and cell-matrix interactions remains to be explored to finally unseat 2D cultures [1]. This study aims to address this gap by proposing a 3D culture platform for hepatic cells based on collagen (Col) hydrogels functionalized with fibronectin (FN). Our model is inspired in the natural matrix: collagen as the main component of the liver matrix and FN as an important biomolecule in cell-cell communication and hepatic cell differentiation [2,3,4]. The main objective of the study is to evaluate the role of FN in the culture of HepaRG cells by assessing the functionality of cells compared to 2D cultures (*Fig. 1*). The final goal will be to use the improved 3D system as a drug screening platform.

Methods: Mechanical and physicochemical characterization. Mechanical properties were determined by rheology and equilibrium water content was also calculated in Col and ColFN with different ratios to finally select the optimal one. Fibronectin was physically incorporated in hydrogels and its retention was assessed by ELISA.

HepaRG cells encapsulation and liver functionality. Cells were encapsulated in Col and ColFN hydrogels, differentiated using 1% of DMSO and compared to monolayers differentiated with the standard protocol (2% DMSO).

The effect of 3D culture on liver functionality was tested. LIVE/DEAD, albumin and urea production were evaluated. Changes in the gene expression of key hepatic markers were tested by qPCR and the expression of hepatic proteins (albumin) was checked by immunofluorescence.

Results: Hydrogels showed tailored mechanical properties with storage modulus values near the liver tissue (600 Pa) and fast gelation times (10 min). Col-FN hydrogels did not show significant changes in their properties. HepaRG cells were alive (90% viability) after 14 days of culture in 3D hydrogels and showed increased urea and albumin

production compared to the 2D. Gene expression revealed significant changes in the expression of genes coding for enzymes important in drug detoxification and liver-specific genes such as albumin in 3D compared to 2D. Encapsulated cells were organized in 3D clusters and expressed liver proteins such as albumin and factor HNF4a (*Fig. 1*).

Discussion: The results demonstrated that the 3D enhanced the liver functionality of encapsulated cells compared with the 2D in less time and DMSO concentration. These hydrogels could be considered as a 3D liver culture platform to replace conventional 2D models with significant potential to be explored.

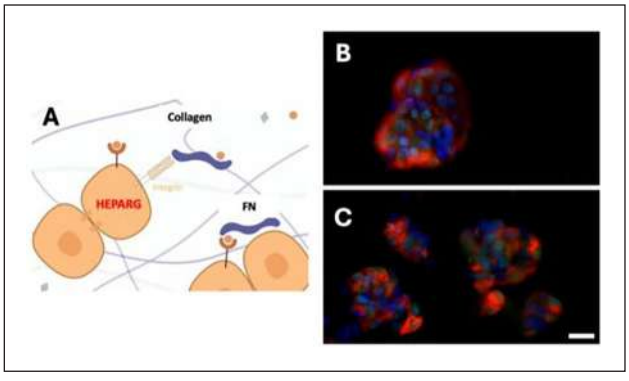

Figure 1. (A) Graphic scheme of the proposed model. (B) Immunofluorescence images of, HNF4a (green) and albumin (red) expression in cells encapsulated in Col and (C) ColFN. Nuclei were stained with Hoechst 33342 (blue).

References

[1] P. Godoy et al., *Arch Toxicol* 87 (8), 1315, 2013.
[2] P. Bedossa and V Paradis, *J Pathol* 200 (4), 504, 2003.
[3] M. Martino et al., *Sci. Transl. Med.*, 3(100), 89, 2011.
[4] R. Li et al., *Biomaterials,* 280, 121266, 2022.

Acknowledgements

Supported by PI21/00223 grant form Institute of Health Carlos III and PID2022-136433OB-C21,-C22/AEI/10.13039/501100011033 and CNS2022-135425 grants from the Spanish State Research Agency. Also supported by Generalitat Valenciana through CIPROM/2022/43 project and grant ACIF/2021/378 awarded to Estela Sanchez.

DEVELOPMENT OF A NOVEL ARTIFICIAL LUNG AND KIDNEY ASSIST DEVICE – FROM FIBER SPECIFICATIONS TO DEVICE DESIGN

Ana Martins Costa (1), Frank Halfwerk (1, 2), Bettina Wiegmann (3, 4, 5), Jan-Niklas Thiel (6), Michael Neidlin (6), Jutta Arens (1)

1. Engineering Organ Support Technologies, University of Twente, Netherlands; 2. Medisch Spectrum Twente, Netherlands; 3. Hannover Medical School, Germany; 4. Implant Research and Development (NIFE), Germany, 5. German Center for Lung Research, Germany, 6. Department of Cardiovascular Engineering, Institute of Applied Medical Engineering, RWTH Aachen University

Introduction: A novel artificial lung and kidney assist device is being developed combining gas exchange and dialysis fibers (RenOx). The RenOx development accounts for 1) fiber specifications to maintain lung and kidney support in a new integrated membrane bundle, and 2) device design considering user requirements and optimal blood flow distribution. Our previous work indicated that lung support can be maintained when 25% of gas exchange fibers are replaced by dialysis fiber layers in an oxygenator. However, the effect of utilizing dialysis fibers in an unconventional outside-in mode in the RenOx (blood flow outside the fibers) still needed to be evaluated. Moreover, these fiber specifications should be considered for the RenOx design.

Objectives: First, this study evaluated RenOx fiber specifications on the efficiency of commercial dialyzer membranes utilized outside-in regarding solute clearance and ultrafiltration coefficient. Secondly, we describe device development steps comprising the optimization of device's blood flow path, design of device parts, and prototyping.

Methods: First, the performance of commercial dialyzers utilized outside-in and in conventional inside-out mode was compared during standardized tests with full blood adapting the ISO 8637:2016. Clearance of urea and creatinine was compared for continuous hemodialysis and hemofiltration. Also, fluid removal was evaluated in terms of dialyzer's ultrafiltration coefficient. Second, for the RenOx development, design requirements specifications were derived based on interviews with users. These specifications were accounted for the design of device concepts. The RenOx's blood flow path design was optimized by means of computational fluid dynamics (CFD) simulations, blood directing angle (50° to 10°) and by considering existing patented blood path designs.

Results: Regarding RenOx fiber specifications, our results show that hemodialyzer's fibers utilized outside-in achieved equal clearance of urea and creatinine as traditional inside-out dialysis fibers. Measured clearance doses (25 mL/kgpatient/h) were comparable to the levels required for continuous renal replacement therapy. However, ultrafiltration coefficient in outside-in mode was about 4 times lower than for

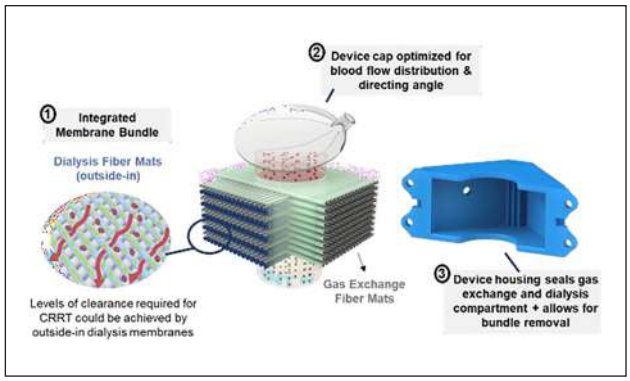

Figure 1. Development of novel lung & kidney assist device.

inside-out. Regarding RenOx development, translation of requirements and fiber specifications resulted in the need for a device with estimated total surface area of 2 m^2 (75% gas exchange fibers = 1.5 m^2, and 25% dialysis fibers = 0.5 m^2) to support 80 kg adult patients. The RenOx blood path design was optimized to guide blood through an inlet and outlet angle that improves blood flow distribution and velocity in the bundle, Fig. 1. This approach was innovative compared to patented models. Device housing was designed considering sealing of gas, blood, and dialysis compartments and the possibility to easily remove the membrane bundle for analysis after tests.

Discussion: Outside-in dialysis fibers could provide sufficient continuous clearance by hemodialysis and hemofiltration in in-vitro tests, but dedicated membranes with an outside selective layer would be needed for improved filtration rates. The estimated surface area for the RenOx of 2 m^2 is comparable to the size of state-of-the-art adult oxygenators. By replacing 25% of gas exchange fibers by dialyzers fibers, the RenOx will still be a compact oxygenator while providing additional kidney support.

Conclusions: A new membrane oxygenator with combined kidney function (RenOx) is under development. Our previous research indicates that a membrane bundle combining 75% of gas exchange fibers and 25% of outside-in dialysis fibers can provide lung and kidney support. In addition, first RenOx prototypes with optimized blood flow distribution are being prepared for further in-vitro and in-vivo testing.

Acknowledgements

This work was supported by the German Research Foundation (DFG) (project number 447746988, part of SPP 2014).

THE WAA-APHERESIS REGISTRY REPORT – AN UPDATE UNTIL 2024.

B Stegmayr (1), E Newman (2), V Witt, K Derfler (3), D Deeren (4), I Bojanic (5), Z Gasova, Z Bhuiyan-Ludvikova, M Blaha, M Lanska, S Blahutova (6), H Prophet, J Kielstein (7), J Audzijoniene, A Griskevicius (8), H Vrielink, K Le Poole (9), A Aandahl (10), T Glatt (11), R Bihariesingh (12), G Berlin, AM Vasilache, J Dykes, S Smargianaki, M Hellberg, C Wallquist, V Strineholm, F Toss, M Ott, E Watz, T Nilsson, G Welander (1), GC Seval, SK Toprak (13).

1. Sweden 2. Australia; 3. Austria; 4. Belgium; 5. Croatia; 6. Czech Republic; 7. Germany; 8. Lithuania; 9. The Netherlands; 10. Norway; 11. South Africa; 12. Suriname; 13. Turkey.

Background and Aim: Therapeutic Apheresis is a group of more than 30 different procedures. Treatment is mainly performed in patients with severe diseases that respond less to conventional therapy alone [1,2].

To learn more about effects and side effects of these various procedures quality assessment registries have been established. One such registry is the World Apheresis Association registry (www.WAA-registry.org) that enables centers from the whole world to participate in registering their experience. During the latest 5 years more than 25 centers have participated in data collection and analyses. The aim of repeated analyses and reports are to evaluate safety and trends of various variables. The aim of this study is to report of data within the WAA-registry from 2004 up to and including 2023.

Material: The joint venture has through the years resulted in data collected of 25 000 patients and more than 160 000 procedures. Safety analyses in relation to procedures, diagnoses and other variables will be reported.

Results: The mean age of 50 years has been stable over the years. Women represent approximately 40% of those treated. Over the years a significant reduction in side effects have been noted. This trend has levelled off during the latest years and eventually there is an increased risk to come. Variables that cause side effects differ such as ICD-10 code diagnoses with M display more moderate AEs than other groups ($p<0.001$) while those with G have more mild AEs than other groups;

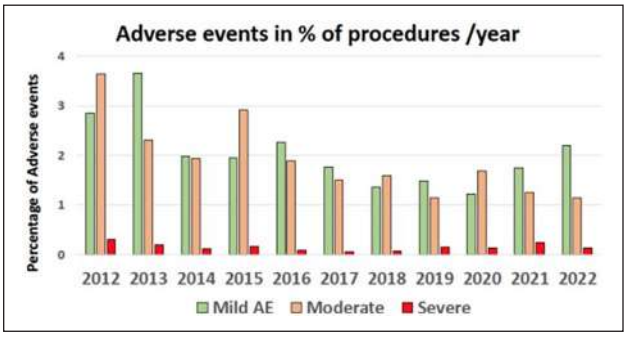

Figure 1. Numbers and rating of reported adverse events. Distribution in percentage of adverse events present during apheresis procedures performed through the years 2012–2022 graded as Mild, Moderate and Severe.

Table 1. Adverse event frequency in 54,164 apheresis procedures in the time frame 2018-2022. Technical and vascular access problems were excluded here.

Symptoms	Mild AE% (n=310)	Moderate AE% (n=729)	Severe AE% (n=63)
Urticaria, conjunctivitis	2	8	25
Hypotension	13	5	24
Tingling, pricking	39	74	11
Late complications, Other	2	1	5
Angina pectoris			3
Hypertension	2	0.5	3
Asystole/Cardiac arrest/			3
Back pain related to apheresis	2	0.7	3
Nausea and/or vomiting	10	4	3
Convulsions, not specified as epilepsy	0.6	0.4	3
Bronchospasm	0.3	0.3	3
Arrhythmia	3		1
Abdominal pain	2	1	1
Vertigo	4	0.1	1

G versus M has more hypotension (p<0.001). Variations exists in replacement fluid. The risk that apheresis causes severe side effects overall is 13/10 000 procedures in 2023.

Discussion & Conclusion: Repeated analyses of quality assessment data may guide safety and efficacy. Changes in adverse events over time help guide risks and benefits with new techniques, diagnoses and procedures.

References

1. Vrielink H, Le Poole K, Stegmayr B, Kielstein J, Berlin G, Ilhan O, Seval GC, Prophet H, Aandahl A, Deeren D, Bojanic I, Blaha M, Lanska M, Gasova Z, Bhuiyan-Ludvikova Z, Blahutova S, Hrdlickova R, Audzijoniene J, Griskevicius A, Glatt T, Strineholm V, Ott M, Nilsson T, Newman E, Derfler K, Witt V, Toss F (2023) The world apheresis association registry, 2023 update. Transfus Apher Sci 62: 103831. doi:10.1016/j.transci.2023.103831.
2. Witt V, Stegmayr B (2024) The WAA-registry. Transfus Apher Sci 10.1016/j.transci.2024.103889: 103889. doi:10.1016/j.transci.2024.103889..

Acknowledgements

We thank all staff and patients at the centers for contribution of data and knowledge to help improve quality and safety of apheresis procedures.

ASSESSING REALISM OF EXTRACORPOREAL MEMBRANE OXYGENATOR SIMULATORS – DEVELOPMENT AND APPLICATION OF AN OBJECTIVE FIDELITY CLASSIFICATION FRAMEWORK

Frank Halfwerk (1,2), Wytze Duinmeijer (1), Jutta Arens (1)

1. Engineering Organ Support Technologies group, University of Twente, The Netherlands; 2. Dept. of cardio-thoracic surgery, Thorax Centrum Twente, Medisch Spectrum Twente, The Netherlands

Introduction: Extracorporeal membrane oxygenation (ECMO) support is a life-saving treatment for severe cardiac and/or pulmonary failure. Because of its high complexity and low patient numbers, complications such as mortality, bleeding, and infections are high. Simulation-based training with ECMO simulators (ECMO sims) is used to train skills such as ECMO cannulation, circuit monitoring, and complex problem solving [1]. Realism (fidelity) is often assessed subjectively, and it is unclear to what extent low-, mid-, and high fidelity ECMO sims are available.

The aim of this study is to develop an objective frame-work for ECMO fidelity classification and apply this to available ECMO sims.

Methods: ECMO sims were identified through literature search in PubMed, Web of Science Core Collection, and Google (Scholar) and is accurate until March 2024. A fidelity framework was developed by a multidisciplinary expert group [1] and incorporated existing fidelity definitions, ECMO components, and ability to customize for patient variation.

Definition-based fidelity was divided into conceptual, functional, physical, and psychological fidelity. ECMO components were identified and scored for each ECMO sim when available. Last, the ability to customize the simulator to patient-specific aspects as skin tone, sex, age, and disease-specific anatomy was scored.

Fidelity domains were divided into tertiles, and labelled low-, mid-, or high-fidelity based on the number of available features, respectively.

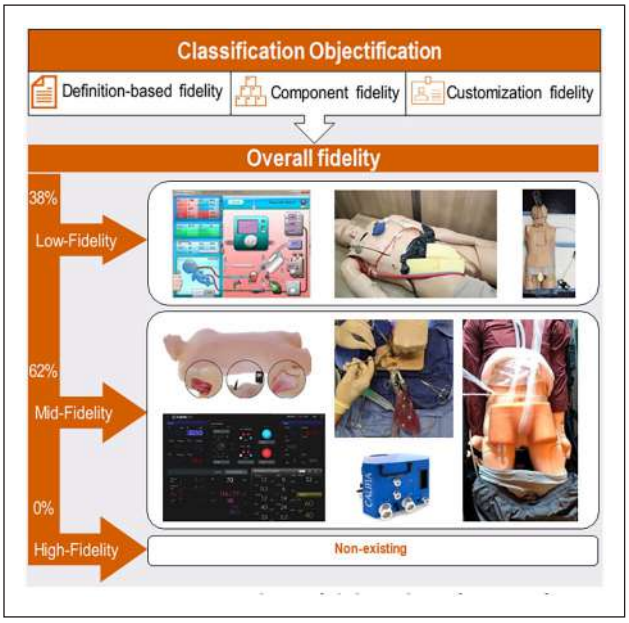

Figure 1. ECMO simulator fidelity classification frame-work with classifications of existing simulators.

Results: 29 of 33 ECMO sims with publicly available information, were suitable for fidelity classification (Figure 1). Definition-based fidelity was low for 34% of ECMO sims, and 45% and 21% scored mid-and high-fidelity, respectively. Based on the ELSO Red Book [2], 10 ECMO process components were identified, e.g. cannulation, circuit priming, monitoring and trouble-shooting, and the use of clinical scenarios. The majority of ECMO sims (69%) had 4 to 7 components covered and scored mid-fidelity, while none scored high-fidelity. ECMO sim customization fidelity was generally low (90%), without high-fidelity customization (0%).

Taking the median for all fidelity domains, 11 (38%) ECMO sims were classified as overall low-fidelity, 18 (62%) as mid-fidelity, and 0 (0%) as high-fidelity.

Discussion: Many ECMO sims are self-claimed to be high-fidelity with a subjective assessment. We developed an objective framework to assess fidelity and found that no high-fidelity simulators are currently available.

Fidelity scoring does not necessarily correlate with a quality mark. To the contrary, basic ECMO cannulation skills acquisition may best be trained on low-fidelity simulators. However, complex team training with distractions, interrupted actions and real-life training with debriefing are likely to benefit from high-fidelity ECMO sims [3] and should be developed. A limitation is that our overview is potentially incomplete, as simulators might have been developed, with public information lacking. We strongly encourage developers and researchers to share design and simulator evaluations publicly, whereafter evaluation may follow.

To conclude, an objective ECMO simulator classification framework was developed, and assessed that no high-fidelity ECMO sims yet exist. This framework may be used to improve the development and assessment of ECMO simulators.

References

1. Duinmeijer et al, J Clin Med, 12:1765, 2023.
2. Vercaemst et al, The ELSO Red Book 6th ed, Ch3, 2022.
3. Halfwerk et al, Int J Healthc Simul, 2023.

A NOVEL DESIGN OF CAVALPULMONARY ASSIST DEVICE FOR THE FONTAN PROCEDURE: INTEGRATING IMPEDANCE AND PERISTALTIC EFFECTS

Burns-Cox (1), C. Yan (1), T. Sun(1), L. Gan (1), A. W. Khir (1)

1. Department of Engineering, Durham University, United Kingdom

Background: Fontan is the standard surgical procedure to treat children with single ventricular defects, which causes systemic complications due to lack of pumping at the cavopulmonary junction [1]. Current commercial ventricular assist devices (VAD) are invasive, may induce high shear stresses with potential hemolysis, and often unsuitable for pediatric use. Therefore a device developed specifically for cavopulmonary support is desirable. In this work, we developed a novel pumping device for the Fontan procedure by integrating the principle of impedance [2] and peristaltic pumping.

Research Methods: A prototype pump was designed and fabricated in-house without any effort to optimise its specification. It was then tested *in vitro*, Fig 1(a), in terms of effect of pumping frequency, background pressure gradients and pump size on output performance.

Results: A prototype of the proposed device for in vitro testing is shown in Fig 1 (b). The proposed device will produce pulsatile flow vs. continuous flow in most commercial VADs. The device produces unidirectional flow without the need for a one-way valve. Also, the device is impeller-free with no blood contact and could be synchronised with the single ventricle using intracardiac electrocardiograms.

Net flow rate (NFR) and maximum pressure head delivery are both reasonably linearly dependent on pumping frequency within normal physiological range. Positive linearity is also observed between NFR and the distance of off-central pumping. The device regulates NFR in favourable pressure head difference and overcomes significant adverse pressure head difference, e.g. 11mmHg, Fig 2. Additionally, the size of the device is shown to have insensitive impact on the performance.

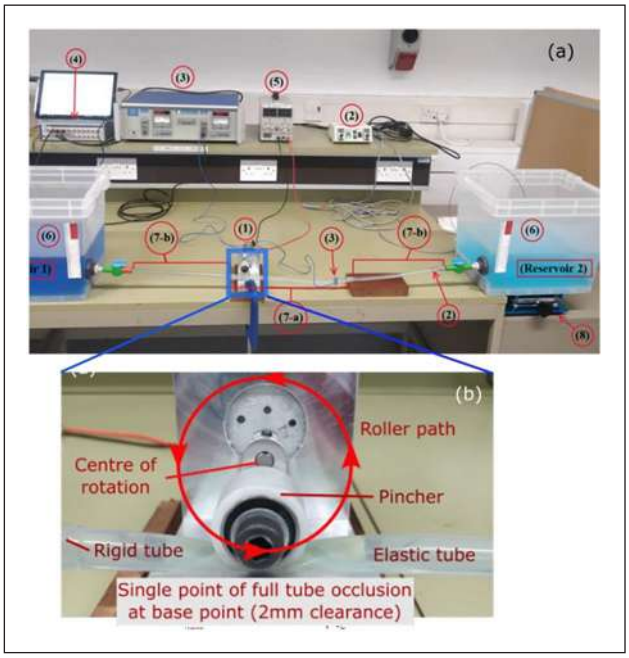

Figure 1. (a) Experimental testbed. (1) Pump, (2) Pressure sensor, (3) Flow sensor, (4) DAQ, (5) Power supply, (6)Reservoirs, (7)Flexible(a) & rigid(b) tubing (b) Rotary pumping mechanism (front view).

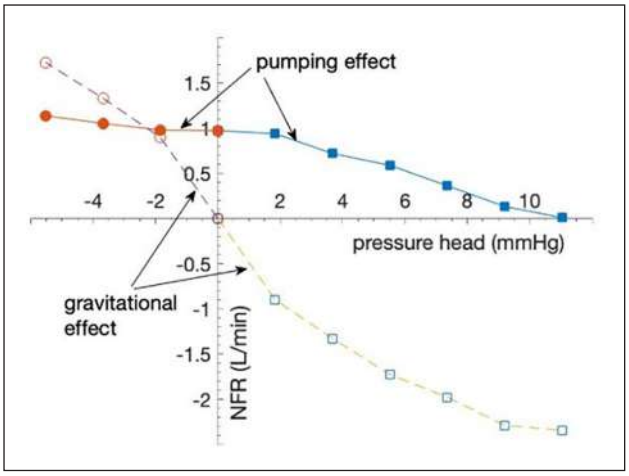

Fig 2. Effect of pressure head on NFR at pumping frequency f=2.5 Hz. Filled symbols are for pumping effect and open symbols are solely due to gravitational effect.

Conclusion: The feasibility of the novel rotary pump integrating impedance and peristaltic pump is demonstrated to perform in normal physiological conditions. The promising results warrant additional work for possible future paediatric cavopulmonary support and merit further investigation towards design optimisation and haemolysis mitigation.

References

1. de Leval, Nat Clin Prac Cardiovasc Med., vol. 2(4), pp. 202–208, 2005
2. Anatol et al, Scientific Reports, 2045–2322, 2022.

INTEGRATING ADVANCED VISUALIZATION AND 3D PRINTING FOR ENHANCED PREOPERATIVE PLANNING

Thai Duy Nguyen (1), Ali Dodge-Khatami (1), Lasse Strudthoff (2), Kai Philip Barbian (2), Sebastian Jansen (2), André Rüffer (1)

1. University Hospital RWTH Aachen, Medical Faculty, Germany; 2. Department of Cardiovascular Engineering, Institute of Applied Medical Engineering, Medical Faculty, RWTH Aachen University, Germany

Introduction: In the field of pediatric cardiac surgery, visualization of congenital heart defects has long been of major importance. From traditional methods such as 2D imaging via echocardiography or cross-sectional imaging, a more 3D focused visualization seems to be the new norm. Recent advances in computed tomography imaging technology such as Photon-counting computed tomography (PCCT) have introduced more precise imaging with lower radiation exposure [1]. In this study, we aim to demonstrate the clinical value of congenital heart defect visualization by highlighting the utility of different modalities in selected complex and redo cases. Through our investigation, we aim to show the practical implications of advanced visualization in pediatric cardiac surgery.

Methods: Visualization was achieved through two primary methods: volume rendering and segmentation followed by 3D printing on a Stratasys Objet 500 machine using elastomeric material. Initial segmentation was performed using Materialise Mimics and 3D Slicer. Volume rendering of cross-sectional imaging data was conducted using Vea software in conjunction with a Meta Quest 2 virtual reality headset.

To assess the impact of visualization on surgical decision-making, we compared our approach to procedure planning before and after the utilization of advanced visualization techniques. This involved analyzing the extent to which visualization influenced our surgical strategy, particularly in complex and redo cases.

Results: Following the utilization of advanced visualization, there was a discernible shift in the surgical approach in several complex cases. Specifically, surgeons reported a more confident and informed decision-making process, leading to adjustments in procedural planning and intraoperative management. In a Swiss cheese VSD case, this provided a completely different perspective, resulting in a second incision near the apex of the heart for direct closure. In a double aortic arch case, the approach was changed to an unconventional right-sided thoracotomy. In redo operations, where the challenges of anatomical distortion and scar tissue were heightened, advanced visualization played a crucial role in guiding surgical strategy. Surgeons reported a more systematic and deliberate approach, leveraging the detailed anatomical models generated through segmentation and 3D printing to anticipate potential challenges and optimize procedural outcomes.

Discussion: The findings highlight the critical role of advanced visualization techniques in pediatric heart surgery, particularly for navigation of complex and repeat procedures. Using both volume rendering and 3D printing, we were able to improve and refine surgical planning.

One of the key observations was the discernible change in surgical approach in complex cases following the use of 3D visualization compared to having only echocardiography or common CT imaging at hand. This was further augmented using elastic 3D printed models as part of the presurgical preparation. These models provided a tangible representation of the anatomy and pathology, allowing to simulate surgical maneuvers prior to entering the operating room. This change suggests that these techniques not only provide clearer anatomical insights, but also enable surgeons to devise more tailored and effective strategies.

We would also like to enhance visualization through emerging technologies such as augmented reality and multi-material printing. Multi-material printing allows the creation of anatomically accurate models that mimic the setting in the operating theatre, providing a tangible and comprehensive representation for preoperative simulation and training purposes. Similarly, augmented reality has the potential to overlay 3D models onto the patient's anatomy in real time, providing for surgical planning and possibly on-site real time measurements, be it cannula sizing for the aorta/vena cavae, conduit sizing for right ventricle to pulmonary artery or LVAD device implantation.

Reference

1. Dirrichs T, Tietz E, Rüffer A, Hanten J, Nguyen TD, Dethlefsen E, Kuhl CK. Photon-counting versus Dual-Source CT of Congenital Heart Defects in Neonates and Infants: Initial Experience. Radiology. 2023 Jun;307(5):e223088. doi: 10.1148/radiol.223088. Epub 2023 May 23. PMID: 37219443.

SIMULATION-BASED TRAINING WITH EXTRACORPOREAL MEMBRANE OXYGENATOR SIMULATORS – A TRAINING NEEDS ANALYSIS

Frank Halfwerk (1,2), Wytze Duinmeijer (1), Marleen Groenier (3), Jutta Arens (1)

1. Engineering Organ Support Technologies group, University of Twente, The Netherlands; 2. Dept. of cardio-thoracic surgery, Thorax Centrum Twente, Medisch Spectrum Twente, The Netherlands; 3. Dept. of Technical Medicine, University of Twente, The Netherlands

Introduction: For patients with severe cardiac and/or pulmonary failure, extracorporeal membrane oxygenation (ECMO) support is a life-saving treatment. Complications such as mortality, bleeding, and infections are high, and are strongly related to annual ECMO case volume.

Simulating ECMO practice with simulation-based training on simulators (ECMO sims) help to train technical skills as ECMO cannulation, and non-technical skills as complex decision making [1]. ECMO sims with a high level of realism (high-fidelity) are currently lacking [1]. Our EduECMO project strives to develop such a high-fidelity patient-centred educational ECMO simulator, where training needs should be investigated.

The aim of this work is to obtain expert input on ECMO practices and ECMO sim training needs to optimize EduECMO sim design.

Methods: INACSL Standards of Best Practice for Simulation [2] were used to conduct a training needs assessment. Invitations to participate in an online survey (Google Forms) were sent to ECMO experts by email. Participants signed informed consent. The study was approved by the University of Twente Ethics Committee (UT-NES 230117).

Results: A total of 41 professionals from 11 countries worldwide responded (Figure 1). Clinical backgrounds were perfusionist (9),

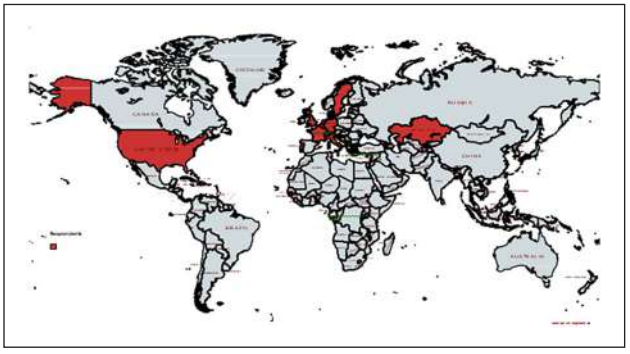

Figure 1. 41 respondents from 11 countries participated in the ECMO training needs survey.

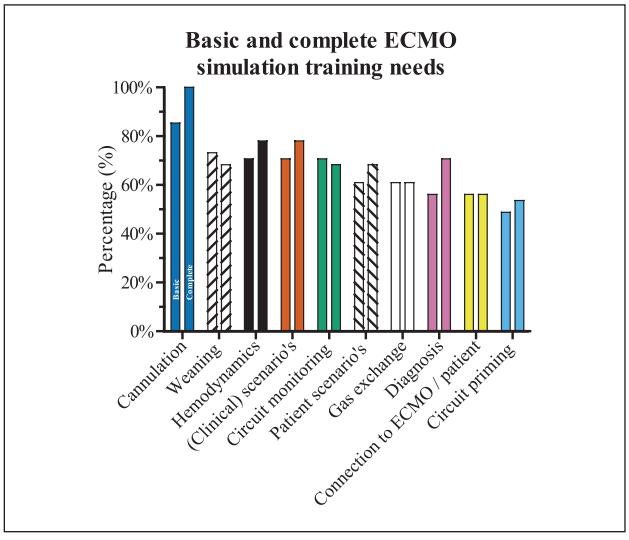

Figure 2. Basic (left columns) and complete (right columns) ECMO simulation training needs as determined by 41 respondents.

intensivist (8), (intensive care) nurse (7), car-diac surgeon (6), anaesthesiologist (5), cardiologist (4), ECMO specialist nurse (1), and physician assistant (1).

18% of respondents are from low-volume centres (< 6 ECMO cases/year), with 42% in mid-volume (6 – 30 ECMO cases/year), and 40% in high-volume centres (> 30 ECMO cases/year).

The majority (83%) had ECMO sim experience, yet only 34% were assessed after training. For both basic and complete ECMO sims, cannulation was deemed most important (85 to 100%), and circuit priming with 49 to 54% the lowest (Figure 2). All respondents (100%) deem at least one patient characteristic as age, sex, skin-tone, or BMI important for basic ECMO sims, with 73% and 20% of respondents requiring mid-to high customization fidelity, respectively.

Discussion: Our international ECMO simulator training needs assessment showed that a minority of international ECMO experts received ECMO training with sub-sequent assessment. In line with previous work [1], ECMO sim training needs are not yet fulfilled. Development of a high-fidelity ECMO simulator (e.g. EduECMO) should incorporate these training needs.

References

1. Duinmeijer et al, J Clin Med, 12:1765, 2023.
2. Sittner et al, Nurs Educ Perspect, 36:294-298, 2012.

ALTERATIONS OF ALBUMIN FUNCTION AFTER KIDNEY TRANSPLANTATION

Kristina Boss (1), Margret Paar (2), Lea Marie Berntsen (1), Max Lennart Westerbarkei (1), Katja Waterstradt (3), Kerstin Schnurr (3), Gerd Klinkmann (4), Steffen Mitzner (5), Karl Oettl (2), Andreas Kribben (1)

1. Department of Nephrology, University Hospital Essen, University Duisburg-Essen, Germany; 2. Division of Medicinal Chemistry, Otto Loewi Research Center, Medical University of Graz, Austria; 3. MedInnovation GmbH Berlin, Germany; 4. Department of Anaesthesiology, Intensive Care Medicine and Pain Therapy, University of Rostock, Germany; 5. Department of Medicine, Division of Nephrology, University of Rostock, Germany

Background: Patients with chronic kidney disease (CKD) have increased morbidity and mortality, which is mainly due to a chronic inflammation [1]. A kidney transplantation (KT) can clearly improve this. It is unclear what part albumin plays in this process and what functional alterations a KT has on albumin.

Methods: Albumin redox state (ARS) was determined by fractionating it into reduced human mercaptalbumin (HMA), reversibly oxidized human non-mercaptalbumin 1 (HNA-1), and irreversibly oxidized human non-mercaptalbumin 2 (HNA-2) by high-performance liquid chromatography. In healthy individuals, albumin circulates roughly in the following proportions: HMA 70–80%, HNA-1 20–30% and HNA-2 2–5% [2].

The binding and detoxification efficiency of albumin (BE and DTE) were assessed by electron paramagnetic resonance spectroscopy using a spin-labelled fatty acid. BE reflects strength and amount of bound fatty acids under certain ethanol concentration. DTE reflects the molecular flexibility of the patient's albumin molecule, thus the ability to change the conformation depending on ethanol concentration. Percentage of BE and DTE are depicted in relation to healthy individuals (100%) [3].

ARS, BE and DTE were measured once immediately before (baseline) and at eight time points until six months after KT.

Results: 42 patients (29 male, median age 43.5 years, median time on dialysis 72 months) were analyzed. Before KT, HMA (median 63.5%, IQR 59.6-67.3%) was lower than in healthy individuals. Accordingly, oxidized albumin fractions were above the level of healthy individuals (median HNA-1 28.9%, IQR 25.9-33.3%; median HNA-2 7.1%, IQR 6.0-8.1%). After KT, HNA-2 increased further, within the first week after KT (median 9.1%, IQR 7.3-11.4%); HMA and HNA-1 accordingly decreased. In most patients, ARS improved during six months after KT.

Binding and detoxification efficiency of albumin showed a similar course. Before KT, they were below the values of healthy individuals (median BE 76%, IQR, 66-84%; median DTE 67%, IQR 48-85%). We found the lowest BE and DTE one week after KT (median BE 40%, IQR 31-49%; median DTE 30%, IQR 19-39%).

Six months after KT, most patients had BE and DTE values similar to the values of healthy individuals.

Conclusion: This is the first multimodal analysis of functional alterations of albumin after kidney transplantation. Albumin redox state, as well as binding and detoxification efficiency of albumin clearly improved after KT, but approach the values of healthy individuals only six months after KT.

References

1. Jager KJ, Kovesdy C, Langham R et al. A single number for advocacy and communication-worldwide more than 850 million individuals have kidney diseases. Kidney Int 2019;96:1048–50
2. Oettl K, Marsche G. Redox state of human serum albumin in terms of cysteine-34 in health and disease. Methods Enzymol. 2010;474: 181–95.
3. Kazmierczak SC, Gurachevsky A, Matthes G.et al. . Electron spin resonance spectroscopy of serum albumin: a novel new test for cancer diagnosis and monitoring. Clin Chem 2006;52:2129–34. 10.1373/clinchem.2006.073148

Acknowledgements

The excellent technical assistance of Doris Payerl is highly appreciated. We thank the Albunet e.V. group for their constructive ideas for this project. This research received external funding from Stiftung Universitätsmedizin Essen (2023 4699 108).

USABILITY CONSIDERATIONS WITH EXPANDING ECLS END-USERS: SHORTCOMINGS AND OPPORTUNITIES

Salim E. Olia, PhD (1), Kelsey Quinonez, BSN (2), Mary Frances Quinn, BSN (2)

1. University of Pennsylvania, USA; 2. Hospital of the University of Pennsylvania -Penn Presbyterian; USA

Introduction: ECLS is a complex, resource-intensive, life-sustaining therapy that requires significant training for any end-users interacting with the ECMO console. The growing use of this technology outside of dedicated ECMO Specialists available at the bedside at all times means an increase in required manipulations or interventions by multi-tasked personnel like an ECMO-trained physician, advanced practice provider, or the bedside nurse. Device usability is critical in low frequency, high risk events that interrupt ECMO support, as the operator is already under extreme stress to diagnosis and restart pump flow while medically supporting the patient simultaneously.

Methods: Two ECMO consoles, the CardioHelp (CH) and Quantum Workstation (QW), were systematically assessed for the steps required

to resolve a false "arterial bubble detected" (ABD) scenario: an alarm that causes the pump to go into zero-flow mode to prevent air from entering the patient, but can be inadvertently triggered by accidental opening of the clamp-on blood flow sensor or injection of echocardiography contrast enhancement agents. Opportunities to deviate from the correct steps were also noted. In the event that a user is unable to clear this alarm, they may elect to manually hand-crank the pump to restore blood flow, so this procedure was also reviewed.

Results: From the default home screen upon ABD, the CH requires the user to manually navigate through two menus and four touches to reset the alarm with the pump automatically returning to previous set speed *(Figure 1)*. While the required menus are highlighted in red, there is no restriction on the user navigating unnecessarily elsewhere. Prior to reset, the speed knob appears to remain functional with RPM changes flashing on the display only to return back after a short delay. In contrast, the QW presents a non-dismissible pop-up screen that is only cleared by acknowledging the ABD, but then necessitates manually returning pump speed to previous settings, requiring up to a total of two touches without any menu navigation *(Figure 1)*. If the screen locks out prior to returning to original speed, this would add an additional two touches to regain access.

Handcranking the CH cartridge is a multistep process requiring i) pivoting of the protective frame arm, ii) disconnecting 1 of 3 sensor cables, iii) gathering enough slack on the heater/cooler lines, iv) clockwise twist to detach from motor, and v) dissimilar tilt up/down pivot

mechanism to attach to the hand crank. The QW uses the same twist latch mechanism between the motor and handcrank, and the pump can be moved without removal of the two pump sensor cables if adequate slack was provided at circuit build.

Discussion: ABD is a critical alarm that interrupts support to prevent air embolism to the patient, but rapid identification and resolution of false positives is crucial to prevent hemodynamic collapse in any ECMO-dependent patient. Device usability and commonality is essential to both retained training and recollection upon presentation for all potential end-users.

The results here also observations seen during formal training sessions and clinically overall. For example, while the CH has visual indicators for the different twist versus pivot mechanism on the motor, the dissimilarity leads to repeated failed attempts to secure. Conversely, while the QW motor and handcrank latch mechanism is identical, the lack of any visual or stylistic indicator as to its operation has led to initial failure to operate until the user is able to appreciate the slider and not push movement. While hardware changes remain a significant hurdle to address post-release and therefore should be comprehensively assessed in advance, software updates may offer a quicker opportunity to rectify unforeseen issues based on clinical feedback.

Figure 1. The touches and menu navigation required to resume pump speed after an ABD alarm for the CardioHelp (CH) and Quantum Workstation (QW).

MAGNETIC HYDROGELS FUNCTIONALISED WITH NATURAL EXTRACTS FOR TISSUE ENGINEERING

Sara Leal Marin (1), Gesine Hentschel (1), Juan Escobar (2), Geovanna Tafurt-García (3), Alex Lopera (2), Juan Vaca (2), Birgit Glasmacher (1)

1. Institute for Multiphase Processes, Leibniz University Hannover, Germany; 2. Grupo de Nanoestructuras y Física Aplicada (NANOUPAR), Universidad Nacional de Colombia sede de La Paz, Cesar, Colombia; 3. Grupo Semilla del Conocimiento del Cesar (Zajuna jwa samu), Universidad Nacional de Colombia sede de La Paz, Cesar, Colombia

Introduction: Hydrogels, water-absorbing polymer networks, mimic the extracellular matrix, supporting cell functions without toxicity. Common materials include collagen, gelatin, and polysaccharides like hyaluronic acid and alginate [1-5]. One challenge with hydrogels is targeted therapy. Magnetic nanoparticles play a crucial role in this area as they can be directed using an external magnetic field. This work developed natural hydrogels embedded with magnetic nanoparticles to potentially release plant extracts like Thymus vulgaris L with antioxidant and antiviral properties [6], as shown in Figure 1.

Methods: *Hydrogel synthesis:* Gelatine (2% w/v) was dissolved with MES and HCl-Tyramine. Then, the pH was adjusted to 6, and NHS and ECD were added. Thereafter, the dissolution was dialysed for two days. Finally, the tyramine conjugate of gelatine was lyophilised. Hydrogels were prepared according to the protocol described by [7].

Magnetite nanoparticles: Magnetite (Fe_3O_4) was synthesised using a co-precipitation method assisted by ultrasound. First, ferric chloride hexahydrate and ferrous chloride tetrahydrate were dissolved in distilled water. The next step consisted of slowly adding sodium hydroxide solution with ultrasound assistance. Magnetic nanoparticles were magnetically separated.

Plant extract: The dried and finely crushed thymus vulgaris L plant parts were used for solid-liquid extraction with sonication at room temperature, using water as solvent. The aqueous extract was concentrated by vacuum distillation and freeze-dried. The extract was mixed with the hydrogel at different concentrations. The rheological properties of the hydrogels were characterised using a rheometer by oscillation and creep test. Magnetic properties were analysed by vibrating sample magnetometry.

Results: Hydrogels demonstrated viscoelastic properties, with their viscosity increasing in correlation with the amount of magnetic nanoparticles incorporated. Magnetic properties showed ferromagnetic behaviour.

Discussion: The successful integration of magnetic particles into the hydrogels will enable the controlled release of the antimicrobial agent Thymus. Given the natural components used, these hydrogels are anticipated to

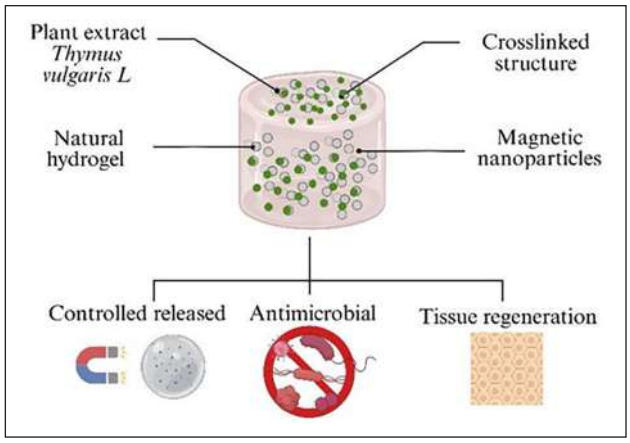

Figure 1. Graphical abstract of magnetic hydrogels. Created with Biorender.com

exhibit good biocompatibility in vitro tests. Additionally, a system will be developed to facilitate the stimulation of the hydrogels during cell culture experiments and to test the control of the release of the plant extract.

References

1. Bao W, et al. Frontiers in chemistry. 2020;8:53
2. Liu M, et al. Bone research. 2017;5:17014
3. Esteghlal S, et al. International Journal of Biological Macromolecules. 2018;114:1-9
4. Zerbinati N, et al. Dermatologic therapy. 2020;33:e13747
5. Suresh S, et al. The International journal of artificial organs. 2018;41:801-810
6. Sanches,. *et al*. Trends Food Sci Tech.. 2021; 117: 218-227.
7. V. Moulisová et al, ACS Omega. 2017; 2:11, 7609–7620.

Acknowledgements

This work was supported by the Caroline Herschel Program of Leibniz University Hannover and the German Federal Ministry of Education and Research project with Colombia (BMBF, 01DN24012).

MECHANICAL CIRCULATORY SUPPORT THROMBOSIS MODELLING ON-A-CHIP DELINEATES MATERIAL AND HEMODYNAMIC EFFECTS

Tiffany Goh (1, 2), Lingzi Gao (1), Jasneil Singh (1), Richard Totaro (3), Ruaidhri Carey (3), Kevin Yang (3), Bruce Cartwright (3), Mark Dennis (3), Lining Arnold Ju (2), Anna Waterhouse (1)

1. School of Medical Sciences, Faculty of Medicine and Health, The University of Sydney, Australia; 2. School of Biomedical Engineering, Faculty of Engineering, The University of Sydney, Australia; 3. Royal Prince Alfred Hospital, Sydney, Australia.

Introduction: The safety and efficacy of mechanical circulatory support (MCS), including extracorporeal membrane oxygenation (ECMO) and ventricular assist devices (VAD), is complicated by blood clot formation (thrombosis) (Fig.1A), which cause fatal complications including device occlusion and failure, patient embolism and stroke [1,2]. Anticoagulants administered to prevent thrombosis cause bleeding risks to patients [1,2]. Thrombosis is induced by the combined effects of foreign artificial material surfaces and pathological hemodynamic conditions of MCS [3]. Thus, to understand biological mechanisms of MCS thrombosis and evaluate the thrombogenicity of MCS design, *in vitro* models need to incorporate both factors at clinically relevant conditions. We demonstrate an *in vitro* model of MCS thrombosis achieving 1) physiologically relevant human and patient whole blood samples, 2) customisable clinical material and flow combinations, 3) detailed real-time visualisation, and 4) higher-throughput screening than traditional models.

Methods: ECMO patient circuits from Royal Prince Alfred Hospital were decannulated, flushed and inspected for thrombus. Computational fluid dynamic modelling was performed on ECMO tubing-connector models at 2 – 6 L min^{-1} to determine thrombosis-relevant flow regimes. Microfluidic models mimicking such conditions were made with ECMO materials polyvinylchloride (PVC) or polycarbonate (PC), within which confocal microscopy recorded real-time thrombosis and platelet activation.

Results: ECMO tubing-connector junctions were common sources of adhered thrombus (Fig.1A). *In situ* modelling correlated these regions to wall shear rates from 500 s^{-1} to 5000 s^{-1}, and velocity gradients. *In vitro* microfluidic experiments showed that shear regimes less than 1000 s^{-1} significantly increased platelet adhesion compared to shear rates above 2000 s^{-1}. In expanding or constricting microfluidics mimicking ECMO tubing-connector velocity gradients, platelet aggregate growth, occlusion and embolism were visualised in real-time (Fig.1B), accurately replicating established clinical phenomena.

We importantly demonstrated the models' ability to experimentally delineate the influence of material properties and flow conditions in activating thrombosis.

This was achieved by real-time spatial quantification of platelet markers e.g. P-selectin, indicating thrombosis activation. We showed increased P-selectin on the platelets adhered to PVC compared to PC (Fig.1C). For the first time, we showed selective P-selectin expression on the leading-edge of individual adhered platelets under shear at 3000 s^{-1}, but not 1000 s^{-1} (Fig.1D).

Discussion: Our model of whole blood, MCS thrombosis achieved material and flow customisability, clinical relevance, and low blood volume for improved throughput. Real-time monitoring provided the advantage of visualising phenomena including occlusion and embolism, and comparing temporal platelet activation under different materials and flow, to improve our understanding of the biological mechanisms underlying MCS thrombosis.

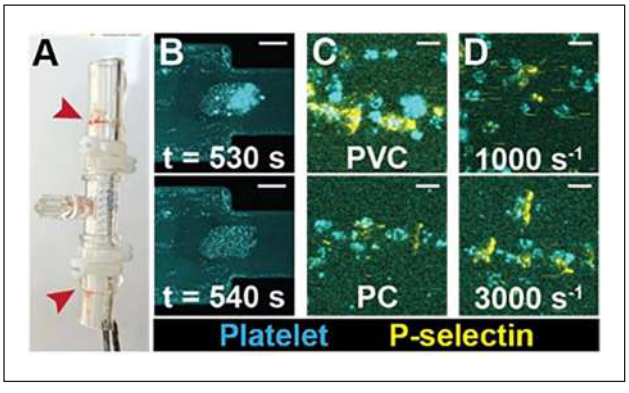

Figure 1. (A) ECMO tubing-connector thrombi. (B) Platelet thrombus embolism in real-time (C) Increased platelet activation on PVC vs. PC. (D) Spatial P-selectin is shear dependent. Scale bar (B)=50µm, (C&D)=5µm.

These results will be useful for guiding future MCS design. For example, our result suggests that low operation flow rates, flow velocity gradients, and the use of PVC over PC should be avoided to reduce activating thrombosis in ECMO, occlusion and embolism. Additionally, future MCS material development could use this model to rapidly screen the hemocompatibility of novel materials under operationally relevant flow conditions, as the model only required microlitres of human blood. Together the detailed biological mechanistic information provided by our model, combined with its customisability, provides a powerful tool for future evaluation of MCS design safety.

References

1. Gaffney et al, BMJ, 341:c5317, 2010
2. Cartwright et al, Sci Rep, 11:7975, 2021
3. Hong et al, Biomater Sci, 8:5824-5845, 2020

APPLICATION OF A TWO-STAGE STENT FOR THE DEVELOPMENT OF TRANSCATHETER AUTOLOGOUS TISSUE-DERIVED PULMONARY VALVE IMPLANTATION.

Yoshiaki Takewa (1), Yusuke Inoue (1), Takeshi Terazawa (1), Yasushi Sato (1), Tomoki Nagayoshi (1), Kazuto Fujimoto (2), Isao Shiraishi (2), Ken Takamatsu (3), Kunio Ohta (3)

1. Advanced Medical Engineering Research Center, Asahikawa Medical University, Japan; 2. Department of Pediatric Cardiology, National Cerebral and Cardiovascular Center, Japan; 3. Tamachi Industries Co. Ltd., Japan

Introduction: We have been developing a novel autologous biological heart valve (biovalve) using a unique technique, called in-body tissue engineering, in which tissue is formed by applying the encapsulation reaction of connective tissue [1, 2]. The biovalve has the potential to grow as we have previously reported [3], and thus has potential application in pediatric valvular heart disease with congenital heart disease. To be used in such patients, the valve must be implanted in a noninvasive method, i.e., transcatheter technique. To achieve this, the diameter of the crimped valve with a stent must be small enough to allow insertion through a peripheral blood vessel. For this purpose, we devised a two-stage deploying technique of stent-combined devices. In this study, we evaluated the feasibility of the device to achieve transcatheter implantation into the pulmonary valve position in a large animal experiment using an adult goat.

Methods: The device developed in this study is divided into two parts: one part consisting of the conduit and stent, and the other part consisting of the valve leaflet and stent, allowing for a reduction in outer diameter when crimping into the vessel. To obtain both parts, The biovalve molds were made of acrylic and metal, implanted with a self-expandable stent each subcutaneously in the back of an adult goat. Around 8 weeks after implantation, the molds with stent were extracted along with the surrounding connective tissue and only the molds were removed, resulting in the final two parts with the stent each. In this way, the minimum outer diameter of each device was reduced from 16 mm to 12 mm, respectively. Using transcatheter technique, a stent with a conduit was first deployed at the pulmonary valve position of an adult goat, followed by a stent with a valve leaflet in the former stent.

Results: The device could be implanted in the pulmonary valve position by conventional transcatheter valve implantation. Postoperative angiographic and echocardiographic monitoring showed good movement of the valve leaflets and no significant stenosis or regurgitation. The goat implanted the biovalve has been well condition (no thromboembolic event or heart failure) beyond 3 months without any anti-coaguration therapy after implantation. We plan to observe the goat's condition and monitor the device function for up to 6 months, after which the valve will be removed to examine its histologic structure and histocompatibility.

Conclusions: The biovalve could be implanted in the pulmonary valve position by our two-stage stenting method. It is expected to be a promising alternative valve for pediatric valvular heart disease with congenital heart disease because of its good histocompatibility in regenerative medicine, ease of application in transcatheter technique, and the advantage of being able to fabricate planned shapes.

References

1. Takewa Y, Yamanami M, Kishimoto Y, Arakawa M, Kanda K, Matsui Y, Oie T, Ishibashi-Ueda H, Tajikawa T, Ohba K, Yaku H, Taenaka Y, Tatsumi E, Nakayama Y. J Artif Organs, Jun;16(2):176-84, 2013
2. Nakayama Y, Takewa Y, Sumikura H, Yamanami M, Matsui Y, Oie T, Kishimoto Y, Arakawa M, Ohmuma K, Tajikawa T, Kanda K, Tatsumi E. J Biomed Mater Res B Appl Biomater., Jan;103(1):1-11, 2015
3. Takewa Y, Sumikura H, Kishimoto S, Naito N, Iizuka K, Akiyama D, Iwai R, Tatsumi E, Nakayama Y, ASAIO J., May/Jun;64(3):395-405, 2018

Acknowledgements

This research was supported by grant MEXT/JSPS KAKENHI Grant Number JP22H03132.

A COMPUTATIONAL ANALYSIS OF VESSEL COLLAPSE DUE TO DRAINAGE CANNULA FLOW DYNAMICS DURING VENO-ARTERIAL ECMO

Mehrdad Khamooshi (1), Avishka Wickramarachchi (2), Aidan Burrell (3), Shaun D. Gregory (1,2)

1. Centre for Biomedical Technologies and School of Mechanical, Medical and Process Engineering. Queensland University of Technology, Brisbane, QLD, Australia 2. Department of Mechanical and Aerospace Engineering, Monash University, Melbourne, Australia 3. Intensive Care Unit, Alfred Hospital, Melbourne, Australia

Introduction: Veno-arterial extracorporeal membrane oxygenation (VA ECMO) is a form of temporary mechanical circulatory support for cardiac and respiratory failure. The drainage cannula is typically inserted into the femoral vein and relies on adequate vessel diameter and wall

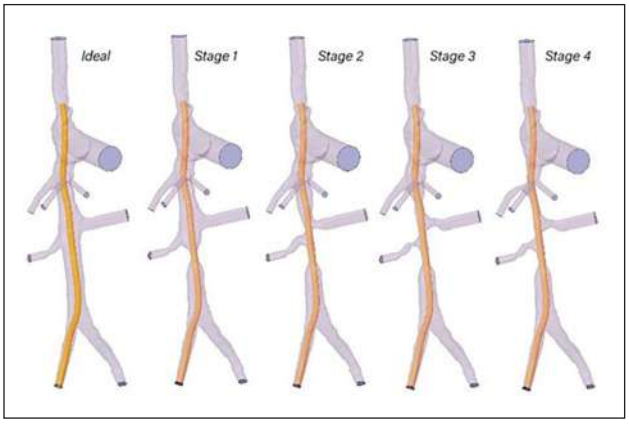

Figure 1. The venous geometry with a cannula at increasing levels of vessel wall collapse. At each stage the holes at the collapse were blocked manually.

Table 1. The vessel wall shear stress values at different stages of collapse.

Column 1	Average WSS (Pa)	Maximum WSS (Pa)
Ideal	0.51	16.4
Stage 1	0.90	39.6
Stage 2	1.74	148.1
Stage 3	3.46	497.9
Stage 4	5.09	537.2

integrity to sustain blood flow. However, under certain conditions the vessel wall can become compromised, leading to partial or complete collapse around the cannula. This study investigates the hemodynamic effects of vessel wall collapse during VA ECMO using computational fluid dynamics (CFD) simulations.

Methods: A patient-specific geometry of the venous system was extracted from a computed tomography scan of a VA ECMO patient. A 25 Fr Maquet drainage cannula was placed within the venous system with the tip positioned in the superior vena cava -right atrium (SVC-RA) junction. To simulate vessel collapse, manual restriction of the vessel wall around the proximal holes of the cannula within the inferior vena cava (IVC) was implemented in four sequential stages (Figure 1). The hemodynamic outcomes at each stage of vessel collapse were compared with the baseline scenario of no vessel wall collapse. The cannula was prescribed with a 4 L/min suction flow rate to reflect standard adult VA ECMO support.

Results: Collapse of the IVC wall narrowed the flow area, leading to increased blood velocity within the restricted regions. Consequently, this caused a significant rise in wall shear stress (WSS) values. Specifically, the maximum WSS under ideal conditions was 16.4 Pa, whereas during stages 1 to 4 of vessel collapse, the values measured were 39.6 Pa, 148.1 Pa, 497.9 Pa, and 537.2 Pa, respectively (Table 1).

Discussion: The increase in wall shear stress resulting from vessel wall collapse in the IVC can cause endothelial damage and initiate thrombosis during VA ECMO. Elevated blood velocities due to narrowed flow areas lead to significantly higher wall shear stress values, particularly at advanced stages of vessel collapse (stage 3 and stage 4). The fibrin/proteinaceous sheath partially enveloping the cannula could occlude some of the hole rows, impairing venous drainage during VA ECMO [1].

Reference

1. Marta Velia, et al. ASAIO J, 69(11):p e471-e472, 2023.

TRIPHASIC ELECTROSPUN SCAFFOLD WITH DYNAMIC CELLS COCULTURE FOR TISSUE ENGINEERING OF BONE-TENDON-MUSCLE JUNCTIONS.

Nicolas Rivoallan (1,2), Morgane Lagier (1), Timothée Baudequin (1), Marc Mueller (2), Pascale Vigneron (1), Rachid Jellali (1), Birgit Glasmacher (2), Cécile Legallais (1)

1. Université de technologie de Compiègne, CNRS, BMBI (Biomechanics and Bioengineering), Centre de recherche Royallieu -CS 60 319 -60 203 Compiègne Cedex; 2. Institute for Multiphase Processes, Leibniz University Hannover, Hannover DE-30823, Germany.

Introduction: Microstructures in electrospun scaffolds are known to guide the differentiation of stem cells. [1-3]. In order to study the bone-tendon-muscle junctions, we propose to generate micrometric walls on a part of the aligned area of a formerly electrospun bi-phasic scaffold (honeycomb / aligned fibres). On this triphasic structure, C2C12 cells were located between the microwalls and cocultured in dynamic condition with C3H10T1/2 seeded on both the honeycombs and the aligned fibers.

Methods: The homemade collector combines patterned regions, gap spinning and regular electrospinning. Photolithography was used to microstructure wafers for the patterned regions and to add PEG walls of 50 µm width spaced of 500 µm on the scaffold. Solutions of 10 and 12%wt/v polycaprolactone were used to produce a two-layered scaffold, the first composed of beads-on-string fibers to increase the thickness of the honeycomb structure [4], the second composed of aligned fibers only (Fig. 1). Elastic moduli of each area of the material were determined using uniaxial tensile testing with video tracking. C3H10T1/2 and C2C12 cells were seeded at a density of 100 000 cells/cm² on the scaffolds without any differentiation factor for one week in static and dynamic conditions. Two programs of strain stimulation were tested. They consist every 11h in 3% and 5% of strain after 5 and 2 days of static culture respectively. The early bone differentiation was evaluated by ALP staining. Immunostaining was used to observe the bone, tendon and muscle fates of both cell lines. Moreover, the scaffolds and the cells were observed on SEM.

Results: Micro walls were well added to obtain the triphasic scaffold. Those different areas showed significantly different mechanical properties with elastic moduli from 80-100 MPa to 130-150 MPa. Tracking highlighted that the aligned phase was the mainly strained during mechanical stimulation corresponding to the tendon and muscle area.

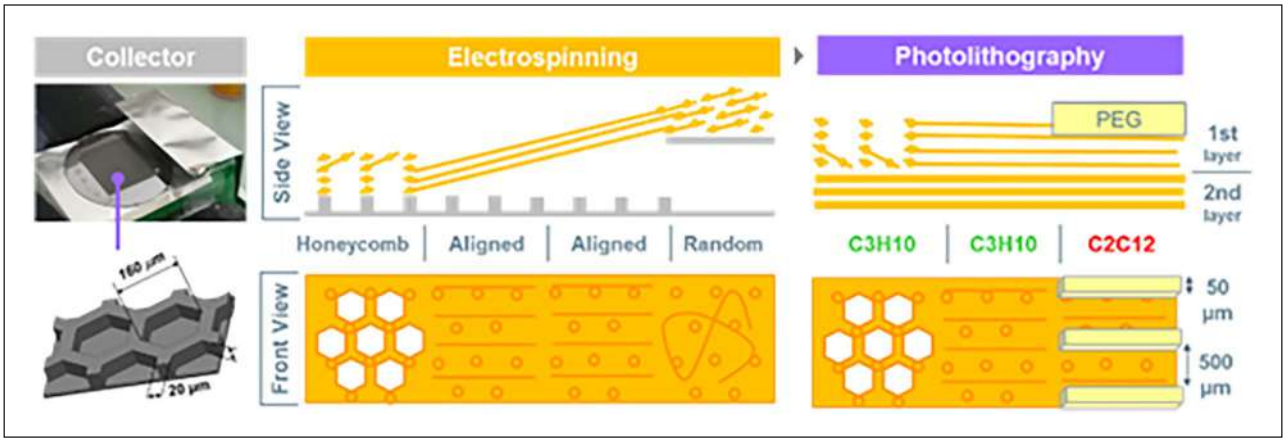

Figure 1. Schematic scaffold manufacture and coculture.

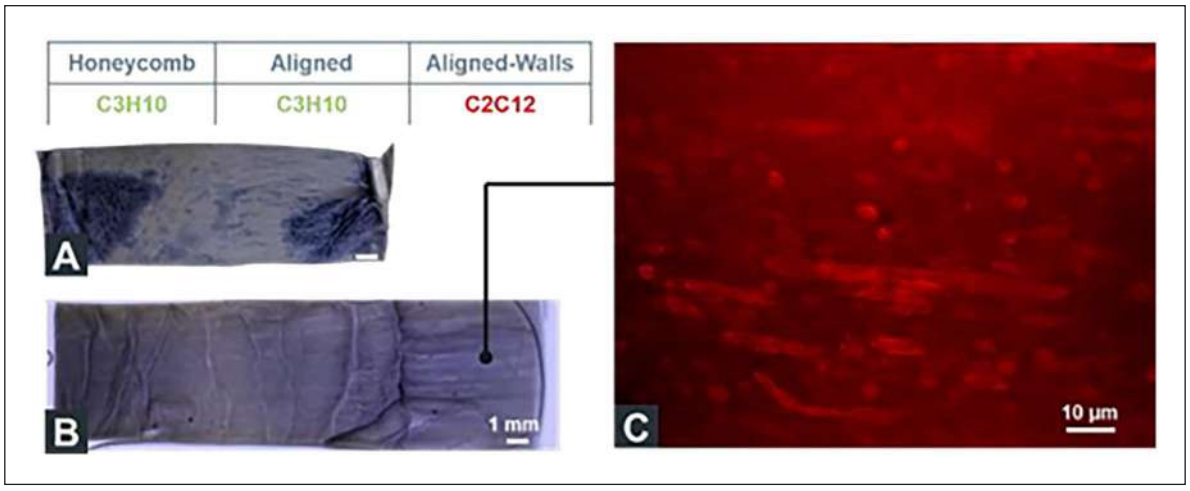

Figure 2. ALP staining after 7 days of dynamic culture in monoculture (A) and coculture (B) conditions. Myotubes immunostained by alpha-actinin (C).

Myotubes were observed by immunostaining where the C2C12 were seeded, showing their correct trend to muscle fate. Unexpectedly, ALP staining was more ubiquitous in the co-culture than in monoculture (Fig. 2). There was thus no clear evidence in this situation that the microstructures can guide C3H10 differentiation towards bone or tendon lineage.

Discussion: This new triphasic microsctuctured scaffold permited to evaluate the capacity of cocultured C2C12 and C3H10 to differentiate into bone, tendon and muscle lineage without any differentiation factor. Our results highlighted that the co-culture attenuated the effect of surface topology on cell differentiation, as previously observed with monoculture. Further investigations are needed to define whether this effect is due to the co-culture medium or by factors released by the cells.

References

1. Garcia Garcia et al, ACS Biomaterials Science and Engineering 4, no 9, 2018
2. Garcia Garcia, et al. Journal of Biomedical Materials Research Part A 109, no 10, 1881-92, 2021
3. Beldjilali-Labro et al, International Journal of Molecular Sciences, 23(1):260, 2022.
4. Nedjari et al, Materials Letters 142, 180-83, 2015

Acknowledgements

This work was supported by a scholarship from Graduierten Akademie from Leibniz University, by fundings from the French Ministry of Higher Education and Research, by Short-Term Research Grants 2023 from the DAAD, and ANR.

EVALUATING OFF-THE-SHELF BALLOONS FOR PARTIAL REBOA

Connor Coughlan-Ward (1), Michael Šeman (1,2), Silvana Marasco (3,4), Shaun Gregory (1,5), Andrew Stephens (1)

1. Cardio-Respiratory Engineering and Technology Laboratory, Department of Mechanical and Aerospace Engineering, Monash University, Australia; 2. School of Public Health and Preventive Medicine, Monash University, Australia; 3. Cardiothoracic Surgery, The Alfred, Australia; 4. Department of Surgery, Monash University, Australia; 5. Centre for Biomedical Technologies and School of Mechanical, Medical, and Process Engineering, Queensland University of Technology, Australia

Introduction: Partial resuscitative endovascular balloon occlusion of the aorta (pREBOA) is a technique for establishing haemostasis in patients with non-compressible torso haemorrhage [1]. Partial inflation of the balloon within the descending aorta leads to incomplete occlusion and subsequent trans-balloon flow, with the aim of striking a balance between haemorrhage and distal ischemia [2]. The preeminent device for pREBOA is the pREBOA-PRO®. However, in emergency situations, pREBOA may be performed with the off-label use of balloons not approved for pREBOA. Traditional compliant balloons easily deform when deflated, resulting in sudden increases in distal flow and potential exsanguination [3,4]. We hypothesize that balloons which share the semi-compliant nature of the pREBOA-PRO® may allow for finer flow titration. This study aimed to compare the capacity of clinically available compliant and semi-compliant balloon (CB and SCB) catheters to titrate flow in a pREBOA setting.

Methods: We present a new measure to assess a balloon's pREBOA ability; optimal working range (OWR). The OWR is the balloon volume range that corresponds to ideal trans-balloon flows (0.3-0.7 L/min). Flows outside this range lead to significantly greater ischemia and rebleeding [4]. This in-vitro study used a continuous flow loop filled with an aqueous glycerol solution. Tubing with a compliance of 0.067 ml/mmHg and inner diameter of 19 mm was used as an aortic model. Initial (uninflated balloon) loop flows ranged from 1.5-3.1 L/min. A 27 mm CB and a 25 mm SCB were compared, with titratability assessed through incremental deflation from full occlusion, using a programmed syringe pump. Data, including intra-balloon pressure and volume, trans-balloon flow rate, and loop pressures, were recorded for analysis.

Results: For all initial flow rates, the OWR was significantly higher for the SCB compared to the CB (mean 1.13 vs. 0.34 ml; $p<0.001$). Linear regression analysis revealed that the slope of the SCB's titration curve was significantly lower than the CB's (0.39 vs. 1.39; $p<0.0001$), indicating superior titratability (Figure 1). Varying initial flow rate had a negligible effect on OWR.

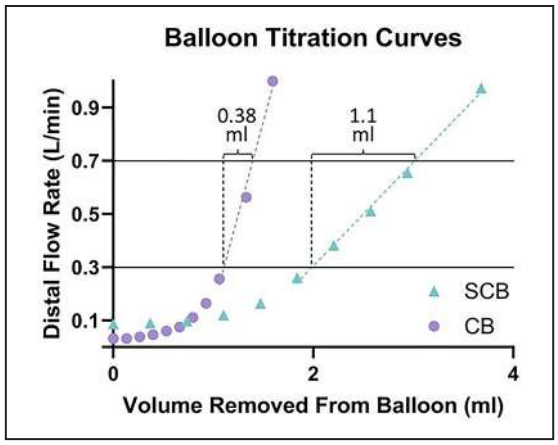

Figure 1. Titration curves of the compliant and semi-compliant balloon (CB and SCB) catheters for an initial flow rate of 2.3 L/min. Horizontal lines at 0.3 and 0.7 L/min represent ideal flow range during pREBOA, optimal working range for each balloon visualized.

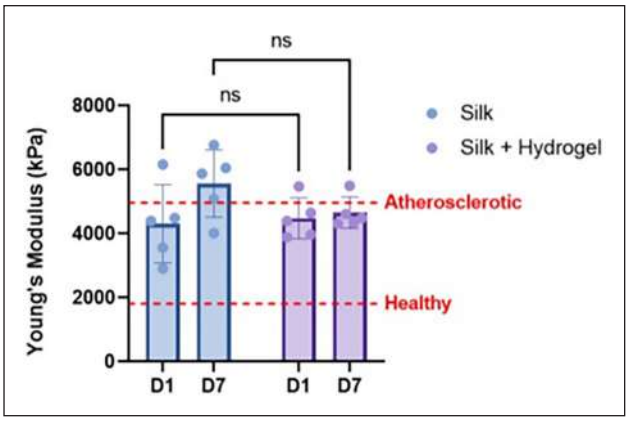

Figure 1. Young's Modulus Plot comparing electrospun silk scaffold with hydrogel-coated electrospun silk scaffolds showing no significant difference between the scaffolds at Day 1 incubation in PBS and Day 7 incubation in PBS. Stiffness of atherosclerotic coronary arteries and healthy coronary arteries were used as comparisons [5].

Discussion: The OWR of the SCB far exceeded that of the CB across all initial flow rates, indicating that SCBs should be considered when performing pREBOA using off-the-shelf equipment. Additionally, we showed that OWR is a measure that can be used for pREBOA evaluation. When considering clinical implementation of pREBOA, the benefits of wider OWRs become apparent. Using a fine adjustment syringe [2] to incrementally titrate practical aliquots of 0.1-0.2 ml [5,4] the OWR of the SCB translates to a minimum of 6-11 "safe" steps, compared to a maximum of 2-4 for the CB. The larger OWR of the SCB enables finer flow control, potentially increasing the likelihood of users achieving ideal trans-balloon flows during balloon titration, which could translate to improved patient outcomes.

References

1. Glaser J et al, Curr Surg Rep, 5:23, 2017.
2. Johnson MA et al, J Trauma Acute Care Surg, 81:S133-S137, 2016.
3. Matsumura Y et al, Eur J Trauma Emerg Surg, 47:1023-1029, 2019.
4. Forte DM et al, J Trauma Acute Care Surg, 87:1015-1025, 2019.
5. Power A et al, J Trauma Surgery Acute CA, 7:e000948, 2022.

ELECTROSPUN SILK SCAFFOLDS TO MIMIC ARTIFICIAL BLOOD VESSELS – HEALTHY AND OBSTRUCTED

Thao Nhu Anne Marie Vuong (1), Sandra Spoa (2), Hien Anh Tran (1), Matthew Moore (3), Ian Chin (3), Timothy Mitchell (3), Steven G. Wise (3), Socrates Dokos (1), Michael Stevens (1), Jelena Rnjak-Kovacina (1)

1. University of New South Wales, Australia; 2. CODEX, Australia; 3. University of Sydney, Australia

Introduction: *In vitro* models of cardiovascular disease serve as invaluable tools for unraveling disease mechanisms, evaluating new therapies, and probing physiological phenomena. A notable limitation of phantoms used in current models lies in their inherent rigidity and cytotoxicity, hindering the exploration of accurate hemodynamics and cell-to-cell interactions crucial in human physiology [1]. Integrating natural polymers like silk as the primary constituent in phantom construction offers a promising solution to this challenge. By leveraging silk's inherent compliance and biocompatibility, we can create biological *in vitro* models that more authentically replicate vessel wall properties, facilitating the investigation of essential cell interactions [2]. This project aims to develop silk-based artificial healthy and obstructed blood vessels as more physiologically relevant phantoms for *in vitro* testing of cardiac devices and pharmaceutical testing.

Methods: Silk-based blood vessel (SBBV) was fabricated by electrospinning a solution of silk [3] (8% w/v) and polyethylene oxide (5% w/v) into fibrous, porous tubular SBBV. Hydrogel-coated electrospun silk scaffolds (HCESS) were created by rotating the SBBVs in a silk hydrogel precursor solution (8% silk, 0.05mM/5mM ruthenium/SPS) and photocrosslinking under visible light for 2.5 minutes. Tensile testing of the SBBVs was conducted on day 1 and 7 of incubation in PBS. Coronary artery smooth muscle cells and NIH3T3 fibroblasts were seeded on flat ⅓5mm SBBVs samples to assess cell interactions. Tensile mechanical properties of silk hydrogels (2-6%) were tested to assess their utility in mimicking the mechanical properties of atherosclerotic plaque.

Results and Discussion: SBBV has been shown to have the modulus of atherosclerotic coronary vessels [Figure 1], but it is difficult to seed cells on porous materials under flow conditions. HCESS addresses this by seeding the vessel walls with hydrogels that support cell encapsulation and do not change the mechanical properties of the vessel. The stiffness of the hydrogel layer can be fine-tuned through the silk concentration within the hydrogel [4].

More optimization is still required to achieve healthy artery mechanical values.

Hydrogels can also be used to create obstructions in the lumen, so flow through obstructed vessels can also be analyzed. The 3% silk hydrogels displayed similar mechanical properties to the fibrotic tissue in coronary plaques, and thus can be used as an obstructive mimic within the vessel. Validation of the hemodynamics experienced within the obstructed and non-obstructed vessels was done against computational fluid dynamic (CFD) studies and produced similar fractional flow reserve (FFR) and flow values.

Conclusion: Integrating silk-based scaffolds into cardiovascular *in vitro* models addresses rigidity limitations, allowing for more accurate replication of vessel properties and cell interactions. HCESS exhibits promising

vessel compliance and support for cell attachment. While further optimization is needed, validation against CFD confirms their utility in mimicking physiological conditions.

References

1. Kainz, W, et al. IEE Tran. Radiat. Plasma. Med. Sci. 2019 Jan; 3(1): 1-23
2. Cui, X et al. Advanced Materials, 2020 Feb; 9(4):
3. Filipe C.E. et al. J Am Coll Cardiol Basic Trans Science. 2018 Feb, 3(1) 38-53
4. Hasturk,O. Biomaterials, 2020; 232
5. Karimi, A. Mater. Sci. Eng C. Mater. Biol. Appl. 2013 Jul. 1;33(5); 2550-4.

IMPACT OF HEMOADSORPTION ON LEVELS AND CHARACTERISTICS OF ALBUMIN – WHERE ARE WE? (PRESENTATION DURING MAIN PROGRAM)

Dr. Maria Taborda-Küpper

CytoSorbents Europe GmbH, Berlin, Germany

Introduction: Albumin has a molecular mass of about 66,470 Da and consists of 585 amino acids, many of which contain sulfur. It is water-soluble, the binding capacity for water is about 18 ml/g. With a serum level of 3.5 -5.2 g/dl it forms the main component of plasma proteins. Albumin is formed in the liver and has a half-life of 12 -21 days in the human body. Human serum albumin is categorized into human mercaptalbumin (HMA) and human non-mercaptalbumin (HNA), according to the redox state of the cysteine residue at position 34.

CytoSorb hemoadsorption provides size-selective and concentration dependent removal of primarily hydrophobic substances from the whole blood. The molecular weight of albumin is beyond the adsorption spectrum of CytoSorb (≤ 60 kDa), however, since there is no definitive cut-off size, substances around this may also be removed.

Screening of the literature should help to clarify remaining questions regarding albumin removal but also concerning any potential impact on albumin characteristics.

Methods: Screening of the existing literature via PubMed and CytoSorbents literature database provided various *in-vitro* and *in-vivo* publications that investigated the impact of hemoadsorption with CytoSorb on albumin levels, but also on the oxidation status of albumin. While *in-vitro* investigations assessed direct removal by the adsorber, human data measuring albumin plasma levels over time primarily analyzed the resulting impact for the patient.

Results: *In vitro*-tests have shown conflicting results regarding removal of albumin by CytoSorb. While some tests did not show any removal, others reported on significant removal (of up to 40%), which was also supported by data from *ex-vivo* perfusion experiments.

In contrast to this, data from patients on the impact of CytoSorb on plasma levels of albumin consistently report no changes with CytoSorb treatment in a variety of patients (cardiac surgery, septic shock, brain death).

Next to this, recent *in-vitro* tests have shown that CytoSorb may have a beneficial impact on the oxidation status of albumin and could thereby increase the proportion of the more functional albumin (HMA).

Discussion: Based on the current understanding it still seems acceptable to not expect any clinically relevant impact on the plasma levels of albumin with CytoSorb therapy over time. This could be explained by the fact that (potential) removal by CytoSorb is rapidly compensated for via an increase in the de-novo-production rate of albumin. Whether this compensatory mechanism might be impaired in certain patient groups remains to be determined, however, critically ill patients in general, as included in the majority of the studies mentioned above, might also experience a reduction in albumin levels due to the underlying disease and not necessarily due to removal by hemoadsorption.

Promising first signals regarding a potential beneficial impact of CytoSorb therapy on the (oxidation) status of albumin needs to be investigated further. The hypothesis that removal of albumin by CytoSorb may be more pronounced for its dysfunctional variations also requires further investigations.

References

1. Bernardi et al., Crit Care 2026; 20(1):96
2. Schaedler et al., PLoS One 2017; 12(1):e0187015
3. Kellum et al., Crit Care Med 2008; 36(1):268-272
4. Mehta et al., World J Crit Care Med 2020;: 9(1):1-12
5. Keles et al., Int J Artif Organs 2019; 42(12):765-769
6. Acar et al., Transplant Proc 2019; 51(7):2420-2424
7. Peng et al., Blood Purif 2022; 51(5):410-416
8. Suefke et al., Ther Apher Dial 2016; 20(5):531-533
9. Iskender et al., J Heart Lung Trans 2017; 37(2):283-91
10. Dominik & Stange. Blood Purif 2021; 50(1):119-12
11. Harm et al., Blood Purif 2020; 49(1):33-43
12. Gemelli et al., Blood Purif 2019; 47(1):10-15
13. Schildboeck et al., Blood Purif 2024; 53(4):231-242
14. Internal data (Dr Hartmann)

Acknowledgements

We thank Dr. Hartmann for conducting experiments on the impact of CytoSorb on the oxidation status of albumin

HEMODIALYSIS WITHOUT AN EXTRACORPOREAL BLOOD CIRCUIT? MODULAR DESIGN CAN MEET PATIENT PREFERENCES & STANDARDS

Fokko Wieringa (1,2)

1. IMEC, Holst Centre, 5656 AE Eindhoven, The Netherlands;
2. Department of Nephrology and Hypertension, University Medical Centre Utrecht, Utrecht, The Netherlands

Methods: The term "hemodialysis" (HD) as defined by international standard IEC 60601-2-16 was used in a PUBMED database query regarding (trans)portable, wearable and (partly) implantable HD systems. 24 out of 159 search results were included and scanned for specific HD devices and/or HD systems in development. We collected additional information about weight, size and development status via the internet and/or by contacting manufacturers. IATA hand baggage criteria formed the border between transportable and portable. Technology Readiness Levels (TRL) values were assigned by combined TRL-scales of the European Union and NATO medical staff. See also Fig. 1.

Results: The query revealed 13 devices/projects: 7 transportable (6xTRL9, 1xTRL5); 2 portable (1xTRL6-7, 1xTRL4); 2

wearable (1xTRL6, 1xfrozen); and 2 partly implantable (1xTRL4-5, 1xTRL2-3). See also Fig. 2.

Three main categories of technical approaches were distinguished: Single-pass, Dialysate regenerating, and Implantable HD filter with extracorporeal dialysate regeneration (in climbing order of mobility). Simplified "typical" system diagrams were derived for these three main categories of typical approaches. Two of these diagrams are depicted in Fig. 2. Technical trade-offs are dominated by water consumption/reclaim, HD filter technology and connection to the vascular system.

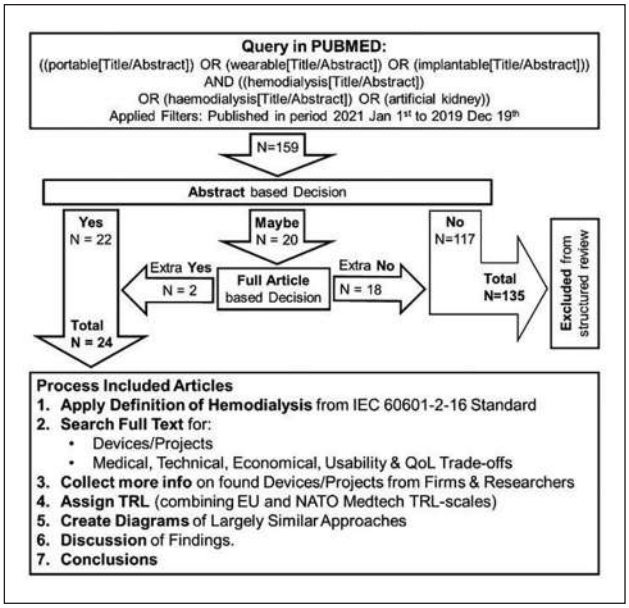

Figure 1. PUBMED query to identify Hemodialysis Systems (or large R&D projects towards them).

Discussion: Compared to Single-pass HD systems, dialysate regenerating HD systems offer a first miniaturization step towards truly portable (or even wearable) HD devices that meet IATA requirements for airplane hand luggage [1]. Such HD systems are in clinical trials for market approval. Ongoing R&D projects, aimed at combining miniaturized implantable HD filters with an extracorporeal dialysate regenerating circuit look promising and the principle falls within the scope of hemodialysis as defined in the IEC60601-2-16 standard.

Conclusions

Dialysate regeneration is an enabler for increased portability/wearability of HD systems. In combination with ongoing R&D projects, targeting long-term implantable HD filters, HD without needles or intravascular catheters seems a technical possibility [2]. But lack of funding severely hampers progress in the field of Kidney Replacement Technologies.

References

1. IATA passenger baggage rules. https://www.iata.org.
2. Ramada DL et al. Portable, wearable and implantable artificial kidney systems: needs, opportunities and challenges. Nat Rev Nephrol 2023;19:481–90.

Acknowledgements

We acknowledge financial support from the European Commission (KIDNEW project, HORIZON-EIC-2022 Pathfinder program, grant agreement no. 101099092), as well as from the NXTGEN HighTech project Biomed04, granted by the Dutch National Growth Fund.

FREE AMINO ACID SUPPLEMENTATION PREVENTS PROTEIN MODIFICATIONS ASSOCIATED WITH CHRONIC KIDNEY DISEASE

Dustin Mikolajetz[1], Silke Laudy[1], Sofía de la Puente Secades[1], Setareh Orth-Alampour[1], Vera Jankowski[1], and Joachim Jankowski[1,2]

1. Institute of Molecular Cardiovascular Research, University Hospital RWTH Aachen, Germany; 2. Experimental Vascular Pathology, Cardiovascular Research Institute Maastricht (CARIM), University of Maastricht, The Netherlands

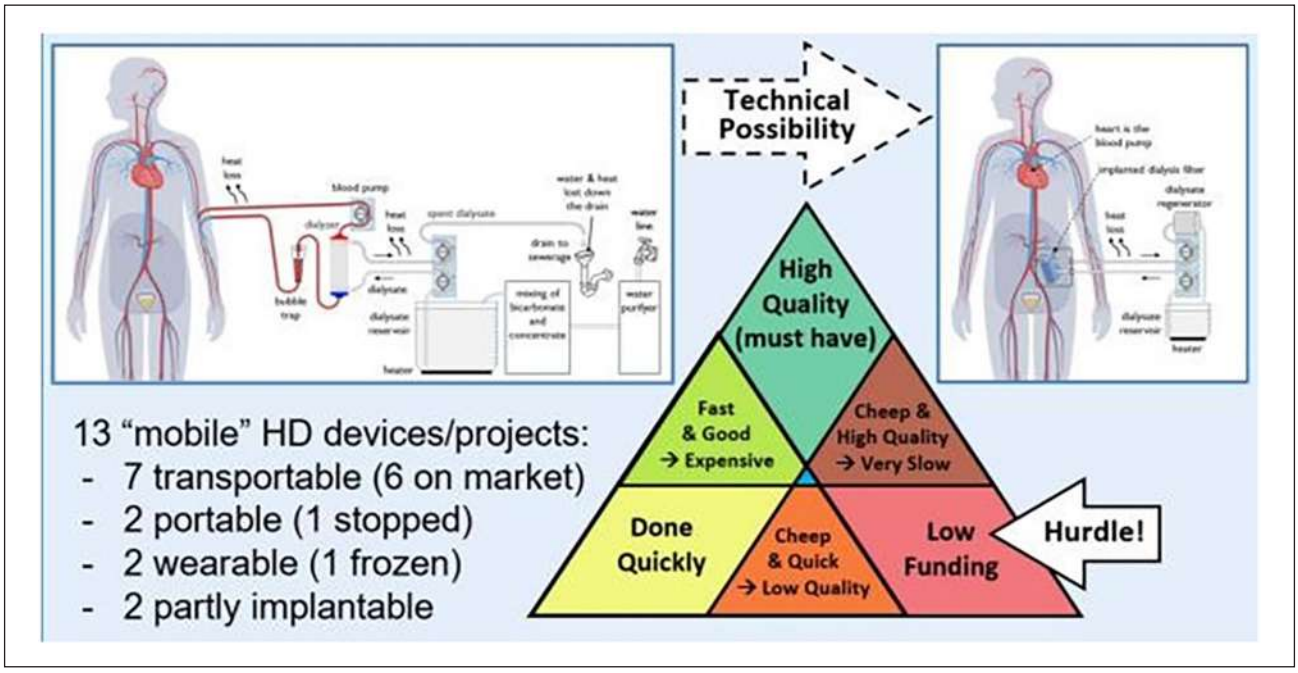

Figure 2. Graphical summary of findings. Presently, single pass systems dominate the market (left diagram). Dialysate regenerating HD systems allow further miniaturization and are in clinical trials. With an implanted HD filter, the blood can stay inside the body and only an extracorporeal dialysate circuit (preferably with dialysate regeneration) is needed (right diagram).

Introduction: Chronic kidney disease (CKD) affects over 10% of the population worldwide. In CKD patients the plasma concentration of uremic toxins is increased due to reduced kidney function [1]. These increased concentrations cause numerous pathological post-translational modifications (PTMs), like carbamylation, guanidinylation or oxidation of proteins, which can lead to an alteration of their conformation, activity or function [1,2]. Specifically, PTMs of proteins like albumin are undesired, since their high mass prevents them to be cleared by the kidney or hemofiltration, ultimately leading to an accumulation of uremic modified proteins [3]. Therefore, preventing PTMs beforehand is of high interest. Here we analyse the effect of amino acid supplementation and their capability to protect proteins from PTMs.

Methods: PTMs were induced in the proteins Carboxypeptidase E and Calpain1 after incubation with different concentrations of o-methylisourea and hydrogen peroxide. Afterwards dialysis and digestion of the protein samples with trypsin was done and analysis with mass spectrometry was performed. Once finding optimal conditions to induce PTMs, amino acids were given to the sample before inducing modification.

Results: Incubation with o-methylisourea led to guanidinylation of Carboxypeptidase E. The modification was only observed at one fragment. This fragment contains the sequence ***ELLVIELSDNPGVHEPGEPEFK**** (87-108). Amino acid marked with * (Lysine) indicates position of modification. Addition of free lysine before the toxin led to prevention of the PTM in the protein.

Incubation with hydrogen peroxide led to oxidation of Calpain1. Modification was observed in multiple fragments: ***LETM*FR*** (682-687), ***M*AIESAGFK*** (642-650), and ***M*EDGEFWM*SFR*** (329-339).

Amino acids marked with * indicates position of modification. In all fragments the methionine residues were oxidized. Addition of free methionine before the toxin led to prevention of the PTM in all fragments.

Discussion: Post-translational modification is an important mechanism in mediating proper protein function, as they can influence multiple aspects of proteins including: folding, binding affinity, translocation or activity. Pathological post-translational modification mediated by uremic toxins might interfere with these tightly regulated mechanism. Therefore, finding an option to prevent these uremic toxin associated PTMs and reducing uremic toxin concentration in CKD patient in general is an anticipated therapy option to improve patient outcome. Here we analyzed the induction of PTMs by incubation of proteins with two uremic toxins. Guanidinylation was successfully induced by o-methylisourea and oxidation by hydrogen peroxide, both modification are known to be more abundant in patients with chronic kidney disease [4]. Moreover, here we showed that free amino acid supplementation is able to prevent toxin induced PTMs and seems to be a promising approach to tackle the problem of PTMs in CKD patient.

The underlying mechanism will be further elucidated, as these preliminary results show first promising effects *in vitro*. The next step is to analyze if amino acid supplementation also prevents CKD associated PTMs in an *in vivo* mouse model.

References

1. Laget, J., *et al.*, *Molecular Aspects of Medicine*, *86*. (2022).
2. Schunk, S., *et al*. *Journal of the American Society of Nephrology*, *32*(12), 1–15 (2021).
3. Sánchez-Ospina, D., *et al. Journal of Clinical Medicine*, *13*(5). (2024)
4. Noels, H., *et al*. *Nature Reviews. Nephrology*. (2024)

Acknowledgements

This work was supported by a grant from the German Research Foundation (DFG, SFB/TRR219 project C-04).

PERSONALIZED ANTICOAGULATION IN DIALYSIS: TARGET OR ILLUSION?

Sunny Eloot (1), Ivan Josipovic (2), Wim Van Biesen (1), Matthieu Boone (2), Floris Vanommeslaeghe (1)

1. Nephrology, Ghent University Hospital, Belgium; 2. Centre for X-ray Tomography (UGCT), Ghent University, Belgium

Introduction: Prevention of clotting in the extracorporeal circuit is an important concern in maintenance hemodialysis (HD) patients. The anticoagulation management is difficult in these patients due to the subtle balance between a prothrombotic state on the one hand, mostly due to inflammation and underlying endothelial dysfunction, and bleeding risk on the other hand, mostly related to medication and uremic thrombocytopathy. Apart from the patient, other aspects, i.e. in the extracorporeal circuit, might enhance clotting as well: mechanical trauma on the blood cells as occurring in the blood pump, shear on the blood cells in narrow channels as in the needles or catheter, blood-air contact as in the venous bubble trap, and blood-membrane contact as in the hemodialyzer.

All these patient and dialysis related variables might result in fluctuating dialyzer outcome over time and, hence, make it difficult to come to a personalized anticoagulation strategy. For a long time there was even a lack of accurate tools to objectively assess dialyzer clotting, such that intrapatient variability of dialyzer outcome was never investigated

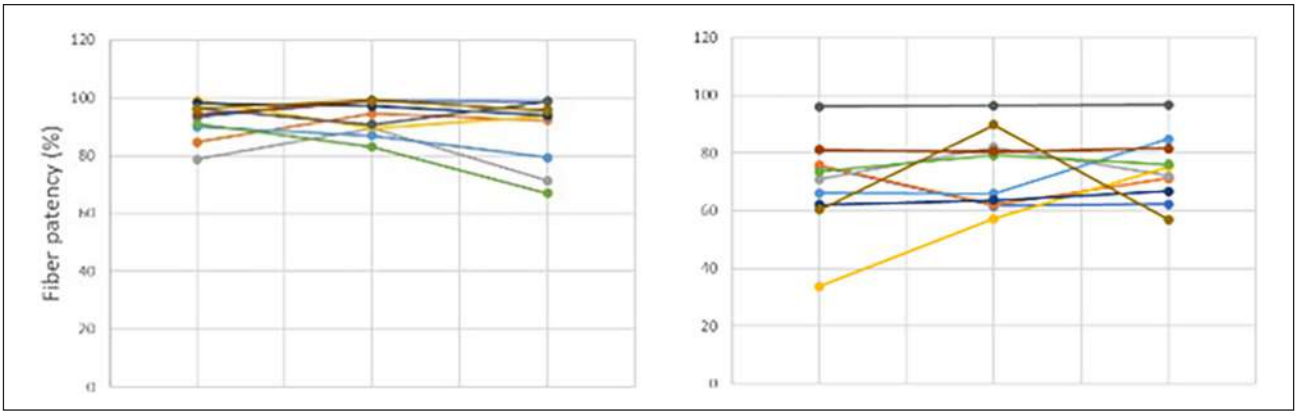

Figure 1. Fiber patency for three consecutive full (left) and 1/4th of regular anticoagulation dose (right).

before. But since recent years, dialyzer fiber patency can be accurately quantified by a, so called gold standard, micro-CT (µCT) scanning of dialyzers post dialysis in a research setting [1,2]. The aim of the present study was therefore to determine intrapatient variability of dialyzer fiber patency as measured by post dialysis µCT scanning.

Methods: Ten stable chronic HD patients were included with a well-functioning vascular access, ultrafiltration rate less than 4L/session, and no known coagulation disorder, active inflammation or malignancy.

Patients were randomized to a cross-over protocol (each arm lasts for 1 week with 3 dialysis sessions) with two different anticoagulation strategies: regular dose *versus* 1/4th of the regular dose. Each patient was his/her own control in this two-arm study over 2 weeks (6 sessions). Low molecular weight heparin was injected as a bolus in the venous blood line at the dialysis start. Patients obtained HD for 240min with an FX800 Cordiax dialyzer on a 5008 dialysis machine (both Fresenius Medical Care, Germany), with blood flow 300mL/min, dialysate flow 500mL/min, and ultrafiltration rates according to the needs of the patients. At the end of the dialysis session, a standard rinsing procedure of the hemodialyzer was performed, and after 16-24h of drying, dialyzers were scanned with µCT technique to quantify fiber patency (25µm resolution) [1]. Octopus Reconstruction software package was used to reconstruct the raw projection data into visualizations of dialyzer cross-sections in which non-blocked fibers were counted using the free package ImageJ (NIH, Bethesda, USA). The number of non-blocked dialyzer fibers was compared with the total number of fibers as quantified previously in three non-used dialyzer samples to determine the percentage fiber patency.

The Intraclass Correlation Coefficient (ICC) was calculated as the inter-patient variance divided by total variance (i.e. inter plus intra-patient variance).

Results: The ten included patients (age 53.0±14.8; 7 male) were dialyzed six times for 240min, with no difference in ultrafiltration rate between the sessions (overall 1.5±0.9L). Dialyzer fiber patency (with fibers at least 50% open) was 94[89;97]% with full anticoagulation and 73[63;81]% with 1/4th of regular anticoagulation (P<0.001)(Figure 1). ICC was 0.531 and 0.493 for fiber patency with full respectively 1/4th of anticoagulation.

Discussion: The low ICC (<0.6) implies a rather large intra-patient variability in dialyzer fiber patency, underscoring the complexity of clotting during dialysis, and the interplay of patient and dialysis related variables impacting clotting. All this, together with the lack of a bed-side tool to quantify clotting, makes it difficult to assess an optimized and personalized anticoagulation strategy in dialysis.

The present ICCs are however useful to determine study power when setting up future interventional clotting studies.

References

1. Vanommeslaeghe et al, Sc Reports, 8:2677, 2018
2. Claudel al, Sem Dialysis, 34:103-115, 2021

GREEN AND EFFICIENT DIALSYIS: A CONTRADICTION IN TERMS?

Sunny Eloot (1), Wim Van Biesen (1), Floris Vanommeslaeghe (1)

1. Nephrology, Ghent University Hospital, Belgium

Introduction: Hemodialysis (HD) is currently performed with dialysate flows in the range 500-700mL/min in HD and hemodiafiltration (HDF) mode. With a standard daytime dialysis scheme of three times four hours a week, and accounting for a 60% efficiency of the reverse osmosis water installation, each patient consumes up to ~31.000-50.000L per year. Lowering dialysate flow may impact the diffusive toxin transport, driven by the concentration gradient. However, also fiber diameter and membrane porosity play a role in the diffusive transport [1]. Hence, for the same blood and dialysate flow, the choice of the dialyzer will determine toxin transport.

The aim of this study was to check if sufficient solute removal can be achieved when using a lower dialysate flow, and as such consuming less water. We therefore quantified instant and overall removal of representative uremic toxins in HDF with high dialysate flow QD in a high flux dialyzer *versus* HD with a medium cut-off dialyzer either without and with lowering QD.

Methods: Ten stable chronic HD patients with a well-functioning vascular access and no active inflammation or malignancy were included. Patients were randomized in a cross-over study with three midweek sessions of 240min with patient's usual blood flow: 1) post dilution HDF with FX800 Cordiax dialyzer (Fresenius Medical Care, Germany), QD 700mL/min, and auto substitution rate (HDF-700); 2) HD with Theranova 400 dialyzer (Baxter, USA) and QD 700mL/min (HD-700); and 3) HD with Theranova 400 and QD 300mL/min (HD-300). All sessions were performed on a 5008 dialysis machine (Fresenius Medical Care, Germany), with ultrafiltration rates according to the needs of the patient.

Blood was sampled 5min after the start of each test session from the arterial and venous dialysis blood lines to calculate dialyzer extraction ratio (ER -%). From the spent dialysate line, sampling was performed at 5, 30, 90, and 240min, to calculate total solute removal (TSR) from the AUC. All blood and dialysate samples were analyzed for urea, phosphate, beta-2-microglobulin (B2M), and myoglobin.

Results: The ten included patients (age 55.6±19.0; 6 male) were dialyzed thrice for 240min, with no difference between the sessions in blood flow [thrice 300mL/min (n=9) and 350mL/min (n=1)], and ultrafiltration rate (i.e. 2.1[1.4;2.6]L, 2.0[1.1;2.4]L, and 2.0[1.4;2.6]L).

Two patients had a central venous catheter, i.e. Bard Hemostar 14.5Fr (Becton Dickinson, USA) and Palindrome 14.5Fr (Medtronic, USA). No adverse or bleeding events were recorded.

Serum concentrations of the four toxins were not different at the dialysis start of the three midweek sessions. Water consumption, ERs and TSRs are shown in Table 1. While ERs were not different among the three strategies, overall TSR was lower with HD-300 *versus* HDF-700, while TSR with HD-700 was not different from TSR with HDF-700.

Discussion: Aiming for a more environmentally friendly dialysis becomes more and more important, and herewith, reducing water consumption is one of the cornerstones. Since a reduction in water consumption might however come at the expense of a decrease in dialysis efficiency, the present study compared water use and toxin removal in different dialysis

Table 1. Extraction Ratio (ER) and Total Solute Removal (TSR).

	Post HDF	HD_700	HD_300	ANOVA
Consumption/session	**189L**	**168L**	**72L**	**P-vlaue**
ER (%)				
Urea	87.7 ± 7.9	87.8 ± 7.8	81.2 ± 9.3	0.180
Phosphorus	83.2 ± 5.5	81.5 ± 6.7	79.3 ± 6.4	0.402
β_2M	50.5 ± 11.0	47.2 ± 11.8	38.8 ± 6.3	0.050
Myoglobin	34.1 ± 9.7	31.7 ± 11.7	25.2 ± 6.1	0.128
TSR				
Urea (g)	53.2 ± 26.3	44.1 ± 17.6	25.3 ± 12.2$^{\alpha}$	**0.018**
Phosphorus (mmol)	61.7 ± 25.8	48.6 ± 22.9	29.9 ± 11.1$^{\alpha}$	**0.012**
β_2M (mg)	273 ± 144	225 ± 188	138 ± 46	0.125
Myoglobin (mg)	5.28 ± 0.77	4.72 ± 0.45	2.37 ± 0.67$^{\beta\gamma}$	**<0.001**

$^{\alpha}$ P<0.05 vs HDF-700; $^{\beta}$ P<0.001 vs HDF-700; $^{\gamma}$ P<0.001 vs HD-700

modalities, using different dialysate flows and dialyzers. Comparing HD with a Theranova dialyzer and 300mL/min dialysate flow resulted in a decrease of 62% in water consumption, but also a decrease in toxin removal of 49-55% as compared to post dilution HDF with an FX800 dialyzer and 700mL/min dialysate flow. Switching from this HDF_700 modality to HD with Theranova dialyzer and 700mL/min dialysate flow reduces toxin removal by 11-21% with a decrease of only 11% in water consumption. A deeper understanding of how different treatment settings affect solute clearance and clinical endpoints should help in rationing water use and tailoring patient-specific recommendations for dialysis modality, dialysis fluid flow, dialyzer membrane, and treatment duration.

Reference

1. Kirsch et al, Nephrol Dial Transpl, 32:165-172, 2017

DEVELOPMENT OF BIOINKS FROM HUMAN PLACENTA ECM FOR 3D BIOPRINTING OF ARTIFICIAL TISSUE CONSTRUCTS

Karl H. Schneider[1,2,5], Marvin Dötzlhofer[1], Felix Pointner[1], Linda Denz[1], Vincent Fitzpatrick[4], Herbert Kiss[3], David Kaplan[4], Bruno K Podesser[1,2,5], Helga Bergmeister[1,2,5]

[1]Center for Biomedical Research, Medical University of Vienna, Austria; [2]Ludwig Boltzmann institute for cardiovascular research, Vienna Austria; [3]Department of Obstetrics and Gynecology, Division of Obstetrics and Feto-Maternal Medicine, Medical University of Vienna, Austria; [4]Department of Biomedical Engineering, Tufts University, Medford, MA, USA; [5]Austrian Cluster for Tissue Regeneration

Introduction: Advancements in tissue engineering rely on bioactive scaffolds that strike a delicate balance between mechanical resilience and cellular support, while also facilitating vascularization and maturation. Although 3D bioprinting offers precise scaffold fabrication, the lack of suitable bioinks remains a challenge for creating functional tissue constructs. Extracellular matrix hydrogels, particularly those derived from human placenta (hpECM), offer a promising combination of natural composition, high bioactivity, and ethical acceptability, enhancing the properties of bioinks for tissue engineering. We envision that hpECM hydrogels and composites could revolutionize the development of innovative bioinks for 3D tissue printing, offering substantial potential for in vitro experimentation and the advancement of future implant technologies.

Materials and Methods: We analysed the biological composition of hpECM hydrogels produced from different parts of the human placenta. Proteome analyses were used to break down the respective matrisome and enabled

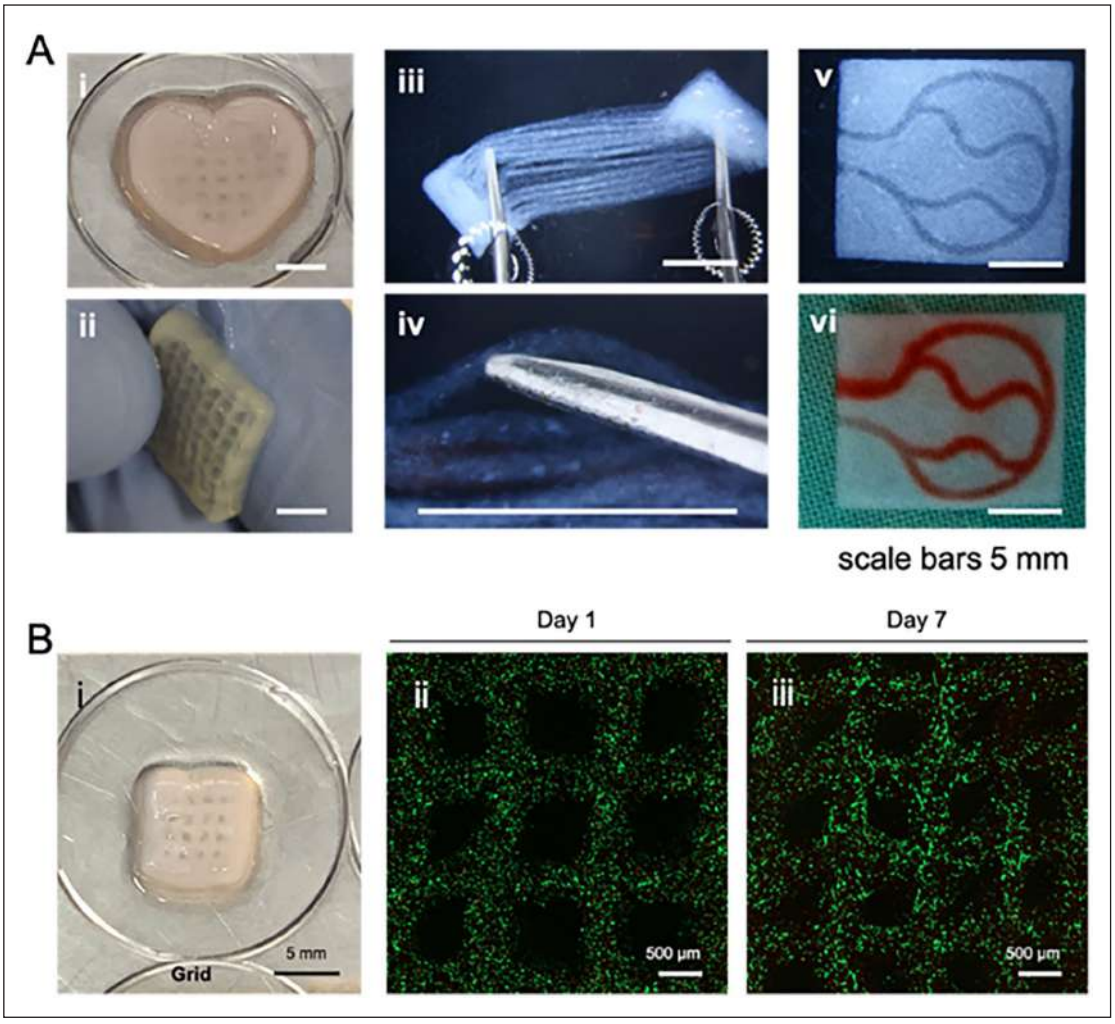

Figure 1. 3D bioprinted scaffolds using hpECM bioink. (A)(i-ii) grids in square and heart shape, (iii-iv, cardiac muscle fiber construct, (v-vi) perfusable loop empty and filled with red dye. (B)(i) grid in square shape, (ii) Calcein AM cell staining day 7, (iii) day 14 showing living cells in green.

an evaluation of the manufacturing process as well as a direct comparison of hpECM hydrogels derived from different placental tissues such as the amnion, the chorion or the umbilical cord. We further were investigating the usability of hpECM hydrogels and various composites with silk or fibrinogen for 3D bioprinting processes. Therefore, printability studies and biomechanical tests were carried out for this purpose. To investigate bioactivity, primary cells were grown in 3D cultures using hpECM bioinks and various prevascularisation experiments were performed.

Results: Our manufacturing protocol results in reproducible hpECM hydrogels with preserved structural and functional proteins and minimal DNA content. Cell studies showed a high cytocompatibility of the hpECM bioinks, and vascularisation experiments demonstrate the importance of the matrix composition for tube formation. A previous study showed the successful enrichment of silk hydrogels with hpECM bioink to enhance bioactivity (1). Biomechanical analysis of these bioinks has now been performed and showed tunability of mechanical strength.

Furthermore, advanced 3D bioprinting with hpECM based bioinks enables the creation of high-resolution constructs, with promoting high cell viabilities as shown in Fig.1.

Outlook: Ongoing efforts are focused on refining tissue models and improving mechanical properties in our bioinks. Studies on prevascularisation have shown that the composition of the bioink matrix has an effect on the formation of microvessels. We hope that these findings will enable us to control vascularization in 3D-printed tissues in the future.

Reference

1. Schneider KH, Goldberg BJ, Hasturk O, Mu X, Dötzlhofer M, Eder G, et al. Silk fibroin, gelatin, and human placenta extracellular matrix-based composite hydrogels for 3D bioprinting and soft tissue engineering. Biomater Res. 2023;27(1):117.

DEGRADABLE WARP-KNITTED SPACER FABRICS FOR MUSCLE TISSUE ENGINEERING.

Leonie Hoffmann (1), Caroline Emonts (1), David Wienen (1), Thomas Gries (1)

1. Institut für Textiltechnik of RWTH Aachen University

Introduction: Extensive muscle defects cannot be structurally and functionally recovered by the body, these lead to a loss of strength and functionality of the affected muscle. The range of motion is decreased and there are permanent defects visible on the body of the patient. [1]

Conservative treatment options such as physical therapy and exoprothesis only offer modest improvement [2]. A surgical approach is the transplantation of functional muscle tissue, which comes with the drawbacks of limited availability and a second operation site [3].

Great possibilities are seen in Tissue Engineering. Important components include both the structural replacement of the extracellular matrix (ECM), and the colonization of this replacement with cells (myocytes) [4]. Another factor is the macroscopic hierarchical structure of natural muscle tissue. To provide potential for hierarchical growth, different cell lines can be printed precisely using the drop on demand technology. Highly biocompatible and bioactive hydrogels can be used as an ECM that is printable. They offer a positive environment for cell growth and proliferation but lack the mechanical stability necessary to cultivate voluminous tissue. Warp-knitted spacer fabrics can be used as a stabilizing scaffold for the hydrogel. They consist of two cover-layers and a pile-system, connecting both layers.

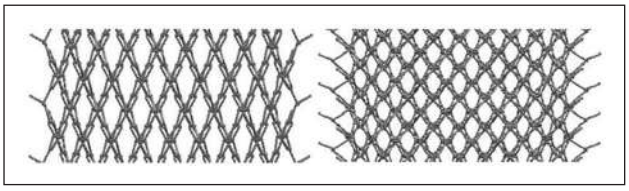

Figure 1. Upper cover layer of spacer textile. Left: Atlas-Mesh (AF), right: 1x2 Mesh (TF).

Table 1. Young's modulus and tensile strength of the analyzed spacer fabrics. Results are given in mean and 95% confidence level. Reference muscle tissue from [5] and [6].

Sample	Young's modulus [N/mm²]	Tensile strength [N/mm²]
AF-10	16.7 (0.4)	4.9 (1.7)
AF-16	10.7 (0.1)	7.0 (0.5)
TF-10	15.8 (0.3)	10.3 (1.3)
TF-16	9.2 (0.2)	7.4 (0.5)
Muscle tissue	1.58	0,9

Methods: This study aims to investigate the potential of degradable warp-knitted spacer fabrics as scaffold material for the use in Tissue Engineered Muscle Repair. The spacer fabrics were produced with biodegradable poly-ε-caprolactone yarns on a doublebar-Raschel-warp-knitting machine. For the cover-layers a 55 dtex f8 multifilament and for the pile yarn a 100 dtex monofilament was used. Spacer fabrics with two different cover-layers and with two different stitch densities were produced. They were evaluated mechanically using uniaxial tensile tests measuring the Youngs modulus and tensile strength. The morphological evaluation contains the pore size of the upper cover area as well as the porosity of the warp-knitted spacer fabric.

Results: The morphological characterization shows significantly larger pores in samples with an atlas-mesh as a cover-layer (Figure 1). Additionally, the share of pores larger than 600 µm is higher in atlas-mesh samples. In contrast, the stitch density does not affect the pore size significantly in the evaluated interval of 10 to 16 stitches/cm.

The mechanical properties of the spacer fabrics also differ significantly regarding the cover-layers (Table 1).

Discussion: Warp-knitted spacer fabrics offer great potential in the field of Tissue Engineering, because of their variable mechanical and morphological properties. The larger pore size of the atlas-mesh cover-layer allows for different filling methods, including the precise printing of hydrogels using the drop on demand technology enabling hierarchically structured cell cultures.

The mechanical properties of all evaluated spacer fabrics exceed those of human muscle tissue, therefore during the degradation enough stability can be provided for a cell-laden hydrogel filling. It was shown, that degradable warp-knitted spacer fabrics have high potential as scaffold materials in muscle tissue engineering.

References

1. Garg et al, Journal of orthopaedic research, 33(1): 40-46, 2015.
2. Greising et al, Tissue engineering. Part B, 25(6): 510-525, 2019.
3. Gorgan et al, Journal of the American Academy of Orthopaedic Surgeons, 19(1): 35-37, 2011.

4. Ikada, Jornal of the Royal Society 3(10): 589-601; 2006
5. Zwirner et al, Journal of Biomechanics, 106, 2020.
6. Zink, Journal of Legal Medicine, 70(3): 163-177, 1972

PUMPLESS IN VITRO OXYGENATOR HAEMOLYSIS SETUP

Nicolas Gendron (1), Marlene Schadow (1), Jan Heyer (1), Ulrich Steinseifer (1), Lasse J. Strudthoff (1) and Johanna C. Clauser (1)

1. Department of Cardiovascular Engineering, Institute of Applied Medical Engineering, University Hospital RWTH Aachen University, Germany

Introduction: In vitro haemolysis tests according to ASTM F 1841-2019 are commonly used to determine the haemolysis of extracorporeal membrane oxygenation (ECMO) devices. However, haemolysis testing for blood oxygenators remains a challenge [1], as current circuits typically require an additional blood pump, which is a primary source of haemolysis. [2]

Based on identified requirements, we propose a novel haemolysis test circuit that operates pump-free to increase the haemolytic signal of oxygenators.

Materials and Methods: Based on the identified limitations of haemolysis tests with oxygenators, we derived and synthesised requirements for a novel test circuit to overcome as many limitations as possible. The identified design requirements are presented below. Oxygenators specifically designed for ECCO2R therapy or paediatric ECMO therapy are designed for low blood flow perfusion. In paediatric ECMO, blood flows in neonates are typically between 0.080 L/kg/min and 0.120 L/kg/min and can be up to 1.7 L/min in infants weighing up to 15 kg [3], while blood flows in ECCO2R are between 0.5 L/min and a maximum of 2.0 L/min [4]. Schöps et al. demonstrated that specific haemolysis in centrifugal pumps is higher at low flow than at high flow [5], suggesting that a haemolysis test circuit that operates pump-free is required to eliminate pump haemolysis and thus improve the haemolysis signal of the oxygenator. To test different oxygenators used in low flow areas, the blood flow of the test circuit must be variably adaptable to the application under test (0.1 L/min to 4 L/min). To reduce the autologous haemolytic signal of the circuit, we reduce sections with causes of high shear rate. Further requirements result from the ASTM F 1841-2019 standard and relate to reproducibility and continuous flow.

Results: A pressure-driven setup was developed to perfuse a test oxygenator continuously without a blood pump. The experimental setup consists of pressurised cylinders that contain water and blood bags. The blood bags are connected by tubes for blood. A predefined pressure builds up in the pressure chambers using gas valves that are controlled by a Raspberry Pi controller. The blood transport tubes are connected via Y-connections and blood flow is regulated via clamp valves in a cross-circuit configuration. A controlled pressure build-up in the chambers compresses the blood bags and enables a controlled blood flow. Level sensors signal to the control unit when the gas and clamp valves for the blood tubes need to be changed to fill the blood bags alternately. The cross circuit guarantees unidirectional flow in the test object and frequent mixing in the reservoirs as they are filled from top but drained from the bottom.

Discussion: The experimental setup represents a novel approach to haemolysis testing, offering the capability to test haemolysis in oxygenators used in low flow areas without having a haemolysis signal either from a resistance adjusting clamp in blood pump testing or from a blood pump in the testing of other components. This unique

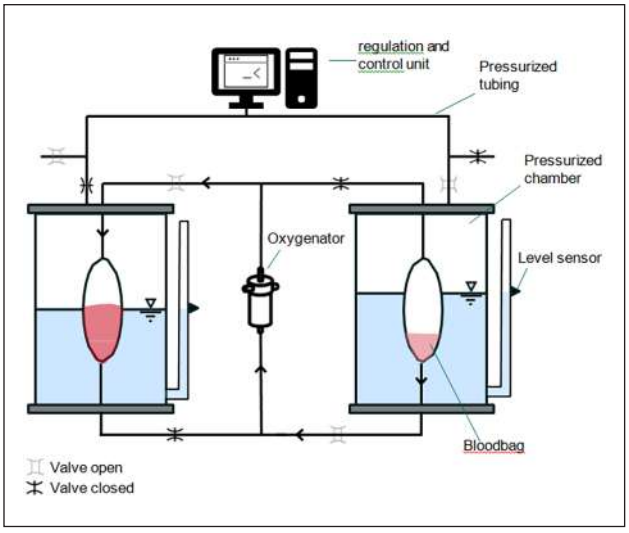

Figure 1. Experimental haemolysis setup

haemolysis test circuit presents a promising alternative for standard haemolysis tests, potentially leading to the standardization of the experimental procedure. However, challenges persist, including the need to further streamline the test setup and conduct more in vitro haemolysis tests to validate its effectiveness thoroughly.

References

1. Von Petersdorff-Campen K. et al. Potential Factors for Poor Reproducibility of In Vitro Hemolysis Testing. ASAIO Journal 68(3):p 384-393, March 2022.
2. Hesselmann F. et al. Three-dimensional membranes for artificial lungs: Comparison of flow-induced hemolysis. *Artificial Organs* 2022;46(3):412–426
3. Rosario et al. Extracorporeal Membrane Oxygenation in Children. *StatPearls Publishing*; 2024, PMID: 34283470
4. Karagiannidis et al. Extracorporeal CO 2 Elimination (ECCO 2 R) for Hypercapnic Respiratory Failure: From Pathophysiology to Clinical Application. *Pneumologie* 2017; 71: 215–220
5. Schöps et al. Hemolysis at low blood flow rates: in-vitro and in-silico evaluation of a centrifugal blood pump. *Journal of Translational Medicine* 2021, 1:

OPTIMAL BLOOD FLOW RATE FOR THE FILTER LIFETIME OF POLYMETHYL METHACRYLATE MEMBRANE FILTER FOR CONTINUOUS RENAL REPLACEMENT THERAPY.

Yoshitaka Kurihara (1), Shunichi Ueki (1), Tomoyo Ebine (1), Hiroshi Tsukao (1,2), Kozue Kobayashi (1,3), Kenichi Kokubo (1,3), Masaru Kubota (1,3)

1. Kitasato University Graduate School of Medical Sciences, Japan; 2. Faculty of Medical Sciences, Juntendo university, Japan 3. Kitasato University School of Allied Health Sciences, Japan;

Introduction: The lifetime of a hemofilter employed in continuous renal replacement therapy (CRRT) is influenced by a multitude factors. These include operational conditions, the anticoagulant used, module structure (hollow fiber diameter, fiber density, length and diameter

of housing, *etc.*), as well as membrane material. Clinical results have demonstrated that filter lifetime is longest at a blood flow rate (QB) of 250 mL/min to 300 mL/min in Australia [1]. In Japan, however, the QB is often selected at approximately 100 mL/min. Additionally, the membranes with adsorption characteristics, such as polymethyl methacrylate (PMMA) membranes, are frequently used to remove inflammatory cytokines. Additionally, nafamostat mesylate, a serine protease inhibitor, is also used as an anticoagulant. Therefore, the optimal QB under CRRT conditions in Japan may differ from that in Australia. The objective of the present study was to determine the optimal QB for filter lifetime under CRRT conditions in Japan.

Methods: Two filters with different hollow fiber inner diameters, CH-1.0N (membrane area, 1.0 m^2; hollow fiber inner diameter, 200 µm) and CH-1.0W (1.0 m^2; 240 µm), were used in *in vitro* hemofiltration experiments. QB was varied from QB = 40 to 160 mL/min at 20 mL/min intervals, and the filter lifetime was determined as the time when transmembrane pressure reached 200 mmHg. To reduce the effects of variation in the likelihood of blood coagulation, porcine blood collected from a single animal was divided into two portions. One portion was used at QB = 100 mL/min and the other at a different QB (40 to 160 mL/min). The lifetime at a given QB was subtracted from the lifetime at 100 mL/min measured with the same blood and divided by the lifetime at 100 mL/min to calculate the percentage prolongation of filter lifetime.

The filtration flow rate and replacement fluid infusion rate were set at 10% of QB. The anticoagulants used were nafamostat mesylate, administered at an initial dose of 20 mg and a continuous dose of 20 mg/h, and trisodium citrate that was added to the replacement fluid to be a final concentration of 8 mM.

Results: The percentage prolongation of filter lifetime peaked at QB = 60 and 80 mL/min for both CH-1.0N and CH-1.0W

($p = 0.0405$, Jonckheere-Terpstra test). CH-1.0W, which has a larger hollow fiber diameter, demonstrated a more pronounced blood flow dependence and a 20-30% increase in the prolongation of filter lifetime. The percentage prolongation of filter lifetime at a QB of 40 mL/min exhibited no consistent trends and a considerable degree of variability, ranging -30 to 30%. For larger QB (100 -160 mL/min), the percentage prolongation of filter lifetime exhibited a small change and a narrow range of variation, ranging from -10 to 10%.

Discussion: In the present study, the filter lifetime due to membrane clogging was compared when a filtration flow rate was 10% of QB. The longest filter lifetime was obtained at QB of 60-80 mL/min. The optimal values were clearly observed at lower flow rates than those reported in clinical studies [1,2], where the filter lifetime increased at over 200 mL/min. In the clinical study conducted in Australia [1], the filtration flow rate was 2 L/h (33 mL/min), which means that if QB was 200 mL/min, the filtration flow rate was 17% of the QB, which is considerably larger than that set in our experiments. In Japan, the filtration flow rate in clinical settings is approximately 10 mL/min. Therefore, it is rational that the optimum QB to prolong filter lifetime was also low in Japan. In the future, it would be beneficial to investigate the effect of changing the ratio of filtration flow rate to QB on the lifetime.

In conclusion, the optimal QB to prolong the filter lifetime was found to be 60-80 mL/min when blood filtration was performed using PMMA membrane filters with a filtration flow rate of 10% of QB.

References

1. Dunn WJ et al, Crit Care Resusc. 16(3):225-231, 2014.
2. Ronco C et al, Crit Care. 19:146, 2015.

IMPELLER POSITION IN THE HEARTMATE 3 AND ITS IMPACT ON NUMERICAL HEMOCOMPATIBILITY ASSESSMENT

Marko Grujic (1), Rosmarie Schoefbeck (1), Bente Thamsen (1), Stefan Jakubek (2), Daniel Zimpfer (1), Marcus Granegger (1)

1. Christian Doppler Laboratory for Mechanical Circulatory Support, Department of Cardiac Surgery, Medical University Vienna, Austria; 2. Division of Control and Process Automation, Institute of Mechanics and Mechatronics, Vienna University of Technology, Austria

Introduction: In magnetically levitated rotodynamic blood pumps (RPBs), such as the HeartMate 3, the impeller position depends on a balance of magnetic and fluid-dynamic forces. Thus, the impeller position is affected by different operating conditions with altered gap clearances around the impeller. These secondary flow channels between the impeller and housing are a major determinant of hemocompatibility [1]. The aim of this study was to measure the impeller position within the Heartmate 3 (HM3) over a wide range of operating conditions and to assess its impact on computational fluid dynamic (CFD) predictions of hemocompatibility.

Methods: Axial impeller position was measured with a laser sensor (Welotec GmbH, AWL7/4) through an acrylic glas replica of the lower volute casing of the HM3. Radial impeller position was determined by the HM3 system and confirmed by high-speed camera recordings. Experiments were conducted for five different speeds (3000 rpm, 4000 rpm, 5000 rpm, 6000 rpm, 7000 rpm) over the entire flow range and with three different water/glycerol mixtures (2.5 mPas, 3.5 mPas, 4.5 mPas).

To assess the impact of impeller position on hemocompatibility the HM3 pump with a centered and a displaced impeller was simulated in CFD at a clinically relevant operating point at 6000 rpm, 3.5 mPas and 5 l/min [2]. Washout time and normalized index of hemolysis (NIH) were calculated using a passive scalar approach [3]. To further investigate hemocompatibility of the pump several parameters including blood volume exposed to shear stresses above thresholds associated with different kinds of blood damage [4] as well as the gap flows were compared.

Results: Figure 1 shows the radial and axial displacement for 3.5 mPa s. The radial impeller displacement is maximum at 0 l/min and decreases with increasing flow rates. Higher viscosities lead to higher radial displacements. The axial displacement is minimal at around 0 l/min and increases with flow rate. For all conditions the tilting angle of the

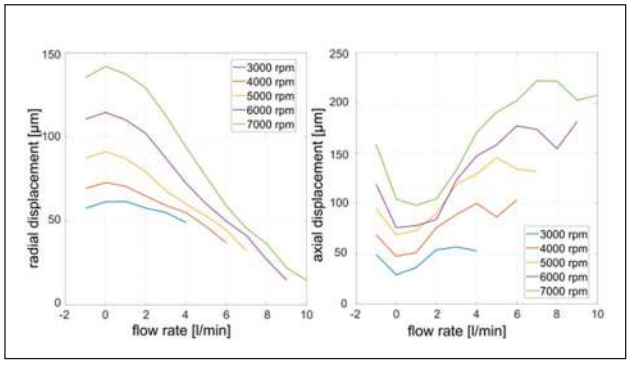

Figure 1. Radial (left) and axial (right) displacement for 3.5 mPa s and speeds form 3000 rpm to 7000 rpm.

impeller axis is less than 1°. Corresponding to experimental data, for CFD analysis the impeller was displaced by 144 µm in axial and 60 µm in radial direction.

CFD analysis revealed comparable values for global pump parameters (pressure head and flow rate) in both simulations (deviations of < 1 %). Numerical assessment of washout and NIH were not influenced substantially by the displaced impeller (< 2%). Most local parameters differed less than 4 %.

Discussion: In this study, the effect of operating conditions on radial and axial displacement of the HM3 impeller are reported to facilitate more accurate numerical predictions of hemocompatibility. Accompanying CFD simulations suggest that in the investigated operating point a displaced impeller has no considerable impact on global pump parameters including washout and NIH. Further assessment and analysis of different operating conditions and the effect of impeller position on local flow phenomena are ongoing. Of note, the impeller was displaced only stationary; hence, dynamic effects were not considered in this study.

References

1. Gil et al., Biomech Model Mechanobiol, 22: 871–883, 2023
2. E Montalto et al., Transplant Proc., 51(1):206-209, 2019
3. Schenkel et al., Computers & Fluids, 86: 185-198, 2013
4. Fraser et al.,J Biomech Eng, 134:081002, 2012

Acknowledgements

The financial support by the Austrian Federal Ministry of Labour and Economy, the National Foundation for Research, Technology and Development and the Christian Doppler Research Association is gratefully acknowledged. The computational results presented have been achieved using the Vienna Scientific Cluster (VSC).

FEASIBILITY OF CARBONIC ANHYDRASE FACILITATED CO2 REMOVAL FOR EXTRACORPOREAL LUNG SUPPORT SYSTEMS USING DOPAMINE AND POLYETHYLENEIMINE SURFACE FUNCTIONALIZATION

Maike Schönborn (1,2), Maria A. Restrepo (2), Lasse J. Strudthoff (1), Ulrich Steinseifer (1), Johanna C. Clauser (1), Matthias Wessling (2,3)

1. Department of Cardiovascular Engineering, Institute of Applied Medical Engineering, University Hospital RWTH Aachen University, Germany; 2. Chemical Process Engineering, Aachener Verfahrenstechnik, RWTH Aachen University, Germany; 3. DWI -Leibniz Institute for Interactive Materials e.V., Germany

Introduction: Extracorporeal membrane oxygenation (ECMO) and extracorporeal CO_2 removal (ECCO2R) offer potential solutions for respiratory failure by providing temporary lung support, using hollow fiber-based oxygenators. CO_2 is mainly transported in the body in form of bicarbonate (HCO_3^-). The enzyme carbonic anhydrase (CA) is naturally localized in the erythrocytes and catalyzes the conversion of bicarbonate (HCO_3^-) into CO_2 and vice versa. The covalent immobilization of CA on the surface of the hollow fiber membrane and the resulting direct conversion of HCO_3^- to CO_2 at the membrane interface facilitates gas exchange [1]. In contrast to previous studies with the same aim, the method employed in this work utilizes an amino group-rich surface, which is commonly used in carbon capture technology, for subsequent enzyme crosslinking. This approach was selected to transfer existing knowledge from another field and further profit from the potential hemocompatibility benefits of the coating.

Methods: Since enzyme cross-linking is not possible without prior surface functionalization, the membrane was modified using a dopamine (DA) and polyethyleneimine (PEI) coating, allowing the enzyme to be cross-linked. Carbonic anhydrase cross-linking was performed using glutaraldehyde. Membranes with different coating compositions were characterized using the spectrophotometrically measurement of esterase enzyme activity. Subsequent testing of the CO2 removal capacity was conducted using PBS buffer as testing liquid. The test setup allowed low cost and continuous testing of different membranes in mini membrane modules (fiber number=90) under constant conditions. Hemocompatibility testing was performed in a static system using platelet-rich plasma (PRP) from abattoir pig blood anticoagulated with sodium citrate. Fixed membrane samples were analyzed using field emission scanning electron microscopy.

Results: We found a PEI/DA coating composition of 10 mg/mL DA and 10 mg/mL PEI with a coating/cross-linking time of 7 h/32 h is a reproducible and scalable method for production of biocatalytic active membranes with high enzyme activity values. Coatings using 600 Da and 800 Da PEI molecular weight showed comparable CO2 removal capacities. Values between 30 % and 60 % were achieved for membrane improvement by the introduction of CA compared to coated membranes without CA. It has been demonstrated that within a storage period of four weeks at a temperature of 4 °C, the CO2 removal capacities and thus the enzyme activity remain constant. Hemocompatibility test showed uncoated membranes exhibited disc-shaped platelet structures, while those with 600 Da PEI/DA showed less adhesion and rougher surfaces with CA cross-linking.

Discussion: Our data shows that a PEI/DA coating composition of 10/10 with 7 h/32 h coating/cross-linking is a feasible method for producing biocatalytic membranes, prioritizing reproducibility over higher enzyme activities. Despite variations in coating quality and flow dynamics, longer coating times prove to be decisive for effective CO2 removal efficiency. The hydrophilized membrane showed biocompatible rough surface with less protein and platelet adhesions and is a promising solution for further surface modification research. The increased diffusion barrier of the coating is effectively compensated by the crosslinking of CA. Yet, an optimization of both coating and enzyme immobilization promises distinct potential for even better gas transfer.

Reference

1. D. T. Arazawa, J. D. Kimmel, and W. J. Federspiel "Kinetics of CO2 exchange with carbonic anhydrase immobilized in fiber membranes in artificial lungs". Journal of materials science. Materials in medicine 26.6 (2015) 193. doi: 10.1007/s10856-015-5525-0.

HIGH-FIDELITY TURBULENCE MODELLING OF THE NEOVAD PAEDIATRIC PUMP

Nathaniel S. Kelly (1), Lee Nissm (1), Shweta Karnik (2), Preston Peak (2), Nobuyuki Kurita (3), O. H. Frazier (2), Yaxin Wang (2), Katharine H. Fraser (1)

1. University of Bath, Bath, UK; 2. Texas Heart Institute, Houston, United States of America; 3. Baylor College of Medicine, Houston, United States of America

Introduction: Around 0.8% of babies born alive have chronic heart failure [1]. The NeoVAD is a prototype left ventricular axial flow pump for neonates to support left ventricular failure. Current work has investigated the optimal blade design of the impeller in this pump using machine learning and global optimization [2]. However, this device is expected to operate in the transitional and turbulent flow regimes, with the implication that turbulent stresses contribute to mechanical blood trauma

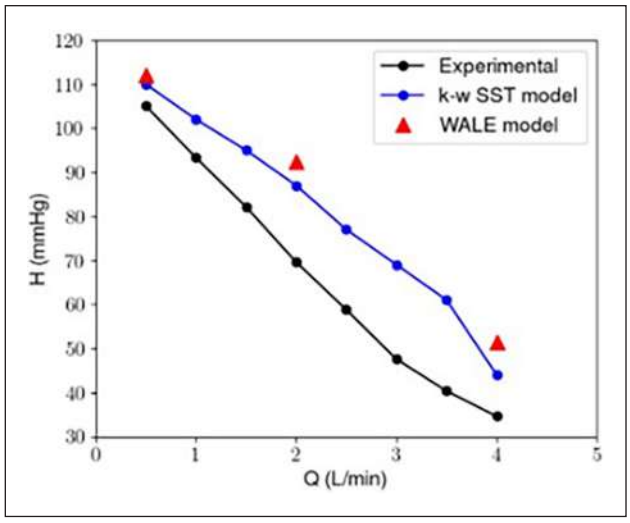

Figure 1. HQ curve for k-ω SST, WALE simulations and experiments.

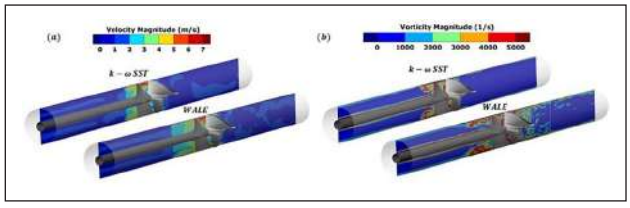

Figure 2. $k-\omega$ SST and WALE CFD simulations of the NeoVAD at 2 l/min. (a) velocity fields (b) vorticity fields.

[3]; higher fidelity computational fluid dynamics (CFD) simulations are needed to model the flow fields. Building on the existing numerical work, this work aimed to use high-fidelity Large Eddy Simulations (LES) to calculate the flow fields found in the NeoVAD pump.

Methods: CFD simulations of the flow through the NeoVAD pump were investigated using OpenFOAM v9. The flow (Q) was simulated from 0.5-4 l/min with a constant impeller speed, equivalent to an impeller tip Re = 32,000. To investigate the effects of the turbulence model on pressure head (H) Unsteady Reynolds Averaging Navier-Stokes (URANS) and LES were used. For turbulence closure the k-ω SST model was chosen for URANS, and the Wall Adapting Local Eddy-viscosity (WALE) model was chosen for LES. URANS models were performed using both a multiple reference frame (MRF) and a sliding mesh approach, with the MRF models used to initialize the transient solutions. Numerical models are compared to experimental pressure measurements from rapid prototyped parts.

Results: CFD simulations using the $k-\omega$ SST model found a slightly lower pressure when compared to the WALE model at all flow rates, Figure 1. At 0.5 l/min, both turbulence models produced pressures similar to experiments. At 2 l/min there was 13.5% absolute difference between the WALE model and experiments.

A qualitative assessment of the flow fields between turbulence models at 2 l/min (Figure 2a and 2b) showed obvious unsteadiness downstream of the diffuser section in the the WALE compared to $k-\omega$ SST model.

Discussion: HQ curves between URANS and LES models showed similar trends at the respective flow rates. Although both turbulence models overpredicted the pressure head we expect the 3D-printed geometries to have surface roughness resulting in underpredicting the correct pressures [4]. The effect of surface roughness is currently under investigation.

These preliminary simulations of LES models indicate that the flow fields are complex at the operating point of interest for paediatrics and URANS is not capable of capturing the turbulent structures that could potentially lead to mechanically induced blood damage.

Future work will include the determination of turbulent shear stresses from URANS and LES models to quantify mechanical blood trauma and include surface roughness in the models.

References

1. Castaldi, B et al. (2023). Journal of Clinical Medicine, 12(7), p.2611.
2. Nissim, L et al. (2023). *Scientific Reports*, 13(1), p.7183.
3. Kameneva, M.V et al.. (2004). ASAIO Journal, 50(5), pp.418–423.
4. Nissim, L et al. (2023) O36. The International Journal of Artificial Organs 46(7), pp 413.

Acknowledgements

Research supported by the National Heart, Lung, and Blood Institute of the National Institute of Health under Award Number 1R01HL153538-04. This work used the Isambard 2 UK National Tier-2 HPC Service (http://gw4.ac.uk/isambard/) operated by GW4 and the UK Met Office, and funded by EPSRC (EP/T022078/1)

THE PORCINE ABATTOIR BLOOD MODEL – VALIDATION OF HEMOCOMPATIBILITY BLOOD PARAMETERS FOR IN-VITRO TESTING

Maike Schönborn (1), Ilona Mager (1), Sofie Hardt (1), Johanna C. Clauser (1)

1. Department of Cardiovascular Engineering, Institute of Applied Medical Engineering, University Hospital RWTH Aachen University, Germany

Introduction: The hemocompatibility remains the major limitation of blood-contacting medical devices. While the evaluation and prediction of flow-related hemolysis can be done either by computational modeling or in-vitro blood experiments, thrombogenicity can hardly be evaluated in vitro and is therefore most often tackled in animal experiments for the first time [1, 2]. This is ethically questionable, expensive, and inefficient for device developing. Therefore, standardized in-vitro test methods for assessing the thrombogenicity of medical devices are required. However, this is currently failing due to required blood volumes > 450 mL, which exceed a human blood donation, and due to the absence of adequate analog fluids. Animal abattoir blood would overcome these limitations but is supposed to be not suitable for medical device thrombogenicity testing due to a lack of comparability to human blood and possible pre-activation from the slaughtering process.

To this end, we investigated a complete DIN EN ISO 10993-4 conform set of hemocompatibility parameters from human donors versus porcine abattoir blood.

Methods: Porcine blood was collected directly at the slaughterhouse after a cut in the jugular vein of the animals. Blood from one animal was separated in two blood bottles and immediately anticoagulated with 2000 IU/L enoxaparin (Clexane) and sodium citrate, (3.13 %, ratio 1:10) respectively. Human blood was collected at the Medical Center of the RWTH Aachen University (EK 23-092) and divided into two separate portions anticoagulated as the porcine blood.

After arrival at the lab, blood count (Idexx ProCyte Dx), blood gas analysis (ABL 800 flex), thromboelastometry (ROTEM®delta), fluorescence activated cell sorting (BD FACS Canto II) with CD61, CD62P, CD45

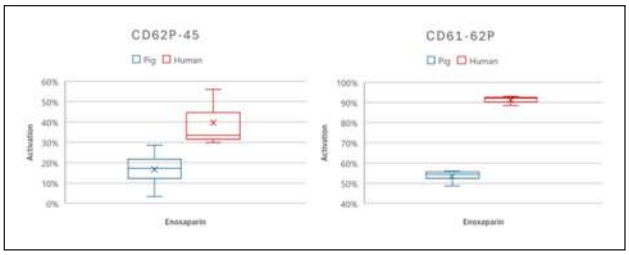

Figure 1. CD62-45 and CD61-62P activation of pig and human blood anticoagulated with enoxaparin.

markers and impedance aggregometry (Multiplate® analyser) were measured in whole blood from both species. Plasma samples were frozen at -80 °C for further ELISA analysis. The ELISA test comprises the analysis of plasma parameters including serotonin, adrenalin, cortisol, PMN Elastase, soluble C5b-9, C3a, β-thromboglobulin, and thrombin-antithrombin-complex.

Results: Blood values of both species were within the ranges of the respective normal values, independent of the way of blood withdrawal. Porcine and human blood platelet activation (CD61-62P) and platelet-leucocyte aggregates (PLAs, CD62-45) measured by FACS (CD61-62P and CD62-45) showed significant differences ($p<0.05$) in the comparison of pre-and post-activation values. While CD61-62P revealed a minimum of 90 % activation for human blood, only around 56 % were achieved by porcine blood. Similarly, CD62-45 activation was about 20 % less for porcine blood compared to human blood (Figure 1).

The aggregometry with collagen activator presented different intra-species values depending on the anticoagulant. Interestingly, and in contrast to reports from literature [3], TRAP activation seemed to be functional for porcine blood as well.

Discussion: Porcine blood is still functional after blood collection at the slaughterhouse. Although presenting some decreased platelet activation potential, coagulation is still intact and generally useful for hemocompatibility testing according to ISO 10993-4. This is an important step towards medical device in-vitro testing with blood volumes >450 mL.

References

1. Sarode, et al, Expert Rev. Med. Devices, 16(7), 603-616, 2019.
2. DIN EN ISO 10993-4, 2017.
3. Heringer et al., PLOS ONE, 14(8), e0222010, 2019.

Acknowledgements

This work was supported by the Flow Cytometry Facility, a core facility of the Interdisciplinary Center for Clinical Research (IZKF) Aachen within the Faculty of Medicine at RWTH Aachen University. We thank Dr. Doris Keller for blood withdrawal and all volunteers who donated blood.

VIRTUAL PATIENT DATA GENERATOR: SYNTHETIC ECMO DATA FOR ENHANCED MEDICAL DEVICE DEVELOPMENT

Micha Landoll (1,2,3), Yifei Huang (1), Ulrich Steinseifer (1), Stephan Strassmann (3), Christian Karagiannidis (3), Michael Neidlin (1)

1. Department of Cardiovascular Engineering, Institute of Applied Medical Engineering, Helmholtz Institute, RWTH Aachen University, Germany; 2. ARDS and ECMO Centre Cologne-Merheim, Dept. of Pneumology and Critical Care Medicine, Kliniken der Stadt Köln gGmbH, Witten/Herdecke University, Germany; 3. Germany Institute for Computational Biomedicine II, University Hospital Aachen, RWTH Aachen University, Germany

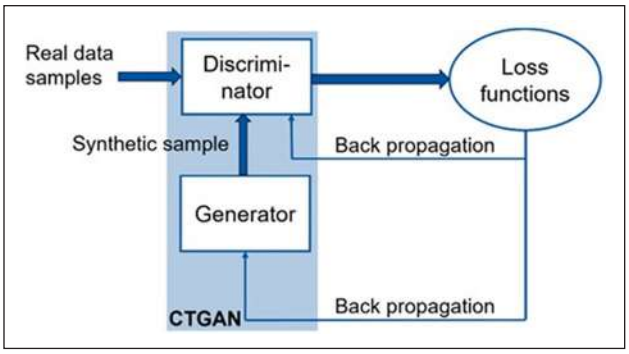

Figure 1. CTGAN Model Architecture with two components: a generator creating synthetic data and a discriminator evaluating its authenticity, working in tandem to produce high-fidelity synthetic data.

Introduction: In silico clinical trials for Extracorporeal Membrane Oxygenation (ECMO) devices, by offering risk-free testing environments, could significantly enhance medical device development. A reliable generation of virtual patient cohorts from clinical data is the first step in such in silico clinical trials [1,2]. The challenge of integrating complex patient data, however, limits these models' predictive power [3]. This study aims to overcome current limitations such as patient privacy concerns and inadequate dataset sizes by generating high quality synthetic patient data from Electronic Health Records (EHR) of ECMO therapy.

Methods: This study employs a Conditional Tabular Generative Adversarial Network (CTGAN) to generate synthetic data from the Electronic Health Records (EHR) of 767 patients during ECMO. It includes time-series data across 59 selected therapy parameters, such as vital signs, blood gases, and organ function indicators. A Conditional Tabular Generative Adversarial Network (CTGAN) was employed to synthesize data (Figure 1), incorporating steps such as data preprocessing, imputation, and hyperparameter tuning. Through its generative adversarial process, this model refines synthetic data to closely mimic real patient records.

Results: The synthetic data showed strong alignment with the original dataset, evidenced by coverage scores averaging 95% (min. 58%) and boundary and synthesis scores of 100%. The mean absolute differences in correlations coefficients between the synthetic and original data were minimal, averaging 5.9% with a maximum deviation of 44.7% (exemplary data subset in figure 2).

Discussion: This synthetic data accurately reflects the original dataset, demonstrating the method's potential to enhance in silico ECMO trials, crucial for patient safety. While scaling to higher dimensional datasets poses challenges, these findings lay a solid foundation for future development. Addressing scalability will further enhance this research's impact, potentially shortening ECMO device development cycles, increasing patient safety and advancing clinical practice. Alongside future explorations in synthetic data benchmarking and patient trajectory modelling, the development of an online platform for virtual patient data generation based on EHR could enhance accessibility to patient data and drive innovation towards in silico clinical trials in ECMO research.

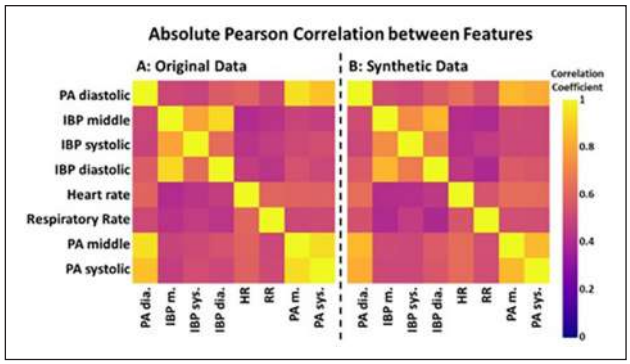

Figure 2. Comparison on exemplary data subset of absolute Pearson correlation coefficients between original (A) and synthetic (B) datasets to evaluate synthetic data generation precision and mirror inter-variable relationships.

References

1. Simalatsar A, Front. Big Data, 6:1085571, 2023.
2. Van Breugel B et al., arXiv:2304.03722, 2023.
3. Chen RJ et al., Nat Biomed Eng, 5:493–497, 2021.

FABRICATION AND CHARACTERIZATION OF FIBER-REINFORCED HYDROGELS FOR TISSUE ENGINEERING APPLICATIONS

Jan Drexler[1], Gesine Hentschel[1], Andre L.C. Conceição[2], Rainer Detsch[3], Aldo R. Boccaccini[3], Birgit Glasmacher[1]

1. Institute for Multiphase Processes, Leibniz University Hannover, Germany; 2. German Electron Synchrotron DESY, Germany; 3. Institute of Biomaterials, University of Erlangen-Nuremberg, Germany

Introduction: The application of hydrogels in tissue engineering is limited due to their low mechanical properties. They can be tuned by incorporating electrospun fibers [1,2]. In addition, the fiber-like morphology of the natural extracellular matrix can be simulated in order to improve cell adhesion. The combination of electrospun fibers and hydrogels may create a biomimetic environment which replicates the water-swollen, fibrous characteristics of natural tissues [1,3]. Here, we present methods for the fabrication and characterization of fiber-reinforced poly(sodium acrylate-co-acrylamide) (PSAAm)-hydrogels. Both layered structures and hydrogels with dispersed short fibers are considered.

Methods: Fiber mats for the layered structures were produced by solution-based electrospinning (SE) and melt electro-spinning (ME) of polycaprolactone (PCL). Solutions for SE were prepared by dissolving 24%w/w PCL (14kDa, Sigma Aldrich) and 6%w/w PCL (80kDa, Sigma Al-drich) in trifluoroethanol (abcr). SE was performed in a uniaxial vertical setup with a rotating drum collector. For ME, PCL (45kDa) was melted at 80°C and subsequently processed into fibers. Short fibers were made from PCL in SE and fatty acid-terminated poly-L-lactide (PLLA) in ME. PLLA fibers were mechanically comminuted using a mortar. Electrospun PCL fiber mats were fabricated according to the procedure for layered structures. The fiber mats were then exposed to UV light (Osram HNS S/E, 11W, 4h) and crushed into short fibers by ultrasonication in isopropanol (Hielscher Electronics UP200S) in an ice bath to prevent melting of the PCL fibers. For the production of layered structures, PSAAm hydrogel precursor and fiber mats were alternately placed in a mold. The short fibers were added to the hydrogel precursor and then dispersed in a water bath for 15min before the reaction starter was added. The morphology of the produced fibers was evaluated by SEM (Hitachi S3400-N).

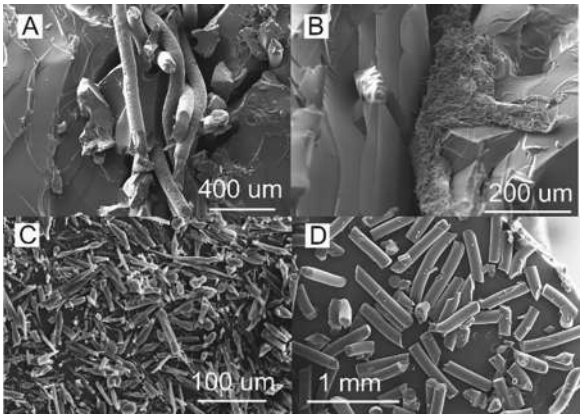

Figure 1. Cross-section of layered structures with PLLA (A) and PCL (B) fiber mats. Short fibers for the incorporation into hydrogels produced from PCL in SE (C) and PLLA in ME (D).

The interface between fiber mat and hydrogel was observed in a sliced cross-section using SEM (Jeol JSM-IT510LA) with a cryostage. Hydrogels with dispersed fibers were measured with SAXS tensor tomography at DESY beamline p62 to investigate crystallinity and molecular orientation.

Results: PCL fiber mats produced for layered structures had fiber diameters of 1±0.6µm (SE) and 87.4±3.7µm (ME). Cryo-SEM of the layered structures showed infiltration of hydrogel into the pores of electrospun fiber mats for ME, but not for SE. Short PCL fibers were 2.2±1.5µm in diameter and 10±6.7µm in length whereas short PLLA fibers were 161.4±21.8µm in diameter and 551±229.3µm in length. SAXS tensor tomography at DESY proved to be capable of volumetric visualization of crystallinity and orientation in hydrogels.

Discussion: Layered structures and hydrogels with dispersed fibers were successfully prepared. Hydrophilization of the SE-PCL mats could improve the infiltration of the hydrogel into the pores. Further work will focus on the mechanical characterization of the reinforced hydrogels and their swelling behavior. The combination of fibers and alginate-based hydrogels is planned in cooperation with the University of Erlangen-Nuremberg.

References

1. Yongcong et al., J Biomed Mater Res, 107A:2694-2705, 2019.
2. Szentivanyi et al., Adv Drug Deliv Rev, 63:209-220, 2011.
3. Grewal and Highley, Biomater Sci, 9(12):4228-4245, 2021.

A NOVEL APPROACH FOR IN DEPTH ANALYSES OF TISSUE SAMPLES – 3D IMAGE MODELLING

Juliane Hermann (1), Vera Jankowski (1), Joachim Jankowski (1,2)

1. Institute for Molecular Cardiovascular Research IMCAR, University hospital, Aachen, Germany; 2. School for Cardiovascular Diseases, Maastricht University, Maastricht, The Netherlands

Introduction: Imaging techniques and the visualization of samples are becoming increasingly important in order to describe clinical pictures and obtain a concrete impression of the condition of a tissue or organ. Imaging with different scales/areas combined in a three-dimensional display provides a significant increase in information and insight that would be lost if limited to one dimension and imaging. A correlation

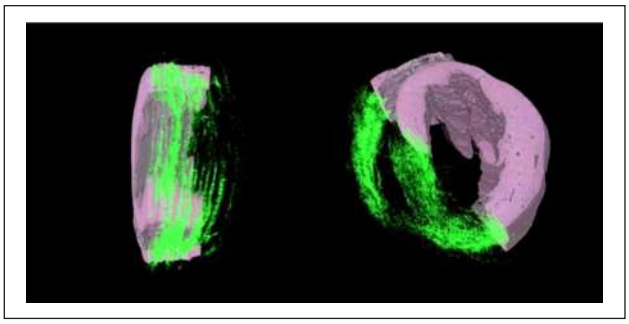

Figure 1. Reconstructed 3-dimensional mice heart in two different viewing angels. In green the mass signal of m/z=1106 is illustrated in combination with HE stained tissue images.

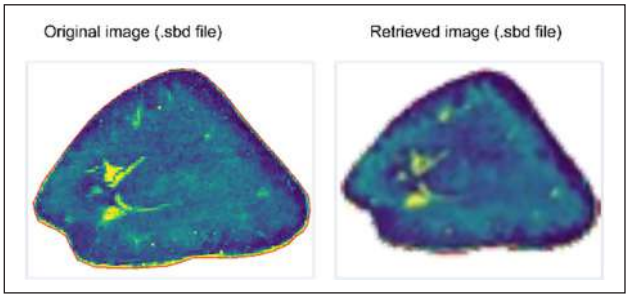

Figure 2. A comparison between an image generated from the original data of a mass spectrometric analysis and the reconstructed representation of such an analysis, which can be implemented in the model.

between the molecular and microscopic levels enables a much more detailed analysis and increase the information content requires a combination of MALDI imaging and histological staining techniques [1]. For this reason, molecular imaging is to be merged with conventional histological imaging and presented as a three-dimensional image, including the including the unique information that characterizes these techniques.

Method: MALDI mass spectrometric imaging (MALDI MSI) is a powerful tool for analyzing biomolecules in tissue samples. The measurements lead to high sensitivity and accuracy in the spatial distribution of biomolecules in tissue samples, with resolution information in the range of 5-10 µm. The histological and mass spectrometric data were combined for the resulting 3D model.

Results: By further developing the algorithm described in the preliminary work, high-resolution histological data generated with a slide scanner could be implemented and displayed as a 3D model **(Figure 1).**

Another success is the implementation of the entire mass spectrometric data set **(Figure 2).**

Discussion: These changes to the underlying algorithm allow an even higher information content of our visualization. The ability to visualize cell levels similar to a microscope and, in addition, to freely select the distribution of mass signals and thus represent proteins, allows us to investigate the complex relationships of the entire organ.

References

1. Hermann J et al, Proteomics Clin Appl. 2021 Jan;15(1): e1900143

Acknowledgements

This work was funded by the 'Deutsche Forschungsgemeinschaft' (DFG, German Research Foundation) by the Transregional Collaborative Research Centre (TRR 219; Project-ID 322900939) to J.J. (subproject S-03 and C-04), and V.J. (subproject S-03, INST 948/4S-1 FU6.6)

IDENTIFICATION OF NOVEL PATHOLOGICAL REGULATORS USING MACHINE LEARNING FOR ANALYSING LC-MS DATA

J. Hermann (1), R. Stojanov (2), A. Todorovska (2), J. Dobreva (2), V. Jankowski (1), J. Jankowski (1,3)

1. Institute for Molecular Cardiovascular Research, University Hospital RWTH Aachen; 2. Faculty of Computer Science and Engineering, University "Ss. Cyril and Methodius" -Skopje, North Macedonia; 3. School for Cardiovascular Diseases and Pathology/ CARIM, Maastricht University, The Netherlands

Introduction: Mass spectrometry is an invaluable analytical technique used to research and elucidate novel mediators and the underlying pathophysiological mechanisms associated with various diseases or disorders. The use of state-of-the-art mass spectrometers facilitates the analysis of a large group of patients and biomaterials, enabling the detection of numerous substances in a single measurement. Nevertheless, determining the key mediators that significantly impact the onset and progression of disease remains elusive, making it a challenge to filter out the relevant substances from the plethora of compounds detected. For this analysis, we aim to develop and apply bioinformatic and biostatistical tools and a machine learning algorithm to identify the molecular features of interest that allow us to combine many LC-MS datasets and identify which signals in the groups have the most substantial statistical impact.

Method: For the data acquisition a LC-MS System was used. The digital signals are transformed in a bucket table and read into the algorithm. The data of each patient is aligned according to the characteristic "time" and "m/z", and the absolute difference in intensity is calculated. The non-matching values are masked to ensure the experiment's integrity, ensuring a unique value is selected for the minimum allowable intensity data values at each experiment iteration.

Results: The initial phase of this project entails the comprehensive examination and analysis of extensive and intricate datasets derived from mass spectrometry. Preliminary findings from a sampling site indicate the algorithm's capability to discern significant discrepancies in mass spectrometry data among individual patients. Furthermore, the algorithm's integration of clinical parameters augments the depth of information obtained. Encouragingly, initial comparisons between patients belonging to disparate groups demonstrate promise.

Initial data **(Figure 3)** from a sample site show that this algorithm can be used to identify MS data that have a significant impact on the disease status.

Discussion: Machine learning facilitates the analysis of extensive and intricate datasets alongside associated parameters, enhancing our capacity to discern disparities pertinent to diseases and their contributing factors. Consequently, this could yield novel insights into diseases' nature and trajectory.

Acknowledgements

This work was funded by the 'Deutsche Forschungsgemeinschaft' (DFG, German Research Foundation) by the Transregional Collaborative Research Centre (TRR 219; Project-ID 322900939) to J.J. (subproject

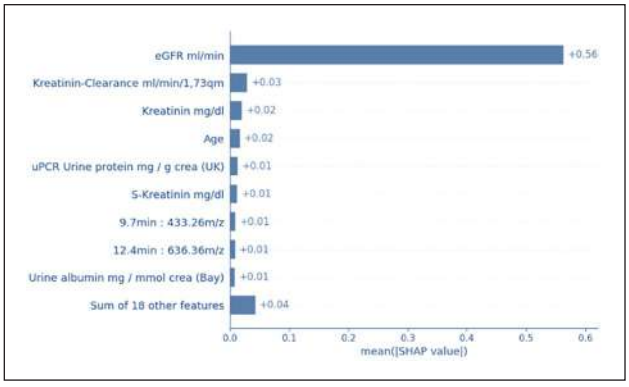

Figure 1. Illustration of the preliminary analysis of LC-MS data, including the associated clinical parameters. The 10 statistically highest influencing factors that could be evaluated in a comparison of two patient groups are presented.

S-03 and C-04), and V.J. (subproject S-03). This article is based upon work from COST Action PerMedik, CA21165, supported by COST (European Cooperation in Science and Technology).

EARLY CLOT DETECTION INSIDE AN OXYGENATOR VIA BIOIMPEDANCE MEASUREMENT

Jan Korte[1], Lasse J. Strudthoff[2], Alexander Theißen, Jannis Focke[2], Lisa Herzog[3], Thomas Gries[3], Rolf Rossaint[1], Christian Bleilevens[1], Tobias Lauwigi[3] and Patrick Winnersbach[1]

1) Department of Anesthesiology, University Hospital RWTH Aachen, Germany; 2) Department of Cardiovascular Engineering, University Hospital RWTH Aachen, Germany; 3) Institut für Textiltechnik (ITA), RWTH Aachen University, Germany

Introduction: ECMO application is associated with various complications, for instance clot formation within the membrane oxygenator (MO). To mitigate complications and consecutive risks, continuous optimization of ECMO technology is imperative. In clinical practice, monitoring techniques such as measuring the pressure difference across the MO (ΔP), are employed to detect clotting events. Yet, existing methods lack predictive capabilities, prompting the need for enhanced early warning systems. Our previous work in bioimpedance analysis demonstrated its potential in detecting blood clot formation, holding promise for improving patient safety [1]. Placing bioimpedance research into an experimental ECMO context, this study investigated the integration of sensor fibers into the "RatOx" [2] to detect clot formation within the MO.

Methods: The RatOx was modified by integrating four sensor-fibers in the middle of the fiber mat bundle (Fig. 1), enabling bioimpedance measurement between the hollow fibers.

The modified RatOx was then perfused with heparinized human blood in an *in vitro* test-circuit. In addition to bioimpedance, ΔP and coagulation parameters were measured in parallel. Two experimental groups were defined (Clotting and Control group) to obtain contrasts in clot formation on the hollow fibers.

Results: In all experiments of the Clotting group, clot formation within the MO was observed. The Control group showed no clot formation. Quantitative analysis of the extent of clot residues on each fiber mats layer was performed through ImageJ. Mean total surface clot deposit area of the Clotting group was 51.88% ± 14.25%, in contrast to 7.28% ± 2.98% in the control group (Figure 2).

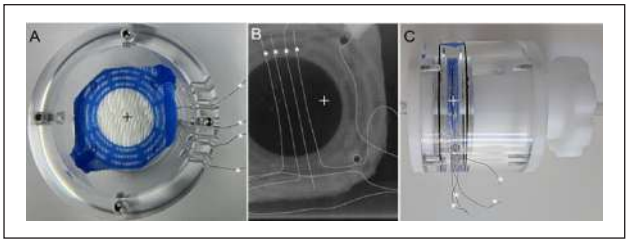

Figure 1. View of modified RatOx. A: Top view. B: Axial CT-scan. C: Lateral view. Hollow fiber mat bundle (+) with integrated sensor fibers.

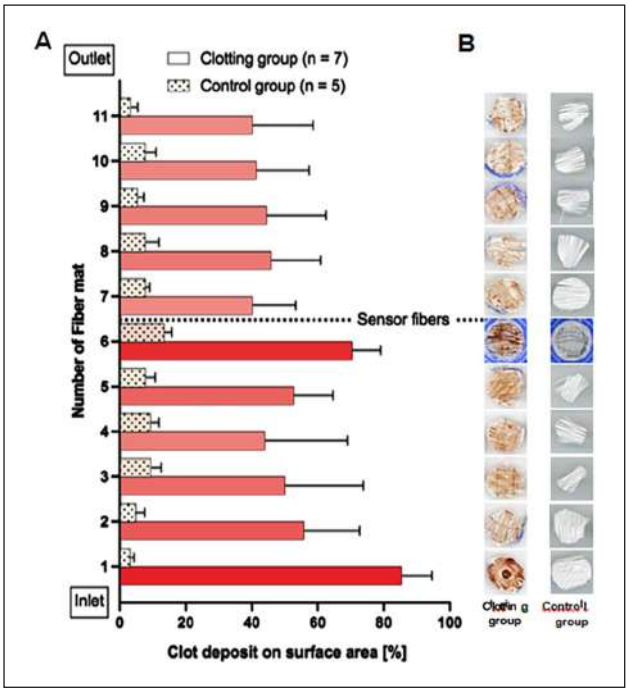

Figure 2. A: The bar chart presents the extent of clot deposit on each layer of the fibre mat in proportion to its total area. B: Exemplary original scans of the fibre mat layers.

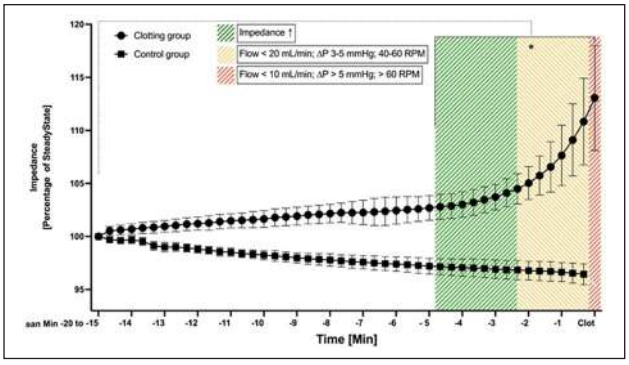

Figure 3. Impedance 15 min retrospectively from experiment termination. Mean ± SEM, ANOVA; * p<0.05 vs. SteadyState.

In the Clotting group impedance significantly increased 5 min prior to fulminant clot formation inside the MO and 2.5 min prior to first changes in hemodynamic parameters.

Discussion: The setup provided significant differences in clot deposition on the MO's fiber mats among the experimental groups. This study demonstrates the feasibility of measuring bioimpedance within a MO using integrated sensor fibers, enabling effective clot detection on the fiber mats. Furthermore, bioimpedance surpasses the clinical standard (ΔP), thus representing a monitoring method for early clot detection.

References

1. Türkmen et al, *Biosensors*, 13(3), 394, 2023**.**
2. Strudthoff et al, *Micromachines, 14, 800,* 2023.

DYNAMIC ANALYSIS OF THE HYDRODYNAMIC BEARING OF A TWO-STAGE PEDIATRIC LEFT VENTRICULAR ASSIST DEVICE

Sarah Linnemeier (1), Rosario Giuffrida (2), Spasoje Miric (3), Daniel Zimpfer (1), Johann W. Kolar (2), Marcus Granegger (1)

1. Medical University of Vienna, Austria; 2. Swiss Federal Institute of Technology Zurich, Switzerland; 3. University of Innsbruck, Austria

Introduction: Ensuring the dynamic stability of hydrodynamically levitated impellers in novel left ventricular assist devices (LVADs) is essential during their design process. The objective of this study was to assess the non-linear behavior of the hydrodynamic journal bearing of a two-stage pediatric LVAD considering the motor characteristics.

Methods: To assess the dynamic properties of the hydrodynamic bearing in combination with the motor characteristics, analytic and in-silico methods were combined. An electric motor was designed to meet the requirements of the two-stage LVAD. The magnetic attraction forces introduced by the motor influence the axial and radial stiffness of the impeller. Such reluctance forces were determined using electromagnetic finite element methods simulations. The hydraulic force acting on the impeller surface was obtained using computational fluid dynamics. This force, together with the radial magnetic attraction force of the motor, was used in the equations of motion which were coupled with the Reynolds equations. The non-linear system, initialized with a position near center, was solved for the impeller position within the bearing clearance [1]. Furthermore, a convective heat transfer simulation was performed to determine the temperature increase of the fluid due to the motor losses in the bearing gap.

Results: The motor is a permanent magnet synchronous machine with a nine-slot, four-pole design (Figure 1).

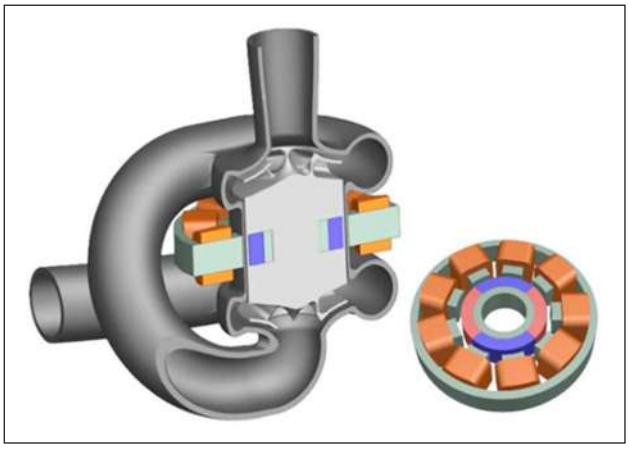

Figure 1. Two-stage LVAD with the motor (left), nine-slot, four-pole motor design (right).

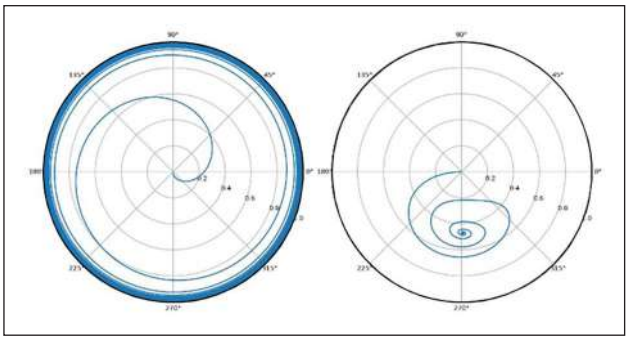

Figure 2. Unstable trajectory of the impeller for the main operating condition (left), equilibrium position with additional external force (right).

The axial reluctance force centers the impeller in the axial direction with a stiffness of -1.74 N/mm,

preventing an axial touchdown during operation. The radial attraction force acts in the direction of the smallest distance between the stator and the impeller with a stiffness of +9.30 N/mm. The maximum hydraulic force acting radially on the impeller surface is 0.03 N. The results of the non-linear analysis indicate that the dynamic forces, the bearing reaction forces and the external forces applied to the impeller are imbalanced, leading to an unstable behavior, pulling the impeller outwards to the housing wall and eventually causing a touchdown. However, introducing an additional external force of 0.65 N at a fixed angle results in an equilibrium position at an eccentricity ratio of 0.47 for the main operating condition of 6400 rpm (Figure 2).

The maximum local temperature increase of the fluid due to the motor losses is 37.2 °C and therefore within the tolerable 2 °C increase.

Discussion: The non-linear analysis of the dynamic behavior of the radial hydrodynamic journal bearing of a two-stage LVAD combined with the motor characteristics indicates that the introduction of an additional external force leads to a stable bearing operation. It has to be considered that the required force and the resulting equilibrium position depend on the rotational speed of the impeller. Future work will explore using the motor to provide this additional force.

Reference

1. Khonsari et al., ASME J. Vib. Acoust, 115(3):303-307, 1993.

Acknowledgements

The authors acknowledge funding from the OptiFlow 3D project (FFG FO999891239).

THE INFLUENCE OF SURFACE PROPERTIES OF NANOCOMPOSITE MEMBRANES ON DIALYSIS PERFORMANCE

Dominika Wójtowicz (1,2), Anna Ścisłowska-Czarnecka (3), Ewa Stodolak-Zych (1)

1. Department of Biomaterials and Composites, Faculty of Materials Science and Ceramics, AGH University of Krakow, al. Mickiewicza 30, 30-059 Krakow, Poland; 2. Clinical Department of Anaesthesiology and Intensive Care, University Hospital in Krakow, ul. Jakubowskiego 2, 30-688 Krakow, Poland; 3. Faculty of Motor Rehabilitation, Bronislaw Czech University of Physical Education in Krakow, Al. Jana Pawła II 78, 31-571 Kraków, Poland

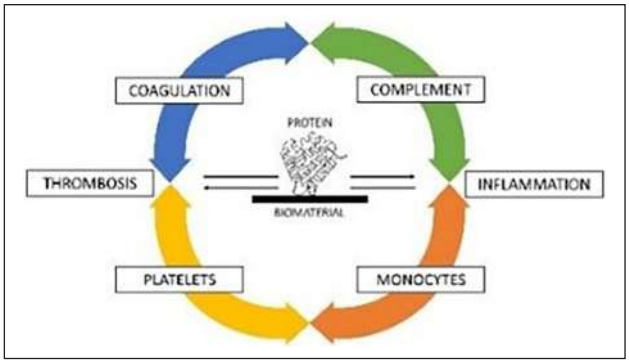

Figure 1. Pathways activated as a response to a contact of biomaterial with blood.

Introduction: Protein adsorption on biomaterials in contact with blood is a significant challenge during renal replacement therapy (RRT) which results in the activation of interrelated pathways, leading to the thrombosis and activation of the immune system (Fig. 1). Determinant for occurrence of fouling are the interactions between a membrane and the charged protein. Understanding the effect of the protein adsorption on solid surfaces is crucial for engineering membranes with enhanced performance parameters and prolonged lifespan [1].

In this study, polysulfone membranes were modified by incorporation of different carbon nanoforms during manufacturing process to alter the surface characteristics to reduce protein fouling without decreasing the dialysis membranes biocompatibility.

Methods: Three nanocomposite polysulfone-based membranes (PSU, Sigma-Aldrich) were manufactured by the liquid-induced phase separation without solvent method using dimethylformamide (DMF, Avantor SA) as the solvent, and water as the non-solvent. As a filler were used different carbon nanoforms: 2%wt. carbon nanotubes (CNT, Nanostructured & Amorphous Materials), 1%wt. graphene oxide (GO, NanoAmor US) and 5%wt. graphite (GR, NanoAmor US).

The membranes microstructure was assessed by the scanning electron microscopy (SEM, Apreo 2) with a subsequent image analysis (ImageJ) to obtain data about their thickness, porosity and pore size distribution. A surface zeta potential (charge) analysis was conducted using Zetasizer (Malvern) and contact angle and surface free energy were determined with DSA25E goniometer (Krüss). Permeability tests were performed on a dialyzer of the own construction to determine the molecular weight cut-off (MWCO) and the pure water flux. Compatibility with biological systems was tested with macrophages and fibroblasts cell cultures and assessed for thrombogenicity.

Results: The carbon nanoforms are present in both a skin and a support layer of asymmetric membranes (100 um thickness), which is proven by changes in Zeta potential. The modified membranes show finger-like pore structure in the support layer and unimodal distribution of pore size in the skin (Fig. 2) and similar skin-to-support ratio (1:3). All nanocomposite membranes have increased surface free energy (up to 50,52 mN/m for CNT) and hydrophobicity (CA from 89,9° to 109,2° for GR). Permeability of membrane by means of the water flux increased only in the case of the membrane modified with CNT. The other additives were less effective in the water flux test. Biocompatibility in *in vitro* tests revealed low cytotoxicity and thrombogenicity of the membranes.

Discussion: The membranes were characterized in terms of four aspects: morphology, surface properties, performance parameters and biocompatibility. In comparison with the pristine PSU membrane, the surface charge of the modified membranes decreases, increasing the magnitude of electrostatics repulsion between the surface and foulants, both charged negatively in a physiological pH of blood.

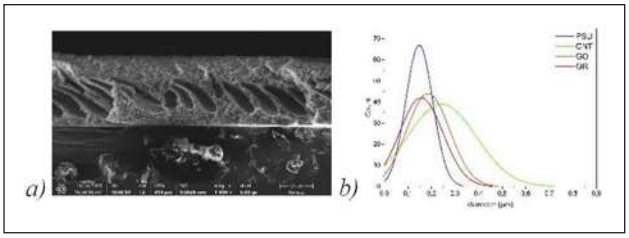

Figure 2. a) CNT-modified membrane cross-section with skin and support layer b) pore size distribution in the skin layer.

Conclusions

The obtained nanocomposite membranes can be an alternative to pure polymeric membranes. The presence of carbon nanoforms affects the surface properties by reducing protein fouling and coagulation.

Reference

1. Florens N, Guebre-Egziabher F, Juillard L. Reconsidering adsorption in hemodialysis: is it just an epiphenomenon? A narrative review. J Nephrol 2022; 35: 33–41.

Acknowledgements

This work was supported by "Initiative of Excellence – Research University" (IDUB) grant ID 4204.

IN VITRO CHARACTERISATION OF MODIFIED MICRO VASCULAR PLUGS AS PULMONARY FLOW RESTRICTORS

Niccolò Crescenti (1, 2), Julia Imhoff (3), Michael Hübler (3), Jörg Siegmar Sachweh (3), Bernhard Semlitsch (2), Rainer Gerhard Kozlik-Feldmann (3), Nora Lang (3), Marcus Granegger (1, 3)

1. Department of Cardiac Surgery, Medical University of Vienna, Austria; 2. Research Unit of Fluid Flow Machinery, Vienna University of Technology, Austria; 3. University Heart & Vascular Center, Hamburg, Germany

Introduction: Hypoplastic Left Heart Syndrome denotes a severe congenital heart disease with high mortality rates due to pulmonary overperfusion and reduced systemic flow. In recent studies, patients who were not eligible for the initial surgical procedure benefitted from the implantation of a modified Micro Vascular Plug (MVP) (Medtronic®) as a pulmonary blood flow restrictor [1]. Due to its high level of unpredictability in its in situ behaviour [2], a steady in vitro setup was used to hydraulically characterise the MVP in different vessel diameters and compliances.

Methods: The pressure drops over a single and a double hole perforated MVP (∅ 9.2 mm unconstrained) were investigated in a steady circulatory loop. The perforations were performed with an injection needle and expanded by the placement and inflation of a 2 mm balloon catheter (Fig.1a). A water-glycerol mixture was prepared to reach a target viscosity of 4.5 cP at room temperature of 25 °C. The pressure drop across the MVP was measured for volume flow rates between 0 to 2 L/min with an increment of 0.1 L/min every 60 seconds. The pressure drop value was averaged over the stable range of measured values. During the tests, different vessel diameters and compliances (inner diameters: 4.8, 5, 6 and 6 mm, the latter with a higher compliance) were used.

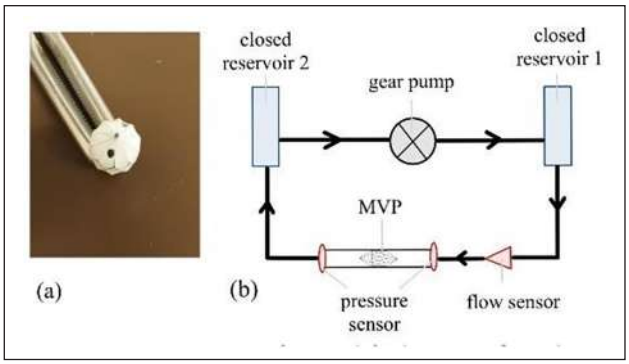

Figure 1. (a) Picture of a modified MVP-7Q with two fenestrations (∅ 2 mm). (b) Schematic drawing of the in vitro experimental setup for measuring pressure drop across the device at steady flow rate from 0-2 L/min.

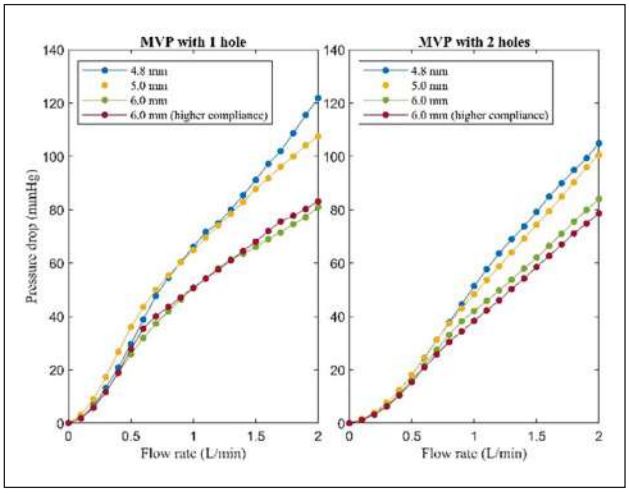

Figure 2. Average pressure drop curves across MVP for flow rates ranging from 0-2 L/min. Influence of perforation choice, tube size and compliance.

Results: The pressure drop increases with smaller vessel diameters (6<5<4.8 mm) and lower compliance (6 mm comp. < 6 mm). Two distinct relationships of the pressure drop on the flow rate can be observed: quadratic at low-volume flow rates and almost linear at high-volume flow rates.

A single hole in the MVP causes a higher pressure drop as compared to two holes. For low-volume flow rates, the percentage difference is about 67%.

Discussion: Tailoring the hydraulic resistance of the MVP to the patients´ cardiovascular condition may improve hemodynamics and patient outcome considerably. We showed that the number of holes significantly affects the hydraulic resistive behaviour of the MVP especially at lower volume flow rates. This finding may be attributable to the flow distribution: At low-volume flow rates (0-0.6 L/min), the differences in the pressure drop between the two groups is explained by the perforation choice (predominant flow proportion passes through the holes). At higher volume flow rates (1.6-2 L/min), the collapse of the MVP leads to a reduction of the effective fenestration size. Therefore, the vessel diameters are primarily causing the differences in pressure drop as para-device flow increases.

References

1. Kizilski et al, Cardiovasc. Eng. Technol., 14:640–654, 2023.
2. Nageotte et al, Pediatr Cardiol., 42(6):1410-1415, 2021.

NEW POLYMERS AS ADDITIVES IN DIALYSIS TREATMENT BLENDED MEMBRANES FOR LONG TERM FILTRATION

Malgorzata Tasior (1), Odyl ter Beek (1), Dimitrios Stamatialis (1)

1. Advanced Organ bioengineering and Therapeutics, Faculty of Science and Technology, TechMed Center, University of Twente, The Netherlands

Introduction: Dialysis is the one of the commonly used therapies for patients with End Stage Kidney Disease. There, a hollow fiber (HF) membrane-based dialyzer is applied for filtering the uremic toxins from patients' blood [1]. These membranes are most based on hydrophobic polymer, such as polysulfone (PES), and hydrophilic polymer additives such as polyvinylpyrrolidone (PVP) [2]. However, during therapy, PVP can be eluted, from the HF resulting in decreased hemocompatibility [3,4] For achieving prolonged dialysis leading to improved toxin removal [5], one needs to fabricate fibers that do not elute hydrophilic additive over the course of the dialysis treatment. Based on earlier studies done by other researchers [6,7] as well as one done in our group [8], here, we

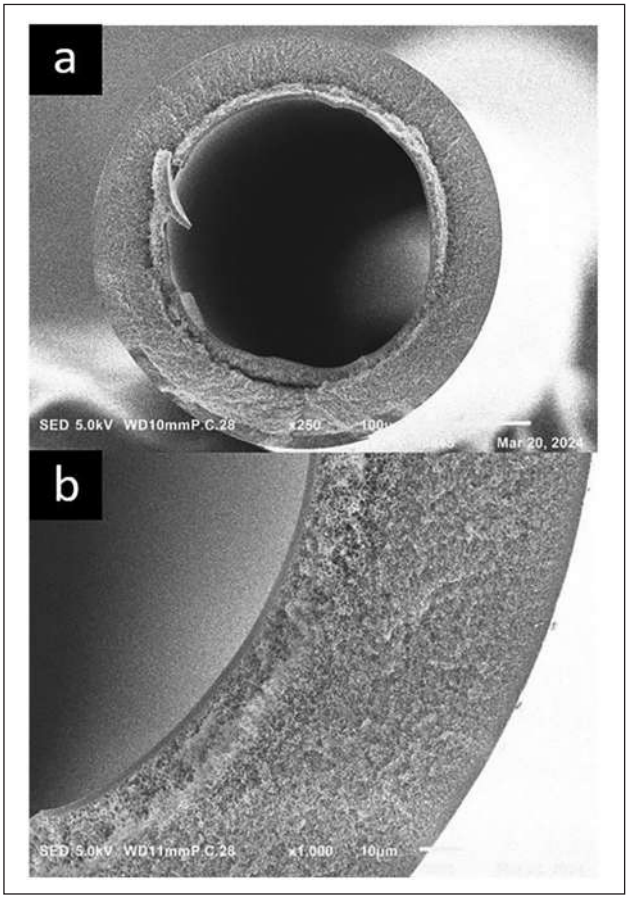

Figure 1. Cross-section of PES/sPPSU/PVP fiber: a) whole fiber cross-section magnification of x250, b) fiber wall, magnification x1000.

Table 1. Inner diameter and ultrafiltration coefficient of PES/sPPSU/PVP and F8HPS.

Fibers	Inner dimeter µm	KUF [mL/(m2*h*mmHg)]
PES/sPPSU/PVP	262 ± 21	11 ± 3
F8HPS[8]	191 ± 9	10 ± 4

investigate the application of sulfonated polymers and copolymers as hydrophilic additive for HF dialysis membranes. We hypothesize that these additives will provide membranes with high flux combined to low additive leakage during long term therapy.

Methods: The polymer dopes consisted of PES (as membrane forming polymer) and PVP, sulfonated polyphenylsulfone (sPPSU) or copolymers (as additives) are dissolved in N-Methyl-2-pyrrolidone (NMP). Various compositions were investigated. HF membranes were prepared by wet spinning using liquid induced phase separation. Various spinning conditions (polymer speed, bore speed, bore composition, pull wheel speed) were investigated. The HF were washed and air dried at room temperature and their morphology was characterized via scanning electron microscopy (SEM). For all membranes we performed clean water flux measurements and for selected membranes we investigated albumin rejection, PVP elution and transport studies with human plasma.

Results: Figure 1 presents typical SEM image of hollow fiber obtained from blend consisting of PES, sPPSU and PVP (PES/sPPSU/PVP). The fibers have spongy structure and selective layer located on the inside of the fiber. The membrane ultrafiltration coefficient (KUF) puts the fibers in low flux range and is comparable to F8HPS (Fresenius) dialyzers. (Table 1). The fibers are mechanically stable and can be used with trans membrane pressure (TMP) up to 2 bars.

Discussion: By adjusting polymer dope and bore composition we can increase further the membranes' KUF and proceed to detailed transport studies. Our first studies indicate that the blend composition and bore liquid can have a significant effect to the membrane morphology, mechanical properties, and overall performance.

References

1. Bello et al, Nat Rev Nephrol, 18:378–395, 2022
2. Yang et al, J of Memb Sci, 326: 322–331, 2009.
3. Namekawa et al, J Artif Organs, 15:185–192, 2012
4. Sato et al, Bioch and Biophy Rep, 28:101140, 2021
5. Davenport, Pediatr Nephrol, 30:2053–2060, 2015
6. Li et al, J of Memb Sci, 513:1-11, 2016
7. Kaleekkal et al, Ch J of Memb Sci, 23: 1236-1244, 2015
8. Ter Beek et al, J of Mem Sc, 604: 118068, 2020

Acknowledgements

This work was financially supported by BASF.

SURFACE MODIFICATION OF CARDIOVASCULAR DEVICES TO REDUCE THE RISK OF THROMBUS FORMATION

Marta Bonora (1), Veronica Viola (1), Stjepan Perak (2), Markus Lunzer (2), Sonja Kopp (3), Michael Mühlberger (3), Barbara Messner (4), Francesco Moscato (1), (5), (6)

1. Center for Medical Physics and Biomedical Engineering, Medical University of Vienna, Austria; 2. UpNano GmbH, Austria; 3. PROFACTOR GmbH, Austria; 4. Department of Cardiac Surgery, Medical University of Vienna, Austria; 5. Ludwig Boltzmann Institute for Cardiovascular Research, Austria; 6. Austrian Cluster for Tissue Regeneration, Austria

Introduction: Blood contacting cardiovascular devices are successfully employed to treat heart failure. Hemocompatibility-related issues due to unphysiological flow and exogenous material still occur and anticoagulant treatment is necessary [1], [2]. In this study, innovative surface manufacturing presenting definable micropatterned geometries, that may reduce adhesion of platelets compared to a fully polished surfaces, are investigated.

Methods: 4 geometries: reverse cones, riblets, grids and spheres have been designed based on 3 criteria: i) hydrophobicity fluid repulsion ii) reduction of accessible area for platelets adhesion iii) improving of the action of the blood flow in washing away platelets from the surface. Micropatterned surfaces are printed via 2 photon polymerization printer (2PP, UpNano GmbH) and replicated via nanoimprinting lithography (NIL, Profactor GmbH). Then, the surfaces are employed in 2 tests corresponding to rationale described: i) wettability measurements via water contact angle (WCA); ii) platelets adhesion tests in static conditions measured via Scanning Electron Microscoppe (SEM).

Results: Geometries are printed in 4 dimensions: Extra-Small (1-3µm), Small (3-9 µm), Medium (6–18 µm), Large (12-36 µm), and wettability test are performed and compared to a flat surface. Large and Medium size of all structures showed a higher hydrophobicity (WCA 120-130°) with respect Extra-Small and Small structures (WCA 100-110°) especially Large riblets showed a superhydrophobic behavior (WCA>150°). All the WCA values resulted at least hydrophobic contrary to the flat surface (WCA 69°).

Secondly, surfaces are incubated with human platelets in a low shear condition (static experiments). Results for Small Cones, Riblets, Grids are showed in Figure 1.

Discussion: We have shown that our micropatterned surface are highly hydrophobic with respect the flat surface as commonly employed in cardiovascular devices. This feature may play an important role in the platelet adhesion reduction since, at the conditions we set, the fluid (blood) is repelled. This result agrees with the results obtained in the static conditions experiments.

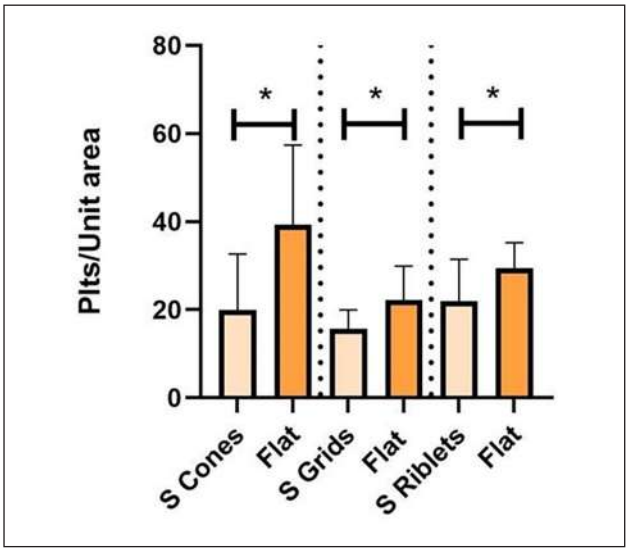

Figure 1. Number of platelets adhering on unit area on Small Cones, Small Grids, and Small riblets compared with flat surfaces. For each microstructured surfaces tested, a flat surface sided is tested. N=6, *p<0.05.

As a next step microfluidic experiments to evaluate the platelet adhesion under shear conditions are currently being established.

References

1. Li, Y. *et al.* A new way to evaluate thrombotic risk in failure heart and ventricular assist devices. *Med Nov Technol Devices* **16**, (2022).
2. Vitale, N. *et al.* Left Ventricular Assist Device Thrombosis: Combined Approach by Echocardiography and Logfiles Review for Diagnosis and Management. *Braz J Cardiovasc Surg* **37**, (2022).

Acknowledgements

The authors acknowledge funding from the OptiFlow 3D project (FFG FO999891239).

MEMBRANE SUPPORTED LIQUID-LIQUID OXYGENATION: A NOVEL APPROACH IN ECLS THERAPIES

Jan Heyer[a], Stepan Sibritsev[b], Paul Vogt[a], Andreas Jupke[b], Ulrich Steinseifer[a], Sebastian V. Jansen[a]

[a]Department of Cardiovascular Engineering, Institute of Applied Medical Engineering, Medical Faculty, RWTH Aachen University, Forckenbeckstr. 55, Aachen, 52074, Germany; [b]Fluid Process Engineering, Aachener Verfahrenstechnik, RWTH Aachen University, Forckenbeckstraße 51, D-52074 Aachen, Germany

Background: Chronic respiratory diseases are the third most frequent cause of death worldwide. The gold standard end-stage therapy is lung transplantation. However, the limited availability of transplantable organs led to an increased research effort in artificial lung systems. Current artificial lung systems use hollow fibre membrane-based oxygenators with limited gas-transfer. Historic oxygenators using a direct liquid-gas or liquid-liquid interface outperformed today's hollow-fibre technology in terms of gas transfer. However, these approaches were no longer pursued due to complications of embolization by gas or liquid particle formation in the bloodstream. The herein presented approach of a membrane-supported liquid-liquid oxygenator combines today's hollow-fibre technology with the historic liquid-liquid approach to achieve a stable interface without risk of embolization with the advantages of a higher gas transfer and the decrease of blood contacting membrane surface.

The concept of membrane-supported liquid-liquid oxygenation is sketched in Figure 1 (right) and compared to a conventional polymethylpenten-membrane (PMP).

Methods: Literature was analyzed regarding a suitable perfluorocarbon fluid for the presented approach of a membrane-supported liquid-liquid oxygenator. The candidate fluids were tested primarily for hemocompatibility. The interface interaction between blood and fluid was analyzed using a Nitsch cell test. Transmembrane pressure was investigated for stable operation in conventional polypropylene fibers as used in the proof-of-principle oxygenator. Based on these results, a proof-of-principle oxygenator was manufactured, tested in vitro for gas transfer and checked for droplet formation in the blood.

Results: Perfluoro-n-hexane was chosen as a hemocompatible carrier fluid for the presented liquid-liquid approach. The Nitsch cell test revealed a stable interface between blood and fluid at Reynolds numbers 285 and 368 with a maximum initial gas transfer of 0.151 mmolO2 min^{-1} and 0.848 mmolCO2 min^{-1}, respectively. A transmembrane pressure of 5 kPa was determined for stable operation in the proof-of-principle oxygenator with O2 and CO2 total gas transfers measured after 10 minutes to be 1.83 mmolO2 and 1.34 mmolCO2, respectively. In the proof-of-principle, no Perfluoro-n-hexane droplets were identified in the blood after the experiment.

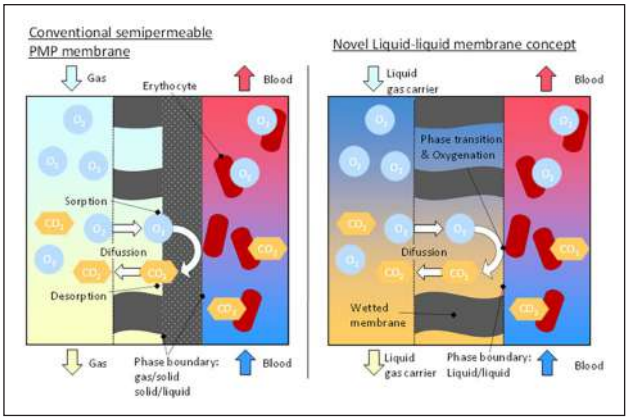

Figure 1. Conventional semipermeable PMP membrane (left) compared to the novel liquid-liquid mambrane concept.

Conclusion: This study demonstrates proof-of-principle of a new membrane-supported liquid-liquid oxygenator. Gas transfer efficiency results were comparable to conventional hollow-fibre technology, while no indication of droplet formation was found. Considering that a non-optimal conventional membrane was utilized for this approach, this is a promising finding indicating that with a more suitable membrane material, the liquid-liquid approach is safe and could exceed hollow-fibre technology by a large margin with respect to gas transfer efficiency.

SEX-DEPENDENT DIFFERENCES IN A LONG-TERM CHRONIC KIDNEY DISEASE MOUSE MODEL

Julia Wollenhaupt (1), Corinna Schulte (1), Dickson Wong (2), Joachim Jankowski (1), Heidi Noels (1)

1. Institute for molecular cardiovascular research, University hospital RWTH Aachen, Germany; 2. Institute for Pathology, University hospital RWTH Aachen, Germany

Introduction: Chronic kidney disease (CKD) is a global health problem that is continuously increasing. CKD is not only impacting the kidney, but also the heart, since it now has been identified as being an independent risk factor for the development of cardiovascular diseases (CVD). The treatment strategies for CVD in women are not as effective as in men, which is probably the result of the fact that most research and clinical trials in the past have only been performed in men. Therefore, this study aimed to characterize in detail the kidney phenotype in both female and male mice in an experimental long-term CKD mouse model along with additional investigation of the heart, liver and vasculature, to uncover the impact on CKD-associated comorbidities.

Methods: Male and female C57BL/6J ApoE -/-mice were fed with an adenine-supplemented diet containing additional high fat and high phosphate concentrations over a period of 20 weeks, resulting in the development of a long-term CKD. The experiment was followed by detailed phenotyping of the kidney and other organs using western blot analysis, FACS analysis, histological stainings, ELISAs and RNA sequencing to provide insights into fibrosis, inflammation, and oxidative stress among others.

Results: We have successfully established a chronic adenine-induced CKD model with CKD development over 20 weeks without any weight loss. Kidney damage was detected in male and female adenine-fed mice, but CKD development was different depending on sex. For example, FACS analysis revealed a higher level of macrophages in kidneys of CKD males compared to females and also RNA sequencing revealed sex-dependent differences in molecular processes in the kidney and heart in CKD.

Discussion: Our results suggests that in male and female mice, the onset, development or progression of CKD is influenced differently depending on sex, with underlying mechanisms currently being investigated in detail at the molecular level. Characterizing sex-dependent differences in CKD-induced effects on the vasculature, heart and liver is ongoing.

VOLUME ADJUSTABLE ARTIFICIAL WOMB FOR EXTREMELY PRETERM INFANTS

Jan Heyer*, Franziska Schubert*, Alexander L. Seitz*, Yannick Steinle*, Jutta Arens†, Thorsten Orlikowsky‡, Ulrich Steinseifer*, Thomas Schmitz-Rode*, Sebastian V. Jansen*, Mark Schoberer‡

** Department of Cardiovascular Engineering, Institute of Applied Medical Engineering, Medical Faculty, RWTH Aachen University, Germany; † Engineering Organ Support Technologies Group, Department of Biomechanical Engineering, Faculty of Engineering Technology, University of Twente, The Netherlands; ‡ Department of Pediatric and Adolescent Medicine, Neonatology, Medical Faculty, University Hospital RWTH Aachen, Germany*

Background: Every year, more than 13 Million children are born prematurely, resulting in 0.9 million deaths. Most affected are Extremely Preterm Infants (gestational age <28 completed weeks). Immaturity causes organ failure and specific morbidities like germinal matrix hemorrhage, etc. Artificial womb and placenta technologies (AWAP) are investigated as a bridge-to-life technology, providing a liquid environment that allows organ maturation under protected and more physiologic conditions. Globally, several research groups are currently developing and testing AWAP. Recent achievements in animal models have demonstrated the potential of this technology. Current approaches usually immobilize the lamb fetuses in bio-bags which expose the animal fetuses to unphysiological gravitational and postural forces. Additionally, current bio-bag environments are continuously flushed with crystalloid solutions. This has proven successful in preventing infections, but causes wash-out of valuable molecules like surfactant phospholipids. We present an adjustable artificial womb that allows fetal movement and includes filtering, disinfecting of the artificial amniotic fluid, and retaining autologous phospholipids.

Methods: Our adjustable artificial womb consists of an outer and inner, liquid filled silicone sac and can adapt to fetal growth. Both sacs are housed in a surrounding liquid-filled chamber. Volume adjustment is achieved by addition or removal of fluid into or from the interspace between the two sacs. The artificial amniotic cavity is attached to a fluid filtering system, which allows to clean the artificial amniotic fluid while retaining autologous phospholipids. Both sacs are embedded in a fluid chamber that controls temperature and generates hydrodynamic pressures equal to in-utero pressures. 7 day in-vitro tests were performed to assess temperature and pressure, cleaning-and filtering abilities, and volume adjustability constancy, which were visualized by MRI-based neonatal manikins (24 and 28 weeks of gestational age).

Results: Results showed constant temperature of (36.9 ± 0.1) °C and no measurable pressure loss over 7 days. The range of the volume of the inner sac was 3.6 – 7.2 L. The increase of the inner sac's volume is shown in Figure 1).

No bacterial contamination occured in the filtered system in contrast to a non-filtered reference sample, and no loss of phospholipids was observed over time.

Conclusion: Our novel artificial womb features a sufficient volume adjustment to allow an extremely preterm fetus to grow and move. Additionally the filtering system proved to be safe and effective in retaining important phospholipids. These are essential steps in artificial womb development. Next steps will include in-vivo testing in animal trials.

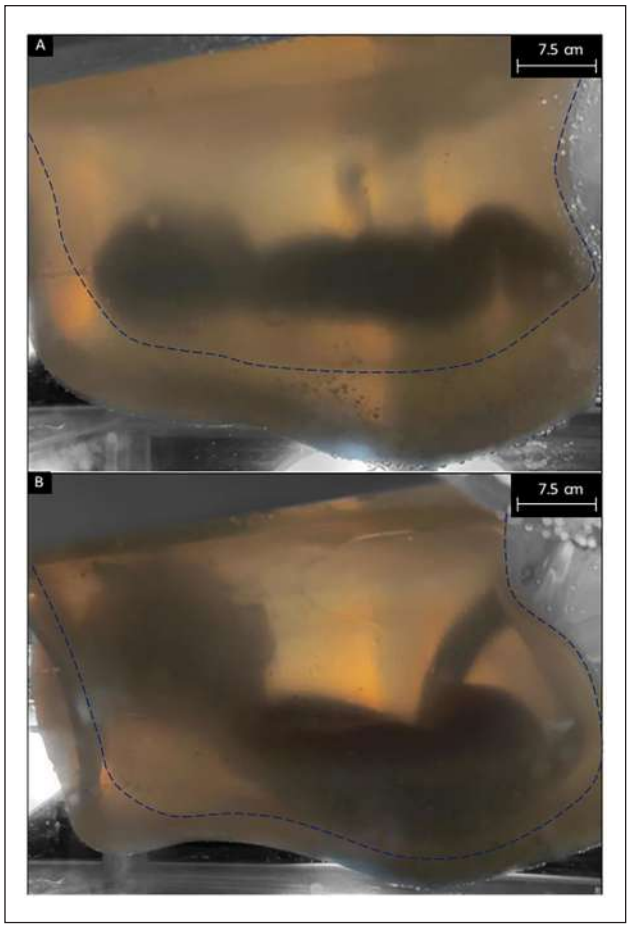

Figure 1. Wisualization of the growth with two manikins of the system from 3.6 L filling volume of the inner sac (dashed line (A)) to 6.8 L filling volume of the inner sac (dashed line (B)).

Acknowledgement

This project was funded by the European Research Council (ERC) under the European Union's Horizon 2020 research and innovation programme (Grant agreement ID 863087)

ON THE MATERIAL RESPONSE TO MECHANICAL SURFACE MODIFICATION: SURFACE PROPERTIES VS MG63 CELLS PROLIFERATION.

Michela Sanguedolce (1), Jessica Dal Col (2), Francesco Modica (3), Vito Basile (3), Cristiana Stellato (2), Luigino Filice (1)

1. Department of Mechanical, Energy and Management Engineering, University of Calabria, CS 87036, Italy; 2. Department of Medicine, Surgery and Dentistry "Scuola Medica Salernitana", University of Salerno, SA 84081, Italy; 3. Institute of Intelligent Industrial Technologies and Systems for Advanced Manufacturing, National Research Council (STIIMA-CNR), BA 70124, Italy.

Introduction: Surface properties of implantable devices both affect their durability and modulate their interactions with the body environment in an interconnected way [1].

In the broad range of available techniques, some of them involve material removal or displacement, most likely with simultaneous material

modification, others involve material deposition. Each surface processing technique – whether mechanical, thermal, or chemical – affects the surface properties of the produced devices in a specific fashion [2]. Among material removal processes, milling, which involves a rotating cutting tool to remove layers of material, is frequently used to define the final shape of the implant starting, for example, from cast parts [3]. Processes like grit-blasting are often used to roughen the surfaces according to different needs, dictated by the specific device location and expected duration.

The identification of the properties of the "ideal" surface is still a major challenge: a good tissue-implant integration would be desirable for the implant's mechanical stability but it could be problematic in the case implant surgical revision or removal are needed. This calls for a better insight into what is happening at the site of implantation. This work aims to identify how different textures generated on a titanium alloy through mechanical processing affect the response of MG63 cells.

Methods: Simply shaped samples of *Ti6Al4V* alloy were processed in triplicates. The used processing techniques are grit-blasting, face milling, and polishing. Milling parameters were varied to assess the effects of different conditions within the same process. Surface topography was analyzed with optical profilometry while microstructure and nanoindentation hardness were studied along the cross-section to characterize altered layers. EDS analysis was used to assess surface composition after processing.

The osteoblast-like MG63 cell line was used for the *in vitro* assays. Cells were cultured in Dulbecco's Modified Eagle Medium supplemented with 10% heat-inactivated fetal bovine serum, 100 units/mL penicillin, 100 µg/mL streptomycin, and 20 mmol/L L-glutamine. Cells were seeded onto the surface of processed *Ti6Al4V* samples and incubated at 37°C in a 5% CO2/95% air-humidified atmosphere for 48 hours. Cell Counting Kit -8 for quantification of viable cell number in proliferation was used, coupled with absorbance measurement at 450 nm. Polystyrene plates were used as control. May Grunwald-Giemsa staining was performed to visualize the cells on *Ti6Al4V* samples.

Results and Discussion: Three types of surface textures were herein compared: grid-like and anisotropic for milling, random and isotropic for grit-blasting, and ideally smooth for polishing. The results of the CCK-8 assay show a higher proliferation on grit blasted samples while proliferation is slowed down on the polished samples. The response to milling texture is affected in a complex trend by processing conditions.

Future developments will cover a thorough analysis of the studied surface modification techniques, in particular milling, taking into account the underlying phenomena that correlate surface texture, microstructure, composition, and contact angle. The long-term goal of the study is to locate a processing window for the modulation of the osteointegration of *Ti6Al4V* implants, as this alloy currently keeps on being the clinical standard of care for bone-contacting implants.

References

1. Ratner et al, Academic Press, 2013.
2. Kalpakjian, Prentice Hall, 2009.
3. Achtelik-franczak & Dobrza, Processes, 2020.

Acknowledgments

This work was supported by Project CalHubRia -T4-AN-09, Piano Operativo Salute, Italian Ministry of Health.

PERFORMANCE EVALUATION OF 3D-MICROSTRUCTURED MEMBRANE MODULES FOR ARTIFICIAL LUNGS

Kai Philip Barbian[1], Jan Heyer[1], Jannis Focke[1], Ulrich Steinseifer[1], Sebastian Victor Jansen[1]

[1]Department of Cardiovascular Engineering, Institute of Applied Medical Engineering, Medical Faculty, RWTH Aachen University, Forckenbeckstr. 55, 52074 Aachen, Germany

Introduction: Hollow fiber membranes (HFM) incorporate significant drawbacks as oxygenator membrane technology. Suboptimal blood flow conditions lead to reduced gas transfer efficiency and increased risk of thrombosis reducing device durability. Moreover, large foreign surface areas are needed for sufficient blood-gas transfer requiring mediation with anticoagulants which puts the patient at risk of internal bleeding [1]. Three dimensional membrane structures, based on triply periodic minimal surfaces (TPMS), have been proposed for usage in oxygenators as they intrinsically separate blood and gas volume and provide increased gas transfer efficiency through passive blood mixing effects [2,3]. In this study, we demonstrate a novel method for manufacturing miniaturized, dense 3D-membrane structures to be able to directly test their performance concerning blood oxygenation against HFM-modules.

Methods: A manufacturing process was established to create dense membranes with TPMS structure out of medical grade silicone. The 3D-membrane modules were created using TPMS unit cell sizes of 2 and 3 mm, which correspond to flow channel widths of 0.71 and 1.06 mm, respectively. Subsequently, the structures were analyzed under digital light microscopy. Afterwards, these modules were assembled into miniature oxygenators.

A miniature HFM-oxygenator with similar membrane surface area, based on a modular platform developed for rodents [4], was manufactured as testing reference. Gas transfer testing according to ISO 7199 and pressure drop measurements were performed using porcine blood on both the 3D-membrane and the HFM modules. Gas transfer efficiency was evaluated by calculating the oxygen transfer coefficient, βO2, for both devices.

Results: The 3D-membrane modules were manufactured successfully with a membrane thickness varying between 80 and 140 µm (cf. Figure 1). In Figure 2, the measurement results for gas transfer efficiency are shown. The 3D-membrane shows comparable oxygen transfer coefficients to the HFM with an increase of 11.16% averaged over all flow rates. Moreover, the pressure loss measured inside the 3D-membrane module was in a similar range and slightly lower than that of the HFM.

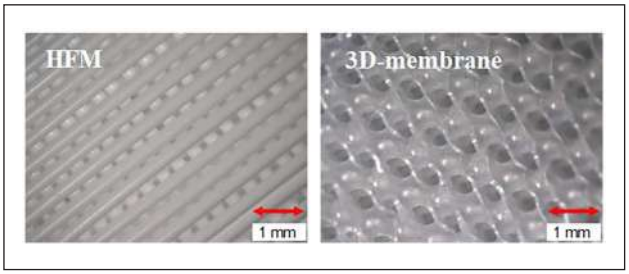

Figure 1. Digital light mircoscopy images of the HFM (left) and the 3D-membrane structure with a TPMS unit cell size of 2 mm (right).

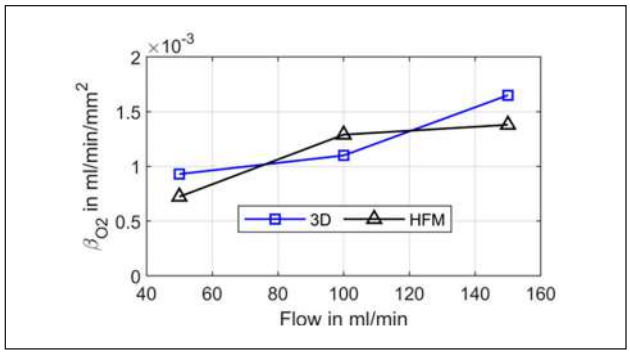

Figure 2. Measurement results of oxygen transfer efficiency for the 3D-membrane oxygenator with 3 mm TPMS unit cells ("3D") and the HFM oxygenator ("HFM").

Discussion: For the first time, we successfully manufactured micro-scale 3D-structured membrane modules and tested them directly against HFM. Comparable gas transfer coefficients as well as slighly lower pressure drops were measured when comparing the 3D-membrane with the HFM. This indicates a more efficient overall device performance being in accordance with findings of earlier studies [2,3]. However, the HFM-module is still superior in terms of low priming volumes. Additional experiments will be performed to obtain statistical certainty. Still, these early results clearly show the capability of the 3D-membrane technology. By further miniaturizing the 3D-membrane to achieve higher efficiencies, a novel membrane concept might be at hand that is superior to the HFM.

References

1. Tonetti et al, 10.1186/s40635-023-00563-x, 2023
2. Femmer et al, 10.1016/j.cej.2015.03.029, 2015
3. Hesselmann et al, 10.1016/j.memsci.2021.119371, 2021
4. Strudthoff et al, 10.3390/mi14040800, 2023

MULTIMODAL IMAGING FOR THE PATIENT-SPECIFIC ASSESSMENT OF NEUROVASCULAR HEMODYNAMICS

Philipp Berg (1,2), Janneck Stahl (1,2), Jana Korte (1,3), Daniel Behme (1,4), Ali Alaraj (5), Sylvia Saalfeld (1,6)

1. Research Campus STIMULATE, University of Magdeburg, Germany; 2. Chair in Healthcare Telematics and Medical Engineering, University of Magdeburg, Germany; 3. Laboratory of Fluid Dynamics and Technical Flows, University of Magdeburg, Germany; 4. Clinic for Neuroradiology, University Hospital Magdeburg, Germany; 5. Department of Neurosurgery, University of Illinois, Chicago, United States; 6. Department for Medical Informatics, University of Kiel, Germany

Introduction: With rising computational resources and higher modeling accuracy the application of image-based blood flow simulations to improve the understanding of cardio-and neurovascular diseases drastically increased over the last decade. However, in most numerical studies the focus is set on limited regions of interest and although they claim to be patient-specific, the modeling only includes a rigid segmentation of the individual vessel lumen [1].

To overcome the strong variability of hemodynamic simulations and regain the trust of the medical community in advanced modeling approaches, a standardized and holistic approach is needed [2].

Methods: Since the accuracy of hemodynamic simulations strongly depends on the imaging resolution, segmentation algorithm and individual image processing experience, high effort is put into a precise and multimodal image acquisition. This includes time-of-flight magnetic resonance imaging (MRI) and digital subtraction angiography (DSA) to capture the arterial vessels and magnetic resonance venography (MRV) for the venous part. Additionally, 2D phase-contrast MRI acquires real patient-specific volume flow rates [3] that are used as boundary conditions for multi-scale modeling [4]. Finally, a robust and reproducible workflow was established ensuring the generation of reliable numerical predictions.

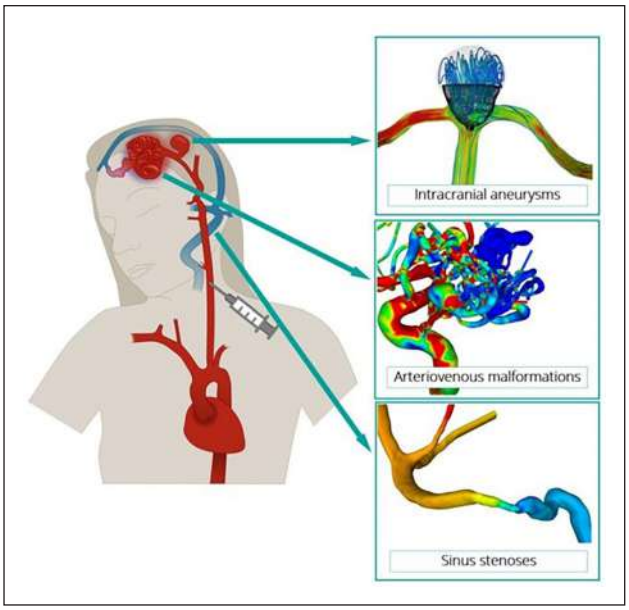

Figure 1. Schematic illustration of multimodal imaging for arterial and venous neurovascular diseases. Patient-specific modeling is used for individualized risk assessment and improvement of treatment planning.

Results: As shown in Fig. 1., highly resolved image-based based blood flow simulations could be carried out using both patient-specific vessel segmentations and boundary conditions. Exemplarily, the flow reduction in a wide-neck bifurcation aneurysm treated with a novel Contour device, the shear distribution of an arteriovenous malformation (AVM) and the pressure drop along a sinus stenos are presented.

Compared to recent studies focusing on limited regions of interest clear advantages of the multimodal approach could be identified. This includes 4D flow fields that allow for a risk-free evaluation of the disease state as well as supports the development of novel treatment approaches and their respective approval.

Discussion: The combination of multiple modalities enables a more robust numerical assessment and the consideration of relevant vascular pathologies. Hence, detailed flow investigation of so far unknow hemodynamic interactions becomes possible, e.g., the analysis of enhanced AVM draining veins [5].

Future work includes further verification and validation of individual processing steps to strengthen the trust among physicians.

References

1. Steinman et al, J Neurointerv Surg, 15(7):621-622, 2023.
2. Berg et al, Neurosurg Focus, 47(1):E15, 2019.
3. Alaraj et al, Stroke, 46:942-947, 2015.
4. Korte et al, Bioengineering, 72:1-24, 2024.
5. Stahl et al, J Neurosurg, 29:1-10, 2024

Acknowledgements

This work is partly funded by the Federal Ministry of Education and Research within the Forschungscampus STIMULATE (grant no. 13GW0473A) and the German Research Foundation (SPP2311, project number: 465189657).

SCALABLE GENERATION OF HUMAN IPSC DRIVED CARDIAC ORGANOIDS IN STIRRED TANK BIOREACTORS

Kurt Pfannkuche (1), Ebru Aksoy (2), Daniel Derichsweiler (3), Sarkawt Hamad (4)

University of Cologne -Medical Faculty. Marga-and-Walter-Boll-Laboratory for Cardiac Tissue Engineering. Germany

Generation of cardiac organoids: Human induced pluripotent stem cells (iPSCs) can be differentiated into various organotypic cells in 2D monolayer and 3D suspension bioreactor cultures. Manipulating Wnt signalling pathways, results in robust differentiation of hiPSCs towards cardiomyocytes [1] and endothelial cells [2] in 2D and 3D culture.

Conventional 2D culture methods are easily reproduced in many laboratories and allow the production of individual cell types. However, new approaches in stem cell therapy, basic research and pharmacology are moving away from simple 2D culture towards more complex microtissues and even macroscopic engineered tissues. An important trend in this respect is the scalable generation of cardiac organoids. Organoid culture allows the complex environment of a tissue to be recapitulated *in vitro*.

We have established a robust protocol to generate human cardiac organoids (COs) in suspension culture from iPSCs. COs are differentiated in stirred tank bioreactors (STBs) under fully controlled conditions.

A critical parameter in STB culture is the stirring of the suspension. In order to reduce shear stress and increase oxygen transfer, we used a novel membrane stirrer module developed by Biothrust GmbH, Aachen, Germany that supports large-scale production of COs.

By this approach, high densities of COs are produced without mechanically damaging the cell clusters. The differentiation of COs was successfully scaled from a 0,25 to a 3 liter STB yielding high quality COs that are used for cardiac cell therapy among other approaches.

Figure 1. Cardiac Organoids in a stirred tank bioreactor agitated by a membrane stirrer (provided by Biothrust GmbH, Aachen)

References

1. Hamad S et al. Theranostics. 25;9(24) (2019)
2. Hamad S et al. Stem Cell Res and Ther. 13(1):251 (2022)

Acknowledgements

This work was supported by grant ZM1-16-B (PERIDIAN) from the State North Rhine-Westphalia in frame of the initiative ZukunftBIO.NRW. Further support was provided by the Marga and Walter Boll Foundation (Kerpen, Germany).

ANISOTROPIC AUXETIC CARDIAC PATCH WITH MODULATED CELL ADHESION AND INFLAMMATORY BEHAVIOUR TO SUPPORT EPICARDIAL THERAPIES

Marjan Enayati[1,2], Christopher Riedmüller[1], Luis Pichelkastner[1], Lukas Weber[1], Sabrina Rohringer[1,2], Martin Stoiber[3], Bruno Podesser[1,2], Karl Schneider[1,2], Helga Bergmeister[1,2]

[1]Center for Biomedical Research and translational Surgery, Medical University of Vienna, Austria, [2]Ludwig Boltzmann Institute for Cardiovascular Research, [3]Center for Medical Physics and Biomedical Engineering, Medical University Vienna, Austria

Introduction: Anisotropic structure of the heart are the key players modulating the cardiac performance. However, after myocardial infarction (MI) and formation of myocardial ischemia, these characteristics varies drastically which could terminate to heart failure. Epicardial restraint constructs such as cardiac patch are a new class cardiac therapy [1]. Cardiac patch of the future should be able to mimic the sophisticated mechanical anisotropic characteristics. 3D-printed synthetic biopolymers are suitable candidate due to their facile tailor ability with adequate mechanics [2]. However, their hydrophobicity and the absence of particular cell recognition sites needs to be improved for a successful regeneration. In this study auxetic (Aux) designs integrated in to the patch to simulate an anisotropic behavior via precise 3D printing bowtie microstructures. To tackle the limited cell adhesion affinity, we utilized human placenta chorion derived extracellular matrix (hpcECM) as a coating to improve cell proliferation and the acceptance of these therapeutic patches in regions of local tissue damage.

Method: Various printing parameters (pressure, temperature, flow rate, digital coding, needle size) were optimized. Morphological and mechanical behavior of the patches (AuxPCL, AuxPCL-hpcECM) were studied via SEM, tensile tests and nano indentation. Roughness and wettability of the patches were studied. Various cell types such as human umbilical vein endothelial cells (HUVEC), endothelial progenitor cells (EPC), H9C2 cardiomyoblasts and human fibroblasts (HFF) were utilized to identify the biocompatibility, hemocompatibility and the role of hpcECM on proliferation and maturation/differentiation of cells via XTT, live dead, hemolysis and clot formation assays at various time points. Furthermore, expression of pro-inflammatory (CD80, CCR7, IL-1a & TNF-a) and anti-inflammatory (CD163, CD206& IL-10) macrophage and cytokine markers were assessed via PCR.

Results: Optimized printing parameters resulted in production of reproducible scaffolds with good structural integrity and pore size of (~0.2 mm^2). Tensile tests showed a clear anisotropic stiffness-ratio with ultimate strain of 7-20%; close to the range of physiological deformations of the myocardium (15-22%). Nano indentation confirmed softer and more elastic micro-environment in the present of hpcECM. A significant increase of initial cell attachment/differentiation (H9C2, HUVECs, HFF cells) mediated by hpcECM coated PCL constructs which led to a more mature cells (EPC, H9C2 cells) were observed. Patches were hemocompatibility with a low hemolysis rate. Pro-inflammatory gene expressions

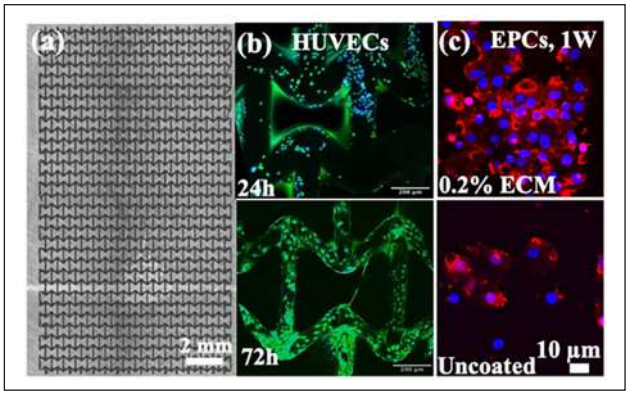

Figure 1. (a) AuxPCL patch, (b) HUVECs proliferation (c) Role of hpcECM on EPCs adhesion and maturation (Prom1 staining)

were showed in all groups at 24 and specifically after 72 hours followed by a significant reduction after 1 week. Immunomodulatory effect of the patches was validated.

Discussion: High resolution 3D printed patch showed promising results for the use of this mechanically tunable biomaterial in cardiac tissue engineering with positive hemocompatibility and immunomodulatory characteristics. Furthermore, hpcECM is capable of providing cells an extracellular matrix based platform with higher cell affinity promoting the proliferation, attachment and cellular metabolic activity of the cells.

References

1. Bar et al., Front. Bioeng. Biotechnol., 8:2020.
2. N. R. Richbourg et al., J Tissue Eng Regen Med., 13:8,2019.

Acknowledgements

This work was partially supported by Ludwig Boltzmann Institute for Cardiovascular Research.

EFFECT OF CANNULA TIP POSITIONS IN PULMONARY ARTERIAL CANNULATION ON BLOOD FLOW AND GAS EXCHANGE USING COMPUTATIONAL FLUID DYNAMICS ANAYLSIS

Shah Eiman Amzar Shah Apandi (1), Annika Schmitz (1), Johannes Greven (2), Jan Spillner (3), Mehdi Behbahani (1)

1. Institute for Bioengineering (IfB), Faculty for Medical Engineering and Techno-Mathematics, FH Aachen University of Applied Sciences, Jülich, Germany; 2. Department of Orthopedics, Trauma and Reconstructive Surgery, RWTH Aachen University, Aachen, Germany; 3. Department of Thoracic Surgery, RWTH Aachen University, Aachen, Germany

Introduction: Pulmonary arterial cannulation presents itself as a viable alternative cannulation strategy for patients at high risk of right ventricular and severe respiratory failure on mechanical circulatory support [1]. However, limited data exists to what effect the position of the cannula tip has on the oxygen perfusion throughout the pulmonary artery (PA). This study aims to evaluate, using computational fluid dynamics, the effect of different cannula tip positions on the oxygenation level in the PA to determine an optimal cannula position.

Methods: The pulmonary artery 3D geometry is a simplified reconstruction using patient CT data as the foundation and Code_Saturne, an

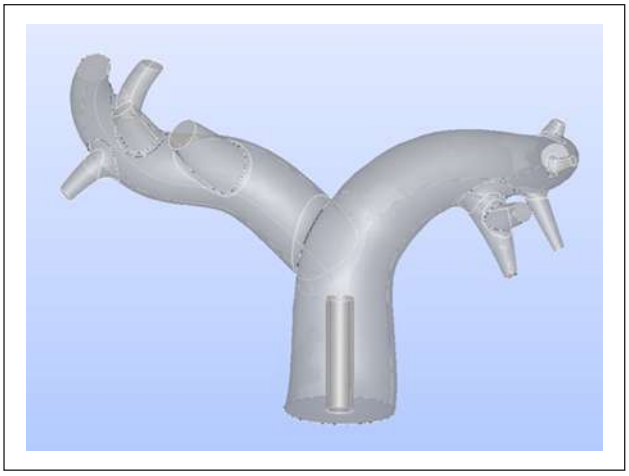

Figure 1. Example of the pulmonary artery 3D geometry with one of the four cannula tip positions.

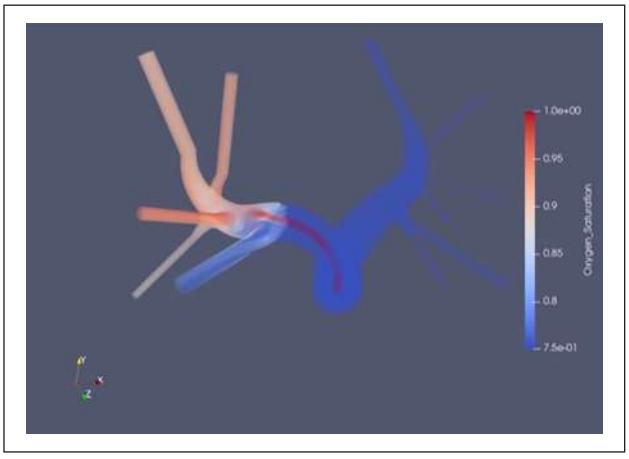

Figure 2. The oxygen saturation distribution in the pulmonary artery with Position 3, the cannula tip positioned directed towards the right pulmonary artery.

open-source software, was used for the computation to simulate the flow field and oxygen concentration distribution. The visualization of the results was performed using ParaView.

Results: Computational results reveal how the position of the cannula tips affect blood flow patterns and consequently the oxygen perfusion in the pulmonary artery. A slight change in the positioning of the cannula can have drastic outcomes on the overall perfusion, for example, position 3, with the cannula tip directed towards the right pulmonary artery (RPA), for which it could be shown that the RPA was almost exclusively saturated with the oxygenated blood (see Figure 2).

Discussion: Results indicate that out of the 4 tested positions, position 2, with the cannula placed at the upper portion of the main PA before the bifurcation, is the most suitable, with both the RPA and LPA achieving adequate mean value and the smallest difference in the concentrations of oxygen. Variations in individual patient geometry is also assumed to have a major impact on the computational results and the modelling accuracy. Furthermore, this computational study used a veno-arterial support level of 50% of the total blood flow rate. Future studies using higher levels of support, such as 75%, can be useful to see whether varying support levels can improve oxygen perfusion and

hence contribute to finding the optimal setting for pulmonary artery ECMO support. Finally, the CFD study demonstrated promising results, however more calculations are necessary to determine optimal perfusion parameters to be used for pulmonary arterial cannulation.

References

1. J. M. Bagan et al, "ECMO with cannulation of femoral vein and pulmonary artery in a patient after heart transplantation and unknown refractory hypoxemia," Journal of Cardiothoracic and Vascular Anesthesia., vol. 31, no. 1, pp. 21-22, 2017.
2. A. Schmitz, "Numerische Strömungsmechanik Analyse der perfundierten Pulmonalarterie", [Master's thesis, FH Aachen], 2024

BRIDGING THE GAPS IN HEMOLYSIS PREDICTION: GENERALIZED K-Ω MODEL OPTIMIZATION AND STRAIN-BASED APPROACH.

Ilaria Guidetti (1), Katharine H. Fraser (2), Maria Laura Costantino (1), Francesco De Gaetano (1)

1. Department of Chemistry, Material and Chemical Engineering, Politecnico di Milano, Milan, Italy; 2. Department of Mechanical Engineering, University of Bath, Bath, United Kingdom

Introduction: Computational prediction of blood damage is still a challenge, hindering the possibility of reducing the design and development time of cardiovascular devices. Since 2008, the FDA is promoting interlaboratory studies aimed at defining a standard for conducting computational fluid dynamics (CFD) simulations and using hemolysis models [1]. Despite efforts, fast and accurate CFD predictions are still a challenge, and a universal hemolysis model has not yet been developed. This study addresses the first shortcoming optimizing the parameters of a Reynolds-averaged Navier-Stokes (RANS) turbulence model and the second implementing a strain-based hemolysis model that accounts for red blood cell (RBC) deformation.

Methods: A 2D axisymmetric model for the sudden expansion (SE) and the conical diffuser (CD) configurations of the FDA nozzle is employed to solve the device flow field with ANSYS Fluent 2021. The tunable parameters of the generalized k-ω (GEKO) turbulence model are optimized for the application and ANSYS Post-CFD 2021 is used to extract the pathlines to implement the Lagrangian hemolysis models. Pathlines are tracked either forward from the inlet, backward from the outlet, or from recirculation zones, normally excluded from path-tracking. Both the stress and the strain-based hemolysis models are implemented in MATLAB® 2023 using a damage dose to account for RBCs' shear history, following the damage accumulation method of Grigioni, and are evaluated with the power-law parameters from Torner and Tobin works [2]-[4]. The stress-based model uses a von Mises-like equivalent shear stress while the strain-based describes the RBC as a deforming droplet through an evolution equation. This model accounts for the tank treading motion and the relaxation time of the RBC membrane and is derived from Arora [5].

Results: The optimized GEKO model parameters improved the flow field prediction, matching the experimental pressure drop with a mean absolute percentage error of only 0.97%. Only two of the power-law parameters sets reported by Torner (FZ and HO) yield modified index of hemolysis (MIH) values in the magnitude order of the experimental results for both models, with the FZ set providing the best results [3]. The inclusion of the recirculation regions (Figure 1) in the path-tracking allows to improve the hemolysis estimation and resolve the prediction errors of the other methodologies. The MIH obtained with the FZ set and this path-tracking method, are shown in Figure 2. Both hemolysis models have similar trends; however, the strain-based is able to correctly predict the MIH for the two conditions at 6 L/min (SE6 and CD6) and slightly overpredicts the 5 L/min condition (CD5).

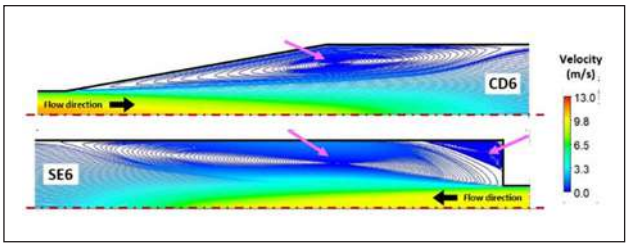

Figure 1. Recirculation regions in the diffuser and in the expansion at 6 L/min (CD6 and SE6 conditions).

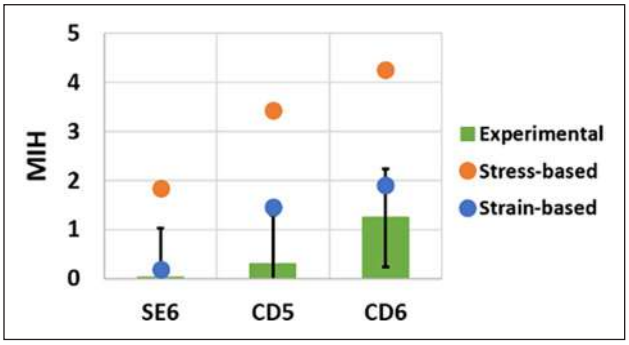

Figure 2. Modified index of hemolysis (MIH) obtained experimentally and with the stress and the strain-based models considering also the recirculation regions.

Discussion: This study improves RANS models prediction capability providing a set of optimized parameters for the GEKO model and introduces a methodology that uses a 2D axisymmetric Lagrangian model for assessing hemolysis in a 3D domain. The results indicate the strain-based model as a viable candidate for the development of a hemolysis model for a wide range of cardiovascular devices. Furthermore, this work explores the impact of recirculation zones and emphasizes the complexities inherent in Lagrangian methods. This lays the groundwork for enhancing hemolysis predictions by incorporating a more comprehensive approach that includes recirculation zones and underscores the necessity for an in-depth examination of the strain-based model and power-law method parameters.

References

1. Website: https://ncihub.cancer.gov/wiki/FDA_CFD .
2. Grigioni et al., Biomech Model Mechan, 4:249-260, 2005.
3. Torner et al., Biomech Model Mechan, 22:401–416, 2022.
4. Tobin et al., Cardiovasc Eng Technol, 11:254-267, 2020.
5. Arora et al., Artificial Organs, 28:1002-1015, 2004.

SYNTHESIS, REACTIVITY, AND BIOLOGICAL ACTIVITY OF NA2CD(SEO4)2·2H2O

Aneliya Kostadinova[1], Dayana benkova[1], Dimitar Dimov[2], Rumyana Yankova[3]

1: Institute of Biophysics and Biomedical Engineering, Bulgarian Academy of Sciences, Sofia 1113, Bulgaria; 2: Institute of Electronics, Bulgarian Academy of Sciences, Sofia,1784, Bulgaria; 3: University "Prof. Dr. Assen Zlatarov" Burgas, 8010, Bulgaria

The molecular structural and geometrical parameters of Na2Cd(SeO4) 2.2H2O nanoparticles were determined by Density Functional Theory.

The electronic structure and net atomic charges were determined. The calculated energies of HOMO and LUMO molecular orbitals were used to determine the descriptor activities of the molecule. The molecular electrostatic potential (MEP) represents the electron density distribution in the molecule and visualizes the differently charged regions with which the molecule would participate in electrophilic or nucleophilic reactions. Thermal analysis has determined the likely mechanism of decomposition of the double salt. Zeta potential analysis and a particle size distribution revealed that Na2Cd(SeO4)2.2H2O is characterized by highly positive charge and nano-dimensions, determining strong biological potency. At concentrations above 0.05 µg/ml, the double selenium salt exhibited strong cytotoxic activities on Hep G2 liver cancer cells, evidenced by significantly decreased cell viability. Moreover, a noticeable alteration in cell morphology was observed, indicated by rounded cell shape, increase in intracellular spaces, and reduction in cell number, all indicative of cell death. Cells decreased noticeably, and the intercellular spaces increased significantly. Owing to its nonlinear optical properties, the double selenium salt Na2Cd(SeO4)2.2H2O holds promise novel and innovative biosensors with potential utilization in biomedicine.

Acknowledgements

This work is supported by grand КП-06-H-77/13 Bulgarian Fund of Scientes.

RABBIT TO HUMAN: TRANSFER LEARNING FOR ECG DELINEATION

Milica Ilic (1), Laurenz Berger (1)(2), Max Haberbusch (1)(2), Lisa Aurora Bernardo (3), Laura Galassi (3)(4), Calogero Oddo (3)(4)(5), Theodor Abart (6), Thomas Schlöglhofer (1)(2)(6), Julia Riebandt (6), Daniel Zimpfer (6), Francesco Moscato (1)(2)(7)

1. Center for Medical Physics and Biomedical Engineering, Medical University of Vienna, Austria; 2. Ludwig Boltzmann Institute for Cardiovascular Research, Austria; 3. The BioRobotics Institute, Scuola Superiore Sant'Anna, Italy; 4. Department of Excellence in Robotics & AI, Scuola Superiore Sant'Anna, Italy; 5. Interdisciplinary Research Center Health Science, Scuola Superiore Sant'Anna, Italy; 6. Department of Cardiac Surgery, Medical University of Vienna, Austria; 7. Austrian Cluster for Tissue Regeneration, Austria

Introduction: Accurate identification of the P-wave, QRS complex, and T-wave of the electrocardiogram (ECG) is important for diagnosing cardiac disorders. Previous work has demonstrated the superiority of deep neural networks (DNNs) over traditional algorithms in ECG delineation [1,2]. Furthermore, transfer learning (TL) has been shown to enhance the performance of DNNs and to decrease the training time needed for the target dataset [3]. In the context of ECGs, TL has already been applied within the same species for arrhythmia classification, but a cross-species approach has not yet been explored. Here, for the first time, we propose using TL from animal to human data for ECG delineation.

Methods: Two datasets were utilized: (1) 9 hours of ECG recordings from 7 rabbits sampled at 1000 Hz [4] with ~ 85 thousand beats, and (2) an 18-hour Holter ECG of one heart failure patient sampled at 250 Hz [5] with ~ 120 thousand beats. The study protocol was approved by the Institutional Review Board (ClinicalTrials.gov Identifier: NCT04641416). All participants provided written informed consent. Datasets were manually annotated for one of four classes: P-wave, T-wave, QRS Complex, or No wave. The models underwent pre-training on the rabbit dataset (80/20 train-test split) to evaluate various architectures. A hyperparameter grid optimization via 5-fold cross-validation was performed. Model performance was assessed on unseen rabbit data. The best-performing model was additionally tested on the human dataset. The final DNN architecture included one 1D convolutional neural network (CNN) layer, three bidirectional long short-term memory (BiLSTM) layers, and a dense output layer. Subsequently, TL was applied to fine-tune the best-performing model on

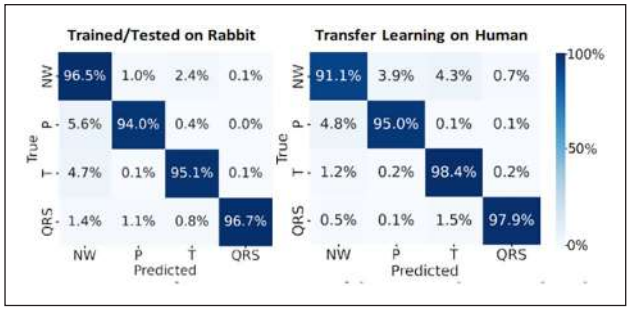

Figure 1. Confusion matrices of the network trained and tested on the rabbit dataset (left) and the transfer learning approach on the human dataset (right). QRS: QRS-complex, T: T-wave, P: P-wave, NW: no wave.

the human dataset. Fine-tuning was performed by freezing specific network layers (e.g., the CNN and first BiLSTM layer) while only retraining the active layers. The efficacy of the TL approach was assessed by accuracy and F1-Score for the human ECGs. All computations were performed using an NVIDIA A100 40 GB GPU.

Results: Pretraining required 5 hours, while the TL approach averaged just 1 hour. The best-performing pretrained

network achieved an accuracy of 95.7% and an F1-Score of 95.8% on unseen rabbit data, and notably lower performance on human data, with an accuracy of only 57.5% and an F1-Score of 53.0%. Employing TL significantly enhanced the delineation performance with an accuracy of 95.9% and an F1-Score of 95.6%.

Discussion: TL was successfully employed for ECG delineation across species going from rabbit to human, while significantly reducing computational training time without sacrificing performance. The current study was focused on a patient-specific approach; however, future work aims at scaling this approach to a larger patient population, thereby enhancing its generalizability.

References

1. Strodthoff et al, IEEE J Biomed Health Inform, 25:1519-1528, 2021.
2. Peimankar et al, Expert Syst Appl, 165:113911, 2021.
3. Weimann et al, Sci Rep, 11:5251, 2021.
4. Haberbusch et al, Proc World Congr Int'l Union Phys Eng Sci Med, 2022.
5. Schlöglhofer et al. J Heart Lung Transplant, 43:251–60, 2024.

Acknowledgements

This work was supported by grant 883859 from the FFG and 824071 from the EU and partially funded by grant #HF2020-000091 from Abbott Laboratories.

INTERACTION OF A VENTRICULAR ASSIST DEVICE WITH PATIENT-SPECIFIC CARDIOVASCULAR SYSTEMS-IN-SILICO STUDY WITH BIDIRECTIONAL COUPLING

Mario Hahne (1), Vincenz Crone (1), Inga Thomas (1), Calvin Wolfgramm (1), Frieder KP Liedtke (1), Frank-Hendrik Wurm (1), Benjamin Torner (1)

1. Institute of Turbomachinery, University of Rostock, Rostock, Germany

Introduction: Ventricular assist devices (VADs) are used to assist the heart function of patients with advanced heart failure. Computational

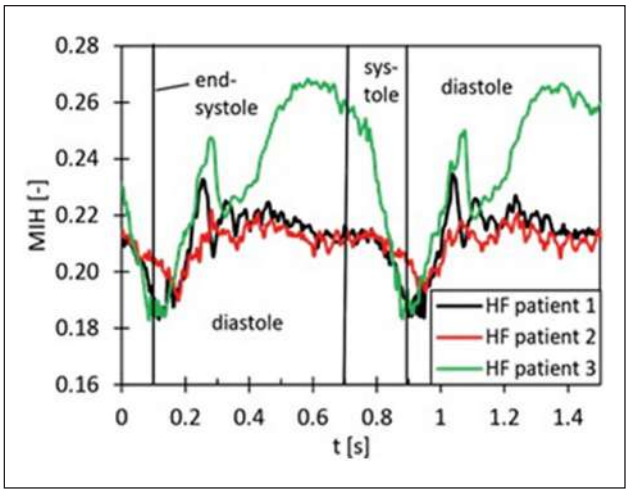

Figure 1. Temporal Progression of the Modified Index of Hemolysis (MIH) over two heartbeats for three VAD-supported Heart Failure (HF) Patients.

fluid dynamics is widely employed in the development and optimization of VADs, particularly for assessing factors such as blood damage. Ensuring the accuracy of these simulations requires precise incorporation of the VAD's operating conditions.

Patients relying on VAD support often exhibit residual cardiac pulsatility, causing the VAD to operate in conjunction with the still-beating heart. This interaction introduces pulsating flow conditions, leading to dynamic changes in operational points from partial load to overload and vice versa. Consequently, VADs may undergo significant variations in pressures and flow rates during operation. In certain patients, specific characteristics of the cardiovascular system can result in non-ideal operation points, potentially increasing blood damage. It is crucial to account for all these factors in flow simulations to accurately represent the complex dynamics involved in VAD operation.

Therefore, this study aims to address this issue by evaluating the flow in a VAD interacting with patient-specific cardiovascular systems in three different heart failure patients.

Method: This study introduces a novel numerical method incorporating a patient-specific cardiovascular system model bidirectionally coupled with a 3D flow simulation of the HeartMate 3. The cardiovascular system is represented by a lumped parameter model, utilizing clinical data from end-stage heart failure patients. Specifically, three heart failure patients with different cardiac activities are considered.

Various parameters of both the cardiovascular system and the VAD are examined. This includes an assessment of flow rates, pressures, VAD heads, efficiencies, and as crucial parameter—the blood damage potential of the VAD. The latter is accounted for using a transport equation for plasma-free hemoglobin.

Results: The head-flow rate curves of the VAD exhibit a pronounced hysteresis, with the degree of hysteresis increasing in correlation with the remaining heart activity. Additionally, a more vigorous heartbeat compels the VAD into less favorable operating conditions, particularly in overload and strong partial load conditions, where stresses and stress exposures reach their maximum, respectively. Both overload and, notably, partial load conditions during pulsating operation result in elevated blood damage potentials, see Fig. 1.

Conclusion: This study yields significant insights into the dynamic behavior of VADs in conjunction with patient-specific cardiovascular systems, highlighting the challenges posed by residual cardiac pulsatility. The findings emphasize the critical role of incorporating patient-specific characteristics in computational simulations for accurate assessments. The novel bidirectional coupling method holds promise in simulating realistic flow environments, closely resembling the actual operational conditions of VADs.

Reference

1. Hahne M, Crone V, Thomas I, Wolfgramm C, Liedtke FKP, Wurm FH, Torner B. Interaction of a Ventricular Assist Device With Patient-Specific Cardiovascular Systems: In-Silico Study With Bidirectional Coupling. ASAIO J. 2024 Mar 27. doi: 10.1097/MAT.0000000000002181

EVALUATION OF Δ9-TETRAHYDROCANNABINOL (THC) AND CANNABIDIOL (CBD) ON AN *IN VITRO* TRIDIMENSIONAL MODEL OF HUMAN LUNG CANCER

Irene Monleón-Guinot (1,2), Víctor Pérez (1), Morgane Millot (1), María Sancho-Tello (1,2), Jose Javier Martín de Llano (1,2), Carmen Carda (1,2,3), Lucía Bravo-Baranda (1,2), Irene Navarro-Esclapés (1), Mauro Llop-Miguel (1), Lara Milián (1,2) and Manuel Mata (1,2,3)

1. Departamento de Patología, Facultad de Medicina y Odontología, Universitat de València, Valencia, Spain; 2. Instituto de Investigación Biomédica INCLIVA, Valencia, Spain; 3. CIBER de Bioingeniería, Biomateriales y Nanomedicina (CIBER-BBN), Spain.

Introduction: Previous research has highlighted the inhibitory effects of cannabinoid agonists on key factors of lung cancer, such as cell proliferation and epithelial-mesenchymal transition (EMT) [1,2]. However, the majority of these studies rely on two-dimensional *in vitro* models that do not consider the tumor microenvironment (TME), which is critical in lung cancer's metastasis and resistance to treatment. Cancer-associated fibroblasts (CAFs) play an important role in tumor progression via EMT, as they have the capability to secrete diverse factors, including transforming growth factor beta (TGF-β).

The aim of this study is to evaluate the effect of two cannabinoid agonists, Δ9-tetrahydrocannabinol (THC) and cannabidiol (CBD), on a three-dimensional *in vitro* model. This model consists of spheroids formed by A549 cells and organoids of A549 combined with either CAFs or normal fibroblasts (NFs), supplemented with TGF-β.

Methods: Spheroids and organoids were formed using the hanging drop method and subsequently embedded in a rat type I collagen hydrogel. After an incubation period of four days, they were either supplemented with 5 ng/ml TGF-β or left untreated, and then treated with the cannabinoid mixture (THC + CBD, 10 µM each) or left untreated, followed by an additional three days of incubation. The spheroids/organoids were subsequently fixed in 4% paraformaldehyde. Immunofluorescence staining was performed to analyze cytokeratin filaments, F-actin was evaluated using rhodamine-conjugated phalloidin, and cell nuclei were stained with DAPI. Finally, the spheroids/organoids were examined using a confocal microscope.

Results: Immunofluorescence analysis showed a consistent morphology in the A549 spheroids under normal conditions, except for those treated with TGF-β, which displayed some small protrusions. Organoids of A549 co-cultured with fibroblasts did not exhibit significant differences in morphology (Figure 1).

Discussion: Our results suggest that while A549 spheroids were affected by TGF-β, organoids were not. This difference could be attributed to the

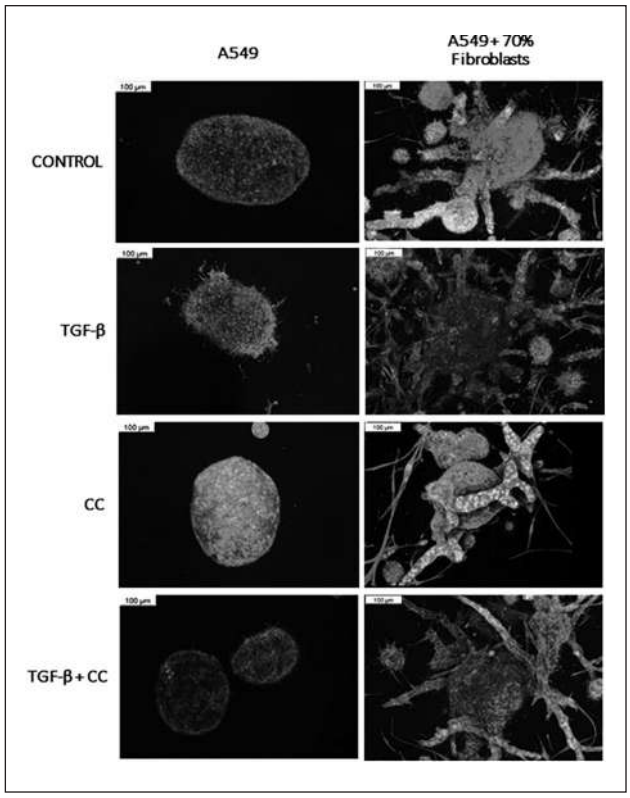

Figure 1. Morphology of human lung cancer organoids from each experimental condition.

endogenous expression of TGF-β in organoids, which may explain why their morphology remained unchanged. When cannabinoids were combined with TGF-β treatment, the phenotype induced by TGF-β in A549 spheroids was reversed. Furthermore, organoids did not show any morphological alterations. Overall, our results offer preliminary insights into the role of cannabinoid agonists in a 3D *in vitro* model of lung cancer.

References

1. Zang Y. et al, Oncol. Lett., 15:8527-8535, 2018.
2. Pacher P. et al, Annu. Rev. Pharmacol. Toxicol., 60:637-659, 2020.

ROSTOCKTESTCASE – OPEN ACCESS GEOMETRY AND HIGH-FIDELITY FLOW SIMULATION RESULTS OF A VENTRICULAR ASSIST DEVICE FOR NUMERICAL VALIDATION

Benjamin Torner (1)

1. Institute of Turbomachinery, University of Rostock, Rostock, Germany

Introduction: Numerical flow simulations in ventricular assist devices (VADs) are crucial for the development and optimization of these devices. They help to evaluate the pump performance, the stress field and to make statements about the hemocompatibility. The flow in a ventricular assist device is rather complex with turbulent flow characteristics and secondary flow structures. Therefore, flow validation of VAD simulation is important to ensure that the applied flow solver, the computational grid, and the simulation setup can represent the VADs flow. Regarding that, the research group "Rotary Blood Pump" at the University of Rostock provides a freely available test case of an axial

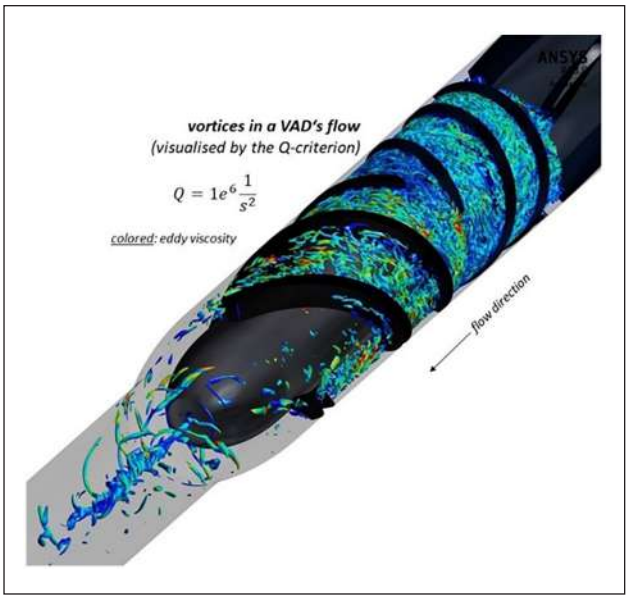

Figure 1. Turbulence-resolving simulation of the flow in an axial ventricular assist device. The iso-surfaces show turbulent eddies, visualized by the Q-criteria.

Figure 2. QR code to the Testcase.

ventricular assist devices on which interested researchers can test their simulation setup and compare their results with the results of a high-fidelity large-eddy simulation of the VAD flow.

Method: The test case is available at: https://unibox.uni-rostock.de/get-link/fi8AE4mYS4kxu8ZY51oxDh/

A documentation of the test case can be found at: https://kbwiki.ercoftac.org/w/index.php/AC7-03

Results: The full 3D geometry of the VAD, as well as detailed information about the grid generation, simulation setup, and experimental validation, can be found at these links. High-fidelity large-eddy simulation results of the stress fields are shown and compared with a state-of-the-art

Reynolds-averaged Navier-Stokes simulation. In addition, blood damage prediction results are published.

Conclusion: The test case offers simulation engineers in the field of cardiac support a validation possibility of their numerical methods. In addition, the simulation methodology in the test case is well documented, providing researchers with a good overview for this purpose.

VISCOELASTIC HYDROGELS AS 3D PLATFORMS FOR CELL CULTURE

José Luis Aparicio-Collado (1), Sandra Igual-Roger (1), Violeta Alagarda-Fernández (1), M. Teresa Donato (2,3,4), Laia Tolosa (2,5), Manuel Salmeron-Sanchez (5,6), Gloria Gallego Ferrer (1,5)

1. Centre for Biomaterials and Tissue Engineering (CBIT), Universitat Politècnica de València, Valencia, Spain; 2. Experimental Hepatology Unit, Health Research Institute La Fe (IISLAFE), Valencia, Spain; 3. Department of Biochemistry and Molecular Biology, School of Medicine, University of Valencia, Valencia, Spain; 4. Biomedical Research Networking Center on Hepatic and Digestive Diseases (CIBER-EHD), Carlos III Health Institute, Valencia, Spain; 5. Biomedical Research Networking Center on Bioengineering, Biomaterials and Nanomedicine (CIBER-BBN), Carlos III Health Institute, Valencia, Spain; 6. Centre for the Cellular Microenvironment, University of Glasgow, Glasgow, United Kingdom.

Introduction: Different approaches have been developed during the last years to generate 3D *in vitro* liver models that replicate the *in vivo* microenvironment to facilitate the understanding of hepatocytes functionality and their alterations in various pathologies. The use of biomaterials naturally found in the liver extracellular matrix (ECM) to generate hydrogels is an interesting approach that promotes cell-cell communication and cell-matrix interactions that resemble the *in vivo* situation (1). Despite different hydrogels have been developed for hepatic disease modeling, only few of them consider how the dynamics in the mechanical properties of the environment influences cell response (2). Most of them devote cell response to substrate stiffness, but do not consider that the liver is a viscoelastic organ in which the cellular response to mechanical stimuli from the ECM depends on the time and frequency of the stimulus (3). This study aims to generate novel *in vitro* models of healthy liver by engineering viscoelastic hydrogels with reversible bonds for the future 3D culture of hepatic cells.

Methods: Synthesis of viscoelastic hydrogels: dual functionalized gelatin (Gel) with norbonene and boric acid (Gel-NB-BA) (8% wt/vol) was mixed with dopamine-functionalized hyaluronic acid (HA) (HA-DOPA) (1,5% wt/vol) in a 90:10 ratio. The final hydrogels were covalently crosslinked due to the thiol-norbonene gelatin crosslinking with PEG4SH during 30 minutes under 365 nm UV light exposure with 10 mM lithium phenyl 2,4,6 trimethyl as photoinitiator. The BA-DOPA interactions by reversible bonding provided the viscoelastic properties.

Grafting analysis: the grafting analysis of the different functional groups bonded to Gel (NB and BA) and HA (DOPA) was confirmed by spectrophotometry.

Mechanical characterization: mechanical properties were determined by rheology. Pieces of fresh pig liver were measured, and the Gel-NB-BA/HA-DOPA hydrogels proportion was adapted to mimic the mechanical properties of the liver.

Cytotoxicity tests: as a first approach to test the cytotoxicity of the hydrogels, L929 murine fibroblasts were encapsulated and cell viability was assessed by a live/dead assay.

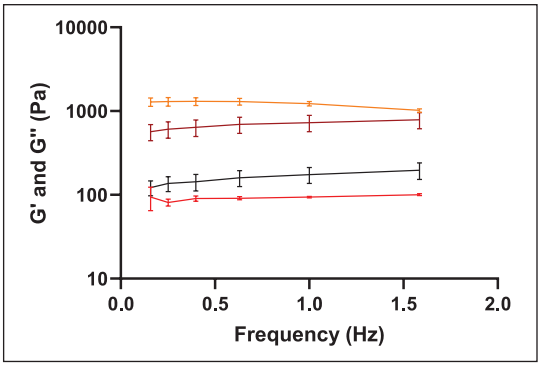

Figure 1. Rheological measurements of Gel-NB-BA/HA-DOPA hydrogels compared with pig liver. G' (orange for hydrogels and dark red for liver) and G'' (black for liver and red for hydrogels) values are represented.

Results and Discussion: Grafting analysis corroborated the incorporation of the different functional groups within the hydrogels precursors (NB, BA, DOPA). The Gel-NB-BA/HA-DOPA hydrogels display viscoelastic properties due to the reversible bonding between BA-DOPA groups in the presence of water (4,5). After assessing the mechanical properties of healthy pig livers by rheology, the hydrogels' proportion was adapted to imitate the biomechanical environment of hepatic tissue (*Figure 1*). Live/dead results proved that UV exposure did not produce any effect on cell viability after 30 minutes of hydrogel crosslinking. These results confirm that the viscoelastic hydrogels are 3D systems with potential applications in liver tissue engineering.

References

1. Unagolla *et al*. Appl Mater Today. 2020; 100479.
2. Kang. Semin Liver Dis. 2020;40(01):84–90.
3. Chaudhuri *et al*. Nature. 2020;584(7822):535–46.
4. Neto *et al*. Small. 2014;10(12):2459–69.
5. Kim *et al*. Biomater Sci Eng. 2021;7(9):4196–208.

Acknowledgements

Supported by PID2022-136433OB-C21, -C22 / AEI/10.13039/501100011033 and CNS2022-135425 grants from the Spanish State Research Agency and PI21/00223 grant form Institute of Health Carlos III. Also supported by Generalitat Valenciana through CIPROM/2022/43 project.

BLOOD DAMAGE POTENTIAL OF RESISTANCE CLAMPS IN IN-VITRO TEST LOOPS

Krishnaraj Narayanaswamy (1), Xiangyu He (1), Andreas Escher (1), Leonie Schmitt (1), Martin Stoiber (2), Daniel Zimpfer (1), Marcus Granegger (1)

1. Christian Doppler Laboratory for Mechanical Circulatory Support, Department of Cardiac Surgery, Medical University of Vienna, Austria; 2. Center for Medical Physics and Biomedical Engineering, Medical University of Vienna, Austria

Introduction: Resistance clamps are important in regulating flow and pressure in in-vitro test loops for blood pumps. However, the narrow cross section introduced by these clamps may contribute to elevated shear stresses. To date, the sole effect of resistance clamps on the in-vitro hemocompatibility assessment of blood pumps has been unclear. The aim of this study was to investigate the hemolytic potential

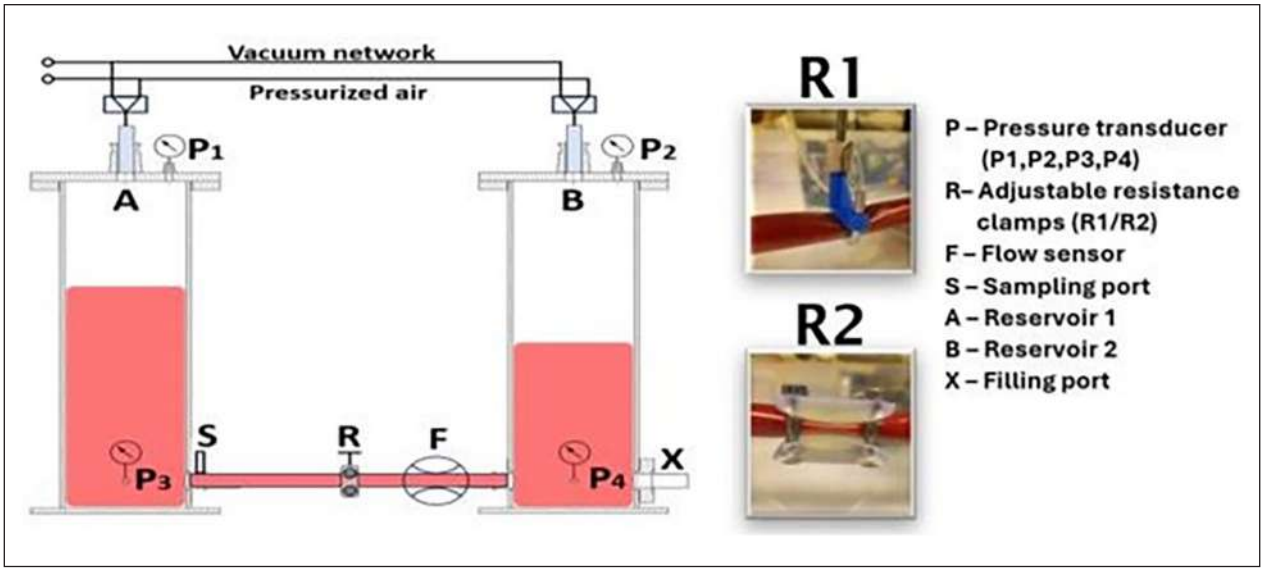

Figure 1. Schematic diagram of the in-vitro test loop (left) and the resistance clamps (R1, R2) (right).

of adjustable resistance clamps at various clinically relevant operating conditions. Computational fluid dynamics (CFD) simulations were performed to understand the flow dynamics and interrelation between this in-vitro hemolytic action and the energy dissipated through the clamps.

Methods: A hydraulic-pneumatic setup was developed consisting of two reservoirs connected by a tubing (Figure 1). Alternating blood flow between the reservoirs was facilitated by controlled pneumatic pressures, while an adjustable resistance clamp (R1/R2 in Figure 1) regulates the flow. Utilizing heparinized bovine blood, hemolysis assessment was conducted under 3 operating conditions with R1: low (7.5L/min at 30mmHg), medium (5L/min at 60mmHg), and high (1.5L/min at 90mmHg) resistances. The influence of sudden (R1) versus gradual (R2) contraction/expansion of tubing was evaluated under medium resistance conditions. Experiments were also conducted to investigate the hemolytic potential of the test loop without a resistance clamp. Further, silicon castings were created to replicate the resistance profiles of the 3 operating conditions, followed by 3D reconstruction. Unsteady RANS simulations were performed in the reconstructed replicas. Hydraulic quantities were computed to calculate the global hydraulic losses together with power-law-based NIH calculation. Further, the interrelation between global hydraulic energy dissipation, in-silico, and in-vitro NIH was evaluated through Pearson correlation coefficients.

Results: The hemolysis contributed by the test loop without clamps was similar to the static control group, with delta fHb of 0.285mg/dl/h. Nine experiments with R1 conducted for 3 operating conditions revealed no significant difference in delta fHb (1.15±0.13mg/dl/h, p>0.81). The NIH increased with increasing resistance: high 14.4mg/100L, medium 4.99mg/100L, and low 2.57mg/100L. Comparative analysis of two-resistance clamps (R1&R2) across five experiments revealed no significant difference in delta fHb and NIH (p=0.55). The pressure drop computed in-silico was in good agreement with the in-vitro results (r=0.999, RMSE<8.7mmHg). A strong correlation was observed between the numerically computed global hydraulic energy dissipation and both in-silico NIH (r=0.9) and in-vitro calculated NIH (r=0.95).

Discussion: Adjustable resistance clamps substantially affect hemolysis outcomes in in-vitro investigations of blood pumps regardless of the investigated shapes or profiles. Clamps with medium resistance are responsible for up to 81% of NIH observed in third-generation blood pumps operated at main operating point [1]. Low/high resistance settings contribute <47% of NIH measured with these blood pumps at off-design conditions. CFD provided a comprehensive understanding of the flow dynamics within the resistance profiles. Consistent with previous studies [2], the strong correlation between the dissipative losses and both in-silico and in-vitro NIH reflects that the dissipated energy may partially be converted into hemolysis. These findings on the hemolytic potential of adjustable resistance clamps may further improve the understanding of in-vitro hemolysis assessments of blood pumps at various operating points.

References

1. Escher et al, IEEE Trans Biomed Eng, 69(8), 2022
2. Escher et al, Adv. Theory Simul, 5,2200117, 2022

Acknowledgement

The financial support by the Austrian Federal Ministry of Labour and Economy, the National Foundation for Research, Technology and Development and the Christian Doppler Research Association is gratefully acknowledged.

INVESTIGATION OF WALL SHEAR STRESS IN AN IBIDI FLOW CHANNEL - APPLICATION NOTE

Sophia Krakowski (1,2), Henri Wolff (1,2), Michael Lommel (1,2), Ulrich Kertzscher (1,2) and Paul Geus (1,2)

1. Deutsches Herzzentrum der Charité, Institute of Computer-assisted Cardiovascular Medicine, Biofluid Mechanics Laboratory, Augustenburger Platz 1, 13353 Berlin, Germany; 2. Charité -Universitätsmedizin Berlin, corporate member of Freie Universität Berlin and Humboldt Universität zu Berlin, Charitéplatz 1, 10117 Berlin, Germany

Introduction: The blood flow in vessels causes shear stress, which is a mechanical force that influences the morphology and behaviour of cells. To study shear stress induced cellular changes, in vitro experiments

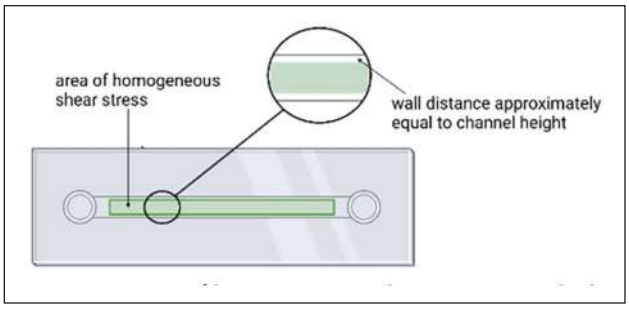

Figure 1. Area of homogeneous shear stress in Ibidi µ-slides according to manufacturer. µ-Slide VI$^{0.4}$ geometry: height= 0.4 mm, width= 3.8 mm. Created with BioRender.com

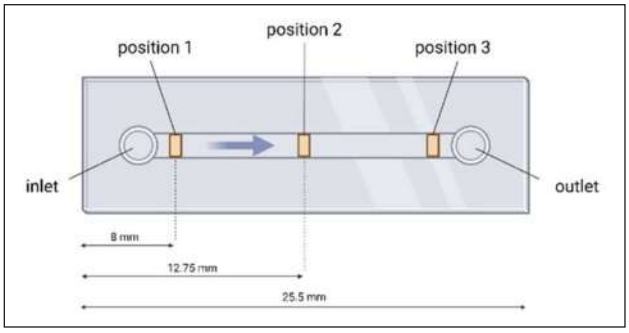

Figure 2. Regions of interest in the µ-Slide *VI*$^{0.4}$. Created with BioRender.com

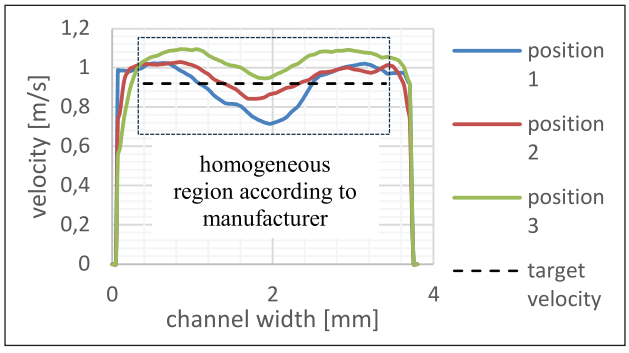

Figure 3. Mean velocities at 3 positions in the channel at 10.7 Pa WSS. The constant target velocity is in accordance with the manufacturer's specifications.

under flow are performed. They simulate the mechanical stimulus in the vessels and induce a more physiological behavior. The µ-Slide VI$^{0.4}$ (Ibidi GmbH) is a commonly used flow chamber for these experiments. According to the manufacturer, there is an area of homogeneous shear stress at the bottom of the chamber (Fig. 1).

However, during our experimental work with the µ-Slide VI$^{0.4}$, we noticed an inhomogeneous flow field at wall shear stresses above 8 Pa. To understand the flow characteristics in detail, we have performed numerical studies, which revealed deviations from the manufacturer's specifications. To validate the simulations, µ-Particle Image Velocimetry (µPIV) experiments were carried out.

Methods: A numerical analysis (Star-CCM+ 16.04.007) was performed for a range of WSS (1-12 Pa). The experimental validation via µPIV measurement was conducted in the center plane of the µ-Slide VI$^{0.4}$ at a shear stress of 10.7 Pa. Microparticles (71-75 µm) were added to the fluid (ultrapure water) and traced using a high-speed camera (12.000 fps). Images of the fluid flow were recorded at short intervals. By calculating the difference in the position of the microparticles between two images, a velocity-vector is created for each traced particle. The flow profile for the considered area can thus be calculated from these vectors. The flow field was analysed at 3 positions in the channel (Fig. 2) and compared to the manufacturer's specifications using a Matlab app (PIVlab) [1].

Results: Figure 3 shows the results of the µPIV experiment at 10.7 Pa. They confirm the inhomogeneous velocity profile predicted in the simulations at 10.7 Pa. The maximum speed deviates from the manufacturer's specifications at all positions (Fig. 2).

Discussion: The µPIV method is limited by the visibility of lower-lying microparticles. Nevertheless, the results allow the validation of the numerical simulations at different flow rates. Thus, for experiments with shear rates ranging from 8 Pa, it is essential that the user considers the inhomogeneous WSS to accurately interpret the test results, as the cells are exposed to different conditions.

Reference

1 Thielicke W and Stamhuis E.J, Journal of Open Research Software 2(1), p. e30, 2014

INTEGRATING CFD AND DEEP LEARNING FOR ENHANCED HEMODYNAMIC PREDICTIONS IN THE LEFT VENTRICLE.

Eneko Lazpita (1), Petros Koumoutsakos (2), Jesús Garicano-Mena (1), Soledad Le Clainche (1)

1. Universidad Politécnica de Madrid, Spain; 2. Harvard University, United States

Introduction: In recent years, cardiovascular disease has remained the leading cause of death worldwide, encouraging the exploration of innovative approaches to address this challenge. In particular, the integration of new engineering perspectives has significantly enhanced cardiovascular research. Techniques such as computational fluid dynamics (CFD) have been used to study hemodynamics within the heart [1], while machine learning tools have been applied to classify and predict these diseases using medical data [2]. Our study builds on these advances by combining left ventricular simulations from commercial CFD software (Star-CCM+) with deep learning architectures based on autoencoders. This combination aims to create high quality, converged databases efficiently and at low computational cost.

Methods: We began our research by using a CFD code to generate a detailed, high-dimensional database of the hemodynamics within the left ventricle using Star-CCM+ software. We modeled the blood as an incompressible laminar fluid and implemented specific inlet and outlet conditions corresponding to the mitral and aortic valves, respectively, based on medical data. In addition, a moving wall boundary condition replicated the ventricular pumping action during a cardiac cycle. These conditions were essential to accurately capture key flow features such as the primary vortex ring. Our simulations were thoroughly validated against reference data and subjected to extensive convergence studies.

After generating a sufficiently converged database, we employed a symmetric autoencoder with a prediction layer in latent space. The encoder consists of three-dimensional convolutional layers, paired

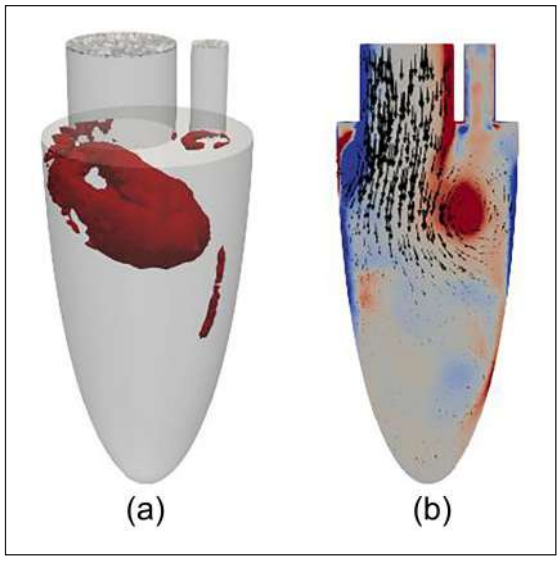

Figure 1. Left ventricle simulation results for t = 0.20 s: a) Q-criterion isosurface, b) Contours of the plane-normal vorticity field with xy velocity vector.

with max-pooling to reduce spatial dimensions while improving learning capabilities. It then transitions to dense layers to further compress the data into a 32-state latent dimension, a technique adapted from Hamidreza et al [3]. In the latent space, we applied a matrix rotation method to predict subsequent temporal states training the frequency λ^k for each state couples.

$$\begin{bmatrix} z_{i+1}^k \\ z_{i+1}^{k+1} \end{bmatrix} = \begin{bmatrix} \cos(\lambda^k \Delta t) - \sin(\lambda^k \Delta t) \\ \sin(\lambda^k \Delta t) - \cos(\lambda^k \Delta t) \end{bmatrix} \begin{bmatrix} z_i^k \\ z_i^{k+1} \end{bmatrix} \quad (1)$$

Results: From the CFD simulations, we extracted data for four heart cycles equispaced in time. Figure 1 illustrates some of these results, including vorticity and velocity fields that highlight the dynamics within the ventricle, such as the vortex ring and blood recirculation. We used this comprehensive database to train our neural network, allowing it to encode the data, predict future time instances in latent space, and reconstruct these new snapshots back into the original space. Our results show that our model can predict over a third of a cardiac cycle with an absolute error of less than 15%. This demonstrates the potential of combining CFD simulations with deep learning techniques to improve predictive accuracy in cardiovascular research, and offers promising directions for future investigation.

We use this database to train our neural network to be able to encode the data, predict following time instances in the latent space, and reconstruct this new snapshots to the original space. Our results show that we are able to predict more than a third of a cycle with an absolute error lower than 15%.

References

1. Zingaro et al, arXiv:2110.02114, 2021.
2. Groun et al, Comput. Biol. Med., 144, 105384, 2022.
3. Hamidreza et al, Expert Syst. Appl., 202, 117038, 2022.

Acknowledgements

The authors acknowledge the grant PID2020-114173RB-I00, TED2021-129774B-C21 and PLEC2022-009235 funded by MCIN/AEI/ 10.13039/501100011033 and by the European Union "NextGenerationEU"/PRTR. The authors gratefully acknowledge the Universidad Politécnica de Madrid (www.upm.es) for providing computing resources on Magerit Supercomputer.

HEMOLYTIC POTENTIAL OF RAPID SPEED VARIATIONS IN THE HEARTMATE 3

Krishnaraj Narayanaswamy (1), Xiangyu He (1), Theodor Abart (1), Barbara Messner (1), Michael Röhrich (2), Stefan Jakubek (3), Daniel Zimpfer (1), Marcus Granegger (1)

1. Christian Doppler Laboratory for Mechanical Circulatory Support, Department of Cardiac Surgery, Medical University of Vienna, Vienna, Austria; 2. Division of Special Anesthesia and Pain Medicine, Department of Anesthesia, Intensive Care Medicine, and Pain Medicine, Medical University of Vienna, Austria; 3. Division of Control and Process Automation, Institute of Mechanics and Mechatronics, TU Wien, Vienna, Austria.

Introduction: The artificial pulse is a special feature introduced to enhance arterial pulsatility with the HeartMate 3 (HM3, Abbott Inc, Chicago, USA). The artificial pulse represents a periodic variation in the impeller speed, with a change of 4000 rpm in 0.35 seconds occurring every 2 seconds. Previous numerical studies have highlighted the importance of the artificial pulse in reducing the low-velocity regions, which may contribute to the low thrombogenicity of the HM3 [1-2]. However, the sudden variation in the speed introduces turbulent flow behavior, which is reflected in the elevated shear stress distribution inside the pump [1]. The aim of this study is to evaluate the impact of the artificial pulse on hemolysis in a hybrid mock circulatory loop.

Methods: We utilized an established hybrid mock circulatory loop [3] to evaluate the blood damage potential of HM3 under three operating conditions: artificial pulse mode, cardiac pulsatile mode, and constant speed mode. The nominal operating point of the HM3 was adjusted to 5600 rpm, and the same targeted mean flow rate of 4.25 L/min in all three conditions. Heparinized bovine blood was utilized for this study, with free hemoglobin (fHb) measured every 30-minutes and the conditions adjusted every 2 hours. Additional to hemolysis, the degradation/fragmentation of high molecular weight (HMW) von Willebrand Factor (vWF) multimers was analyzed for every 2 hours through gel electrophoresis and western blotting.

Results: Overall, six experiments were conducted for the hemolysis assessment with 12 measurements per experiment. The achieved mean flow rate was 4.25 ± 0.007 L/min, and the mean pressure head was 75.3 ± 0.08 mmHg (Figure 1). The calculated delta-free hemoglobin revealed no significant difference between the conditions ($p > 0.74$), with an NIH of 6.1 ± 0.09 mg/100L. The degradation of HMW vWF multimers was analyzed in 4 experiments with 4 samples each. Qualitative results showed a linear degradation in the multimers over a 6-hour period.

Discussion: In this study, we showed that the artificial pulse feature has no significant impact on hemolysis compared with continuous and pulsatile flow conditions in HM3. The similar delta fHb values between the three conditions reflect the relationship between shear stress and exposure time, which was globally similar among the three conditions. In detail, approximately 20% of the blood volume passing through the pump during one artificial pulse (0.5 Hz) was exposed to different levels of shear stresses. The combined effect of the volume of blood exposed to shear stress during low flow, due to the reduction in speed (0.15 s) and high flow, due to the increase in speed (0.2 s), together with the exposure time may balance each other out, resulting in a similar delta fHb comparing to continuous flow. On the other hand, the mean flow rate through the pump remains constant, resulting in no significant difference in the calculated NIH between the three conditions.

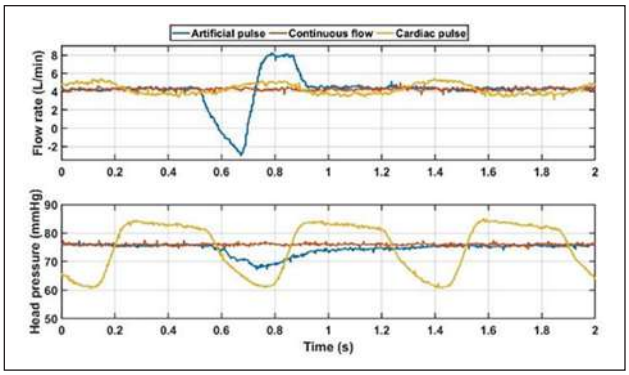

Figure 1. The measured flow rate and pressure head from the hybrid mock circulatory loop for the three operating conditions.

The observation on the vWF multimer showed qualitatively similar behavior in degradation between the conditions; a quantitative analysis is ongoing.

References

1. Wiegmann.L et al, Artif. Organs, 43(4):363-376, 2018
2. Fang.P et al, Front. Cardio Med, 2022
3. Bender.M et al, IEEE. Trans. Biomed Eng, 2023

Acknowledgement

The financial support by the Austrian Federal Ministry of Labour and Economy, the National Foundation for Research, Technology and Development and the Christian Doppler Research Association is gratefully acknowledged.

THE ARTIFICIAL PLACENTA: DEVELOPMENT OF A LUNG AND KIDNEY ASSIST DEVICE FOR CRITICALLY ILL PRETERM NEONATES

Danny van Galen (1), Niels Rochow (2), Ulrich Haag (3), Christoph Fusch (2), Ana Martins Costa (1), Frank Halfwerk (1,4), Jutta Arens (1), on behalf of the ArtPlac Research Consortium (5)

1. Dept. of Biomechanical Engineering, Engineering Organ Support Technologies group, University of Twente, Enschede, the Netherlands; 2. Dept. of Neonatology, Klinikum Nurnberg, Nuremberg, Germany; 3. Getinge, Hechingen, Germany; 4. Dept. of Cardiothoracic Surgery, Thorax Centrum Twente, Medisch Spectrum Twente, Enschede, the Netherlands; 5. HORIZON-EIC-2022-PATHFINDEROPEN-01, Grant agreement ID: 101099596

Introduction: Neonatal mortality declined worldwide in recent years, yet preterm birth is still the leading cause of death among newborns [1]. Many of these cases are caused by immaturity of the lungs, sometimes compounded by kidney failure [2,3].

Currently available therapies including mechanical ventilation, extracorporeal membrane oxygenation (ECMO), and continuous renal replacement therapy (CRRT) do not fully address the needs of extremely preterm infants (>24 weeks gestational age). These technologies are highly invasive, associated with lifelong disability, and require multiple human-machine interfaces that limit family integration [4,5].

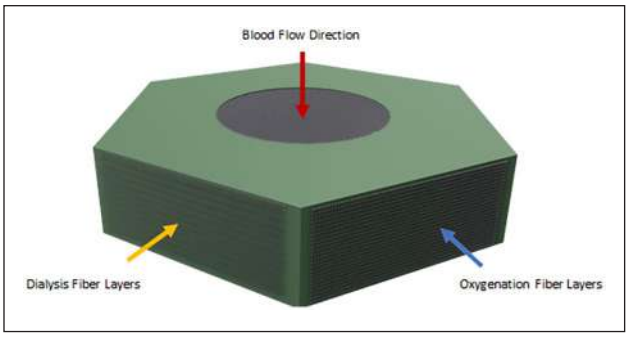

Figure 1. 3D render illustrating the configuration of oxygenation and dialysis hollow fiber mats encapsu-lated in potting material for phase separation of fluids and gas forming a hexagonal membrane bundle design.

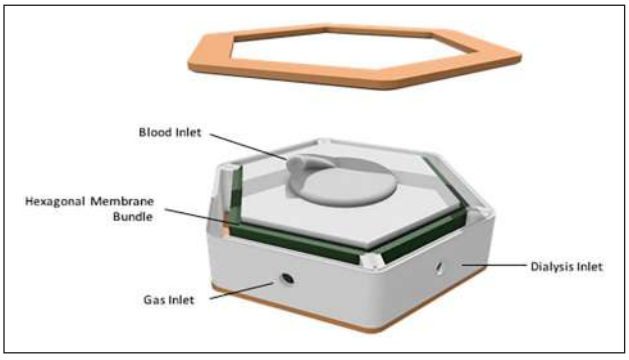

Figure 2. Initial concept design of the combined lung and kidney assist device.

The ArtPlac project aims to develop a combined lung-kidney assist device to prevent lifelong disability through a less invasive, infant-and family-centered approach. This abstract describes an initial ArtPlac design.

Methods: User requirements were defined based on stakeholder analysis and translated into design requirements. Initial concepts for the blood inlet/outlet geometry and device housing were generated and converted into 3D designs.

Results: The device should be connected through the umbilical vessels, eliminating additional vascular access to the neonate. Furthermore, the system should be pumpless and driven solely by the neonate's heart to minimize the risk of hemolysis. To handle three fluids (blood, gas, dialysate), the fiber bundle is designed in a hexagonal shape with a 60° angle between respective layers of oxygenation and dialysis hollow fiber mats (figure 1). To avoid dead water areas in the fiber bundle, potting will be performed in a round fashion in a single production step.

Discussion: Incorporating user requirements, a novel hexagonal membrane design combines oxygenation and dialysis in one housing (figure 2). Upcoming design challenges are to minimize pressure drop and to limit hemodilution by keeping the priming volume as low as possible.

With ArtPlac, we envision a revolutionary treatment approach to improve survival and quality of life in neonatal intensive care.

References

1. Cao et al, JAMA Pediatr, 176 (8):787-796, 2022.
2. David Sharrow et al, Levels & Trends in Child Mortality -Report 2023 -Estimates developed by the United Nations Inter-agency Group for Child Mortality Estimation: 6,2024.

3. Nada et al, Semin Fetal Neonatal Med 22 (2): 90-97, 2017.
4. Stoll et al, JAMA 314 (10): 1039-51, 2015.
5. Amodeo et al, Eur J of Pediatr, 180 (6): 1675-1692, 2021.

Acknowledgements

ArtPlac is supported by Horizon EIC Pathfinder Open 2022.

SELECTIVE REMOVAL OF GLYCATED AND OXIDIZED ALBUMIN BY ADSOPTION: MISSION IMPOSSIBLE?

Jens Hartmann, Claudia Schildböck, Stephan Harm

University for Continuing Education Krems, Austria

Introduction: In addition to its function as a transport protein, albumin has other important tasks that are particularly important for patients undergoing therapeutic apheresis. Albumin not only contributes significantly to colloid osmotic pressure, but is also an important buffer in the event of oxidative stress.

Pathological modifications of albumin can occur in various clinical pictures. These include the reversible oxidation of the Cys-34 position from human mercaptalbumin (HMA) to human non-mercaptalbumin 1 (HNA-1), or non-reversible oxidation to HNA-2. Furthermore, glycation of albumin occurs, particularly in diabetic patients, due to the increased glucose level in the blood. These changes have an impact on the functions of albumin and thus contribute to a worsening of the patient's condition.

Procedures based on adsorption on polystyrene-divinylbenzene (PS-DVB) adsorbents remove a certain amount of albumin as a side effect.

The aim of this study was to investigate whether PS-DVB adsorbents selectively adsorb oxygenated albumin and/or glycated albumin.

Methods: Oxidized albumin was generated by incubation of fresh frozen plasma (FFP) and human serum albumin (HSA) with cystine for 2 days (HNA-1) or with H2O2 for 3 hours (HNA-2) at 37 °C with subsequent dialysis to remove excess cystine.

Glycated albumin was produced by incubation of FFP and HSA with glucose (4.5 g/dL) for 3 weeks and subsequent dialysis to remove excess glucose.

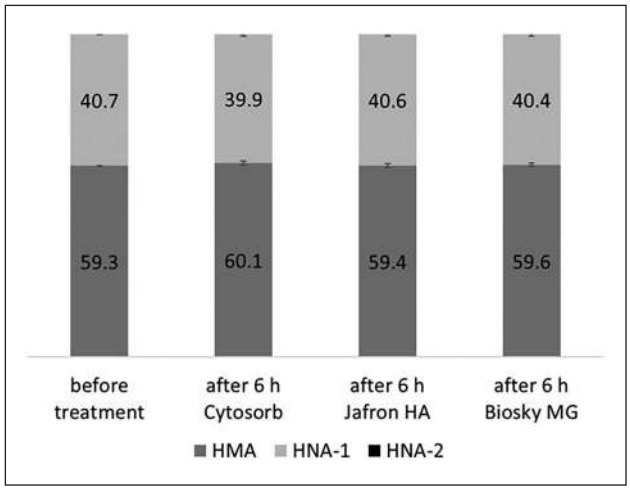

Figure 1. Amount of HMA, HNA-1 and HNA-2 in plasma before and after an 6 hour in-vitro treatment of human plasma. The values are given as a percentage (n=3).

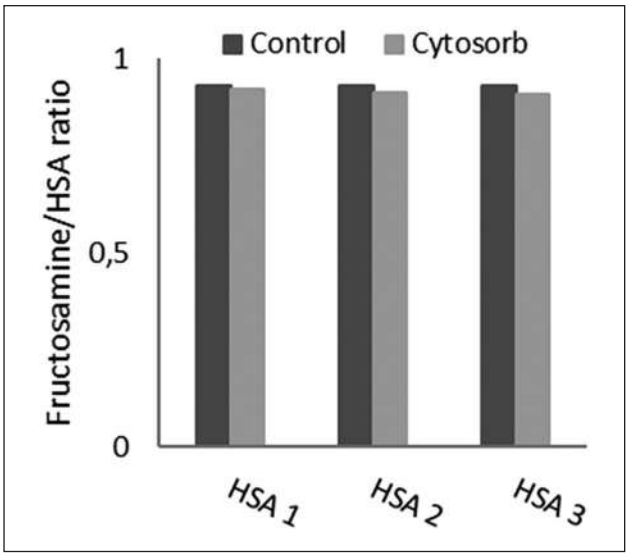

Figure 2. Fructcosamine to HSA ratio after 2 hours incubation with Cytosorb and without adsorbent (control).

The adsorption tests in FFP and HSA were carried out with 10 % v/v PS-DVB adsorbent (Cytosorb, Jafron HA and Biosky MG) for 2 hours at 37 °C (n=3).

The HMA, HNA-1 and HMA-2 were quantified using HPLC according to Imai et al [1]. Glycated albumin was quantified by a photometric fructosamine test kit.

Results: None of the adsorbents tested can selectively remove oxidized or glycated HSA. Furthermore, the adsorbents have no oxidative or reducing effect on HSA.

Discussion: Our results are not consistent with *in-vivo* studies that have demonstrated a transient improvement in the redox status of albumin during treatment [2]. It can be assumed that the elimination of various toxins and the stabilization of the patient in the ICU may lead to an improvement in the redox status of albumin *in vivo*, which is not observed *in vitro*.

The changes in albumin investigated in this study have no influence on the affinity of albumin to hydrophobic neutral resins based on PS-DVB.

References

1. Imai et al., Adv Exerc Sport Physiol, 11(3): 109-113, 2005.
2. Oettl et al, Ther Apher Dial, 13(5):431-436, 2009.

ELECTROSPUN PCL/PEG NANOFIBERS FOR IN VIVO WOUND HEALING STUDY

Katarina Virijević (1,2), Marko Živanović (1), Jelena Pavić (1), Nenad Filipović (2,3)

1. Institute for Information Technologies, University of Kragujevac, Kragujevac, Serbia; 2. BioIRC -Bioengineering Research and Development Center, Kragujevac, Serbia; 3. Faculty of Engineering, University of Kragujevac, Kragujevac, Serbia

Abstract: In this study, we present the electrospun PCL/PEG antibiotic-bea ring scaffolds that exhibit outstanding results in promoting and facili-ita ting *in vivo* wound treatment.

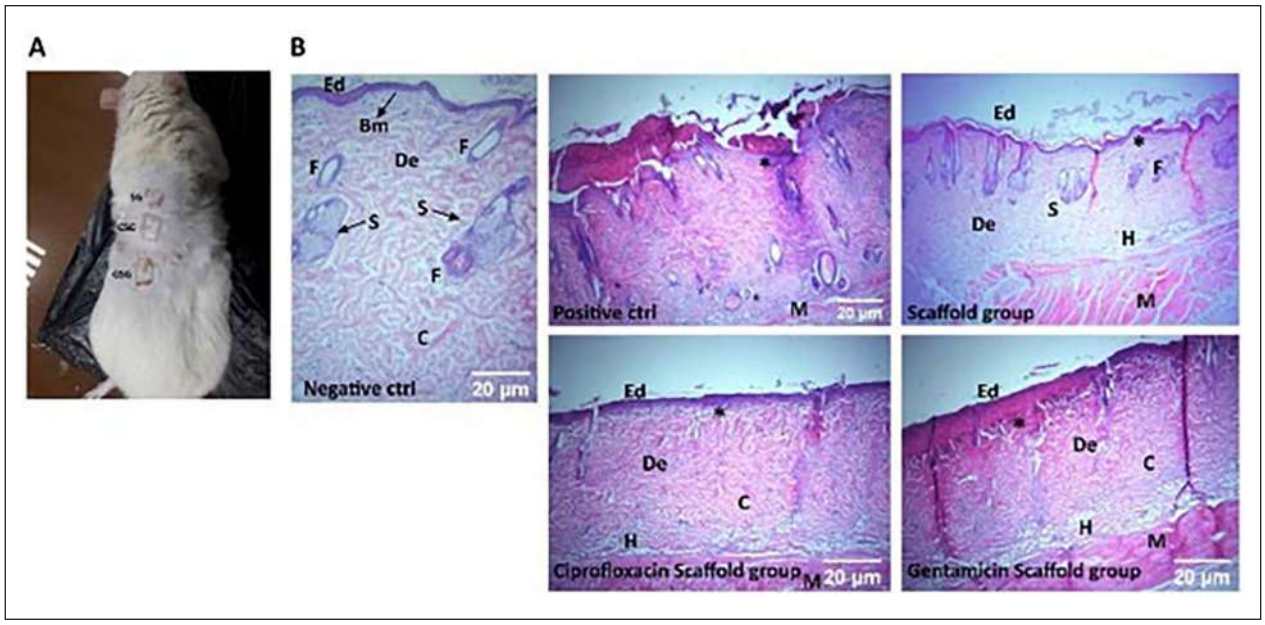

Figure 1. In vivo application of selected scaffold in wound healing process. A) Macroscopic analysis of wound healing in areas treated with scaffold alone compared to treatment with scaffolds loaded with ciprofloxacin or gentamicin. B) Representative images of H&E staining of paraffin-embedded sections of negative, positive control after treatments of the scaffold with incorporated ciprofloxacin and gentamicin (original magnification x40 and x20). SG: Scaffold Group, CSG: Ciprofloxacin Scaffold Group, GSG: Gentamicin Scaffold Group. Ed: epidermis, Bm: Basement membrane, De: dermis, F: hair follicles, S: sebaceous gland, C: collagen fibers, V: blood vessel, H: hypodermis, M: muscle fibers, * burn area.

Introduction: Poly(ε-caprolactone) (PCL) and poly(ethylene glycol) (PEG) polymer scaffolds are garnering increasing attention for their potential applications in *vivo* experiments, particularly in the field of tissue engineering and regenerative medicine.[1,2]

Materials and Methods: Polycaprolactone (PCL) (average Mw ~80,000) and poly(ethylene)glycol (PEG) (average Mw ~4,000). Chloroform (CHCl3) was from Macron Fine Chemica ls, while N,N-dimethylformamide (DMF), Antibiotics ciprofloxacin (CIP), and gentamicin sulfate (GEN) were from Fujian Fukang Pharmaceutical, China. Table 1 presents the chemical composition of the used polymer solution.

Results: In order to investigate the role of the electrospun-derived PCL/PEG antibiotic-bearing scaffolds in the process of wound healing, we conducted an *in vivo* study on male Wistar albino rats. As illustrated in **Figure 1A**, macroscopic evaluation of the wound area revealed accelerated wound closure due to PCL/PEG antibiotic-bearing scaffold treatment compared to scaffold alone treatment in areas of burned skin. Microscopic pictures of healthy skin (before burn), burned skin (after burn), as well as treated skin stained with hematoxylin and eosin were demonstrated in **Figure1B**.

Discussion: The results of wound healing were significantly better in the group treated with PCL/PEG antibiotic-bearing scaffolds, especially in the group treated with ciprofloxacin. Remarkable healing was noted with a decrease in inflammatory cells with an increase in fibroblast proliferation and angiogenesis. A lower number of polymorphonuclear cells and a more organized arrangement of collagen fibers were recorded in the dermis, which is a clear sign of enhanced skin regeneration. Therefore, these results demonstrated that the treatment with ciprofloxacin-bearing scaffolds can significantly promote the wound healing process.

Table 1. The chemical composition of the polymer

Polymer composition	Solvent system	Polymer concentration
PCL: PEG 70:30	CHCL3:DMF 70:30	18%

References

1. Movahedi, M.; Asefnejad, A.; Rafienia, M.; Khorasani, M.
2. T. Potential of Novel Electrospun Core-Shell Structured Polyurethane/Starch (Hyaluronic Acid) Nanofibers for Skin Tissue Engineering: In Vitro and in Vivo Evaluation. *Int J Biol Macromol* **2020**, *146*, 627–637.
3. Wu, T.; Zhang, J.; Wang, Y.; Li, D.; Sun, B.; El-Hamshary, H.; Mo, X. Fabrication and Preliminary Study of a Biomimetic Tri-Layer Tubular Graft Based on Fibers and Fiber Yarns for Vascular Tissue Engineering. *Mater Sci Eng C* **2018**, *82*, 121–129.

Acknowledgments:

The research was funded by the Institute for Information Technologies Kragujevac, University of Kragujevac (451-03-47/2023-01/200378).

PRESSURE SURVEILLANCE IN EXTRACORPOREAL CIRCUITS: RELEVANCE IN HAEMODIALYSIS AND HEMODIAFILTRATION

Gita F. Choirot, Wolfgang Kleinekofort

RheinMain University of Applied Sciences Am Brückweg 26, 65428 Rüsselsheim, Germany

Introduction: Pressure measurement in extracorporeal circuits is established as a standard surveillance technique during blood-based therapies (1). In the last years, pressure measurement based on simple threshold monitoring was replaced by intelligent algorithms that reduce false positive alarm. However, it is helpful to understand on a physical as well as physiological basis that changes in treatment settings lead to different types of pressure changes.

Methods: Detailed analysis of arterial pressure PA, venous pressure PV, dialyzer inlet pressure DIP, and transmembrane pressure TMP during haemodialysis was performed using a patient data base. Main causes of pressure changes were identified, analysed and replicated during simulated hemodialysis therapies with an FMC 6008 haemodialysis device with a patient simulator.

Results: Pressure variations during haemodialysis and hemodiafiltration are mainly the result of changes in blood flow QB, flow resistance R of the extracorporeal circuit and blood viscosity η. Higher blood flow is nonlinear correlated with PA and PV. Fast changes in blood viscosity η are directly related to changes in ultrafiltration setting. Long-term changes in η depend on the individual ability of the patient to refill blood volume from intracellular and extracellular fluid compartments. Isolated increase in DIP is a direct mirror of the flow resistance of the hemodialyzer.

Discussion: Slowly drifting pressure trends can be found in almost every haemodialysis and hemodiafiltration treatment (2). It is important to notice that any variation in extracorporeal pressures originate in both physiological and physical changes. Patient movements lead to symmetrical variations in PA and PV, whereas blood pressure plays only a minor role.

References

1. Polaschegg H.-D. (2010). Venous needle dislodgement: the pitfalls of venous pressure measurement and possible alternatives, a review. Journal of Renal Care 36(1), 41-48.
2. Ficheux, A., Gayrard, N., Szwarc, I., Duranton, F., Vetromile, F., Brunet, P., ... & Argiles, A. (2020). Measuring intradialyser transmembrane and hydrostatic pressures: pitfalls and relevance in haemodialysis and haemodiafiltration. Clinical Kidney Journal, 13(4), 580-586.

SYSTEM LEVEL ANALYSIS OF VENTRICLE ASSIST DEVICES FOR RIGHT VENTRICLE FAILURE

Canberk Yildirim (1), Goksel Guven (2), Osama Soliman (3), Erhan Tenekecioglu (4), Sakir Akin (5), Kadir Caliskan (5), Kerem Pekkan (6)

1. Istanbul Bilgi University, TR; 2. Hacettepe University, TR; 3. University of Galway, IR; 4. University of Health Sciences, TR; 5. Erasmus Medical Center, NL; 6. Koc University, TR

Introduction: Discussing heart failure, the left ventricle (LV) is mainly considered, and the right ventricle (RV) is overlooked. However, the function of this "forgotten ventricle" also plays a crucial role in several disease conditions. These RV failure states are commonly treated via commercially available ventricle assist devices (VADs). Even so, as a major limitation, these VADs are suitable for systemic support with higher pressure and resistance, thus, utilization of LVADs in pulmonary circulation may lead to unphysiological hemodynamics and suction in RV. Therefore, in this study, we aim to *in silico* investigate commercially available LVADs in RV support and then optimize these devices to be more suitable for pulmonary circulation via target hemodynamics. Our previously developed adult lumped parameter model network [1] was modified to simulate four most common RV failure cases: *(1)* pulmonary thromboembolism, *(2)* isolated RV infarction, *(3)* RV failure secondary to LV failure and *(4)* RV failure after LVAD implantation. Heartmate 3 (HM3) was characterized and used as the commercial VAD in this study.

Methods: Euler turbomachinery equation, including friction losses, was used for VAD characterization as follows:

$$Q = \frac{\rho w^2(\sigma r_2^2 - r_1^2) - \Delta P_{th} - \Delta P_{loss}}{\frac{\rho w r_2 \cot\beta_2}{2\pi r_2 b_2 - t z b_2} - \frac{\rho w r_1 \cot\beta_1}{2\pi r_1 b_1 - t z b_1}} \quad (1)$$

where Q is the pump flow rate, ΔPth and ΔPloss are the theoretical pump pressure and losses, respectively. Indices 1 and 2 represent the inlet and outlet of the associated design parameter as shown in Table 1, with the values used for HM3. ΔPloss is the total friction loss of impeller, diffuser, volute and inlet and outlet tubing.

Disease cases were generated via modifying our previously developed healthy adult model's [1] compliances, systemic/pulmonary vascular resistances, and heart rate. In this abstract, results for pump implanted acute state of disease cases *(1)* and *(2)* are demonstrated. Disease cases *(3)* and *(4)* results will be presented during the meeting. Furthermore, chronic state of each disease case is generated via considering cardiovascular system's physiological response to RV failure through a novel optimization-based remodeling framework that aims to conserve the *key health indicator (KHI)* of cardiovascular circulation.

Results: Table 2 shows the *in silico* HM3 implanted (RV to pulmonary artery, rotational speed = 4000 rpm) acute states of disease case *(1)* and disease case *(2)*.

Discussion: Our results showed that a commercially available pump utilization in RV support improves hemodynamics in acute state as expected, despite undesired pulmonary pressure increase. Via tracking the KHI, change in this key hemodynamics will better reflect to generate chronic RV failure state and a more suitable VAD for right side can be designed through hemodynamic target-based optimization of parameters in Table 1. Therefore, our tool numerically investigates the RV failure for the first time in literature as our knowledge, has a potential to contribute to the emergence of more physiological and suitable for right site support devices. These system level studies are crucial towards achieving a dedicated RV support device with optimal physiological response.

Table 1. Inlet (1) and outlet (2) design parameters.

Parameter	HM3
Blade angle – β (1-2)	24° – 35°
Impeller radius – r (1-2)	3.2 – 9.6 mm
Blade width – b	4.6 mm
Blade thickness – t	3 mm
Blade number – z	4

Table 2. P_{AO}: aortic pressure, P_{RV}: RV pressure, P_{PA}: pulmonary pressure, P_{RA}: right atrial pressure. All pressures are in mmHg. CI: cardiac index (l/min/m²)

	Healthy	(1)	(2)	(1)+ HM3	(2)+ HM3
P_{AO}	133/66	84/57	83/57	105/70	106/71
P_{RV}	25/7	58/10	42/10	42/13	35/8
P_{PA}	25/10.5	57/14	45/15	85/17	77/15
CI	3.64	1.8	1.8	2.45	2.5

References

1. Sisli et al, Ann Biomed Eng, 12: 2853-2872, 2023.

Acknowledgements

This work is supported by the European Research Council (ERC) Proof of Concept Grant -BloodTurbine project #966765.

IS THIS THE SUMMIT OF EXTRACORPOREAL GAS EXCHANGE PERFORMANCE?

Foivos L. Mouzakis (1), Ali Kashefi (1), Flutura Hima (2), Khosrow Mottaghy (1), Jan Spillner (2)

1. ECC Lab, Institute of Physiology, Medical Faculty, RWTH Aachen University, Germany; 2. Department of Thoracic Surgery, Medical Faculty, RWTH Aachen University, Germany

Introduction: Modern extracorporeal life support (ECLS) applications often incorporate extracorporeal gas exchange systems that carry out the necessary oxygen and carbon dioxide transfer between blood and gas phases. Customarily, these systems are outfitted with artificial semi-permeable membranes that keep the liquid and gas phases apart, yet without impeding gas exchange between them. This exchange is a mass transfer manifestation that can be neatly exemplified by Equation 1:

$$\dot{Q}_j = K_j \cdot A_m \cdot \Delta p_j (b-g)$$

where, K_j the overall mass transfer coefficient, A_m the effective surface area of the membrane and Δp_j the concentration gradient between blood -gas phase (expressed in partial pressure).

Amplification of one or more of these parameters ought to augment the product and result in enhanced gas exchange performance. Nevertheless, any increase in the membrane's surface area will be accompanied by protracted blood -foreign surface interaction and elevated risk of blood trauma. Likewise, mass transfer coefficient is already optimized, both in terms of material permeability [1,2] and fluid dynamic efficiency (packing density, hydraulic diameter, etc.).

Hence, the sole manipulated variable remaining is the difference in the partial pressure of gas between the two fluid phases. For instance, implementation of pure oxygen (FiO_2 = 1.0) as sweep gas instead of air (FiO_2 = 0.21), will most definitely improve oxygen transfer rate (OTR). Similarly, the concentration of oxygen can be artificially increased by employing a mechanism that constricts the oxygenator's gas outlet, leading to pressure buildup in the oxygenator's gas compartment (see Figure 1).

Methods: This novel approach makes use of modern, purely diffusive membrane materials, and takes advantage of the elevated concentration gradient ensuing from hyperbaric gas supply. An assortment of silicone membrane gas exchangers were tested in vitro as per a modified protocol in pursuance of assessing their gas exchange efficiency under both regular (normo-) and hyperbaric aeration conditions.

Results: The findings point to a stark performance gain when pressurization of the gas compartment is involved; a 40% rise above atmospheric pressure (300 mmHg) elevates oxygen transfer rate (OTR) by nearly 30%. Carbon dioxide transfer rate (CTR) does not benefit as much from this principle, yet it retains a competitive edge when higher gas flow/blood flow ratios are employed. Moreover, implementation of purely diffusive membranes warrants a bubble-free circulation.

Discussion: Further optimization of the introduced method ought to pave the way for in vivo animal trials, which in turn may potentially unveil new realms of gas exchange performance for therapies associated with extracorporeal circulation.

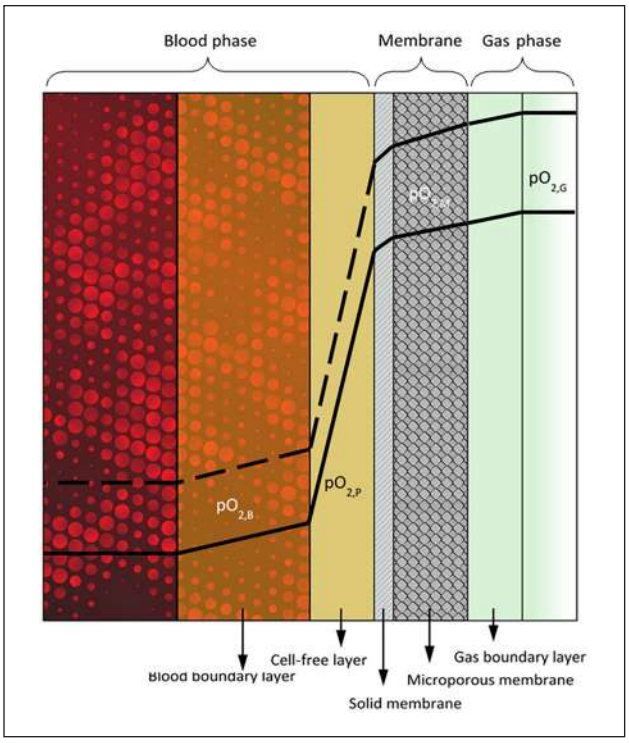

Figure 1. Graphic illustration of the diverse strata spanning between blood and gas phases during extracorporeal membrane gas exchange. Simultaneously, a qualitative representation of the resistance to gas transfer in terms of oxygen partial pressure (pO2). Continuous and dashed lines denote normobaric and hyperbaric gas delivery, respectively.

References

1. Robb, Ann N Y Acad Sci, 146(1):119-37, 1968.
2. Allen et al, J. Membr. Sci. *2*:153-163, 1977.

A METHOD OF PREVENTING BLOOD VOLUME DECREASE DUE TO HIGH GAS FLOW RATE DURING ECMO HEMOCOMPATIBILITY EVALUATION

Wanning Ge(1), Tingting Wu(1), Yuxin Zhu(1), Xianshan Qi(2) , Chia-Hao Hsu(2), Po-Lin Hsu(2)

1. Artificial Organ Technology Lab, School of Mechanical and Electrical Engineering, Soochow University, China;2. magAssist Co., Ltd., China

Introduction: For ECMO development, blood damage shall be evaluated [1]. For registration purpose the system shall be tested by its claimed maximum blood flow rate and maximum gas flow rate per ISO 7199 standard. However, the required high gas flow would induce reduced blood loop volume during the hemocompatibility tests. Blood volume is one of the parameters used for MIH or NIH calculation. According to the authors' experience after one of the 6-hour hemocompatibility tests, the blood volume of the loop reduced from 700mL to 400mL, hematocrit increased from 38% to 45%, and the humidity of the oxygenator gas outlet increased from 16%HR to 90%HR. Blood volume measurement per some timeframe during the

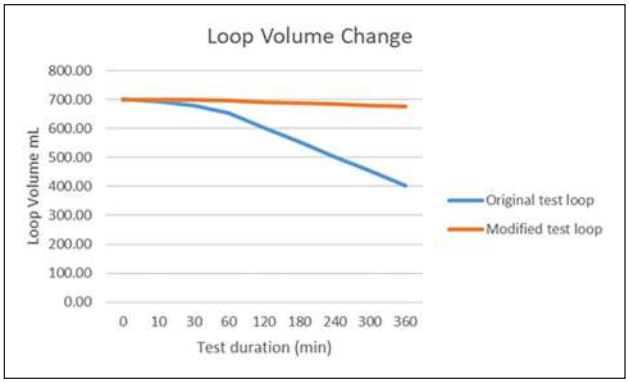

Figure 1. Loop blood volume change over test duration

tests is manageable, but it's always better if the blood volume can be kept constant. This study proposed a test method while minimizing blood volume change due to the high sweep gas flow rate.

Methods: The head-to-head comparison was conducted with 2 sets of test samples. Before the gas inlet, a warm(37°C） water-filled gas washing bottle was added to one of the test samples. So that the gas swept into the oxygenator was with high humidity. All blood loops were kept with the same blood volume (700mL per loop), and the same operating condition(7L/min blood flow rate,14L/min gas flow rate, 150mmHg oxygenator backpressure), and blood was prepared per ISO 7199 standard. The study was performed for 6 hours. The blood bag was merged into a big beaker filled with water. The water height level was then marked. The blood volume loss was measured by the volume of water added to maintain the water height level.

Results: It is shown in Figure 1 that the blood volume decrease of the original test loop was about 15 times of the modified test loop. The blood volume was reduced by 50ml/h and 4ml/h for the pure gas loop, and warm moistened gas loop respectively. The blood volume change may be due to the humidity and temperature difference between the gas and blood, which may cause the water exchange through the membrane.

Discussion: This study investigated the difference in sweep gas humidity influence on the blood volume while evaluating ECMO system hemocompatibility. The study was a feasibility study. The relationship between the sweep gas humidity, temperature, and blood volume change would need further quantified investigation. The influence of humid gas on hemocompatibility results should be further evaluated with quantified gas humidity.

Conclusion: The experiments indicated that the humidity and temperature of the sweep gas will influence blood volume change during ECMO hemolysis tests. Applying warm, humid sweep gas during ECMO clinical use might help maintain the patient's fluid balance.

Reference

1. Chan CHH et al, Membranes (Basel), 1(5):313, 2021.

ADMINISTRATION OF MOLECULAR HYDROGEN IN EXTRACORPOREAL CIRCULATION AND ITS IMPACT. AN IN VITRO STUDY

Foivos L. Mouzakis (1), Ayla Al wafai (2), Flutura Hima (2), Ali Kashefi (1), Johannes Greven (2), Lothar Rink (3), Emiel P.C. van der Vorst (4-7), Joachim Jankowski (4,5,8), Khosrow Mottaghy (1), Jan Spillner (2)

1. ECC Lab, Institute of Physiology, Medical Faculty, RWTH Aachen University, Germany; 2. Department of Thoracic Surgery, Medical Faculty, RWTH Aachen University, Germany; 3. Institute of Immunology, Medical Faculty, RWTH Aachen University, Germany; 4. Institute for Molecular Cardiovascular Research (IMCAR), RWTH Aachen University, Germany; 5. Aachen-Maastricht Institute for CardioRenal Disease (AMICARE), RWTH Aachen University, Germany; 6. Interdisciplinary Center for Clinical Research (IZKF), RWTH Aachen University; 7. Institute for Cardiovascular Prevention (IPEK), Ludwig-Maximilians-Universität München, Germany; 8. Department of Pathology, Cardiovascular Research Institute Maastricht (CARIM), University of Maastricht, The Netherlands

Introduction: Extracorporeal circulation (ECC) is frequently implemented in a vast array of modalities such as hemodialysis, cardiopulmonary bypass, extracorporeal membrane oxygenation (ECMO) etc. Patients receiving any such therapy are frequently encumbered with chronic inflammation, which is inherently accompanied by oxidative stress [1]. ECC treatments themselves though are also responsible for sustaining or promoting inflammation [2]. On these grounds, a study has been designed, aiming at investigating the oxidative and inflammatory stress triggered by ECC and by pathogens, and at assessing the therapeutic potential of molecular hydrogen (H2).

Methods: Five identical experimental circuits have been assembled consisting of a roller pump, a collapsible reservoir and tubing. On top of these components, three of these systems additionally encompassed a miniature gas exchanger module facilitating the delivery of a gaseous admixture containing O_2-CO_2-N_2 (only one of them received additionally ca. 7.5 % H_2). All systems were primed with fully heparinized blood from healthy adult donors, whereas a small amount was maintained for the duration of the experiment (6 h) as negative control. A lipopolysaccharide (LPS) solution (250 ng/ml) was infused into two of the circuits, one of them being the gas-flushed, in order to trigger an inflammatory reaction. Blood samples drawn at the beginning and at the end of each experimental session (n=7) realized the assessment of specific biomarkers. These have been settled upon, based on their pertinence and their recurring surfacing in relevant literature [3,4]. Myeloperoxidase (MPO), thioredoxin-1 (TRX-1), monocyte chemoattractant protein-1 (MCP-1, and malondialdehyde (MDA) are often related to oxidative stress, whereas interleukin 6 (IL-6) is a prime indicator of inflammation.

Results: Preliminary results reveal a similar trend between the analysed biomarkers indicating a progressive oxidative and inflammatory response between the 6 systems. Circulation has definitely triggered inflammation and blood trauma, but the staggering influence of LPS in this outcome is indisputable. Accordingly, hydrogen's remedial potential becomes immediately apparent in view of the consistently lower biomarker concentrations in the H_2-handled circuit.

Discussion: Having established the feasibility of in vitro gas exchange investigations with hydrogen, this study nears to conclusion, but not before setting distinct objectives for future research. The dosage, the duration, and the pattern of hydrogen administration ought to be further investigated, in order to ascertain the optimal protocol for patient treatment. Once in vivo trials are approved, the protocol can be further tailored to the specific disorder being handled.

References

1. Himmelfarb et al, Kidney International, 62(5):1524–1538, 2002.
2. Nakayama et al, Ren Replace Ther, 2(23), 2016.
3. Satta et al, Ren Replace Ther, 7(37), 2021.
4. Nakayama et al, Nephrol Dial Transplant, 25:3026–3033, 2010.

Acknowledgements

The authors would like to express their gratitude towards Qun Zhao for his contribution to data acquisition and analysis.

ANATOMY AND PHYSIOLOGY BASED MOCK LOOP FOR CARDIAC IMPLANT DEVELOPMENT

Isabell Schulz (1,2), Vera Froese (1,2), Michael Lommel (1,2) Ulrich Kertzscher (1,2), Tim Bierewirtz (1,2)

1 Deutsches Herzzentrum der Charité, Institute of Computer-assisted Cardiovascular Medicine, Biofluid Mechanics Laboratory, Augustenburger Platz 1, 13353 Berlin, Germany.
2 Charité – Universitätsmedizin Berlin, corporate member of Freie Universität Berlin and Humboldt Universität zu Berlin, Charitéplatz 1, 10117 Berlin, Germany.

Introduction: The integration of biological organs into *in vitro* mock loops is essential to simulate the operating conditions of medical devices under realistic testing conditions in the development phase which usually requires animal testing. A multifunctional mock loop connected to a porcine heart has been developed to mimic the natural movement of the heart. The current focus of this test bench is on the anchoring of pacemaker electrodes. The current focus of this mock loop is to support the development of cardiac electrodes.

Methods: The operating principle of the *in vitro* mock loop is to drive the movement of the ventricular walls throughout the cardiac cycle, mimicking the pulsatile pumping function of the heart. To achieve this, the system is able to pressurize the ventricles while excluding the atria from external loads. The system consists of a fluid-filled chamber that houses the ventricles and is sealed to isolate the atria from external stress loads. The heart is held in place by two thermally molded polyurethane foils supported by radially shiftable pins pointing towards the coronary sulcus. The thermoformability of the foils allows the mock loop to handle the high variability of the hearts. In between those foils a vacuum is generated. The chamber is connected a computer-controlled piston pump that cyclically injects and withdraws fluid in and out of the chamber, hence directly actuating the ventricular walls. The atriae and the large arteries are connected to the two circuits (cardiac and pulmonary circulation) with silicone tubes and 3D printed connectors. Each circuit consists of an open and a closed reservoir, a pressure sensor, a flow sensor, and a resistor. The current state of the test bench is shown in Figure 1.

Figure 1. Mock loop for the development of cardiac implants using a slaughterhouse porcine heart, showing the heart housed in the fluid-filled chamber.

Results: An initial pilot experiment was conducted to demonstrate the functionality of the mock loop. A representative example of the pressure and flow measured in the mock loop was recorded, which was consistent with typical systemic in vivo waveforms. It was possible to generate pressure and flow conditions corresponding to the diastole and systole of the beating human heart.

Discussion: From a technical point of view, the main challenge of the approach is to seal the pressurized fluid chamber around the coronary sulcus and to fix the heart within the mock loop In this regard, the design of two thermally molded vacuum sealing foils together with shiftable pins allowed a simple, efficient and reliable sealing and mounting of the heart, allowing physiological ventricular stroke volumes. Together with the hydraulic modules used in the mock loop this results in the achievement of appropriate hemodynamic conditions in the setup. Further improvements to the mock loop are required and will be implemented in the coming months.

Acknowledgements

This project is co-financed by the European Regional Development Fund (ERDF).

FROM LAB TO LARGE SCALE: MIXED MATRIX MEMBRANES FOR PROTEIN-BOUND UREMIC TOXIN REMOVAL

Marc Torrents Yeste [1], O.E.M ter Beek [1], Dimitrios Stamatialis [1]

1Advanced Organ bioengineering and Therapeutics, Faculty of Science and Technology, TechMed Center, University of Twente, The Netherlands

Introduction: Hemodialysis is nowadays the most used therapy for treating End-Stage Renal Disease (ESRD) patients, due to the low availability of transplant organs, which are the best option [1]. However, this treatment presents some drawbacks, it is non-continuous (3 times a week for 4 hours each session) [1,2]. Moreover, commercial filters show a poor capability on removing Protein-Bound Uremic Toxins (PBUTs) such as Indoxyl sulfate (IS) and Hippuric acid (HA). This results in an accumulation of these toxins which is associated to the high mortality rate of ESRD patients [3]. To achieve a better removal of PBUTs, a different type of dialyzer should be used. Our previous studies showed that the application so called Mixed Matrix Membranes (MMM) which combines filtration and adsorption [4] can provide improved the removal of these toxins]. This study highlights the production and testing of MMM with human plasma and full human blood and the route to upscaling their production. The latter could enhance the application of these MMMs into clinical practice.

Methods: Different polymer ratios of membrane forming polymers Polyethersulfone (PES) / Polyvinylpirrolidone(PVP) and spinning settings were used.

The dual layer MMM was fabricated by extruding polymer dope solutions (PVP / PES) – particle free and particle based – through a spinneret into a coagulation bath with a non-solvent (water). There, the fibers solidify by immersion precipitation and washed for 3 days to remove the solvent (NMP). Afterwards, the fibers are stretched and dried at room temperature.

Table 1. Polymer ratios of MMM dope solutions. *60 wt% of the polymer weight. For 10g of PES and PVP, 6g of ACP were added.

Layer	PVP wt%	PES wt%	NMP wt%	ACP wt%
Inner	5	17	78	-
Outer	1,4	14	84,6	*60

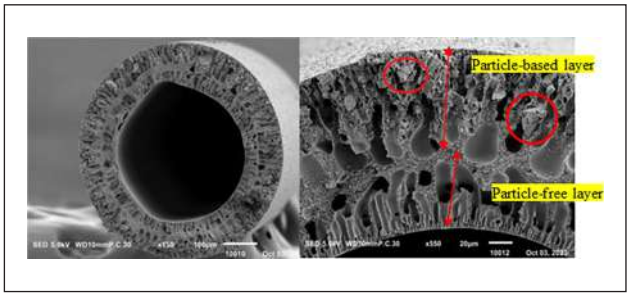

Figure 1. SEM images of the produced MMM. Left magnification x150, Right: magnification x550.

Table 2. PBUTs removal from human plasma and full human blood comparison between MMM and FX1000 in-house laboratory-scale filters.

	Fibers used	IS [mg·m^{-2}]	HA [mg·m^{-2}]
Human Plasma	FX1000	377 ± 91[4]	2674 ± 564[4]
	MMM	500 ± 176[4]	2478 ± 361[4]
Full human blood	FX1000		
	MMM	1471 ± 364	3060 ± 480

Laboratory scale mini dialyzers were used to test the PBUTs removal capacity of MMM compared to fibers of commercial dialyzers.

Results and Discussion: Figure 1 presents SEM images of the cross-section of the MMM showing the dual-layered structure and the presence of AC. They have ultrafiltration coefficient (Kuf) of 23 ± 5 mL/(m^2·h·mmHg), within the range of high-flux commercial filters, such as Fresenius FX1000. However, their inner diameter is almost 100% larger.

Table 2 compares the PBUT removal of the MMM to FX1000. The removal by the MMM was mainly due to adsorption.

References

1. Stamatialis, Dimitrios, ed. Biomedical membranes and (bio) artificial organs. Vol. 2. World Scientific, 2017
2. Ter Beek, Odyl, et al. Separation and Purification Technology 225 (2019): 60-73
3. Pavlenko, Denys, et al. Scientific reports (2016)
4. Kim, DooLi, et al. Journal of Membrane Science 609 (2020)

Acknowledgements

This work is part of the project Biomed04 'Artificial Organs'. This project receives a Growth Fund contribution from the program NXTGEN HIGHTECH.

EXPLORING THE DEVELOPMENT OF A WIRELESS IMPLANTABLE PULSATILE MECHANICAL VENTRICULAR DEVICE

Chengwei Yan, TianYuan Sun, Lian Gan, Khir W Ashraf

Department of Engineering, Durham University, United Kingdom

Introduction: Prolonged use of continuous flow left ventricular assist device (LVAD) may lead to complications related to diminished pulsatility, reducing the chance of heart rehabilitation, increasing the incidence of aortic valve insufficiency and aortic adhesions, raising the risk of bleeding, and increasing the incidence of right heart failure [1]. First-generation LVAD, the use of gas-driven pulsatile flow resulted in large device volumes, making them susceptible to infections (HeartMate XVE) and mechanical failures (LionHeart), leading to their obsolescence. Currently, magnetically levitated LVAD, primarily HeartMate III, achieve pulsatile pumping by altering the rotor speed. However, intraoperative bleeding and postoperative gastric bleeding remain potential threats to patient safety. Moreover, the secondary flow channels generated between the continuous-flow rotor and the housing can lead to intra-pump thrombosis, which was a major reason for the discontinuation of the HeartWare HVAD by Medtronic. Currently, the only pulsatile-flow device available with FDA approval is the Berlin Heart-Excor, which is primarily indicated for pediatric use.. Therefore, the aim of this work is to introduce a novel VAD that, while generating pulsatile flow, has a smaller footprint and can be driven wirelessly.

Methodology: The proposed device involves a flexible diaphragm the incompases magnets which are being pulled and pushed towards the base and top of the pumping chamber using electromagnetic elements (Fig 1). This experiment uses the FengXing Serial Testing machine as the experimental equipment. We used 3D printed molds to fix the number

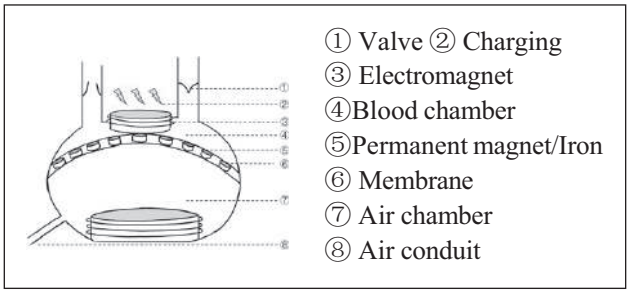

Figure 1. Working principle.

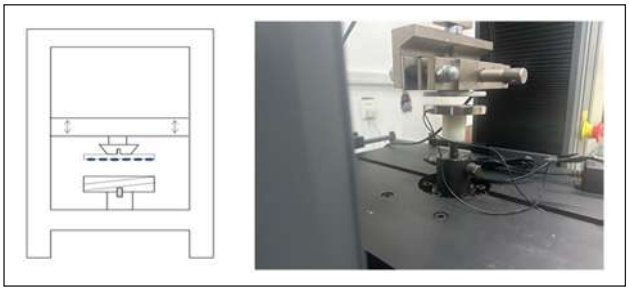

Figure 2. Schematic Diagram (Left) and Physical Representation (Right). By adjusting the size of the electromagnet below and the number and arrangement of permanent magnets above to explore the optimal dimensions and quantities of both electromagnets and permanent magnets.

of permanent magnets and varied the size of Kakcom electromagnets for conducting tension tests. Experimental curves are analyzed to explore the optimal operating scheme for magnet rotation within the constraints of implantation in the abdominal cavity.

$$F_{magnetic\ attraction} = P_{Aortic\ pressure} \times A_{cross\text{-}sectional\ area} + G_{blood+magnet}$$

Results: Maintaining the voltage at 12V and ensuring that the height of the electromagnet does not exceed 10mm, a single electromagnet interacting with one layer (comprising 8 permanent magnets) can meet the requirement of 5.5N force.

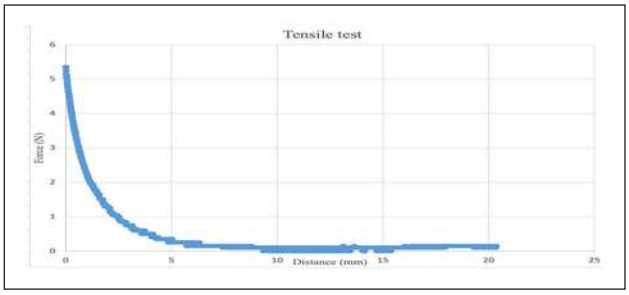

Figure 3. Force-Distance curve. At distance 10mm the magnetic system does not generate any force.

Discussion and Conclusions: The proposed design provides a novel approach for a wireless pulsatile pump, utilizing an electro-magnetic arrangement. Altering the internal structure of electromagnets and adjusting the arrangement and number of permanent magnets, greater electromagnetic force can be achieved. The initial results pave the way for realizing a compact pulsatile-flow VAD, and warrant further investigations towards the control, pulsatility power and hemolysis aspects.

Reference

1. Wu T, Khir A W, Kütting M, et al. A review of implantable pulsatile blood pumps: Engineering perspectives[J]. The International Journal of Artificial Organs, 2020, 43(9): 559-569.

AUTOMATED TEST BENCH FOR CATETHER-BASED ELECTRICAL IMPEDANCE MEASUREMENTS OF BLOOD

Daniel Voss, Steffen Leonhardt, Marian Walter

Chair for Medical Information Technology, RWTH Aachen University, Germany

Introduction: Electrical bioimpedance techniques play a crucial role in clinical diagnostics, providing insight into diverse health parameters [1]. A precise characterization of blood is for example required for the advancement of impedance-based left ventricular volume estimation methods [2]. The available literature on blood properties is, however, sparse, as settling effects at rest and orientation changes during flow complicate the measurements. In particular, systematic measurements with an electrode catheter which is applicable in a clinical setting are missing.

Methods: We have developed an automated test bench, which is capable of measuring blood impedance while being able to manipulate flow and temperature. This test bench comprises of three component groups:

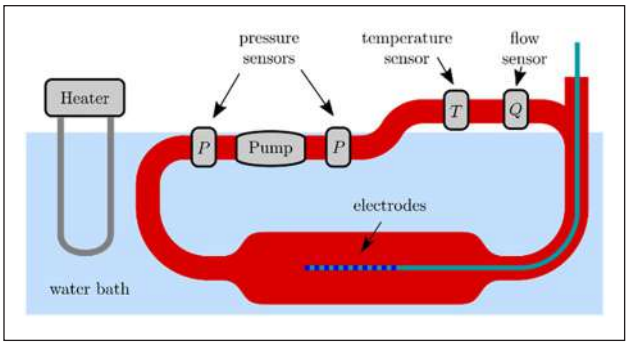

Figure 1. Schematic drawing of the test bench.

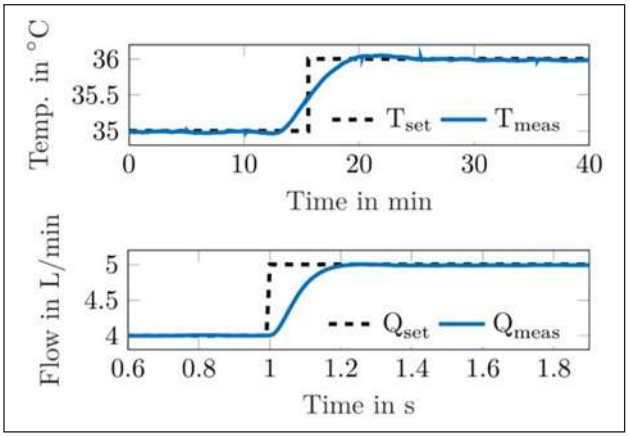

Figure 2. Step response for a temperature reference step (top) and for a flow reference step (bottom).

The test bench hardware; signal processing and control; and the measurement instrumentation.

The hardware consists of a hemocompatible blood loop with pump and sensors, and the water bath with a heater (incl. internal temperature sensor), in which the blood loop is partially submerged (Fig. 1).

The blood loop consists of 1/2" PVC tubing and an enlarged measurement region with a diameter of 32 mm. Two pressure sensors, a NTC temperature sensor in the blood stream and a flow sensor are used to measure the operation conditions. The system is actuated by a left ventricular assist device to regulate the blood flow and a heater in the water bath to control the temperature.

Signal processing and control are performed on a real-time PC (Microautobox II, dSpace, Paderborn, Germany). For the hydraulic subsystem the state is determined by a Kalman filter designed with a pump model and a time-varying hydraulic load model, which is estimated online for better robustness against setup changes. This state is then used by a linear quadratic regulator to control the pump. The temperature control is performed by a model predictive controller which

uses a thermal system model derived from first principles and parametrized by system identification.

The final component group of the test bench is the impedance measurement instrumentation. We use a multi-channel impedance analyzer (ISX-3, Sciospec, Bennewitz, Germany) connected to a commercial 7F, 10 electrode diagnostic catheter via a custom made adapter. With this setup, one can freely select the electrodes for the measurement, thus

enabling 2, 3 and 4 electrode measurements as well as investigations of the effects of electrode spacing on the measurements.

Results: The test bench is capable of controlling the temperature in the blood loop to 0.04 °C from 4 °C above room temperature up to 41 °C. The flow is within 0.1 L/min for steady-state set-point. The transient response to step input changes is shown in Fig. 2.

The step responses show a rise time of 80 ms for the flow and a rise time of 10 min for the temperature.

Discussion: A hemocompatible test bench has been designed to measure the electrical properties of flowing blood with a diagnostic catheter. The test bench has closed-loop control for flow and temperature with high performance and thus facilitates fast automated data acquisition.

Reference

1. Martinsen and Heiskanen, Bioimpedance and Bioelctricity Basics, Elsevier, 2023.
2. Baan et al., Circulation 70, No. 5, 812-823,1984

Acknowledgements

This research was funded by the German Research Foundation, grant no. 452009371, LE 817/44-1.

HEMODYNAMIC LONGITUDINAL ANALYSIS OF THE EFFICACY OF THE CONTOUR NEUROVASCULAR SYSTEM BASED ON IN VIVO DATA

Jana Korte (1, 2), Franziska Gaidzik (1, 2), Lena Spitz (2, 3), Daniel Behme (2, 4), Mariya Pravdivtseva (5), Naomi Larsen (5), Philipp Berg (2,6)

1. Department of Fluid Dynamics and Technical Flows, University of Magdeburg, Germany; 2. Research Campus STIMULATE, University of Magdeburg, Germany; 3. Department of Simulation and Graphics, University of Magdeburg, Germany; 4. University Hospital Magdeburg, University of Magdeburg, Germany; 5. University Hospital Kiel, University of Kiel, Germany; 6. Department of Medical Engineering, University of Magdeburg, Germany

Introduction: Intracranial aneurysms (IAs) are dilatations of the neurovascular system which occur in 3% of the western population [1]. IAs carry the risk of rupture, which can lead to fatal consequences like stroke. Different shapes of IAs exist, which can be differently treated to prevent IA rupture. For example, side wall aneurysms can be treated with flow diverting stents [2]. Wide necked bifurcation aneurysms (WNBA) can be treated with the novel Contour Neurovascular System (Contour) [3]. In this study, the effect of the Contour is analyzed numerically using computational fluid dynamics (CFD). CFD simulations are based on patient specific in vivo data of WBNAs and the placed Contour. Post treatment data exists in different temporal ranges after placement, which allows for the longitudinal analysis of the effectiveness.

Methods: Thirteen WBNA cases, all treated with a Contour, were considered in this study. In vivo data was captured with digital subtraction angiography and computed tomography in varying quantity and temporal ranges (ranging from 1 month to 3 years and 2 to 5 post-images per case) after placement for each case. Medical images were segmented and prepared for simulations, respectively. The exact shape and placement of the Contour could be captured, nevertheless artifacts led to non-usable data. Thus, original Contour computer-aided design files were placed and shaped as seen in the in vivo data [3]. Moreover, due to low flow of contrast agent into the IA head, post-treatment data did not reveal the IA head shape. The pre-treatment IA head was hence stitched onto the post treatment vessel. For each case, pre-and post-treatment CFD simulations were performed using the solver Star CCM+ with laminar flow conditions. Blood was modeled with the Carreau-Yasuda Model and a constant density of 1055kg/m³. Morphological changes of the IA ostium were analyzed in an associated study and compared with the hemodynamic effects of the Contour onto intra-aneurysmal flow.

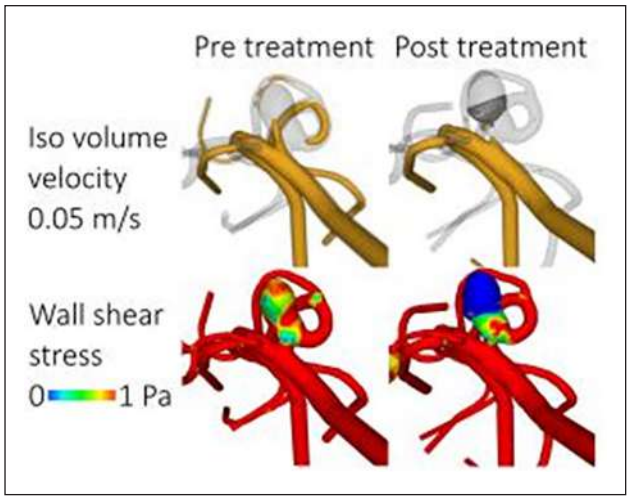

Figure 1. Exemplarily visualization of the velocity iso volume and wall shear stress pre-and post-treatment for one case.

Results: Hemodynamic flow parameters like velocity and kinetic energy show reduction after placement of the Contour, when compared to the pre-treatment state for each case.

Additionally, wall shear stress and oscillatory shear index were reduced after treatment. Looking at the longitudinal change, parameters stay low over time.

Discussion: The reduction of hemodynamic parameters shows the efficacy of the Contour in long term and based on in vivo data. Hemodynamic reduction was up to now only demonstrated in vitro [3, 4]. Compared to other devices like flow diverting stents, the Contour gives the advantage of not occluding small vessels close to the IA [2]. The longitudinal analysis is important to analyze the long-term effect, which was not evaluated in recent research yet due to the novelty of the device. Morphological and hemodynamic results show that there is no reverse effect of the Contour in the long term and that its efficacy can be demonstrated. Limitation of this study are the non-visible and thus stitched IA head of the post-treatment data as well as the manual adjustment of the Contour placement, which can lead to differences from the real placement.

References

1. Wiebers et al, Lancet, 362:103–10, 2003.
2. Briganti et al, Neuroradiol J, 28:365–75, 2015.
3. Korte, Gaidzik et al, JNIS, 10.1136, 2023.
4. Pravdivtseva et al, Interv Neuroradiol, 10.117, 2023.

Acknowledgements

This work was supported by the German Research Foundation within the SPP 2311 (grant no. 465189657) and the German Federal Ministry of Education and Research within the Research Campus STIMULATE (grant no. 13GW0473A).

EMERGENCY RECONSTRUCTION OF THE SYSTEMIC CIRCULATION AFTER THE CHEST INJURY WITH TERRORISM OF THE GUNSHOT

Tomoyuki Yambe (1), Yasuyuki Shiraishi (1), Francis Chikweto (1), Kenichiro Yambe (2), Toshihiko Kijima(3)

1. Tohoku University, Japan; 2. Tohoku Medical and Pharmaceutical University, Japan; 3. C&T Medical Labo, Japan

Introduction: In Japan, very shoking news was reported that the former prime minister had been dead with heart injury with gunshot of a terrorist. Japan had been called as the sefety country because the gun was strictly limited. However, the hand made gun was shooted near the former minister. Only 25 cases was reported in the research papers in Japan, so, almost hospitals did not have the experiences of the gunshot cases. If the emergency open chest surgery and open heart massage with emergency use assist circulation system, there will be possibility to have a small chance of recover. This challenging theme was the aim of this study.

Material and methods: As soon as possible, systemic circulation must be started even in the situation of the chast injury with gunshot. However, cardiopulmonary resuscitation will not be possible wspecially in the situation of the massive bleeding. Stop of the bleeding will be most important issue, so, open chest surgery will be needed. If we will open the chest within the one minute, diirect open cheat cardiac massage will be possible.

If the open chest surgery through fifth intercostal space will able to be realized, direct massage will covered the heart and bleeding from heart may be able to be covered by the palm. Massive blood transfusion will be required and surgical team must be gathered.

One team inserted the blood transfusion line and one team must perform intubation, and another team must inserted catheter into the femoral artery and vein.

Yes, we can inserted the inflow cannulae directly into the left ventricle during cardiac massage, so, we can carry out the left heart bypass assist circulation or construct extracorporeal menmrane oxygenater (ECMO) system.

In this study, direct puncture system into the left ventricle with dilater through the puncture wire was developed and figure showed the open chest cavity and model heart with cardiac massage and cover the wound of the heart injury the puncture system.

Figure 1. As soon as possible, open chest surgery will be needed and direct cardiac massage will be able to be embodied.

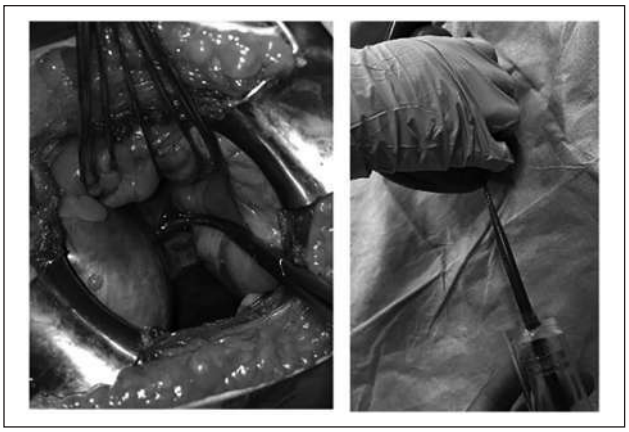

Figure 2. The open chest cavity, and model heart with cardiac massage and covering the wound of the heart with palm, and newly developed puncture system.

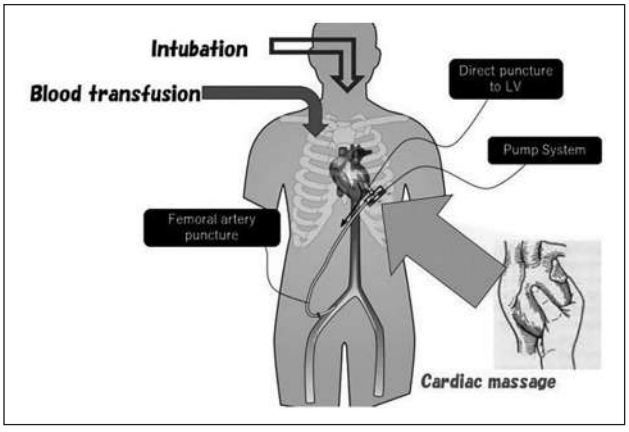

Figure 3. Direct puncture LV assist system during the covering the wound of the heart by palm.

Results: By the use of the healthy adult goats, animal experiments was performed and satisfactory hemodynamic derivatives, pump output was obtained

Discussion: In the emergency case of the gunshot to the heart, direct massage will covered the heart and bleeding from heart may be able to be covered by the palm. One team inserted the blood transfusion line and one team must perform intubation, and another team must inserted catheter into the femoral artery and vein.

Yes, it may be possible to help patient after gunshot in near future.

BRIDGING THE KNOWLEDGE GAP BETWEEN SCIENTIFIC DISCOVERY AND CLINICAL APPLICATION: A CRUCIAL STEP FOR EFFECTIVE HEALTHCARE

Gerd Klinkmann (1,2,3), Steffen Mitzner (2,4), Joerg Vienken (5)

1. Department of Anaesthesiology, Intensive Care Medicine and Pain Therapy, University Medical Center Rostock, Germany; 2. Fraunhofer Institute for Cell Therapy and Immunology, Department of Extracorporeal Therapy Systems, Germany; 3. International Renal

Research Institute of Vicenza (IRRIV), Italy; 4. Division of Nephrology, Department of Internal Medicine, University Medical Center Rostock, Germany; 5. MedTech Consultants, Germany

Introduction: Albumin finds widespread application in critical care and various conditions to augment plasma volume, replace losses, and restore serum albumin levels in hypoalbuminemic states [1-3]. This utility stems from the prevailing notion that albumin's oncotic pressure effects outweigh other biological, physiological, or clinical considerations. However, as a naturally occurring protein, albumin possesses additional vital biological properties beyond its oncotic and volume-expanding effects [4]. Recognizing these effects is crucial for clinicians to grasp the full scope of human albumin solution therapy's potential impacts.

Findings: The Saline vs. Albumin Fluid Evaluation (SAFE) study has shown that the use of albumin as an infusion solution in the field of volume therapy is safe almost everywhere, with the exception of hypooncotic albumin in craniocerebral trauma [5]. While there are clear indications for patients with liver cirrhosis, there is still a lack of large-scale studies for other areas of application that could unequivocally demonstrate a clinically relevant advantage beyond hemodynamic efficacy. In large-volume paracentesis, spontaneous bacterial peritonitis and hepatorenal syndrome, the use of albumin is clearly recommended and established in randomized controlled trials due to its clinical benefit. The use of albumin can be considered in septic shock [6,7]. For many applications in volume therapy, albumin can be used above all when other measures for hemodynamic stabilization have already been exhausted, both in hypovolemia and in conservative volume management. The question of whether the correction of pronounced hypoalbuminemia by administering exogenous albumin improves the poorer outcome is also the subject of ongoing studies. In the future, considering the functional properties of albumin beyond solely focusing on its concentration could have profound implications for clinical practice, shaping both diagnostic and therapeutic strategies, as we advance towards more personalized therapy.

Conclusion: The biological effects of albumin in critical illness are not fully understood, yet they may extend beyond its role as an intravenous fluid. In this keynote lecture (Albunet Symposium), the evidence regarding albumin's biological and physiological impacts beyond its function in plasma volume expansion, and examine potential mechanistic effects of albumin as a disease modifier in critically ill patients will be outlined.

References

1. Caironi P, Gattinoni L. The clinical use of albumin: the point of view of a specialist in intensive care. Blood Transfus 2009; 7: 259-67.
2. Vincent JL, et al. Albumin administration in the acutely ill: what is new and where next? Crit Care 2014; 18: 231. Erratum in: Crit Care 2014; 18: 630.
3. Garcovich M, et al. Clinical use of albumin in hepatology. Blood Transfus 2009; 7: 268-77.
4. Adamson RH, et al. Albumin modulates S1P delivery from red blood cells in perfused microvessels: mechanism of the protein effect. Am J Physiol Heart Circ Physiol 2014; 306: H1011-7.
5. Finfer S, et al. SAFE Study Investigators. A comparison of albumin and saline for fluid resuscitation in the intensive care unit. N Engl J Med. 2004 May 27;350(22):2247-56
6. Caironi P, ALBIOS Study Investigators. Albumin replacement in patients with severe sepsis or septic shock. N Engl J Med. 2014 Apr 10;370(15):1412-21.
7. Evans L, et al. Surviving Sepsis Campaign: International Guidelines for the Management of Sepsis and Septic Shock 2021. Crit Care Med. 2021 Nov 1;49(11):1974-1982.

Acknowledgements

We thank the Albunet e.V. group for their constructive ideas for this project.

SIMULATING ARTERIOVENOUS FISTULA SOUNDS: A FLUID STRUCTURE INTERACTION APPROACH

Sofia Poloni (1), Luca Soliveri (2), David Bruneau (3), Andrea Remuzzi (1), Michela Bozzetto (2), Kristian Valen-Sendstad (4)

1. University of Bergamo, Italy; 2. Istituto di Ricerche Farmacologiche Mario Negri IRCCS, Italy; 3. University of Toronto, Canada; 4. Simula Research Laboratory, Norway.

Introduction: The arteriovenous fistula (AVF) remains the preferred vascular access for hemodialysis, but its effectiveness is compromised by frequent failure due to adverse vascular remodeling [1]. Recent research has unveiled that the presence of transitional flow within the vein, coupled with its interaction with the vessel wall, induces high-frequency wall vibrations [2] and sounds. The qualitative auscultation of AVF sounds is used in clinical settings for the assessment of AVF functionality [3]. However, the relationship between these sounds and hemodynamic conditions remains unclear. Hence, this study aims to establish a method to translate fluid pressure and wall vibration data derived from fluid-structure interaction (FSI) simulations into sounds.

Methods: In this study, six patients with radio-cephalic AVF were examined. Following the AVF's functional maturation (3-8 weeks post-surgery), MRI scans were conducted to create patient-specific 3D models. These models were utilized for high-fidelity FSI simulations using a fully coupled 2nd order accurate space/time centred scheme [4]. The

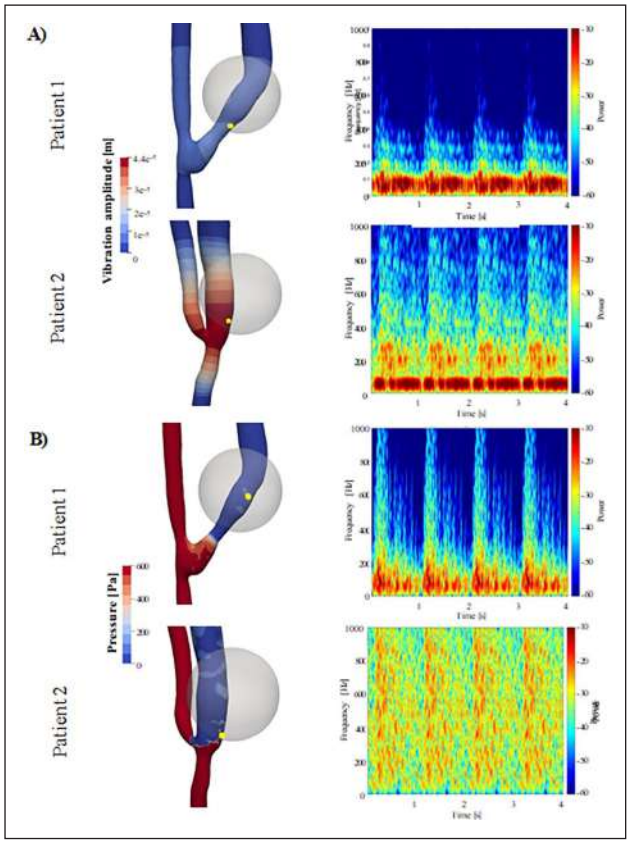

Figure 1. Surface maps with associated spectrograms of point-wise generated sounds of A) time-averaged vibration amplitude and B) systolic peak pressure for two representative patients.

simulation data were converted into sounds, assuming the magnitude of hemodynamic data as the sound intensity and the same sampling frequency of the simulation. The resulting sounds, filtered at 25 Hz, were repeated over four cardiac cycles to compare with clinical measurements and spectrograms were generated. Specifically, the location within the venous segment exhibiting the highest vibration amplitude was selected to represent vibration behavior and sonified. Similarly, the point within the vein experiencing the highest pressure fluctuations was selected for sound generation.

Results: Vibration and pressure sounds were successfully generated at specific points of interest for all AVFs. Within the same patient the sonification of pressure and displacement produces different tones with higher frequencies detected in the pressure sounds. The six participants presented varying AVF geometries, hemodynamics, and outcomes in wall vibrations, leading to individualized sound profiles. Illustrated in Figure 1 are two representative cases. AVFs with decreased vibration amplitudes (as for Patient 1) produced sounds characterized by lower frequencies and intensity. Conversely, heightened peak pressure (Patient 2) led to spectrograms displaying higher frequencies.

Discussion: All sounds generated from FSI results were considered similar to those recorded in clinical practice [5]. Preliminary findings revealed differences in generated sounds potentially related to AVFs geometry and hemodynamics. Understanding the relation between computationally generated sounds and related hemodynamic phenotypes could clarify the origin and the specific determinants of certain sound features detected in clinical settings, connecting frequency bands with AVF clinical conditions. This approach could further facilitate the validation of AVF sound analysis as a monitoring technique.

References

1. Bozzetto M et al, JVA, 24.5: 1061-1068, 2023.
2. Bozzetto M et al, Phys Eng Sci Med, 1-11, 2023.
3. Lok CE et al, Am J Kidney Dis, 75.4: 1-164, 2020.
4. Bergersen A W et al, JOSS, 5.50: 2089, 2020.
5. Tsuboi M et al, JVA, 23.3: 390-397, 2022.

OPTIMIZATION OF DANAPAROID INCORPORATION TO DIALYSIS MEMBRANES FOR LONG TERM HEMOCOMPATIBILITY

Roberto Nese[1], Odyl ter Beek[1], Dimitrios Stamatialis[1]

[1]Advanced Organ bioengineering and Therapeutics, Faculty of Science and Technology, TechMed Center, University of Twente, The Netherlands

Introduction: Hemodialysis is one of the main life-saving therapy for patients with end stage renal disease (ESRD) until an organ transplantation becomes available. Currently, ESRD patients undergo non-continuous dialysis therapies (usually for 4 hours, 3 times per week) mainly due to practical, logistical and health-related reasons[1][2]. This leads to a limited toxin removal efficiency because uremic toxins keep accumulating in blood between each dialysis treatments. To enhance patient outcomes and improve their quality of life, more continuous therapies like home or portable hemodialysis are needed, which require membranes with long-term hemocompatibility. Besides, despite advancements in biocompatible materials and membranes, systemic anticoagulation is still required, creating challenges for patients who cannot tolerate anticoagulant administration. Our approach consists in incorporating Glycosaminoglycans (GAGs) to hollow fiber membranes to improve their hemocompatibility. GAGs are long linear polysaccharides that can be found in human's kidney glomerulus, providing natural anticoagulating properties. Our group has recently performed first studies of incorporating various GAGs into hollow fiber membranes, showing that Danaparoid (DP), which is a mixture of different GAGs, can provide improved blood compatibility of polymeric membranes compared to other types of GAGs[3]. In this study we investigated the optimal strategies to incorporate DP to hollow fiber membranes. Ideally, DP should be concentrated in the layer of the membrane that comes into contact with blood and does not leak from this location during therapy.

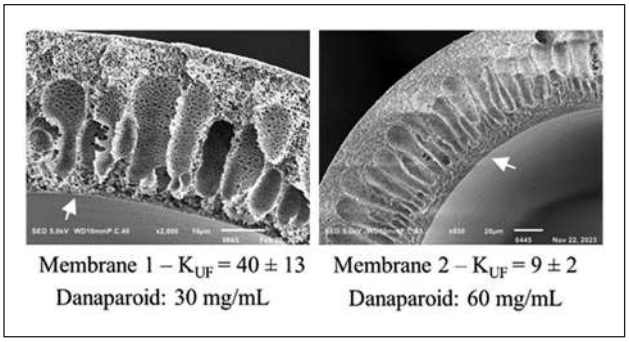

Figure 1. SEM images of hollow fiber membranes and Ultrafiltration coefficient (K_{UF}).

Methods: We investigated two different strategies to incorporate GAGs: blending in polymer solution and post-treatment coatings. Polymer dope for membrane fabrication consists of polyethersulfone (PES; 16 -20%), polyvinylpyrrolidone (PVP; 2%) and N-methyl-2-pyrrolidone (NMP; 75 – 79%). DP is dissolved in water at various concentrations and added to the polymer solution. The hollow fiber membranes fabrication conditions are tuned to produce fibers with a small diameter and good mechanical properties. The hollow fiber membranes are fabricated using a conventional spinning setup. Coatings of GAGs is performed with a post-treatment approach.

Results: Figure 1 shows SEM images of two hollow fiber membranes that we fabricated with blended GAGs at different concentrations. Membrane 1 has a higher ultrafiltration coefficient (KUF) due to the lower concentration of DP, which result in a thinner and less compacted selective layer (SL, highlighted by the white arrows). By staining the GAGs within the fibers, we detected the presence of them mainly on the SL of the hollow fiber membranes. To assess the effects of GAGs coating to hollow fiber membranes, we performed preliminary tests of coatings with commercial dialysis membranes. Clean water flux results indicate that the coatings need to be tuned to avoid significant decrease of the KUF.

Discussion: We found that blending is the simplest way to incorporate GAGs to hollow fiber membranes. However, more investigation on the spinning parameters and on the drying process of the fibers are necessary to improve the mechanical properties and permeability of the membranes.

References

1. Stamatialis, Dimitrios, ed. Biomedical membranes and (bio) artificial organs. Vol. 2. World Scientific, 2017. ISBN: 9813221755
2. Shan, Liang, et al. Journal of materials chemistry B 8.5 (2020): 878-894.
3. Kim, DooLi, et al. Journal of Membrane Science (2024): 122669.

Acknowledgements

This work is part of the project Biomed-04 'Artificial Organs'. This project receives a Growth Fund contribution from the program NXTGEN HIGHTECH.

TOWARDS PREDICTIONS OF HAEMORRHAGIC VERSUS THROMBOEMBOLIC EVENTS FROM ROTARY BLOOD PUMPS.

James Wootton (1), Tom Williams (1), O. H. Frazier (2), Yaxin Wang (2), Katharine H. Fraser (1)

1. Department of Mechanical Engineering, Centre for Bioengineering and Biomedical Technologies, University of Bath, UK; 2. Innovative Device and Engineering Applications, Texas Heart Institute, USA

Introduction: Haemorrhagic and thromboembolic events are post-surgical complications in LVAD patients. Fluid dynamic stresses cause activation and damage to blood components, creating a delicate balance between bleeding and clotting. A numerical model may enable a better understanding of the propensity for bleeding and clotting in patients with different LVADs.

Methods: Eight steady state, convection-diffusion-reaction equations were solved for: free haemoglobin (pfHb), von Willebrand factor (vWf) (collapsed, unfolded and fragmented forms) [1], platelets (nonactivated, activated and receptor shed) [2,3], and an example platelet agonist. Source terms for pfHb, mechanical activation and receptor shedding from platelets, used power law functions of shear stress and time. Chemical platelet activation was proportional to agonist concentration above a threshold. Rate constants for vWf unfolding and collapsing were dependent on the local flow type: rotating, shearing or extensional. Fragmentation of unfolded vWf occurred above a critical shear depending on the pfHb concentration [4]. Platelets attached to the walls according to a thrombus susceptibility potential modified from [2]. Blood flow was solved in Ansys Fluent with reaction equations implemented as User Defined Functions. Individual models were first compared with literature results from stenosis-like geometries [1,5,6]. The model was then used to estimate clotting in the HeartMate II and compared with [7].

Results: Haemolysis results predicted the right order when a shear stress threshold (250 Pa) was introduced (fig 2). Results for shear induced vWf unfolding were in good agreement with the literature in both symmetric (fig 3) and asymmetric (not shown) stenosed flows. Qualitative agreement in regions of high platelet deposition was found (fig 4). The relative numbers of platelets deposited in the different regions of the HeartMate II was similar to the relative numbers of thrombus formations (note the bearing was not modelled in this work.)

Discussion: While the model still requires some tuning, it was able to predict the LVAD region with most thrombi. In future the model could be used for design optimization.

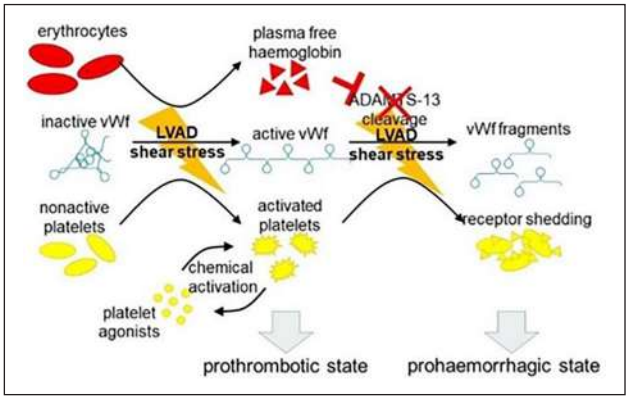

Figure 1. Fluid shear stress leads to prothrombotic and prohaemorrhagic states in patients with blood pumps.

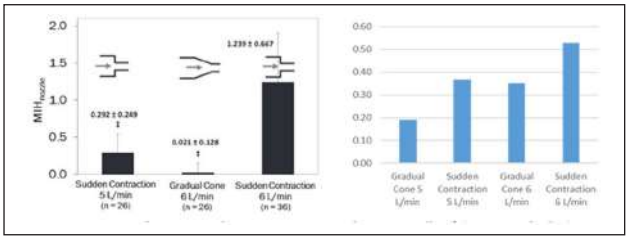

Figure 2. Haemolysis in nozzle [5] (left), model (right).

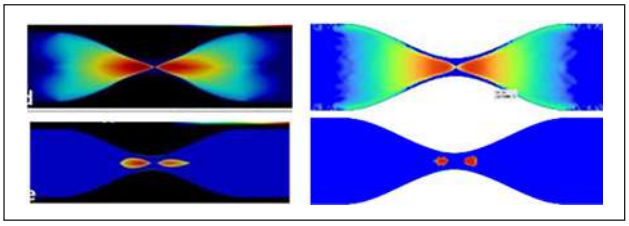

Figure 3. Flow type (top) and vWf unfolding rate (bottom) from literature [1] (left) and our model (right).

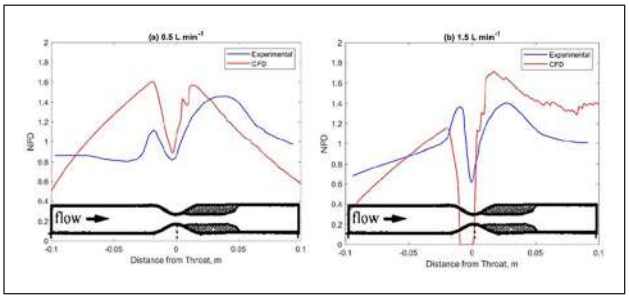

Figure 4. Platelet deposition comparison with [6].

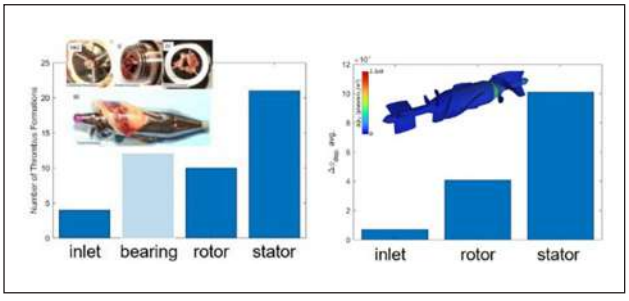

Figure 5. Clinical thrombi [7] (left) compared with platelet deposition in model (right).

References

1. Zhussupbekov et al, Ann Biomed Eng, 49:2646-58, 2021
2. Taylor et al, Biomech Model Mechanobi, 15:1713-31, 2016
3. Chen et al, ASAIO J, 64:773-8, 2018
4. Bartoli et al, Ann Thorac Surg, 105:807-14, 2018
5. Herbertson et al, Artif Organs, 39:237-59, 2014
6. Schoephoerster et al, Art Thromb Vasc, 13:1806-13, 1993
7. Rowlands et al, ASAIO J, 66:992-9, 2020

Acknowledgements

National Heart, Lung, and Blood Institute of the National Institute of Health under Award Number 1R01HL153538.

PRECLINICAL ASSESSMENT OF A DOUBLE-INFLOW SINGLE-OUTFLOW CAVOPULMONARY ASSIST DEVICE

Pascal Schmidt (1), Leon Ballabani (1), Bente Thamsen (1), Andreas Escher (2), Michael Röhrich (3), Michael Hübler (4), Daniel Zimpfer (1), Marcus Granegger (1,4)

1. Department of Cardiac Surgery, Medical University of Vienna, Austria; 2. Institute for Medical Engineering and Science, Massachusetts Institute of Technology, Cambridge, USA; 3. Department of Anesthesia, Critical Care and Pain Therapy, Medical University of Vienna, Austria; 4. University Heart & Vascular Center, Hamburg, Germany

Introduction: The Fontan circulation serves as a palliative treatment for patients with congenital univentricular heart disease. Established through a series of three surgeries, it reinstates functional blood oxygenation and improves survival rates. The Fontan circulation is, however, prone to progressive hemodynamic deterioration. Therefore, the development of novel mechanical circulatory support systems is of pivotal importance given the shortage of donor organs. Escher et al. [1] showcased promising preclinical results with a double-inflow double-outflow Cavopulmonary Assist Device (CPAD), moreover, revealing the potential to enhance implantability by transitioning the design to a single-outflow concept [2]. This study covers the preclinical in silico and in vitro evaluation of the updated single-outflow CPAD (Figure 1) regarding hydraulic performance and hemocompatibility over a broad range of caval inflow ratios (IRs). In addition, a flow estimator was developed to monitor hemodynamics in future chronic animal trials.

Materials & Methods: Numerical and experimental test setups were employed to assess hydraulic performance in terms of pressure-flow characteristics under varied IRs (IVC/SVC: 1/1; 2/1; 3/1; and 1/2) and operating conditions (rotational speed: 1500rpm – 3500rpm; and total flow: 0 – 10 L/min). Further, the current consumption of the CPAD was experimentally determined to establish a flow estimator based on current, rotational speed, and viscosity. The normalized index of hemolysis (NIH) over 30-min intervals was obtained experimentally at the nominal operating point (4 L/min, 2500 rpm) under two different IRs (IVC/SVC: 1/1 and 3/1) in a paired test setting using the same blood (hematocrit: 35%) per test (n=5). Moreover, the NIH was numerically computed for the same conditions utilizing a previously established methodology [3].

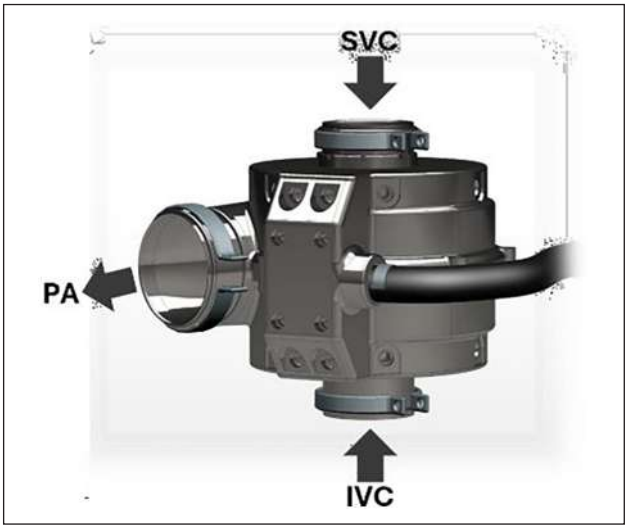

Figure 1. 2nd Generation CPAD with depiction of superior (SVC) and inferior vena cava (IVC) inflows and pulmonary artery (PA) outflow.

Results: Both in silico and in vitro analyses indicated a negligible impact of the analyzed IRs on hydraulic and hemolytic CPAD performance. Experimental analysis showed no significant influence ($p > 0.98$) on the current consumption and pressure head generated for all chosen operating conditions. Therefore, a flow estimator, independent of IR, was developed and cross-validated (RMSE < 0.13 L/min, $R2 > 0.99$). Further, the experimental NIH evaluation revealed a non-significant ($p = 0.79$) difference of 8.9% between both conditions (IR = 3/1: 8.5 mg/100L; IR = 1/1: 7.7 mg/100L), while numerical analysis showed a variation of 5.9% (IR = 3/1: 1.06 mg/100L; IR = 1/1: 0.99 mg/100L).

Discussion: The single-outflow CPAD meets hydraulic benchmarks set by its predecessor, while demonstrating a low hemolytic behavior (compared to clinically established blood pumps [3]). The updated design and the displayed robustness against different IRs further promote the implantability within the heterogenous Fontan patient population. The successfully developed flow estimator will be essential for pump control and monitoring in future pre-clinical in vivo trials.

References

1. Escher, A. et al., Seminars in Thoracic and Cardiovascular Surgery. 34:238-248, 2022
2. Karner, B., et al., ASAIO Journal, 69(11): 1016-1024, 2023
3. Escher, A. et al., IEEE Transactions on Biomedical Engineering. 69(8):2423-2432, 2022.

Acknowledgements

The computational results presented have been using the Vienna Scientific Cluster (VSC). This study was supported by the GIGAX Foundation and the Ever Foundation.

IN VITRO CHARACTERIZATION OF NOVEL 'PEPTIDE B'

Josefin Soppert, Giulia Bagarolo, Emona Staudacher, Marie-Luise Berres, Joachim Jankowski, Heidi Noels

University Hospital RWTH Aachen, Germany

Background: The portal vein is an essential compartment of the gut-liver axis. Mediators entering the portal vein and transported into the liver have far-reaching consequences on liver function and hepatic diseases. 'Gut-mediated effects' on the liver are modulated by the integrity of the gut barrier, which is affected by portal venous pressure among other factors. To study gut-liver crosstalk, portal vein and peripheral blood of patients with severe portal hypertension and liver pathology undergoing transjugular intrahepatic portosystemic stent (TIPS) were profiled by mass spectrometry. Two peptides were enriched in portal compared to peripheral blood. MS sequencing identified these features as peptides derived from the parent proteins 'protein kinase c-beta type' (from here on referred to as: 'peptide β') and 'protocadherin fat' [1].

Hypothesis: These novel peptides might be gut-derived mediators with functional consequences on the liver.

Aim: The effect of the novel peptides on liver inflammation and fibrosis, two crucial processes underlying chronic liver disease, will be examined *in vitro* using hepatocytes, hepatic stellate cells and macrophages.

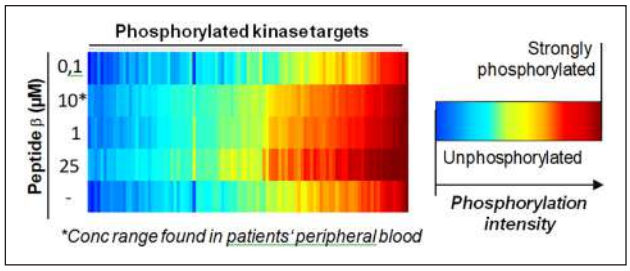

Figure 1. Heat map of the kinase activity assay from dose response with peptide β. HepG2s were lysed 15min after stimulation. The heat map displays intensities (AU) of phosphorylation levels of a range of kinase targets.

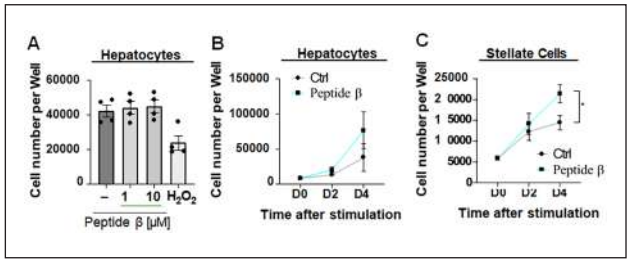

Figure 2. Peptide β is pro-proliferative in hepatic stellate cells. Cells were treated with 1µM peptide β. (A) Metabolic activity in HepG2s after 1 day (n=4). (B) Proliferation in HepG2s (n=5). (C) Proliferation in TWNT-4s (n=5). Mean with SEM.

Methods: Kinase activity profiles with increasing concentrations of peptide β (0-10µM) were analysed after 15 minutes of incubation using a commercial "kinase activity assay". Cell viability (MTT) and proliferation assay (CyQUANT, Invitrogen) was performed according to manufacturer's instructions. For gene expression, cells were processed for RNA isolation, cDNA synthesis and quantitative real-time PCR according to standard protocols, analyzing markers for myofibroblast activation and fibrosis (α-SMA, Col1α1 and TGF-β1, MMP-2, TIMP-1, Vimentin).

Results: Kinase activity profiling in hepatocytes (HepG2) revealed an impact of peptide β on cellular signaling at clinically relevant concentrations **(Figure 1**).

In hepatocytes, peptide β does not affect cellular viability/metabolic activity **(Figure 2A-B**). In contrast, peptide β is pro-proliferative in hepatic stellate cells (HSCs) (**Figure 2C**)

Peptide β significantly reduced gene expression levels of α-SMA, Col1α1 and TGF-β1 in human hepatic stellate cells (**data not shown**), indicating a less activated and ECM-producing myofibroblast-like phenotype. Gene expression of vimentin, MMP-2 and TIMP-1 were unchanged (**data not shown).**

Discussion: We revealed a novel peptide that is increased in the portal vein of patients with portal hypertension ('peptide β'). Peptide β impacts cellular signaling and function at concentrations found in patients' blood. Peptide β reduces the activation into a myofibroblast-like phenotype and decreases collagen production, while it increases the pro-proliferative capacity of hepatic stellate cells. Both effects might be mutually interrelated. Transdifferentiated, highly ECM-producing myofibroblasts are less proliferative than activated proto-myofibroblasts [2]. Although peptide β limits the myofibroblast-like phenotype, we suggest a profibrotic nature of the novel peptide β because of its pro-proliferative effects on stellate cells. Direct effects of peptide β on inflammation in liver cells remain to be elucidated. Furthermore, it is uncertain whether the peptide derived from the 'protocadherin fat' parent protein exhibits functional consequences on any liver cell.

References

1. Bagarolo et al, Submitted, 2024
2. Gibb et al, Circ Res, 127(3):427-447, 2020.

QUESTIONING A PARADIGM: SHOULD DIALYSIS MEMBRANES BE IMPERMEABLE FOR ALBUMIN.

Joerg Vienken (1), Gerd Klinkmann (2)

1. MedTech Consultants, Germany; 2. University Clinic Rostock, Germany

Introduction: Since longtime manufacturers of dialysis membranes are faced by requirements of the nephrological community that the cut-off of dialysis membranes should be below the molecular weight of albumin, i. below 66,000. Further, a loss of albumin per dialysis session should not exceed 4g/session. Maintenance of the vital colloid osmotic pressure as well as binding and transport of water insoluble substances and pharmaceutical drugs are arguments favoring the opinion that albumin levels should be kept in the normal range and not be deteriorated by filtration through dialysis membranes.

Here, the hypothesis will be tested whether an albumin-loss through dialysis membranes might not be a disadvantage. Support for this statement are provided by recent findings.

Findings: Albuminurea in PD and HD: Published investigations have shown that patients on PD exhibit a considerable protein loss per day. Losses are in the range of >6g/day. Thus, the term albuminurea in PD has been coined in this context [1]. A retrospective meta-analysis compar-ing patients treated with PD and HD further showed that serum **pre**-albumin levels are approximately 6mg/dl higher in PD-compared to HD-patients. It is presumed that hepatic synthesis of albumin by the healthy liver is stimulated by PD´s albumin loss [2]. Despite the fact, that serum albumin levels are about 0,3g/dl lower in PD-than in HD-patients, the liver is obviously able to compensate for theses losses. Further, no survival advantage of HD versus PD could be found after a completion of a 2-year treatment period [3], questioning the role of albumin in this context.

Strategies to develop dialysis membranes are deter-mined by improving the molecular weight cut-off of membranes. A sieving coefficient (SC) for albumin far below SC=0,5 has become even a paradigm. With the recent advent of clinical high-volume hemodiafiltration, removal of only individual single uremic retention solutes has turned out to be insufficient. Current opinions preferentially address the removal of families of molecules with different molecular weights, because those might interact synergistically with the result of an increased toxic potential.

Consequently, membranes with a higher molecular weight cut-off would be needed to allow for this increased performance, possibly exceeding the cut-off range of albumin. Recent clinical trials on >690 HD-Patients in Japan were performed to prove the benefit of

protein permeable membranes in terms of long-term survival. Patients were treated here in a 7 years follow-up with three subgroups of high-flux dialysis membranes differing in the capacity to show an albumin loss per session (albumin loss 3g or more, 1-3g and less than 3g). Albumin leakage of >3g or more per HD session provided a better prognosis and thus, showed highly beneficial effects on mortality in maintenance HD-patients.

Conclusion: Following these findings the paradigm of protein-impermeable dialysis membranes should be reconsidered. Results on patient mortality comparing HD and PD, and on membranes with high molecular weight cut-off prove the hypothesis that protein permeable dialysis membranes have beneficial effects on patient performance.

References

1. Lu W et al, Clin Exper Nephrol,23:551-560 (2019)
2. Goldwasser P et al.; Kidney Int, 62:276-281 (2002)
3. Klinger M et al; K, Adv Clin Exp Med, 28:133.135 (2019)
4. Nagai K et al,; Ther Apher Dial, 21:378-386 (2017)

AN OPTICAL SENSOR FOR CONTINUOUS HEMOLYSIS MEASUREMENT

Patrick Borchers (1), Steffen Leonhardt (1), Marian Walter (1)

1. Chair for Medical Information Technology, RWTH Aachen University, Germany

Introduction: Hemolysis induced by blood pumps is routinely evaluated by in-vitro testing according to the ASTM-F1841 standard [1]. This usually involves taking blood samples from a test bench once per hour and assessing hemolysis by determining plasma-free hemoglobin (pfHb). However, the manual sample processing is time-consuming, resource demanding, and prone to errors. Therefore, this work proposes an optical sensor to continuously measure hemolysis in whole blood without the need for blood sampling. Such a sensor could also be integrated into the graft of left ventricular assist devices (LVADs) to continuously monitor hemolysis and oxygen saturation (sO2) in LVAD patients.

Methods: The optical hemolysis sensor (c. f. Figure 1) contains four LEDs (645 nm, 730 nm, 810 nm, and 940 nm) and two photodiodes, with barriers in between. The LEDs and photodiodes are soldered to circuit boards, that are connected to 3D-printed half-shells. The half-shells are clamped around a transparent plastic tube adapter for ½ inch tubes. The LEDs were switched on one after each other for 250 ms and the reflected light intensity was measured at the photodiode on the same side.

The voltage change due to hemolysis $U_{hemolysis}$ of each LED was calculated by correcting the measured sensor voltage U_{sensor} for oxygen saturation:

$$U_{hemolysis} = U_{sensor} - f(sO_2) \quad (1)$$

Thereby, $f(sO_2)$ is a third order polynomial for each LED describing the dependence between sO_2 and U_{sensor} as shown in Figure 2 (left).

The sO_2 was estimated from the sensor voltages at 810 nm (U_{810}) and 940 nm (U_{940}) (c. f. Figure 2 (right)):

$$sO_2 = 430.2 \cdot \left(\frac{U_{810}}{U_{940}}\right) - 242.7 \quad (2)$$

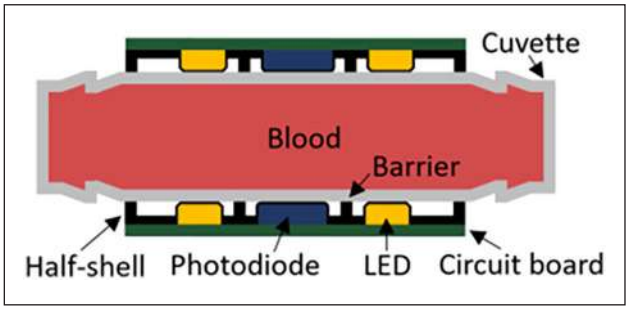

Figure 1. Structure of the optical hemolysis sensor.

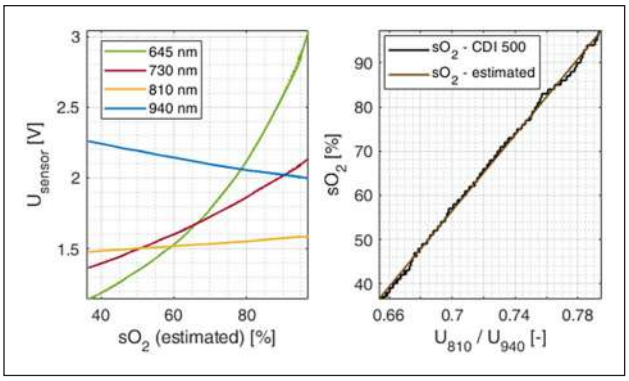

Figure 2. Dependence of the estimated sO_2 on U_{sensor} (left) and sO_2 estimation from sensor signals (right).

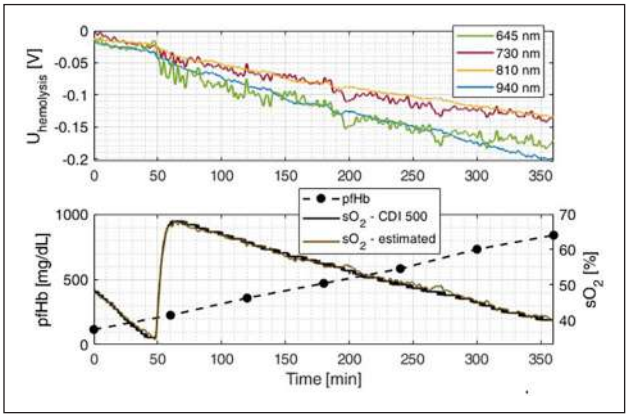

Figure 3. sO_2, pfHb, and $U_{hemolysis}$ during a 6-hour hemolysis trial. sO_2 was changed at t = 50 min.

The sensor was evaluated using a test bench according to the ASTM F1841 standard [1]. The test bench was extended by an oxygenator and a CDI 500 device to vary and measure the oxygen saturation. Porcine blood with a hematocrit of 35 % was circulated at a flow rate of 5 L/min for six hours using a Sputnik LVAD.

Results: During 6 hours, pfHb increased linearly from 116 mg/dL to 839 mg/dL (Figure 3), while $U_{hemolysis}$ decreased linearly for all wavelengths. The correlation coefficient between these was at least -0.96.

Discussion: The strong negative correlation between pfHb and $U_{hemolysis}$ for all wavelength could be explained by the increase of the scattering coefficient of blood due to hemolysis [2]. The findings are also in accordance with Neudel et al. [3], which aimed for the determination of sO_2 and hematocrit, but regarded hemolysis as a disturbance. However, further trials have to be conducted to assess the reproducibility and accuracy of the developed hemolysis sensor.

References

1. ASTM International, ASTM F1841 – 19, 2019.
2. V. Tuchin et al, Opt Express, 12:2966-71, 2004
3. F. Neudel et al, Med. Eng. & Physics, 24:301–307, 2002

Acknowledgements

This work was supported by grant 409796053 from the German Research Foundation (DFG).

THE EFFECT OF DIFFERENT EXERCISE INTENSITIES ON THE HEMODYNAMICS IN ABDOMINAL AORTIC ANEURYSM

Haoyao Cao (1), Chengxin Weng (2), Ding Yuan (2), Tinghui Zheng (1)

1. Department of Mechanics & Engineering, College Architecture & Environment, Sichuan University, China; 2. Division of Vascular Surgery, Department of General Surgery, West China Hospital, Sichuan University, China

Introduction: The European Society for Vascular Surgery guidelines first proposed exercise as one of the treatments for the patients with abdominal aortic aneurysm (AAA) in 2019 [1]. Generally, exercise is believed to improve the cardiovascular function of patients and inhibit the growth of AAA [2]. The previous studies have already compared between the exercise group and resting group [3, 4]. However, there are various ways to exercise in the daily life, and what intensity of exercise can benefit the AAA patients is still a question for the doctors. Furthermore, considering the risk of the AAA, it is difficult to find the answer in clinical practice. Therefore, this study aims to explore the effect of exercise intensity on the hemodynamic environment of AAA by numerical simulation, providing theoretical support and detailed supplementation for exercise prescription.

Methods: Eight patient-specific AAA models are reconstructed based on the computed tomography images. There were three exercise intensities: resting state, continuous low-intensity exercise and continuous moderate-intensity exercise. For each AAA model, the impact of three boundary conditions on the flow field, the time averaged wall shear stress (TAWSS) and oscillatory shear index (OSI) are analyzed, respectively. For each exercise intensity, the hemodynamic environment of AAAs with different morphologies are compared.

Results: The results show that both low-and moderate-intensity exercise can increase the flow velocity in the AAA, maintain more flow in a forward direction within one cardiac cycle, and reduce the proportions of low TAWSS (<0.4 Pa) and high OSI (>0.3) areas to the surface area of AAA. The decrease value in abnormal hemodynamic area proportions is related to the morphology of the AAA. As the intensity of exercise increases, the area of low TAWSS and high OSI area gradually decrease. However, there are obvious disordered flow, such as vortex in the flow field of AAAs with continuous moderate-intensity exercise.

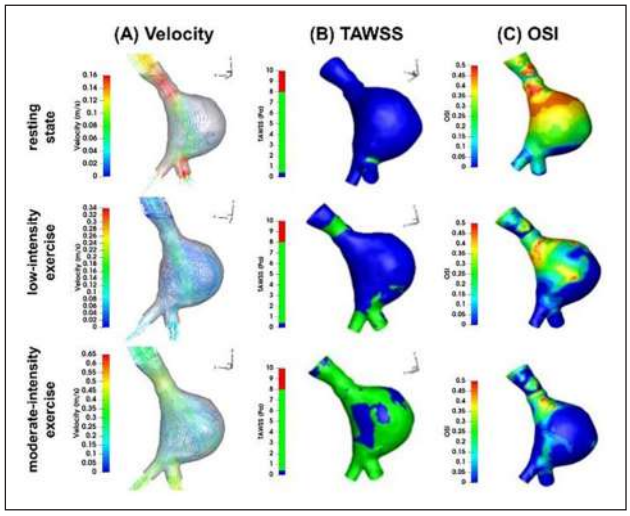

Figure 1. (A) Streamlines of the blood flow of patient 2 (systole period); (B) Time average wall shear stress (TAWSS) distribution contour map on the vessel wall of patient 2;(C) Oscillatory Shear Index (OSI) distribution contour map on the vessel wall of patient 2.

Discussion: Compared with the medium-intensity exercise and the resting state, the continuous low-intensity exercise may be the best way for the patients to keep a normal hemodynamic environment in the AAA, which has the potential to become a non-invasive management method. At the same time, when designing the exercise treatment plans, the intensity of exercise and the morphology of the AAA should be considered.

References

1. Wanhainen A. et al, European Journal of Vascular and Endovascular Surgery, 2020. 59(3).
2. Tew G.A et al, Archives of Physical Medicine and Rehabilitation, 2012. 93(12): p. 2148-2153.
3. Nakayama A et al, Journal of the American Heart Association, 2018. 7(5).
4. Barakat H.M et al, Annals of Surgery, 2016. 264(1): p. 47-53.

Acknowledgements

This work was supported by grant 12072214 from the National Natural Science Foundation of China.

A NOVEL MODULAR MOCK CIRCULATION LOOP

Tianyuan Sun, Chengwei Yan, Lian Gan , Ashraf W Khir

Department of Engineering, Durham University, United Kingdom

Introduction: Mock Circulatory loops (MCLs) have been a fundamental tool during the development and testing of ventricular assist devices (VADs). MCLs have also been very useful in hemodynamic studies. However, current MCLs have several limitations: a) Some local and vital circulations are missing (coronary and lower body circulations), b) Although the auto-regulation response has been represented in some MCLs, they rely depend on Hoffman clamps to adjust parameters such as resistance, which leads to a decrease in the precision of the experimental data, c) current designs present MCLs as one large test-bed, which is inflexible. Therefore, the aims of this research are to a) introduce coronary, cerebral and lower body circulations, b) Develop a modular MCL that allows the user to select different modules for testing different types of VADs or various hemodynamic studies, c) MCL that is automatically controlled by calculating and applying the auto-regulation parameters.

Methodology: The modulars used in this study were constructed using average dimensions of the major vessels of each circulatory, computer aided design (CAD) software, 3D printing and silicone perfusion and vacuum demoulding. The were selected and modelled using. The MCL was divided into 6 circulatory modulars as shown in the Table 1. Each part was connected through solenoid valves and controlled by National Instrument control unit (CompactRIO) and HMI (Human Machine Interface) modules. The Ursino mathematical model [1] will be used for determining arterial resistance, heart rate and feeding these values for implementation into the MCL. The operator can select different modulars from the HMI according to different tests. The NI Compact RIO will automatically control the connection between the modulars based on the user's inputs, to achieve different functions for different tests. The basic logic flow is shown in Figure 1.

Table 1. Circulatory systems covered in this research.

No.	Circulation System (Include Vein)
1	Pulmonary Circulation
2	Coronary Circulation
3	Basic Heart Circulation
4	Cerebral Circulation
5	Lower Body Circulation
6	Renal Circulation

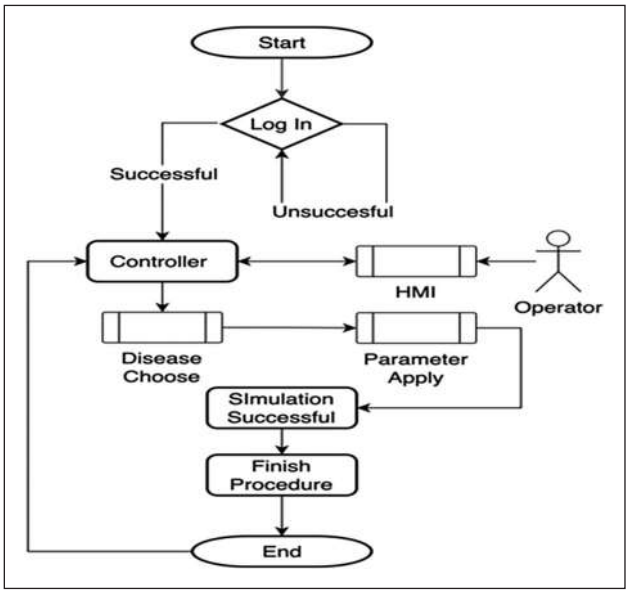

Figure 1. The flow chart of main control logic of this MCL.

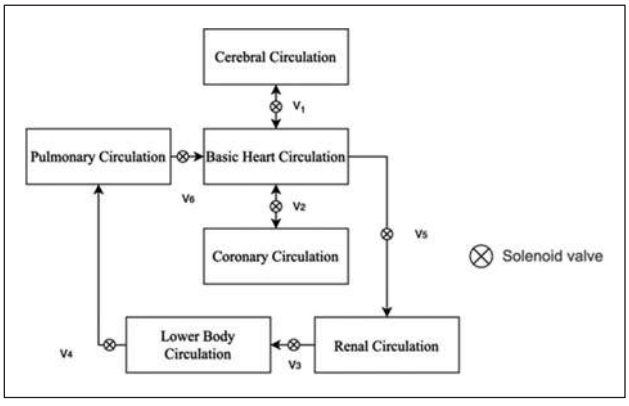

Figure 2. This image shows how each part is connected and modularised.

Results: Based on the objective of the investigation, the operator selects the required clinical scenario from the HMI control screen. The system automatically turns off the irrelevant solenoid valve and changes the corresponding arterial (compliance and resistance) and cardiac (HR, stroke volume and pulsatility) parameters.

Conclusion: The hemodynamic auto-regulation parameters of the human circulation including lower and upper limbs were successfully simulated in vitro. The MCL results of this design closely replicate the physiological circulation and can be reliably used for the in-vitro testing of VADs. The modular design allows for using the MCL for different testing and diagnostic procedures and clinical scenarios.

Reference

1. Ursino, "A mathematical model of the carotid baroregulation in pulsating conditions." IEEE Transactions on Biomedical Engineering 46.4: 382-392,1999.

HISTOLOGICAL STUDY OF THE CHONDROGENIC REGENERATION CAPACITY OF A GELATIN-HYALURONIC ACID MICROGEL IN A PORCINE MODEL OF ARTICULAR CARTILAGE INJURY

Lara Milián[1,2], Manuel Mata [1,2,3], José Luis Gómez Ribelles[4,3], Joaquín Ródenas Rochina[4], Ignacio Alcorisa[4], Julia Pla Salom[4], José Antonio Gómez Tejedor[4,3], Gloria Gallego Ferrer[4,3], Juan Carlos Monllau[5,6], Carmen Carda[1,2,3], María Sancho-Tello[1,2] (*)

1. Departamento de Patología, Facultad de Medicina y Odontología, Universitat de València,Spain, 2. INCLIVA Biomedical Research Institute, Spain, 3 Centro de Investigación Biomédica en Red de Bioingeniería Biomateriales y Nanomedicina, Instituto de Salud Carlos III, Spain; 4 Centre for Biomaterials and Tissue Engineering (CBIT), Universitat Politècnica de València, Spain; 5. Department of Orthopedic Surgery, 6. Universitat Autonoma de Barcelona, Spain.
E-mail (corresponding author): maria.sancho-tello@uv.es

Introduction/aim: The histological characteristics of hyaline cartilage, mainly its avascular nature, dictate its poor regenerative capacity. High-grade local cartilage injuries induce unbalanced mechanical stresses within the joint which exacerbate the damage and often progress to osteoarthritis. The regeneration of articular cartilage requires of three key elements: (i) the recruitment of chondrogenic cells to the defect site; (ii) the use of a biomaterial able of generating a three-dimensional environment capable of providing the necessary biomechanical cues; and finally, (iii) provide the essential biochemical factors to induce cells towards the adoption of the hyaline cartilage chondrocyte phenotype.

In this work we combined subchondral bone damage by microdrilling to produce bleeding at the defect site and create a pathway for migration of mesenchymal stem cells from the subchondral bone, with the use of a mixture of gelatin and hyaluronic acid microspheres containing platelet-rich plasma to provide a chondrogenic friendly environment with the idea to improved cartilage regeneration.

Methods: We use a model of joint damage developed in pigs. We included 2 experimental groups, one treated with microdrilling and the other with microdrilling in combination with the microgel containing platelet-rich plasma (PRP). We used 8 animals for each experimental group. The animals were sacrificed after nine months, and the histological characteristics of the regenerated cartilage as well as the biomechanical properties were evaluated. Neocartilage morphology was characterized by thickness, cell density, and interdigitation of the cartilage and subchondral bone. Microscopic features of the cartilage were also evaluated using the ICRS grading scaling as previously described [1], using hematoxylin-eosin and toluidine blue histological stains.

Results: The results show a great variability between the different animals of the two experimental series, since we observed cases in which

the regenerated tissue has all the characteristics of hyaline cartilage, while in other animals, although the regenerated tissue filled the defect, its structure was more like fibrous tissue or fibrocartilage.

Although the series in which only the subchondral bone was damaged seems to present poorer results, we only found significant differences in terms of cartilage thickness (in the group with microdrilling and microgel it was greater than in the group with only microdrilling). Other quantitative variables analyzed did not show significant differences. We also did not find variations in relation to the biomechanical characteristics of the groups analyzed, being similar in terms of hardness and recovery.

Conclusion: It seems that the use of the microgel loaded with PRP represents an improvement over the use of microdrilling alone because, on the one hand, the thickness of the cartilage of the animals included in this experimental group is greater, while, on the other hand, the area of the matrix with high glycosaminoglycan content is thicker. It would be necessary to increase the "n" to demonstrate if there are significant differences between groups.

Reference

1. Zurriaga Carda J et al. J Biomed Mater Res B Appl Biomater, 108(4):1428-1438, 2020.

Acknowledgements

This work was supported by the projects PDC2021-121658-C21 and C22, funded by MCIN/AEI/10.13039/501100011033 and by the European Union "NextGenerationEU"/PRTR.

IMPROVEMENT OF CLINICAL SYMPTOMS BY APPLYING PRE-DILUTION ON-LINE HEMODIAFILTRATION (HDF) WITH VARIOUS COMMERCIAL DIAFILTERS

Akihiro C. Yamashita[1], Kenji Sakurai[2]

1. Department of Chemical Science and Technology, Hosei University, Tokyo, Japan; 2. Hashimoto Clinic, Sagamihara, Japan

Objectives: There are two major dilution techniques in hemodiafiltration (HDF) therapy, i.e., pre-dilution and post-dilution. Most HDF treatments are performed in post-dilution mode, employing higher blood flow rates (Q_B) in European countries, whereas pre-dilution is predominantly performed in Japan under relatively lower Q_B. This paper discusses the correlation between solute removal and clinical symptoms for further success of the treatment.

Method: The purpose of HDF treatments in European countries is to remove β2-microglobulin (β2-MG, MW 11,800) without losing much albumin (MW 66,000) to reduce the risk of ESKD patients. Since the purpose of Japanese HDF is to remove solutes much greater than β2-MG (up to a1-MG, MW 33,000) under Q_B of 200-250 mL/min, employing pre-dilution on-line technique to control the amount of albumin loss more easily. We then performed pre-dilution on-line HDF with various commercial diafilters under above mentioned Q_B and the total dialysis fluid flow rate of 500 mL/min in order to remove various clinical symptoms.

Results and Discussions: We found a great difference between European HDF and Japanese HDF in terms of α1-MG removal and albumin leakage (Fig.1). Since we have experienced a correlation between the reduction rate of α1-MG and the improvement of various clinical symptoms, such as shoulder pains, numbness, and restless legs syndrome (RLS)[1)], we tried to remove α1-MG actively, sacrificing a relatively large amount of albumin with no nutritional problems so far. Although the reduction

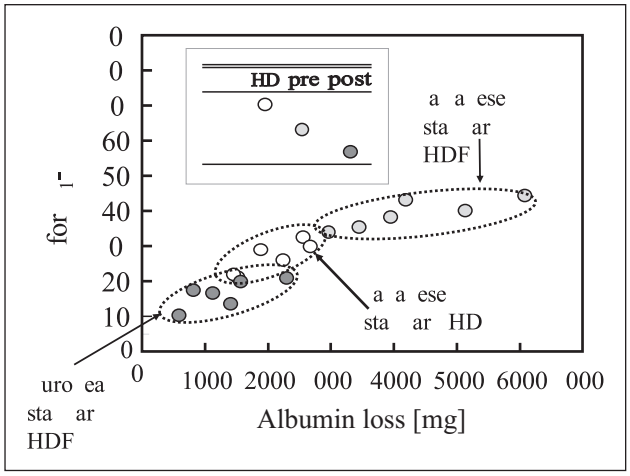

Figure 1. Relationship between RR for a_1-MG and albumin loss Comparison of European standard HDF and Japanese standard HD.

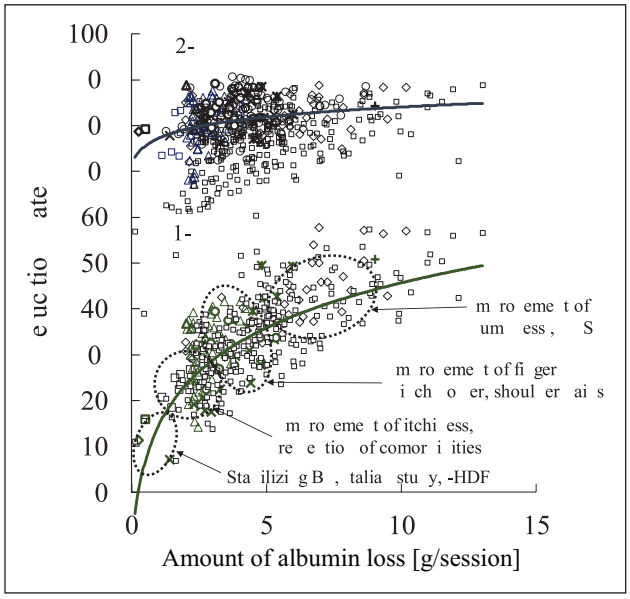

Figure 2. Relationship between the reduction rate for β_2-MG / α_1-MG and amount of albumin loss.

rate of β2-MG was about 80%, no correlation was found between the reduction rate of β2-MG and the improvement of clinical symptoms. Removing α1-MG or even greater solutes is important to improve clinical symptoms (Fig.2). However, since the reduction rate of α1-MG was also correlated with the amount of albumin leakage, attention must be paid for the choice of diafilters or membranes[2)].

Conclusions: It is important to remove α1-MG effectively to improve clinical symptoms; however, one cannot remove α1-MG without losing albumin. Also, the choice of diafilters is as important as the convective (or substitution) volume in HDF.

References

1. Yamashita AC, Sakurai K: Choice of Dialyzers for HDF, *Contributions to Nephrology*, **168**, 146-152, Basel Karger, 2010.

2. Yamashita AC, Sakurai K: Clinical effect of pre-dilution hemodiafiltration based on the permeation of the hemodiafilter, *Contributions to Nephrology*, **185**, 1-7, Basel, Karger, 2015.

EFFECT OF ELECTRIC CHARGE OF THE DIALYSIS MEMBRANE ON THE TRANSPORT OF CHARGED AND NON-CHARGED MOLECULES

Akihiro C. Yamashita

Department of Chemical Science and Technology, Hosei University, Tokyo, Japan

Objectives: An electric charge of the dialysis membrane is known to be an important character of solute permeability. The objective of this study is to evaluate the permeability of a strongly negatively charged dialysis membrane, AN-69® ST for charged and non-charged molecules.

Materials and Method: A flat sheet AN-69® ST dialysis membrane, known to have a strong negative charge of -70 mV, was taken from S-2400 multi-plate dialyzer (Baxter Health Care Co., Dear Field, IL, U.S.A.) for evaluation. A small piece of the membrane was set between a pair of horizontal diffusion chambers, the volume of each chamber of 50.0 mL and the effective transport area of 4.78 cm² (Permcell®, Fig.1). Transport studies were made at various temperatures by filling one chamber with an aqueous solution that included the solute of interest (donner) and the other with the solvent with no solute of interest (receptor). Test solutes were creatinine (MW 113), benzoic acid (BA, MW 122, pKa = 4.1) and methylene blue (MB, MW 320) as an electrically neutral, a negatively charged and a positively charged solute, respectively.

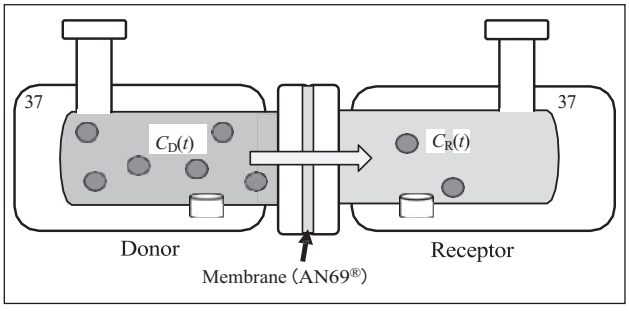

Figure 1. Horizontal diffusion chamber (Permcell®) Volume of each chamber: V = 50.0 mL Effective membrane area: A = 4.78 cm²

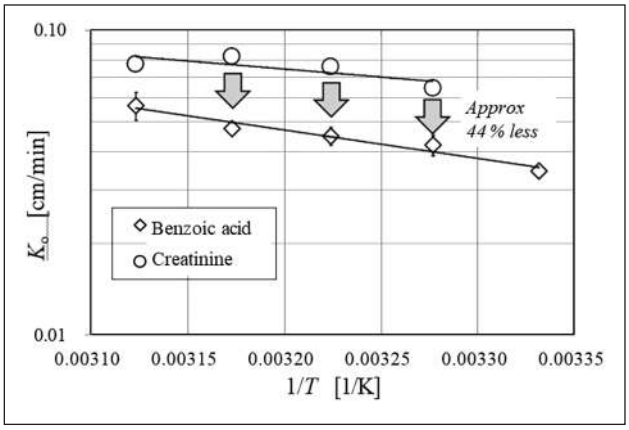

Figure 2. Arrhenius plot of *Ko* for benzoic acid and creatinine

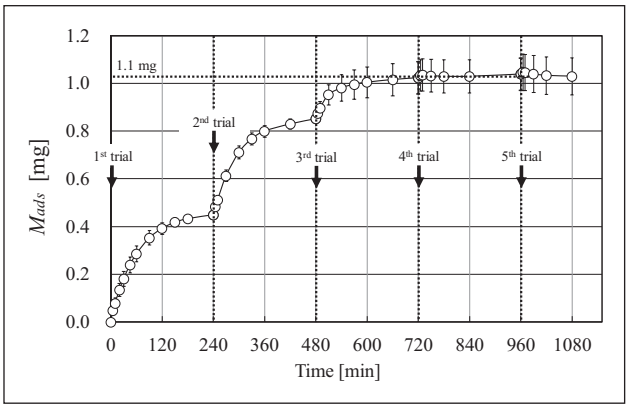

Figure 3. Cumulative amount of MB adsorbed by AN69®. (Initial conc. CD(0) = 0.010 mg/mL, repeated 5 times every 240 min).

Results and Discussion: Although MW of creatine and that of BA are similar, the permeability for the latter was approximately 44% less than that for the former (Fig.2). Then it seemed that the electric charge of the membrane influenced on the permeability even for a small solute like BA. When MB was employed as a test solute, almost no transport was observed across the membrane in 4 hrs while the concentration of MB decreased from 1.0 to 0.1 mg/dL, suggesting that most MB molecules (0.42 mg) were adsorbed by the membrane (Fig.3). After repeating the same experiments five times, virtually no adsorption was observed, achieving the adsorption maxima of 1.1 mg of MB. The permeability of the membrane with the adsorption maxima for creatinine was 20 % less than that of the intact membrane. Then the electric status of the dialysis membrane is as important as the physico-chemical structure of the membrane[1].

Conclusions: A strongly negatively charged membrane adsorbed small positively charged molecule, which reduced the permeability for creatinine, a neutral molecule.

Reference

1) Yamashita AC, Kakee T, Ono T, *et al.*: Semi-quantitative evaluation of asymmetricity of dialysis membrane using forward and backward ultrafiltration, *Membranes* **12**, 624, 2022.

HIGH DENSITY CULTURE SYSTEM BASED ON ALGINATE-AGAROSE SPHERES FOR THE COLLECTION AND CHARACTERIZATION OF THE SECRETOME OF MESENCHYMAL CELLS

Lucía Bravo (1,2)*, Mauro Llop-Miguel (1), Irene Monleón-Guinot (1,2), María Sancho-Tello (1,2), José Javier Martín de Llano (1,2), Carmen Carda (1,2,3), Lara Milián (1,2) and Manuel Mata (1,2,3)

1. Department of Pathology, Faculty of Medicine and Dentistry, Universitat de València, 46010 Valencia, Spain; 2. INCLIVA Biomedical Research Institute, 46010 Valencia, Spain; 3. Biomedical Research Networking Center of Respiratory Diseases (CIBERES), 28029 Madrid, Spain.

Introduction: The use of the secretome of mesenchymal stem cells (MSCs) as a substitute for cell therapy in the regeneration of articular

cartilage has recently gained importance due to the potential problems involved in the use of cells in regenerative therapies. This hypothesis is based on the fact that the effects observed with the use of MSCs could be due to the substances released rather than to the introduction of the cells themselves [1]. Our aim is to develop a secretome, a conditioned medium enriched with the essential factors for the regeneration of hyaline cartilage, while avoiding the need to introduce stem cells into the body and the potential associated risks.

Methods: We developed a three-dimensional (3D) culture platform to achieve our goal. We used MSCs, specifically human dental pulp stem cells (hDPSCs). Cells were encapsulated in microspheres of a hydrogel composed of alginate and agarose, two polymers that, in combination, allowed the culture. To carry out this encapsulation, we generated a suspension of both polymers and cells, which were generated in a spherical shape thanks to the use of a peristaltic pump (Figure 1). Once generated, we kept them in a bioreactor for long periods, which was made possible by the continuous addition and removal of culture medium. Additionally, we controlled critical parameters such as temperature, humidity, and the percentage of CO2 to which the cells were exposed. After a defined proliferation period, we induced hDPSCs differentiation with a fetal bovine serum (FBS)-free differentiation medium [2], a relevant feature for potential clinical translation. Once the microspheres were generated and cultured, we evaluated their elastic modulus in the presence and absence of cells using a Zwick Roell elastomer. We measured the dimensions of the microspheres to verify their homogeneity. We collected the conditioned medium to perform various experiments to determine whether the factors released by the cells were suitable to achieve the desired tissue regeneration.

Results: Our method for generating microspheres guarantees a consistent size and optimal cell density, obtaining microspheres of 2.4 ± 0.5 mm in diameter. More than 90% cell viability was observed after 6 weeks of culture. The elastic modulus measurement exhibited a significant increase in hydrogel stiffness in the presence of cells, showing a 2.3-fold increase in differentiation media and a 1.5-fold increase in proliferation. Additionally, the use of a bioreactor for culture allowed us to establish a constant rate of medium turnover, further supporting sustained cellular activity.

Discussion: Our findings indicate that the culture system designed preserved the structural integrity of the microspheres, and the stiffness of the hydrogel even showed an increase in the presence of cells, which suggested a potential secretion of specific components by the cells. Moreover, the sustained cell viability suggests that the hydrogel does not hinder nutrient entry or gas exchange, further supporting its suitability for our purposes.

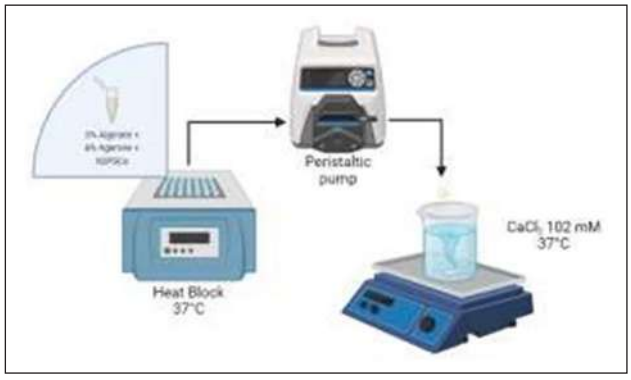

Figure 1. Manufacturing of alginate-agarose microspheres.

References

1. Chang et al, Adv. Healthc. Mater. 10(7), e2001689, 2021.
2. Monaco et al, Front. Bioeng. Biotechnol. 8, 243, 2020.

THE ROLE OF NANOMATERIALS IN THE FABRICATION OF MEDICAL DEVICES

Giuseppe D'Avenio, Carla Daniele, Mauro Grigioni

National Centre for Innovative Technologies in Public Health, Italian National Institute of Health (ISS), Italy

Introduction: The increasing diffusion of nanomaterials (NMs), i.e., materials with at least one external dimension <100 nm, is impacting also the fabrication of medical devices (MDs). The unique properties of materials at the nanoscale are often unexpected, given the corresponding properties that these materials (e.g., gold) present in bulk form.

The remarkable characteristics of nanomaterials (above all, the tunability of their physicochemical properties as a function of their size) are very attractive for biomedical applications, given that it is possible to enhance the biocompatibility of MDs by using NMs.

Besides the theoretical advantages, though, also the associated risks must be carefully considered.

Methods: The principal literature search was performed on the Web of Science Core Collection database. The intersection The intersection of the results pertaining to the keywords "medical device" and "nanomaterial" provided the basis for the analysis of the relevant evidence. The aim was to select the papers which made explicit consideration of MD application(s), in short or long term, of nanomaterials.

The analysis enabled to list the broad areas of application, such as dentistry, orthopedics, etc., without attempting to evaluate the quality of the specific papers in a given area: the low number of the latter's papers would have prevented us from performing a finer-grained analysis.

Not all of the papers from the basic search were found to be useful to give a picture of current nanostructured MDs, for which a proof of principle has been demonstrated. The raw data from the basic literature search have been filtered, discarding non-relevant papers. Other causes for exclusion were insufficient maturity of the application or insufficient focus on application to MDs.

Results: Nine broad application areas have been identified for current (or demonstrably feasible) diagnostic and/or therapeutic applications of nanostructured medical devices. In some of these applications, the release of nanoparticles is explicitly designed (e.g., to improve the antibactericidal properties of the coating of implantable MDs): this approach is somewhat contrasting with the cautionary approach adopted by the Medical Device Regulation (MDR) [1], though, since medical devices incorporating or composed of nanomaterials are categorized under Class III, the highest risk class, if there is a high or medium potential for internal exposure (Rule 19).

Discussion: The MDR reflects the necessity for increased oversight of medical devices containing nanomaterials. Traditionally, ISO 10993 series standards (e.g., [2]) address the biocompatibility and toxicity of biomaterials, but the scope of these standards does not foresee the use of nanostructured materials.

In this regard, ISO published in 2017 a technical report providing guidance for evaluating nanomaterials in MDs [3]. The report highlights that many traditional tests used for evaluating MD biocompatibility may fail in the presence of nano-objects, due to interactions of the latter with dyes used in assays such as MTT, XTT, lactate dehydrogenase, and

dichlorofluorescin. For example, regarding cytotoxicity testing according to ISO 10993-5, up to 14% false increases in viability, induced by the NP-dye reaction in the MTT assay, were observed in ref. [4], with a potential underestimation of toxicity.

As underlined in [3], corroboration of several test results from different methodologies might be required for a scientifically sound interpretation.

A remarkable recommendation for designing a test plan is that "In general, nanomaterials themselves need to be evaluated instead of extracts as usually used when testing biomaterials or medical devices". Nanosized extracts may exhibit physicochemical alterations compared to the original nano-objects within the MD, thus extracting them from a final product can lead to inaccuracies in safety assessment.

The cautious risk classification approach outlined in MDR for nanostructured MDs appears the most appropriate, given the absence of relevant standards and the numerous unresolved research issues.

References

1. Regulation (EU) 2017/745 of the European Parliament and of the Council of 5 April 2017 on Medical Devices, Amending Directive 2001/83/EC, Regulation (EC) No 178/2002 and Regulation (EC) No 1223/2009 and Repealing Council Directives 90/385/EEC and 93/42/EEC (Text with EEA Relevance) (OJ L 117 05.05.2017, p. 1, ELI). http://data.europa.eu/eli/reg/2017/745/oj
2. ISO 10993-1:2018; Biological Evaluation of Medical Devices Evaluation and Testing within a Risk Management Process. ISO:Geneva, Switzerland, 2018.
3. ISO/TR 10993-22:2017; Biological Evaluation of Medical Devices—Part 22: Guidance on Nanomaterials. ISO: Geneva, Switzerland, 2017.
4. Lupu, A.R.; Popescu, T. Toxicol. Vitr. **2013**, 27, 1445–1450

NUMERICAL MODELING TO PREDICT OXYGENATION AND FILTRATION RATES IN A COMBINED OXYGENATOR AND DIALYSIS DEVICE

Imane El Jirari (1), Lisa Prahl Wittberg (1), on behalf of the ArtPlac Research Consortium (2)

1. FLOW, Department of Engineering Mechanics, KTH Royal Institute of Technology, Stockholm, Sweden; 2. HORIZON-EIC-2022-PATHFINDEROPEN-01, Grant agreement ID: 101099596

Introduction: Mortality in premature infant population suffering from severe lung or kidney failure is high. Current treatments are less adapted to neonatal physiology, invasive and have side-effects. The Artificial Placenta (ArtPlac) preclinical project aims to provide a miniaturized assist device providing simultaneous pulmonary and renal support. The model configuration of the lung and kidney assists device (LKAD) will be adopted for either microfluid or hollow-fiber approach. The in-development procedure promises a low invasive support and mortality rates as well as a reduced risk occurrence of lifelong disabilities. Moreover, the innovative umbilical cannulation will provide large bore access.

One aspect of the device development lies in the oxygenation and filtration performance, achieving an efficient gas exchange while keeping resistance within the device low and minimizing device induced complications such as blood clot formation and hemolysis. To assess the computational framework to be applied on the device and associated sensitivity, a preliminary analysis was carried out on a generic geometry, evaluating the influence of methodology on species transport.

Methods: A computational fluid dynamics (CFD) analysis was carried out to mathematically assess the mass transport through membranes between gas or dialysate and blood as well as overall in-device hemodynamic performance. The models were implemented with the commercial Comsol Multiphysics software. A parametric analysis was conducted to assess the sensitivity of physical quantities of interest (related to both hemodynamics and species transport rates) to the inputs, including the influence of blood structural/rheological model, flow unsteadiness (temporal and spatial gradients), fiber arrangement, membrane porosity and species diffusivity. The oxygen transport in blood is governed by convection-diffusion equation:

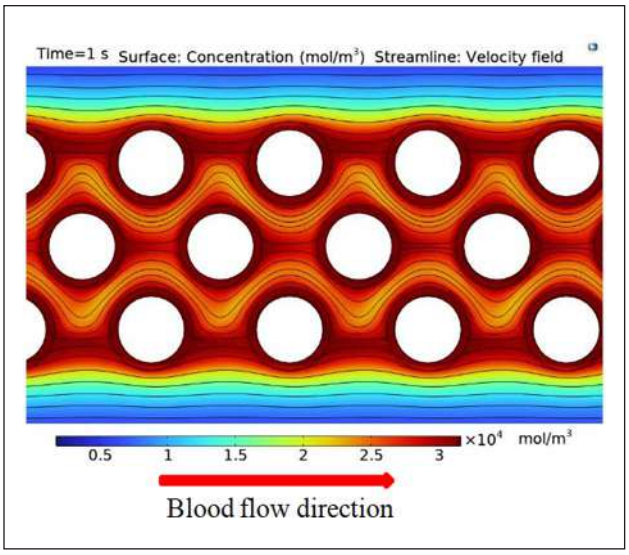

Figure 1. Oxygen concentration distribution in hollow fibre membranes and blood. Oxygen-rich gas enters through the hollow fibres, diffuses through the gas-permeable membrane and into surrounding blood.

$$v \cdot \nabla PO_2 = D_b \cdot \nabla^2 PO_2 \quad (1)$$

where v is blood velocity, PO_2 oxygen patrial pressure and Db oxygen diffusivity in blood. To consider the fraction of oxygen bound to hemoglobin, the effective diffusivity approach first introduced in reference [1] was employed:

$$D_{eff} = \frac{D_b}{1 + 1.34 \frac{c[Hb] dSO_2}{\alpha dPO_2}}$$

where c[Hb] is hemoglobin concentration, α oxygen solubility in blood and the derivative dSO_2/dPO_2 is the slope of the oxygen-hemoglobin dissociation curve.

Results and Discussion: Figure 1 shows oxygen concentration distribution in membrane and in homogeneous blood. The influence of oxygen diffusivity was found to be significant. Indeed, oxygen concentration varied by a factor of two depending on the assigned oxygen diffusivity (i.e. molecular diffusivity *versus* effective diffusivity). The influence of particulate nature of blood was observed to be negligible at the flow scale considered in this geometry.

Further investigations are needed, and will include hematocrit variation, investigation of simultaneous oxygenation and filtration plus varying fiber cross-section shape, found to be a promising approach to optimize mass transfer [2].

References

1. Vaslef et al, ASAIO Journal, 40:990-996, 1994.
2. Ecker et al, Membranes, 11(5):374-389, 2021.

Acknowledgements

ArtPlac is coordinated by Klinikum Nurnberg, Germany and funded by Horizon Europe programme under the European Innovation Council (EIC). Grant agreement ID: 101099596.

DEVELOPMENT OF A LOW-COST, HIGH-FIDELITY SIMULATOR FOR CARDIAC SURGERY

Oskar Leschinsky (1), Clara Großmann, MD (2), Farhad Bakthiary, MD, PhD (1) Kaveh Eghbalzadeh, MD, PhD (1)

1. University Hospital Bonn, Department of Cardiothoracic Surgery, Bonn, Germany 2. University Hospital Cologne, Department of Cardiology, Cologne, Germany

Introduction: The objective of this project was to develop a model of the human heart that is as anatomically and hemodynamically accurate as possible, while maintaining a low investment and maintenance cost. The model can be employed as a simulator for various cardiac surgery operations and offers a life like surgical training ground.

Methods: In order to achieve a low-cost approach and simple reproducibility, only components that are widely available were used. A microcontroller is used to inflate a balloon in the left ventricle of a pig heart. The displacement causes the ventricle to eject simulated blood and visibly 'contract'. The blood is then drained into a reservoir via a tube in the aortic stump. Another balloon simulates the Windkessel effect of the aorta, a pressure sensor measures the aortic pressure and displays it in real time on a monitor. Peripheral resistance can be regulated using a rotary valve in front of a reservoir. Pressure in the air balloon in the ventricle, analogous to inotropy, can be adjusted via a pressure reducer. The compressed air can be supplied by a compressor or a ZGV connection.

Results:

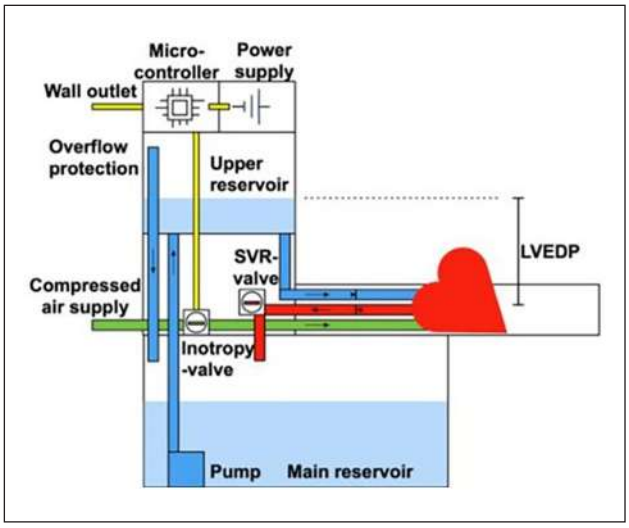

Figure 1. Schematic drawing of the simulator Yellow: Power/ Electronics, Blue: Blood inflow/Red: Blood outflow, Green: Pressured air.

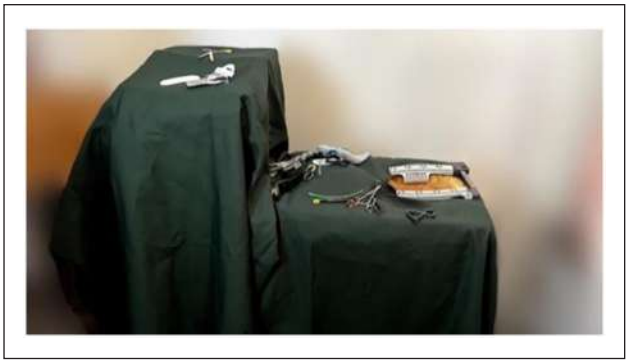

Figure 2. Simulator covered with surgical drapes.

Figure 3. Surgical field, simulated OPCAB procedure, exposed LAD, proximal tourniquet occlusion.

Discussion: This simulator falls within a range of other cardiac surgery simulators. High-fidelity setups such as those previously published create a realistic environment for training using purposely designed hardware and controllers [1, 2].This simulator is our first prototype aiming for the same fidelity and realism and improving upon them by using a working hemodynamic model while utilizing only widely available and affordable parts. So far, it is the first development stage, as we plan multiple additions for an added spectrum of procedures and additional realism during the sessions. The implementation of a cardiopulmonary bypass is the next step as it could enable different kind of cardiac surgeries. As a subsequent phase, the implementation of right heart perfusion would further enhance the level of realism concerning the hemodynamic model. The absence of these features at the current stage limits the simulator's ability to allow trainees to experience a wide variety of cardiac surgery procedures.

Despite these limitations, simulators like ours play a crucial role in skill development and training, but they cannot fully replace hands-on experience in real surgical settings. Moreover, continued refinement and innovation will be essential to bridge the gap between simulation and real-world practice in cardiac surgery training.

References

1. Ramphal PS, Coore DN, Craven MP, Forbes NF, Newman SM, Coye AA, et al. A high fidelity tissue-based cardiac surgical simulator. Eur J Cardiothorac Surg. 2005;27(5):910-6.

2. Reuthebuch O, Lang A, Groscurth P, Lachat M, Turina M, Zund G. Advanced training model for beating heart coronary artery surgery: the Zurich heart-trainer. Eur J Cardiothorac Surg. 2002;22(2):244-8.

WIRELESS-CONTROLLED BIDIRECTIONAL PUMPING SYSTEM FOR ARTIFICIAL ORGANS WITH HYDRAULIC ACTUATION

Simone Onorati (1), Michele Ibrahimi (1), Federica Semproni (1), Stefano Pane (1), Veronica Iacovacci (1), Arianna Menciassi (1)

1. The BioRobotics Institute, Scuola Superiore Sant'Anna, Pontedera (Pisa), Italy

Introduction: Hydraulic soft actuation is often adopted to activate implantable systems like artificial organs, thanks to its intrinsic safety, versatility and power efficiency [1], [2]. However, the associated flow control systems proposed up to now are still far from being implantable, lacking miniaturization, powering from an on-board battery and/or wireless communication with the user [3], [4]. In this work, we introduce a portable, standalone and low-power bidirectional pumping system dedicated to implantable soft robots. A preliminary validation with an artificial urinary bladder is also presented.

Methods: The device consists of three functional blocks (Fig. 1a): an electrohydraulic switch, the electronic circuit and a battery. The switch includes a small DC pump (M200M, TCS Micropumps, UK) and a small DC motor (1512U003SR 324:1, Faulhaber, Germany) connected to a custom camshaft. This can compress four soft tubes (Fig. 1b), allowing thus fluid flow between a reservoir and the soft actuator(s) in both directions, as well as passive flow blocking (retaining the actuators' pressure, *p*). As such, the switch can act at the same time as a set of valves and as a bidirectional pump, by including only two active components. The electronic circuit includes an Arduino Nano 33 BLE controller, which (*i*) activates the pump and the motor via a driver (DRV8833, Texas Instruments, US), (*ii*) stops the flow at a preset *p* threshold by measuring *p(t)* with a digital sensor, and

(*iii*) interacts with a phone app via Bluetooth, receiving commands and providing feedback. A small lithium battery (3.1 Wh, 3.7 V) powers the device.

The performances of the electrohydraulic switch, in terms of flow blocking and tubes' *p* retention by the custom camshaft, were tested by externally pressurizing each one of the four occluded soft tubes with a minimal flow rate (1 mL/min), up to 30 kPa (i.e. twice the pump's maximum *p* of 15.5 kPa), and recording the *p(t)* trend with an external sensor. The device was then employed to actuate a detrusor muscle in an artificial bladder [4] (Fig. 1c). In four voiding tests, the Voiding Efficiency (VE: the % of output water) and the Actuation Time (AT: time to reach the set *p* threshold of 15.5 kPa in the actuators and switch to block mode) were measured.

Results: The occluded soft tubes showed a linear *p(t)* increase during their pressurization, indicating no appreciable losses, and a contained *p* loss (mean of -2.2% from 30 kPa) in the first minute after stopping the flow. The mean VE of the artificial bladder system was 83.6%; this is comparable to the previous work from the authors [4], where the control module was bulkier (140 x 90 x 70 mm vs. 106 x 47 x 36 mm). The mean AT was 38 s (although the total VE was obtained with further pump reactivations, until injecting ~ 40 mL per actuator).

Each switch of flow mode, realized by a 90° rotation of the shaft, consumes ~ 190 mJ = 53 µWh (~ 255 mW for 0.75 s); each actuator filling in the above example, ~ 26.7 mWh (~ 2.53 W for 38 s); in idle mode, the board consumes 12.3 mW (mostly due to the BLE module). The circuit in [4] required instead ~ 4 W while pumping, and ~ 150 mW when idle. In the artificial detrusor case, assuming seven two-way pumping acts (i.e. urinations) of 4 min overall per day, the battery would last 48 hours.

Discussion: Thanks to its reduced size, its low power usage, and its wireless-based design, the proposed device marks the first step towards the feasible implementation of fully implantable hydraulic soft robotic systems.

References

1. D. Zrinscak et al, Prog. Biomed. Eng., 5:012002, 2023.
2. R. Tiwari et al, J. Intell. Mater. Syst. Struct., 23(3):301-312, 2012.
3. M. A. Bell et al, Adv. Intell. Syst., 4:2100094, 2022.
4. G. Casagrande et al, Soft Robot., 10(2):269-279, 2023.

SUCCESS PREDICTION OF FLOW DIVERTER TREATMENT FOR INTRACRANIAL MEDIA BIFURCATION ANEURYSMS

Janneck Stahl (1,2), Matthias Gawlitza (3), Philipp Berg (1,2)

1. Research Campus STIMULATE, University of Magdeburg, Magdeburg, Germany; 2. Chair in Healthcare Telematics and Medical Engineering, University of Magdeburg, Magdeburg, Germany; 3. Department of Neuroradiology, University Clinic Leipzig, Leipzig, Germany

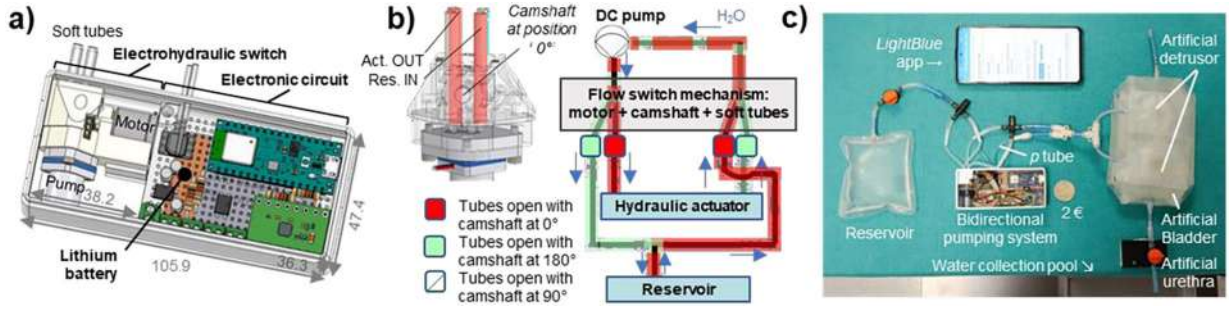

Figure 1. The bidirectional pumping system for implantable applications. a) Design overview. The whole device weights 120 g. b) Concept of the electro-hydraulic switch. c) Device application to support an active artificial urinary bladder.

Introduction: The treatment of intracranial aneurysms (IA) using flow diverters (FD) is associated with high rates of complete aneurysm occlusion. Particularly for side wall aneurysms, this was proven in clinical and technical hemodynamic studies [1,2]. However, there is still an active debate regarding its value in the treatment of bifurcation IA [3]. Despite prior clinical indication, there are cases in which the IA with implanted FD remains almost unaffected long-term after treatment. The aim of the study is to examine possible hemodynamic causes for treatment failure on the basis of retrospective cases and thus to predict the success of FD treatment.

Methods: Eight bifurcation IA patients treated with a state-of-the-art FD device (p48 HPC, phenox GmbH, Bochum, Germany) are included. Four patients show successful treatment whereas four demonstrated no occlusion of the IA after follow-up. Patient-specific surface models are extracted based on pre-interventional 3D digital subtraction angiography. Utilizing an in-house fast virtual stenting approach [4], post-interventional treatment stages are virtually created. Image-based blood flow simulations are conducted allowing the comparison of pre- and post-interventional hemodynamics of both failed and successfully treated IA.

Results: The hemodynamics stresses in the IA sac are reduced for all cases despite of the treatment success. Inflowing blood causing higher wall shear stresses at the inflow zone are reduced (see Figure 1). The flow diversion effect indicated by the ostium inflow and the inflow concentration index is reduced almost similar in both cohorts. However, the clinically failed cases demonstrate lower shear rates caused by reduced flow velocities in the bifurcating branch without FD. Successful cases indicate higher shear stresses in the non-stented branch regardless of the treatment (see Figure 1).

Discussion: This study investigates hemodynamic changes in IA treated with FD devices. In a retrospective analysis clinically successful and failed cases are collected. Image-based blood flow simulations may indicate hemodynamic differences in the bifurcation branches, which are not captured in a clinical setting so far. This could support the predictability of clinically failed treatments for bifurcation IA using FD.

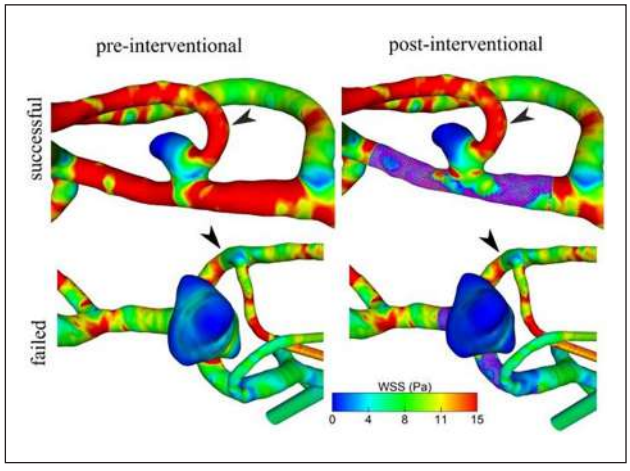

Figure 1. Qualitative hemodynamic comparison of pre-and post-interventional stages of an exemplary successful and failed case. The wall shear stress at the inflow zone is reduced due to the deployed FD (purple) for both cases. The arrows indicate lower shear stresses in the bifurcation branches without FD in the failed case.

References

1. Lv et al., Neuroradiol J, 29(1):66-71, 2016.
2. Stahl et al., Comput Biol Med, 156:106720, 2023.
3. Michelozzi et al., J Neurosurg, 131(6):1751-1762, 2018.
4. Berg et al., Elsevier, 371–411, 2017.

Acknowledgements

This work is partly funded by the Federal Ministry of Education and Research within the Forschungscampus STIMULATE (grant no. 13GW0473A) and the German Research Foundation (SPP2311, project number: 465189657).

FIBROUS SUBSTRATES FOR CORNEAL REGNERATION STIMULATION WITH ENHANCED UV RESISTANCE

Roksana Kurpanik *[1], Roksana Zielińska*[3], Natalia Wróbel*[3], Dominika Wójtowicz*[2], Ewa Stodolak-Zych*[1]

*[1]*Department of Biomaterials and Composites, AGH University Of Krakow, Poland*
*[2]*Department of Ceramics and Refractories, AGH University Of Krakow, Poland*
*[3]*Faculty of Electrical Engineering, Automatics, Computer Science and Biomedical Engineering, AGH University Of Krakow, Poland*

Background: Factors such as trauma, infection or oxidative stress caused by overexposure to sunlight are reported as the main factors disrupting proper signaling between corneal cells, inhibiting its regeneration [1]. Therefore, it is crucial that the fibrous substrate intended for its regeneration provides not only support for migrating corneal limbal stem cells, but also has high antibacterial and UV-protective properties. There are a number of modifiers that meet these criteria, however, not all of them provide high transparency. Both carbon materials and amino acids, due to their high biocompatibility, are used to reduce implantation complications in case of various eye implants. They also do not affect the transparency of the substrate modified with them and absorb light in the UV range. However, their ability to protect the eye from harmful external environmental factors (including bacteria and UVR), still remains unexplored.

The aim of the study was to obtain electrospun core-shell fibers modified with the addition of carbon dots functionalized with amino acids and to evaluate them for antibacterial properties and light transmission in the UV range.

Materials & Methods: Carbon dots (CDs) were prepared using the microwave method. Citric acid and urea (in the ratio of 1:1) were chosen as precursors for the carbon dots, which were dissolved in 50µl of distilled water. Then, they were placed in a microwave oven setting maximum power and a time of 2min, until a brown liquid was obtained. The dots were then functionalized by adding 10mg of an amino acid (cysteine, tyrosine, tryptophan) to 1 ml of CDs solution and incubating at 37°C.for 24 hours. Then, the core-shell fibers based on PCL-PVP were prepared using the coaxial electrospinning method, described in the previous work [2]. Carbon dots were used as a fiber core modifier. Characterization of the CDs included measurements of particle size using the DLS method (Zetasizer Nano ZS, Malvern) and morphology (AFM, TopoMetrix Discoverer TMX 2000 system). Amino acids were characterized for UV light transmission (UV-Vis, Shimazu) and antioxidant properties using DPPH protocol. The nonwovens microstrucuture was observed under scanning electron mcroscope (NOVA NanoSEM 200, FEI), translucency (UV-Vis, Shimazu) and antimicrobial properties by diffuse-disk method on the *E.coli* and *S.aureus* strains.

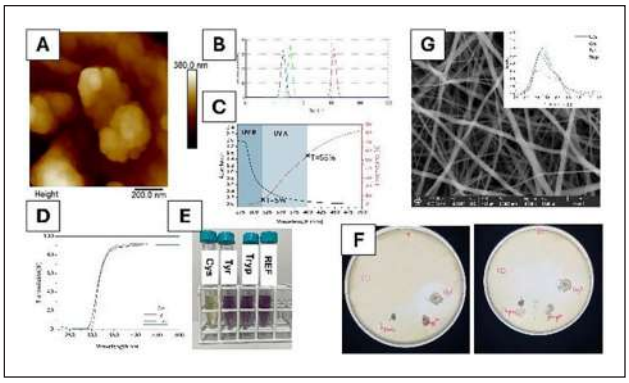

Figure 1. AFM scan (A), size distribution by volume (B) and absorption and transmission spectra of CDs (C), transmission spectra (D) and antioxidant activity (E) of amino acids, antibacterial activity of the functionalized CDs (F), nonwoven microstructure and fibers size distribution (G).

Results and Discussion: Tests conducted showed the presence of carbon dots with a bi-modal distribution -1 -10nm and about 100nm (Figure 1A,B). The obtained dots showed high UVR absorption in the UVB range and partial absorption in UVA (Figure 1C). On the other hand, in the case of amino acids, both UV filter effect and antioxidant activity were observed (Figure 1D,E). Functionalization with amino acids has given the dots bactericidal qualities -especially against both bacteria (Figure 1D). Further encapsulation of the functionalized carbon dots contributed to nano-and submicrometer-sized electrospun fibers in the 0.2 -1.0um range (Figure 1G).

Conclusions: The study showed the high potential of bio-functionalized carbon dots as a modifier of substrates for corneal regeneration. The results obtained indicate high UV absorption, as well as effective antibacterial activity against *E.coli* and *S.aureus* strains. In addition, nonwoven fabrics modified with these additives show high transparency in the visible range, making them an suitable carrier for CDs.

References

1. Notara, M. et al. Sci Rep 2018, 8 (1), 1–12.
2. Kurpanik R. et al. J Mechan Behavior of Biomed Mat 2024 152 art. no. 106437, 1–19.

Acknowledgements

This work was supported by "Initiative of Excellence – Research University" (IDUB) grant ID 4204.

COMPUTATIONAL FLUID DYNAMICS SIMULATION OF 3RD GENERATION ROTODYNAMIC BLOOD PUMPS UNDER REALISTIC DYNAMIC OPERATING CONDITIONS

Bente Thamsen (1), Rosmarie Schöfbeck (1), Simon Klocker (1,2), Marko Grujic (1), Theodor Abart (1), Adrian Wisniewski (3), Bernhard Semlitsch (2), Daniel Zimpfer (1), Marcus Granegger (1)

1. Christian Doppler Laboratory for Mechanical Circulatory Support, Department of Cardiac Surgery, Medical University of Vienna, Austria; 2. Department of Fluid Flow Machinery, Technical University of Vienna, Austria; 3. Berlin Heart GmbH, Berlin, Germany.

Introduction: Rotodynamic blood pumps (RBPs) provide support that directly depends on the pulsatile hemodynamic conditions set by the cardiovascular interface. Although designed for a single static operating point, these pumps are operated in a highly transient manner. Computational Fluid Dynamics (CFD) simulations are successfully used to investigate RBPs in static conditions, but for dynamic operation there is no standard methodology with a broad range of setups used so far [1-3]. Aim of this study was to establish a CFD framework to adequately and efficiently capture the realistic fluid dynamics within an RBP working in tandem with the native heart through thorough experimental validation using a hybrid mock loop [4].

Methods: Using two different RBPs, the Heartmate 3 (HM3) for adult patients and a functional model of a next generation RBP (NGP) in pediatric use, three different clinical cases (high/low pulsatility adult, typical pulsatility pediatric) were investigated. Measured data from the hybrid mock loop were translated into numerical models of the pumps and their peripheries [4, 5]. In the simulations, fluid density and viscosity as well as a pulsatile inlet mass flow were specified based on the experiments (fluid: 1120kg/m³ density and 3.5mPas dynamic viscosity). To identify an appropriate setup, the effects of different CFD settings (time step size, simulation of rotation, turbulence model) on the results were analyzed for the HM3. The computed dynamic pressure-flow behavior for both pumps was validated on the basis of the experimental results. In addition, the influences of surface roughness and inflow conditions were investigated experimentally.

Results: As shown in Figure 1, dynamic pressure-flow loops could be qualitatively replicated with CFD for both pumps in typical conditions (NGP: RMSE=5.19mmHg; HM3: RMSE=8.34mmHg). For the HM3, the pressures were widely overpredicted. The Frozen Rotor scheme showed a substantial dependence on impeller position, but the Mixing Plane model allowed a similarly good prediction (RMSE=8.15mmHg) of global hydraulic performance as the Sliding Mesh model. Consideration of turbulence did not influence the global results. Surface roughness in the volute casing had no impact on the measured pressures.

Discussion & Conclusion: We developed a framework to capture the realistic fluid dynamics within two different RBPs at three different clinically relevant, pulsatile operating conditions. In conducting such

Table 1. Investigated setup parameters.

Time step	Rotation	Turbulence
2°, 4°, 8°, 16°	Sliding Mesh, Mixing Plane, Frozen Rotor	k-omega SST, laminar

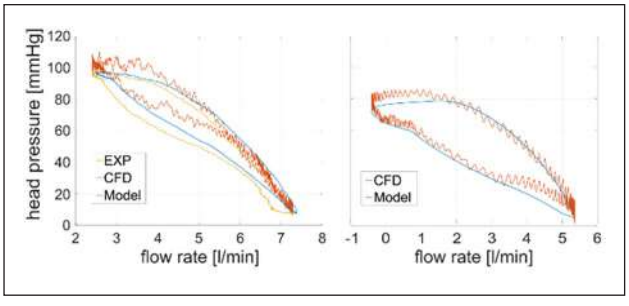

Figure 1. Dynamic pressure-flow loops. Left: HM3: data from experiment, CFD and numerical model; Right: NGP numerical model vs. CFD.

dynamic simulations, it is crucial to meticulously validate the accuracy of the results. While using Sliding Mesh enables the analysis of local flow features within a cardiac cycle, Mixing Plane can be used to describe global performance. The deviations for the HM3, especially in the high flow regime, may stem from the magnetic levitation system, which involves a non-fixed rotor position, that is not reflected in CFD.

References

1. Wiegmann et al, Artif Organs, 43(4), 2019.
2. Chen et al, Int J Numer Method Biomed Eng, 34(2), 2018.
3. Song et al, J. Biomech. Eng. 126:180–7, 2004.
4. Bender et al, IEEE Trans Biomed Eng, online, 2023.
5. Boes et al, IEEE Trans Biomed Eng, 66(6):1618-27, 2019.

Acknowledgements

The financial support by the Austrian Federal Ministry of Labour and Economy, the National Foundation for Research, Technology and Development and the Christian Doppler Research Association is gratefully acknowledged. The computational results presented have been achieved using the Vienna Scientific Cluster (VSC).

STUDYING HEMODYNAMIC SUPPORT DURING LUNG TRANSPLANTATION IN AN ANIMAL MODEL: DO WE NEED THE MECHANICAL PUMP?

Michaela Orlitová(1), Dieter Van Beersel(1), Anna E Frick(1), Kristof Van de Voorde (2), Karlien Degezelle(2), Joachim Hellinck(1), Melanie Nolmans(1), Xin Jin(3), Bart M Vanaudenaerde(3), Robin Vos(3), Dirk E Van Raemdonck(3), Laurens J Ceulemans(3), Piet Claus(1), Arne P Neyrinck (1), Tom Verbelen (1)

1. Department of Cardiovascular Sciences, KU Leuven, Leuven, Belgium; 2. Department of Cardiac Surgery, division perfusion, UZ Leuven, Leuven, Belgium; 3. Department of Chronic Diseases and Metabolism, Laboratory of Respiratory Diseases and Thoracic Surgery (BREATHE), KU Leuven, Leuven, Belgium

Introduction: The gold standard for intraoperative hemodynamic and respiratory support during sequential single-lung transplantation (SSLTx) is veno-arterial extracorporeal membrane oxygenation (VA-ECMO). It is used to prevent right ventricular (RV) failure and severe pulmonary ischemia-reperfusion injury (IRI). However, its use is not risk free: blood

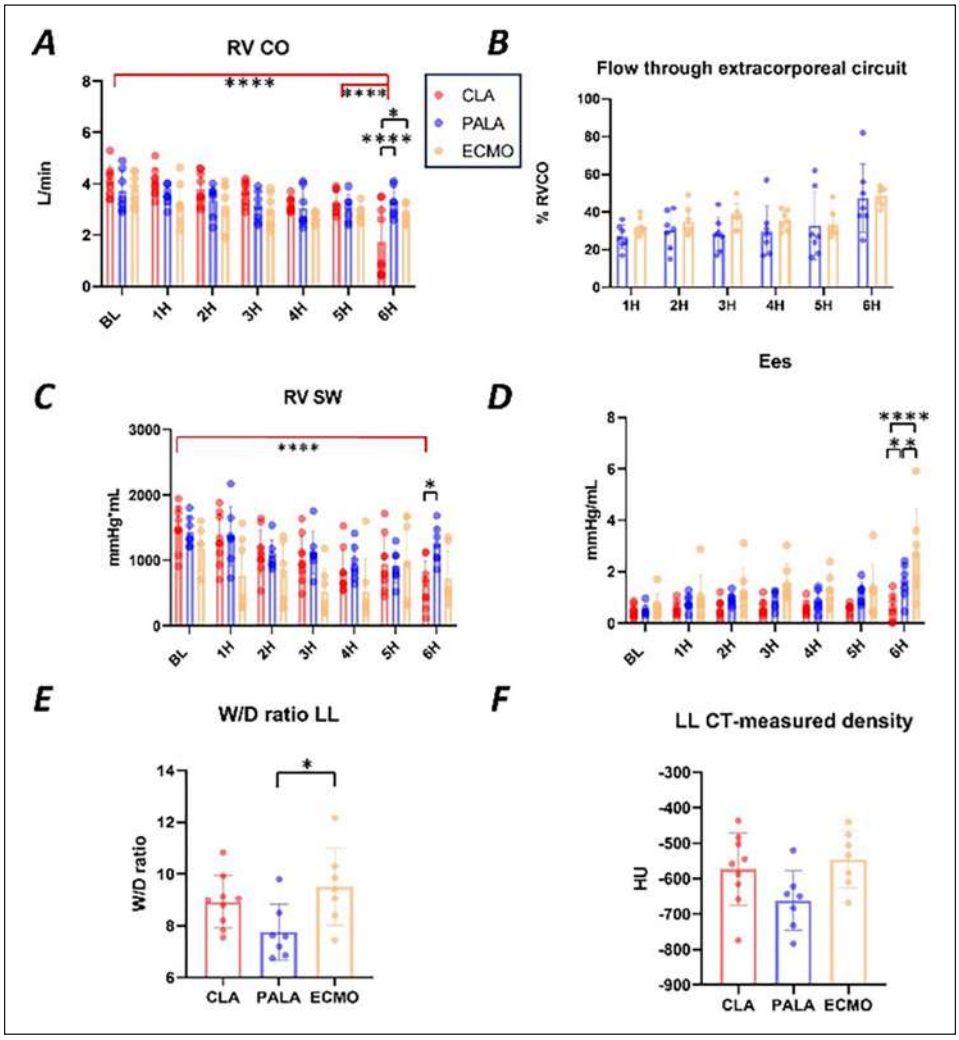

Figure 1. RV CO, right ventricular cardiac output; SW, stroke work; Ees, end systolic elastance; W/D wet-to-dry; LL, left lung; CT, computed tomography; HU, Hounsfield units.

activation and trauma, cannulation complications, unclear association with incidence of severe primary graft dysfunction. We aimed to compare traditional VA-ECMO with a novel approach, using a pumpless artificial lung as a shunt between pulmonary artery (PA) and left atrium (LA), in our porcine model simulating hemodynamics of SSLTx.

Methods: The left lung (LL) hilum was clamped in situ for 3 hours (LL ischemia, 1H – 3H) and reperfused for 2 hours (4H – 5H). Consequently, the contralateral non-ischemic lung was clamped for 1 hour (6H), creating the hemodynamic and respiratory challenge. In the clamping group ([CLA], n=9), no extracorporeal life support (ECLS) was used. In the intervention groups an oxygenator (Hemovent GmbH, Aachen, Germany) was inserted between PA and LA ([PALA], n=7); or a centrally cannulated VA-ECMO was placed ([ECMO], n=7). ECLS was initiated when LL was clamped. Conductance catheter (CC) was placed in RV. We measured: CC data, mean PA pressure (mPAP), RV cardiac output (CO), ECLS circuit flow, LL wet-to-dry (W/D) ratio and LL computed tomography (CT)-measured density. One-or Two-way ANOVA were used.

Results: RV failure developed in 5/9 animals in [CLA], but not in [PALA] or [ECMO]. There was no difference in mPAP between groups. RVCO was higher at 6H in [PALA] and [ECMO] vs. [CLA] (fig. 1A; p=0.0001, p= 0.04, respectively). There was no difference between ECLS circuit flow between [PALA] and [ECMO] (fig. 1B; p=ns). RV stroke work decreased significantly in [CLA] at 6H compared to baseline, and was at 6H higher in [PALA] vs. [CLA] (fig. 1C p=<0.0001, p=0.0396, respectively). RV end-systolic elastance at 6H was higher in both [PALA] and [ECMO] compared to [CLA] (fig. 1D, p=0.033, p=<0.0001), and was higher in [ECMO] vs. [PALA] (p=0.0167). W/D ratio was lower in [PALA] vs. [ECMO] (fig. 1E, p= 0.0315), a same trend was observed in LL CT-density (fig.1F p=0.0631).

Discussion: Both PALA and ECMO prevented RV failure in our animal model. Pumpless PALA strategy is non-inferior to traditional ECMO configuration in providing sufficient hemodynamic support. Avoiding passage of blood cells through a extracorporeal pump and using a shorter extracorporeal circuit might even be protective towards lungs suffering from IRI, as reflected by our results. Further hemodynamic, tissue and molecular analyses should clarify this relationship.

A JOURNEY FROM BECOMING A DIABETES TYPE 1 PATIENT TO REALIZING A CE-MARKED ARTIFICIAL PANCREAS

Robin Koops (1,2)

1. Diabetes type 1 patient, Diabetes Fund, the Netherlands; 2. CEO INREDA Diabetics, the Netherlands

Introduction: This abstract unites 2 perspectives: from a patient and from an inventor/entrepreneur. When diagnosed with diabetes type 1, my quality of life drastically decreased. As a technologist I wanted to understand what was happening to me. And the more I started to understand the mechanisms of my disease (helped by wonderful medical doctors), the more I got convinced there should be a way to replace the natural blood glucose regulation of the pancreas with an artificial device. As I used to run a small firm designing and building custom machines, I decided to use my engineering & entrepreneurial skills to design & build an AP (starting in my garage).

Methods: From 2004 on, I built several AP iterations, starting with a laptop-controlled setup. As a patient I could experiment on myself, which facilitated quick iterations. This resulted in a CE-marked bihormonal (insulin & glucagon) fully closed-loop (FCL) automated AP. We assessed long-term performance & safety in a 1-year, multicentre (8 Dutch outpatient clinics), prospective, single-arm intervention trial in adults (18–75y) with type 1 diabetes who, as a baseline, had used flash or continuous

Figure 1. The belt clip-on artificial pancreas system.

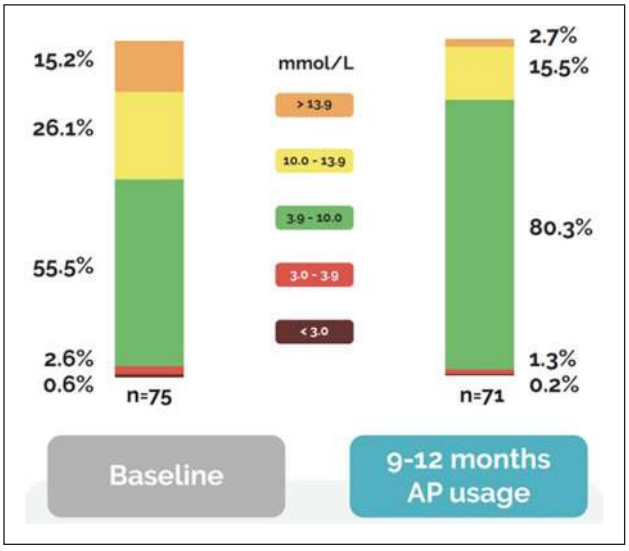

Figure 2. Left the ≥ 3 months baseline. Right the results observed after 9-12 months AP usage in daily life.

glucose monitoring ≥ 3 months. Primary endpoint was time in range (TIR; glucose concentration 3.9–10.0 mmol/L) after 1 year, also Problem Areas in Diabetes (PAID) questionnaires quantified the patient burden [1]. Dutch Trial Register study ID: NL9578.

Results: Time *in* Range (TIR, desired) improved from 55.5% to 80.3%, while Time *below* Range (TBR, to be avoided) was reduced from 3.2% to 1.5%. Time *above* Range (TAR, also to be avoided) was reduced from 41.3% to 18.2%. See also Fig. 2. PAID-scores strongly improved from 30.0 (IQR 18.8–41.3) at preintervention to 10.0 (IQR 3.8–21.3; p<0.0001) at 12 months.

Discussion: This 1-year trial demonstrates that the tested bihormonal FCL system facilitated very good glycaemic control in a real-world daily-life setting and could be safely used by patients who completed 1 year of treatment. The FCL system offers a strong potential to relieve individuals with diabetes type 1 from constantly making treatment decisions and burdensome carbohydrate counting.

Reference

1. AC van Bon et al. Bihormonal fully closed-loop system for the treatment of type 1 diabetes: a real-world multicentre, prospective, single-arm trial in the Netherlands. Lancet Digit Health 2024; 6: e272–80. Published Online March 4, 2024. https://doi.org/10.1016/S2589-7500(24)00002-5

Acknowledgements

The study was funded by Inreda Diabetic. I thank all participating diabetes care teams for their support, and health insurer, Menzis (Enschede, Netherlands), for reimbursing our FCL treatment as regular care. I cherish all study participants for their valuable contribution. I thank the Boerhaave museum in Leiden, that put my artificial pancreas on display next to the artificial kidney of Dr. Kolff. And special thanks to my wife Irene for supporting me throughout this demanding journey.

ASSUMPTION-RELATED SENSITIVITY ANALYSIS IN A FLUID-STRUCTURE INTERACTION STUDY OF AN ARTERIOVENOUS FISTULA.

Daniel Jodko (1, 2), Tracie Barber (2)

1. Lodz University of Technology, Poland; 2. University of New South Wales, Australia

Introduction: Since the two-way coupled fluid-structure interaction (FSI) methodology has become a widely accepted numerical tool for solving biomedical engineering problems, several questions have arisen regarding the assumptions that should be made when using FSI [1]. This study focused on the assumption-related sensitivity FSI analysis of an arteriovenous fistula (AVF) case representing the widely accepted vascular access for hemodialysis, in which highly disturbed non-physiological blood flow is observed and mutual fluid-wall interaction is unneglectable [2].

Methods: Important assumptions playing a critical role in FSI simulations were analyzed: 1) damping of loose connective tissue (LCT) embedding the AVF vasculature, 2) Newtonian/non-Newtonian blood rheology, 3) outlet pressure conditions and dealing with pressurization phase; 4) compliance of LCT; 5) compliance of blood vessel walls.

Results: The spatial and temporal distributions of hemodynamic parameters (fluid domain) and stress, strain, and deformation (structural domain) obtained for different settings were compared. Fig. 1 shows the influence of the magnitude of damping on the maximal and averaged wall displacement. Dealing with the pressurization phase significantly affected WSS (fig. 2), however, correct coping with initial undesirable deformation provided similar WSS as rigid-walled simulation. The choice of material properties considerably influenced wall extension and resulting hemodynamics (e.g. turbulence kinetic energy).

Discussion: All of the investigated assumptions affected the temporal quantitative results to some extent. 1) Lower damping may lead to wall vibrations (fig. 1); 2) As for high shear strain the Newtonian and non-Newtonian models overlap, blood rheology played a minor role here; 3) As data concerning the geometry of vasculature are acquired in the pre-stressed state, correct coping with the pressurization phase is necessary;

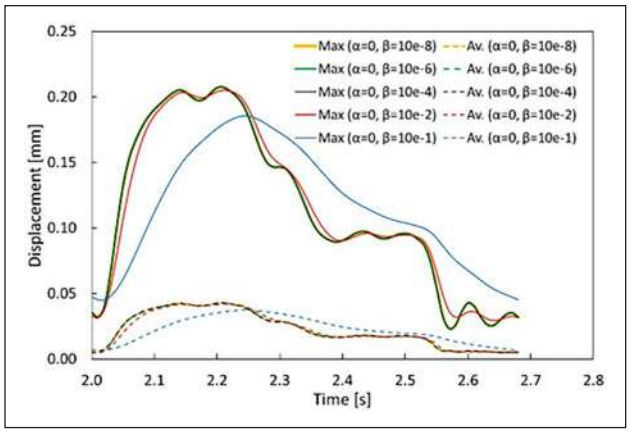

Figure 1. Influence of cushioning effect of LCT (modelled with a wide range of Rayleigh damping coefficients) on the maximum (solid lines) and average wall displacement (dashed lines).

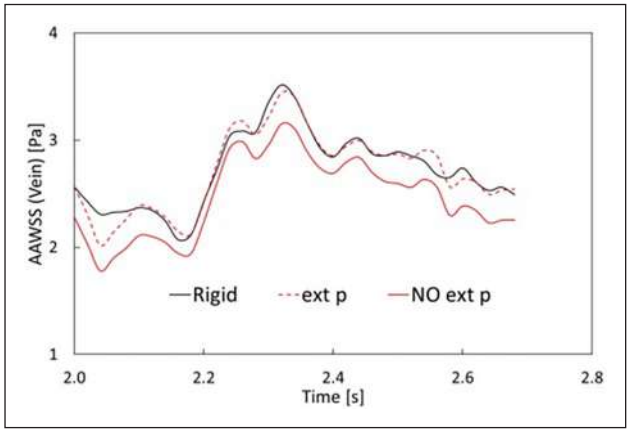

Figure 2. AAWSS determined in the AVF with the rigid-walled simulation and the FSI approach with (ext p) and without (NO ext p) coping with the pressurization phase.

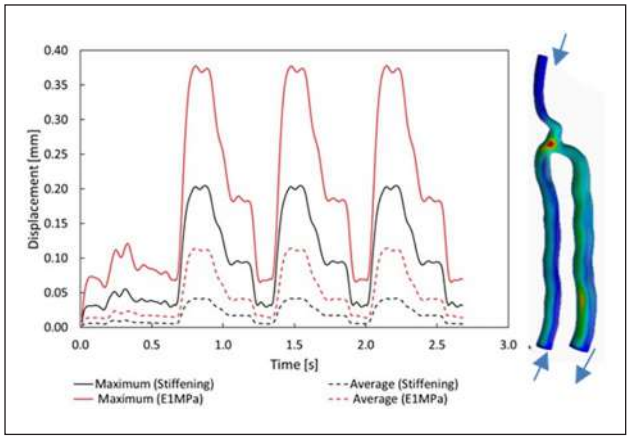

Figure 3. Wall displacement for the pressure peak for different material properties defining venous wall.

4&5) The total wall compliance resulting from the elasticity of LCT and material properties of tissue remains unknown but significantly affects wall extension and temporal progression of hemodynamic parameters. However, properly performed FSI provides comparable time-averaged results as the rigid wall approach that has to be considered due to the high computational cost of FSI.

References

1. Jodko et al., Int. J. Numer. Method. Biomed. Eng., 2022.
2. Bozzetto et al., Cardiovasc. Phys. Eng. Sci. Med. 47(1):187-197, 2024.

Acknowledgements

This project was supported by the Bekker program from the Polish National Agency for Academic Exchange.

ARTERIOVENOUS FISTULA MATURATION – A FLUID-STRUCTURE INTERACTION FOLLOW-UP STUDY.

Daniel Jodko (1, 2), Tracie Barber (2)

1. Lodz University of Technology, Poland; 2. University of New South Wales, Australia

Introduction: Arteriovenous fistula (AVF) is a widely accepted vascular access in haemodialyzed patients. AVF is formed by suturing the patient's artery and vein. Creating such an artificial connection (anastomosis) is followed by a maturation process (MP) associated with significant hemodynamic changes. MP is crucial, however, 20-60% of newly created AVFs fail to mature which is associated with the mutual interaction of non-physiological blood flow and AFV vasculature [1]. This bidirectional fluid-structure interaction (FSI) study addresses blood flow through the maturing AVF. This extends the findings obtained in a preliminary study based on rigid wall simulations [2].

Methods: A single AVF was followed up for 15 weeks and examined 1.5 years after surgery. Geometric and flow data were collected using the safe ultrasonic methodology described in [2]. Velocity curves were used as inlet boundary conditions. Blood pressure pulsations were modelled. The stiffness of the artery, suture, and vein was varied and the stiffening of the venous wall was modelled over time. The mechanical response and attenuation of the loose connective tissue surrounding the AVF were taken into account (Fig. 1).

While obtaining geometric data, the patient's vascular system is subjected to initial stress. To compensate for unwanted deformations caused by pressure, external pressure was applied. Blood was treated as a non-Newtonian fluid. The SST turbulence model was used.

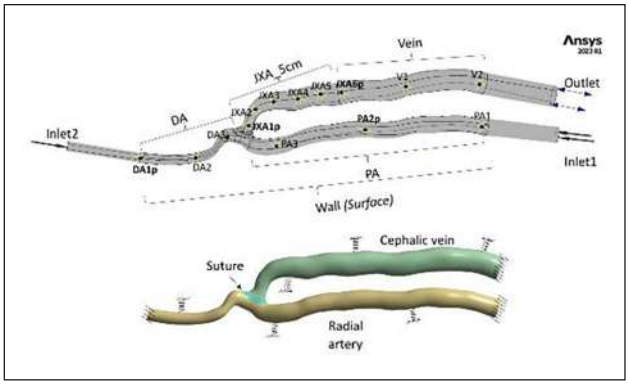

Figure 1. Fluid and wall of the fully matured AVF.

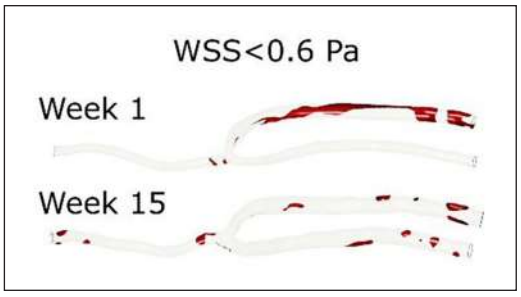

Figure 2. Low-WSS zones (max outflow).

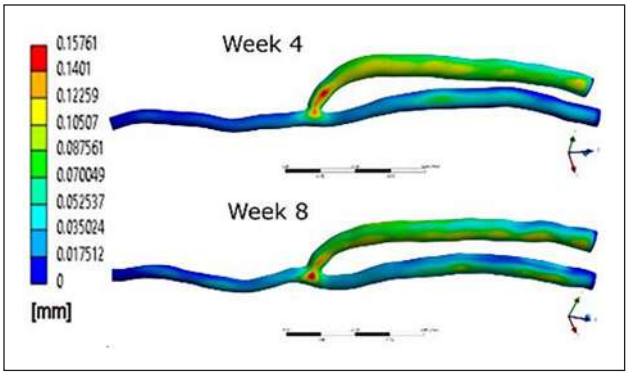

Figure 3. Migration of maximal deformation zone.

Results: The FSI methodology allowed us to take into account the interaction of blood flow and blood vessel walls. In the third cardiac cycle, temporal hemodynamics, wall deformation, and von Mises stress were analyzed. Changes in time-weighted parameters were monitored within the maturation and later. The two combining arterial blood streams generated two opposing rotating

vortices at the anastomosis, increasing the local blood velocity and lowering the blood pressure throughout the MP process. Blood flow disturbances were visualized with coherent structures. Large fluctuations in blood vorticity, shear strain, and TKE were found in the JXA region (Fig. 1) where peak values of these parameters were determined. Extreme WSS>20 Pa was present near the anastomosis over the entire cardiac cycle at every stage of the MP. The absence of stagnation, associated with sufficient washout, was confirmed by small zones occupied by low WSS (<0.6 Pa) covering 10% of the entire vasculature for a short time (Fig. 2). Changes in time-averaged WSS were monitored in all parts of the AVF.

The largest wall deformation (0.277 mm) was found in the JXA in 1st week due to the highest compliance of the venous wall. After 4 weeks of venous stiffening, the maximal extension zone moved to the artery (Fig. 3).

Discussion: Blood flow disturbances occurred at all stages of MP. Extreme WSS increases the risk of internal remodelling, but stenosis has not developed within 1.5 years. The studied AVF, due to continuous washout, was a well-functioning fistula without thrombosis. The deformation of the wall depends on the MP stage.

References

1. Bozzetto et al., Cardiovasc. Phys. Eng. Sci. Med. 47(1):187-197, 2024.
2. Colley et al., Biomech. Model. Mechanobiol., 21:1217– 1232, 2022.

Acknowledgments

This project was supported by the Bekker program from the Polish National Agency for Academic Exchange.

BLOOD SUBSTITUTE FLUID FOR EXPERIMENTAL FLOW VISUALIZATION IN INTRACRANIAL ANEURYSMS.

Christina Maria Winkler (1,2), Gesine Hentschel (1,2), Marc Müller (1,2), Philipp Berg (3,4), Péter Kováts (5), Katharina Zähringer (5), Florian Rummel (6), Birgit Glasmacher (1,2)

1. Institute for Multiphase Processes, Leibniz University Hannover, Germany; 2. NIFE – Lower Saxony Center for Biomedical Engineering, Implant Research and Development, Hannover, Germany; 3. Research Campus STIMULATE, Otto-von-Guericke-Universität Magdeburg, Germany, 4. Chair in Healthcare Telematics & Medical Engineering, Otto-von-Guericke-Universität Magdeburg, Germany; 5. The Laboratory of Fluid Dynamics & Technical Flows, Otto-von-Guericke-Universität Magdeburg, Germany; 6. NETZSCH-Gerätebau GmbH, Selb, Germany
e-Mail: winkler@imp.uni-hannover.de

Introduction: In order to investigate blood flow in brain aneurysms, cerebral hemodynamics are modelled using computational fluid dynamics (CFD) and validated with experimental in vitro flow tests, in particular using particle image velocimetry (PIV) [1,2]. Since blood is intransparent, the laser light can only penetrate a few micrometers into the boundary flow. Thus, it is unsuitable for PIV measurements. The aim is to develop PIV-compatible blood substitute fluids that simulate the multiphase nature of blood (blood cells and blood plasma) and adapt rheologically to blood.

Methods: The artificial erythrocytes (beads) are modelled with a microfluid systems (MKS) aiming for a diameter of 7 µm and a biconcave shape. The continuous phase is olive oil, the disperse phases are the hydrogel solutions. The beads consist of the natural hydrogel agarose and the photopolymer NOA60 [3]. In addition, PIV seeding particles (Polyamid spericals) are integrated into the beads to make them visible during the PIV measurements. The influence of fluid flow of the continuous and disperse phase on the diameter size of the beads and their monodispersity are investigated. The bead shape is formed by the flat design of the MKS channels (0.5 x 400 mm) [3]. The generated beads are separated from the oil by washing and sinking and finally transferred to a 36% (v/v) glycerol-water mixture. The visibility of the beads in the blood substitute fluids is analyzed in initial PIV experiments.

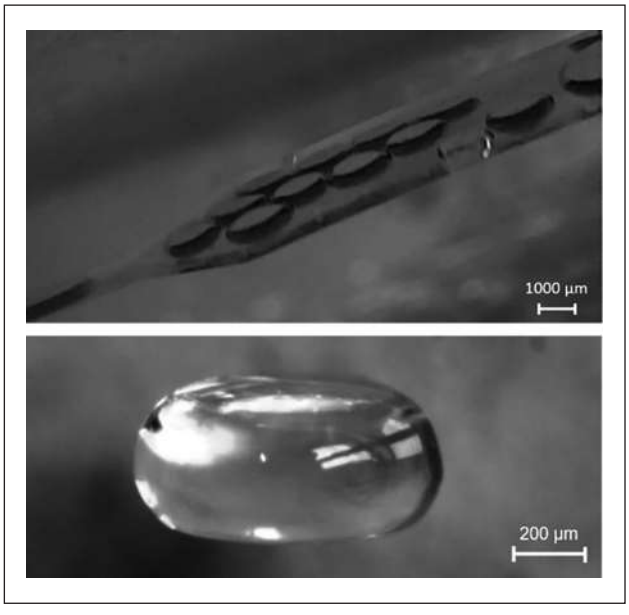

Figure 1. Light microscopic images of the synthesized disc-shaped Agarose beads in MKS (above) and a disc-shaped NOA60 bead (below).

Results: Several blood substitute fluids were successfully produced, including artificial plasma from a glycerol-water mixture, mixed with spherical and disc-shaped agarose beads as well as disc-shaped NOA60 beads. The smallest beads show diameters of up to 29 µm at a volume flow rate of 70 ml/h. Disc-shaped beads can be successfully synthesized with the flat channel structure (cf. fig. 1). The developed blood substitute fluids can be used for PIV measurements for 24 days with the agarose beads and for several months with the NOA60 beads. Initial PIV measurements showed that the agarose beads could only be tracked using the modified measurement method called shadow imaging.

Discussion: The results show that multiphase blood replacement fluids could be successfully developed for PIV measurements. The size and quantity of the artificial erythrocytes produced will be optimized in further work. The blood replacement fluids can be used for future studies to investigate hemodynamics in brain aneurysms.

References

1. C. Roloff, P. Berg. “Effect of flow diverter stent malposition on intracranial aneurysm hemodynamics-An experimental framework using stereoscopic particle image velocimetry”. PLoS One, vol. 17, no. 3., 2022. DOI: 10.1371/journal.pone.0264688.
2. C.M. Winkler, A. I. Kuhn, G. Hentschel, B. Glasmacher, “A review on novel channel materials for Particle Image Velocimetry measurements -Usability of hydrogels in cardiovascular applications,” Gels, vol. 8, no. 8, 2022. DOI: 10.3390/gels8080502.
3. D. Dendukuri, K. Tsoi, T. A. Hatton und P. S. Doyle, “Controlled synthesis of nonspherical microparticles using microfluidics,” Langmuir, vol. 21, no. 6, pp. 2113–2116,
4. 2005. DOI: 10.1021/la047368k.

Acknowledgements

The authors would like to thank the “Caroline Herschel Program” of the Equal Opportunities Office at Leibniz University Hannover for the financial support.

BIOMECHANICAL INVESTIGATION: COMPARISON OF YARN MATERIALS IN TUBULAR FABRICS FOR USE AS VASCULAR PROSTHESES WITH INCREASED COMPLIANCE

Pauline Riedl (1), David Wienen (1), Thomas Gries (1)

1. Institut für Textiltechnik, RWTH Aachen University, Aachen, Germany

Introduction: The development of innovative synthetic vascular prostheses is crucial to face challenges based on the rising numbers of cardiovascular diseases worldwide. The main cause for cardiovascular diseases is arteriosclerosis, which can lead to severely impaired blood vessels. These can be treated with various invasive and non-invasive treatment methods, such as medication, angioplasty and surgical interventions which include stent insertion, vascular replacements, or bypass procedures. However, there is a growing need for appropriate synthetic options based on the shortcomings of autologous vascular

grafts, including limited availability, potential morbidity at the donor site, and the need for additional surgical sites.

Synthetic grafts have proven effective for medium-to large-diameter vessels, but encounter difficulties when applied to smaller vessels. In particular, synthetic vascular grafts often face challenges such as restenosis, thrombus formation, and compliance mismatch, leading to problems such as intimal hyperplasia or disease progression.[1]

To bridge the mechanical gap between autologous blood vessels and synthetic grafts, an innovative approach involves the integration of elastic materials in the circumferential direction to enhance elasticity and compliance.[2]

In this study, tubular woven structures are produced from yarns based on polyethylene terephthalate (PET) and thermoplastic polyurethane (TPU) filaments using shuttle weaving technology. The aim is the development of compliant vascular grafts.

Methods: Tubular samples with diameters between 5 mm to 9 mm were produced in weaving trials on a shuttle weaving loom using ultra-fine PET and elastic TPU multifilaments. Melt spinning experiments were carried out at Institut für Textiltechnik of RWTH Aachen University, Germany, to develop processable elastic TPU yarns with different finenesses and mechanical properties. The influence of yarn characteristics on the mechanical properties of the samples focusing on compliance was investigated.

In the main tests, a non-elastic weft yarn as well as several elastic yarns were used.

The samples were tested on both mechanical and morphological properties, using microscopy and circumferential tensile tests. The tensile tests were carried out up to material failure or the force limit of the testing machine. Samples with elastic weft yarns were

as well tested in cyclic tests in a force range corresponding to an inner pressure of 20-200 mmHg. The regions of the force-elongation-diagram and the maximum tensile force were examined and the results of tensile tests were converted into compliance values. The influence of the number of cycles on the compliance was evaluated. Also, the porosity of the samples was analyzed.

Results: The sample production with the selected materials in low porosity woven tubes was successful. It was necessary to adapt the weaving process to the respective weft yarns in order to achieve a stable process. The varying yarn finenesses were balanced out by adjusting the yarn densities.

The maximum tensile forces could not be determined of all samples due to exceeding the stability of the test setup. The compliance of tubular structures was successfully increased by using elastic weft yarns. Therefore, an application of such structures as biomimetic vascular grafts is indicated. The mechanical properties showed a settling behavior in the first cycles of testing and satisfactory residual elasticity over the entire test. The next step will be to validate the compliance results with a test setup that allows a higher number of cycles and more application-oriented testing.

References

1. Hu et al., Biomater Transl., 3(1):81-98, 2022
2. Kancevicha et al., Scientific Journal of Riga Technical University, 6:9-13, 2011

Acknowledgements

We thank Ms Seidel for her help in the experiments.
This work was supported by the German Federal Ministry for Economic Affairs and Energy for funding the research project within the framework of the Central Innovation Program for SMEs (ElaWeaveGraft, KK5055950AP3).

STABLE PEG-BASED POLYMER BRUSHES AS ANTI-FOULING LAYERS FOR BLOOD FILTRATION

Larissa dos Santos Silva Araújo[1,2], Lionel Bureau[1,2]

1. Laboratoire Interdisciplinaire de Physique (LIPhy), France; 2. Centre National de la Recherche Scientifique (CNRS), France

Introduction: Polyethylene glycol (PEG)-based brushes have been at the forefront of biological applications and nanomedicine due to their anti-fouling properties, low toxicity, wide availability, and use history in medicine and drug delivery materials [1]. In addition to the biocompatibility of such thin films, the macromolecules present a cost-effective possibility of functionalization, allowing the use of different monomers and architectural modifications according to the specific application [2].

In this work, we present a blood compatible noncharged PEG brushes for the application in a filtration membrane of an implantable kidney device (KIDNEW).

Methods: Poly(ethylene glycol) methyl ether methacrylate (PEGMA) brushes of different molecular weight were grafted in Silicon wafers by surface initiated activator regenerated by electron transfer atom transfer radical polymerization (ARGET-ATRP).

The optimization of synthesis conditions was conducted by approaching different strategies to anchor the brushes to the surfaces, concentration of monomer and catalyst, initiator, time of reaction and ligand [3]. The brushes' characterization was performed by ellipsometry and Atomic Force Microscopy (AFM).

Anti-fouling properties were probed in static and dynamic conditions for physiological concentrations of albumin. Quartz Crystal Microbalance with dissipation (QCM-D) allowed an insight on the protein resistance properties. Stability assay was performed by monitoring the thickness of the brushes after immersion of the coated silicon wafer in phosphate-buffered saline solutions over time.

Results: PEGMA brushes from 3 to 120 nm thicknesses were obtained. Static protein adsorption assay and QCM-D demonstrated the effectiveness in preventing adsorption of fresh and aged brushes. In addition, anchors were found to play an important role in the brushes' long-term stability. The investigations pointed to the degrafting in 90 days of brushes synthesized from 3-aminopropyl triethoxysilane (APTES). Increased stability was expected for poly(glycidyl methacrylate) (PGMA)

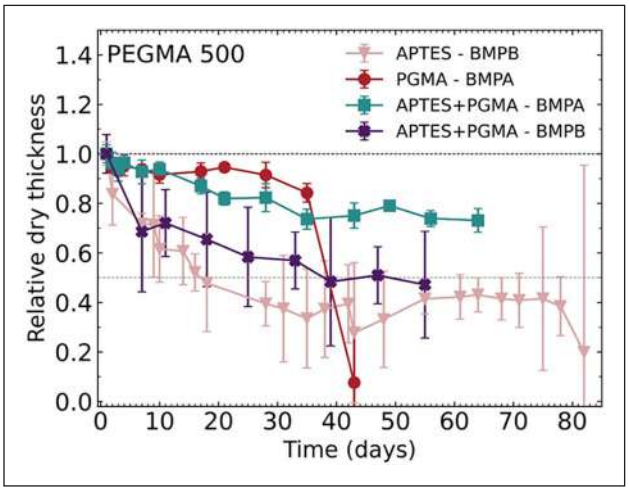

Figure 1. Stability assay for PEGMA500 brush: Relative dry thickness of the brushes after immersion in PBS for evaluation of surface anchoring and initiator.

macroinitiator based coatings, but complete degradation was also observed after 40 days. Interestingly, coupling the silane and the macroinitiator optimized the long-term stability, as depicted in Figure 1. The 2-bromo-2-methylpropionyl bromide (BMPB) and 2-bromo-2-methylpropionic acid (BMPA) initiators were also evaluated.

Discussion: Protein adsorption experiments with fresh and a four-month aged brush with bovine serum albumin in concentrations between 1.0 and 7.0% revealed the remarkable anti-fouling properties of PEGMA brushes. Aiming the application in an implantable device, the long-term stability is a crucial parameter. The results evidenced strong hydrolysis process occurring in APTES surface-initiated brushes. The presence of an additional hydrophobic layer of polymer PGMA provides long-term stability by preventing the nucleophilic interaction with water [4]. The substitution of BMPB for BMPA also influenced the stability of the coatings. Altogether, the simple synthetic procedure, physicochemical characteristics, anti-fouling properties and stability of PEGMA brushes make these coatings attractive functional candidates to integrate a blood filtration device.

References

1. Bernhard C et al. Phys Chem Chem Phys;19:28182–8, 2017.
2. Krishnamoorthy M et al. Chem Rev;114:10976–1026, 2014.
3. Telford AM, Neto C, Meagher L. Polymer; 54:5490–8, 2013.
4. Brió Pérez M et al. Macromolecules; 56:8856–65, 2023.

Acknowledgements

This work was supported by grant from the EIC Pathfinder Open Project No: 101099092.

PEDIATRIC AND ADULT FULLY IMPLANTABLE MAGNETICALLY LEVITATED TOTAL ARTIFICIAL HEART

Alexandru Plesoianu (1), Ionut Nistor (1,2), Alberto Bacusca (1,3), Grigore Tinica (1,3), Carmen Plesoianu (1,3)

1. "Grigore T. Popa" University of Medicine and Pharmacy Iasi, Romania; 2. "Dr. C. I. Parhon" Clinical Hospital Iasi, Romania; 3. "Dr. George IM Georgescu" Cardiovascular Diseases Institute Iasi, Romania

Introduction: Total artificial hearts (TAHs) are pioneering solutions addressing the critical challenges of biventricular heart failure. They offer a vital alternative for thousands of patients who are ineligible or remain on the waiting list for heart transplantation [1]. However, the reliability and side effects associated with current devices restrict their application to fewer than 200 cases annually [2]. The project's objective was to design an innovative TAH capable of sustaining enough blood for children and adults while reducing the risks of thrombosis, hemolysis, infection, and malfunction compared to existing TAHs. Key features focused on durability, wireless operation, affordability, and simplicity.

Methods: We employed mathematical modeling to define the pump parameters necessary for the required blood flow. Pumps designed in CFturbo were analyzed using Ansys CFX. Prototypes created in Fusion 360 were manufactured using SLA 3D printing at a resolution of

100 microns and machined from polymethyl methacrylate using a VHF k5+ 5-axis CNC milling machine. We constructed a test bench to conduct in vitro tests in accordance with ASTM F1841-19e1. Anatomical fitting and in silico tests were performed using V-Patient software.

Results: TAH system measuring 50 by 55mm includes a radial pump unit actuated by a radial bearingless slice motor that is powered by a subcutaneous electronic driver and a waterproof wearable smart battery. The motor measures 55 mm in diameter and 15 mm in thickness.

Figure 1. Size comparation Top from left: 5 years old heart model, resulted artificial heart, Bivacor TAH model; Bottom: Subcutaneous driver, smart battery, Medtronic Protecta XT CRT

Initial in vitro tests using water at 21°C yielded a mean flow of 11.43 liters per minute on the left side and 11.06 liters per minute on the right side. The 3D geometry of the TAH fits optimally in the space of the ventricles. CFD analysis indicated a maximum shear stress of 1.92 Pa and an efficiency of 53% for the left pump. The smart battery provides minimal user interface (battery level and alarms). Detailed information about the system functionality is displayed on a mobile phone via a proprietary app.

Discussion: The compact size of our artificial heart is approximately three times smaller than that of the Bivacor TAH, offering significant advantages for implantation in both children and adults. The wireless operation reduces the risk of infection and enhances patient mobility. Autonomy is further supported by reserve batteries. The impeller clearance of 1 mm minimizes damage to blood cells, thereby reducing the risks of thrombosis and hemolysis. We are developing a new model targeting a 5 liters per minute flow rate to better serve both pediatric and adult patients. Ongoing in vitro testing aims to further assess hemolysis levels. The thermal effect of the TET system on tissues is also under investigation.

References

1. Bakhtiyar SS et al, JAMA Cardiol, (11):1227-1235, 2020.
2. Arabía FA et al, Transplant Proc, 55(7):1664-1673, 2023.

NUMERICAL ASSESSMENT OF THE EFFICIENCY OF A NEW MINIMALLY INVASIVE PROBE FOR THE ISOLATION OF CIRCULATING TUMOR CELLS

Felix Hehnen (1,2), Henri Wolff (1,2), Sophia Krakowski (1,2), Gabi Bondzio (3), Michael Lommel (1,2), Ulrich Kertzscher (1,2) and Paul Friedrich Geus (1,2)

1. Deutsches Herzzentrum der Charité, Institute of Computer-assisted Cardiovascular Medicine, Biofluid Mechanics Laboratory, Augustenburger Platz 1, Berlin 13353, Germany; 2. Charité – Universitätsmedizin Berlin, corporate member of Freie Universität Berlin and Humboldt-Universität zu Berlin, Institute of Computer-assisted Cardiovascular Medicine, Charitéplatz 1, 10117 Berlin, Germany; 3. Invicol GmbH, Köpenicker Straße 325, Berlin 12555, Germany

Isolation of CTCs: Liquid biopsy, particularly the isolation of circulating tumor cells (CTCs) from blood, is a promising approach in the fight against cancer. CTCs are cells that have been shed from the primary tumor or metastatic deposits and circulate through the bloodstream. The analysis of CTCs and their quantification in blood can be used to diagnose cancer, for prognostic evaluation, treatment stratification and treatment monitoring, as shown in the review by Lin et al. [1]. However, the reliable isolation of CTCs continues to be a technical challenge [2,3]. This is due to their rarity in blood: it is assumed that there are less than 10 CTCs / mL in cancer patients [4].

To overcome the limitations of current isolation methods, screening large blood volumes in vivo was recommended to increase CTC yield [5]. Therefor the company Invicol (Berlin, Germany) developed the BMProbe™: A minimally invasive device with a twisted geometry to increase the interaction with blood and the screened blood volume.

CFD study: In this study, using multiple Computational Fluid Dynamics (CFD) simulations, the efficiency of the BMProbe™ is quantified. In the following, the term efficiency refers to the ability of the probe to isolate CTCs from the bloodstream. Since a direct simulation of cell attachment has many limitations, high computational costs and is usually associated with inaccuracies, the efficiency in this study is determined indirectly via three parameters that are known to have an influence on cell attachment. These parameters include the screened blood volume, the residence time of cells near the probe´s surface and the transport of cells to the probe´s surface (negative wall normal rate). Further, the influence that the geometry of the BMProbe™, the vein diameter and the blood flow velocity have on the efficiency of the BMProbe™ is presented.

Results: The numerical data suggests that the geometry has a strong influence on cell binding efficiency. Increasing the number of windings improves the transport of cells to the surface (negative wall normal rate) and the screened blood volume but decreases the residence time of particles in the close vicinity of the probe. When compared to experimental data, the screened blood volume and the wall normal rate indicate cell attachment very well, whereas the residence time does not show a significant impact on the attachment of cells. For the 32-windings BMProbe™, the screened blood volume is determined to be 130 mL – 313 mL, depending on the vein diameter, which is a multiple of the volume achieved by common CTC isolation techniques.

References

1. Lin, D.; Shen, L.; Luo, M.; Zhang, K.; Li, J.; Yang, Q.; Zhu, F.; Zhou, D.; Zheng, S.; Chen, Y.; et al. Circulating Tumor Cells: Biology and Clinical Significance. Signal Transduct. Target. Ther. 2021, 6, doi:10.1038/s41392-021-00817-8.
2. Raufi, A.G.; May, M.S.; Hadfield, M.J.; Seyhan, A.A.; El-Deiry, W.S. Advances in Liquid Biopsy Technology and Implications for Pancreatic Cancer. Int. J. Mol. Sci. 2023, 24, doi:10.3390/ijms24044238
3. Vidlarova, M.; Rehulkova, A.; Stejskal, P.; Prokopova, A.; Slavik, H.; Hajduch, M.; Srovnal, J. Recent Advances in Methods for Circulating Tumor Cell Detection. Int. J. Mol. Sci. 2023, 24, doi:10.3390/ijms24043902.
4. Haber, D.A.; Velculescu, V.E. Blood-Based Analyses of Cancer: Circulating Tumor Cells and Circulating Tumor DNA. Cancer Discov. 2014, 4, 650–661, doi:10.1158/2159-8290.CD-13-1014.
5. Batool, S.M.; Yekula, A.; Khanna, P.; Hsia, T.; Gamblin, A.S.; Ekanayake, E.; Escobedo, A.K.; You, D.G.; Castro, C.M.; Im, H.; et al. The Liquid Biopsy Consortium: Challenges and Opportunities for Early Cancer Detection and Monitoring. Cell Reports Med. 2023, 4, 101198, doi:10.1016/j.xcrm.2023.101198

Acknowledgements

This research was funded by the Investitionsbank Berlin and the European Regional Development Fund (grant no. 10194288).

INTRODUCTION OF THE NOVEL CONCEPT OF SIZING FLUID POTTING

Felix Hund[a], Jan Heyer[a], Ulrich Steinseifer[a], Thomas Schmitz-Rode[a], Mark Schoberer[b], Sebastian V. Jansen[a]

[a] Department of Cardiovascular Engineering, Institute of Applied Medical Engineering, Medical Faculty, RWTH Aachen University, Forckenbeckstr. 55, Aachen, 52074, Germany
[b] Pediatric Clinic, Neonatology Section, RWTH Aachen University and University Hospital, Aachen, Germany

Background: The treatment of extremely premature infants with immature lung function is a key challenge in neonatal intensive care. Avoiding pulmonary gas ventilation by use of an artificial placenta (AP) is a lung protective alternative treatment concept for this patient group. The AP basically is an oxygenator integrated into the umbilical vascular circulation. Current approaches for oxygenators in the AP context are commercial oxygenators adapted for this purpose and oxygenators with a constant gas exchange surface area or special developed prototypes for this purpose, e.g. the Neonatox. The blood volume and needed gas supply of the extremely premature infant doubles during the treatment process between 24 and 28 weeks of gestation. Current technologies do not fulfil the resulting need for an adjustable system to tackle this growth. The presented approach introduces the novel concept of sizing fluid potting to generate a dual-chambered stacked oxygenator for a volume-adjustable AP.

Methods: The novel concept is based on using a sizing fluid with a higher density than the potting fluid to create a defined lumen. Therefore, round potting in the acceleration field rotating around its center axis was chosen. The Potting process can be divided into three steps: Potting of the outer sealing of the device following the round potting process, adding the sizing fluid to determine the size of the outer chamber and finally potting the inner wall to divide the two concentric chambers. After defining requirements for usable fluids with either a high density or a changeable aggregate state, the resulting candidate fluids were tested for their applicability with hollow fibre membranes used in conventional oxygenator models and potting materials.

This novel process with the desired sizing fluid was used to generate the targeted dual chamber design. A reproduction test was done to evaluate the defined potting method. The test consists of the corresponding chambers' inner and outer potting diameters and their target parameters.

The dual chamber fiber bundle was further tested in a specially designed prototype for its gas transfer efficiency according to DIN EN ISO 7199 with blood flows between 50 ml/min and 200 ml/min in steps of 25 ml/min. Switching to the additional chamber was performed at 100 ml/min when oxygen saturation dropped below 80 %.

Results: Perfluorodecaline was chosen as a sizing fluid. The fluid is fully removable from the tested hollow fibre membranes, polypropylene (PP) and polymethylpentene (PMP), and does not interact with the silicone used for potting (Elastosil 620 A/B). A fibre bundle with resulting compartments of 5 ml priming volume each is shown in Figure 1.

In vitro testing according to ISO7199 showed an increase in transmitted oxygen over time after switching from the inner to both compartments. The resulting oxygen transfer with its corresponding blood flows is shown in Figure 2.

Conclusion: This study demonstrates proof-of-concept for a manufacturing process of concentric multi-chamber oxygenators with stacked fiber bundles using a sizing fluid. Reproducibility was demonstrated on hollow fiber bundles with corresponding compartments of 5 ml priming volume each. Sufficient gas transfer results for use as an artificial placenta could be shown.

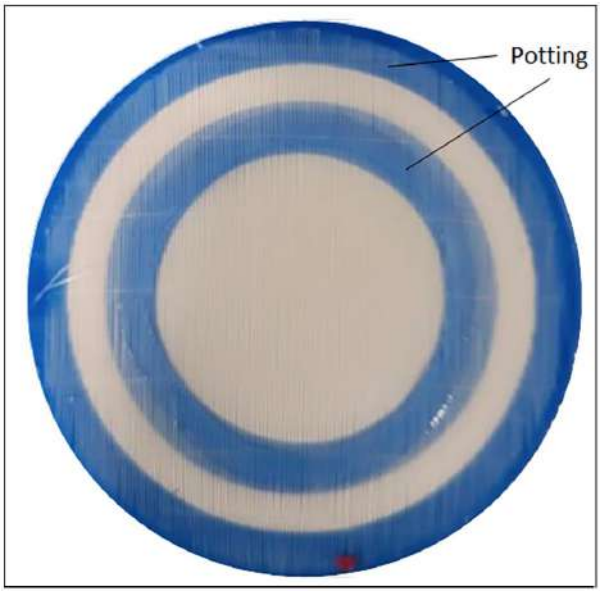

Figure 1. Dual chambered fibre bundle.

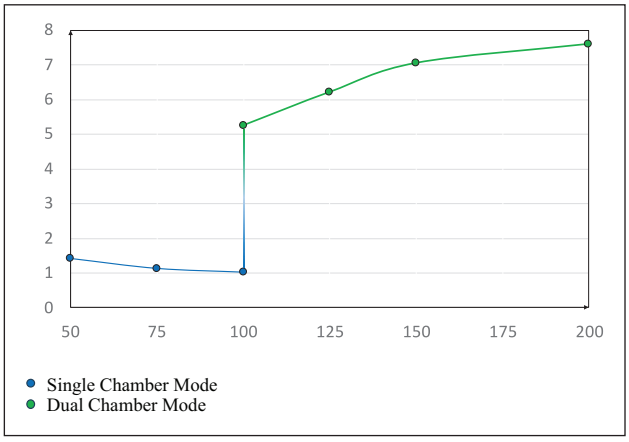

Figure 2. Transferred oxygen overflow in single (blue) and dual chamber mode (green).

INFLUENCE OF TITANIUM SURFACE ROUGHNESS ON A NANOSCALE ON THE ZETA POTENTIAL AND PLATELET ADHESION

Isabell Esslinger (1,2), Michael Lommel (1,2), Florian Kießlich (1,2), Ulrich Kertzscher (1,2), Tim Bierewirtz (1,2)

1. Deutsches Herzzentrum der Charité, Institute of Computer-assisted Cardiovascular Medicine, Biofluid Mechanics Laboratory, Augustenburger Platz 1, 13353, Berlin, Germany; 2. Charité – Universitätsmedizin Berlin, corporate member of Freie Universität Berlin and Humboldt-Universität zu Berlin, Charitéplatz 1, 10117 Berlin, Germany

Introduction: Thromboembolic complications still arise on blood contacting surfaces like titanium in implants. Surface characteristics like charge and topography are known to have an influence on the subsequent deposition of proteins and platelets. A study of Borghi et al. [1] showed an influence of different surface roughness values on a nanoscale on the surface charge behavior of titanium without considering hemocompatibility aspects. Therefore, the aim of this study was to compare different surface roughness values in a nanoscale range in terms of platelet adhesion and surface charge.

Methods: Titanium samples with four different surface roughness levels were polished and roughened on a nanometer scale and Ra values were measured. Samples were tested for platelet adhesion (covered surface area (CSA), N=8) in flow chambers with human whole blood using fluorescence imaging and zeta potential measurements were conducted over a broad range of pH values and interpolated to obtain zeta potential values at the pH of blood (7.4, pHBlood). Platelet adhesion tests were evaluated in terms of p-values and the Wilcoxon test effect size and the trend of the zeta potential values at pHBlood and the CSA was compared for the different roughness values.

Results: R_a-values were between 35 (polished) and 156 nm. The CSA between the samples did not differ significantly. However, strong and medium effect sizes were present, and the polished sample had the lowest mean CSA, see Figure 1. A similar trend was observed for the zeta potential measurements at pHBlood, with the polished surface showing the lowest value of -53 mV.

Discussion: Our findings introduce novel insights on the correlation of surface roughness, surface charge and platelet adhesion. Despite the deviations of the results of the platelet adhesion test (which is a commonly faced problem due to donor variability), the trend of our results is consistent with literature [2,3]. At the same time, the polished samples showed the most negative zeta potential at physiological blood pH of 7.4, which is also consistent with studies investigating similar surfaces in terms of surface roughness [4,5]. Interestingly, the interpolated zeta potentials for pH of 7.4 follow a similar trend as the mean CSA of platelets of our blood experiments, as depicted in Figure 1. This trend suggests that the change of zeta potential due to nanoscale roughness variation is an important factor on the extend of platelet adhesion

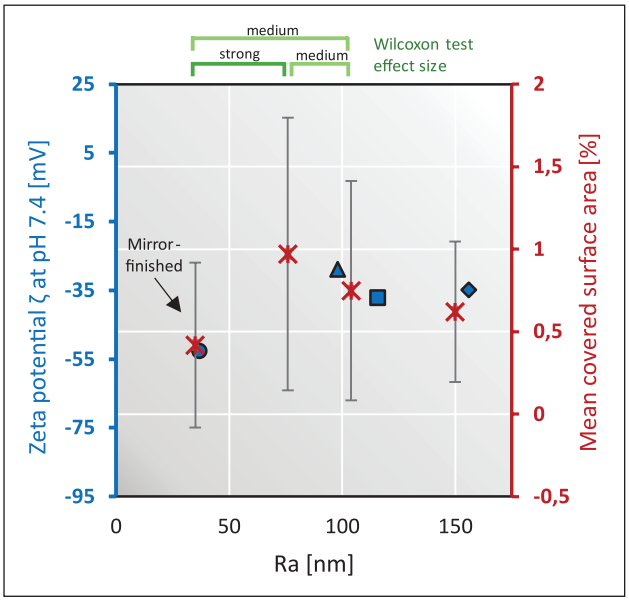

Figure 1. Zeta potential ζ at pH_{Blood} and mean covered surface area with platelets including standard deviation and Wilcoxon test effect sizes over roughness values R_a for all samples.

on titanium surfaces. Smooth surfaces are generally considered less thrombogenic because of less geometric features protruding inside or outside of the surface baseline and due to less specific surface area [3]. However, our findings suggest that the decreasing surface charge due to a lower nanoscale roughness might be an additional explanation for the improved hemocompatibility.

References

1. Borghi et al., PLOS One, 8(7):1-14, 2013.
2. Linneweber et al., Artif Organs, 31(5):345-51, 2007.
3. Schuster et al., TMS 2015 144th Annual Meeting & Exhibtion, pp. 653-660, 2015.
4. Ferraris et al., Front Bioeng Biotechnol., 6:1-7, 2018.
5. Spriano et al., Mater Sci Eng C.,74:542-55, 2017.

APPLICABILITY OF STRESS-BASED AND STRAIN-BASED HEMOLYSIS MODELS FOR SHORT-TERM STRESS PEAKS IN ROTARY BLOOD PUMPS: AN EXPERIMENTAL STUDY IN MICROCHANNELS

Michael Lommel (1,2), Vera Froese (1,2), Henri Wolff (1,2), Nico Dirkes (3), Katharina Vellguth (1,2), Marek Behr (3), and Ulrich Kertzscher (1,2)

1. Deutsches Herzzentrum der Charité, Institute of Computer-assisted Cardiovascular Medicine, Augustenburger Platz 1, 13353 Berlin, Germany; 2. Charité – Universitätsmedizin Berlin; 2. Charitéplatz 1, 10117 Berlin Germany; 3. Chair for Computational Analysis of Technical Systems, RWTH Aachen University, Aachen, Germany

Introduction: In the development process of blood-carrying medical devices, such as rotary blood pumps (RBPs), it is important to predict hemolysis -flow-induced damage to red blood cells (RBCs) -at an early development stage. Several models exist that predict the index of hemolysis (IH) based on the flow field obtained from computational fluid dynamics (CFD) simulations [1]. Commonly used stress-based models with a scalar shear stress (SSS) formulation, like the power-law model, have unclear validity, especially for complex flows [2,3]. Alternatively, strain-based models estimate hemolysis from local velocity gradients affecting RBC deformation. These models have been investigated in fewer studies than stress-based models [1,2].

This study compares the experimentally measured IH of three microchannels to the IH predictions of these models using CFD simulations.

Methods: We conducted experiments with human whole blood in three microchannels, each representing a different flow scenario typical for critical regions of RBPs (figure 1).

Results: Experiments showed for all three microchannels low and statistically not significantly deviating hemolysis values. The CFD simulations determined SSS of up to 1500 Pa, with high-stress exposure times in the range of milliseconds. Stress-based models overestimated hemolysis by up to three orders of magnitude and differed significantly across microchannels. The strain-based model predicted low and approximately equal hemolysis for all channels, agreeing with experimental observations (see table 1).

Discussion: The results suggest that for short-term stress exposure (< 5 ms) the stress-based hemolysis models are not suitable. The strain-based model, which considers the time-dependent red blood cells' deformation, is more appropriate in our flow scenario. This implies a similar relationship for RBPs, where such flow scenarios are typical for the high-stress areas.

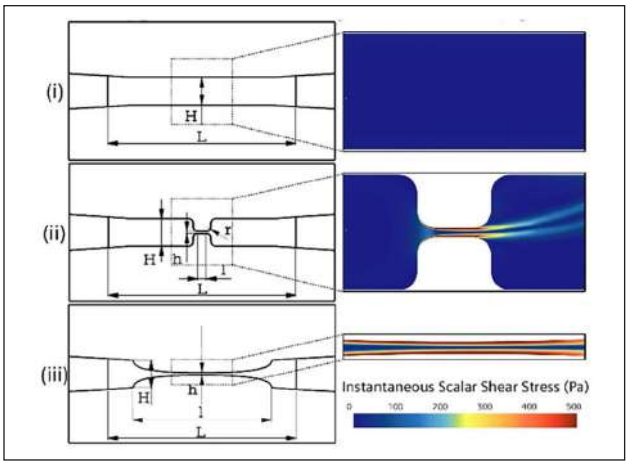

Figure 1. Left: The three channels investigated. Right: CFD SSS field. (i): Reference (ii): Sudden (iii): Smooth. Hemolysis was measured after circulating the blood up to 1200 times through the channels. Using CFD simulations and virtual massless particles, we traced trajectories and used the velocity gradient along the trajectories as input for the hemolysis models. Two stress-based models with different SSS formulations ([2] and [4]), and one strain-based model were used [5].

Table 1. Hemolysis results from 1200 pass-throughs with experiments (Exp.), two stress-based models (Stress 1: [4], Stress 2: [2]), and the strain-based model (Strain [5]).

Method	IH in %		
	Reference	Sudden	Smooth
Exp.	5.0e-2	5.3e-2	4.1e-2
Stress 1	6.25e-3	7.2e-1	1.49
Stress 2	7.77e-2	76.49	16.44
Strain	1.93e-3	1.69e-3	1.79e-3

Acknowledgements

This study was supported by the Investitionsbank Berlin and the European Regional Development Fund (funding code: 10168084). This study was supported by the Deutsche Forschungsgemeinschaft (DFG, German Research Foundation) through grant 333849990/GRK2379 (IRTG Modern Inverse Problems).

References

1. Yu et al., Artif Organs, 41:603-621, 2017.
2. Faghih et al., Biomech Model Mechanobiol, 18:845-881, 2019.
3. Grigioni et al., Artif Organs, 28:467-475, 2004.
4. Bludszuweit, Artif Organs, 19:583-589, 1995.
5. Dirkes et al., Comput Methods Appl Mech Eng, 426, 2024.

BAROREFLEX CONTROL IMPLEMENTATION AND PERFORMANCE EVALUATION OF A CARDIOVASCULAR HYBRID MOCK CIRCULATION LOOP.

Francesco De Gaetano (1), Ilaria Guidetti (1) and Maria Laura Costantino (1),

Department of Chemistry, Material and Chemical Engineering, Politecnico di Milano, Milan, Italy

Introduction: Mock circulatory loops (MCL) are used to multiple purposes like training and research including the in vitro assessment of VADs and other cardiac assist devices. Usually, conventional hydraulic MCL are used but the versatility is limited because whenever different patient conditions need to be tested, hardware changes are required. Numerical MCL instead allow for a wide reproducibility and controllability of the cardio-vascular system features by means of lumped parameter modeling. The concept of merging numerical and physical models was exploited in the last years leading to a new concept of circulatory models called hybrid MCL (H-MCL). The aim of this work is the development of a H-MCL providing realistic hemodynamic waveforms in different scenarios including rest, exercise, infarction, with and without cardiovascular device support.

Methods: The mock circulatory loop here presented is a hardware-in-the-loop system. The numerical model of the human circulatory system, implemented in MATLAB Simulink, provides a real-time simulation. The lumped parameter model is made by the following blocks: Left and Right Heart (time-varying elastance model with internal resistance for both atrium and ventricle), Pulmonary and Systemic Circulation (each described as a five Windkessel element model for the arterial system and a classic Windkessel model for the venous one), and the baroreflex control. The baroreflex control implemented is meant to act on arterial pulmonary resistances, systemic peripheral resistances, venous unstressed volume and heart rate according to the Colacino [1] and Ursino [2] model.

The hydraulic part is mainly composed of two cylindrical PMMA tanks. The tanks can be any anatomic district of interest. In our case, we use a numerical model of the CVS and for that reason the two chambers are meant to be the left ventricle and the aorta, if the left cannulation is chosen, or right ventricle and pulmonary artery in case of right cannulation choice.

The validity of the numerical model was assessed changing real-time HF and CF when baroreflex control is activated. Then, different patients' conditions were simulated varying pressure tracings consistently with the input parameters chosen by the user.

The accuracy in the experimental measures has been evaluated considering two functional indexes: pressure error difference and stroke work.

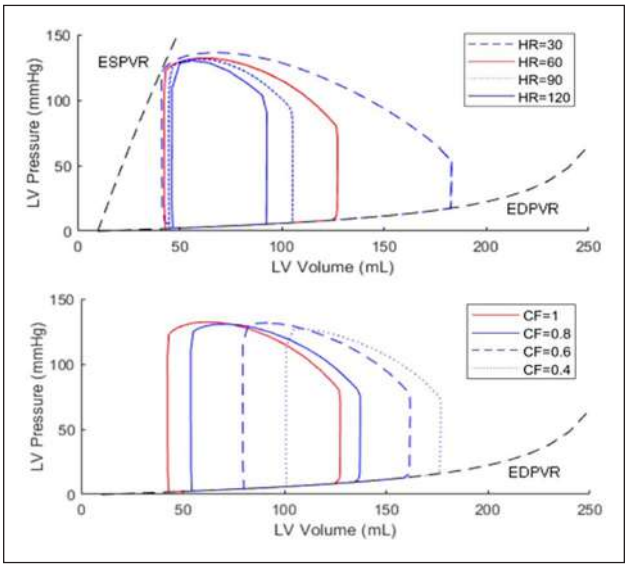

Figure 1. PV loop variations considering HR variability (upper figure) and CF variability (lower figure).

Results: The model we implement is capable of restoring the physiological pressure tracing (if the myocardium is not severely impaired) a few cycles after the real-time modifications of HR and CF, when the baroreflex control is activated. PV loop analysis (Figure 1) gives additional worth to the numerical model. Increasing the HR, the end-diastolic volume reduces, leading to a reduction of the SW. Varying the CF from healthy to pathological, SW decreases with the reduction of contractility causing reduced ejection, lower blood pressure, higher end-systolic volume and as a consequence reduced ventricu-lar filling. The comparison between experimental and numerical pressure shows that the controller is capable of making the experimental pressure wave-forms follow the numerical tracings.

Discussion: The flexibility of our mock loop has been checked: several parameters can be changed and monitored, mimicking several clinical scenarios. This is an extremely useful tool for clinicians, allowing them to understand which device or selected device configuration is most appropriate for the simulated patient.

References

1. Colacino et al., Asaio Journal, 53(3):263–277, 2007.
2. Ursino et al., American Journal of Physiology-Heart and Circulatory Physiology, 275(5):H1733–H1747, 1998.

ANALYSIS OF COMBINED EXTRACORPOREAL LUNG AND KIDNEY SUPPORT USING A COMPUTATIONAL CARDIOVASCULAR MODEL

Jan-Niklas Thiel (1), Ana M. Costa (2), Bettina Wiegmann (3), Jutta Arens (2), Michael Neidlin (1)

1. Department of Cardiovascular Engineering, Institute of Applied Medical Engineering, Helmholtz Institute, RWTH Aachen University, Aachen, Germany; 2. Engineering Organ Support Technologies, University of Twente, Enschede, Netherlands; 3. Department of Cardiothoracic, Transplantation and Vascular Surgery and Lower Saxony Center of Biomedical Engineering, Implant Research and Development (NIFE) and German Center for Lung Research (DZL), BREATH, Hannover Medical School, Hannover, Germany

Introduction: Extracorporeal membrane oxygenation (ECMO) is commonly used in intensive care to support cardiac and respiratory failure, yet up to 70 % of these patients also suffer from acute kidney injury. Treatment for this complication involves connecting continuous renal replacement therapy (CRRT) to the ECMO circuit. To date, its connection configuration varies depending on the operator's practice and proficiency, without any gold standard. This study aims to develop a cardiovascular model to investigate the interactions between ECMO and CRRT circuits in veno-arterial ECMO (VA-ECMO) patients, see Figure 1. Using Global Sensitivity Analysis (GSA), the study focuses on improving model fitting by assessing parameter importance, ultimately quantifying the effects of CRRT connection schemes and ECMO pump speed.

Methods: A computational cardiovascular model was extended by both ECMO and CRRT systems with external pumps, filters, and additional cannulas. A GSA was conducted using Sobol indices to identify the model parameters most relevant for the fitting. The model was fitted to six patients with the identified parameters and using gradient-based optimization with multistart. The influence of different CRRT connection modalities and ECMO flows was then investigated for one patient. For this, a GSA was performed including CRRT connection schemes and ECMO pump speed as input parameters, allowing to quantify their influence on clinical

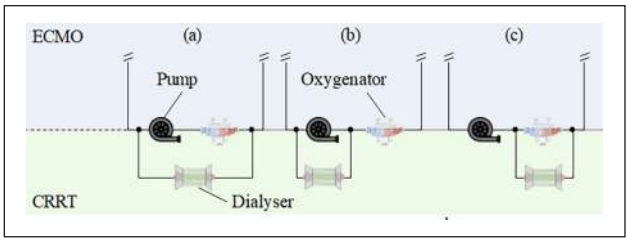

Figure 1. Example for combination of CRRT and ECMO.

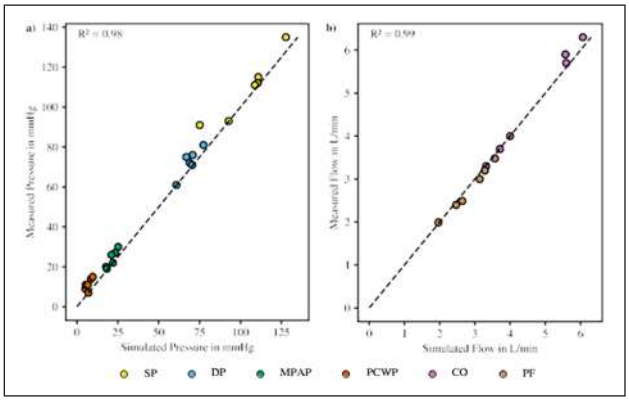

Figure 2. Simulated against measured pressures in a) and flows in b) for six patients. SP, DP: systolic and diastolic pressure of aorta. MPAP: mean pulmonary artery pressure. PCWP: pulmonary capillary wedge pressure. CO: cardiac output. PF: pump flow.

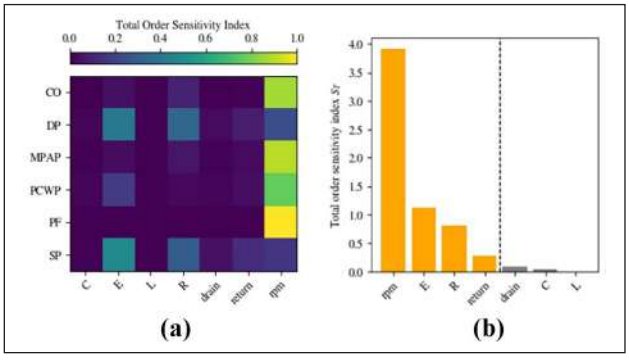

Figure 3. Total effect of model parameters, CRRT connection and ECMO rpm in a) and their cumulative effect in b). Parameters grouped into cardiovascular compliances (C), inertias (L) and resistances (R), and cardiac properties (E).

outputs. Input samples for each GSA were created using Saltelli sampling and their size is chosen so that convergence is achieved.

Results: Figure 2 presents scatterplots of the model predictions against clinical data for various pressures in a) and flows in b) for six patients. These show a strong correlation with R^2 values of 0.98 for pressures and 0.99 for flows.

Figure 3 a) illustrates the total effect of model parameters on outputs, while b) quantifies their cumulative total effects. Pump speed (rpm), cardiac properties, vascular resistances, and location of the CRRT return cannula have a high influence, in contrast to all other parameters.

Discussion: Applying GSA to a cardiovascular model with ECMO and CRRT revealed that using a subset of parameters reduces computational cost without losing predictive accuracy. This model can reliably simulate physiological conditions of VA-or VV-ECMO patients. It was found that the position of the CRRT return cannula has a sig-nificant influence on hemodynamic markers. This aids physicians in selecting the optimal CRRT and ECMO combination based on the patient and ECMO flow.

Acknowledgements

This project is funded by the DFG SPP2014 "Towards the Artificial Lung" -PN: 447746988.

A NOVEL POLYMERIC HEART VALVE: MANUFACTURING AND HYDRODYNAMIC ASSESSMENT

Michael Šeman (1,2,3,4), Andrew Stephens (2), Mehrdad Khamooshi (2,5), Rezan Jafary (2), David Kaye (2,3,6), William Chan (3,4,6,7), Connor Coughlan-Ward (2), Shaun Gregory (2,5), Dion Stub (1,2,3,6)

1: School of Public Health and Preventative Medicine, Monash University, Australia
2: Cardio-Respiratory Engineering and Technology Laboratory, Department of Mechanical and Aerospace Engineering, Monash University, Australia
3: Department of Cardiology, Alfred Health, Australia 4: Department of Cardiology, Western Health, Australia
5: Centre for Biomedical Technologies, Queensland University of Technology, Brisbane, Australia 6: Baker Heart and Diabetes Institute, Australia
7: Department of Medicine, Western Health, Melbourne Medical School, University of Melbourne, Australia

Introduction: The prevalence of valvular heart disease is increasing worldwide and is a major cause of morbidity and mortality [1]. Valve replacement, with mechanical or biological prosthetic valves, is a well-established treatment option for patients with significant valvulopathy. Polymeric heart valves (PHV) have been suggested as having the potential to replace mechanical and biological valves in the future [2]. Existing PHV manufacturing methods are varied and may result in inconsistent results.

Methods: We present a novel dip-casting approach for creating trileaflet PHV. We describe the preparation of a multi-solvent polyurethane solution that optimises the casting process. We evaluated the hydrodynamic performance of the crafted 25-mm polyurethane valve in a pulse duplicator according to ISO standards [3] and compared the results to a 25-mm St Jude Masters aortic mechanical valve and a 26-mm Medtronic Evolut bioprosthetic valve. Valves were tested at 70 bpm and at cardiac output of 3, 5 and 7 L/min. Effective orifice area (EOA), mean transvalvular pressure gradient (TPG) and regurgitant fraction (RF) were assessed compared between valves.

Results: The polyurethane valve (see Figure 1) markedly exceeded the minimum performance requirements for bioprosthetic aortic heart valves. The polyurethane valve had significantly higher EOA (ranging from 2.7 ± 0.1 to 3.5 ± 0.1 cm^2) across the cardiac output range, compared to the Mechanical and Evolut valves (2.1 ± 0.1 to 2.8 ± 0.1 cm^2 and 2.5 ± 0.1 to 3.2 ± 0.1 cm^2, respectively; $p < 0.001$). For all tested cardiac outputs, TPG was significantly lower in the polyurethane valve (ranging from 3.6 ± 0.1 to 4.7 ± 0.1 mmHg) compared to the Mechanical and Evolut valves (4.4 ± 0.1 to 7.4 ± 0.1 mmHg and 4.1 ± 0.1 to 5.6 ± 0.1 mmHg, respectively; $p < 0.001$). Measures of RF were at least 40% lower

Figure 1. Final dip-casted 25-mm polyurethane valve.

for the polyurethane valve compared to the Mechanical and Evolut valves across all tested cardiac outputs ($p < 0.001$).

Discussion: This study presents a novel dip-casting approach for the manufacture of prosthetic polyurethane heart valves. The hydrodynamic performance was very promising demonstrating superior EOA, TPG, and RF compared to existing clinically approved mechanical and bioprosthetic valves. Thus, this innovative method of dip-casting offers considerable promise as a viable approach for manufacturing prosthetic heart valves.

References

1. d'Arcy JL et al, Heart.97(2):91-3. 2011.
2. Rezvova MA et al, Int J Mol Sci, 24(4), 2013.
3. ISO standards, ISO5840-2, 2021.

REAL-TIME PLATELET OBSERVATION SETUP FOR IN-VITRO HEMOCOMPATIBILITY TESTING

Marlene Schadow (1), Corentin Raveleau (2), Simon Mendez (2), Franck Nicoud (2,3), Ulrich Steinseifer (1), Michael Neidlin (1), Johanna C. Clauser (1)

1. Department of Cardiovascular Engineering, Institute of Applied Medical Engineering, RWTH Aachen University, University Hospital Aachen; Germany 2. IMAG, University of Montpellier, CNRS France 3. Institut Universitaire de France, IUF, France

Introduction: Poor hemocompatibility of artificial materials is still a bottleneck in medical engineering. A current approach is the microstructuring of substrate surfaces to reduce platelet adhesion as an initialization of thrombus formation. Although the advantage has already been demonstrated [1-3], the underlying mechanism is still not fully understood. The aim of this study is to investigate the mechanism by analyzing the flow behavior of platelets in a systematic study including in-vitro testing as well as a computational study addressed by Raveleau et al.

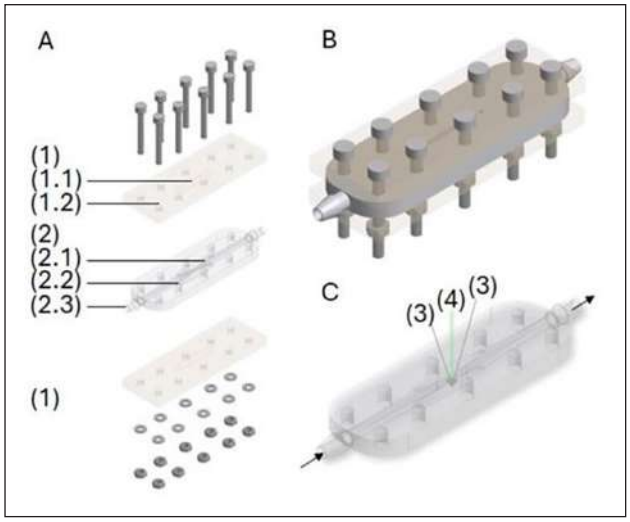

Figure 1. The design of a flow chamber for the novel application in a µPTV setup.

Particle Image or Particle Tracking Velocimetry (PIV or PTV) are the gold standard for flow visualization, analyzing movement of particles in a fluid in a wide range of applications. This abstract presents the preliminary unpublished outcomes of a real-time platelet observation setup using µPTV with platelets as tracer particles for in-vitro hemocompatibility testing including the protocols to produce the test fluid, the design and manufacture of a flow chamber and the application in the µPTV setup.

Methods & Results: The test fluid is prepared using platelets isolated from citrated porcine whole blood by gel filtration and buffered in calcium-free PBS. The cells are then stained with 1,1'-Dihexadecyl-3,3,3',3'-Tetramethylindocarbo-cyanine Perchlorate (DilC16), resulting in homogeneous fluorescence staining of the cell membranes without compensating platelet function.

(A) The flow chamber consists of (1) two identical sample plates and (2) a semi-closed flow channel. (1) The sample plates are PMMA sheets designed with (1.1) a sealing groove and (1.2) passage holes, whereas the sample can be permanently fixed in the area within the sealing groove. (2) The flow channel is a one-step 3D-print using KeySplint Soft ® clear, as a translucent, semi-flexible material. It has a continuous transition from a circular inlet to (2.1) a rectangular channel at the sample area with openings at the top and bottom to the sample plates to allow uniform light entry and exit for µPTV measurement. (2.2) 1 mm from the opening, a sealing lip is placed, (B) which makes it possible to seal the flow chamber only by clamping the sample plates to the channel with screws. (2.3) The inlet and outlet were designed with male barb connectors integrated into the device. (C) In the µPTV application, the stained platelets in the flow are stimulated with (4) a 532 nm laser at the sample area. The light emitted by the cells is recorded in 400 x magnification with (3) 4000 Hz stereo cameras using a 575 nm filter. To compensate for the difference in refractive index between flow chamber materials and the fluid, a calibration of the refractive shift through the sample plate was performed.

In conclusion a proof-of-concept was demonstrated showing the recording of the flow pattern over a surface and status recordings of the total deposition of platelets in the context of dynamic in-vitro hemocompatibility testing.

Discussion: Using the novel µPTV test setup, the impact of microstructures on platelet flow behaviour can be systematically investigated in the future.

The results will allow for improving the hemocompatibility of blood contacting medical devices by specifically tailored structured surfaces.

References

1. Koh et al, Biomaterials, 31:1533-1545,2010,
2. Chen et al, LColloids Surf B Biointerfaces, 85:2-7, 2010
3. Jokinen et al, Advanced Materials, 30:1705104,2018

Acknowledgements

This work is part of the THROMBOSURF project co-funded by Deutsche Forschungsgemeinschaft (Project number: 490779571) and Agence Nationale de la Recherche (ANR.21.CE45-0035-02).

DEVELOPMENT OF OUTSIDE-IN FILTRATION HOLLOW FIBERS FOR THE ARTPLAC DEVICE.

L. Romano (1), R. Luiten (1), R. Selvaganapathy (2), N. Rochow (3), C. Fusch(3), J. Arens (4), O.E.M. ter Beek (1) D. Stamatialis (1) on behalf of the ArtPlac Research Consortium (5)

1. Faculty of Science and Technology, Advanced Organ bioengineering and Therapeutics (AOT), University of Twente, Enschede; 2. Department of Mechanical Engineering, McMaster University, Hamilton, ON -Canada; 3. Department of Neonatology, Klinikum Nurnberg, Nuremberg, German; 4. Faculty of Engineering Technologies, Department of Biomechanical Engineering, Engineering Organ Support Technologies, University of Twente, Enschede, the Netherlands; 5. HORIZON-EIC-2022-PATHFINDEROPEN-01, Grant agreement ID: 101099596

Introduction: Despite medical progress, around 1 million premature babies worldwide still die yearly due to complications such as lung or kidney failure [1]. Current treatments (mechanical ventilation, extracorporeal membrane oxygenation, and dialysis) are invasive have side-effects leading to lifelong disabilities. We propose the development of an artificial placenta (ArtPlac), connected to the umbilical vessel like the natural placenta in utero [2,3]. This innovative device aims to integrate lung and kidney assistant into a single unit by combining blood oxy-genator fibers with dialysis hollow fibers (HF) in a bundle both working in outside-in mode (OIF) [Fig. 1]. Unlike the traditional dialysis mode, the baby's blood will flow around the fibers and either oxygen or dialysate fluid will flow inside the fiber. This combination would offer a compact device with low blood priming volume and adding dialyzer function [4,5]. In this study, we investigate the development of the HF suitable for outside-in dialysis for this neonatal application.

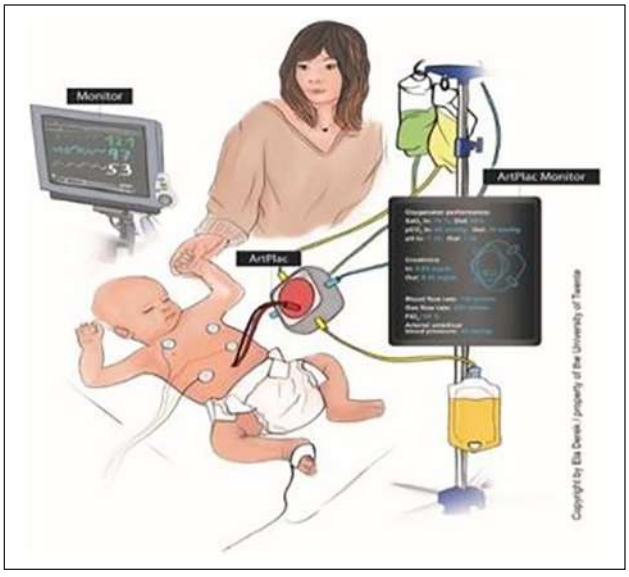

Figure 1. ArtPlac – one device attached to the umbilical cord combining lung and kidney support.

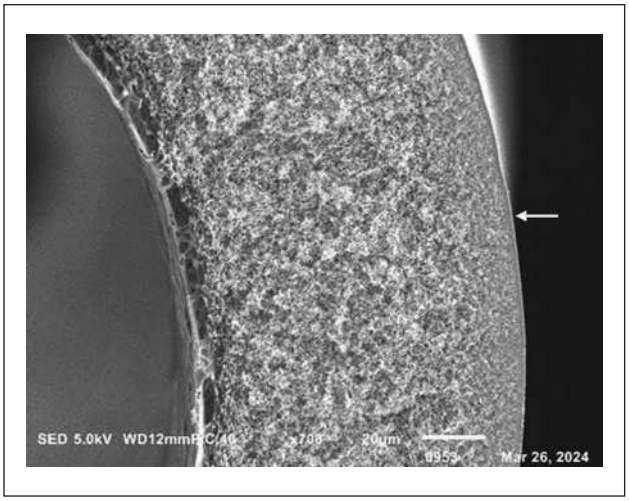

Figure 2. SEM image of the cross section of HF for OIF. The white arrow indicates the outer selective layer.

Methods: The hollow fibers (HF) were prepared using PES Ultrason (BASF, Ludwigshafen, Germany), a mixture of PVP K90, K30 (BASF, Ludwigshafen, Germany) and NMP (Acros Organics, Geel, Belgium) by dry-wet spinning**.** Scanning Electron Microscopy (SEM) was employed for fiber morphology characterization. The membrane ultrafiltration coefficient was determined via Clean-Water Flux (CWF) measurements.

Results: Figure 2 presents typical SEM images of new HF for OIF. They have sponge-like pore morphology with an outer selective layer, in contact with the blood, and porous inner layer, in contact with the dialysis fluid. These membranes have an ultrafiltration coefficient of 7 mL/(m^2·h·mmHg) and are considered as low-flux dialyzer membranes.

Discussion: The sponge-like pore morphology and the measured ultrafiltration coefficient of the HF present promising characteristics for their potential use within the ArtPlac device. To maximize membrane performance, we are working on the development of an optimal fiber design.

References

1. Howson, C. P. et al. Reprod Health 10, S1,2013
2. Dabaghi, M. Et al. Adv Sci 7, 2001860, 2020
3. Niels Rochow et al, J Artif Organs, 36 (6): 377-391,2013
4. Schoberer et al, J Artif Organs, 36(6):512-6, 2012
5. S.S. Dukhin et al, J Memb Sci, 464: 173-178, 2014

Acknowledgements

This project has received funding from the European Union's Horizon Europe research and innovation programme (EIC Pathfinder) under grant agreement № 101099596.

MAGNETIC HYDROGELS AS DRUG DELIVERY VEHICLES FOR POTENTIAL CANCER TREATMENT

Esteban Rodriguez (1), Vanessa Narvaez (1), Sara Cotes (1), Valeria Rodriguez (1), Alex Lopera (1), Marcela Arenas (1), Carlos Orozco (2), Flor Bravo (1), Diego Garzón-Alvarado (3), Carlos Caicedo (3), Oscar Suarez (4), Nestor Rojas (5), Juan Vaca-González (1)

1. Universidad Nacional de Colombia, Sede de La Paz, Colombia; 2. Instituto Nacional de Cancerología, Colombia; 3. Universidad Nacional de Colombia, Sede Bogotá, Colombia; 4. Universidad Nacional de Colombia, Sede Orinoquia, Colombia; 5. Universidad Nacional de Colombia, Sede Medellín, Colombia.

Introduction: Pancreatic cancer, a major challenge in oncology, ranks seventh in cancer-related deaths globally due to late diagnosis and limited treatments [1]. Magnetic hydrogels offer a promising solution, enabling precise drug delivery to tumors via integrated magnetic nanoparticles (NPs). This approach minimizes side effects by concentrating drugs at the tumor site [2]. Magnetic hydrogels also provide versatility in tailored treatments due to their biocompatibility and tunable properties [3]. HA-Gel/Fe_3O_4/Gem, a magnetic hyaluronic acid -gelatin hydrogel loaded with gemcitabine, shows potential for sustained release and non-invasive administration, offering hope in combating pancreatic cancer by prolonging therapeutic efficacy through targeted drug delivery.

Methods: *Hydrogel synthesis:* Either HA or Gel (2% w/v) was dissolved with MES and HCl-Tyramine. Then, NHS and ECD were added. Thereafter, the dissolution was dialyzed and then lyophilized. A mixture containing 80% (v/v) of HA-Gel and 10% (v/v) of HRP was prepared. After, the HA-Gel-HRP solution was cross-linked with 10% (v/v) of H_2O_2.

Synthesis of magnetite (Fe_3O_4) NPs: They were synthesized by co-precipitation method assisted by ultrasound. Ferric chloride hexahydrate ($Cl_3FeH_{12}O_6$) and ferrous chloride tetrahydrate ($FeCl_2H_8O_4$) were dissolved in distilled water at N_2 bubbling. Then, NaOH was added dropwise while sonicating. NPs were magnetically separated, while non-magnetic NPs were harvested by centrifugation. Finally, samples were washed and dried overnight.

Synthesis of magnetic hydrogels: Fe_3O_4 NPs were dispersed in CF-KRB buffer under sonication. Then, Gel-HRP was added while sonicating. Finally, H_2O_2 was added dropwise under sonication.

Characterization of NPs: The crystal structure of magnetite was analyzed by X-ray diffraction (XRD). The size, shape and morphology of Fe_3O_4 NPs were determined using a dual beam FIB-SEM. The superparamagnetic behavior of Fe_3O_4 NPs were recorded by a vibrating sample magnetometer (VSM).

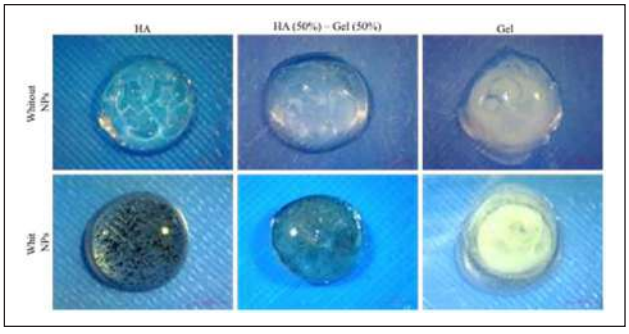

Figure 1. Hydrogels. A) HA -Gel hydrogels. B) Magnetic hydrogels.

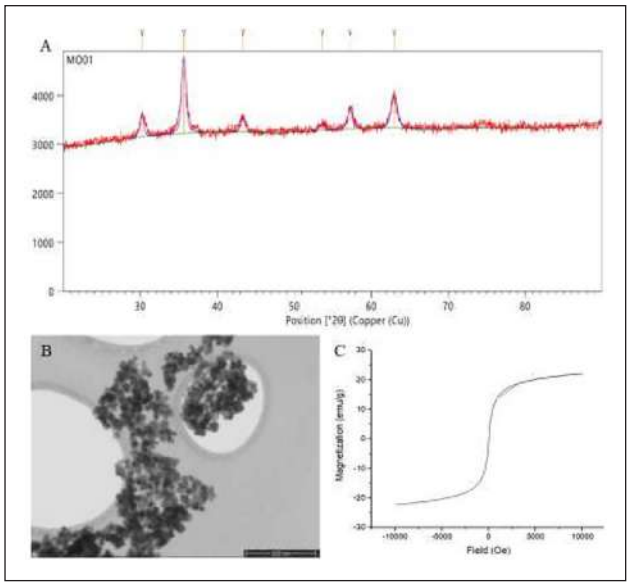

Figure 2. Fe_3O_4 characterization. A) X-ray. B) STEM. C) Hysteresis curve.

Results: Figure 1 shows hydrogels without and with NPs (0.6%) embedded within HA (100%), HA-Gel (50%/50%) and Gel (100%). Figure 2A shows the diffraction peaks for Fe_3O_4 NPs that can be indexed to the cubic phase of magnetite without any secondary phase. Figure 2B shows the formation of Fe_3O_4 NPs with sizes less than 100 nm. Figure 2C shows the hysteresis curve for Fe_3O_4 NPs.

Discussion: These scaffolds hold promise for cancer treatment by enabling targeted delivery of anticancer drugs to tumor sites. Magnetic guidance ensures precise localization, enhancing therapeutic efficacy while minimizing off-target effects. Their biocompatibility and tunable properties offer a versatile platform for personalized cancer therapy, fostering hope for improved outcomes.

References

1. C. J. Herting et al,Cancer Metastasis Rev 40:675–689,2021
2. A. M. Shabana et al, International Journal of Pharmaceutics, 593:1-14, 2021.
3. K. Shi et al, Nano Res., 12:6, 1389–1399, 2019.

Acknowledgements

We thank Cecoltec (HOME (cecoltec.com)) for their help in the XRD analysis.

FULL SCALE OXYGENATOR GAS TRANSFER MODELING: PARAMETERS FOR A REDUCED ORDER MODEL APPROACH

Jannis Mathias Focke[1], Kai Philip Barbian[1], Paul-Luca Bonke[1], Ulrich Steinseifer[1], Jutta Arens[2], Michael Neidlin[1]

1Department of Cardiovascular Engineering, Institute of Applied Medical Engineering, RWTH Aachen University, Aachen, Germany 2Engineering Organ Support Technologies Group, Department of Biomechanical Engineering, Faculty of Engineering Technology, University of Twente, Enschede, the Netherlands

Introduction: Oxygenators, so-called artificial lungs, support patients with severe lung diseases by leading blood through bundles of thousands of

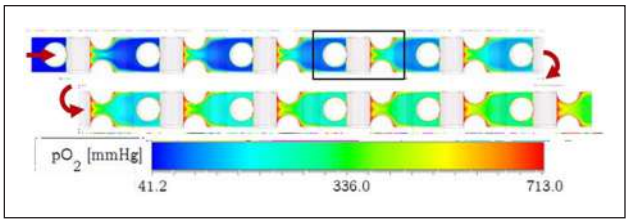

Figure 1. Microscale gas transfer simulation of a cross stacked fiber arrangement. Averaged gas transfer rates were determined for multiple sections (black frame) along the flow path.

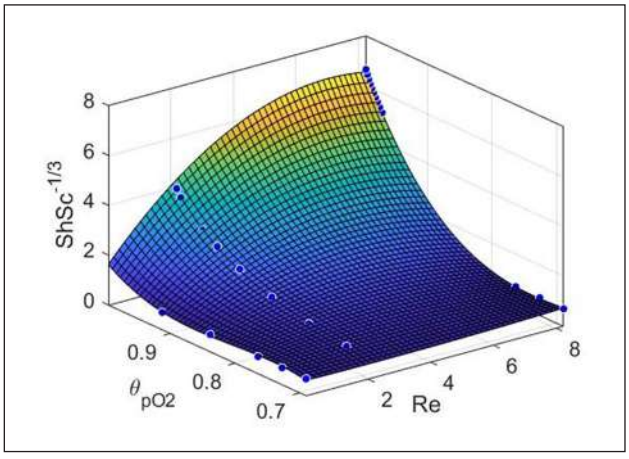

Figure 2. Polynomial mass transfer correlation for the fiber arrangement found in the RatOx oxygenator.

fiber membranes. Hemocompatibility is a major challenge, mainly associated with the large surface area and priming volume [1]. New and more efficient oxygenator designs are required to tackle those challenges. Computational models that allow an a priori estimation of gas transfer are a key step to facilitate the rapid development and testing of new device concepts. Particularly the interaction between local flows conditions, fiber arrangement and gas transfer needs to be considered on a macroscopic device scale. Such models do not exist yet. The aim of this study was to extend a reduced order model [2] to incorporate the effect of different fiber arrangements. Therefore, gas transfer rates of isolated arrangements were correlated with flow conditions and local gas concentration differences. This correlation was applied to a porous medium domain of an experimental oxygenator [3].

Methods: We have used a recently developed and validated 3D computational fluid dynamics model of microscopic gas transfer and blood flow around various hollow fiber arrangement (Figure 1). Then, these microscopic simulations of different fiber arrangements and different blood gas concentrations were used to obtain gas transfer rates.

These were translated into dimensionless Sherwood numbers (Sh) and correlated to dimensionless flow conditions (Reynolds number, Re and Schmidt number Sc) and a newly introduced dimensionless concentration difference (θ), using a polynomial curve fitting approach. This mass transfer correlation was implemented into a porous medium model and tested on the RatOx oxygenator [3].

Results: The polynomial function shows very high oxygen transfer for high velocities and high differences in partial pressure (Figure 2). For very high flow rates and for low partial pressure differences oxygen transfer is low. The correlation was implemented into the CFD model.

Discussion: Our newly introduced dimensionless concentration difference allowed us to better capture the intricate interplay between geometry, flow physics and gas transfer. The derived dimensionless relationship allows an easy implementation into widely used porous medium models and drastically accelerate development times of novel hollow fiber oxygenators.

References

1. Nguyen Thi et al, Acta Mater, 152:19-46, 2022.
2. Zhang et al, J Membr Sci, 288:268-279, 2007.
3. Strudthoff et al, Micromachines, 14(4):800, 2023.

Acknowledgements

This work was supported by the German Research Foundation (DFG) project number 42281948.

TOWARDS BIOHYBRID LUNG DEVELOPMENT: ANALYSIS OF CLINICALLY RELEVANT WORKING CONDITIONS ON THE ENDOTHELIAL CELLS ON GAS EXCHANGE MEMBRANES

G Sitarz[1,2,9], M Pflaum[1,2,3,9], A Brüggemann[1,2], K Barbian[4,9], L Budde[8,2], M Wessling[5,9], M Neidlin[4,9], J Arens[7,9], S Jansen[6,9], U Steinseifer[4,9], A Ruhparwar[1,2,3], B Wiegmann[1,2,3,9]

1 Hannover Medical School, Department of Cardiothoracic-, Transplantation-and Vascular Surgery, Germany; 2 NIFE – Lower Saxony Center for Biomedical Engineering, Implant Research and Development, Germany; 3 German Center for Lung Research (DZL), Germany; 4 RWTH Aachen University, Institute of Applied Medical Engineering, Germany; 5 RWTH Aachen University, Chemical Process Engineering, Germany; 6 RWTH Aachen Universität, Department of Cardiovascular Engineering, Aachen, Germany; 7 University of Twente, Department of Biomechanical Engineering, Twente, Netherlands; 8 Leibniz University Hannover, Institute of Mechatronic Systems (imes), Germany; 9 Member of the DFG priority program SPP 2014, Germany

Introduction: The development of the implantable biohybrid lung (BHL) is intended to offer an alternative to lung transplantation, which is currently the only treatment option for patients with end-stage lung disease. Based on the same functional principle as extracorporeal membrane oxygenation (ECMO), gas exchange in the BHL is achieved by diffusion via the gas exchange hollow fiber membranes (HFM). However, these are covered with a layer of endothelial cells to prevent obstruction due to blood clotting and thrombus formation, which is normally caused by the inevitable blood contact with the artificial surfaces of conventional ECMOs. In future BHL, endothelial cells must withstand a supraphysiological high oxygen gradient between the oxygen-rich gas in the HFM and the hypercapnic/hypoxic patient blood. Thus, we investigated the influence of this clinically relevant oxygen tension under static and dynamic conditions on the endothelial cells.

Methods: Prior to seeding with 1.52 x 10^5 EC/cm², hydrophobic PMP membranes (foil for static experiments and HFM for flow exposure) were coated with 2 µg/cm² fibronectin to facilitate EC adhesion [2, 3]. After reaching confluence, ECs were pre-cultured for 24 hours under blood gas levels of severe respiratory insufficiency (50 mmHg pO2, 80 mmHg pCO2) and then exposed to hyperoxia (>95% pO2) for 24 hours. In a custom-built miniature oxygenator, the endothelialised HFM were gently adapted to the flow conditions by applying an increasing ramping flow rate profile, starting at 2 ml/min and doubling every 30 minutes up to a maximum of 15 ml/min.

Remaining ECs were detected with the nuclear dye Hoechst 33342 and the vital dye calcein. Immunostaining agents were applied for the

detection of extracellular matrix Collagen type-IV and cell junction protein VE-Cadherin via confocal laser scanning microscopy (CLSM). Expression level change of oxidative stress (HMOX1, GCLM) -or inflammation (ELAM, VCAM, ICAM) related genes were measured

via qRT-PCR. Apoptosis (AnnexinV/PJ) and reactive oxygen species (ROS) accumulation (CellRox) were investigated using flow cytometry, and compared to menadione (50 µM, 4 h) treated ECs as positive control.

Results: On film and HFM samples, CLSM imaging confirmed confluent and viable EC-monolayers with intercellular junctions and *de novo* synthesized Collagen-IV under pre-cultivation or hyperoxia condition. In addition, no change in prothrombotic and proinflammatory gene regulation was detected. Under hyperoxia, genes associated with oxidative and flow stress were correspondingly upregulated.

The proportion of apoptotic ECs was not significantly increased in response to the high oxygen tension, while the level of ROS production was elevated. However, the ROS level of menadione-treated ECs, used as positive control, exceeded this level significantly.

Discussion: We have shown that the high oxygen tension, prevailing in the future BHL can be tolerated by the membrane seeded ECs, for at least 24h. The ECs responded to these clinically relevant conditions with an upregulation of genes related to stress and ROS-coping mechanisms, which may explain the fact that no lethal damage of the ECs could be detected.

Thus, the results of this study underline the feasibility of the biohybrid lung application under clinical conditions.

References

1. Hess et al, Tissue Engineering: Part A 16 (10) , 2010
2. Pflaum et al, Membranes 12 (35), 2022
3. Almesto et al, Bioengineering 10 (72), 2023

DESIGN AND IN VITRO TESTING OF A VALVELESS UNDULATING DISPLACEMENT PUMP FOR EXTRACORPORAL MEMBRANE OXYGENATION

Tim Bierewirtz (1,2), Michael Lommel (1,2) and Ulrich Kertzscher (1,2)

1. Deutsches Herzzentrum der Charité, Institute of Computer-assisted Cardiovascular Medicine, Biofluid Mechanics Laboratory, Augustenburger Platz 1, 13353, Berlin, Germany; 2. Charité – Universitätsmedizin Berlin, corporate member of Freie Universität Berlin and Humboldt-Universität zu Berlin, Charitéplatz 1, 10117 Berlin, Germany

Introduction: Extracorporeal membrane oxygenation (ECMO) temporarily supports critically ill patients with cardiopulmonary support. Commonly used centrifugal pumps in ECMO systems pump blood at high pressures of up to 700 mmHg and flow rates that can fall below 1 l/min. Depending on the patient's needs, there is a wide range of operating points regarding head pressure and flow, which are often far outside the optimized design point of the pumps, increasing the risk for adverse events.[1]

Positive displacement pumps may offer an alternative, as their flow rates are more independent of the head pressure and mostly determined by the stroke volume times the pumping rate.

In this study, we propose a valveless, undulating displacement pumping concept with an adjustable pump gap and stroke volume that is operated by kinematic driven by a standard rotary motor. The concept might offer a blood gentle pumping principle over a broad operation range.

Methods: Stereolithography (SLA) 3D Printed parts were used as flow guiding and structural mechanical components. A kinematic, including two spherical polymer friction bearings and a ball cup friction bearing, was designed to transform the rotary motion of the motor into the undulating motion needed for the proposed pumping principle. A polyurethane foil of 200 µm thickness was thermoformed to serve as a pump sealing between the pump housing and the moving pumping part, designed to be stretched only to a minimal extend.

Pumping tests were performed with water-glycerol mixture (60/40 wt.) as blood mimicking fluid. Head pressures and flow rates were recorded for different pumping rates and pump adjustments.

Results: The kinematic allowed an adjustable undulating amplitude and pumping gap, leading to stroke volumes between 20 and 25 ml. Depending on the stroke rate, the set pumping rate and the set pumping gap, flow rates of up to 3.8 L/min against head pressures of up to 210 mmHg could be reached, ultimately leading to bending of some structural components.

Discussion: The tested undulating pump allows pumping of blood mimicking fluid with moderate flow rates of 3.8 L/min and head pressures of up to 210 mmHg after the positive displacement pump principle, without the need of valves or a driving membrane. The pumping limits were rather reached because of structural weaknesses of some kinematic parts as well as imperfect tolerances due to 3D printing, than by the underlying pumping principle. The shape of the thermoformed polyurethane foil is concepted to meet a compromise between manufacturability, mountability, washout, back flow and minimized foil stretching, but should be optimized for a fixed stroke volume.

This initially realized pump has rather generic dimensions and motion profiles since this is the very first realization effort. However, it shows promising results that indicate an early proof of concept of the pumping principle.

Therefore, a redesign of the pump is currently conducted, including stronger structural parts of the kinematic, attuned pump dimensions and pump rates as well as optimized foil shape.

With this, the overall hemocompatibility of the pump concerning blood damage and the risk of thrombus formation, especially over a broad range of operation points, needs to be assessed in future studies.

Reference

1. Gross-Hardt, Sascha et al. "Low-flow assessment of current ECMO/ECCO2R rotary blood pumps and the potential effect on hemocompatibility." Critical care (London, England) vol. 23,1 348. 6 Nov. 2019, doi:10.1186/s13054-019-2622-3

THREE-DIMENSIONAL SKELETAL MUSCLE MODELS AND ELECTRICAL STIMULATION IN MYOTONIC DYSTROPHY TYPE 1: APLICATIONS FOR MUSCLE-ON-A-CHIP DEVICE

Lis Quevedo (1), Juan Vaca (2), Diego Garzón (1), Angélica Ramirez (3)

1. Universidad Nacional de Colombia, Sede Bogotá, Colombia; 2. Universidad Nacional de Colombia, Sede de la Paz, Colombia; 3. Universidad Militar Nueva Granada, Colombia.

Introduction: Myotonic dystrophy type 1 (DM1) is a hereditary, progressive, degenerative disease and is the most prevalent myopathy in adults. Clinically, symptoms include myotonia, chronic fatigue, and muscular weakness [1-2]. Electrical stimulation (ES) emerges as a technique to replace electrical potentials and preserve muscular tissue functions.

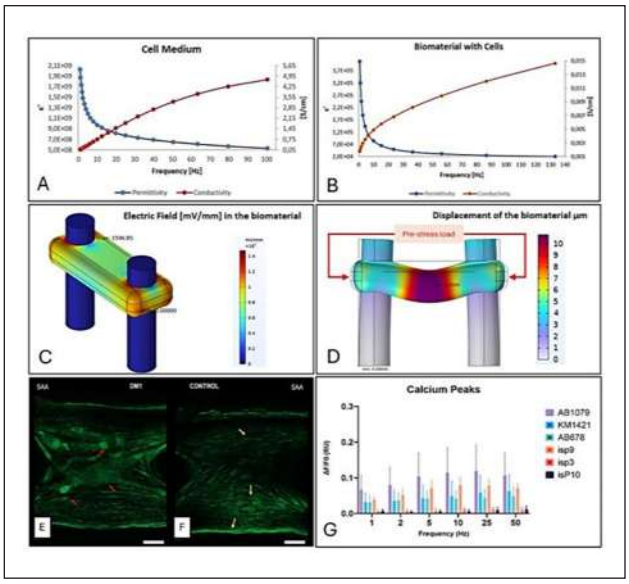

Figure 1. (A-B) Dielectric properties; (C-D) Computational model; (E-G) Experimental validation. SAA (Sarcomeric alpha Actinin)

However, the effect of this strategy on muscle fiber adaptations remains unknown [3]. On the other hand, contemporary advancements in human-based three-dimensional (3D) cell culture techniques have facilitated preclinical research by enhancing the reproduction of neuromuscular diseases [4]. Nowadays, there is no consensus about the range of electrical parameters that should be used when applying them to 3D muscle constructs, this variability presents a difficulty in comparing results between the studies [5].

Methodology: This study presents a combined computational and experimental approach. Initially, electrochemical impedance spectroscopy was employed to characterize the electrical properties (conductivity and permittivity) of 3D tissue constructs. Secondly, a multi-physical computational model integrating solid mechanics and electrostatics was formulated using COMSOL to quantify the electric field (EF) intensity within specific domains, and the consequent biomaterial displacement resulting from 3D muscle contraction induced by an EF. Finally, human DM1 and AB1079 cells (control) were cultured in Matrigel to validate the computational model. The 3D cultures were subjected to ES, calcium fluorescence, and immunostaining assays for functional and structural characterization of the tissues. The videos and images obtained were processed in Python and statistically analyzed with the Mann-Whitney U test.

Results: This is the first attempt to estimate the dielectric properties of both the cell medium and the biomaterial (Figure 1 A-B). The cell culture medium is a conductor material due to its low electric resistance. Conversely, the biomaterial, Matrigel, reveal its high resistance to current flow and moderate polarization. Regarding to the computational simulation, an EF was obtained in the biomaterial of a magnitude of 1506mV/mm and a displacement of 11.83 µm. The structural characterization of the 3D cultures, differences were detected such as the length and nuclear fusion phenotypes of the myofibers (See Figure 1 E-F). Furthermore, the 3D tissues developed from DM1, and control group presented opening of calcium channels in response to ES (See Figure 1G)

Discussion: This research calculates the dielectric properties of cell medium and biomaterial, allowing for accurate EF estimation within cell cultures, when ES is applied. The computational model facilitates the integration of electric and mechanical stimulations, elucidating their relationship in muscle contraction. The findings highlight the potential of the DM1 model as a platform for understanding EF effects on skeletal muscle. Overall, the study emphasizes the integration of technology and engineering into health research, showcasing the time-efficient benefits of combined experimental and computational approaches for generating 3D skeletal muscle models.

References

1. Ozimski, L.L., et al. Biol Rev, 96:716–730, 2021.
2. Smith C.A., et al. Curr Treat Options Neurol, 18:1-15, 2016.
3. Fernández-Costa, J.M., et al. Dis Model Mech, 16, 2023.
4. Maffioletti, S. M., et al. Cell Rep, 23:899–908, 2018.
5. Carter, S., et al. Pflügers Archiv, 471:413-429, 2019.

THE LIFE CYCLE OF MEDICAL DEVICES AS A DETERMINANT FOR HEALTHCARE SUSTAINABILITY

Joerg Vienken (1), Carlo Boccato (2)

1. MedTech Consultant, Usingen, Germany; 2. Freelance Consultant, Milan, Italy

Introduction: The concept of sustainability is generally understood to be associated with pollution, waste removal and energy consumption. However, these aspects must be extended to societal and economic issues when talking about medical devices and related successful healthcare. A successful healthcare therapy finally reduces cost and resources. A determining factor for medical devices in healthcare sustainability bases on their life cycle. It starts already with the conceptual design of the device, includes selection of suitable polymers, adaptation of device design to clinical needs and concepts for easy-to-use devices in patient application, not to forget final disposal of possibly contaminated products. This paper will test the hypothesis whether a careful control of the medical device life cycle will contribute to healthcare sustainability.

Medical device design and production: During production of medical devices resources such as energy related to Green House Gas Generation (GHG), and cost for transportation of components are to be provided. It has been estimated that the healthcare sector is responsible for the production of 4,4% of global GHG emissions.

Most medical devices and their necessary packaging are made of plastics, which represent 3% of the worldwide production of plastics and refer to about 14 million metric tons. In medical devices, mostly composite materials are applied which makes a final deposition after clinical use as “simple” waste difficult. They cannot be disassembled easily, such that their fate ends in the landfill, despite the fact, that these materials might be infectious. Incineration might be a solution, but some polymers, such as silicone and PVC need high temperatures (>750°C) to either become inflammable or exclude formation of HCL.

Medical devices should be made from polymers with the qualification “medical grade”. No generally accepted definition of “medical grade” exists, nor is it defined in the international pharmacopeias. As a result, compliance with ISO 10993 series is taken by manufacturers of medical devices by focusing exclusively on biocompatibility pattern. Further the role of perfluoroalkyl substances (PFAS) has become a matter of debate. Although they are used in many medical devices for the sake of easy clinical application, (e.g., in surface modifications of catheters), the EU and other authorities are considering their total ban.

Medical devices face an expiry date of either 2 or 3 years. Degradation of polymers during storage and use, e.g. after exposure to harsh environmental conditions. Among them are UV light, high temperatures, or unsuitable applications. These mechanisms should be carefully anticipated during life cycle assessment to avoid waste of valuable resources.

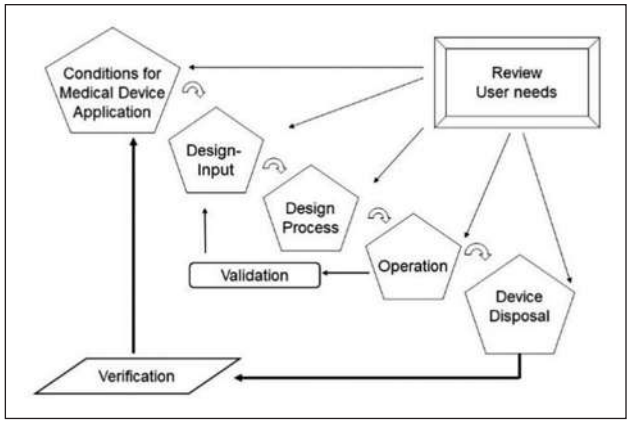

Figure 1. The medical device along the length of its life cycle under sustainability conditions seen from an engineering point of view. All leverage steps need validation and include a final verification for quality and risks. (adapted from C. Boccato et al; IJAO 2024).

Reuse or discard?: Already during the conceptual phase of a medical devices, the bioengineer should perform a Health-Technology (HTA) and a life cycle assessment under the premise of the 4R-loops of circular economy. 4R stands for reuse, repair, remanufacture and recycle of medical devices components. Such analyses will finally allow for decisions, whether a device should be easily dis-assembled or discarded after clinical use. Cost issues and environmental protection play here a decisive role.

Conclusion: Patient expectations for a better health and longevity are closely related to the clinical performance of medical devices which depends on its life-cycle. Careful consideration of the device´s life cycle is also important to assess the sustainability both for the environment and for the whole healthcare system. The establishment of an HTA-program during all steps of device production and application will contribute considerably to health care sustainability of medical devices.

RODENT SIZED OXYGENATOR–IN VITRO AND IN VIVO APPLICATIONS OF THE "RATOX"

Lasse J. Strudthoff[1], Jannis Focke[1], Felix Hesselmann[1], Andreas Kaesler[1], Ana Martins Costa[2], Peter Schlanstein[1], Thomas Schmitz-Rode[3], Ulrich Steinseifer[1], Niklas Steuer[1], Bettina Wiegmann[4], Jutta Arens[2], Sebastian V. Jansen[1]

1. Department of Cardiovascular Engineering, University Hospital RWTH Aachen, Germany; 2. Department of Biomechanical Engineering, University Twente, Netherlands; 3. Institute of Applied Medical Engineering, University Hospital RWTH Aachen, Germany; 4. Department for Cardiothoracic, Transplantation & Vascular Surgery, Hanover Medical School, Germany

Introduction: Research, development and the therapy itself have been progressing slow in extracorporeal life support (ECLS). The last disruptive breakthrough in the technology has been the introduction of hybrid polymethylpentene fibers with a plasma-tight outer layer two decades ago. One of the reasons for the slow progress is the lack of comprehensive and low-cost testing environments and modelling options. The same is true for clinical studies due to ethical considerations. All in all, research is impeded by lack of experimental models.

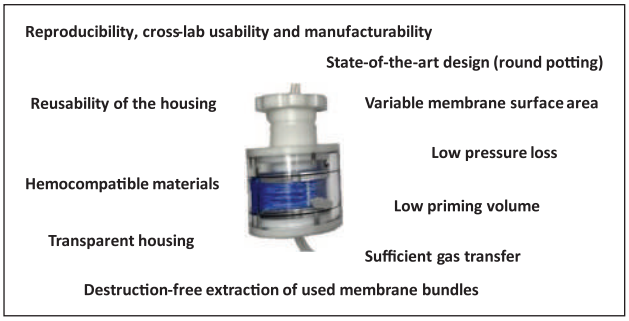

Figure 1. Photography of the RatOx oxygenator and key design requirements.

In other fields of medical and pharmaceutical research, rodent models, especially mice and rats, offer an effective, low-cost and feasible means for experiments. In ECLS, there has not yet been a miniaturization of the relevant components that allowed for broad and standardized application across laboratories. Our group has developed an oxygenator to close this gap.

The "RatOx" oxygenator is designed with the specifications listed in Fig. 1. We then tested the oxygenator performance in vitro [1]. Further, several groups have already begun using the RatOx in vivo, which is part of the current report.

Methods: The RatOx has an adjustable fiber module size between 10 cm^2 and 600 cm^2 gas transfer surface area, suitable for various rodents like mice, rats, or hamsters. The calculated priming volume, is kept between 1 and 6 ml, depending on the fiber module size. While in ECLS, mostly PMP fibers are used, any type of fiber mat can be mounted. The material of the casing is hemocompatible, sterilizable, reusable, and partly transparent. Applying DIN EN ISO 7199, experiments to establish the gas transfer efficacy were conducted in two independent research facilities. Further, we actively sought out groups capable of conducting in vivo experiments with the oxygenator.

Results: In its largest configuration and at a blood flow of 100 ml/min, the RatOx effectively transfers 5.5 ml O_2 / min and –5.5 ml CO_2 / min, respectively. For the same operating point, results from the independent laboratory showed transfer rates of 6.27 ml O_2 / min and –8.2 ml CO_2 / min, respectively. The measured priming volume for this the largest fiber module is 5.4 ml, and in a single fiber-mat configuration 1.1 ml of priming volume.

The RatOx is currently being investigated in eight external groups, six of which are attempting different forms of in vivo experiments. Our longest successful ECMO-run was 8h in a rat, we are currently aiming at a multi-day run of 72h in rats within one year. One group has already published their results for a post-mortem approach [2]. Five of six groups use Sprague-Dawley rats, on group uses specifically altered RatOx-oxygenators in hamsters.

Discussion: All current endeavors with the RatOx have proven extremely challenging but feasible. The RatOx is well received by the investigators, functioning well and easy in the handling. Most of all, its design promises reproducible results.

The RatOx oxygenator was developed to eventually become a standard device for any group and any research question in the vast field of ECLS to be investigated. We have already proven its effectiveness in vitro and post-mortem in rats and are currently pursuing several in-vivo investigations in cooperation with leading international groups. We are aiming for further studies to be performed using the RatOx. We could prove in vitro that the RatOx can be produced by an independent group without loss in effectiveness.

References

1. Strudthoff et al, Micromachines, 14, 800, 2023.
2. Deininger et al, Animals, 13, 3532, 2023.

DEVELOPMENT OF HEMODIALYSIS MEMBRANES FOR OUTSIDE-IN FILTRATION

Ramada, D. (1), Adema, B. (1), ter Beek, O. (1), Stamatialis, D. (1)

1. Department of Advanced Organ bioengineering and Therapeutics-Technical Medical Centre, University of Twente, The Netherlands

Introduction: Standard dialyzers used in hemodialysis (HD) therapy function by flowing the patients' blood through the lumen of each fiber, while the dialysate passes along the inter-fiber space. In this "inside-out" configuration, red blood cell accumulation at the device's entrance can occur, forming clots and effectively reducing the efficacy and longevity of the dialyzer. Changing the filtration mode—blood flowing in the space between fibers and dialysate flowing inside the fiber lumen—reduces the chance of blockages and potentially extends the duration of hemodialysis treatment [1]. For this "outside-in" filtration mode (OIF), the membrane morphology must also be adapted and reversed, so the selective biocompatible layer is on the outer fiber surface, in contact with the blood [2].

Methods: Outside-in hollow fibers were prepared by dry-wet spinning using polyethersulfone/polyvinylpyrrolidone polymer (PES/PVP) blends. The hollow fibers' physical (SEM, mechanical properties, and surface chemistry) and transport properties (molecular weight cutoff, toxin removal from human plasma spiked with creatinine, indoxyl sulphate and hippuric acid) were studied and compared with commercial HF membranes.

Table 1. Properties of selected hollow fiber membranes.

	P10P4	P8P4
ID/OD/Wall (µm)	280/440/95	240/409/101
K_{UF} (mL/(m^2.hmmHg))	13 ± 1	28 ± 3
Cr removal (mg/m^2)	1307 ± 112	1412 ± 139
HA removal (mg/m^2)	1122 ± 203	1024 ± 214
IS removal (mg/m^2)	332 ± 55	266 ± 58

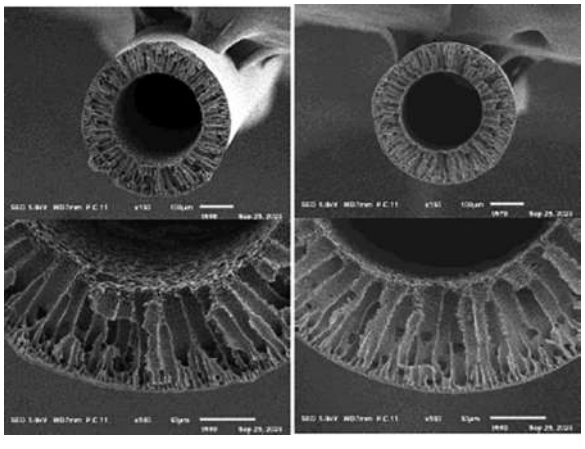

Figure 1. SEM images of the 2 fibers tested. Left image shows the fiber P10P4 (10% PES and 4% PVP) while the right image shows the fiber P8P4 (8% PES and 4% PVP).

Results: Figure 1 presents typical SEM images of two membranes selected for their representative characteristics, of all the fabricated membranes. They both have a smooth selective layer on the outside and a highly porous layer on the inside.

While the ultrafiltration coefficient of the membranes is quite different (due to different polymer concentrations, table 1), both membranes remove similar amounts of creatinine (Cr), hippuric acid (HA) and indoxyl sulphate (IS) for human plasma, while losing < 10% of the total protein content, in outside-in mode.

Discussion: This study describes the development of membranes for OIF HD. With optimizations to the polymer composition (to improve mechanical properties) and dialyzer design (suitable for OIF), we expect to improve the performance even further of these membranes.

References

1. Dukhin, S., et al., Outside-in hemofiltration for prolonged operation without clogging, Journal of Membrane Science, 464 (2014), p. 173-178.
2. Ramada, D.L. *et al.* (2023) 'Portable, wearable and implantable artificial kidney systems: Needs, opportunities and challenges', *Nature Reviews Nephrology*, 19(8), pp. 481–490.

Acknowledgements.

We thank Mr. Marc Ankone for his help in the mechanical properties' experiments.
D. Ramada acknowledges the financial support of the Top Sector Life Sciences & Health (Health~Holland), NODIAL project 21OP+035).

NOVEL DUAL-ACTION COATING FOR VASCULAR GRAFTS

Philippe Reymond[1], Daniela LaGrange[1], Jean-Pierre Giliberto[1], Rita Marchi[1], Olivier Felix[2], Michel Tschopp[2], Marie-Luce Piallat[1], Jean-Christophe Tille[1], Christoph Huber[1], Gero Decher[2], Pierre Fontana[1], Beat Walpoth[1]

1University & University Hospital, Geneva, Switzerland
2University of Strasbourg & C.N.R.S. Institut Charles Sadron, Strasbourg, France

Introduction: Surgical revascularisations (CABG/distal peripheral/AV shunts) are performed with autologous arteries and/or veins due to poor clinical patency results of commercial small-calibre (<5mm ID) vascular prostheses (ePTFE/PET), mainly due to early thrombosis and late intimal hyperplasia. [1] Therefore we have developed a dual-action coating which is anti-thrombogenic and endothelial cell-favouring.

Methods: Our dual-action coating is based on cell-favouring layer-by-layer (LbL) coating with end-point attached heparin. The coating was applied to small calibre, micro-porous, degradable polycaprolactone (PCL) electro-spun vascular grafts and patches and compared to uncoated samples. [2] *In vitro* 6mm patches were tested for coagulation tests (thrombin time/partial thrombin time/anti-Xa assays) and thrombin generation tests up to 7-days. Cell cultures were performed up to 7 days with endothelial and smooth muscle cells (spindle and rhomboid). *In vivo* uncoated and coated, 2mm ID vascular grafts were implanted in 18 rats in the abdominal aorta and followed up to 1, 3 and 12-weeks (n=3 per coating and implantation duration) [3].

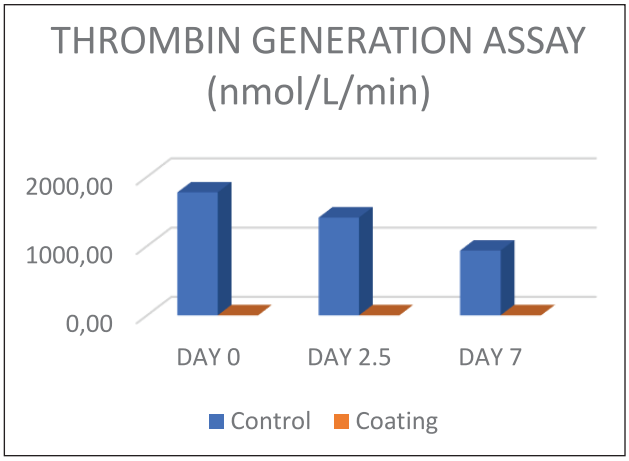

Figure 1.

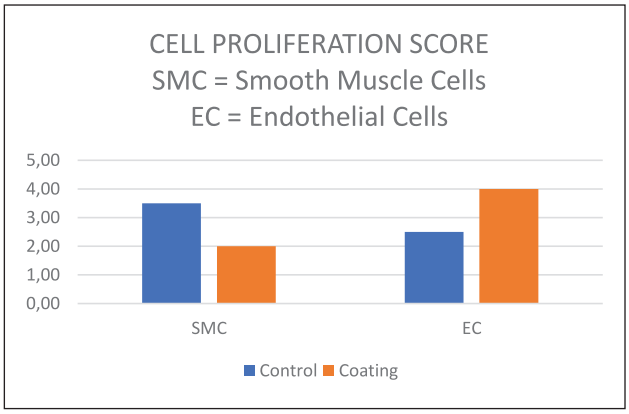

Figure 2.

Results: The *in vitro* coagulation tests showed heparin (anti-Xa) in the coated patches and no thrombin generation. The uncoated patches showed no heparin, clot formations and high thrombin generation (high levels of EPT (nmol/l/m)) Fig.1. Higher endothelial cell proliferation on the coated patches were found at 7-days in cell culture as well as a reduction of smooth muscle cells. Fig. 2. The *in vivo* animal tests showed 100% patency in the coated grafts and one occlusion in the uncoated grafts. The endothelialization was faster and confluent at 12 weeks in the coated compared to the uncoated grafts.

Discussion: The *in vitro* and *in vivo* anti-thrombotic and endothelial cell proliferating effects on micro-porous, degradable, vascular grafts of our novel dual-action coating have shown promising results. As future perspectives, the same approach will be used on ePTFE grafts which would allow their application for small calibre revascularization procedures such as coronary, peripheral vascular and access surgery for hemodialysis.

Furthermore, such a coating could be applied to all MedTech devices in contact with blood.

References

1. R. J. Halbert, et al. KIDNEY360 1: 1437–1446, 2020
2. B. Nottelet, et al. J Biomed Mater Res A. 89(4):865-75, 2009
3. S. de Valence, et al. Biomaterials 33: 38-47, 2012

ON THE DEVELOPMENT OF A BENCHMARK MAGLEV BLOOD PUMP AND INFLUENCE OF MANUFACTURING TOLERANCE ON PUMP PERFORMANCE.

Peng WU[1,2], Guan-Ting DU[2], Yu-Qiao BAI[2], Zhi-Cheng DONG[2], Shu LI[3]

1. Jiangsu Key Laboratory for Design and Manufacture of Micro-Nano Biomedical Instruments, School of Mechanical Engineering, Southeast University, Nanjing, China; 2. Artificial Organ Technology Laboratory, School of Mechanical and Electric Engineering, Soochow University, Suzhou, China; 3. National Institutes for Food and Drug Control, Institute for Medical Device Control, Beijing, China

Introduction: In recent years, blood pumps have become an effective therapy to treat patients with heart failure [1,2]. A blood pump should have good hydraulic performance on one hand, while its level of blood damage should be reduced to improve clinical treatment efficacy on the other hand. In-vitro blood damage test is an important means to evaluate the blood compatibility of newly developed blood pumps, and the control group is one of the key elements during in-vitro blood test. Up to now, the latest generation of blood pumps has employed maglev bearing, which can avoid problems such as friction, heat and secondary blood damage caused by mechanical bearings. However, the control group of blood pump has often been arbitrary. Legacy blood pumps with mechanical bearings have often been employed [3], with high level of blood damage, and large standard deviations of experimental data. At present, a benchmark blood pump that reflects the latest technological trend and provides a neutral and credible comparison as a control group is still lacking.

Methods: Therefore, this study aims at designing a maglev blood pump benchmark model and investigating the influence of manufacturing tolerance on the uncertainty of blood pump performance, so as to provide a reliable control group for in-vitro testing of blood pumps.

Results: The benchmark blood pump was developed in collaboration with National Institutes for Food and Drug Control of China. Magnetic bearing was employed, which can effectively reduce the secondary blood damage caused by mechanical bearings. The technological features of new-generation maglev blood pump such as short and long blades, semi-open impeller, large blade angles and spiral volute were employed. Preliminary hydraulic and hemolysis tests showed that the hydraulic performance of the blood pump benchmark model has reached the design goal, and the hemolysis level was significantly reduced compared with the FDA blood pump. With the non-intrusive polynomial chaos expansion (NIPCE) method, a surrogate model for the prediction of blood pump performance was established, and the influence of volute and impeller manufacturing tolerance on the performance of the benchmark blood pump was studied.

Discussion: The developed blood pump benchmark model will be beneficial for improving the reliability of in-vitro experimental data, and contribute to the development and evaluation of new generation blood pumps.

References

1. Kirklin JK et al, The Journal of Heart and Lung Transplantation, 36(10): 1080-1086,2017.
2. Kormos RL et al, The Journal of Heart and Lung Transplantation, 2019, 38(2): 114-126.
3. Malinauskas RA et a, Asaio Journal, 63(2): 150-160, 2017

Acknowledgements

The authors would like to acknowledge the support from National Natural Science Foundation of China (Grant Nos. 12072216) and the Mobility Program of the Sino-German Center (Grant No. M-0231).